ISSN 0021-9673

VOL. 588 NOS. 1 + 2 DECEMBER 27, 1991

COMPLETE IN ONE ISSUE

JOURNAL OF CHROMATOGRAPHY

INCLUDING ELECTROPHORESIS AND OTHER SEPARATION METHODS

ELSEVIER

JOURNAL OF CHROMATOGRAPHY

INCLUDING ELECTROPHORESIS AND OTHER SEPARATION METHODS

Scope. The *Journal of Chromatography* publishes papers on all aspects of chromatography, electrophoresis and related methods. Contributions consist mainly of research papers dealing with chromatographic theory, instrumental development and their applications. The section *Biomedical Applications*, which is under separate editorship, deals with the following aspects: developments in and applications of chromatographic and electrophoretic techniques related to clinical diagnosis or alterations during medical treatment; screening and profiling of body fluids or tissues with special reference to metabolic disorders; results from basic medical research with direct consequences in clinical practice; drug level monitoring and pharmacokinetic studies; clinical toxicology; analytical studies in occupational medicine.

Submission of Papers. Manuscripts (in English; *four* copies are required) should be submitted to: Editorial Office of *Journal of Chromatography*, P.O. Box 681, 1000 AR Amsterdam, Netherlands, Telefax (+31-20) 5862 304, or to: The Editor of *Journal of Chromatography, Biomedical Applications*, P.O. Box 681, 1000 AR Amsterdam, Netherlands. Review articles are invited or proposed by letter to the Editors. An outline of the proposed review should first be forwarded to the Editors for preliminary discussion prior to preparation. Submission of an article is understood to imply that the article is original and unpublished and is not being considered for publication elsewhere. For copyright regulations, see below.

Publication. The *Journal of Chromatography* (incl. *Biomedical Applications*) has 39 volumes in 1992. The subscription prices for 1992 are:

J. Chromatogr. (incl. *Cum. Indexes, Vols. 551–600*) + *Biomed. Appl.* (Vols. 573–611):
Dfl. 7722.00 plus Dfl. 1209.00 (p.p.h.) (total *ca.* US$ 4421.25)

J. Chromatogr. (incl. *Cum. Indexes, Vols. 551–600*) only (Vols. 585–611):
Dfl. 6210.00 plus Dfl. 837.00 (p.p.h.) (total *ca.* US$ 3488.50)

Biomed. Appl. only (Vols. 573–584):
Dfl. 2760.00 plus Dfl. 372.00 (p.p.h.) (total *ca.* US$ 1550.50).

Subscription Orders. The Dutch guilder price is definitive. The US$ price is subject to exchange-rate fluctuations and is given as a guide. Subscriptions are accepted on a prepaid basis only, unless different terms have been previously agreed upon. Subscription orders can be entered only by calender year (Jan.–Dec.) and should be sent to Elsevier Science Publishers, Journal Department, P.O. Box 211, 1000 AE Amsterdam, Netherlands, Tel. (+31-20) 5803 642, Telefax (+31-20) 5803 598, or to your usual subscription agent. Postage and handling charges include surface delivery except to the following countries where air delivery via SAL (Surface Air Lift) mail is ensured: Argentina, Australia, Brazil, Canada, China, Hong Kong, India, Israel, Japan*, Malaysia, Mexico, New Zealand, Pakistan, Singapore, South Africa, South Korea, Taiwan, Thailand, USA. *For Japan air delivery (SAL) requires 25% additional charge of the normal postage and handling charge. For all other countries airmail rates are available upon request. Claims for missing issues must be made within three months of our publication (mailing) date, otherwise such claims cannot be honoured free of charge. Back volumes of the *Journal of Chromatography* (Vols. 1–572) are available at Dfl. 208.00 (plus postage). Customers in the USA and Canada wishing information on this and other Elsevier journals, please contact Journal Information Center, Elsevier Science Publishing Co. Inc., 655 Avenue of the Americas, New York, NY 10010, USA, Tel. (+1-212) 633 3764, Telefax (+1-212) 633 3764.

Abstracts/Contents Lists published in Analytical Abstracts, Biochemical Abstracts, Biological Abstracts, Chemical Abstracts, Chemical Titles, Chromatography Abstracts, Clinical Chemistry Lookout, Current Contents/Life Sciences, Current Contents/Physical, Chemical & Earth Sciences, Deep-Sea Research/Part B: Oceanographic Literature Review, Excerpta Medica, Index Medicus, Mass Spectrometry Bulletin, PASCAL-CNRS, Pharmaceutical Abstracts, Referativnyi Zhurnal, Research Alert, Science Citation Index and Trends in Biotechnology.

See inside back cover for Publication Schedule, Information for Authors and information on Advertisements.

0021-9673/91/$03.50

This issue is printed on acid-free paper.

Printed in the Netherlands

CONTENTS

(Abstracts/Contents Lists published in Analytical Abstracts, Biochemical Abstracts, Biological Abstracts, Chemical Abstracts, Chemical Titles, Chromatography Abstracts, Current Contents/Life Sciences, Current Contents/Physical, Chemical & Earth Sciences, Deep-Sea Research/Part B: Oceanographic Literature Review, Excerpta Medica, Index Medicus, Mass Spectrometry Bulletin, PASCAL-CRNS, Referativnyi Zhurnal, Research Alert and Science Citation Index)

REGULAR PAPERS

Column Liquid Chromatography

(Continued overleaf)

Contents (continued)

Gas Chromatography

(Continued overleaf)

BOOK REVIEWS

In articles with more than one author, the name of the author to whom correspondence should be addressed is indicated in the article heading by a 6-pointed asterisk (*).

JOURNAL OF CHROMATOGRAPHY

VOL. 588 (1991)

JOURNAL of CHROMATOGRAPHY

INCLUDING ELECTROPHORESIS AND OTHER SEPARATION METHODS

ELSEVIER
AMSTERDAM — LONDON — NEW YORK — TOKYO

0021-9673/91/$03.50

Printed in the Netherlands

Journal of Chromatography, 588 (1991) 1–14
Elsevier Science Publishers B.V., Amsterdam

CHROM. 23 603

Effect of the sample solvent on band profiles in preparative liquid chromatography using non-aqueous reversed-phase high-performance liquid chromatography

Pavel Jandera* and Georges Guiochon*

**Department of Chemistry, University of Tennessee, Knoxville, TN 37996-1501 and Division of Analytical Chemistry, Oak Ridge National Laboratory, Oak Ridge, TN 37831-6120 (USA)*

(First received February 20th, 1991; revised manuscript received June 25th, 1991)

ABSTRACT

If a solvent with a higher elution strength than the mobile phase is used to dissolve poorly soluble samples in preparative chromatography, significant deformation of the band profiles occurs, especially when the column is overloaded. Eventually, band splitting may take place. This behavior was observed in non-aqueous reversed-phase chromatography of cholesterol and other low-polarity sample compounds dissolved in a non-polar solvent, such as dichloromethane, at concentrations exceeding their solubilities in the mobile phase, a higher polarity solvent such as acetonitrile. In this chromatographic system, the dependence of the band deformation and of its splitting on the volume and concentration of the sample, the composition of the mobile phase and the column temperature were investigated. A model taking into account the dependence of the solubility of the sample components in the sample solvent and in the eluent and of the equilibrium isotherm of these components between the stationary and mobile phases on the composition of these two solvents (eluent and sample solvent) was worked out. The possible formation of supersaturated solutions was also considered in the model. This model permits the computer simulation of the band profiles for a single compound or for mixtures dissolved in a solvent different from the mobile phase. The results of the simulations are in qualitative agreement with the behavior observed experimentally.

INTRODUCTION

The main objective of optimization in preparative liquid chromatography is to obtain the lowest production cost. Academics, who lack reliable data for cost estimates, settle for finding the conditions permitting the maximum throughput of the purified material [1]. For this latter purpose, the sample load should be large. This may be difficult if the sample is not well soluble in the mobile phase. Two procedures are often used in an attempt to overcome this problem, the so-called "dry injection" of a solid sample [2] or the dissolution of the sample in another solvent in which it is more soluble than in the mobile phase. In the latter instance, great caution must be exercised to avoid the use of a solvent stronger than the mobile phase.

Very hydrophobic compounds, insoluble in water and poorly soluble in polar organic solvents such as methanol or acetonitrile, can be separated on alumina or silica, which are the preferred stationary phases for preparative applications involving these compounds. Mobile phases of low polarity must be used to achieve an adequate retention for a successful separation or purification. Partly water-saturated aliphatic hydrocarbons or dichloromethane are suitable for this purpose, but it is difficult to maintain good reproducibility in these chromatographic systems unless the trace concentrations of water in the solvents are carefully controlled, such as by using a "moisture control system" [3], a procedure which could be difficult and costly to use under

* On leave from the Institute of Chemical Technology, Pardubice, Czechoslovakia.

0021-9673/91/$03.50

preparative conditions. An aliphatic hydrocarbon containing 0.01–1% of a polar solvent such as propanol can be used as the mobile phase, but then the solvents used for the preparation of the mobile phase should be carefully dried to achieve good reproducibility [4,5].

The problems encountered with the control of the water content in normal-phase systems have led to attempts to separate strongly hydrophobic compounds by reversed-phase chromatography. In contrast to the polar adsorbents, the retention of these compounds on C_{18} or C_8 chemically bonded phases is large and non-aqueous eluents such as pure acetonitrile or its mixtures with chloroform, dichloromethane or tetrahydrofuran should be used to accomplish the elution in an acceptable time. For example, non-aqueous reversed-phase (NARP) systems [6] have been applied to the separations of fats [6], carotenoids [7] and sterols [8]. Under such conditions, homologs or isomers of the hydrocarbon groups may be much better resolved than on silica, which is another incentive to use NARP in preparative separations. The solubility of hydrophobic compounds in the mobile phase required for an adequate retention and a good resolution in non-aqueous reversed-phase chromatography is usually poor.

This problem is minor in analytical applications and NARP has become a popular approach. In preparative chromatography, however, mass overload of the column cannot be achieved without a high degree of volume overload when the sample is dissolved in the mobile phase. This does not permit a high production rate. Gradient elution in non-aqueous reversed-phase chromatography cannot be expected to resolve the solubility problem, as the solubility of hydrophobic samples is much lower in the weaker, starting eluent than in the stronger eluent used to generate the gradient or even than the eluent used for the isochronic, isocratic analysis.

Nevertheless, attempts are often made to overcome the limitation due to the low solubility of the sample in the eluent by using a stronger, low-polarity solvent to dissolve the sample. Considerable success has been achieved in the trace analysis of aqueous samples by reversed-phase chromatography by using the opposite approach, a mobile phase stronger than the sample solvent. Large volumes of the samples can be separated without a significant increase in band broadening because of the strong concentrating effect referred to as the sample focusing effect. Although the use of a sample solvent stronger than the mobile phase is not recommended, it usually causes only slight problems in analytical high-performance liquid chromatography (HPLC), where small sample amounts are injected. In preparative chromatography, on the other hand, the chromatograms obtained under these conditions exhibit often band profiles which are considerably deformed in unusual ways and sometimes split peaks appear [7,9]. This phenomenon leads to important separation difficulties and to a dramatic decrease in production rate [9].

In this paper, we report on an experimental and theoretical investigation of column overloading in non-aqueous reversed-phase chromatography, using cholesterol as a sample dissolved in mixtures of dichloromethane and acetonitrile.

THEORETICAL

From the theoretical point of view, the problem studied involves the simultaneous injection of a pulse of the component of interest (cholesterol) and of a pulse of the non-retained sample solvent (dichloromethane) in the mobile phase (acetonitrile). The dichloromethane band moves along the column at the mobile phase velocity, it broadens because of axial dispersion and of the finite rate of diffusion in the mobile phase and it dilutes. The profile of this band is easy to calculate at all times. The behavior of the cholesterol pulse is more complex because the presence of dichloromethane in the mobile phase changes greatly the local retention and solubility of cholesterol. Both the cholesterol solubility and its isotherm depend strongly on the dichloromethane concentration in the mobile phase. Thus, both are functions of the distance migrated by the solute along the column and of time. The effects of this dependence must be accounted for.

The semi-ideal model of non-linear chromatography was used for the calculation of band profiles [10–13]. This model assumes finite mass-transfer kinetics with rate constants and dispersion coefficients which are independent of the solute concentration in the mobile phase. It is expressed by a

system of partial differential equations, stating the mass balance of each sample component involved except the weak solvent, and of algebraic equations, stating the competitive isotherms of these components. This system of equations can be solved by numerical calculations.

The isotherm relates the concentrations of cholesterol in both phases at equilibrium. In the problem under investigation, the isotherm depends on the local composition of the mobile phase. The solute is introduced into the column with a pulse of the sample solvent (dichloromethane) which progressively dilutes and spreads in the mobile phase (acetonitrile); the pulse of the non-retained dichloromethane moves faster than the pulse of cholesterol. Accordingly, the isotherm changes as the environment of cholesterol is being changed from pure dichloromethane to pure acetonitrile. In contrast to the classical problem of isocratic elution, the isotherm coefficients are a function of the time and the position in the column, as during a step gradient elution. The original computer program [10,13] was adapted to take into account this dependence.

A further modification was needed to account for the fact that the solubility of the component studied decreases rapidly with decreasing dichloromethane concentration. A limiting condition was introduced in the calculation algorithm to prevent the propagation from one column space element (plate) to the next of an amount of the solute which would exceed the amount permitted by its solubility in the local mobile phase. In the last set of simulations, the calculation algorithm was further refined to take into account the possible formation of supersaturated solutions of the sample solutes, as will be discussed later.

EXPERIMENTAL

Instrumentation

An HP 1090M liquid chromatograph (Hewlett-Packard, Palo Alto, CA, USA), equipped with a 3DR solvent-delivery system, an automatic sample injector with a 250-μl sample loop, a temperature-controlled column compartment, a diode-array UV detector and a data work-station, was used both to record the band profiles of large-size samples and to acquire the data necessary for the determination of the equilibrium isotherms.

Column

We used Nucleosil 500-C_{18}, a wide-pore, spherical C_{18}-bonded silica, with an average particle size of 7 μm, available from Macherey-Nagel (Düren, Germany). The specific surface area of the support is 35 m^2/g (average pore diameter 50 nm). This material was packed in the laboratory into a stainless-steel column (250 mm × 4.6 mm I.D.) using a high-pressure slurry technique.

The column efficiency was 17 000 theoretical plates for benzene and *n*-butylbenzene as the test solutes in 100% acetonitrile at 35°C and 1 ml/min (h = 2.1). The column dead volume measured with acetone as the unretained compound was V_M = 3.174 ml in acetonitrile containing 0–20% of dichloromethane as the mobile phase. The total column porosity was ε_T = 0.764 and the phase ratio V_S/V_M = 0.308 (V_S is the volume of the stationary phase in the column).

Mobile phase and solutes

Spectroscopic-grade acetonitrile and dichloromethane (Burdick & Jackson, Muskegon, MI, USA) were filtered through a 0.45-μm filter (Millipore, Milford, MA, USA) and used to prepare the mobile phase by mixing in various ratios from 100:0 to 20:80. The mobile phase was de-gassed continuously in the liquid chromatograph by stripping with helium. The flow-rate was 1 ml/min in all experiments. Cholesterol (99% grade; Sigma, St. Louis, MO, USA) and tridecylbenzene (99%; Aldrich, Milwaukee, WI, USA) were used as the sample solutes.

Measurement of experimental band profiles

Samples of 5–250 μl of 32.3 and 70.8 g/l cholesterol solutions and of 91.4 g/l tridecylbenzene solution in dichloromethane were injected onto the column using the automatic sample injector. Acetonitrile and 5% and 10% solutions of dichloromethane in acetonitrile were used as the mobile phases at constant temperature (35, 40 or 45 ± 1°C).

Determination of equilibrium isotherms

The equilibrium isotherms were measured using the frontal analysis method as described previously

[12]. The mobile phase (0–80% solutions of dichloromethane in acetonitrile) was stored in one of the solvent flasks of the solvent-delivery system and a solution of cholesterol in the same mobile phase in another flask. The gradient-delivery system was used to mix and pump the solutions needed for the frontal analysis experiments. Caution was paid that the concentration of cholesterol in these solutions, C_m, was always at least 10% below the solubility limit in a given mobile phase, to avoid possible precipitation of cholesterol in the instrument lines (Table I).

The flow-rate ratio of the liquids pumped from the two flasks, which controls the concentration of cholesterol delivered continuously to the column, was changed from 0 to 100% in 10% steps. Time was allowed for the stabilization of the detector signal, recorded at 215 nm, after each concentration change. The flow-rate (1 ml/min) and the temperature (35°C) were kept constant during all the experiments.

In each experiment, the concentration of cholesterol in the stationary phase, q_i, was determined from the integral mass balance equation, using the experimental retention volume (inflection point of the breakthrough curve), corrected for the volume of the tubing between the mixing point of the liquids pumped in each channel and the top of the column, as described previously in more detail [12].

TABLE I

SOLUBILITY AND ISOTHERM PARAMETERS OF CHOLESTEROL

ϕ = Concentration (%, v/v) of dichloromethane in acetonitrile; x_s = solubility (g/l) of cholesterol; c_m = concentration (g/l) of cholesterol solutions used for frontal analysis measurements (see procedure under Experimental); a_1, a_2, b = best values of the parameters of the isotherm obtained by fitting the experimental data to eqn. 3. Column: 250 × 4.6 mm I.D. Nucleosil 500-C_{18} (7 μm); 35°C.

ϕ	x_s	c_m	a_1	a_2	b (l/g)
0	0.872	0.728	6.958	13.924	11.645
5	1.582	1.372	5.166	9.922	7.447
10	2.241	2.097	4.259	7.558	4.472
20	3.932	3.285	2.638	3.624	0.781
30	6.794	5.822	1.617	1.762	0.433
40		10.106	1.055	0.963	0.246
50		15.72	0.690	0.452	0.127
60		25.31	0.572	0.237	0.162
80		34.71	0.338	0.141	0.130
100	>160	–	0.2[a]	0.1[a]	0.13[a]

[a] Values extrapolated from eqns. 4–6.

Determination of solubility of cholesterol

An excess of cholesterol was stirred with a mixture of acetonitrile and dichloromethane in an ultrasonic bath for 10 min and allowed to stand overnight. A 20-μl sample of the supernatant saturated solution was analyzed, using pure acetonitrile as the mobile phase, at 1 ml/min and 35°C. The solubility of cholesterol in the saturated solution, x_s, was evaluated from the results of three repeated analyses, using a calibration graph based on the integrated peak areas (Table I).

Computer

Computations were performed on a VAX 8650 computer (Digital Equipment, Marlboro, MA, USA) at the Computer Center of the University of Tennessee. Because the computation time needed to calculate a band profile is proportional to the square of the plate number of the column [10–12] and takes several hours for a 17 000-plate column, an efficiency of only 2000–5000 theoretical plates was considered in most of these calculations.

RESULTS AND DISCUSSION

Experimental band profiles

If cholesterol is injected as a very dilute solution in pure acetonitrile as the mobile phase, its capacity factor is 6.4. When larger samples are injected, the band becomes asymmetric and its shape becomes progressively unusual.

Figs. 1 and 2 show the experimental band profiles observed at 35°C for 5–250-μl samples of 32.3 (Fig. 1) and 70.8 g/l (Fig. 2) solutions of cholesterol dissolved in pure dichloromethane, with 100% acetonitrile as the mobile phase. These concentrations are respectively 37 times and 81 times higher than the solubility of cholesterol in the pure acetonitrile reported in Table I.

In both figures and for a sample size of 5 μl (profiles 1), the cholesterol band exhibits the typical shape, with a sharp front and tailing rear end, which correspond to column overloading with a component having a convex upward isotherm. For larger

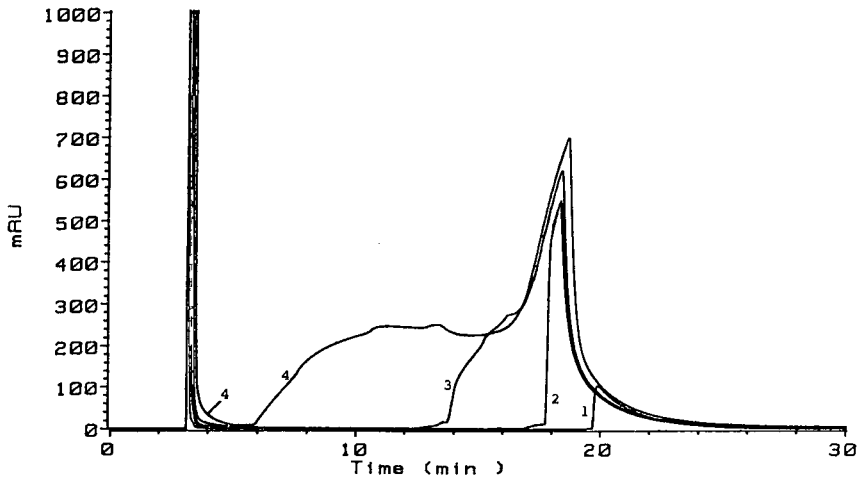

Fig. 1. Experimental band profiles of samples of cholesterol dissolved in dichloromethane. Column, 250 × 4.6 mm I.D., Nucleosil 500-C_{18} (7 μm); mobile phase, acetonitrile; temperature, 35°C; mobile phase flow-rate, 1 ml/min; detection, UV at 215 nm; sample concentration, 32.3 g/l of cholesterol. Sample volume: 1 = 5; 2 = 20; 3 = 50; 4 = 100 μl.

sample sizes, the profile becomes different. The front shock layer does not extend from the baseline to the band maximum, but the top of the band front is slanted (profiles 2 in both figures). When the sample size is increased further (profiles 3 in both figures), a hump appears, preceding the band maximum. With increasing sample sizes (profiles 4 in both figures), this hump grows and appears earlier and earlier. The retention time of the peak maximum is nearly constant in Fig. 1 (profiles 2–4); it increases slowly with increasing sample size in Fig. 2 (profiles 2–5). From the detector calibration graph we calculated that the maximum band height in Figs. 1 and 2 corresponds to *ca.* 80% of the cholesterol solubility in dichloromethane.

This behavior contrasts with that observed previ-

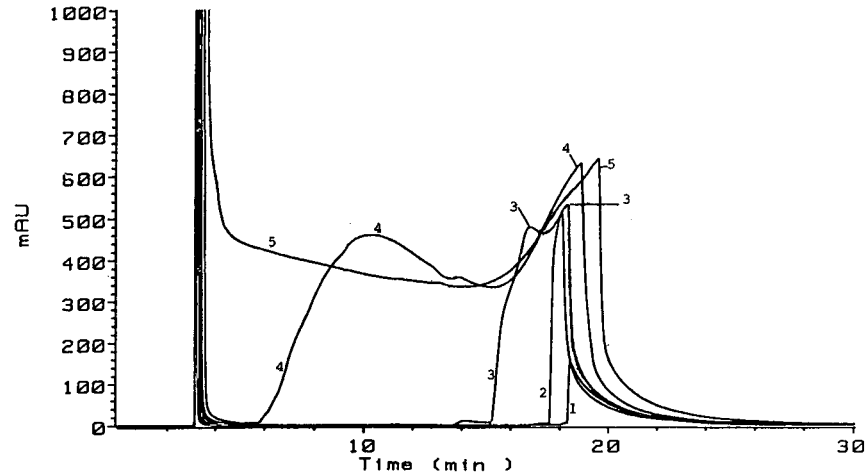

Fig. 2. Experimental band profiles of samples of cholesterol dissolved in dichloromethane. Conditions as in Fig. 1, except cholesterol concentration, 70.8 g/l, and sample volume: 1 = 5; 2 = 10; 3 = 30; 4 = 100; 5 = 250 μl.

TABLE II

HEIGHTS OF THE "DEAD VOLUME" PEAK

c_s = Concentration (g/l) of cholesterol in dichloromethane as the sample solvent; h_5–h_{100} = heights of the "dead volume" peak (in milliabsorbance units) in the chromatograms of samples with volumes of 5, 20, 30, 50 and 100 μl, respectively (see Figs. 1 and 2).

c_s	h_5	h_{20}	h_{30}	h_{50}	h_{100}
32.3	800	1700	1870	1950	2050
70.8	640	1450	1750	2050	2500

ously [13,14]. The most striking characteristic of these chromatograms, however, is their second mode, a feature which is exceedingly rare in chromatography. With profile 2 in both figures, a second peak appears at the column dead volume. Its relative importance increases with increasing sample size. The hump of the main band merges eventually with the dragging tail of the dead volume peak at large sample sizes (profile 5 in Fig. 2).

Dichloromethane is not retained and is eluted at the column dead volume. However, the first peak, eluted at the dead volume, cannot be attributed to this solvent alone. The presence of cholesterol in the "dead volume" peak is proven by the following observations: (a) the UV spectra recorded for this peak are very similar to the spectrum of cholesterol in dichloromethane; (b) the "dead volume" peak increases with increasing concentration of cholesterol in a sample of constant volume (50 or 100 μl) whereas the concentration of dichloromethane in the sample actually decreases, in contrast to lower sample volumes where only dichloromethane with no cholesterol is present in the "dead volume" peak (Table II); (c) re-injection of a fraction collected during the elution of the "dead volume" peak gives a peak at the cholesterol time.

Similar behavior was observed with samples of solutions of tridecylbenzene in dichloromethane (Fig. 3). The nearly symmetrical peak obtained for the low-volume samples (profiles 1 and 2) indicates that the sorption isotherm is almost linear in this size range and suggests that band deformation and splitting may occur even under conditions where the column is not overloaded. Most probably the tridecylbenzene contains some isomeric and homologous impurities to which the smaller peaks in the earlier part of the chromatogram can be attributed. However, as for the chromatograms in Figs. 1 and 2, when the sample size is increased, a new peak appears at the "dead volume" and a hump is observed at the front of the retained band; it grows and eventually merges with the dead volume peak, whereas the retention time of the band maximum remains nearly constant and, at very high sample sizes, begins to increase with increasing sample size.

Quantitative study of the chromatograms in Figs. 1 and 2 shows that the hump appears for a

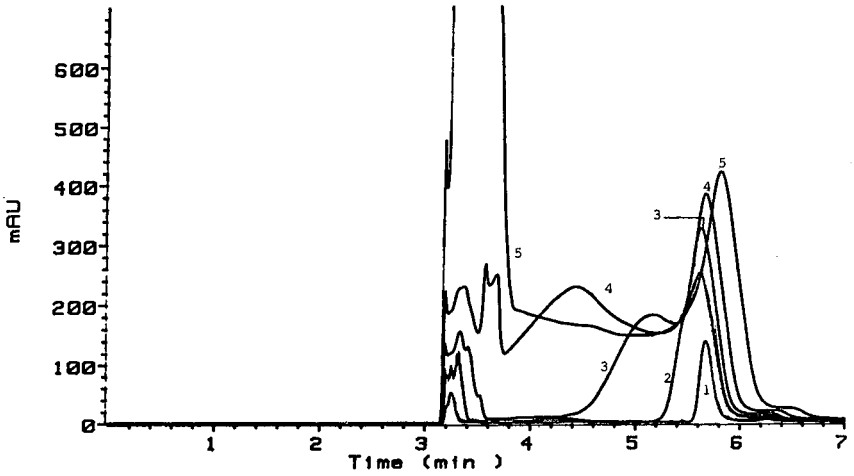

Fig. 3. Experimental band profiles of samples of tridecylbenzene dissolved in dichloromethane. Conditions as in Fig. 1, except sample concentration, 91.4 g/l, detection wavelength, 230 nm, and sample volume: 1 = 5; 2 = 20; 3 = 50; 4 = 100; 5 = 250 μl.

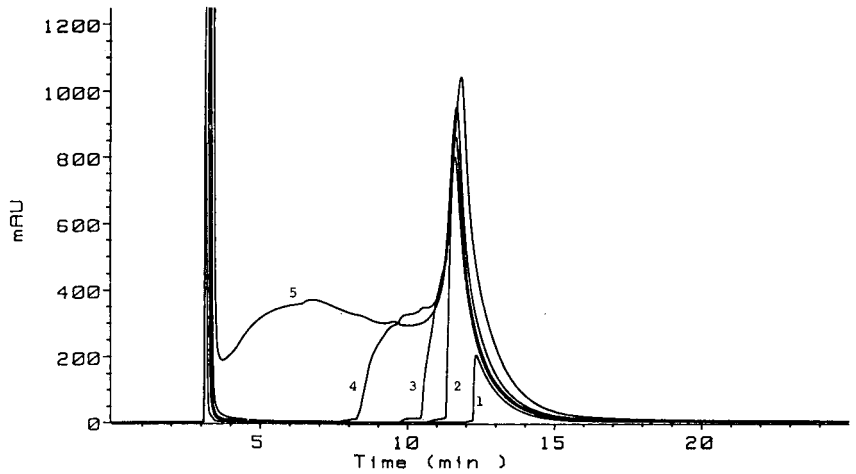

Fig. 4. Experimental band profiles of samples of cholesterol dissolved in dichloromethane. Conditions as in Fig. 1 (including sample volumes), except temperature, 45°C.

sample volume of 50 μl with the 32.3 g/l cholesterol solution (Fig. 1, profile 3) and for a sample volume of 30 μl with the 70.8 g/l solutions (Fig. 2, profile 3), corresponding to sample amounts of 1.5 and 2.1 mg, respectively. The behavior of the front of the retained band ceases to be normal when the sample exceeds *ca.* 0.7 mg. However, the amount of cholesterol injected does not control the phenomenon entirely. The amount of cholesterol for which splitting and band deformation begin to occur increases with decreasing sample concentration.

To investigate further the effect of the experimental conditions, band profiles of samples of increasing volume of a 32.3 g/l cholesterol solution in dichloromethane were recorded at 40 and 45°C (Fig. 4) with pure acetonitrile as the mobile phase, and at 35°C (Fig. 5) with 5% and 10% dichloromethane solutions in acetonitrile as the mobile

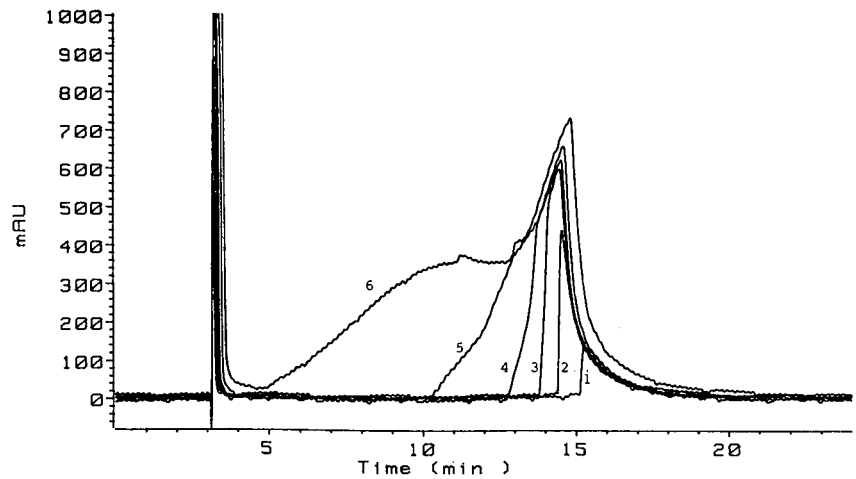

Fig. 5. Experimental band profiles of samples of cholesterol dissolved in dichloromethane. Conditions as in Fig. 1 (including sample volumes), except the mobile phase, acetonitrile-dichloromethane (95:5).

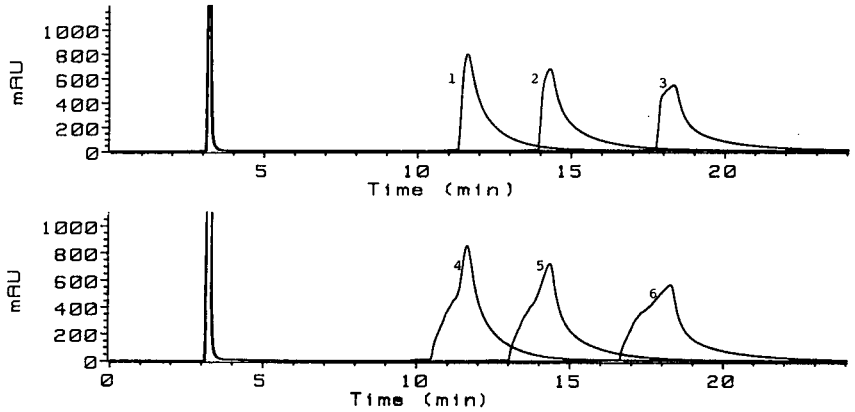

Fig. 6. Experimental band profiles of samples of cholesterol dissolved in dichloromethane. Conditions as in Fig. 1. Band profiles of 20 μl (top, 1–3) and 30 μl (bottom, 4–6) samples of a 32.3 g/l cholesterol solution, measured at (1, 4) 45°C, (2, 5) 40°C and (3, 6) 35°C.

phase. Increasing the temperature or the concentration of dichloromethane results in an increase in the cholesterol solubility and a decrease in the retention times. The aforementioned behavior of the band profiles is still observed, however. Fig. 6 shows the band profiles for the same sample sizes at 35, 40 and 45°C and Fig. 5 compares the band profiles in acetonitrile containing 0, 5 and 10% dichloromethane. The profiles in Figs. 4 and 5 show the same trends as those in Figs. 1 and 2. The profiles in Figs. 6 and 7 show that, at constant sample size, the intensity of the band deformation decreases slightly with increasing temperature and increasing dichloromethane concentration.

The phenomena observed cannot be explained by the appearance of system peaks, because pure acetonitrile was used in most experiments reported here and because dichloromethane is not retained under the chromatographic conditions used. The probable cause of these results is the variation of the solubility of cholesterol in the mobile phase during the migration of the dichloromethane band, as already suggested by Khachik *et al.* [7] to explain similar observations. In this instance, the band

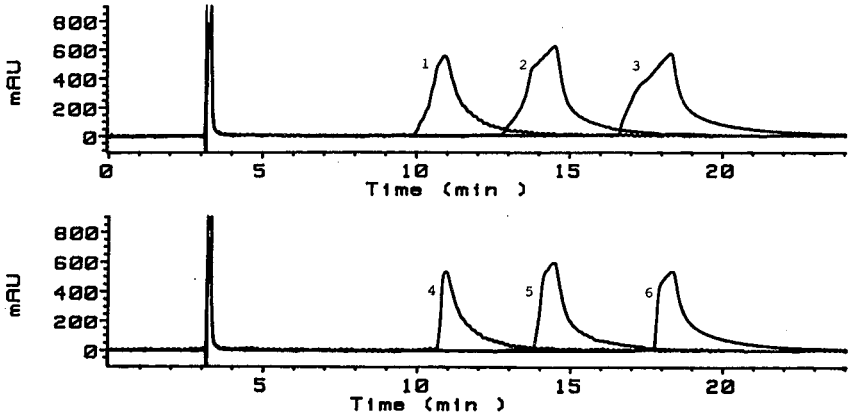

Fig. 7. Experimental band profiles of samples of cholesterol dissolved in dichloromethane. Conditions as in Fig. 1. Band profiles of 30 μl (top, 1–3) and 20 μl (bottom, 4–6) samples of a 32.3 g/l cholesterol solution, eluted with acetonitrile containing (1, 4) 10%, (2, 5) 5% and (3, 6) no dichloromethane.

profile could depend on the shape of the sorption isotherm, the solubility of the sample in the solvent mixtures, the exact injection profile of the sample and the possible formation of supersaturated solutions close to the solubility limits. The formation of supersaturated solutions of cholesterol in the solvents used was observed during the study.

These factors are taken into account in an approximate model which can be used for simulation of the behavior observed. First, an appropriate description of the experimental isotherms is needed.

Equilibrium isotherms

The equilibrium isotherms of cholesterol were measured in various mobile phases containing 0–80% dichloromethane in acetonitrile, in order to collect the data necessary to perform the calculations. As an example, the experimental data points are reported in Fig. 8 (symbols) for pure acetonitrile. These points were fitted to the Langmuir isotherm equation:

$$q_i = \frac{ac_i}{1 + bc_i} \quad (1)$$

where q_i and c_i are the stationary and mobile phase concentrations, respectively, and a and b are numerical parameters. The result was not satisfactory (Table III). An attempt to fit these data to the bi-Langmuir isotherm:

$$q_i = \frac{a_1c_i}{1 + b_1c_i} + \frac{a_2c_i}{1 + b_2c_i} \quad (2)$$

where a_1, b_1, a_2 and b_2 are numerical parameters, was also unsuccessful. Small and sometimes negative values of b_2 were obtained.

As the plots of the experimental isotherms appeared to be nearly linear in the high-concentration range, the data were fitted to the sum of a Langmuir and a linear isotherm, *i.e.*, a bi-Langmuir isotherm with the parameter $b_2 = 0$:

$$q_i = \frac{a_1c_i}{1 + bc_i} + a_2c_i \quad (3)$$

This last isotherm gives values of q_i which are in much better agreement with the experimental results

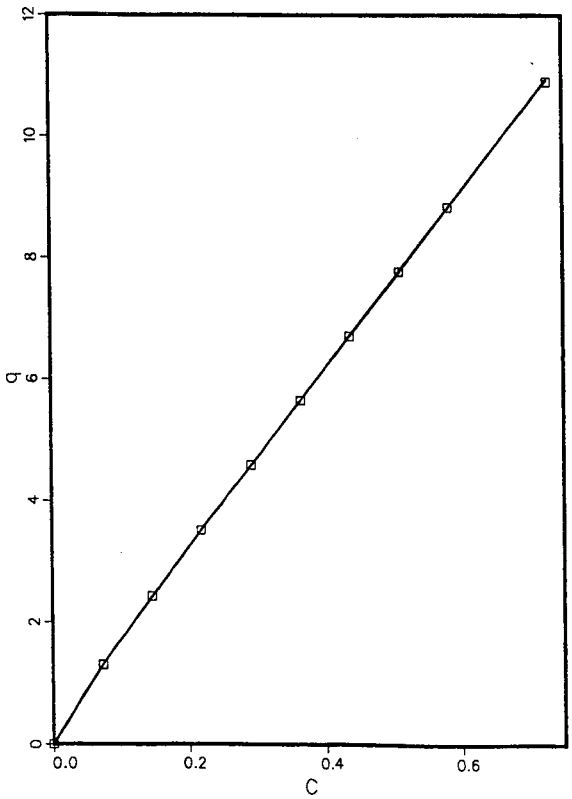

Fig. 8. Experimental isotherm of cholesterol in acetonitrile at 35°C. Symbols, data points by frontal analysis. Solid line, best fit to eqn. 3 (parameters a_1, a_2, b in Table I). c and q = concentrations (g/l) of cholesterol in the mobile and stationary phase, respectively.

TABLE III

EXPERIMENTAL AND PREDICTED CONCENTRATIONS OF CHOLESTEROL IN THE STATIONARY PHASE

c_s = Concentration (g/l) of cholesterol in acetonitrile as the mobile phase; q_i (E) = concentration (g/l) of cholesterol in the stationary phase determined experimentally by frontal analysis; q_i (C-1) = concentration (g/l) of cholesterol in the stationary phase calculated from the eqn. 1 (Langmuir isotherm); q_i (C-3) = concentration (g/l) of cholesterol in the stationary phase calculated from the eqn. 3 (combined isotherm). Column and temperature as in Table I.

c_s	q_i (E)	q_i (C-1)	q_i (C-3)
0.0728	1.296	1.234	1.298
0.1456	2.426	2.425	2.424
0.2183	3.514	3.574	3.511
0.2911	4.583	4.685	4.583
0.3639	5.645	5.759	5.648
0.4366	6.706	6.798	6.709
0.5094	7.766	7.803	7.767
0.5822	8.826	8.776	8.823
0.7278	10.898	10.633	10.932

than the first isotherm (eqn. 1), as shown in Table III. Deviations between the experimental and calculated values of the amount adsorbed at equilibrium are always less than 0.003 g/l of packing material with eqn. 3 whereas they exceed 0.1 g/l with eqn. 1. The same results were obtained for all the concentrations of dichloromethane used. The composite isotherm (eqn. 3) fitted the data very well.

The best values of a_1, a_2 and b in the equilibrium isotherms obtained for the different mobile phase compositions at which measurements were carried out are reported in Table I. The linear regression of the logarithms of the experimental parameters a_1, a_2 and b on the dichloromethane concentration, ϕ, yielded the following equations which account well for the mobile phase dependence of these parameters:

$$\log a_1 = 0.770 - 0.02056\,\phi \quad (4)$$

$$\log a_2 = 1.096 - 0.03145\,\phi \quad (5)$$

$$\log b = 0.748 - 0.04491\,\phi \quad (6)$$

Thus, a general isotherm (eqn. 3) valid over a wide range of mobile phase compositions can be formulated.

Because of too low a cholesterol retention, it was impossible to determine accurately the isotherm parameters in acetonitrile solutions with more than 80% of dichloromethane. The values of a_1, a_2 and b in pure dichloromethane necessary for the calculations discussed later were derived by extrapolation from the data measured at lower dichloromethane concentrations (see Table I).

We have at present no justification for the isotherm used, except that it fits the whole set of data extremely well. It also accounts well for the band profiles observed, which are controlled by the Langmuir term, dominant at low concentrations in spite of the little deviation observed from linear behavior [10]. The properties of the chromatographic system and of the sample solute could explain the isotherm: a bimodal surface energy distribution, a mixed retention mechanism or an accidental compensation between effects leading to the curvature of the isotherm in opposite directions (*e.g.*, surface saturation and adsorbate–adsorbate interactions). Some features of the chromatograms in Fig. 2, such as the very steep rear part of the profile, could suggest that the isotherm has an inflection point at high concentrations. For this reason, we carried out the isotherm measurements in the whole range of concentrations accessible, up to 90% of the mobile phase saturation at all compositions of this phase. Although we cannot rule out an inflection, and especially not one in the supersaturated range, we have found none. Further, measurements are not possible in the supersaturated range, even if such solutions may have a transitory existence in the column.

A calculation based on the molecular weight of cholesterol, 386.7, on the assumption of spherical molecules, on the specific surface area of the silica used (35 m^2/g), the packing density of the column (0.5 g/ml) and the volume of octadecylsilica (0.979 ml) gives an estimate of the monomolecular layer capacity of the column for cholesterol, 42 mg. Using the isotherm (eqn. 3) and the appropriate parameters from Table I, it is found that this amount would be adsorbed at equilibrium with a 3 g/l solution of cholesterol in acetonitrile, which is approximately three times the solubility of cholesterol. Again, this concentration exceeds considerably the limits within which measurements are possible.

Simulation calculations of cholesterol band profiles

Not surprisingly, calculations of the band profiles of cholesterol samples performed using the classical algorithm [9–13] and the isotherm parameters measured in pure acetonitrile (Table I) give profiles (not shown) typical of a convex upward isotherm and similar to typical Langmuirian band profiles as those reported previously [12–14]. Whatever the combination of concentration and volume used, these profiles are not like those recorded during the experiments (Figs. 1–7). The agreement with experimental profiles is not improved when the algorithm is modified to take into account the dependence of the isotherm coefficients on the local composition of the mobile phase, *i.e.*, both on the time and the position of the solute in the column, but not the limited solubility of cholesterol in acetonitrile. Thus, neither the equilibrium isotherm nor the passage of the dichloromethane band can explain the anomalous band profiles reported in Figs. 1–7.

When the constraint of a limited solubility of the sample in the mobile phase was included in the calculation algorithm, a completely different picture

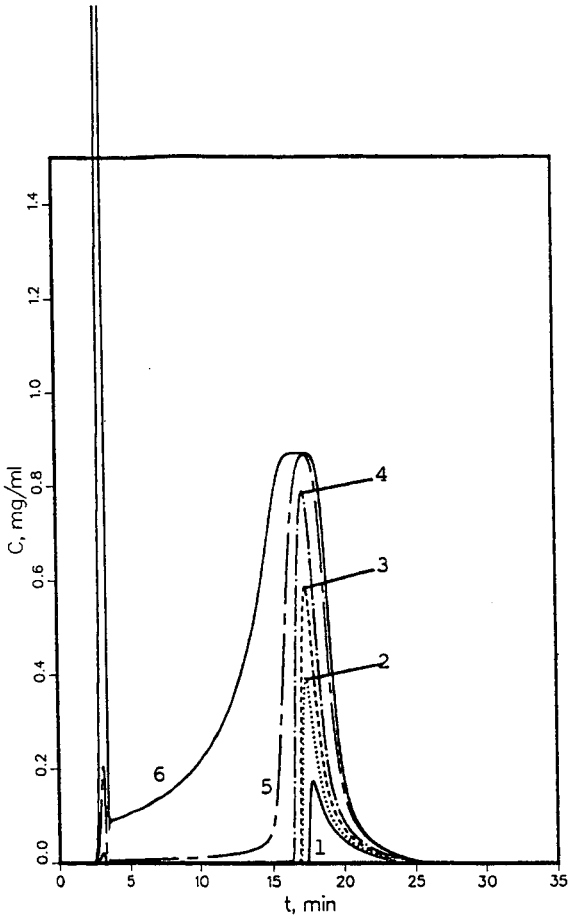

Fig. 9. Calculated band profiles of samples of cholesterol dissolved in dichloromethane. Simulated conditions as in Fig. 1; solubility and isotherm parameters as in Table I. t = Time (min); c = concentration of cholesterol (g/l). Sample volume: 1 = 10; 2 = 20; 3 = 30; 4 = 50; 5 = 100; 6 = 250 μl.

arose. Fig. 9 shows the band profiles calculated for 10–250-μl samples of a 32.3 g/l solution of cholesterol in pure dichloromethane, eluted with pure acetonitrile. These calculations were made assuming a rectangular profile of the sample plug. Some important similarities are apparent between these calculated profiles and the experimental band profiles reported in Figs. 1 and 2.

First, the calculated chromatograms corresponding to large size samples show a split peak, the second mode appearing at the column dead volume. This effect is first observed for a sample volume of 50 μl (profile 4); it increases with increasing sample volume. Second, the retention time of the band maximum remains constant. Finally, when the sample size increases, the front of the main mode band becomes increasingly skewed and eventually merges with the dragging tail of the "dead volume" peak (profiles 5 and 6). On the other hand, two major features of the calculated and experimental bands differ. The experimental bands do not exhibit a concentration plateau; the progressive formation of the hump on the band front and its profile are not correctly simulated.

Extra-column contributions affect both the retention times and the band profiles in preparative chromatography [15]. To investigate the possible influence of an actual injection profile differing markedly from a rectangular plug, a profile composed of a vertical front and an exponential rear was used in calculations. This profile describes better the actual sample pulse. However, the results of the calculations were not significantly changed, even for large sample volumes.

Finally, the formation of supersaturated solutions of cholesterol observed during the solubility measurements was taken into account as a possible contribution to the deformation of the retained band. The sample solution may become supersaturated as it starts to mix with the mobile phase before sorption equilibrium is attained. However, once the sorption equilibrium has been reached, a fresh portion of the mobile phase coming into contact with the solute in the stationary phase will not accommodate a concentration of the solute higher than the saturation. To take into account this phenomenon, we assumed in the calculation algorithm that the propagation of the sample from one column element to the next is possible up to a certain "supersaturated" solubility, higher than the experimental saturation on the band front. Below that supersaturation, we used the extrapolated isotherm. Above it, we assume precipitation in the column element. On the other hand, the solubility was set as the limiting concentration in the mobile phase for the adsorption equilibrium, on the band rear.

The supersaturated solubility cannot be measured. It was set arbitrarily at 150% of the solubility in the saturated solution. Fig. 10 shows simulated chromatograms for 20–500-μl samples of a 70 g/l solution of cholesterol in dichloromethane, with acetonitrile as the mobile phase. Only the 20-μl

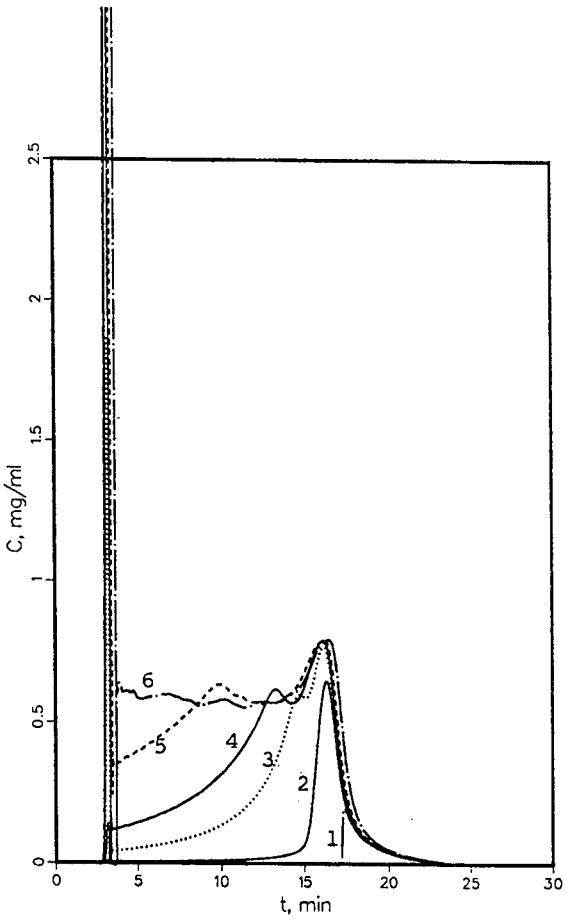

Fig. 10. Calculated band profiles of samples of cholesterol dissolved in dichloromethane. Simulated conditions as in Fig. 1; the formation of supersaturated solutions with maximum concentration equal to 150% of the experimental solubility in the mobile phase was assumed. Solubility and isotherm parameters as in Table I. t = Time (min); c = concentration of cholesterol (g/l). Sample volume: 1 = 20; 2 = 50; 3 = 100; 4 = 150; 5 = 250; 6 = 500 μl.

sample (profile 1) yielded a non-split Langmuirian band profile. All the chromatograms corresponding to larger sample volumes show a "dead volume" peak in addition to the retained band. The front of the retained peak is slanted for the 50-μl sample (profile 2), which also exhibits a shallow leader as the bands for the corresponding size samples in Figs. 1 and 2. A hump appears at the front of the peak of the 100-μl sample (profile 3). The size of this hump increases and its retention decreases with increasing volume, from 100 to 250 μl (profiles 3–5). The hump eventually merges with the rear of the "dead volume" peak for the 500-μl sample (profile 6), in good qualitative agreement with the experimental behavior.

The effect of the sample volume on the deformation of the retained bands is larger in the experimental results than predicted by the calculations. This could be attributed to the arbitrary selection of the value of the "supersaturated" solubility. The qualitative agreement of the simulations with the experiments gives some support to the formation of supersaturated solutions as the origin of the "hump" on the retained sample bands.

Mechanism of band deformation

On the basis of the results, the behavior of large samples injected as solutions in a solvent which is stronger than the mobile phase can be explained principally by their interaction with the bolus of strong solvent. In this bolus, the solubility of the sample components is considerably increased. The elution strength of the sample solvent is high. When the composition of the mobile phase forming the local environment of the sample solute changes as a result of the migration and the progressive dilution of the strong solvent bolus, the sample solubility and its retention decrease rapidly. Supersaturated solutions can form when the solubility decreases and contribute to the faster migration of part of the sample. This combination of effects causes a complex band profile.

After the injection into the mobile phase of a dichloromethane solution of cholesterol, a steep gradient of decreasing elution strength is induced by the sample itself. The wave of dichloromethane propagates along the column, carrying along part of the sample. As long as the volume of the sample is small enough, dispersion dilutes both the sample and the solvent and the whole sample amount is brought into contact with a mobile phase of lower elution strength, so that it eventually elutes in much the same way as if it was injected dissolved in the mobile phase.

When large volumes of sample solution are injected, however, the bolus of dichloromethane is wider and dilutes more slowly in the mobile phase. Part of the sample is carried along with the bolus and, as its retention in presence of pure dichloromethane is negligibly small, it is eluted with it in a

"dead volume" peak. At the rear edge of the diffusing dichloromethane band, the solubility of cholesterol drops rapidly, because acetonitrile is a poor sample solvent. A supersaturated solution of cholesterol in acetonitrile is formed first. This supersaturated solution is unstable but does not precipitate instantly. It propagates along the column, and part of this cholesterol precipitates at some distance from the top of the column, so that the local cholesterol concentration in the stationary phase becomes higher than that which corresponds to the sorption isotherm. This portion of cholesterol is subsequently re-dissolved and diluted by the fresh mobile phase, in which it migrates along the remaining part of the column. Eventually it elutes and forms a hump at the front edge of the peak of the retained portion of the cholesterol sample. Because of the dilution during the re-dissolution process, the height of the hump is lower than the height of the sharp peak eluted after the hump. This sharp peak obviously can be attributed to the band of the originally saturated solution of cholesterol in acetonitrile, formed at the top of the column and moving all the distance along the column in the mobile phase.

During the re-dissolution of the precipitated cholesterol in the mobile phase, the formation of a supersaturated sample solution is most unlikely. The part of the column in which the precipitation occurs and consequently the width of the hump increases with increasing sample size. Eventually, for large enough sizes, the precipitation and re-dissolution take place in the whole column volume, resulting in a merging of the retained band and the dead volume peak.

For very large sizes (Fig. 2), the profile of the supersaturated part of the retained sample band shows a sloping front and a steep rear end, the same profile which is expected with anti-Langmuirian isotherms. Possibly the isotherm is concave in the supersaturated concentration range, but it is just impossible to measure isotherms in supersaturated solutions as the rate of precipitation is too high and uncontrollable.

Obviously, the band splitting and deformation observed here would make it very difficult to separate and purify efficiently cholesterol from other related compounds at high sample loads in a non-aqueous reversed-phase chromatographic system. This conclusion extends to many similar systems.

CONCLUSIONS

The use of a sample solvent with a higher elution strength than the mobile phase to increase the throughput in preparative liquid chromatography of poorly soluble samples may seem a good idea but leads to serious deformations and to the splitting of the sample component bands. This phenomenon limits drastically the amount of sample which can be injected, and hence the production rate. This result is of special importance in the preparative applications of non-aqueous reversed-phase HPLC of hydrophobic compounds, such as steroids.

On the basis of the results, this behavior can be explained by the abrupt and simultaneous decrease in the sample-component solubility and the change in their equilibrium isotherms which take place when the sample components are separated from the sample solvent during the early phase of their migration along the column. The possible formation of supersaturated solutions of sample solutes in the mobile phase may contribute significantly to the band deformation and the occurrence of humps on the front of the retained sample peak. The results of the simulation calculations based on this model yielded band profiles in good qualitative agreement with the experiments. Obviously, however, this agreement is not a proof of the validity of the entire model. Some features of the elution band of cholesterol, especially its sharp rear profile, are not explained satisfactorily.

The phenomena causing the band deformation interfere with the separation process and are detrimental to the production of purified material in preparative liquid chromatography, as the solutes are spread almost over the entire column at larger sample loads [9].

For these reasons, the use of sample solvents having an elution strength much stronger than the mobile phase should be avoided in preparative chromatography, especially at high sample loads. The injection of a large volume of a saturated solution of the sample in the mobile phase seems to be the best approach to column overloading. If the maximum production rate so achieved is considered to be insufficient, another chromatographic system

in which the mobile phase is a better sample solvent should be searched for. From this point of view, in spite of its own problems, preparative normal-phase chromatography, using polar adsorbents with low-polarity mobile phases containing a small concentration of a polar organic modifier, should most often be considered as a preferred alternative to non-aqueous reversed-phase chromatography for the separation or purification of hydrophobic compounds.

ACKNOWLEDGEMENTS

We thank Sadroddin Golshan-Shirazi (University of Tennessee) for fruitful discussions and for his assistance in modifying the simulation program. We are grateful to Henri Colin (Prochrom, Champigneulle, France) for useful discussions. We acknowledge the gift by Hewlett-Packard of a Model 1090A liquid chromatograph with a diode-array detector and a data work-station.

This work was supported in part by grant CHE-8901382 from the National Science Foundation and by the cooperative agreement between the University of Tennessee and the Oak Ridge National Laboratory. We acknowledge support of our computational effort by the University of Tennessee Computing Center.

REFERENCES

1 G. Guiochon and A. Katti, *Chromatographia*, 24 (1987) 165.
2 J. Kříž, M. Březina and L. Vodička, *J. Chromatogr.*, 248 (1982) 303.
3 W. Boehme and H. Engelhardt, *J. Chromatogr.*, 133 (1977) 67.
4 P. Jandera, M. Janderová and J. Churáček, *J. Chromatogr.*, 148 (1978) 79.
5 L. Svoboda and P. Jandera, *Chem. Listy (Chem. Papers, Prague)*, 79 (1985) 201.
6 N. A. Parris, *J. Chromatogr.*, 157 (1978) 161.
7 F. Khachik, G. R. Beecher, J. T. Vanderslice and G. Furrow, *Anal. Chem.*, 60 (1988) 807.
8 D. J. Chitwood and G. W. Patterson, *J. Liq. Chromatogr.*, 14 (1991) 151.
9 H. Colin, personal communication.
10 G. Guiochon, S. Golshan-Shirazi and A. Jaulmes, *Anal. Chem.*, 60 (1988) 1856.
11 G. Guiochon and S. Ghodbane, *J. Phys. Chem.*, 92 (1988) 3682.
12 S. Golshan-Shirazi, S. Ghodbane and G. Guiochon, *Anal. Chem.*, 60 (1988) 2630.
13 S. Golshan-Shirazi and G. Guiochon, *Anal. Chem.*, 60 (1988) 2634.
14 A. M. Katti, Z. Ma and G. Guiochon, *AIChE J.*, 36 (1990) 1722.
15 E. V. Dose and G. Guiochon, *Anal. Chem.*, 62 (1990) 1723.

Journal of Chromatography, 588 (1991) 15–24
Elsevier Science Publishers B.V., Amsterdam

CHROM. 23 659

Assessment of a thermospray interface for the coupling of high-performance liquid chromatography and Fourier transform infrared spectrometry

Alan M. Robertson and David Littlejohn*

Department of Pure and Applied Chemistry, Thomas Graham Building, University of Strathclyde, Cathedral Street, Glasgow G1 1XL (UK)

Michael Brown

Unicam Ltd., York Street , Cambridge CB1 2PX (UK)

Christopher J. Dowle

ICI Wilton Materials Research Centre, P.O. Box 90, Middlesbrough TS6 8JE (UK)

(First received April 17th, 1991; revised manuscript received July 30th, 1991)

ABSTRACT

A thermospray interface has been developed to couple high-performance liquid chromatography (HPLC) with Fourier transform infrared (FT-IR) spectrometry. The system has been constructed for operation in normal- and reversed-phase HPLC. The HPLC effluent is thermally desolvated and deposited on to a moving metal substrate, which continually transfers the solutes into the diffuse reflectance (DRIFT) accessory of an FT-IR spectrometer, enabling identification by measurement of the IR reflectance spectrum. Various aspects of the interface design have been investigated and optimised, and the interface has been applied to the analysis of several types of compound, with molecular identification being indicated for the antioxidant Irganox 565 at concentrations lower than 50 $\mu g\ ml^{-1}$.

INTRODUCTION

Over the past decade, the use of combined techniques for solving complex analytical problems has become increasingly popular. This is particularly true in the interfacing of chromatography and molecular spectroscopy. Application of techniques such as gas chromatography–mass spectrometry (GC–MS) is relatively commonplace. Various procedures have been proposed to couple high-performance liquid chromatography (HPLC) with Fourier transform infrared (FT-IR) spectrometry, however this combination has proved much more difficult to achieve than other combined techniques.

Much research work has centred on the use of flow cells [1–3], which can be used in conjunction with some organic solvents. However most solvents commonly used in HPLC possess intense IR absorption bands in important wavelength regions, rendering some spectral regions opaque. In order to maintain a sufficiently high IR transmittance over these regions, the pathlength of the flow cell must be kept short. Hence the sensitivity and amount of qualitative information obtained from a flow cell interface for HPLC–FT-IR may be limited. More favourable results can be obtained if solvent elimination is applied prior to FT-IR detection [4–13].

One of the first solvent elimination techniques de-

0021-9673/91/$03.50

veloped for use in normal-phase HPLC was described by Kuehl and Griffiths [4]. Concentrated portions of the HPLC effluent were deposited into a series of diffuse reflectance cups filled with KBr powder, held in a carousel arrangement. After solvent evaporation, the cup was brought into the IR beam path of the FT-IR spectrometer, and the diffuse reflectance (DRIFT) FT-IR spectrum recorded. Although this system showed good sensitivity, it did not allow continuous analysis of the chromatographic effluent, and a component could be missed or more than one component collected in a single cup. More recently, Wood [5] demonstrated the feasibility of using a particle-beam HPLC–FT-IR interface with normal-phase HPLC solvents, depositing the effluent on to a KBr plate substrate. The most serious limitation of these solvent elimination techniques is that they cannot be used with aqueous based solvents commonly used in reversed-phase HPLC, as water must be removed for any method using KBr as a deposition medium; thus limiting separations to normal-phase or some size-exclusion chromatography.

Various suggestions have been made to circumvent the problems associated with aqueous solvents. Kalasinsky *et al.* [6] removed water from the HPLC column effluent by the continuous addition of 2,2-dimethoxypropane to produce acetone and methanol, which were easily evaporated after deposition on to KCl powder. However, 2,2-dimethoxypropane is expensive and fairly high flow-rates are required. A method of replacing the conventional metal halide substrate with a stainless steel wire mesh was described by Fujimoto *et al.* [7]. Solutes were trapped in the metal net as the solvent was evaporated using a heated gas flow. Unfortunately, the interface was used with an extremely low mobile phase flow-rate of 0.4 μl min^{-1}.

Gagel and Bieman [8,9] have reported a method for narrowbore HPLC–FT-IR where the HPLC effluent is continuously deposited on to and evaporated from the surface of a rotating reflective disc using a nitrogen gas nebuliser. After deposition, the solutes are analysed by rotating the disc in the sample compartment of an FT-IR spectrometer, while the reflectance-absorbance (R-A) spectra are collected. The system displays good sensitivity (110 ng for caffeine) and can deal with gradient elution for up to a 50% aqueous mobile phase. Somson *et al.* [10] proposed a spray jet assembly interface for narrowbore HPLC–FT-IR spectrometry using heated nitrogen gas to promote evaporation of the solvent. After deposition on to a linearly moving zinc selenide substrate, the deposited compounds were analysed by FT-IR microscopy. The system could be used with up to 20% aqueous effluents in methanol and exhibited high sensitivity (20 ng) for phenanthrenequinone). However, the interface was used with a relatively low mobile phase flow-rate of 20 μl min^{-1}. A monodisperse aerosol generation interface (MAGIC) combining LC with FT-IR spectrometry has been described by Robertson, De Haseth and Browner [11]. The interface can be used with 100% aqueous solvents and flow-rates of up to 0.3 ml min^{-1} with no effluent heating. The sensitivity of this system is around 100 ng for methyl red however, the deposition efficiency is low (about 10%). Buffers can also be used with this system, but spectral subtraction remains necessary. Details of an HPLC–FT-IR interface consisting of a thermospray, moving belt and an optical reflectance accessory have been reported by Jansen [12]. Applications included analysis of various polymers and polymer additives and detection limits in the 100 ng range were claimed. The system can be used with 30% water in methanol at a flow-rate of 0.5 ml min^{-1}, but no information was provided on thermospray deposition efficiency or solute spot size and spreading effects.

Recently, we reported preliminary details of a thermospray interface for coupling HPLC with FT-IR spectrometry using diffuse reflectance optics and a moving ribbon substrate [13], which can be used in both normal- and reversed-phase HPLC. The column effluent is vaporised using a thermospray similar to that used by Vestal to couple HPLC to mass spectrometry [14,15], and deposited on to a moving metal substrate similar in concept to the transportation device used by Yang *et al.* [16], which continually transfers the de-solvated solutes into the diffuse reflectance accessory of the FT-IR spectrometer. The interface has been used with 100% aqueous effluents at flow-rates of 0.5 ml min^{-1}. Various aspects of the interface design have been investigated further and the system has been evaluated to illustrate the qualitative and quantitative capabilities of HPLC–FT-IR in the analysis of several types of compounds.

EXPERIMENTAL

Schematic diagrams of the HPLC–FT-IR interface assembly and thermospray are shown in Figs. 1 and 2.

Apparatus

The HPLC system was a Philips PU 4100 liquid chromatograph (Cambridge, UK) utilising a Rheodyne 7125 syringe loading injector (Berkeley, CA, USA) with a 20- or 50-μl sample loop. The analytical columns were either a Hichrom stainless-steel (250 mm × 4.6 mm I.D.) Spherisorb S50DS2 column or a stainless-steel (250 mm × 4.6 mm I.D.) Spherisorb S5NH column (Berkshire, UK). Various compositions of methanol–acetonitrile–water mobile phases were pumped through the columns at flow-rates of 1 or 0.5 ml min^{-1}. A Philips PU 4110 UV–visible detector or Philips PU 4026 differential refractive index detector was used during HPLC method development prior to FT-IR spectrometric detection. A smooth stainless-steel ribbon (width 13 mm, thickness 0.02 mm), which moved with a constant speed of either 1 or 1.5 cm min^{-1}, was used as a substrate for thermospray deposition and transport of solutes.

IR spectrometric data were obtained using either a Philips PU 9800 FT-IR spectrometer or Nicolet system 800 FT-IR spectrometer (Madison, WI, USA), both equipped with a Spectra-Tech Collector diffuse reflectance accessory (Stamford, CT, USA). The Philips instrument was equipped with a deuterated triglycine sulphate (DTGS) detector, and the Nicolet instrument with a medium range mercury-cadmium-telluride (MCT) detector. IR data, in the form of single-scan interferograms, were collected at 8 cm^{-1} resolution and stored using standard Philips (now Unicam) FT-IR computer software. Interferograms were transformed to IR transmittance spectra using the fast Fourier transform algorithm, post-run. Background spectra were collected from the deposition trace on the substrate surface prior to the area of interest. Specially developed Philips (now Unicam) computer software was used to process this data and construct FT-IR functional group chromatograms (FGCs). These were obtained by calculating the integrated IR transmittance across various wavenumber windows (corresponding to particular functional groups), as a function of time.

Effluent from the HPLC was transferred to the thermospray through stainless-steel tubing (250 μm

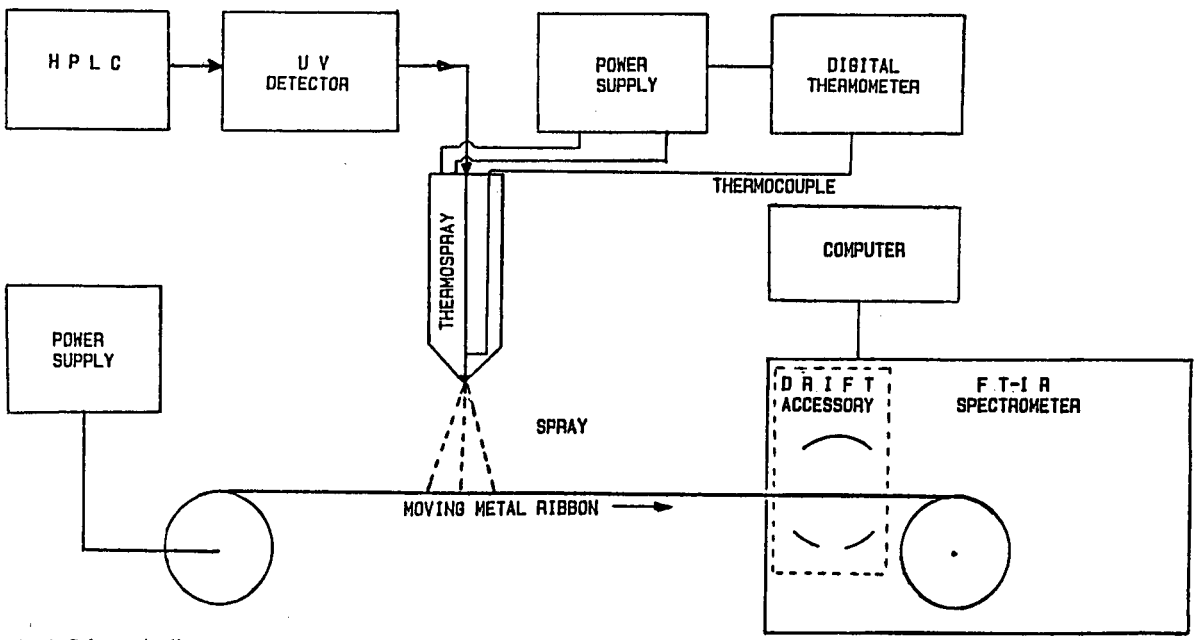

Fig. 1. Schematic diagram of HPLC–FT-IR interface assembly.

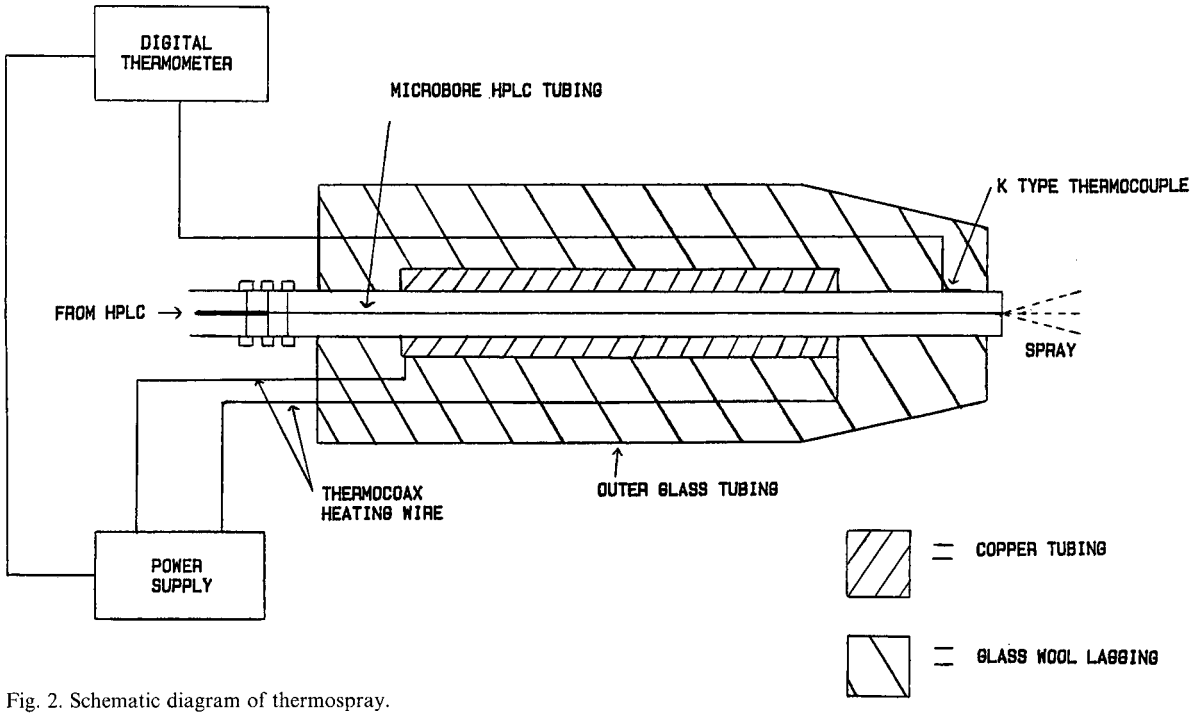

Fig. 2. Schematic diagram of thermospray.

I.D., 1.5 mm O.D.) coupled to a 30 cm length of narrow-bore stainless-steel tubing (125 μm I.D., 1.5 mm O.D.). The narrow bore tubing was inserted into a 10 cm length of copper tubing (1.5 mm I.D. $\times$ 4 mm O.D.). Philips thermocoax heating wire was brazed around the outside of this copper tubing. The narrow-bore tubing protruded 1.5 cm from the heating assembly. A Philips KS 4400 temperature regulator/voltage controller (Eindhoven, Netherlands) and a Fluke type 52 digital thermometer (Watford, UK) were used in conjunction with a Farnell "L" series, 120-W (variable) power supply (Wetherby, UK) to provide power to, and control the temperature of, the thermospray. A "K" type thermocouple was laser soldered 1 cm from the tip of the thermospray necessitating the use of a PCS transmitter isolation amplifier (Philips, Eindhoven, Netherlands) in order to isolate the thermocouple from the thermocoax heating wire in the thermospray.

Amino acids, saccharides and carboxylic acids were obtained from Aldrich (Milwaukee, WI, USA). Phenolic antioxidants were provided courtesy of ICI Wilton Materials Research Centre, (Cleveland, UK). HPLC-grade methanol and acetonitrile were obtained from Rathburn (Walkerburn, UK), and water was distilled prior to analysis.

RESULTS AND DISCUSSION

Interface optimisation

In order to maintain chromatographic resolution and derive maximum sensitivity from the HPLC–FT-IR interface, the area over which solutes are deposited by the thermospray should be optimised to match that of the IR beam in the DRIFT accessory (2.25 mm diameter). The deposition area depends not only on the speed of the moving substrate, but also on the thermospray temperature and height above the moving surface. The thermospray temperature and height must be optimised for a particular mobile phase composition and flow-rate. In order to measure the efficiency of thermospray deposition, a known concentration of solute was injected (in duplicate) on to the HPLC column, deposited by the thermospray on to the substrate surface, and the peak area measured for UV detection at 275 nm. The deposited solute was then dissolved in 1 ml of

chloroform–methanol (50:50), injected on to the HPLC column, and the peak area measured for UV detection at 275 nm. The thermospray deposition efficiency was then calculated as a percentage by comparison of the UV peak area absorbance for both measurements.

Irganox 565 is a phenolic antioxidant found in various plastics, and was selected as a test solution in this study to allow comparison of IR and UV absorption measurements during the investigation of the thermospray interface. The effects of varying the thermospray height on the IR absorbance of Irganox 565 at 2915 cm^{-1} and the thermospray deposition efficiency, are shown in Figs. 3 and 4, respectively. It is clear that both parameters improve as the thermospray approaches the substrate surface. The area over which the solute is deposited on the substrate surface decreases with thermospray height and provided the thermospray temperature is sufficiently high, it is uniformly deposited. If the thermospray temperature is too low, solute may be deposited in a non-uniform manner in the form of "rings", with high concentrations of solute at the outer edges of these "rings".

The effects of varying the thermospray temperature on the magnitude of the absorbance at 2915 cm^{-1} and the thermospray deposition efficiency, are illustrated in Figs. 5 and 6, respectively, for Irganox 565. The results indicate that the greatest IR absorbance is obtained at a thermospray temperature of 158°C. The deposition efficiency remained high at lower thermospray tempeatures because a "wet" spray was produced and more solute adhered to the substrate surface. Unfortunately, a "wet" spray also caused solute spreading and hence, a reduced absorbance. The initial increase in the absorbance is mainly due to a reduction in solute "spot size" on the substrate surface. Solute spreading and "ringing"' effects are eliminated with increased thermospray temperature and an optimum spot size

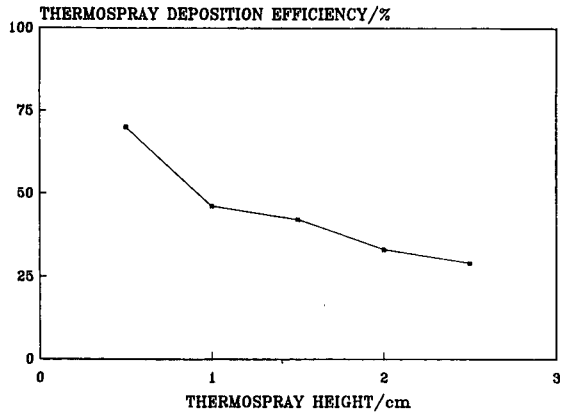

Fig. 4. Effect of varying the thermospray height on the thermospray deposition efficiency for the analysis of Irganox 565. Conditions as in Fig. 3.

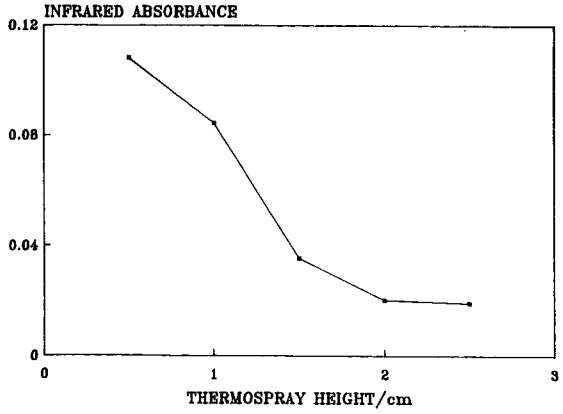

Fig. 3. Effect of varying the thermospray height on the magnitude of the IR absorbance at 2915 cm^{-1} for the analysis of Irganox 565 obtained using the MCT detector. Conditions: mobile phase, 100% methanol; flow-rate 1 ml min^{-1}; sample concentration, 300 μg ml^{-1}; column, S50DS2; thermospray temperature, 154°C (controlled to ± 0.5°C); substrate speed, 1.5 cm min^{-1}.

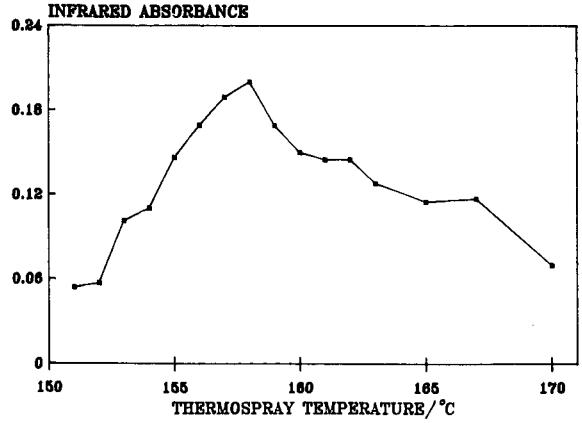

Fig. 5. Effect of varying the thermospray temperature on the magnitude of the IR absorbance at 2915 cm^{-1} for the analysis of Irganox 565. Conditions as in Fig. 3 except that the thermospray height was 0.5 cm.

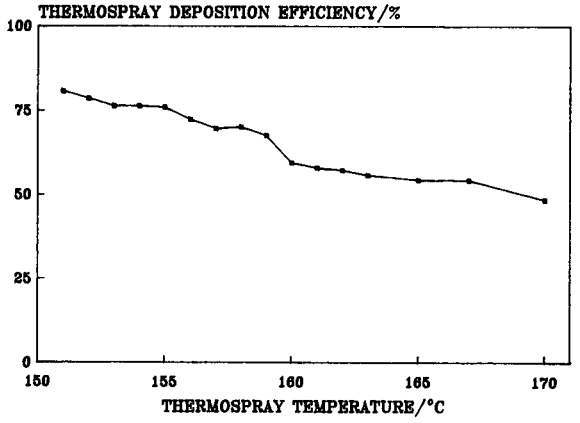

Fig. 6. Effect of varying the thermospray temperature on the thermospray deposition efficiency for the analysis of Irganox 565. Conditions as in Fig. 3 except that the thermospray height was 0.5 cm.

of 3.5 × 2.5 mm was achieved at 158°C. The optimum thermospray temperature changes if any alteration is made to the composition of the mobile phase. An increase in the thermospray temperature is accompanied by a corresponding increase in the back pressure to the HPLC pump from the thermospray. This pressure increase suggests that solute may progressively coat the inner walls of the thermospray tubing, and this may be the reason why the thermospray deposition efficiency never reaches 100%. It is also possible that some solute may be lost to the atmosphere.

In order to investigate the reproducibility of thermospray deposition, a 1 mg ml^{-1} solution of Irganox 565 was injected on to the HPLC column and deposited ten times on to the moving substrate (using thermospray temperature control). The values of the IR absorbance and the percentrage thermospray deposition efficiency measurements were 0.188 ± 0.024 and 76.6 ± 10.3% (n = 10), respectively. Although, the relative standard deviation (R.S.D.) values of 12.8% and 13.5% for the absorbance and deposition measurements are relatively high, they represent a major improvement in reproducibility of thermospray deposition compared to the performance without thermospray temperature control (typical R.S.D. levels of 50%). Further improvements to the interface design and temperature control should give additional improvement in the deposition reproducibility.

Quantitative analysis

The general trend in the literature when outlining the detection limit performance of a proposed solvent elimination interface for HPLC–FT-IR is to quote the minimum identifiable quantitity (MIQ) of a particular compound. However, if the magnitude of the chromatographic injection volume is a limiting factor and relatively low mobile phase flowrates are used [as in narrow-bore HPLC (7–10)], and no solute preconcentration techniques are applied, it is more relevant to discuss detection limits in terms of concentration of solute in the injected liquid.

Fig. 7 shows the calibration graph for the HPLC analysis of Irganox 565 at various concentrations, using FT-IR spectrometric detection. A linear relationship is indicated between the IR absorbance at 2915 cm^{-1} and the Irganox 565 concentration.

Fig. 8 shows an overlay of FT-IR spectra for Irganox 565 obtained after thermospray deposition of a 50 $\mu g\ ml^{-1}$ concentration and direct deposition of a 500 $\mu g\ ml^{-1}$ standard on to the moving substrate. A comparison of the spectra indicates that no degradation of the Irganox 565 has occurred and that identification of this solute can be achieved down to at least the 50 $\mu g\ ml^{-1}$ level. IR detection has no advantage over UV detection for this compound, particularly as the detection limit at 275 nm is around 1 $\mu g\ ml^{-1}$. The main advantage of IR detection is in the identification of solutes which exhibit less sensitive UV absorption. Quantitative

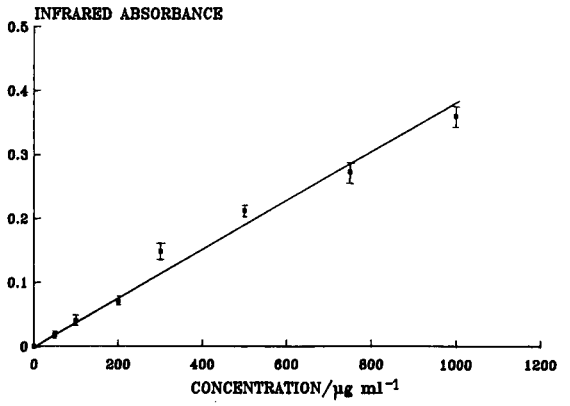

Fig. 7. Calibration graph for HPLC–FT-IR analysis of Irganox 565, indicating mean ± one S.D. of 4 results. Conditions as in Fig. 3 except that thermospray height was 0.5 cm.

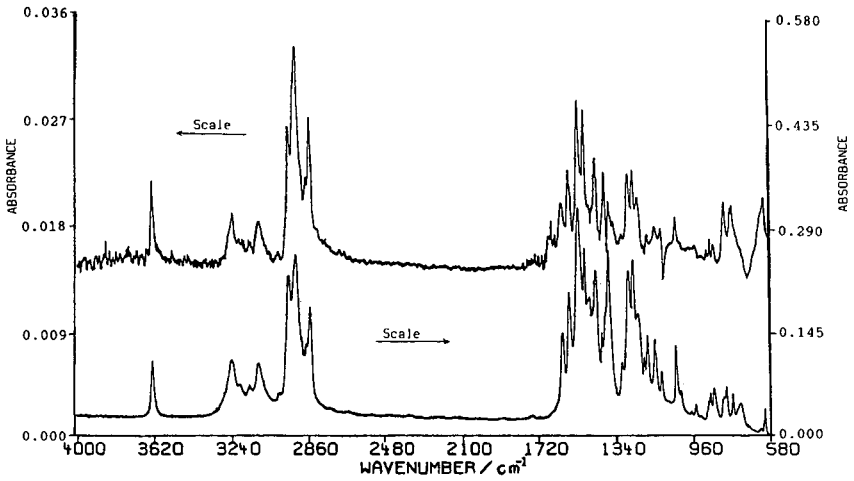

Fig. 8. Spectral overlay of the HPLC–FT-IR interface spectrum (upper) and the standard FT-IR spectrum (lower) for Irganox 565. Conditions as in Fig. 3 except that the thermospray height was 0.5 cm and the sample concentration was 50 μg ml^{-1}.

measurements were therefore obtained for a number of other compounds and it was possible to detect unambiguously individual saccharides and aliphatic carboxylic acids at 200 μg ml^{-1} and amino acids at 100 μg ml^{-1}. Lower limits of detection are likely to be achieved with better thermospray temperature control.

Qualitative analysis

The examples described so far illustrate the use of the HPLC–FT-IR interface for the analysis of compounds which can be detected by both UV-visible and FT-IR absorption spectrometry. However, some compounds do not possess a UV chromophore, and although procedures such as sample derivatization can improve detection, they are often time consuming and laborious. The refractive index (RI) detector is a common alternative "universal" detector for compounds without a UV chromophore, although it is subject to slight variations in temperature and lacks the high sensitivity of UV-visible absorption. An RI detector was used in this work to develop HPLC methods for the analysis of non-UV absorbing saccharides and aliphatic carboxylic acids. The methods were then applied to assess the potential of FT-IR detection for these compounds. Fig. 9 shows the FT-IR functional group chromatogram for the analysis of four saccharides, based on measurement of the carbonyl stretch at the wavenumber window 1750–1600 cm^{-1}. All four saccharides have been detected, however Fig. 10 indicates that exact molecular identification cannot be achieved by comparison of interface derived and standard FT-IR spectra. Although the general features of the spectra are similar, there are significant differences in the "fingerprint" region below 1500 cm^{-1}. Most notable is a loss of spectral detail for the interface spectrum.

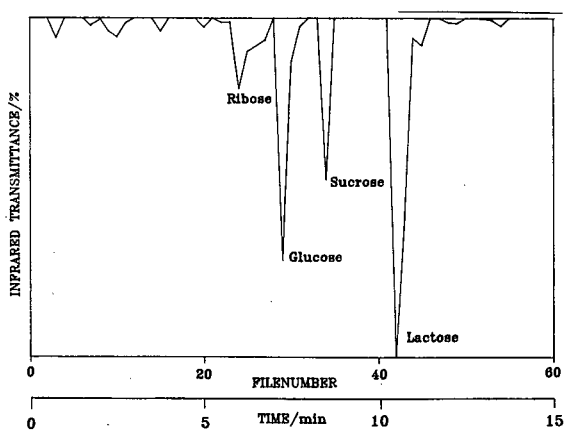

Fig. 9. FT-IR functional group chromatogram for the analysis of various saccharides obtained using the DTGS detector. Functional group, carbonyl stretch; wavenumber window, 1750–1600 cm^{-1}; conditions: mobile phase composition, acetonitrile–water (70:30); flow-rate, 1 ml min^{-1}; thermospray temperature, 180–186°C (no fine temperature control); thermospray height, 0.5 cm; column S5NH; individual saccharide concentration, 1 mg ml^{-1}; substrate speed, 1.0 cm min^{-1}.

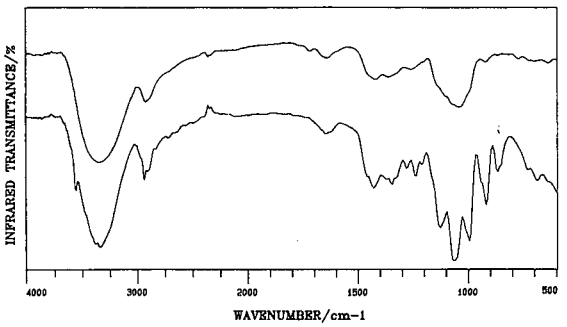

Fig. 10. Spectral overlay of the HPLC–FT-IR interface spectrum (upper) and standard FT-IR spectrum (lower) for sucrose. Conditions as in Fig. 9. Upper spectrum transmission scale multiplied by a factor of two.

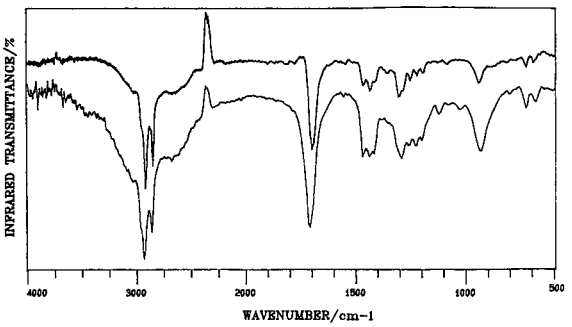

Fig. 12. Spectral overlay of HPLC–FT-IR interface spectrum (upper) and standard FT-IR spectrum (lower) for undecanoic acid. Conditions as in Fig. 11.

The differences in the spectra could be due to formation of a saccharide "glass" on the substrate surface following thermospray deposition.

The FT-IR functional group chromatogram for the analysis of five aliphatic carboxylic acids is shown in Fig. 11, based on measurement of the carbonyl stretch at 1750–1600 cm^{-1}. An overlay of the interface and standard FT-IR spectra for undecanoic acid is given in Fig. 12. No sample derivatization procedures were required for this analysis and

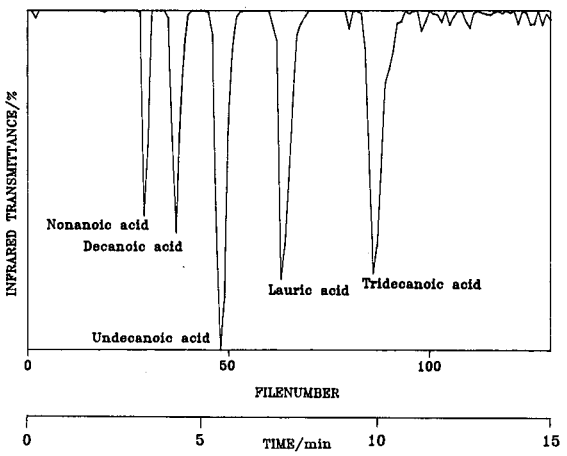

Fig. 11. FT-IR functional group chromatogram for the analysis of various aliphatic carboxylic acids obtained using the DTGS detector. Functional group, carbonyl stretch; wavenumber window, 1750–1600 cm^{-1}; conditions: mobile phase, acetonitrile–water (80:20); flow-rate, 1 ml min^{-1}; thermospray temperature, 165–170°C (no fine temperature control); thermospray height, 0.5 cm; column S50DS2; individual carboxylic acid concentration, 1 mg ml^{-1}; substrate speed, 1.5 cm min^{-1}.

molecular identification could be achieved for each of the carboxylic acids by comparison of interface and standard FT-IR spectra, indicating that passage through the thermospray caused little or no thermal sample degradation of the solutes studied. Even if sample degradation occurs for some thermally unstable solutes, this may not necessarily be a problem providing standard compounds are degraded to the same extent as the solutes in the samples and a suitably sensitive spectral feature remains. In effect, utilising this method of detection for thermally unstable solutes would be analogous to sample derivatization, without the need for preliminary sample preparation.

We have outlined previously both the "universal" and selective detection capabilities of HPLC–FT-IR [13] for the analysis of amino acids separated in a 100% aqueous mobile phase. The advantages of both detection modes has also been illustrated in the analysis of several antioxidants. Fig. 13 shows the FT-IR functional group chromatogram for the analysis of seven antioxidants. This result was obtained by monitoring the hydrocarbon stretch at 3100–2800 cm^{-1}, which is common to each solute. Only six antioxidants have been detected because of loss of chromatographic resolution derived from solute spreading during thermospray deposition. The first component to be eluted from the HPLC column after 3.3 min is in fact a composite of Irganox 3114 and Irganox 1035. The results were obtained prior to the incorporation of precise thermospray temperature control. Introduction of this feature limits solute spreading effects, and therefore

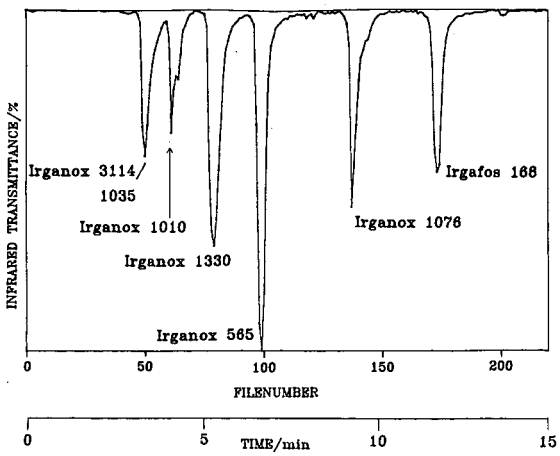

Fig. 13. FT-IR functional group chromatogram for the analysis of various phenolic antioxidants obtained using the DTGS detector. Functional group, hydrocarbon stretch; wavenumber window, 3100–2800 cm^{-1}; conditions as in Fig. 3 except that thermospray temperature was 150–154°C (no fine temperature control) and individual antioxidant concentrations were 1 mg ml^{-1}.

should minimise the loss of chromatographic resolution derived from the interface system.

In contrast, Fig. 14 illustrates the selective detection of Irgafos 168 obtained by monitoring the wavenumber window at 1100–1050 cm^{-1} covering the C-O-P vibration. Molecular identification of Irganox 1330, by comparison of interface derived and standard FT-IR spectra, is illustrated in Fig. 15. There is good comparison of the features of both spectra indicating there has been not thermal degradation of this antioxidant during passage through the thermospray.

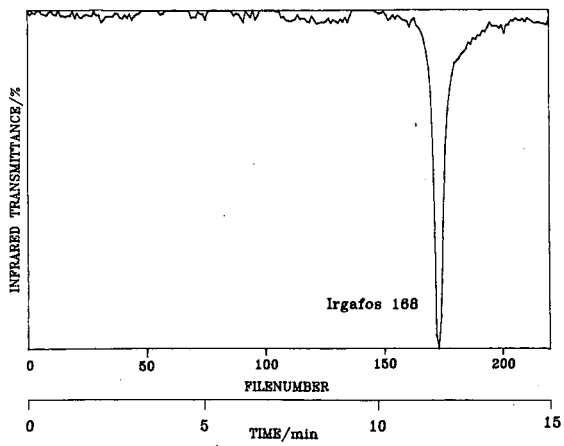

Fig. 14. FT-IR functional group chromatogram for the analysis of various phenolic antioxidants. Wavenumber window, 1100–1050 cm^{-1} (covering C-O-P vibration). Conditions as in Fig. 3 except that thermospray temperature was 150–154°C (no fine temperature control) and individual antioxidant concentrations were 1 mg ml^{-1}.

CONCLUSIONS

The development of a thermospray HPLC–FT-IR interface which can be used with most normal- and reversed-phase solvent compositions, has provided a means of obtaining qualitative information unavailable from more conventional detection methods in HPLC. The "universal" and selective detection characteristics of FT-IR detection have been illustrated for antioxidants and amino acids, and the quantitative capacilities of the system have been demonstrated. The results indicate that identification of the antioxidant Irganox 565 is possible at concentrations lower than 50 μg ml^{-1}. The interface has been applied to the analysis of non-UV absorbing species such as aliphatic carboxylic acids and saccharides, with little or no sample degradation at thermospray temperatures of 165 to 186°C. Molecular identification of each of the solutes (except saccharides) has been confirmed by comparison of interface derived and standard FT-IR spectra.

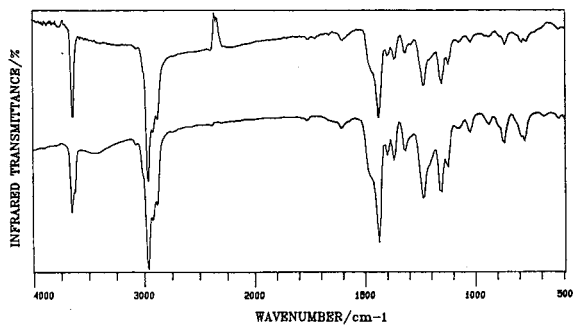

Fig. 15. Spectral overlay of HPLC–FT-IR interface spectrum (upper) and standard FT-IR spectrum (lower) for Irganox 1330. Conditions as in Fig. 3 except that thermospray temperature was 150–154°C and sample concentration was 1 mg ml^{-1}.

REFERENCES

1 K. Jinno, in E. S. Yeung (Editor), *Detectors For Liquid Chromatography*, Wiley, New York, 1986, p. 74.
2 P. R. Griffiths and J. A. de Haseth, in J. D. Winefordner and P. J. Elving (Editors), *Fourier Transform Infrared Spectroscopy*, Wiley, New York, 1986, p. 611.
3 J. W. Hellgeth and L. T. Taylor, *Anal. Chem.*, 59 (1987) 295.
4 D. Kuehl and P. R. Griffiths, *J. Chromatogr. Sci.*, 17 (1979) 471.
5 D. J. Wood, *Spectrosc. International*, 2 (1990) 36.
6 V. F. Kalasinsky, K. G. Whitehead, R. C. Kenton, J. A. S. Smith and K. S. Kalasinsky, *J. Chromatogr. Sci.*, 25 (1987) 273.
7 C. Fujimoto, T. Oosuka and K. Jinno, *Anal. Chim. Acta.*, 178 (1985) 159.
8 J. J. Gagal and K. Biemann, *Anal. Chem.*, 59 (1987) 1266.
9 J. J. Gagel and K. Biemann, *Mikrochim. Acta.*, 2 (1988) 185.
10 G. W. Somson, R. J. van de Nesse, C. Gooijer, U. A. Th. Brinkman, N. H. Velthorst, T. Visser, P. R. Kootstra and A. P. J. M. de Jong, *J. Chromatogr.*, 552 (1991) 635.
11 R. M. Robertson, J. A. de Haseth and R. F. Browner, *Appl. Spectrosc.*, 44 (1990) 8.
12 J. A. J. Jansen, *Fresenius' Z. Anal. Chem.*, 337 (1990) 398.
13 A. M. Robertson, L. Wylie, D. Littlejohn, R. J. Watling and C. J. Dowle, *Anal. Proc.*, 28 (1991) 8.
14 M. L. Vestal and G. J. Fergusson, *Anal. Chem.*, 57 (1985) 2373.
15 J. A. Koropchak and H. Aryamanya-Mugisha, *Anal. Chem.*, 60 (1988) 1838.
16 L. Yang, G. J. Fergusson and M. L. Vestal, *Anal. Chem.*, 56 (1984) 2632.

Journal of Chromatography, 588 (1991) 25–31
Elsevier Science Publishers B.V., Amsterdam

CHROM. 23 671

High-performance liquid chromatography on polypyrrole-modified silica

Hailin Ge and G. G. Wallace*

The University of Wollongong, P.O. Box 1144, Wollongong, NSW 2500 (Australia)

(First received January 25th, 1991; revised manuscript received August 6th, 1991)

ABSTRACT

Bare silica and C_{18}-bonded silica were modified with polypyrrole chloride and polypyrrole chloride–dodecyl sulfate. The packing materials were characterised using scanning electron microscopy, energy dispersive X-ray analysis, elemental analysis and surface area analysis. Both reversed-phase and anion-exchange chromatographic behaviour were determined using a selection of test compounds.

INTRODUCTION

Silica is the most popular supporting material used in liquid chromatography at present [1]. It is readily available in appropriate particle sizes, pore sizes, pore volumes and surface areas for high-performance liquid chromatography (HPLC). Furthermore, it can be modified to provide stationary phases with different interaction modes. Functional groups such as alkyl, phenyl, amino and cyano groups have been bonded to silica. Such functional groups attached have included polar compounds such as safrole [2], electron donor–acceptors such as caffeine [3–5], hydrogen bonding ligands such as pyridyl [6], metallic compounds such as copper (II) [7] and zirconium oxide [8], compounds for protein separations such as melittin [9], concanavalin A [10] and N-hydroxysuccinimide ester [11], and compounds for chiral separations such as L-proline [12], acetylquinine [13] and cellulose [14].

More recently, polymer-coated silica gels have become popular since they combine the mechanical properties of silica with the dynamic chemical properties of polymers. For example, poly(alkyl aspartamide) [15], alkyl polysiloxanes [16], polyvinylpyrrolidone [17], poly(2-sulfoethyl aspartamide) [18], polyethyleneimine [19,20], polyamine [21], poly(butadiene-maleic acid) [22] and polyvinylimidazole [23] have been coated on silica gels. More complicated polymer-coated silica stationary phases such as polymer-diol-silica [24] and C_{18}-polymer-silica [25] have also been synthesised. The polymer coating not only improves the selectivity but also the chemical stability of the stationary phases.

Conducting polymers such as polypyrrole are known to posses unique physical and chemical properties [26]. They are conductive, electroactive and stable in aqueous as well as organic solvents. Conducting polymers coated on to reticulated vitreous carbon have previously been utilised as chromatographic stationary phases in these laboratories. Both reversed-phase as well as anion-exchange chromatographic interactions were reported [27–29]. However, to date these polymers have not been coated on silica substrates.

In this work, bare silica (termed silica) and C_{18}-bonded silica (termed C_{18}) have been coated with polypyrrole chloride (PP/Cl) or polypyrrole chloride–dodecylsulfate (PP/Cl/DS) and selectivity differences were considered. Characterisation of the coated phases was carried out using scanning electron microscopy (SEM), energy dispersive X-ray (EDX) analysis, elemental analysis and surface area analysis: Both reversed-phase and anion-exchange chromatography were characterised.

0021-9673/91/$03.50

TABLE I

HPLC CHARACTERISATION CONDITIONS

Column	C_{18} based	Silica based
Mobile phase	methanol–water (65:35)	methanol–water (50:50)
Flow-rate-(ml/min)	0.50	0.30
Test compounds	Benzene 50 ppm	
	Toluene 50 ppm	
	Dimethylphthalate (DMP) 10 ppm	
	Diethylphthalate (DEP) 10 ppm	
	Phenol 30 ppm	
	Benzoic acid 20 ppm	
	Aniline 20 ppm	
	N,N-Dimethylaniline (DMA) 20 ppm	
	Theophylline 10 ppm	
	Caffeine 10 ppm	

EXPERIMENTAL

Reagents and materials

Analytical reagent (AR) grade chemicals were used unless otherwise stated. Silica gel (10-μm Spherisorb, PhaseSep) and C_{18}-bonded silica gels (10-μm ODS-Hypersil, Shandon) were used as substrates in separate parts of this work. Pyrrole was distilled before use. Sodium chloride and sodium dodecyl sulfate (SDS) were used as supporting electrolytes, *i.e.* counterion sources and a 1.5 *M* $FeCl_3$ laboratory reagent (LR) grade solution was used to induce polymerisation. The chromatographic test compounds (Table I) were the same as those used previously [27]. Methanol and purified water were used as solvents. Ammonium acetate and a phosphate buffer (mixture of Na_2HPO_4 and NaH_2PO_4) were added to the mobile phase as required.

Instrumentation

SEM and EDX were carried out using a Hitachi S-450 scanning electron microscope (Hitachi, Japan), connected to a TN-2000 Microtrace detector (United Science, USA). Elemental analysis results were obtained from the Analytical Laboratory, Australian National University. Surface areas of stationary phases were measured on an Area Metre II (Strohlein Instruments, Germany). The HPLC experiments were conducted using a Kortec K350 HPLC Pump (ICI, Australia), an ERC-7210 spectrophotometric detector at 254 nm (ERMA Optical Works, Japan) and a Rheodyne 7512 injector (USA) with a 20-μl sample loop.

Column preparation

The polymer-modified stationary phases were prepared as follows: (1) 1 g of silica or C_{18} was placed in a 100-ml beaker; (2) 1 ml distilled pyrrole was added to the beaker, and stirred for 10 min with a glass rod; (3) 100 ml of distilled water were placed in the beaker, and 0.01 mole of counterions (Cl^- or DS^-) were added as required. The mixture was stirred with a magnetic stirrer to form a suspension; (4) 1 ml of 1.5 *M* $FeCl_3$ solution was added and the solution was stirred vigorously for 30 min; (5) the coated particles were collected using a büchner filter and washed with 200 ml of water; (6) all packings were dried at 62°C in vacuum for 3 h before use.

The packing procedures employed for this column system have been described previously [30]. All columns were washed with methanol for 8 h before use.

RESULTS AND DISCUSSION

Preliminary characterisation of the polypyrrole-

TABLE II

ELEMENTAL ANALYSIS OF VARIOUS PACKINGS

Packing	C%	H%	N%	Cl%	S%	Polymer%[a]
C_{18}	9.45	1.80	0.0	0.0	0.0	0.0
PP/Cl/C_{18}	11.82	1.99	0.69	0.64	0.0	3.9
PP/Cl/DS/C_{18}	12.59	2.10	0.59	0.46	0.31	4.8
Silica	0.0	0.0	0.0	0.0	0.0	0.0
PP/Cl/silica	4.91	0.33	1.16	0.99	0.0	7.4

[a] Polymer% (w/w) was calculated from the weight difference between polypyrrole-modified supports and bare supports.

coated phases was carried out to ensure that the silica and C_{18} were in fact coated using the polymerisation procedure. Polypyrrole chloride-modified silica, polypyrrole chloride-modified C_{18} and polypyrrole chloride–dodecylsulfate-modified C_{18} were termed PP/Cl/silica, PP/Cl/C_{18} and PP/Cl/DS/C_{18}, respectively. Elemental analysis (Table II) indicated that the polypyrrole loadings on C_{18} were relatively low.

It was verified that using C_{18} both DS^- and Cl^- ions were incorporated when the polymer was formed from a SDS–$FeCl_3$ solution.

It was found that the polymer coating changed the specific surface area in all cases (Table III). Surface areas were determined by BET. After placing a sample bottle and an empty reference bottle into a liquid nitrogen bath, a pressure difference between the two bottles was recorded and the specific surface area of the phases was calculated according to a manufacturer provided chart. With the C_{18} material change in surface area was more obvious when the surfactant SDS was present. However, the results indicated that the surface area of the porous silica and C_{18} materials did not change dramatically with the polymer coating. These changes may in fact be due to complications that arise from the use of nitrogen in measuring the surface area of polar phases.

A micrograph of a polypyrrole-coated C_{18} packing is shown in Fig. 1. The other polypyrrole-modified packings have similar micrographs. Although the characteristic black colour of the polypyrrole-coated particles was visible to the naked eye, no significant difference was observed using SEM.

Counterions in polypyrrole-coated stationary phases were detected using EDX analysis. Not only the counterion but also the silica background signals appeared on all spectra (Fig. 2). When poly-

TABLE III

SURFACE AREA ANALYSIS OF VARIOUS PACKINGS

Packing	Specific surface area (m^2/g)	Estimated[a] polymer thickness (nm)
C_{18}	98.5	–
PP/Cl/C_{18}	96.5	0.26
PP/Cl/DS/C_{18}	83.4	0.33
Silica	149	–
PP/Cl/silica	137	0.33

[a] Assuming polymer density = 1.5 g/cm² [26,31] polymer thickness = polymer%/(polymer density × specific surface area).

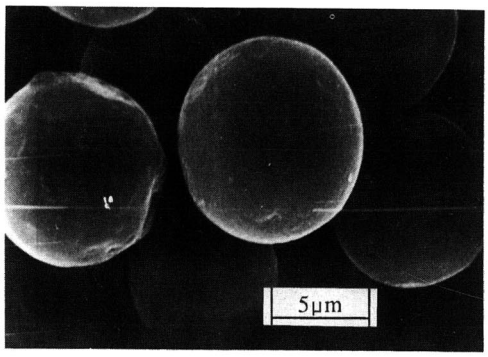

Fig. 1. Scanning electron micrograph of silica-based polypyrrole packings. Sample: PP/Cl/DS on 10-μm Hypersil ODS.

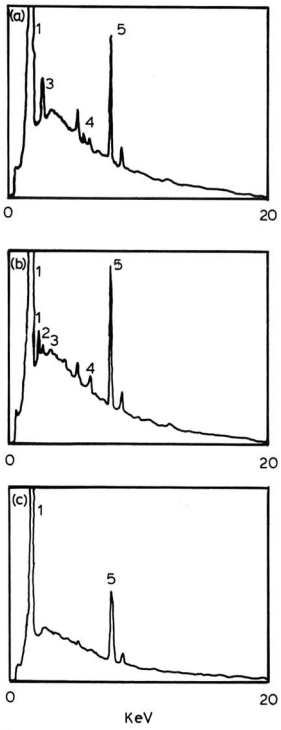

Fig. 2. EDX spectra of silica-based polypyrrole packings. Spectrum on (a) PP/Cl/C_{18}, (b) PP/Cl/DS/C_{18} and (c) C_{18}. Responses due to (1) Si, (2) S, (3) Cl, (4) Fe and (5) Cu. EDX condition: high voltage = 20 kV; accumulation time = 200 s.

TABLE IV

CHROMATOGRAPHIC INTERACTIONS ON POLYPYRROLE CHLORIDE-COATED SILICA

Column: PP/Cl/silica 64 mm × 1.6 mm I.D.

Test compounds	In methanol–water (50:50)		In methanol–water (50:50) with 0.1 *M* ammonium acetate	
	k'	Relative k' *vs.* benzene	k'	Relative k' *vs.* benzene
Benzene	0.41	1.0	0.28	1.0
Toluene	0.67	1.6	0.59	2.1
DMP	0.83	2.0	0.63	2.2
DEP	0.85	2.1	0.64	2.8
Phenol	0.38	0.92	0.31	1.1
Benzoic acid	∞	∞	9.6	34
Aniline	3.3	8.0	0.18	0.63
DMA	9.1	22	0.86	3.0

mers were chemically synthesised using $FeCl_3$, Cl^- as well as $FeCl_4^-$ was incorporated as a counterion which was confirmed by the existence of Fe signals in the spectra. This has also been reported by other workers [32]. The addition of DS^- to the monomer solution resulted in incorporation of DS^-.

Reversed-phase chromatographic characterisation

Chromatographic interactions on polypyrrole-modified silica and C_{18} stationary phases were characterised using the test compounds already listed. A comparison of chromatographic interactions on bare silica and polypyrrole-modified silica is summarized in Table IV and a comparison of chromatographic interactions on C_{18} and polypyrrole-modified C_{18} summarized in Table V. The relative capacity factor (k') *vs.* benzene was calculated by dividing capacity factors of test compounds by the capacity factor of benzene.

Polymer-coated silica. Using bare silica none of the test compounds investigated were retained except for aniline and N,N-dimethylaniline (DMA). These compounds are known to interact with the silanol groups on silica surfaces [1].

Retention of all compounds on polypyrrole-modified silica was observed (Table IV), which indicated that a reversed-phase chromatographic interaction was generated by PP/Cl. Retention of all compounds except benzoic acid, aniline and DMA was low and the results were comparable with other

TABLE V

CHROMATOGRAPHIC INTERACTIONS ON POLYPYRROLE-COATED C_{18}

Mobile phase: methanol–water (65:35); 0.5 ml/min.

Test compounds	C_{18}		PP/Cl/C_{18}		PP/Cl/DS/C_{18}	
	k'	Relative k' *vs.* benzene	k'	Relative k' *vs.* benzene	k'	Relative k' *vs.* benzene
Benzene	2.02	1.00	1.86	1.00	1.87	1.00
Toluene	3.66	1.81	3.33	1.79	3.40	1.82
DMP	0.89	0.44	1.25	0.67	0.87	0.47
DEP	2.13	1.05	2.71	1.46	1.90	1.02
Phenol	0.60	0.30	0.70	0.38	0.61	0.33
Benzoic acid	0.12	0.06	∞	∞	∞	∞
Aniline	0.84	0.42	0.63	0.34	2.42	1.29
DMA	4.29	2.12	3.19	1.72	11.3	6.00
Theophylline	0.26	0.13	6.23	3.35	0.70	0.37
Caffeine	0.31	0.15	6.04	3.24	1.14	0.61

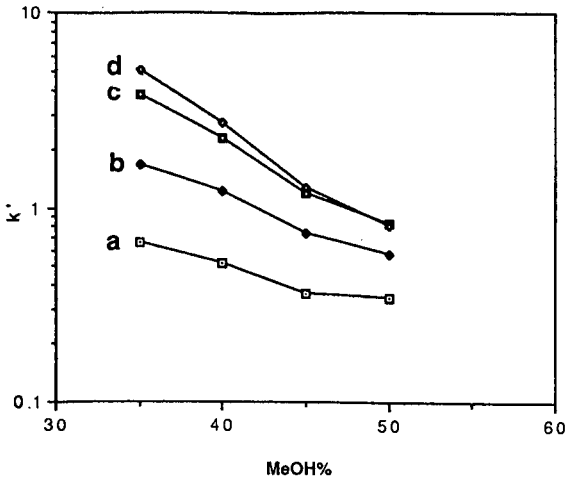

Fig. 3. Capacity factors of benzene, toluene, DMP and DEP *vs.* methanol (MeOH) concentration in the mobile phase. Column: PP/Cl/silica in a 64 mm × 1.6 mm I.D. column; detector: UV at 254 nm; sample: a = 50 ppm benzene; b = 50 ppm toluene; c = 10 ppm DMP; d = 10 ppm DEP.

polypyrrole columns previously investigated [27]. These results indicated that PP/Cl contributed only minor hydrophobic effects. Retention increased with decreased methanol concentration (Fig. 3) which is typical of reversed-phase behaviour. As expected, PP/Cl also introduced a certain degree of polarity to the silica surface, probably from the polar part of the polymer matrix. The low retention values obtained for phenol confirmed that PP/Cl had very low levels of interaction with unisolated acidic molecules. Both aniline and DMA were retained which verified that polypyrrole was capable of basic interactions. This is due to the fact that electrons are lost during polymerisation and positive sites are formed on the polymer. Amines with unshared electron pairs can then access these sites.

The addition of salt (0.10 *M* phosphate buffer) to the mobile phase (methanol–water, 50:50) reduced the capacity factors for aniline and DMA. This was due to solvation of the positive sites on the polymer matrix as has been reported previously for other stationary phases [33].

Polymer-coated C_{18} phases. Capacity factors on the polypyrrole-modified C_{18} columns for benzene, toluene, dimethylphthalate (DMP), diethylphthalate (DEP) and phenol compounds, were similar to those obtained using non-coated C_{18} packings. There were two possible reasons for this. The polypyrrole coating was porous enough to allow molecules to pass through and to interact with the C_{18} coating and/or the C_{18} surface was not fully covered. Although the polypyrrole coating did not alter the selectivity of the C_{18} stationary phase it did contribute to the retention properties.

Capacity factors obtained for benzene and toluene decreased marginally with both polymer coatings. This indicated that polypyrrole-coated C_{18} was less hydrophobic than the C_{18} packing. Capacity factors for DMP and DEP were slightly increased on PP/CL/C_{18} but remained unchanged on PP/Cl/DS/C_{18}. This indicated that the PP/Cl/C_{18} was less hydrophobic than PP/Cl/DS/C_{18}. This was propably due to the contribution of the non-polar end of the surfactant causing an increase in the hydrophobicity of the stationary phase. Phenol was not retained significantly on any of the coated and uncoated C_{18} phases investigated. Aniline and DMA were retained significantly on all stationary phases. Chromatograms obtained on C_{18} phases revealed that both of these compounds gave tailing responses. Polypyrrole coating of the C_{18} material reduced this tailing but did not eliminate it. However, the presence of the PP/Cl/DS coatings on C_{18} resulted in increased levels of interaction with aniline and DMA. This may have been due to the polar end of the surfactant. A similar effect was reported previously by others who have incorporated surfactants into conducting polymers [34].

Anion-exchange chromatographic characterisation

Benzoic acid was permanently retained on polypyrrole-modified phases unless a salt was induced in the eluent but it was eluted in the void volume on C_{18} and bare silica columns. This indicated that the polypyrrole coating had anion-exchange capabilities as reported previously [27–29].

The effect of pH on retention by ion exchange was investigated. It was found that the capacity factor for benzoic acid increased with decreasing pH of the phosphate buffer (Fig. 4).

The effect of ionic strength on ion exchange was also investigated. The capacity factor of benzoic acid decreased with an increasing ionic strength of the buffer (Fig. 5). The retention of aniline and DMA were not altered significantly (Fig. 5).

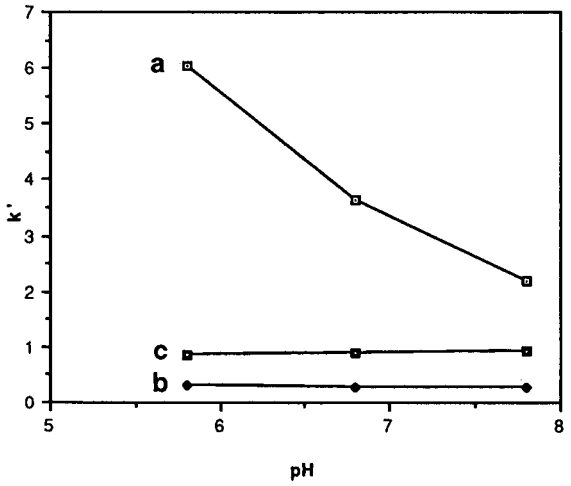

Fig. 4. Capacity factors *vs.* pH of the mobile phase. Column: PP/Cl/silica in a 64 mm × 1.6 mm I.D. column; detector: UV at 254 nm; sample: a = 20 ppm benzoic acid; b = 20 ppm aniline; c = 20 ppm DMA.

Chromatographic performance

Using optimized conditions from Figs. 3, 4 and 5, it was found that the polypyrrole-modified silica column was not efficient enough to separate a group of test compounds. Chromatographic separations were carried out using polypyrrole-modified C_{18} phase (Fig. 6). The polypyrrole-modified C_{18} column displayed different selectivity to the C_{18} column. Retention on C_{18} column was summarized in Table V. For example, although benzoic acid eluted first on the C_{18} column, it did not elute from the PP/Cl/C_{18} column. In addition, phenol and aniline could be separated on the C_{18} column, but not on the PP/Cl/C_{18} column. Furthermore, benzene and DEP as well as aniline and DMP could be separated on the PP/Cl/C_{18} column but not on the C_{18} columns. Basic drugs, caffeine and theophylline, were separated on the PP/Cl/C_{18} column (Fig. 6a) but they were eluted almost in the void volume under the same conditions using a C_{18} column. This verified that the polypyrrole coatings can provide unique selectivities when used in chromatography.

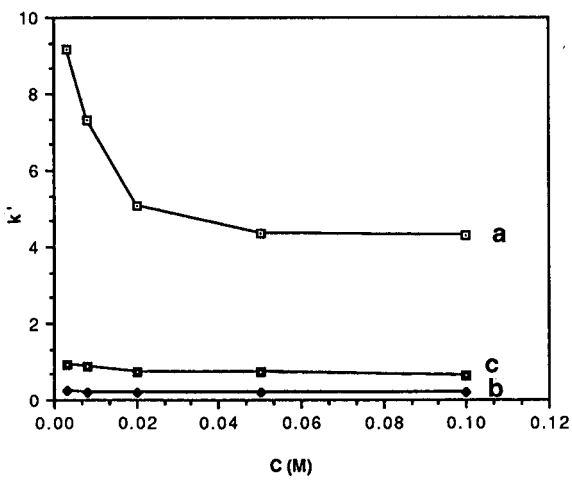

Fig. 5. Capacity factors *vs.* ionic strength of the mobile phase. Column: PP/Cl/silica in a 64 mm × 1.6 mm I.D. self-compressed column [30]: detector: UV at 254 nm; sample: a = 20 ppm benzoic acid; b = 20 ppm aniline; c = 20 ppm DMA.

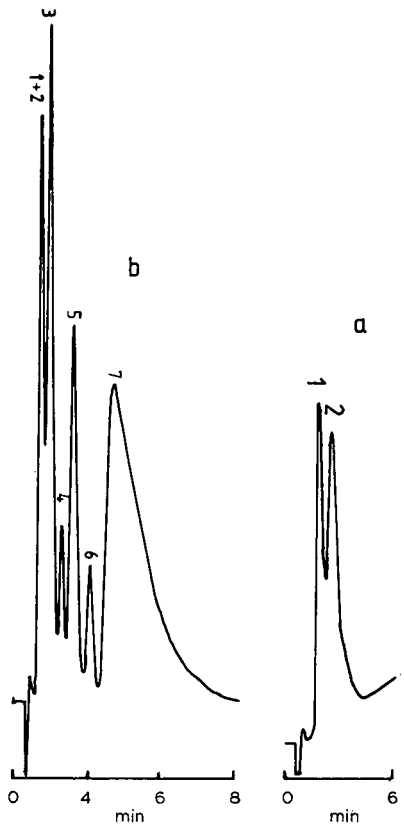

Fig. 6. Separations on a polypyrrole-coated C_{18} stationary phase. Column: PP/Cl/C_{18} in a 64 mm × 3.2 mm I.D. self-compressed column [30]; eluent: methanol–water (65:35) at 0.3 ml/min; detector: UV at 254 nm. Responses due to: (a) 1 = 5 ppm theophylline and 2 = 5 ppm caffeine; (b) 1 = 15 ppm phenol, 2 = 5 ppm aniline, 3 = 5 ppm DMP, 4 = 50 ppm benzene, 5 = 5 ppm DEP, 6 = 50 ppm toluene and 7 = 5 ppm DMA.

CONCLUSIONS

Using a chemical polymerisation procedure, silica-based packing materials were coated with conducting polymers. Elemental analysis indicated that the polymer loading was low on the C_{18}-based supports but slightly higher on the bare silica packings.

Changes in chromatographic interactions were found when polypyrrole-modified C_{18} columns were examined. Similar behaviour was observed on polypyrrole-modified bare silica. Mixed mode phases capable of anion exchange as well as hydrophobic interactions were obtained.

REFERENCES

1 L. C. Sander and S. A. Wise, *CRC Critical Rev. in Anal. Chem.*, 18 (1987) 299.
2 T. G. Den and S. L. Lee, *J. Chromatogr.*, 408 (1987) 323.
3 L. Nondek, *J. Chromatogr.*, 373 (1986) 61.
4 G. Felix, C. Bertrand and F. Van Gastel, *Chromatographia*, 20 (1985) 155.
5 G. Felix and C. Bertrand, *J. Chromatogr.*, 319 (1985) 432.
6 S. S. Yang and R. K. Gilpin, *J. Chromatogr.*, 408 (1987) 93.
7 M. Lienne, P. Gareil, R. Rosset, J. F. Husson, M. Emmelin and B. Neff, *J. Chromatogr.*, 395 (1987) 255.
8 R. W. Stout, S. I. Sivakoff, R. D. Ricker, H. C. Palmer, M. A. Jackson and T. J. Odiorne, *J. Chromatogr.*, 352 (1986) 381.
9 W. S. Foster and H. W. Jarrett, *J. Chromatogr.*, 403 (1987) 99.
10 S. Honda, S. Suzuki, T. Nitta and K. Kadehi, *J. Chromatogr.*, 438 (1988) 73.
11 H. W. Jarrett, *J. Chromatogr.*, 405 (1987) 179.
12 C. H. Shieh, B. L. Karger, L. R. Gelber and B. Feibush, *J. Chromatogr.*, 406 (1987) 343.
13 C. Petterson and C. Gioeli, *J. Chromatogr.*, 398 (1987) 247.
14 Y. Okamoto, R. Aburatani, S. I. Miura and K. Hatada, *J. Liq. Chromatogr.*, 10 (1987) 1613.
15 A. J. Alpert, *J. Chromatogr.*, 359 (1986) 85.
16 H. Figge, A. Deege, J. Köhler and G. Schomburg, *J. Chromatogr.*, 351 (1986) 393.
17 I. Krasilnikov and V. Borisova, *J. Chromatogr.*, 446 (1988) 211.
18 A. J. Alpert and P. C. Andrews, *J. Chromatogr.*, 443 (1988) 85.
19 W. Kopaciewicz, M. A. Rounds and F. E. Regnier, *J. Chromatogr.*, 318 (1985) 157.
20 G. Jilge, K. K. Unger, U. Esser, H.-J. Schafer, G. Rathgeber and W. Muller, *J. Chromatogr.*, 476 (1989) 37.
21 L. A. Kennedy, W. Kopaciewicz and F. E. Regnier, *J. Chromatogr.*, 359 (1986) 73.
22 P. Kolla, J. Kohler and G. Schomburg, *Chromatographia*, 23 (1987) 465.
23 M. Millot and B. Sebille, *J. Chromatogr.*, 408 (1987) 263.
24 G. Szabo, K. Offenmuller and E. Csato, *Anal. Chem.*, 60 (1988) 213.
25 Y. Ohtsu, H. Fukui, T. Kanda, K. Nakamura, M. Nakano and Y. Fujiyama, *Chromatographia*, 24 (1987) 380.
26 T. A. Skotheim (Editor), *Handbook of Conducting Polymers*, Vols. 1 and 2, Marcel Dekker, New York, 1986.
27 H. Ge and G. G. Wallace, *J. Liq. Chromatogr.*, 13 (1990) 3245.
28 H. Ge and G. G. Wallace, *Anal. Chem.*, 61 (1989) 2391.
29 H. Ge and G. G. Wallace, *Anal. Chem.*, 61 (1989) 198.
30 H. Ge and G. G. Wallace, *J. Liq. Chrom.*, 14 (1991) 1615.
31 R. Qian and J. Qiu, *Polymer J.*, 19 (1987) 157.
32 S. P. Armes, *Synth. Met.*, 20 (1987) 365.
33 J. N. King and J. S. Fritz, *Anal. Chem.*, 59 (1987) 703.
34 F. T. A. Vork and L. J. J. Janssen, *Electrochim. Acta*, 33 (1988) 1513.

Journal of Chromatography, 588 (1991) 33–39
Elsevier Science Publishers B.V., Amsterdam

CHROM. 23 629

High-performance liquid chromatographic determination of products of autoxidation of isopropylbenzene derivatives

Stefan Baj* and Zdzisław Kulicki

Department of Organic Chemistry and Technology, Silesian Technical University, Gliwice (Poland)

(First received August 7th, 1990; revised manuscript received July 15th, 1991)

ABSTRACT

The application of high-performance liquid chromatography to the qualitative and quantitative determination of the products of the autoxidation of cumene, *p*-cymene and 1,3- and 1,4-diisopropylbenzene is described.

INTRODUCTION

The autoxidation of isopropyl derivatives of benzene to hydroperoxides is the first reaction step in the process for the manufacture of phenols [1]. The autoxidation products are complicated mixtures containing unreacted hydrocarbons and compounds such as hydroperoxides, alcohols, ketones and many other oxygen derivatives. When two or more isopropyl groups are present on the benzene ring, the compositions of the mixtures are especially complicated. An example of such a process is the autoxidation of 1,4-diisopropylbenzene:

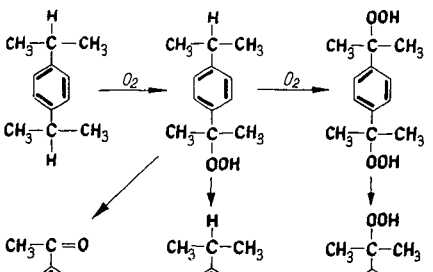

Such mixtures are not easily separated and analysed by conventional techniques. Gas chromatography (GC) [2–6] is not useful because some compounds are non-volatile and thermally unstable. Thin-layer chromatography (TLC) [7,8] and conventional column chromatography [9,10] offer insufficient separation efficiency and are slow. NMR techniques [10–12] offer unsatisfactory precision. IR [13–16], polarographic [17], density measurement [18] and iodimetric titration [19,20] methods enable only some of the components of the mixtures to be determined.

In contrast, high-performance liquid chromatography (HPLC [21–23] is a versatile, efficient and relatively rapid separation method for non-volatile, thermally labile compounds and is ideal for the separation and study of the mixtures from autoxidation reactions.

In this paper the separation and determination of components of the autoxidation products of cumene, 1,3- and 1,4-diisopropylbenzene and *p*-cymene is reported. Isocratic elution was employed because of its simplicity and potential use in routine analysis.

0021-9673/91/$03.50

EXPERIMENTAL

Materials and reagents

The solvents hexane, isopropanol and chloroform were of HPLC grade.

Standards

Cumyl hydroperoxide (technical product) was purified [24] and 1-methyl-1-phenylethanol [25], 1,3- and 1,4-diisopropylbenzene [26] and *p*-cymene derivatives [27,28] were prepared by published methods. Acetophenone was of analytical-reagent grade.

High-performance liquid chromatography

HPLC analyses were conducted utilizing an Philips LC XPD chromatograph, a Reodyne Model 7125 syringe-loading sample injector with a 20-μl loop and 25 cm × 4.6 mm I.D. stainless-steel column filled with LiChrosorb 60 (5 μm) or Partisil 10 (10 μm). The mobile phases were isopropanol–hexane mixtures at a flow-rate 1.0 cm^3/min. Samples for injection (20 μl) were solutions in the mobile phase. Compounds were detected at 257 nm with a LC XPD UV–VIS detector and integrated with a CDP4 integrator.

Quantitative procedures

Calibration was carried out according to one of two methods: external standardization using the external standard mode CDP4 integrator and internal standardization. In the external standardization mode, full 20-μl loop repetitive injections of single-concentration standard solution were used for single-point calibration, based on principles where the test samples are "bracketed" by standards injected before and after test. An internal standard method was also used for comparison. The ratio of the peak area of the analysed compounds to that of the internal standard was used to construct a calibration graph. A number of possible internal standard were explored for quantification of each compound. The criteria applied in assessing a suitable candidate were the UV absorbance in the region of 257 nm, chemical similarity to analysed compounds, a capacity factor (k') close to each component and complete separation from other sample components.

For all mixtures examined 1-methyl-1-phenylethanol was chosen as the internal standard except for the autoxidation products of cumene, where cumyl hydroperoxide was used.

RESULTS AND DISCUSSION

Selection of eluents

The conditions of analysis were investigated for the purpose of establishing routine analytical HPLC. It was important to know if there was any decomposition of hydroperoxides in the presence of LiChrosorb Si 60. The behaviour of cumyl hydroperoxide in the presence of LiChrosorb Si 60 (10 μm was examined. A 1-g amount of cumyl hydroperoxide was dissolved in 5 cm^3 of *n*-hexane and stirred with 1-g of LiChrosorb Si 60 (10 μm) for 8 h at room temperature. In the organic phase the hydroperoxide was determined by HPLC and iodimetric titration. HPLC did not provide evidence of hydroperoxide decomposition products. Iodimetric titration showed no change in hydroperoxide concentration.

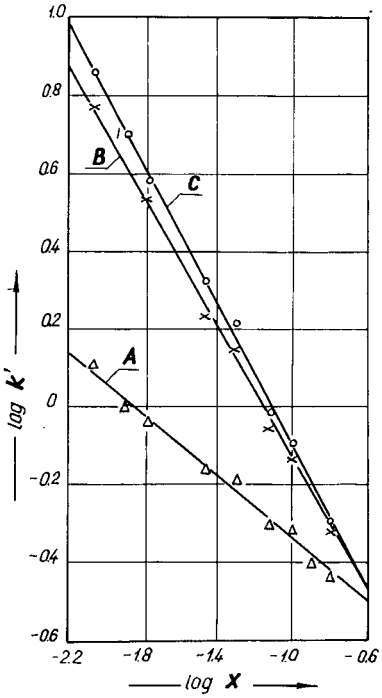

Fig. 1. Relationship between log k' of autoxidation products of cumene and log x, where x = molar ratio of isopropanol to *n*-hexane. (A) Acetophenone; (B) cumene hydroperoxide; (C) 1-methyl-1-phenylethanol.

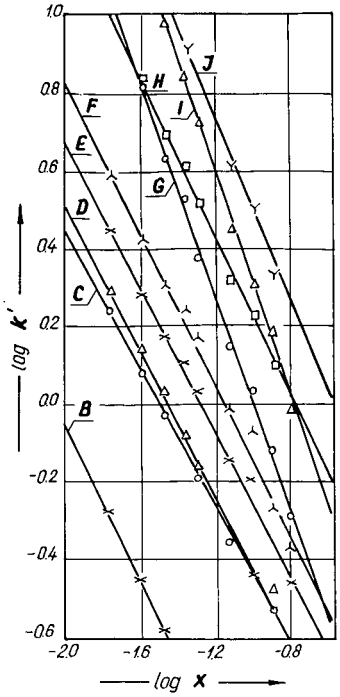

Fig. 2. Relationship between log k' of autoxidation products of 1,3-diisopropylbenzene and log x, where x = molar ratio of isopropanol to *n*-hexane. (C) 1,3-Di(1-methylethyl)benzene monohydroperoxide; (E) 1-methyl-[3-(1-methylethyl)phenyl]-1-hydroxyethane; (F) 1-methyl-1-phenylethanol; (G) 1,3-di(1-methylethyl)benzene dihydroperoxide; (H) 1-[3-(1-hydroxymethylethyl)phenyl]-1-methylethane hydroperoxide. (A), (B), (D), (I) and (J) are unidentified compounds.

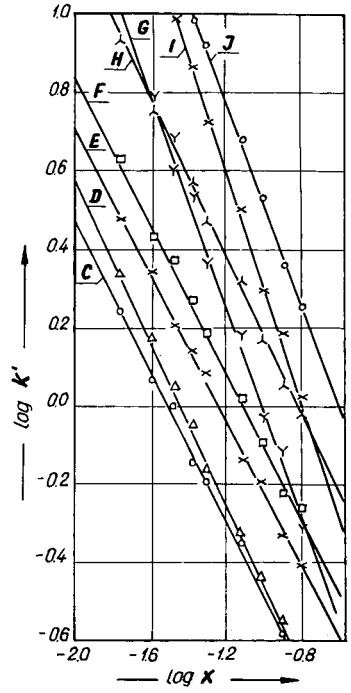

Fig. 3. Relationship between log k' of autoxidation products of 1,4-diisopropylbenzene and log x, where x = molar ratio of isopropanol to *n*-hexane. (C) 1,4-Di(1-methylethyl)benzene monohydroperoxide; (E) 1-methyl-[4-(1-methylethyl)phenyl]-1-hydroxyethane; (F) 1-methyl-1-phenylethanol; (G) 1,4-di(1-methylethyl)bezene dihydroperoxide; (H) 1-[4-(1-hydroxymethylethyl)phenyl]-1-methylethane hydroperoxide. (A), (B), (D), (I) and (J) are unidentified compounds.

The performance of three solvent systems as eluents was examined: *n*-hexane–isopropanol, *n*-hexane–chloroform and chloroform–isopropanol. *n*-Hexane–isopropanol provided the best resolution. The dependence of log k' on log (molar ratio of components) is shown in Fig. 1–4.

For quantitative analyses, solvent compositions having $1 < k' < 10$ were chosen, because for $k' < 1$ poor resolution and a poorly defined baseline and for $k' > 10$ broad peaks were observed.

TABLE I

EXTERNAL STANDARD CALIBRATION: LINEAR REGRESSION BY LEAST-SQUARES METHOD FOR A PLOT OF PEAK AREA *VERSUS* MASS INJECTED FOR AUTOXIDATION PRODUCTS OF CUMENE

Number of calibration points for each compounds, $n = 7$; number of replicates of each injection, $m = 5$.

Compounds	Range (μg)	Slope, a	Intercept, b	Correlation coefficient, r
Acetophenone	0.1–1.0	$1.1201 \cdot 10^{10}$	14042	0.998
Cumene hydroperoxide	1.0–10.0	$1.2783 \cdot 10^{9}$	4152	0.999
1-Methyl-1-phenylethanol	1.0–5.0	$1.3795 \cdot 10^{9}$	1731	0.999

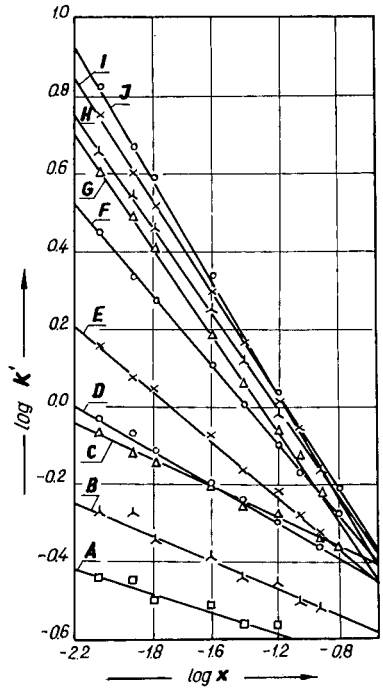

Fig. 4. Relationship between log k' of autoxidation products of p-cymene and log x, where x = molar ratio of isopropanol to n-hexane. (B) [4-(1-Methylethyl)phenyl]methane hydroperoxide; (C) 4-methylacetophenone; (F) 1-methyl-1-(4-methylphenyl)ethane hydroperoxide; (G) 1-methyl-4-(hydroxy-1-methylethyl)benzene; (J) 1-methyl-1-phenylethanol. (A), (B), (E), (H) and (I) are unidentified compounds.

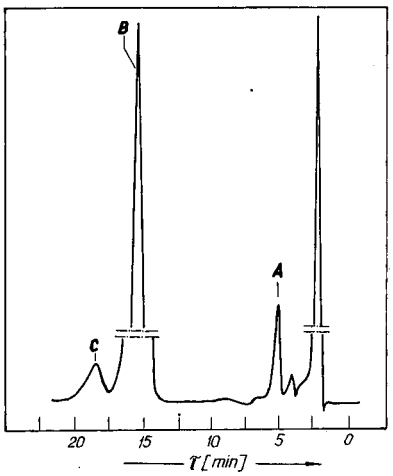

Fig. 5. Typical chromatogram of autoxidation products of cumene. Peaks: A = acetophenone; B = cumene hydroperoxide; C = 1-methyl-1-phenylethanol. Eluent, isopropanol–hexane (0.5:99.5); column Partisil 10 (10 μm) (25 cm); flow-rate, 1.0 ml/min.

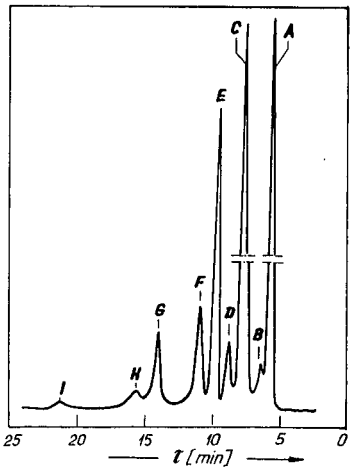

Fig. 6. Typical chromatogram of autoxidation products of 1,3-diisopropylbenzene. Peaks: A = 1,3-diisopropylbenzene; C = 1,3-di(1-methylethyl)benzene monohydroperoxide; D = 1,3-dihydroxybenzene; E = 1,3-di(1-methylethyl)benzene dihydroperoxide; F = 1-methyl-1-phenylethanol; G = 1-[3-(1-hydroxy-1-methyl)phenyl]-1-methylethane hydroperoxide; H = 1-methyl-[3-(1-methylethyl)phenyl]-1-hydroxyethane. B and I are unidentified compounds. Eluent, isopropanol–hexane (2.0:98.0); column, LiChrosorb Si 60 (5 μm) (25 cm); flow-rate, 1.0 ml/min.

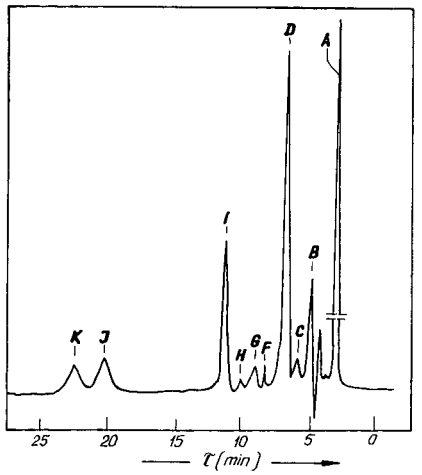

Fig. 7. Typical chromatogram of autoxidation products of 1,4-diisopropylbenzene. Peaks: A = 1,4-diisopropylbenzene; D = 1,4-di(1-methylethyl)benzene monohydroperoxide; F = 1,4-dihydroxybenzene; H = 1-methyl-1-phenylethanol: I = 1,4-di(1-methylethyl)benzene dihydroperoxide; J = 1-[4-(1-hydroxy-1-methylethyl)phenyl-1-methylethane hydroperoxide; K = 1-methyl-[4-(1-methylethyl)phenyl]-1-hydroxyethane. B, C, E and G are unidentified compounds. Eluent, isopropanol–hexane (2.0:98.0); column, LiChrosorb Si 60 (5 μm) (25 cm); flow-rate, 1.0 ml/min.

TABLE II

EXTERNAL STANDARD CALIBRATION: LINEAR REGRESSION BY LEAST-SQUARES METHOD FOR A PLOT OF PEAK AREA *VERSUS* MASS INJECTED FOR AUTOXIDATION PRODUCTS OF 1,3-DIISOPROPYLBENZENE

Number of calibration points for each compounds, $n = 7$; number of replicates of each injection, $m = 5$.

Compounds	Range (μg)	Slope, *a*	Intercept, *b*	Correlation coefficient, *r*
1,3-Di(1-methylethyl)benzene monohydroperoxide	1.0–10.0	$1.2193 \cdot 10^9$	2735	0.997
1-[3-(1-Hydroxy-1-methylethyl)phenyl]-1-methylethane hydroperoxide	1.0–5.0	$1.3145 \cdot 10^9$	3275	0.998
1-Methyl-[3-(1-methylethyl)phenyl]-1-hydroxyethane	1.0–5.0	$1.2831 \cdot 10^9$	4142	0.995
1,3-Di(1-methylethyl)benzene dihydroperoxide	1.0–10.0	$1.3543 \cdot 10^9$	5027	0.999
1,3-Dihydroxybenzene	0.5–1.0	$1.4579 \cdot 10^9$	10271	0.931

TABLE III

EXTERNAL STANDARD CALIBRATION: LINEAR REGRESSION BY LEAST-SQUARES METHOD FOR A PLOT OF PEAK AREA *VERSUS* MASS INJECTED FOR AUTOXIDATION PRODUCTS OF 1,4-DIISOPROPYLBENZENE

Number of calibration points for each compounds, $n = 7$; number of replicates of each injection, $m = 5$.

Compounds	Range (μg)	Slope, *a*	Intercept, *b*	Correlation coefficient, *r*
1,4-Di(1-methylethyl)benzene monohydroperoxide	1.0–10.0	$1.3124 \cdot 10^9$	5431	0.998
1-[4-(1-Hydroxy-1-methylethyl)phenyl]-1-methylethane hydroperoxide	1.0–5.0	$1.3941 \cdot 10^9$	3725	0.989
1-Methyl-[4-(1-methylethyl)phenyl]-1-hydroxyethane	1.0–5.0	$1.2945 \cdot 10^9$	4211	0.995
1,4-Di(1-methylethyl)benzene dihydroperoxide	1.0–10.0	$1.4133 \cdot 10^9$	10182	0.985
1,4-Dihydroxybenzene	0.5–1.0	$1.5183 \cdot 10^9$	15041	0.981

TABLE IV

EXTERNAL STANDARD CALIBRATION: LINEAR REGRESSION BY LEAST-SQUARES METHOD FOR A PLOT OF PEAK AREA *VERSUS* MASS INJECTED FOR AUTOXIDATION PRODUCTS OF *p*-CYMENE

Number of calibration points for each compounds, $n = 7$; number of replicates of each injection, $m = 5$.

Compounds	Range (μg)	Slope, *a*	Intercept, *b*	Correlation coefficient, *r*
1-Methyl-1-(4-methylphenyl)ethane hydroperoxide	1.0–5.0	$1.601 \cdot 10^9$	993	0.998
[4-(1-Methylethyl)phenyl]methane hydroperoxide	1.0–5.0	$1.336 \cdot 10^9$	735	0.995
4-Methylacetophenone	0.5–1.0	$2.736 \cdot 10^{10}$	7232	0.989
1-Methyl-4-(1-hydroxy-1-methylethyl) benzene	1.0–5.0	$1.405 \cdot 10^9$	7210	0.989
4-(1-Methylethyl)benzoic acid	0.5–2.0	$2.351 \cdot 10^9$	1351	0.897
4-Methylbenzoic acid	0.5–2.0	$2.532 \cdot 10^9$	10073	0.899
1-Hydroxy-4-methylbenzene	0.1–1.0	$2.103 \cdot 10^9$	12131	0.889

TABLE V

REPRODUCIBILITY OF EXTERNAL STANDARD METHOD FOR DETERMINATION OF AUTOXIDATION PRODUCTS OF CUMENE, 1,3-DIISOPROPYLBENZENE 1,4-DIISOPROPYLBENZENE AND *p*-CYMENE

Number of injections for each determination, $m = 8$.

Compounds	Amount added (μg)	Mean amount found (μg)	S.D. (μg)	R.S.D. (%)	Amount added (μg)	Mean amount found (μg)	S.D. (μg)	R.S.D. (%)
Autoxidation products of cumene								
Acetophenone	0.10	0.11	0.005	4.55	1.01	0.98	0.027	2.76
Cumene hydroperoxide	1.00	0.98	0.023	2.35	10.09	10.11	0.112	1.11
1-Methyl-1-phenylethanol	1.00	1.05	0.022	2.10	5.03	5.05	0.104	2.06
Autoxidation products of 1,3-diisopropylbenzene								
1,3-Di(1-methylethyl)benzene monohydroperoxide	1.02	1.03	0.022	2.14	10.01	10.51	0.198	1.88
1-[3-(1-Hydroxy-1-methylethyl)phenyl]-1-methylethane hydroperoxide	1.00	1.10	0.019	1.73	5.330	5.37	0.079	1.47
1-Methyl-[3-(1-methylethyl)phenyl]-1-hydroxyethane	1.02	0.95	0.028	2.95	4.99	5.42	0.069	1.27
1,3-Di(1-methylethyl)benzene dihydroperoxide	1.04	1.03	0.035	3.40	10.01	10.34	0.196	1.90
1,3-Dihydroxybenzene	0.51	1.07	0.027	2.52	1.35	1.29	0.032	2.48
Autoxidation products of 1,4-diisopropylbenzene								
1,4-Di(1-methylethyl)benzene monohydroperoxide	1.00	1.05	0.021	2.00	10.00	9.27	0.186	2.01
1-[4-(1-Hydroxy-1-methylethyl)phenyl]-1-methylethane hydroperoxide	1.01	1.02	0.019	1.86	5.02	5.15	0.141	2.74
1-Methyl-[4-(1-methylethyl)phenyl]-1-hydroxyethane	1.05	0.97	0.023	2.37	4.99	5.01	0.101	2.02
1,4-Di(methylethyl)benzene dihydroperoxide	1.00	0.98	0.020	2.04	10.04	10.08	0.197	1.95
1,4-Dihydroxybenzene	0.50	0.49	0.017	3.47	1.03	1.11	0.038	3.42
Autoxidation products of p-cymene								
1-Methyl-1-(4-methylphenyl)ethane hydroperoxide	1.02	1.03	0.023	2.33	5.01	5.21	0.139	2.67
[4-(1-Methylethyl)phenyl]methane hydroperoxide	1.01	1.05	0.021	2.00	5.05	5.03	0.095	1.89
4-methylacetophenone	0.49	0.97	0.039	4.02	0.98	0.99	0.025	2.52
1-Methyl-4-(1-hydroxy-1-methylethyl)-benzene	1.04	0.93	0.021	2.26	4.89	5.02	0.012	2.39
4-(1-Methylethyl)benzoic acid	0.51	0.49	0.019	3.73	2.00	1.98	0.024	1.21
4-Methylbenzoic acid	0.50	0.48	0.022	4.58	2.03	2.01	0.039	1.94
1-Hydroxy-4-methylbenzene	0.11	0.10	0.003	3.00	1.00	1.01	0.051	4.95

For the determination of the autoxidation products of cumene and *p*-cymene, the composition of the eluent was *n*-hexane–isopropanol (99.5:0.5, v/v) and for the autoxidation products of 1,3- and 1,4-diisopropylbenzenes the composition was 98.0:2.0 (v/v).

Figs. 5–8 are typical chromatograms of crude autoxidation products of cumene, 1,3- and 1,4-diisopropylbenzene and *p*-cymene.

Quantification

External and internal standard calibration gave a linear response for the peak-area ratio for standard concentrations over the range 1–10 μg/ml. The parameters derived from least-squares regression for the external standard method are given in Tables I–IV. The internal-standard method was also linear.

The relative standard deviations (R.S.D.) of replicate injections for the external standard method

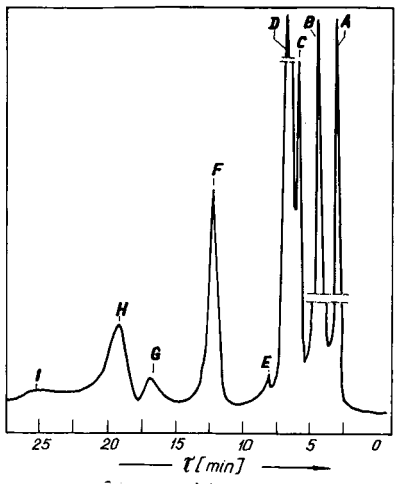

Fig. 8. Typical chromatogram of autoxidation products of *p*-cymene. Peaks: A = *p*-cymene; B = [4-(1-methylethyl)phenyl]methane hydroperoxide; C = 4-methylacetophenone; D = 1-methyl-1-(4-methylphenyl)ethane hydroperoxide; E = 1-methyl-4-(1-hydroxy-1-methyl)benzene; F = 1-methyl-1-phenylethanol; G = 4-(1-methylethyl)benzoic acid; H = 4-methylbenzoic acid; I = 1-hydroxy-4-methylbenzene. Eluent isopropanol–hexane (0.50:99.50); column, Partisil 10 (10 μm) (25 cm); flow-rate, 1.0 ml/min.

are given in Table V. The method gave the possibility of determining the main products of the autoxidation of alkylaromatic compounds with good precision.

CONCLUSIONS

The possibility of the application of HPLC to the determination of the autoxidation products of some alkylaromatic compounds was studied. The method gave good results for the analysis of mixtures containing very unstable compounds such as hydroperoxides. The proposed procedure is rapid and simple.

ACKNOWLEDGEMENTS

We thank Dr. Ing. Aleksandra Burghardt, Institute of Organic Chemistry and Technology of Silesian Technical University, for samples of standards of *p*-cymene autoxidation products.

REFERENCES

1 G. Franz, *Ullmanns Encyklopädie der Technischen Chemie*, Band 17, Verlag Chemie, Weinheim, 1972, p. 483.
2 N. V. Shumilov, T. I. Bugai and A. S. Yablokova, *Mater. Nauchno-Tekh. Konf. Kazan. Khim.-Tekhnol. Inst. Kazan. Zavoda Org. Sint., 2nd, 1972* (1973) 162.
3 R. Pies, V. Sibaiova and V. Sulik, *Ropa Uhlie*, 17 (1975) 233.
4 G. S. Kirichenko and L. K. Plamova, *Zh. Anal. Khim.*, 35 (1980) 758.
5 G. S. Kirichenko and L. K. Plamova, *Zh. Anal. Khim.*, 35 (1980) 1799.
6 A. Yu. Bruk, K. A. Gaishun, R. I. Godynskaya and V. A. Markova, *Neftepererab. Neftekhim.*, 9 (1983) 30.
7 L. P. Novitskaya, *Zh. Anal. Khim.*, 44 (1989) 1138.
8 P. R. Ivanienko and A. S. Walga, *Zavod. Lab.*, 7 (1964) 797.
9 A. Graham, in *Proceedings of the 7th World Petroleum Congress, Mexico, 1967*, Elsevier, New York, 1967, p. 341.
10 G. A. Ward, *Int. Lab.*, 1 (1971) 72.
11 L. Cavalli and G. Cancellieri, *Analyst (London)*, 100 (1975) 46.
12 M. Skrzyński, K. Gorczyńska and E. Bednarek, *J. Mol. Struct.*, 143 (1986) 541.
13 G. F. Okuner and L. G. Morozova, *Mater. Nauchno-Tekh. Konf. Kazan. Khim.-Tekhnol. Inst. Kazan. Zavoda Org. Sint., 2nd, 1972*, (1973) 168.
14 A. Worknoj and A. Worknoj, *Chem. Anal. (Warsaw)*, 21 (1976) 1069.
15 O. Landauer, C. Matescu and V. Porausanu, *Bul. Inst. Politeh. "Gheorghe Gheorghiu-Dej" Bucuresti*, 38 (1976) 25.
16 O. Landauer, C. Matescu and V. Porausanu, *Bul. Inst. Politeh. "Gheorghe Gheorghiu-Dej" Bucuresti*, 39 (1977) 43.
17 Z. Gregorowicz, J. Cebula and P. Górka, *Fresenius' Z. Anal. Chem.*, 284 (1977) 287.
18 K. Gorczyńska, H. Malikowska, H. Walędziak and A. Szostak, *Chem. Anal. (Warsaw)*, 20 (1975) 1099.
19 J. M. Kolthoff and A. J. Medalia, *J. Am. Chem. Soc.*, 71 (1949) 3781.
20 *Jpn. Pat.*, 80 62, 355 (1980).
21 L. Topolova, Kh. Dimitrov and M. Aleksandrova, *Izv. Akad. Nauk SSSR, Ser. Khim.*, 19 (1986) 520.
22 C. P. Patel and S. Lilly, *LC · GC*, 6 (1988) 424.
23 B. J. Beltra and J. Beltran de Hevedia, *Afinidad*, 46 (1989) 185.
24 W. Karmiński, Z. Kulicki and Z. Stec, *Chemia Stosow.*, 24 (1969) 17.
25 G. P. J. Armstrong, R. H. Hall and D. C. Quin, *J. Chem. Soc.*, (1950) 666 and 670.
26 L. A. Sinovitch, I. M. Zinoveva, W. W. Lezneva, W. W. Fedorova, B. A. Worobeva and A. G. Kostiuk, *Usp. Khim. Org. Perekisnych Soedin. Autook. Dokl. Ves. Konf. 3rd, 1965*, (1969) 137.
27 H. Dressler, *US Pat.*, 4 108 907 (1978).
28 F. Matsunaga and O. Norio, *Eur. Pat.*, 21 665 (1980).

Journal of Chromatography, 588 (1991) 41–45
Elsevier Science Publishers B.V., Amsterdam

CHROM. 23 612

High-performance liquid chromatography of diastereomeric flavanone glycosides in *Citrus* on a β-cyclodextrin-bonded stationary phase (Cyclobond I)

Martin Krause and Rudolf Galensa*

Institut für Lebensmittelchemie der Technischen Universität Braunschweig, Schleinitzstrasse 20, 3300 Braunschweig (Germany)

(First received May 2nd, 1991; revised manuscript received July 8th, 1991)

ABSTRACT

The flavavone glycosides prunin, naringin, neohesperidin and narirutin were separated into their diastereomers by high-performance liquid chromatography elution in the reversed-phase mode on a β-cyclodextrin bonded stationary phase (Cyclobond I). Application to the analysis of *Citrus* extracts showed that immature grapefruit fruits contained almost entirely (2*S*)-naringin and (2*S*)-prunin, whereas in grapefruit juice both diastereomers of naringin and narirutin were present (about 60% *S* and 40% *R* isomers). In bitter-orange juice only (2*S*)-neohesperidin was detected and sweet orange juice contained racemic narirutin. Benzoylated flavanone glycosides (naringin, prunin) were also separated on Cylcobond I in the normal-phase mode.

INTRODUCTION

Flavonoids are widely distributed in the plant kingdom [1]. Some flavanone glycosides, however, are unique to *Citrus* [2] and have been considered to be potential taxonomic markers [3]. For example, naringin, the chief bitter constituent in grapefruit (*Citrus paradisi*), is an indicator substance to detect grapefruit juice in sweet orange (*Citrus sinensis*) juice [4–6]. The C-2 position of the flavanone moiety is a chiral centre and (2*R*)- and (2*S*)-flavanone glycosides are diastereomeric by virtue of the carbohydrate present. From chiroptical studies it was concluded that naturally occurring flavanone glycosides have the 2*S* configuration [7]. Gaffield and Lundin [8] also reported that only immature grapefruit contained (2*S*)-naringin whereas both diastereomers were present in the mature fruit. These results were obtained by circular dichroism and NMR spectroscopy.

In recent years, high-performance liquid chromatography (HPLC) has become the technique of choice for the analysis of flavonoids, especially in complex phenolic mixtures of plant extracts [9]. Most of the HPLC separations have been performed on reversed-phase (RP) stationary phases [9]. Although diastereomeric flavanone glycosides differ in their physico-chemical properties, no separation of the isomers by reversed-phase chromatography has been reported. Recently, we reported the resolution of flavanone glycosides on a cellulose triacetate-based chiral stationary phase [10]. Unfortunately, different flavanone diglycosides could not be separated from each other on this stationary phase. *Citrus* extracts often contain more than one flavanone diglycoside (*e.g.*, naringin and narirutin in grapefruit), and therefore their analysis was impossible.

Although benzoylated flavanone glycosides have been resolved into their diastereomers on a silica gel stationary phase by HPLC [5,11], it is advantageous to have an analytical method without a preceding derivatization step.

Cyclodextrin-bonded stationary phases have been used for the separation of enantiomers, diastereomers, structural isomers and other compounds

0021-9673/91/$03.50

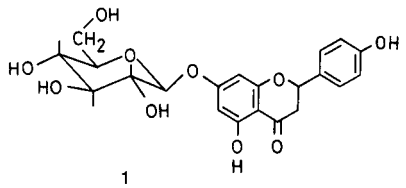

1

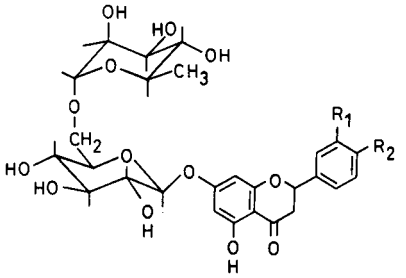

2a: R_1 = H, R_2 = OH

2b: R_1 = OH, R_2 = OCH_3

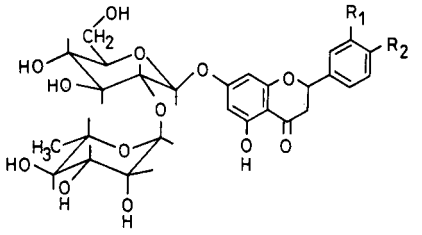

3a: R_1 = H, R_2 = OH

3b: R_1 = OH, R_2 = OCH_3

Fig. 1. Structures of flavanone glycosides. 1 = Prunin (naringenin-7-O-glucoside); 2a = narirutin (naringenin-7-O-rutinoside); 2b = hesperidin (hesperetin-7-O-rutinoside); 3a = naringin (naringenin-7-O-neohesperidoside); 3b = neohesperidin (hesperetin-7-O-neohesperidoside).

[12–15]. In this paper we report the direct separation of flavanone glycosides (prunin, naringin, narirutin and neohesperidin, Fig. 1) on a β-cyclodextrin-bonded stationary phase (Cyclobond I) in the reversed-phase mode and its application to *Citrus* extracts. Some benzoylated flavanone glycosides were also resolved in the normal-phase mode on Cyclobond I.

EXPERIMENTAL

Materials

Flavanone glycosides were of HPLC grade and purchased from Roth (Karlsruhe, Germany). The benzoylated flavanone glycosides were prepared as described previously [5,16]. Methanol, acetic acid, isooctane and diethyl ether were of analytical-reagent or HPLC grade and purchased from Baker (Gross-Gerau, Germany). Immature grapefruit (2–3 cm diameter) was a gift from Professor Dr. C. Hoeppe (Kassel, Germany) and bitter-orange juice from Dr. V. Ara (Hannover, Germany). Other samples were from commercial sources.

HPLC

The liquid chromatograph consisted of two Model 114 M pumps (Beckman, Munich, Germany), a high-pressure mixing chamber, a sampling valve (Altex 210; Beckman) equipped with a 20-μl sample loop and a Pye Unicam variable-wavelength UV detector set at 280 nm (Philips, Kassel, Germany). The peaks were recorded with a C-R6A integrator (Shimadzu, Duisburg, Germany). Peak identity was also confirmed with an HP 1040 diode-array detector (Hewlett-Packard, Waldbronn, Germany). The analytical column used was a 250 × 4.6 mm I.D. Cyclobond I (β-cyclodextrin; ASTEC, ICT, Germany). The following gradient was applied: 1 min A [water–methanol–acetic acid (90:10:0.5)]–B (methanol) (95:5), then linear from 5% to 50% B in 25 min. The flow-rate was 1 ml/min.

The configurations of the flavanone glycoside diastereomers were determined by enzymatic hydrolysis of the enriched isomers and determination of the enantiomeric aglycone on a chiral stationary phase [10].

Sample preparation

A 5-ml volume of *Citrus* juice was applied to a polyamide cartridge (Macherey-Nagel, Düren, Germany). After washing with 12 ml of water, the flavonoids were eluted with 6 ml of methanol. Water was added to give a final volume of 10 ml. Immature grapefruit and marmalade were extracted with methanol, the extract was evaporated to dryness and the residue transferred with water to the polyamide cartridge. Washing and elution steps were the same as for the juices.

RESULTS AND DISCUSSION

Fig. 2 shows two chromatograms of a mixture of flavanone glycosides. All four flavanone diglycosides

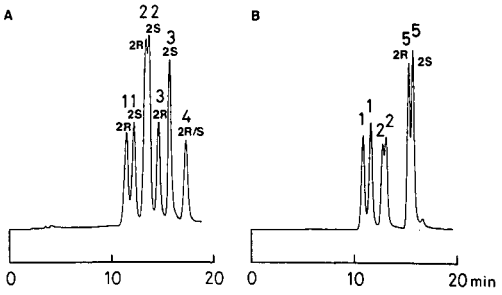

Fig. 2. HPLC of diastereomeric flavanone glycosides on Cyclobond I with gradient elution (see text). Peaks: 1 = naringin; 2 = narirutin; 3 = neohesperidin; 4 = hesperidin; 5 = prunin.

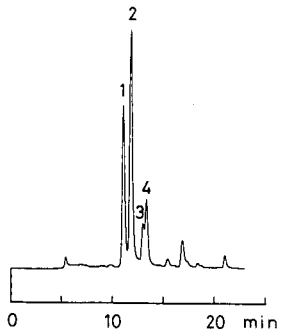

Fig. 4. HPLC of an extract of a commercial grapefruit juice extract. Peaks: 1 = (2*R*)-naringin; 2 = (2*S*)-naringin; 3 = (2*R*)-narirutin; 4 = (2*S*)-narirutin.

(naringin, nariruitin, neohesperidin and hesperidin) are separated from each other (Fig. 2A). The resolution of their diastereomers, however, depends on the sugar moiety. Naringin and neohesperidin (sugar moiety: neohesperidose) are much better separated than the rutinosides. Narirutin is only partially resolved and hesperidin not at all. Naringenin-7-O-glucoside (prunin) is also separated into diastereomers, as shown in Fig. 2B.

A chromatogram of an immature grapefruit fruit (diameter 2–3 cm) extract is shown in Fig. 3. Only about 2% of the naringin has the 2*R* configuration. The same result was reported by Gaffield and Lundin [8], who studied the composition of naringin diastereomers in grapefruit during ripening. They found that as the fruits mature, the amount of (2*S*)-naringin increased up to a final composition of 60% *S* and 40% *R* [8]. These results, obtained by circular dichroism and NMR spectroscopy after the isolation of naringin, could be confirmed by HPLC. Freshly squeezed grapefruit juice (ripe fruit) contained 66% (2*S*)- and 34% (2*R*)-naringin and a grapefruit juice from a commercial source 60% (2*S*)- and 40% (2*R*)-naringin. Fig. 4 illustrates the analysis of a commercial grapefruit juice. The diastereomeric compositions of narirutin and naringin were almost the same.

Prunin (naringenin-7-O-glucoside) has recently been identified in immature grapefruit, but has not been detected in mature grapefruit [17]. Raymond and Maier [18] isolated a chalcone cyclase from grapefruit and it was believed that glycosidation and rhamnosylation of naringin occur before flavanone formation in *Citrus* tissues. However, recently Lewinsohn *et al.* [19] suggested that glycosidation occurs at the stage of the flavanone and the monoglycoside prunin is an intermediate in the biosynthesis of naringin in *Citrus*. The convertion of exogene-

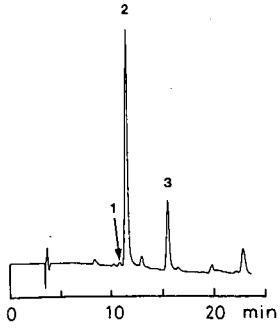

Fig. 3. HPLC of an immature grapefruit extract. Peaks: 1 = (2*R*)-naringin; 2 = (2*S*)-naringin; 3 = (2*S*)-prunin.

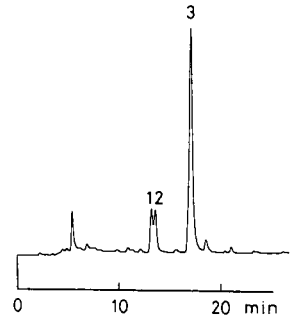

Fig. 5. HPLC of a sweet orange juice extract. Peaks: 1 = (2*R*)-narirutin; 2 = (2*S*)-narirutin; 3 = (2*R*/*S*)-hesperidin.

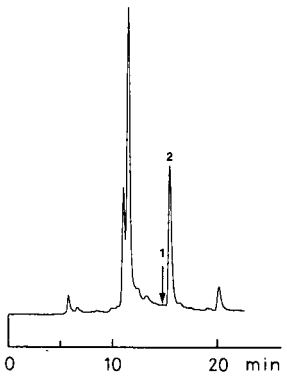

Fig. 6. HPLC of a bitter-orange juice extract. Peaks: 1 = (2*R*)-neohesperidin; 2 = (2*S*)-neohesperidin.

ous naringenin to prunin and further to naringin by grapefruit cell cultures has also been reported [20]. Fig. 3 shows that prunin is present in immature grapefruit almost exclusively as the 2*S* isomer.

Sweet oranges (*Citrus sinensis*) contain only flavanone rutinosides such as narirutin and hesperidin [2]. Fig. 5 shows a chromatogram of an orange juice extract. Narirutin is present with both diastereomers and hesperidin isomers cannot be separated with this method.

Bitter oranges (*Citrus aurantium* subsp. *aurantium*) are used for processing marmelade. In contrast to sweet oranges (*Citrus sinensis*), they contain the flavanone neohesperidosides naringin, neohesperidin and neoeriocitrin [2,21]. The results of the HPLC analysis are shown in Fig. 6. As naringin and neoriocitrin co-elute, their diastereomeric composition cannot be determined; neohesperidin is only detected in the 2*S* configuration. Horrowitz and Jurd [22] reported that the tendency for chalcone formation of flavanone glycosides depends on the substitution pattern of the flavanone. A free 4′-hydroxy group of a flavanone (*e.g.*, naringenin aglycone in naringin and narirutin) favours the reaction. Neohesperidin has a 4′-methoxy group and is therefore more stable than naringin and narirutin. This also has implications for the racemization of flavanone glycosides. The aglycone in naringin was easily racemized by heating (2*S*)-naringin at 70°C in an aqueous methanolic solution. Neohesperidin did not racemize under these conditions, but was racemized in dilute alkaline solution. In a marmalade extract (Fig. 7), most of neohesperidin is still in the 2*S* configuration, despite the heat-processing conditions. It should be mentioned additionally that in commercially available neohesperidin the 2*S* isomer also dominates (Fig. 2).

Cyclodextrin-bonded stationary phases have similar properties to a diol column when used in the normal-phase mode [13,23]. The separation of ben-

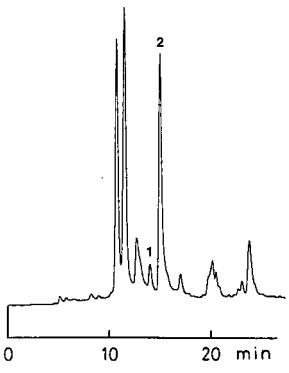

Fig. 7. HPLC of a marmalade extract. Peaks: 1 = (2*R*)-neohesperidin; 2 = (2*S*)-neohesperidin.

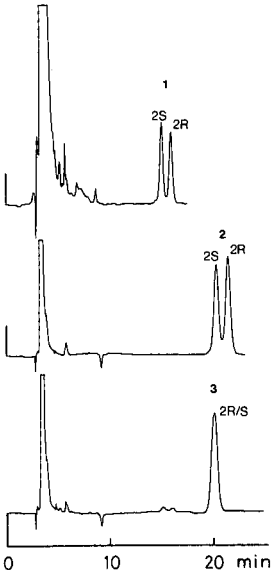

Fig. 8. HPLC of benzoylated flavanone glycosides on Cyclobond I. Mobile phase: isooctane–diethyl ether–methanol (55:40:5 v/v/v) at a flow-rate of 1 ml/min; detection at 231 nm. Peaks: 1 = prunin benzoate; 2 = naringin benzoate; 3 = narirutin benzoate.

zoylated diastereomeric flavanone glycosides has been performed on silica gel [7,11]. Fig. 8 shows that the resolution of benzoylated naringin and prunin can also be achieved on Cyclobond I, while narirutin benzoate is unresolved.

In conclusion, on Cyclobond I the direct HPLC separation of flavanone glycoside diastereomers in the reversed-phase mode and the resolution of their benzoates in the normal-phase mode are possible. Applying gradient elution, the diastereomeric composition of flavanone glycosides in *Citrus* can be determined, with the exception of hesperidin.

With the described HPLC method, the formation of flavanone glycosides can be analysed easily with respect to their C-2 stereochemistry and this may also be of interest in biochemical or enzymatic studies of *Citrus*.

ACKNOWLEDGEMENTS

We thank Professor C. Hoeppe (Kassel, Germany) for providing the immature grapefruit and Dr. V. Ara (Hannover, Germany) for a gift of bitter orange juice.

REFERENCES

1 J. B. Harborne, T. J. Mabry and H. Mabry, *The Flavonoids*, Chapman & Hall, London, 1975.
2 B. A. Bohm, in J. B. Harborne, T. J. Mabry and H. Mabry (Editors), *The Flavonoids*, Chapman & Hall, London, 1975, pp. 561–631.
3 S. Ranganna, V. S. Govindarajan and K. V. R. Ramana, *CRC Crit. Rev. Food Sci. Nutr.*, 18 (1983) 313.
4 R. Galensa and K. Herrman, *Dtsch. Lebensm.-Rdsch.*, 76 (1980) 270.
5 F. Siewek, R. Galensa and V. Ara, *Ind. Obst-Gemüseverwert.*, 70 (1985) 11.
6 G. Greiner and S. Wallrauch, *Flüss. Obst.*, 12 (1984) 626.
7 W. Gaffield, *Tetrahedron*, 26 (1970) 4093.
8 W. Gaffield and R. E. Lundin, *Bioorg. Chem.*, 4 (1975) 259.
9 D. J. Daigle and E. J. Conkerton, *J. Liq. Chromatogr.*, 11 (1988) 309.
10 M. Krause and R. Galensa, *J. Chromatogr.*, 502 (1990) 287.
11 D. Treutter, R. Galensa, W. Feucht and P. P. S. Schmid, *Physiol. Plant.*, 65 (1985) 95.
12 T. J. Ward and D. W. Armstrong, *J. Chromatogr. Sci.*, 40 (1988) 131.
13 C. A. Chang, Q. Wu and L. Tan, *J. Chromatogr.*, 361 (1986) 199.
14 D. W. Armstrong and W. DeMond, *J. Chromatogr. Sci.*, 22 (1984) 411.
15 D. W. Armstrong, W. DeMond, A. Alak, W. L. Hinze, T. E. Riehl and K. H. Bui, *Anal. Chem.*, 57 (1985) 234.
16 R. Galensa, *Z. Lebensm.-Unters.-Forsch.*, 176 (1983) 417.
17 M. A. Berhow and C. E. Vandercook, *Phytochemistry*, 28 (1989) 1627.
18 W. R. Raymond and V. P. Maier, *Phytochemistry*, 16 (1977) 1535.
19 E. Lewinsohn, L. Britsch, Y. Mazur and J. Gressel, *Plant Physiol.*, 91 (1989) 1323.
20 E. Lewinsohn, E. Berman, Y. Mazur and J. Gressel, *Phytochemistry*, 25 (1986) 2531.
21 R. L. Rouseff, S. F. Martin and C. O. Youtsey, *J. Agric. Food Chem.*, 35 (1987) 1027.
22 R. M. Horrowitz and L. Jurd, *J. Org. Chem.*, 26 (1961) 2446.
23 T. J. Ward and D. W. Armstrong, *J. Liq. Chromatogr.*, 9 (1986) 407.

Journal of Chromatography, 588 (1991) 47–52
Elsevier Science Publishers B.V., Amsterdam

CHROM. 23 613

Detection of zearalenone in cereal extracts using high-performance liquid chromatography with post-column derivatization

Michael T. Hetmanski* and Keith A. Scudamore

MAFF, Central Science Laboratory, London Road, Slough, Berkshire SL3 7HJ (UK)

(First received May 1st, 1991; revised manuscript received July 9th, 1991)

ABSTRACT

Post-column derivatization has been used to enhance the fluorescence response of the *Fusarium* mycotoxins zearalenone and zearalenol when determined by reversed-phase high-performance liquid chromatography. Derivatization is based on reaction with aluminium chloride and this results in a more selective response for these toxins. The method was tested on a number of cereals and animal feeds.

INTRODUCTION

Zearalenone is a fungal metabolite produced by a number of *Fusarium* species, and was originally isolated from *Fusarium roseum* and *Fusarium graminearum* [1]. Although not acutely toxic, zearalenone has been found to produce oestrogenic effects in animals and is suspected of causing infertility problems, especially in pigs [2]. Zearalenol is a structurally related *Fusarium* metabolite and produces similar oestrogenic effects [3]. The structural formulae for zearalenone and zearalenol are illustrated in Fig. 1.

A number of analytical methods have been developed for the determination of zearalenone and zearalenol in animal feedstuffs and human foods. Thin-layer chromatography (TLC) has been used for determination of zearalenone alone [4] or in multi-mycotoxin screening procedures [5,6]. However, the detection limits for zearalenone are relatively high, as it has a weak native fluorescence under UV light and, in order to improve the sensitivity of TLC, a number of reagents have been used to produce coloured spots when viewed under daylight or UV light. These include sulphuric acid [4], potassium hexacyanoferrate(III) and iron(III) chloride [4], bis-diazotized benzidine [7], aluminium chloride [5] and Fast Violet B [8].

More recently, high-performance liquid chromatographic (HPLC) methods have been developed for the determination of zearalenone, but owing to interference from co-extracted substances, extensive clean-up of the sample extracts is necessary prior to HPLC analysis to take full advantage of the sensitivity of modern detectors. This requires lengthy and time-consuming clean-up techniques such as liquid–

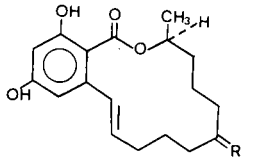

Name	R
Zearalenone	=O
Zearalenol	-OH

Fig. 1. Structural formulae of zearalenone (F-2) and zearalenol (ZAL).

liquid partition together with silica gel column chromatography to achieve detection levels as low as 10 μg/kg [8–10]. Even after clean-up using these methods, the final extracts produced are often unsatisfactory for the determination of zearalenone at this level. Hence any technique which improves selectivity and sensitivity would be advantageous.

Gas chromatography–mass spectrometry (GC–MS) has also been used and, when operated in the selected ion monitoring (SIM) mode, detection of zearalenone is both sensitive and selective [8]. A further development is the use of GC–tandem MS (GC–MS–MS), where multiple reaction monitoring (MRM) of daughter ions offers a highly specific detection method for zearalenone [11], but this type of instrumentation is expensive and may not be available to many laboratories. Recently, immunoassays have been developed for the determination of zearalenone, and an enzyme-linked immunosorbent assay (ELISA) method has been published for the determination of zearalenone in corn [12]. However, these methods will require further evaluation before general acceptance for routine use.

A post-column reaction using aqueous iodine to enhance the fluorescence of aflatoxins B_1 and G_1 is now commonly utilized in aflatoxin analysis, when analysed by reversed-phase HPLC [13]. Aluminium chloride is known to enhance the fluorescence of zearalenone on TLC plates [5], and this reaction has been applied to the determination of zearalenone and zearalenol in sample extracts using the apparatus developed for the post-column derivatization of aflatoxins.

This on-stream reaction has been found to enhance the fluorescence of zearalenone and zearalenol by a factor of five without increasing the background signals from sample co-extractives.

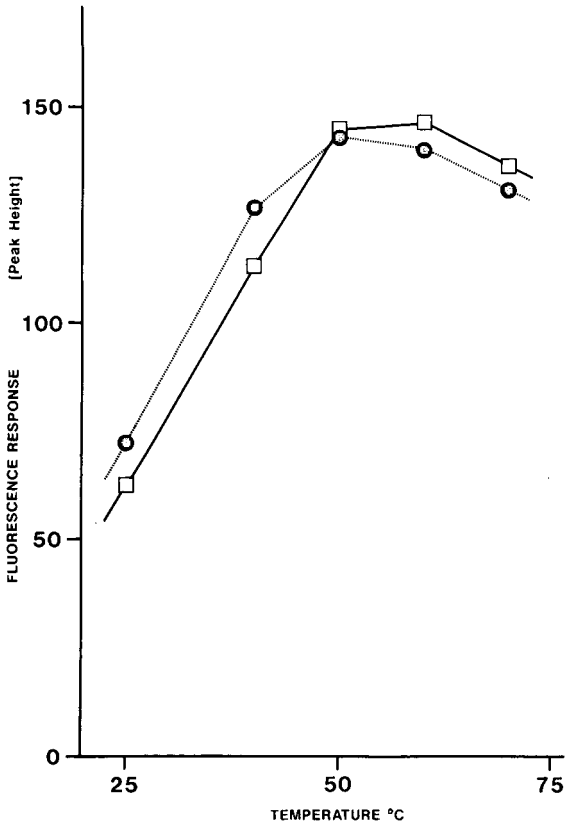

Fig. 2. Effect of temperature on the post-column derivatization of (□) zearalenone and (●) zearalenol.

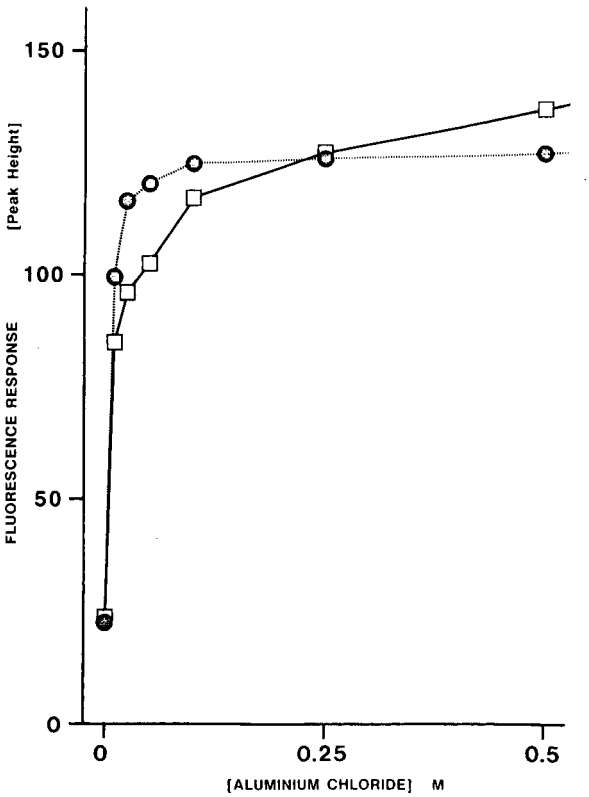

Fig. 3. Effect of aluminium chloride concentration on the post-column derivatization of (□) zearalenone and (●) zearalenol.

EXPERIMENTAL

Apparatus

High-performance liquid chromatography. The instrumentation consisted of pumps, system controller and U6K injector (Waters Assoc., Harrow, UK), a Shimadzu RF 530 fluorescence detector (Dyson Instruments, Houghton-le-Spring, UK) and a stainless-steel column packed with Spherisorb 5-μm ODS-1 (250 mm × 4.6 mm I.D.) (Hi-Chrom, Reading, UK), or similar HPLC equipment.

Post-column reaction system [13]. This was composed of an SSI stainless-steel tee-piece (1/16 in. × 0.0015 in.) (Jones Chromatography, Hengoed, UK), a PTFE coil (5000 mm × 0.3 mm I.D.) heated in a water-bath and an HPLC pump.

Materials

Solvents. Methanol and water of HPLC grade obtained from Rathburn Chemicals (Walkerburn, UK) or equivalent materials were used.

Aluminium chloride solution for post-column reaction. Aluminium chloride hexahydrate, 99.999% (Gold Label, Aldrich, Gillingham, UK) dissolved in methanol–water (3:1) to make a 0.25 *M* solution was used.

Mycotoxin standards. Zearalenone and zearalenol were obtained from Sigma (Poole, UK) and working standard solutions of 0.1 and 1.0 μg/ml zearalenone and 1.0 and 10.0 μg/ml zearalenol in methanol–water (80:20) were prepared.

High-performance liquid chromatography

HPLC was carried out using a Spherisorb 5-μm ODS-1 column with methanol–water (80:20) as

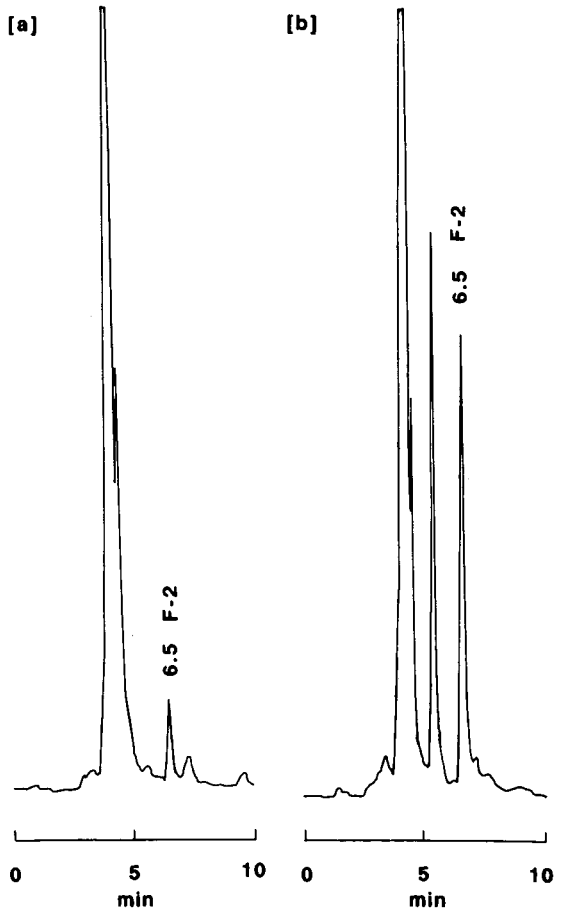

Fig. 4. HPLC of a mycotoxin-free maize extract with zearalenone standard equivalent to 100 μg/kg added, (a) without derivatization and (b) after post-column derivatization with 0.25 *M* aluminium chloride solution.

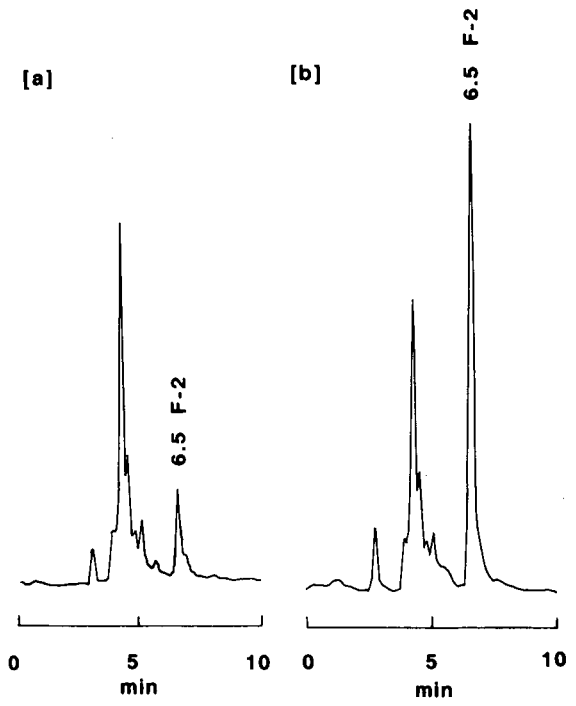

Fig. 5. HPLC of a mycotoxin-free wheat extract with zearalenone standard equivalent to 100 μg/kg added, (a) without derivatization and (b) after post-column derivatization with 0.25 *M* aluminium chloride solution.

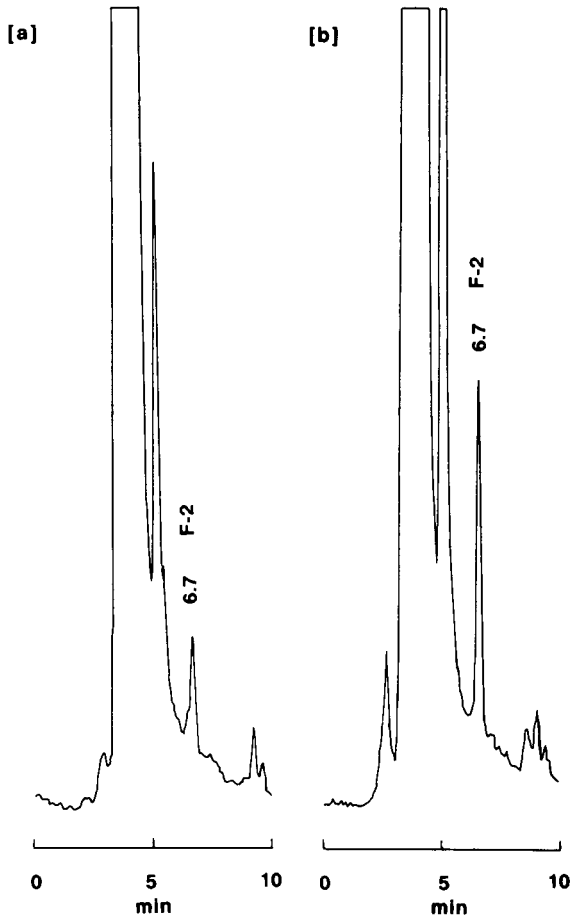

Fig. 6. HPLC of a compound feed extract naturally contaminated with zearalenone at a level of 50 μg/kg, (a) without derivatization and (b) after post-column derivatization with aluminium chloride solution.

eluent at a flow-rate of 1.0 ml/min. Detection of zearalenone and zearalenol was by fluorescence after post-column derivatization. A solution of aluminium chloride hexahydrate was pumped at 0.5 ml/min into the column eluent via a tee-piece as used previously for aflatoxins [13]. The combined column eluate and aluminium chloride solution was passed through a heated PTFE reaction coil held at 50°C in a water-bath and into the cell of the fluorescence detector, with the excitation wavelength set at 285 nm and emission wavelength at 440 nm. The system was flushed out by pumping methanol–water (3:1) to displace the aluminium chloride hexahydrate solution at the end of each working day as a precaution against corrosion and precipitation of aluminium chloride in the HPLC equipment.

Extraction and clean-up of commodity extracts

Extracts for examination were prepared either using a method published by Patterson and Roberts [5] for the multiple screening of a range of mycotoxins or gel permeation chromatography as described previously for aflatoxins [14].

RESULTS AND DISCUSSION

The increase in response for zearalenone and zearalenol obtained by post-column derivatization with aluminium chloride solution was found to be dependent both on the temperature of the reaction coil and on the concentration of aluminium chloride solution used. Fig. 2 shows the post-column fluorescence for zearalenone and zearalenol (25 and 250 ng, respectively) using 0.25 *M* aluminium chloride solution with reaction coil temperatures from 25 to 70°C. The optimum temperature for this reaction occurs between 50 and 60°C for zearalenone, and is slightly lower for zearalenol.

The effect of the concentration of aluminium chloride is shown in Fig. 3. A rapid increase in sensitivity occurred up to *ca.* 0.1 *M* concentration, after which the fluorescence increased linearly but at a slower rate. The maximum response for zearalenone (25 ng) was not reached. However, 0.25 *M* was selected as the working concentration, as a large increase in aluminium chloride concentration would be required for a relatively small further increase in fluorescence. The effect of concentration on the post-column response for zearalenol (250 ng) was similar, although the optimum response was apparently reached at a lower concentration.

Extracts prepared from non-mouldy, mycotoxin-free samples of maize and wheat using gel permeation chromatography [14] were examined with and without the post-column reaction. Figs. 4 and 5 show the chromatograms from these extracts of non-mouldy maize and wheat, respectively, to which zearalenone standard representing a level equivalent to 100 μg/kg in the original sample had been added. The selectivity of the post-column reaction, (a) without derivatization and (b) using 0.25 *M* alumi-

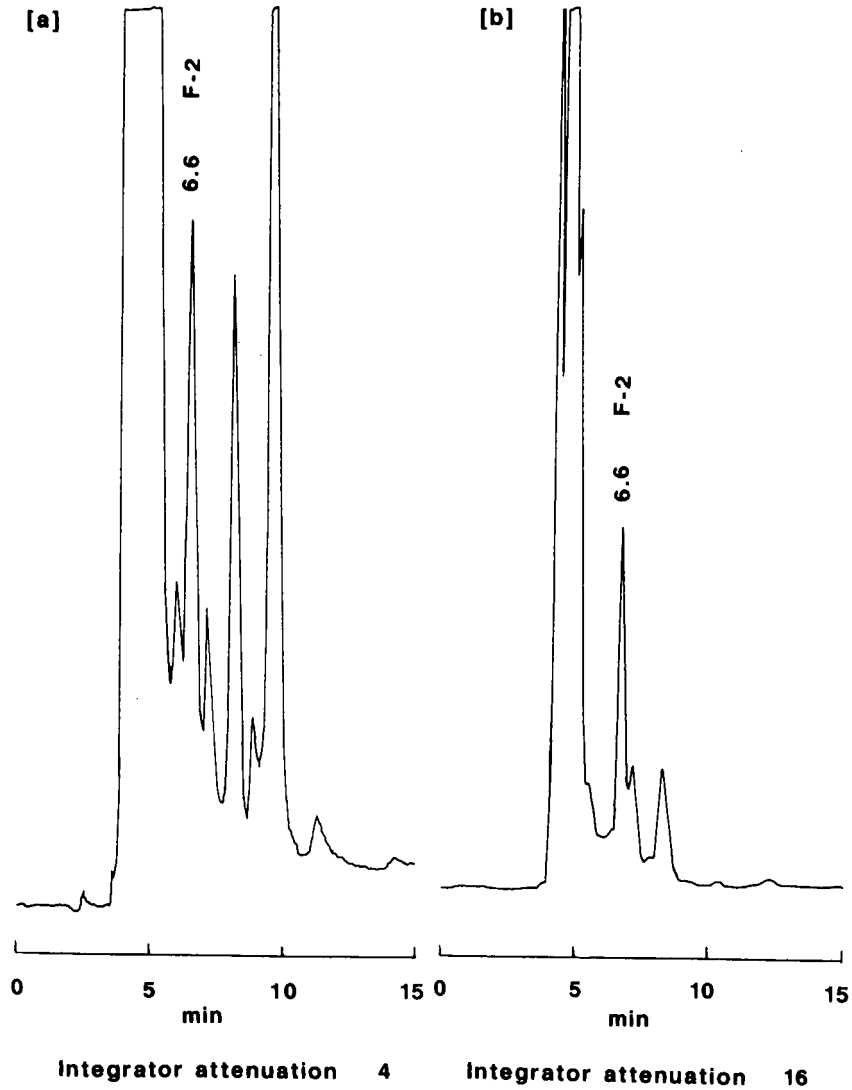

Fig. 7. HPLC of maize gluten extract naturally contaminated with zearalenone at a level of 150 μg/kg, (a) without derivatization and (b) after post-column derivatization with aluminium chloride solution.

nium chloride, is illustrated. Although the peak for zearalenone has increased *ca.* fivefold, the level of background interference from co-extractives is almost unaltered. However, with maize (Fig. 4) and also in the compound feed sample (Fig. 6), the response for a compound eluting about 1 min before zearalenone and close to the retention time of zearalenol is considerably enhanced by derivatization. The identity of this compound is unknown. However, it would potentially interfere with the determination of zearalenol.

A number of samples of cereals and animal feedstuffs were examined for zearalenone after clean-up either by gel permeation chromatography or using the method of Patterson and Roberts [5]. The chromatograms obtained for extracts of an animal feed sample prepared by the latter procedure are shown in Fig. 6. The sample contained *ca.* 50 μg/kg

of zearalenone, and the increase in response for zearalenone relative to the background interference from co-extractives permits a low limit of detection to be achieved and facilitates quantification at this level.

A sample of maize gluten naturally contaminated with zearalenone at a level of *ca.* 150 μg/g was extracted and prepared using gel permeation chromatography [14] and the chromatograms obtained without derivatization and after reaction with aluminium chloride are shown in Fig. 7. The volume of extract injected was the same in each instance but the sensitivity of the detector output was reduced to enable the peak of zearalenone after derivatization (Fig. 7b) to be compared directly. The peak for zearalenone after derivatization was considerably smaller than expected, and it is almost certain that another peak co-eluted with zearalenone, giving an artificially large response when monitored without derivatization as shown in Fig. 7a. After derivatization there is reduced interference at this retention time, and a more accurate response for zearalenone is obtained. The interference from other co-extractives is much reduced relative to the response for zearalenone.

Attempts to elucidate the nature of the chemical reaction involved in derivatization have proved unsuccessful to date. Collection of the zearalenone and zearalenol peaks eluting from the detector after post-column derivatization followed by extraction with chloroform, concentration and TLC resulted in a mixture of spots, including some corresponding to unreacted zearalenone and zearalenol. Aluminium chloride is a powerful Lewis acid and it may form a conjugate with zearalenone and zearalenol under the HPLC derivatization conditions. We have found a similar increase in sensitivity after derivatization with aluminium chloride for the mycotoxin sterigmatocystin.

CONCLUSIONS

The post-column reaction of zearalenone and zearalenol with aluminium chloride under the conditions described leads to an increase in fluorescence response of up to fivefold for these mycotoxins, without significantly affecting the level of background interference from co-extractives from cereal and animal feed samples. The post-column derivatization technique should be applicable to the determination of zearalenone and zearalenol in sample extracts prepared by a range of alternative analytical procedures and represents a significant improvement in limits of detection compared with most currently used procedures.

REFERENCES

1 C. J. Mirocha, C. M. Christensen and G. H. Nelson, in S. Kadis, A. Ceigler and S. S. Ajl (Editors), *Microbial Toxins*, Vol. VII, Academic Press, New York, 1971, p. 107.
2 W. F. O. Marasas, S. J. van Rensburg and C. J. Mirocha, *J. Agric. Food Chem.*, 27 (1979) 1108.
3 C. J. Mirocha, S. V. Pathre, J. C. Behrens and B. Schauerhamer, *Appl. Environ. Microbiol.*, 35 (1978) 986.
4 C. J. Mirocha, B. Schauerhamer and S. V. Pathre, *J. Assoc. Off. Anal. Chem.*, 57 (1974) 1104.
5 D. S. P. Patterson and B. A. Roberts, *J. Assoc. Off. Anal. Chem.*, 62 (1979) 1265.
6 L. Stoloff, S. Nesheim, L. Yin, J. V. Rodricks, M. Stack and A. D. Campbell, *J. Assoc. Off. Anal. Chem.*, 54 (1971) 91.
7 M. Malaiyandi, J. P. Barrette and P. L. Wavrock, *J. Assoc. Off. Anal. Chem.*, 59 (1976) 959.
8 P. M. Scott, T. Panalaks, S. Kanhere and W. F. Miles, *J. Assoc. Off. Anal. Chem.*, 61 (1978) 593.
9 G. M. Ware and C. W. Thorpe, *J. Assoc. Off. Anal. Chem.*, 61 (1978) 1058.
10 M. Malaiyandi and J. P. Barrette, *J. Environ. Sci. Health*, B13 (1978) 381.
11 J. Plasencia, C. J. Mirocha, R. Pawlosky and J. F. Smith, *J. Assoc. Off. Anal. Chem.*, 73 (1990) 973.
12 R. Warner, B. P. Ram, L. P. Hart and J. J. Pestka, *J. Agric. Food Chem.*, 34 (1986) 714.
13 L. G. M. Th. Tuinstra and W. Hasnoot, *J. Chromatogr.*, 282 (1983) 457.
14 M. T. Hetmanski and K. A. Scudamore, *Food Addit. Contam.*, 6 (1989) 35.

Journal of Chromatography, 588 (1991) 53–59
Elsevier Science Publishers B.V., Amsterdam

CHROM. 23 668

Separation of neutral mono- and oligosaccharides derivatized with ethyl *p*-aminobenzoate by high-performance liquid chromatography on an amine-bonded vinyl alcohol copolymer column

Takashi Akiyama*

Laboratory of Serology and Biochemistry, National Research Institute of Police Science, 6 Sanban-cho, Chiyoda-ku, Tokyo 102 (Japan)

(First received May 15th, 1991; revised manuscript received August 2nd, 1991)

ABSTRACT

A number of mono- and oligosaccharides derivatized with an ultraviolet-absorbing compound, ethyl *p*-aminobenzoate, were separated by high-performance liquid chromatography on an Asahipak NH2P-50 amine-bonded vinyl alcohol copolymer column. The derivatized mono- and oligosaccharides were sufficiently separated with isocratic elution and the separation efficiency for the derivatives was better than that for the underivatized counterparts. The column was remarkably stable relative to a conventional amine-bonded silica column and no decrease in the retention of the derivatives due to dissociation of the stationary phase was observed.

INTRODUCTION

High-performance liquid chromatography (HPLC) has been employed to separate oligosaccharides, and amine-bonded silica columns have mostly been used because of its high resolution and short analysis times [1–9]. However, the column has the disadvantage that considerable amounts of amine-bonded phase and silica itself dissociate into the mobile phase, which causes a gradual decrease in retention [10]. An amine-bonded silica column is frequently used with acetonitrile–water mobile phases, oligosaccharides usually being separated without derivatization [11]. Although measurements of refractive index and intrinsic ultraviolet (UV) absorption have been widely used for the detection of underivatized oligosaccharides, the sensitivity of these detection methods is low relative to that for oligosaccharides derivatized with UV-absorbing or fluorescent compounds [12,13].

In this paper, the separation of mono- and oligosaccharides derivatized with a UV-absorbing compound, ethyl *p*-aminobenzoate (EAB), on an Asahipak NH2P-50 stable amine-bonded vinyl alcohol copolymer column is described.

EXPERIMENTAL

Materials

Monosaccharides, dextran (200–300 kilodalton) and ethyl *p*-aminobenzoate (EAB) was purchased from Wako (Osaka, Japan). Malto-, isomalto-, cello- and N-acetylchitooligosaccharides were obtained from Seikagaku Kogyo (Tokyo, Japan). The isomaltooligosaccharide series were also prepared by partial acid hydrolysis of dextran according to the slightly modified method of Yamashita *et al.* [14]: to a Pyrex tube with a PTFE-lined screw-cap containing 0.5 g of dextran were added 5 ml of 0.2

* Present address: Hokkaido National Agricultural Experiment Station, Hitujigakoa, Toyohira-ku, Sapporo 061-01, Japan.

0021-9673/91/$03.50

M HCl, followed by hydrolysis for 3 h at 100°C and the hydrolysate was passed through a Dowex 1-X8 (OH^-) resin column (5 cm × 1 cm I.D.) to remove the acid. N-Acetylchitooligosaccharides were further purified by gel permeation chromatography on a Bio-Gel P-4 (Bio-Rad Labs., Richmond, CA, USA) column (100 cm × 1.5 cm I.D.) equilibrated with water. Sodium cyanoborohydride ($NaBH_3CN$) was purchased from Aldrich (Milwaukee, WI, USA). All other chemicals and solvents were of analytical-reagent or HPLC grade.

High-performance liquid chromatography

The HPLC system consisted of the following components from Waters Assoc (Milford, MA, USA): a multi-solvent delivery system (Model M600), a universal injector (Model U6K), a variable-wavelength detector (Model 450) and a differential refractometer (Model 410), with a computing integrator (Model C-R6A) from Shimadzu (Kyoto, Japan). Separations were done on an Asahipak NH2P-50 column (250 mm × 4.6 mm I.D.) packed with an amine-bonded vinyl alcohol copolymer gel (5 μm) (Asahikasei, Tokyo, Japan), and the column temperature was kept at 25°C if not specified otherwise. The mobile phase was acetonitrile–water. All elutions were done isocratically at a flow-rate of 0.5 ml/min.

Derivatization of mono- and oligosaccharides with EAB

The procedure employed for labelling of mono- and oligosaccharides at their reducing end with EAB was done by the method of Wang *et al.* [15] with slight modification. To a Pyrex tube with a PTFE-lined screw-cap containing 10 μl of 0.3 *M* mono- and oligosaccharides were added 40 μl of 1.4 *M* $NaBH_3CN$ in distilled water, 350 μl of 0.6 *M* EAB in methanol and 40 μl of glacial acetic acid and the mixture was heated at 80°C. After 1 h, the reaction mixture was cooled and 1 ml of distilled water was added. The aqueous phase was extracted with four 1-ml volumes of chloroform to remove excess of EAB and the aqueous phase containing derivatized mono- and oligosaccharides was lyophilized.

RESULTS AND DISCUSSION

Although the main feature of the Asahipak NH2P-50 amine-bonded vinyl alcohol copolymer column appears to be the separation of oligosaccharides by size, as reported for an amine-bonded silica column [11], the column could be employed for the resolution of both underivatized and EAB-derivatized mono- and disaccharides. The HPLC elution profiles of underivatized mono- and disaccharides eluted with acetonitrile–water (65:35) are shown in Fig. 1; it was not possible to separate glucose from N-acetylchitobiose and maltose from cellobiose (Fig. 1A), or arabinose from N-acetylglucosamine

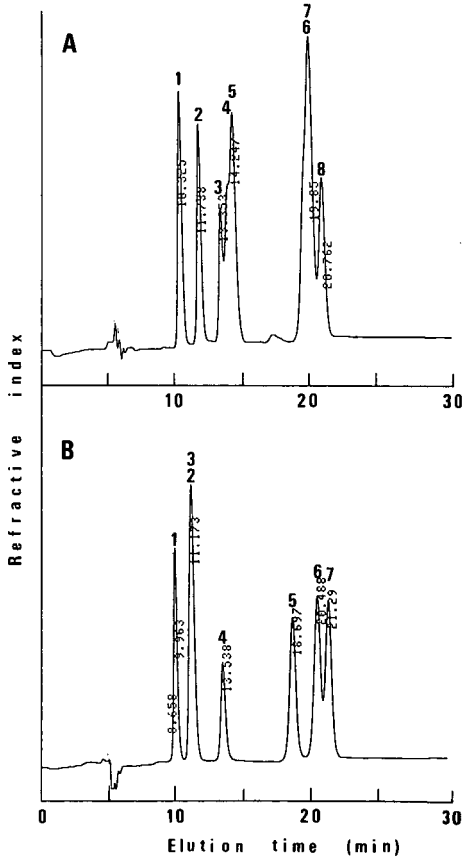

Fig. 1. Elution profiles of underivatized mono- and disaccharides. Peaks: (A) 1 = fucose; 2 = xylose; 3 = mannose; 4 = glucose; 5 = N-acetylchitobiose; 6 = maltose; 7 = cellobiose; 8 = isomaltose; (B) 1 = rhamnose; 2 = arabinose; 3 = N-acetylglucosamine; 4 = galactose; 5 = lactose; 6 = melibiose; 7 = gentiobiose. Column, Asahipak NH2P-50; mobile phase, acetonitrile–water (75:25); flow-rate, 0.5 ml/min.

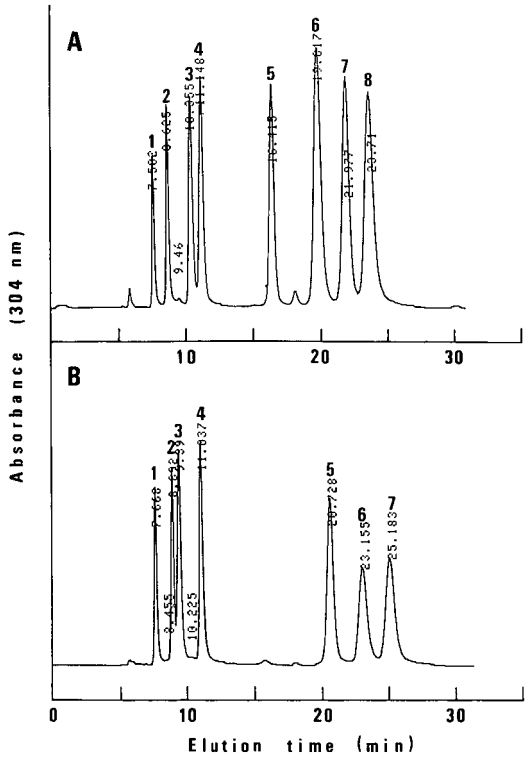

Fig. 2. Elution profiles of mono- and disaccharide EAB derivatives. Peaks: (A) 1 = fucose; 2 = xylose; 3 = mannose; 4 = glucose; 5 = N-acetylchitobiose; 6 = maltose; 7 = cellobiose; 8 = isomaltose derivatives; (B) 1 = rhamnose; 2 = arabinose; 3 = N-acetylglucosamine; 4 = galactose; 5 = lactose; 6 = melibiose; 7 = gentiobiose EAB derivatives. Column, Asahipak NH2P-50; mobile phase, acetonitrile–water (85:15); flow-rate, 0.5 ml/min.

(Fig. 1B). However, much greater resolution was obtained when the corresponding mono- and oligosaccharides were derivatized with EAB and eluted with acetonitrile–water (75:25) (Fig. 2A and B). The major mechanism for the retention of mono- and oligosaccharide EAB derivatives seems to be due to hydrogen bonding between the hydroxyl groups of the sugar residue and the amine group of the stationary phase [7,8]. However, as a substantial improvement in the separation of mono- and disaccharides was obtained by derivatization with EAB, a subtle interaction between the aromatic ring of EAB derivatives and the stationary phase appears to be responsible for the improved resolution.

The retention times of mono- and disaccharide EAB derivatives separated with two mobile phases are summarized in Table I. Monosaccharide EAB derivatives generally exhibited shorter retention times than disaccharide derivatives and were eluted in following 6-deoxyhexose (fucose and rhamnose), pentose (xylose and arabinose), N-acetylhexosamine (N-acetylglucosamine) and hexose (mannose, glucose and galactose) EAB derivatives, and this order was independent of the mobile phase used. As suggested in the HPLC of underivatized monosaccharides [10], the absence of a hydroxyl group at the C-6 position of 6-deoxyhexose EAB and pentose EAB appears to be primarily associated with the shorter retention times of these derivatives. On the other hand, disaccharide EAB derivatives were sufficiently separated with acetonitrile–water (85:15), and large increases in the retention times and peak widths were observed when the derivatives were eluted with acetonitrile–water (90:10).

The HPLC elution profiles of the isomalto-, malto- and cellooligosaccharide EAB series, which have a common constituent sugar (glucose) and different linkage types, are shown in Fig. 3. The isomaltooligosaccharide EAB series, which have an α-1–6-linkage (Fig. 3A) showed longer retention times than the maltooligosaccharide EAB series, which have an α-1–4-linkage (Fig. 3B), suggesting that the presence of an α-1–6-linkage in the structures seems to be correlated with the increase in the retention times, as reported for underivatized oligosaccharides [10]. In contrast, only minimal differences in the retention times were observed between the malto- and cellooligosaccharide EAB series (β-1–4-linkage), indicating that an anomeric configuration of the linkage is not likely to be responsible for changes in retention (Fig. 3C).

The HPLC elution profiles of the cello- and N-acetylchitooligosaccharide EAB series, which have a common β-1–4-linkage and different constituent sugars, glucose and N-acetylglucosamine, are shown in Fig. 4. The N-acetylchitooligosaccharide EAB series (Fig. 4B) exhibited considerably shorter retention times than the cellooligosaccharide EAB series (Fig. 4A). As the replacement of a hydroxyl group at the C-2 position with an acetoamide group is only the difference between the two oligosaccharide EAB series, the structural difference could be correlated with shift in the retention times, as indicated by Mellis and Baenziger [16].

Fig. 5 shows the HPLC elution profiles of mono-

TABLE I

RETENTION TIMES OF MONO- AND DISACCHARIDE EAB DERIVATIVES

EAB derivative	Structure	Retention time (min)	
		Acetonitrile–water (85:15)	Acetonitrile–water (90:10)
Monosaccharides			
Fucose	Fuc	7.6	10.3
Rhamnose	Rha	7.7	10.5
Xylose	Xyl	8.6	12.8
Arabinose	Ara	8.9	12.6
Mannose	Man	10.4	18.6
Galactose	Gal	11.6	20.9
Glucose	Glc	11.1	21.3
N-Acetylglucosamine	GlcNAc	9.4	16.4
Disaccharides			
Lactose	Galβ-1–4Glc	20.7	57.3
Melibiose	Galα-1–6Glc	23.2	63.3
Gentiobiose	Glcβ-1–6Glc	25.1	75.0
Cellobiose	Glcβ-1–4Glc	22.0	61.9
Maltose	Glcα-1–4Glc	19.8	50.0
Isomaltose	Glcα-1–4Glc	19.8	50.0
Isomaltose	Glcα-1–6Glc	23.7	69.2
N,N′-Diacetylchitobiose	GlcNAcβ-1–4GlcNAc	16.4	36.6

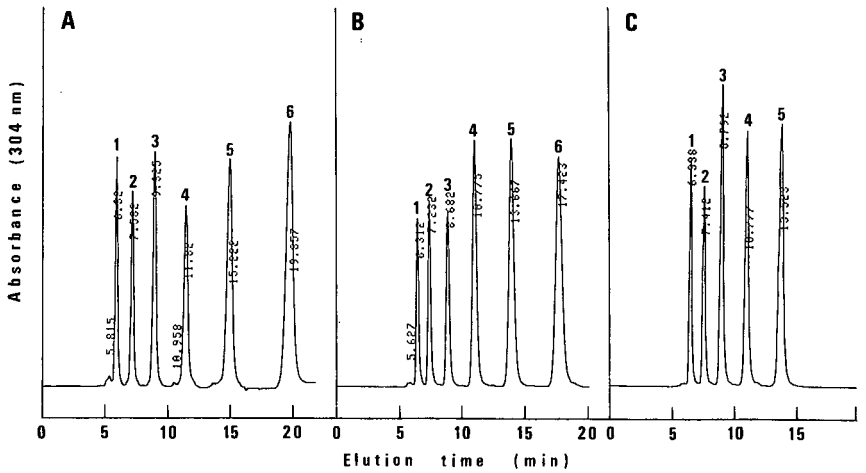

Fig. 3. Effect of linkage type on separation of oligosaccharide EAB series. (A) Isomaltooligosaccharide EAB series (Glcα-1–6Glc); (B) maltooligosaccharide EAB series (Glcα-1–4Glc); (C) cellooligosaccharide EAB series (Glcβ-1–4Glc). The number above each peak indicates the number of sugar residues present. Column, Asahipak NH2P-50; mobile phase, acetonitrile–water (70:30); flow-rate, 0.5 ml/min.

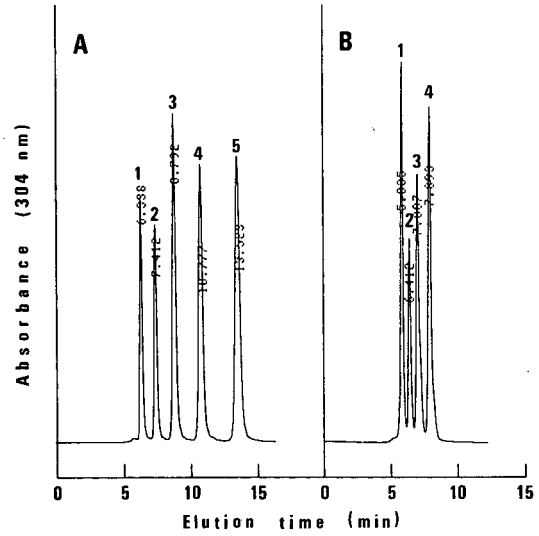

Fig. 4. Effect of constituent sugars on separation of oligosaccharide EAB series. (A) Cellooligosaccharide EAB series (Glcβ-1–4Glc); (B) N-acetylchitooligosaccharide EAB series (GlcNAcβ-1–4GlcNAc). The number above each peak indicates the number of sugar residues present. Column, Asahipak NH2P-50; mobile phase, acetonitrile–water (70:30); flow-rate, 0.5 ml/min.

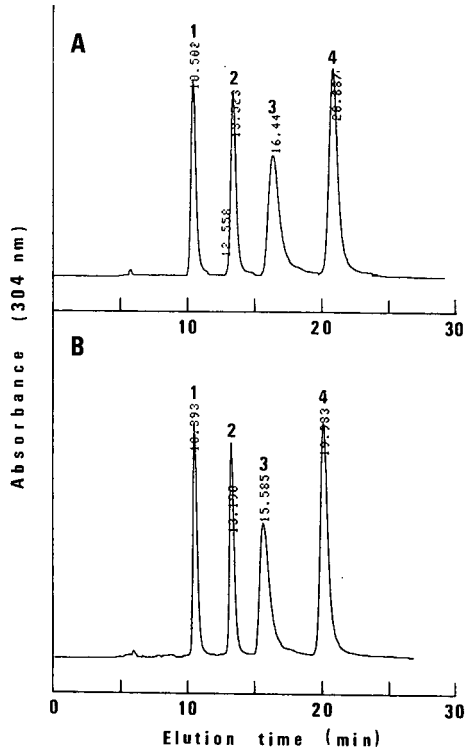

Fig. 5. Effect of temperature on separation of monosaccharide EAB derivatives: (A) 25°C; (B) 45°C. Peaks: 1 = rhamnose; 2 = arabinose; 3 = N-acetylglucosamine; 4 = galactose EAB derivatives. Column, Asahipak NH2P-50; mobile phase, acetonitrile–water (90:10); flow-rate, 0.5 ml/min.

saccharide EAB derivatives separated at different column temperatures. Although variations in the column temperature led to the different elution profiles in the HPLC of underivatized oligosaccharides [9,17], only slight differences in the elution profiles and the retention times of monosaccharide EAB derivatives were observed when operating temperature was increased from 25 to 45°C (Fig. 5A and B).

The HPLC profiles of underivatized and EAB-derivatized isomaltooligosaccharide series derived from dextran by partial acid hydrolysis are compared in Fig. 6. The underivatized isomaltooligosaccharide series having up to nine sugar residues were separated as single peaks with acetonitrile–water (65:35) in less than 50 min (Fig. 6A). Although a similar separation of the underivatized isomaltooligosaccharide series was achieved by HPLC on a C_{18}-bonded vinyl alcohol copolymer column, alkaline eluents were necessary to circumvent an undesirable separation of α- and β-anomeric peaks [18]. On the other hand, isomaltooligosaccharide EAB derivatives possessing up to thirteen or more sugar residues were well resolved with acetonitrile–water (65:35) (Fig. 6B). Isomaltooligosaccharides that was derivatized with EAB showed longer retention times than underivatized oligosaccharides in size fractionation on a Bio-Gel P-4 column [19], whereas isomaltooligosaccharide EAB derivatives showed lower retention times than the underivatized counterparts in HPLC on an Asahipak NH2P-50 column. The decrease in the retention times of the derivatives appears to be due to the interaction between the aromatic ring of EAB derivatives and the stationary phase.

Fig. 7 shows the dependence of the retention times of isomaltooligosaccharide EAB derivatives on the acetonitrile concentration in the mobile phase. At the highest acetonitrile concentration examined (70%), isomaltooligosaccharide EAB derivatives having nine sugar residues were well resolved in 50 min (Fig. 7A), whereas the derivatives with thirteen or more sugar residues were separated at a

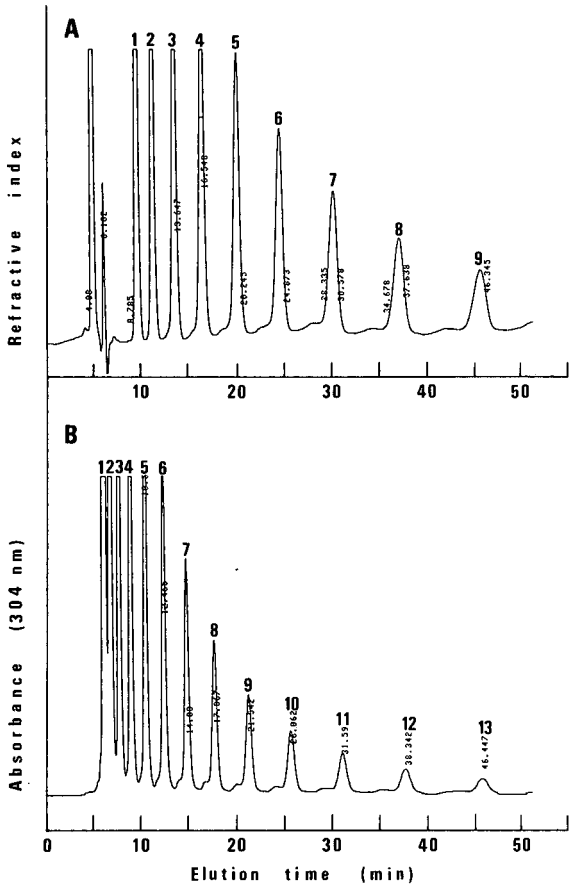

Fig. 6. Elution profiles of underivatized and EAB-derivatized isomaltooligosaccharide series, (A) before derivatization and (B) after derivatization with EAB. The number above each peak indicates the number of sugar residues present. Column, Asahipak NH2P-50; mobile phase, acetonitrile–water (65:35); flow-rate, 0.5 ml/min.

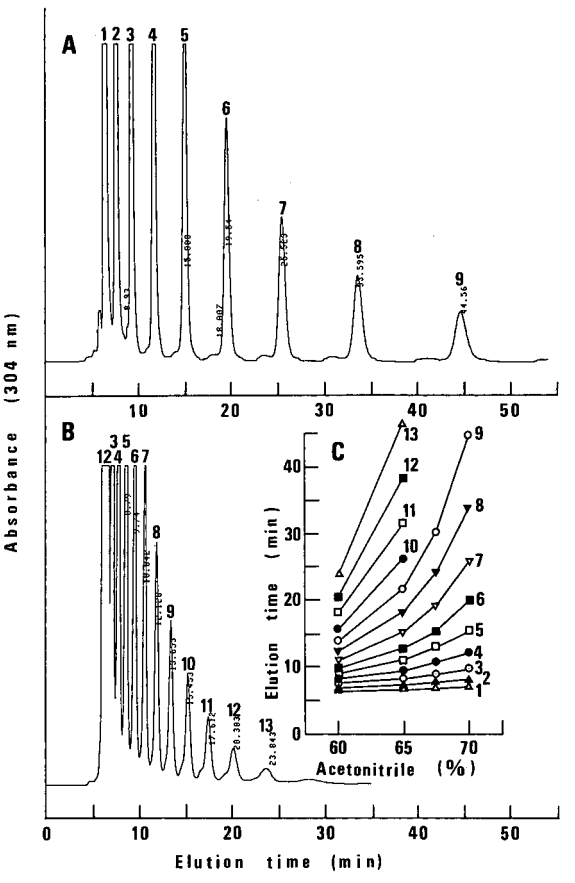

Fig. 7. Effect of acetonitrile concentration in the mobile phase on retention times of isomaltooligosaccharide EAB series, (A) 70% and (B) 60%, and (C) relationship between acetonitrile concentration and retention times of the derivatives. The numbers indicate the number of sugar residues present. Column, Asahipak NH2P-50; flow-rate, 0.5 ml/min.

60% acetonitrile concentration in 25 min (Fig. 7B). Further, the relationship between the retention times of the derivatives and acetonitrile concentration in the mobile phase is summarized in Fig. 7C; increasing concentrations of acetonitrile resulted in a regular increase in the retention times of the derivatives, and the increase in retention approximated to an exponential increase in the range of 60–70% acetonitrile.

In conclusion, mono- and oligosaccharides derivatized with EAB were well resolved with a simple isocratic method. Further, the resolution of the underivatized mono- and oligosaccharides was greatly improved by derivatization with EAB. The column was clearly stable in comparison with conventional amine-bonded silica columns, and no decrease in the retention times of the derivatives was observed during the course of this study. The stable Asahipack NH2P-50 column could be useful for the preparation not only of mono- and oligosaccharide EAB derivatives, but also of their underivatized counterparts, free from dissociation products.

REFERENCES

1 J. C. Linden and C. L. Lawhead, *J. Chromatogr.*, 105 (1975) 125.
2 R. B. Meagher S.J. and A. Furst, *J. Chromatogr.*, 117 (1976) 211.
3 R. Schwarzenbach, *J. Chromatogr.*, 140 (1977) 304.
4 A. D. Jones, I. W. Burns, S. G. Selling and J. A. Cox, *J. Chromatogr.*, 144 (1977) 169.
5 L. W. Doner, *Carbohydr. Res.*, 70 (1979) 209.
6 J. Wong-Chong and F. A. Martin, *J. Agric. Food Chem.*, 27 (1979) 927.
7 H. Binder, *J. Chromatogr.*, 189 (1980) 414.
8 M. D'Amboise, D. Noel and T. Hanai, *Carbohydr. Res.*, 79 (1980) 1.
9 V. Kahle and K. Tesarik, *J. Chromatogr.*, 191 (1980) 721.
10 W. M. Blanken, M. L. E. Bergh, P. L. Koppen and D. H. van Den Eijnden, *Anal. Biochem.*, 145 (1985) 322.
11 L. A. Verhaar and B. F. M. Kuster, *J. Chromatogr.*, 234 (1982) 57.
12 P. F. Daniel, *Methods Enzymol.*, 138 (1987) 94.
13 S. Hase, T. Ibuki and T. Ikenaka, *J. Biochem.*, 95 (1984) 197.
14 K. Yamashita, T. Mizouchi and A. Kobata, *Methods Enzymol.*, 83 (1882) 105.
15 W. T. Wang, N. C. Ledonne, Jr., B. Ackerman and C. C. Sweeley, *Anal. Biochem.*, 141 (1984) 366.
16 S. J. Mellis and J. U. Baenziger, *Anal. Biochem.*, 114 (1981) 276.
17 K. Koizumi, T. Utamura, Y. Kubota and S. Hizuki, *J. Chromatogr.*, 409 (1987) 396.
18 K. Koizumi and T. Utamura, *J. Chromatogr.*, 436 (1988) 328.
19 F. Matsuura and A. Imaoka, *Glycoconjugate J.*, 5 (1988) 13.

Journal of Chromatography, 588 (1991) 61–71
Elsevier Science Publishers B.V., Amsterdam

CHROM. 23 650

Precolumn fluorescence tagging reagent for carboxylic acids in high-performance liquid chromatography: 4-substituted-7-aminoalkylamino-2,1,3-benzoxadiazoles

Toshimasa Toyo'oka*, Mumio Ishibashi and Yasushi Takeda

Division of Drugs, National Institute of Hygienic Sciences, 1–18–1 Kamiyoga, Setagaya-ku, Tokyo 158 (Japan)

Kenichiro Nakashima and Shuzo Akiyama

Faculty of Pharmaceutical Sciences, Nagasaki University, 1–14 Bunkyo-Machi, Nagasaki 852 (Japan)

Sonoko Uzu and Kazuhiro Imai

Branch Hospital Pharmacy, University of Tokyo, 3–28–6 Mejirodai, Bunkyo-ku, Tokyo 112 (Japan)

(First received May 6th, 1991; revised manuscript received July 23rd, 1991)

ABSTRACT

Four new 2,1,3-benzoxadiazole amine reagents having different functional groups at the 4- and 7-positions, [4-nitro-7-N-piperazino-2,1,3-benzoxadiazole (NBD-PZ), 4-(N,N-dimethylaminosulphonyl)-7-N-piperazino-2,1,3-benzoxadiazole (DBD-PZ), 4-(N,N-dimethylaminosulphonyl)-7-N-cadaverino-2,1,3-benzoxadiazole (DBD-CD) and ammonium 7-N-piperazino-2,1,3-benzoxadiazole-4-sulphonate (SBD-PZ)] were synthesized as fluorogenic tagging reagents for carboxylic acids in high-performance liquid chromatography. The reagents, except SBD-PZ, reacted with carboxylic acid at room temperature in the presence of activation agents to produce fluorescent adducts. The maximum wavelengths of arachidic acid tagged with DBD-PZ, DBD-CD and NBD-PZ were 569 nm (excitation, 440 nm), 561 nm (excitation, 437 nm) and 541 nm (excitation, 470 nm), respectively. Among various activation agents tested [diethyl phosphorocyanidate (DEPC), diphenyl phosphoroyl azide (DPPA), 1-ethyl-3-(3-dimethylaminopropyl)carbodiimide (EDC)–pyridine, 2,2′-dipyridyl disulphide–triphenylphosphine (Mukaiyama A) and 2-chloro-1-methylpyridinium iodide–triethylamine (Mukaiyama B)], DEPC and Mukaiyama A were more effective than the others. When the piperazino reagents (DBD-PZ and NBD-PZ) were used as the tagging reagents, the derivatization reaction in the presence of Mukaiyama A was faster than that in the presence of DEPC. Although the reaction in the presence of Mukaiyama A was completed after 30 min, an unknown peak derived from the activation agent appeared on the chromatograms. The fluorescence peak intensities were compared in the presence of DEPC. The order of the fluorescence peak areas obtained after reaction for 6 h in the presence of DEPC was DBD-PZ > DBD-CD > NBD-PZ. Thirteen saturated free fatty acids (FFAs) derivatized with DBD-PZ (or DBD-CD) and DEPC (or Mukaiyama A) in acetonitrile were separated completely by linear gradient elution on a reversed-phase ODS column. Eight drugs (ibuprofen, indomethacin, dinoprost, prostaglandin E_1, dehydrocholic acid, ursodesoxycholic acid, hydrocartisone succinate and prednisolone succinate) were also tagged with DBD-PZ in the presence of DEPC and separated by isocratic elution. The detection limits (signal-to-noise ratio = 3) of FFAs tagged with DBD-PZ were in the range 3.2–4.7 fmol, whereas those of drugs were in the range 3.9–14 fmol.

INTRODUCTION

The sensitive detection of biologically active compounds with carboxylic acid groups such as fatty acids, prostaglandins and bile acid is difficult absorptiometrically owing to the weak UV and visible absorption. For the trace analysis of these compounds, fluorescence tagging followed by fluorimetric detection of the adducts is one of the plausible methods [1,2]. Various fluorescence tagging re-

0021-9673/91/$03.50

agents have been developed for the determination of carboxylic acids [3–17], but many of these have some disadvantages. Coumarin-type derivatives, such as 4-bromomethyl-7-methoxycoumarin (Br-Mmc) [3–5] and 4-bromomethyl-7-acetoxycoumarin (Br-Mac) [6,7], which are popular as fluorescence tagging reagents for carboxylic acids, are unstable to moisture, and aqueous reaction media should therefore be avoided in the derivatization step. Moreover, the reagents require a base catalyst such as K_2CO_3 for accelerating the reaction. Therefore, the derivatization reaction is usually carried out in aprotic solvents such as acetone at 50–60°C in the presence of a crown ether as a phase-transfer catalyst, which also increases the solubility of the base catalyst K_2CO_3 or $KHCO_3$. This derivatization procedure is complicated and the reaction is sometimes unsuccessful. Diazomethane-type reagents such as 9-anthryldiazomethane (ADAM) [12,13] and 1-pyrenyldiazomethane (PDAM) [14], on the other hand, are unstable in reaction solvents such as acetonitrile and methanol. In contrast, dansyl semipiperazide (DNS-PZ) [15] and monodansyl cadaverine (MDC) [16], aliphatic amine-type reagents, are suitable for carboxylic acid analysis owing to their excellent stability and selectivity toward the carboxylic acid moiety and the sensitivity of the adducts.

In a previous study [18], 4-(aminosulphonyl)-7-N-piperazino-2,1,3-benzoxadiazole (ABD-PZ), 4-(aminosulphonyl)-7-N-cadaverino-2,1,3-benzoxadiazole (ABD-CD) and 4-(aminosulphonyl-7-N-ethylenediamino-2,1,3-benzoxadiazole (ABD-ED) were synthesized and applied as precolumn tagging reagents to fatty acids in high-performance liquid chromatography (HPLC). The adducts of fatty acids with these reagents exhibited longer excitation (λ_{ex} 430–440 nm) and emission maxima (λ_{em} 570–580 nm) than those with other reagents (*e.g.*, Br-Mmc, λ_{ex} 360 nm and λ_{em} 410 nm; Br-Mac λ_{ex} 365 nm and λ_{em} 460 nm; MDC, λ_{ex} 340 nm and λ_{em} 518 nm; DNS-PZ, λ_{ex} 350 nm and λ_{em} 530 nm). The fluorescence characteristics of the adducts might be advantageous for the determination of carboxylic acids, as the other compounds having intrinsic fluorescence would not interfere.

This paper described further syntheses of similar new fluorogenic tagging reagents having a benzofurazan (2,1,3-benzoxadiazole) structure. Their reactivity toward fatty acids in the presence of various activation agents, the fluorescence properties and HPLC separation of the adducts with fatty acids and some drugs containing a COOH moiety in their structure were investigated. The effect of functional groups at the 4- and 7-positions in 2,1,3-benzoxadiazole reagents on the derivatization reaction and fluorescence properties of the adducts are also discussed.

EXPERIMENTAL

Materials and reagents

ABD-PZ and ABD-CD were synthesized as described previously [18]. Ammonium 7-fluoro-2,1,3-benzoxazole-4-sulphonate (SBD-F) [19], 4-(aminosulphonyl)-7-fluoro-2,1,3-benzoxadiazole (ABD-F) [20] and 4-fluoro-7-nitro-2,1,3-benzoxadiazole (NBD-F) [21] were purchased from Wako (Osaka, Japan). 4-(N,N-Dimethylaminosulphonyl)-7-fluoro-2,1,3-benzoxadiazole (DBD-F) [22,23] was obtained from Tokyo Kasei (Tokyo, Japan). Four saturated free fatty acids [myristic acid ($C_{14:0}$), palmitic acid ($C_{16:0}$), stearic acid ($C_{18:0}$) and arachidic acid ($C_{20:0}$)] were obtained from Wako, lauric acid ($C_{12:0}$), margaric acid ($C_{17:0}$), behenic acid ($C_{22:0}$) and lignoceric acid ($C_{24:0}$) from Tokyo Kasei and tridecanoic acid ($C_{13:0}$), *n*-pentadecanoic acid ($C_{15:0}$), nonadecanoic acid ($C_{19:0}$), heneicosanoic acid ($C_{21:0}$) and tricosanoic acid ($C_{23:0}$) from Nacalai Tesque (Kyoto, Japan). Dinoprost (prostaglandin $F_{2\alpha}$), ibuprofen, indomethacin and ursodesoxycholic acid were donated by Mochida Pharmaceutical (Tokyo, Japan), Kyowa Hakko Kogyo (Tokyo, Japan), Sumitomo Pharmaceuticals (Tokyo, Japan) and Tokyo Tanabe Seiyaku (Tokyo, Japan), respectively. Prostaglandin E_1 (Sigma, St. Louis, MO, USA), cadaverine (Sigma), piperazine (Wako), triphenylphosphine (Wako), dehydrocholic acid (Wako), diethyl phosphorocyanidate (DEPC) (Wako), diphenyl phosphoroyl azide (DPPA) (Tokyo Kasei), 2,2′-dipyridyl disulphide (Tokyo Kasei), 2-chloro-1-methylpyridinium iodide (Tokyo Kasei) and 1-ethyl-3-(3-dimethylaminopropyl)carbodiimide hydrochloride (EDC) for peptide synthesis (Nacalai Tesque) were used as received. Hydrocortisone succinate and prednisolone succinate were of biochemical-reagent grade (Wako). Acetonitrile and water were of HPLC

grade (Wako). All other chemicals were of analytical-reagent grade and were used as received.

Apparatus

Proton nuclear magnetic resonance (^{1}H NMR) spectra were recorded on a Varian (Palo Alto, CA, USA) Jemini-300 spectrometer at 300 MHz using tetramethylsilane as internal standard. For describing NMR characteristics, the following abbreviations are used: s = singlet, d = doublet, q = quartet and m = multiplet. For measurement of excitation and emission spectra, a Hitachi (Tokyo, Japan) Model 650-60 fluorescence spectrometer with a 1-cm quartz cell was employed without spectral correction. Melting points were measured with a Yanagimoto (Tokyo, Japan) micro melting point apparatus.

The high-performance liquid chromatograph consisted of two Model LC-9A pumps (Shimadzu, Kyoto, Japan) and an SCL-6B system controller (Shimadzu). All samples were injected using an SIL-6B autoinjector (Shimadzu). The analytical column was 5-μm Inertsil ODS-2 (150 × 4.6 mm I.D.) (GL Sciences, Tokyo, Japan). The column was maintained at 40°C with a Model 655A-52 column oven (Hitachi). A Shimadzu RF-550 fluorescence monitor equipped with a 12-μl flow cell was employed for the detection of the eluate from the column. The peak areas obtained from the fluorescence monitor were calculated with a C-R4A chromatopac (Shimadzu). All mobile phases were degassed with an on-line degasser (DGU-3A, Shimadzu). The flow-rate of the eluent was 1.0 ml/min.

Syntheses of DBD-PZ, DBD-CD, NBD-PZ and SBD-PZ

DBD-F (123 mg, 0.5 mmol) in 20 ml of acetonitrile was added dropwise to a stirred solution of piperazine (129 mg, 1.5 mmol) or cadaverine (153 mg, 1.5 mmol) in 20 ml of acetonitrile at room temperature (20–30°C). After stirring for 30 min at room temperature, acetonitrile in the reaction mixture was evaporated under reduced pressure. The residue was dissolved in 5% hydrochloric acid (50 ml) and extracted with 3 × 50 ml of ethyl acetate. The ethyl acetate solution was discarded and the pH of the aqueous solution including DBD-amine derivative (DBD-PZ or DBD-CD) was adjusted to 13–14 with 5% NaOH solution. Then 50 ml of ethyl acetate were added to the alkaline solution to extract DBD-amine derivative. The same extraction procedure was repeated five times. The combined ethyl acetate extracts were washed with 20 ml of water, dried over anhydrous sodium sulphate and evaporated *in vacuo*.

DBD-PZ: orange crystals; m.p. 121–122°C; yield 60%; NMR (ppm) in C^2HCl_3, 7.89 (1H, d, *J*ab = 8.15 Hz, a), 6.33 (1H, d, *J*ab = 8.15 Hz, b), 3.89 (4H, m, c), 3.15 (4H, m, d), 2.89 (6H, s, e); Analysis, calculated for $C_{12}H_{17}N_5O_3S$, C 46.29, H 5.50, N 22.49; found, C 46.34, H 5.49, N 22,17%.

DBD-CD: orange crystals; m.p. 100–101°C; yield 30%; NMR (ppm) in C^2HCl_3, 7.90 (1H, d, *J*ab = 8.01, a), 6.12 (1H, d, *J*ab = 8.01, b), 3.41 (2H, q, c), 2.87 (6H, s, h), 2.79 (2H, m, g), 1.81 (2H, m, d), 1.56 (4H, m, e + f); analysis, calculated for $C_{13}N_{21}N_5O_3S$, C 47.69, H 6.46, N 21.39; found, C 47.24, H 6.39, N 21.51%

NBD-F (92 mg, 0.5 mmol) in 20 ml of acetonitrile and piperazine (129 mg, 1.5 mmol) in 20 ml of acetonitrile were reacted and treated as in the same manner for DBD-F and piperazine.

NBD-PZ: dark red crystals; m.p. 230–231°C; yield 62% NMR (ppm) in [$^2H_6$] dimethyl sulphoxide ([$^2H_6$]DMSO) 8.46 (1H, d, *J*ab = 9.23Hz, a), 6.65 (1H, d, *J*ab = 9.23Hz, b), 4.09 (4H, m, c), 2.93 (4H, m, d); analysis, calculated for $C_{10}H_{11}N_5O_3$, C 48.19, H 4.45, N 28.10; found, C 48.13, H 4.42, N 27.84%.

SBD-F (118 mg, 0.5 mmol) in 40 ml of ethanol and piperazine (215 mg, 2.5 mmol) in 20 ml of ethanol were reacted for 24 h at room temperature. Ethanol in the reaction mixture was evaporated under reduced pressure. The residue was dissolved in 20 ml of water and some impurities were extracted with 50 ml of ethyl acetate. The same extraction procedure was repeated twice. The ethyl acetate extract was discarded and the aqueous solution was evaporated *in vacuo* with heating at 50–60°C. The residue including crude SBD-PZ was chromatographed on a Bio-Gel P-2 (200–400 mesh) column (60 cm × 1.5 cm I.D.) (Bio-Rad Labs, Richmond, CA, USA) with water as eluent. The fluorescent fractions corresponding to SBD-PZ were collected, evaporated and crystallized.

SBD-PZ: orange crystals; m.p. >290°C (unknown); yield 20%; NMR (ppm) in [$^2H_6$] DMSO, 7.61 (1H, d, *J*ab = 7.65Hz, a), 6.65 (1H, d,

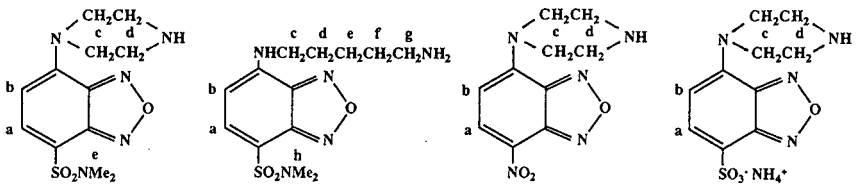

*J*ab = 7.65Hz, b), 3.75 (4H, m,c), 3.26 (4H, m, d); Analysis calculated for $C_{10}H_{15}N_5O_4S$, C 39.86, H 5.02, N 23.24; found, C 39.85, H 4.68, N 22.87%.

Spectral measurements of NBD-PZ, DBD-PZ, DBD-CD and SBD-PZ and their adducts

Excitation and emission spectra of 1 μM of each reagent (NBD-PZ, DBD-PZ, DBD-CD or SBD-PZ) in acetonitrile–water (9:1) were measured by a manual method. The fluorescence intensities of the reagents were determined at maximum excitation and emission wavelengths.

DEPC (70 mM) was added to 0.4 ml of dimethylformamide (DMF) solution containing the reagent (5 mM each) and arachidic acid (0.5 mM). After reaction at room temperature for 2 h, 5 μl of the solution were injected into the HPLC column. The peak corresponding to the adduct separated from those of the reagent and DEPC was collected in 2 ml for spectral measurement.

Time course for the derivatization reaction in the presence of DEPC

DEPC (70 mM) was mixed with 0.4 ml of DMF or acetonitrile containing the reagent (5 mM each of NBD-PZ, DBD-PZ, DBD-CD) and arachidic acid (50 μM) in a brown-glass vial. The vials were capped tightly and allowed to stand for 585 min at room temperature in the dark. At the fixed time intervals, an aliquot of the solution was automatically injected onto the column for HPLC and the fluorescence peak area corresponding to the adduct was calculated with an integrator.

Comparison of activation agents for the derivatization reaction

DBD-PZ (5 mM) was reacted with arachidic acid (50 μM) in 0.4 ml of DMF or acetonitrile at room temperature in the presence of each activation agent [DEPC (70 mM), DPPA (70 mM), EDC (35 mM) and pyridine (20 μl), 2,2'-dipyridyl disulphide (35 mM) and triphenylphosphine (35 mM) (designated Mukaiyama A) or 2-chloro-1-methylpyridinium iodide (35 mM) and triethylamine (20 μl) (designated Mukaiyama B)] in the same solvent (acetonitrile or DMF). After reaction for 6 h, an aliquot of the solution was injected onto the column and the fluorescent peaks corresponding to the adduct were compared with each other.

Effect of reaction solvent and concentration of activation agent on derivatization

Arachidic acid (50 μM) activated with DEPC (70 mM) or Mukaiyama A (10 mM) was reacted with DBD-PZ (5 mM) in acetonitrile, DMF or ethanol. Arachidic acid (50 μM) in acetontrile was also reacted with DBD-PZ (5 mM) in the presence of DEPC or Mukaiyama A at three different concentrations. The reaction solutions were allowed to stand for 585 min at room temperature in the dark. At fixed time interval, an aliquot of the solution was injected onto the HPLC column.

HPLC separation of fatty acids or drugs tagged with DBD-amines (DBD-PZ or DBD-CD)

To a 1-ml brown-glass vial was added 0.2 ml of DBD-amine (10 mM each of DBD-PZ of DBD-CD) in DMF or acetonitrile and 0.2 ml of mixed fatty acids (10 μM of each) in DMF containing DEPC (140 mM) or Mukaiyama A (70 mM). The reaction solution in the vial was allowed to stand for 6 h at room temperature. After reaction for 6 h at room temperature, 1 μl of the reaction solution was injected into the column. Linear gradient elution from 70% to 98% acetonitrile over 60 min and then isocratic elution with 98% acetonitrile for 20 min were adopted for the separation of fatty acids labelled with DBD-amines. The eluate was monitored at 569 nm (excitation at 440 nm) for the adducts with DBD-PZ and at 561 nm (excitation at 437 nm) for the adducts with DBD-CD.

Eight drugs (5 μM each of ibuprofen, indometha-

cin, dehydrocholic acid, ursodesoxycholic acid, hydrocortisone succinate, prednisolone succinate, dinoprost and prostaglandin E_1) and DBD-PZ (5 m*M*) in 0.4 ml of acetonitrile were reacted in the presence of DEPC (70 m*M*). After reaction for 6 h at room temperature, 1 μl of the solution was injected onto the HPLC column. The isocratic elution conditions were 65% acetonitrile for the adducts of ibuprofen and indomethacin, 50% acetonitrile for dehydrocholic acid and ursodesoxycholic acid and 45% acetonitrile for prednisolone succinate, hydrocortisone succinate, dinoprost and prostaglandin E_1.

RESULTS AND DISCUSSION

Fluoresence characteristics of 2,1,3-benzoxadiazole amine reagents and their adducts

To obtain the effective detection wavelengths of the adducts with carboxylic acid compounds, the fluorescence excitation and emission spectra of the reagents and their adducts with arachidic acid (Ar) were measured in acetonitrile–water (9:1) by a manual method. As shown in Table I, the excitation maxima of the adducts (DBD-PZ–Ar and DBD-CD–Ar) with arachidic acid were shifted towards the red compared with the reagents themselves, the shifts being 19 and 7 nm, respectively. Red shifts of the emission maxima were also observed in the solution of DBD-PZ–Ar (14 nm). Similar shifts were observed in the adducts of arachidic acid with ABD-PZ and ABD-CD [18]. In contrast, no shifts of the excitation and emission maxima were observed in the solution of NBD-PZ–Ar (Table I). On the other hand, no fluorescent product was obtained from the derivatization of arachidic acid with SBD-PZ.

The relative fluorescence intensities of the reagents themselves were also determined in the same medium. As indicated in Table I, the intensities of cadaverino reagents were higher than those of the corresponding piperazino reagents judging from the comparison between DBD-CD and DBD-PZ. Further, a dimethylaminosulphonyl group at the 4-position exhibits about a threefold higher fluorescence intensity than a nitro group [DBD-PZ (59.6) *versus* NBD-PZ (19.0)] and an aminosulphonyl group [DBD-CD (100) *versus* ABD-CD (32.6) and DBD-PZ (59.6) *versus* ABD-PZ (17.0)]. The fluorescence intensity of SBD-PZ was the weakest among all the reagents. Therefore, its is obvious that both the fluorescence wavelengths and the fluorescence intensity depend on the functional groups at the 4- and 7-positions in the 2,1,3-benzoxadiazole structure.

The shift of the fluorescence wavelengths between the reagent (DBD amine) and its adduct might be preferable for the determination of carboxylic acids, because the effect of the reagent would be less in the detection of the adducts.

Derivatization reaction with 2,1,3-benzoxadiazole amine reagents in the presence of activation agents

The 2,1,3-benzoxadiazole amine reagents essentially require the activation of carboxylic acids before the derivatization with the reagents. Various activation agents have been developed for the purpose of peptide syntheses. Some of them, *e.g.*, DEPC [24] and EDC [25], are miscible with solvents such acetonitrile, ethanol and DMF. As water-miscible solvents are suitable as a reaction medium for the determination of carboxylic acids in biological samples, the following five activation agents were selected in this work: DEPC [24], DPPA [26], EDC [25], Mukaiyama A (2,2′-dipyridyl disulphide and

TABLE I

MAXIMAL WAVELENGTHS OF SYNTHESIZED REAGENTS AND THEIR ADDUCTS WITH ARACHIDIC ACID

Reagent	λ_{max}		Relative fluorescence intensity	Adduct	λ_{max}	
	ex.	em.			ex.	em.
NBD-PZ	470	541	19.0	NBD-PZ-Ar	470	541
DBD-PZ	421	555	59.6	DBD-PZ-Ar	440	569
DBD-CD	430	560	100[a]	DBD-CD-Ar	437	561
SBD-PZ	399	576	5.6			

[a] The fluorescence intensity of DBD-CD was arbitrarily taken as 100%.

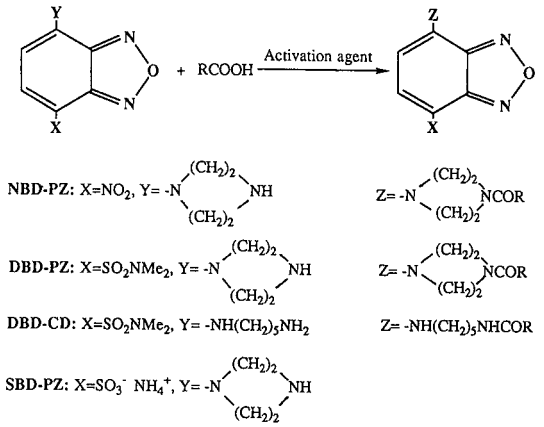

Fig. 1. Structures of the synthesized fluorescence reagents and their reaction with carboxylic acids in the presence of an activation agent.

triphenylphosphine) [27] and Mukaiyama B (2-chloro-1-methylpyridinium iodide and triethylamine) [28]. The scheme for the reaction of the 2,1,3-benzoxadiazole amine reagents with activated carboxylic acid is shown in Fig. 1.

The reactivity toward arachidic acid, which was selected as a representative carboxylic acid, was examined with three 2,1,3-benzoxadiazole amine reagents in the presence of DEPC, an activation agent. As depicted in Fig. 2, the production of the adducts with cadaverino reagents (DBD-CD) at room temperature reached a plateau after 15 min over the 585-min period tested. The derivatization reaction patterns with cadaverino reagents were almost identical in both acetonitrile and DMF (Fig. 2A and B), whereas the production of the adducts with piperazino reagents (NBD-PZ and DBD-PZ) gradually increased with increasing reaction time, and was constant after 5 h. Therefore, the rate of reaction with piperazino reagents seems to be slower than that with cadaverino reagents. With piperazino reagents, the reaction in acetonitrile gave higher fluorescent peaks than in DMF at all points (Fig. 2A and B). Among all the reagents tested, the fluorescence intensity of the adduct obtained from DBD-PZ in acetonitrile was the highest after reaction for 2 h (Fig. 2B). Therefore, the derivatization reaction with the reagents depends on the solvent in the reaction medium. This phenomenon was especially notable in the reaction with piperazino reagents (DBD-PZ and NBD-PZ). Although similar

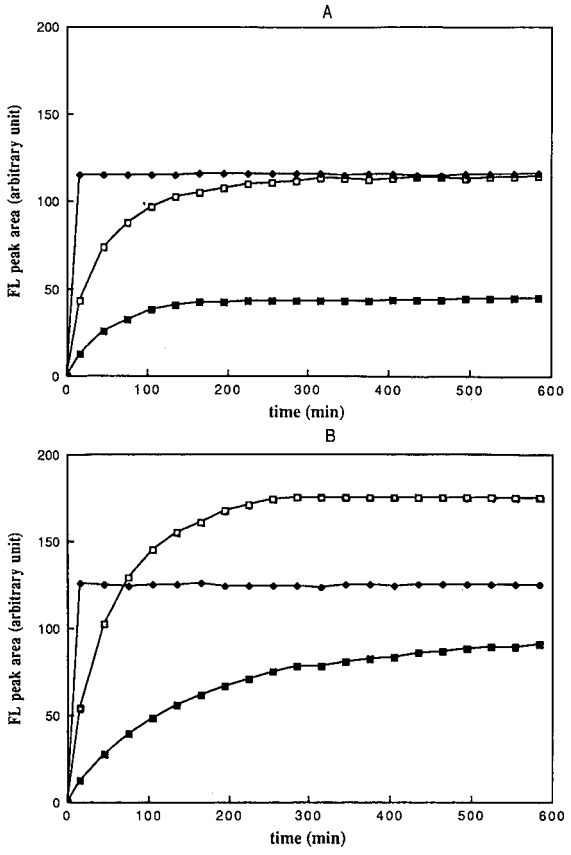

Fig. 2. Time course of the reaction of arachidic acid with various fluorescence reagents in the presence of DEPC. (A) in DMF; (B) in acetonitrile. □ = DBD-PZ; ◆ = DBD-CD; ■ = NBD-PZ. Arachidic acid (50 μM) and fluorescence tagging reagents (5 mM) in 0.4 ml of DMF (or acetonitrile) were reacted at room temperature in the presence of DEPC (70 mM). At fixed time intervals, an aliquot of the reaction solution was injected onto the HPLC column. Column, Inertsil ODS-2 (150 × 4.6 mm I.D.; 5 μm) at 40°C; flow-rate, 1.0 ml/min; isocratic elution with acetonitrile–water (9:1); fluorescence detection, λ_{ex} 470 nm and λ_{em} 541 nm for NBD-PZ–Ar, λ_{ex} 440 nm and λ_{em} 569 nm for DBD-PZ–Ar, λ_{ex} 437 nm and λ_{em} 561 nm for DBD-CD–Ar.

curves were also obtained with the reactions of ABD-PZ and ABD-CD [18], the maximum peak areas were 30–40% of those with DBD-PZ and DBD-CD. The reaction pattern with DBD-CD in the presence of DEPC (or with DBD-PZ in the presence of Mukaiyama A) seems to be comparable to that with MDC and DEPC reported by Lee *et al.* [16].

The effect of activation agents on the derivatization reaction was investigated with DBD-PZ in both acetonitrile and DMF. The relative activation

TABLE II

EFFECT OF ACTIVATION AGENTS ON THE DERIVATIZATION OF ARACHIDIC ACID WITH DBD-PZ

Activation agent	Relative peak area (%)	
	In acetonitrile	In DMF
DEPC	100[a]	63.2
DPPA	50.2	21.7
EDC–pyridine	81.6	71.2
Mukaiyama A	90.2	78.6
Mukaiyama B	24.4	25.9

[a] The peak area with DEPC in acetonitrile was arbitrarily taken as 100%.

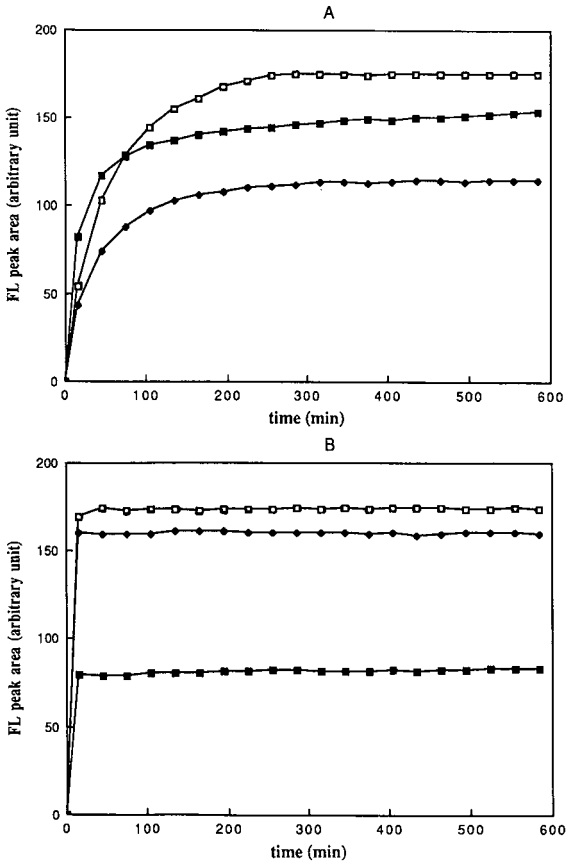

Fig. 3. Time course of the reaction of arachidic acid with DBD-PZ in various solvents. (A) DEPC (70 m*M*); (B) Mukaiyama A (10 m*M*). □ = acetonitrile; ◆ = DMF; ■ = ethanol. Arachidic acid (50 μM) and DBD-PZ (5 m*M*) in three solvents were reacted at room temperature in the presence of activation agents. Fluorescence detection; λ_{ex} 440 nm and λ_{em} 569 nm. Other HPLC conditions in Fig. 2.

capability was evaluated in terms of the fluorescent peak area of the adducts as shown in Table II. Among all the activation agents, DEPC and Mukaiyama A exhibited the highest activation in acetonitrile and DMF, respectively. The activation with Mukaiyama B was similar in both solvents. The order of activation in acetonitrile was DEPC > Mukaiyama A > EDC–pyridine > DPPA > Mukaiyama B. In DMF, the order was Mukaiyama A > EDC–pyridine > DEPC > Mukaiyama B > DPPA. Judging from the results in Table II both DEPC and Mukaiyama A were selected hereafter as the activation agents for carboxylic acids.

To decide a suitable reaction solvent, the derivatization reaction of arachidic acid with DBD-PZ was compared in three solvents (acetonitrile, ethanol and DMF). All three solvents dissolved DBD-PZ at relatively high concentration (>1000 ppm). As illustrated in Fig. 3, acetonitrile was the most effective solvent in the derivatization reaction with both DEPC and Mukaiyama A. The relative peak areas of the adduct with Mukaiyama A in DMF were about 90% of those in acetonitrile. The low fluorescent peaks with Mukaiyama A in ethanol seem to be due to side-reactions. The low production of the adduct might also depend on the amount of water in the solvent used as the medium. With DEPC, the order of the fluorescent peaks after reaction for 2 h was acetonitrile > ethanol > DMF. From these results, acetonitrile is the most effective solvent for the tagging reaction with DBD-PZ. However, the reaction solvent must also be selected by considering the solubility of the target carboxylic acid in real samples.

The derivatization reaction was compared at three different concentrations of DEPC and Mukaiyama A in acetonitrile. As shown in Fig. 4A, the adducts at 42 and 70 m*M* DEPC at room temperature gradually increased with increasing reaction time and reached a plateau after 5 h. With 14 m*M* DEPC, the reaction was slower than those at the other two DEPC concentrations and a constant peak area was not obtained even after 585 min. Consequently, a concentration of DEPC higher than 42 m*M* is necessary in order to obtain a constant peak area. On the other hand, the curves derived from Mukaiyama A were similar at three different concentrations (2, 10 and 35 m*M*) (Fig. 4B). The reaction of arachidic acid with DBD-CD in the

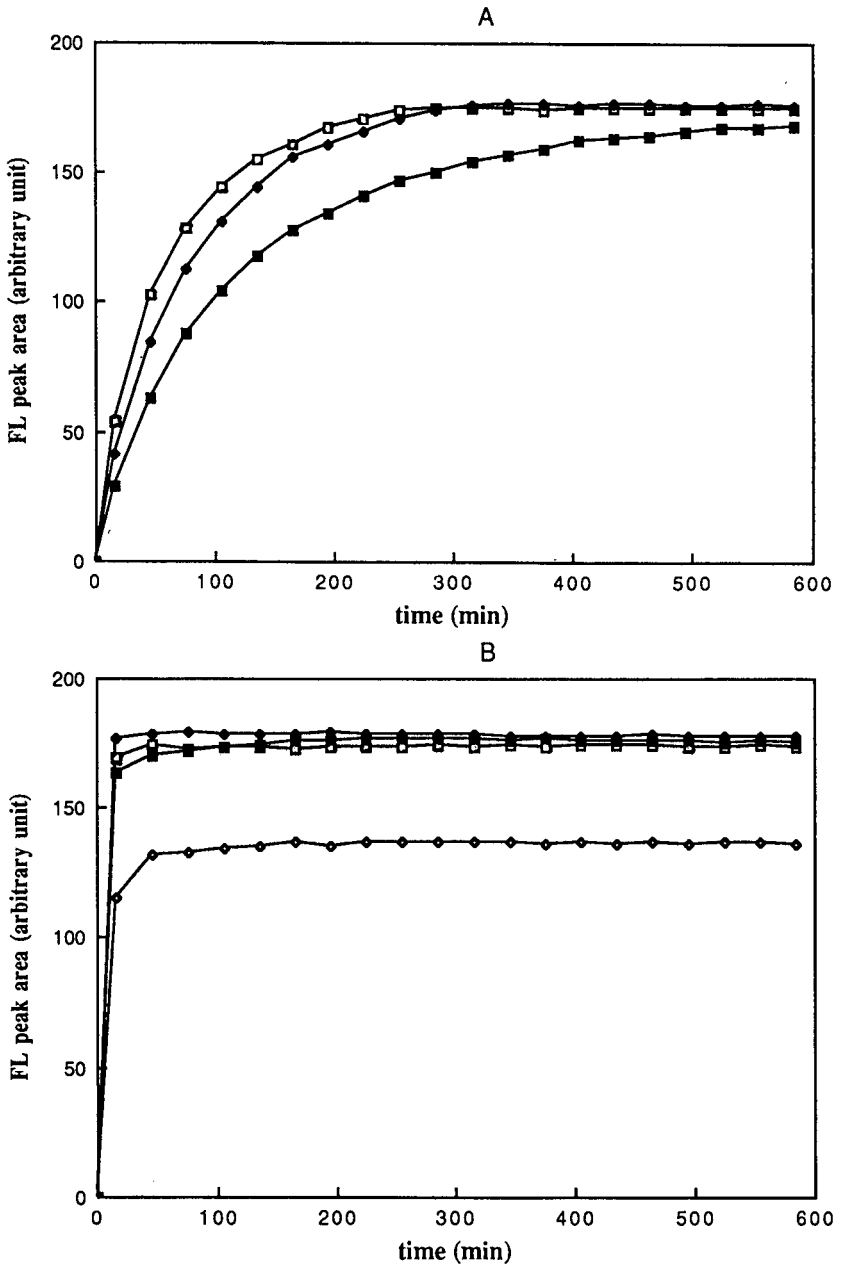

Fig. 4. Time course of the reaction of arachidic acid with various concentrations of activation agents in acetonitrile. (A) ⊔ = with DBD-PZ and DEPC (70 m*M*); ◆ = with DBD-PZ and DEPC (42 m*M*); ■ = with DBD-PZ and DEPC (14 m*M*). (B) □ = with DBD-PZ and Mukaiyama A (35 m*M*); ◆ = with DBD-PZ and Mukaiyama A (10 m*M*); ■ = with DBD-PZ and Mukaiyama A (2 m*M*); ◇ = with DBD-CD and Mukaiyama A (35 m*M*). Arachidic acid (50 μM) and DBD-amine reagents (5 m*M*) in acetonitrile were reacted at room temperature in the presence of various concentration of activation agents. Fluorescence detection, λ_{ex} 440 nm and λ_{em} 569 nm for DBD-PZ–Ar, λ_{ex} 437 nm and λ_{em} 561 nm for DBD-CD–Ar. Other HPLC conditions in Fig. 2.

presence of Mukaiyama A was completed after 45 min, the same as those with DBD-PZ. However, the fluorescent peak areas of the adduct were about 25% lower than that with DBD-PZ at all points (Fig. 4B).

According to the time-course study described above, the adducts derived from DBD-PZ and DBD-CD in the presence of DEPC were stable for at least 6 h in both acetonitrile and DMF (Figs. 2, 3A and 4A). Therefore, reaction for 6 h at room temperature was selected for the derivatization of carboxylic acids with DBD-PZ or DBD-CD (10 m*M*) in the presence of DEPC (70 m*M*). As good stability of the adducts and faster reactions were observed in the reaction of carboxylic acids with DBD-PZ and DBD-CD in the presence of Mukai-

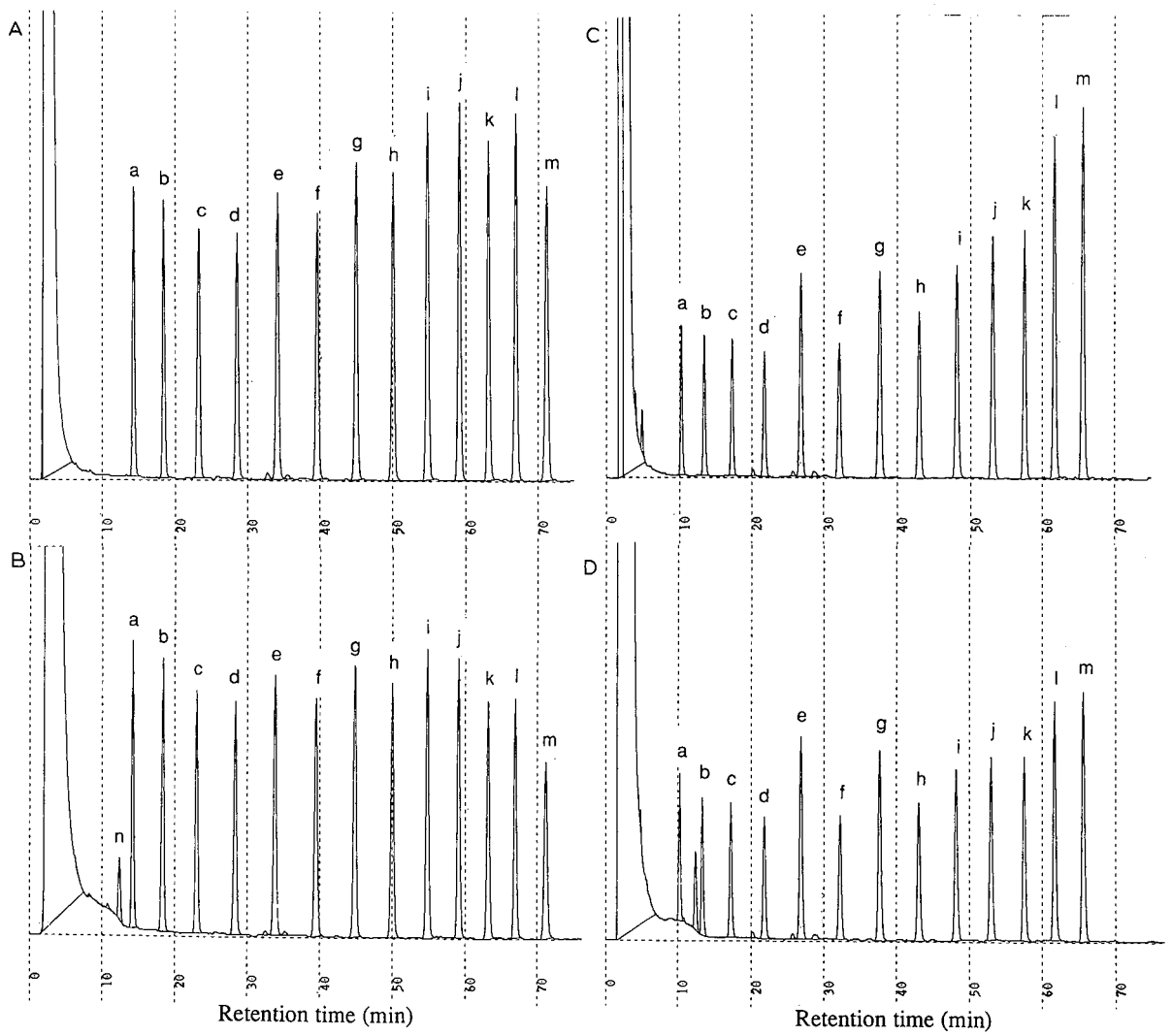

Fig. 5. Chromatograms of fatty acids labelled with DBD-amines in acetonitrile. (A) With DBD-PZ and DEPC (70 m*M*); (B) with DBD-PZ and Mukaiyama A (35 m*M*); C with DBD-CD and DEPC (70 m*M*); (D) with DBD-CD and Mukaiyama A (35 m*M*). Each peak corresponds to 5 pmol of fatty acid. (a) $C_{12:0}$ (b) $C_{13:0}$; (c) $C_{14:0}$; (d) $C_{15:0}$; (e) $C_{16:0}$; (f) $C_{17:0}$; (g) $C_{18:0}$; (h) $C_{19:0}$; (i) $C_{20:0}$; (j) $C_{21:0}$; (k) $C_{22:0}$; (l) $C_{23:0}$; (m) $C_{24:0}$; (n) unknown. Arachidic acid (5 μM) and DBD-amine reagents (5 m*M*) in acetonitrile were reacted at room temperature in the presence of activation agents. Linear gradient elution from acetonitrile–water (7:3) to acetonitrile–water (98:2) over 60 min and then isocractic elution with acetonitrile–water (98:2) for 20 min. Other HPLC conditions as in Fig. 4.

yama A (Figs. 2, 3B and 4B), reaction for 45 min was adopted for the derivatization in the presence of Mukaiyama A (35 m*M*). Judging from the reaction period affording the maximum fluorescence yield, Mukaiyama A might be more suitable than DEPC as an activation agent.

HPLC analyses of fatty acids and drugs tagged with DBD-amines

The HPLC separation of thirteen saturated free fatty acids (FFAs) and of eight drugs tagged with DBD-amine reagents (DBD-PZ and DBD-CD) in the presence of DEPC or Mukaiyama A were carried out on a reversed-phase column (Inertsil ODS-2). Fig. 5A and C show the separation of 5 pmol of each FFA, tagged with DBD-PZ or DBD-CD in the presence of DEPC, with mixtures of acetonitrile and water as the eluents. Peak separations of the adducts with each fluorescence reagent were completed within 75 min by a simple linear gradient. The FFAs tagged with DBD-PZ showed higher peaks compared than those of DBD-CD. Similar peak heights were observed among the DBD-PZ–FFAs in spite of the change in the solvent composition (Fig. 5A). For the adducts with DBD-CD in the presence of DEPC, the differences in the peak heights were larger than those with DBD-PZ (Fig. 5A *versus* C). Similar results were also obtained with the use of Mukaiyama A as an activating agent for carboxylic acids. However, an unknown peak (peak *n* in Fig. 5B and D) derived from the activating agent appeared on the chromatograms. With respect to the activation agents, DEPC and Mukaiyama A gave similar peak heights in the reaction with DBD-PZ (or DBD-CD) (Fig. 5A *versus* B and Fig. 5C *versus* D). Consequently, both activating agents are applicable to the determina-

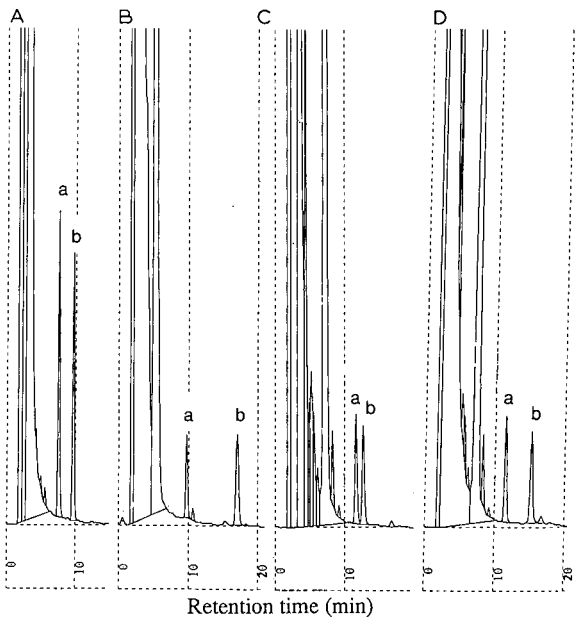

Fig. 6. Chromatograms of drugs derivatized with DBD-PZ in the presence of DEPC in acetonitrile. (A) (a) indomethacin and (b) ibuprofen; (B) (a) dehydrocholic acid and (b) ursodesoxycholic acid; (C) (a) prednisolone succinate and (b) hydrocortisone succinate; (D) (a) dinoprost (prostaglandin $F_{2\alpha}$) and (b) prostaglandin E_1. Each peak corresponds to 5 pmol of drug. Isocratic elution; (A) acetonitrile–water (65:35); (B) acetonitrile–water (5:5); (C) and (D) acetonitrile–water (45:55). Other HPLC conditions as those in Fig. 5.

TABLE III

DETECTION LIMITS OF FREE FATTY ACIDS AND DRUGS LABELLED WITH DBD-PZ AND DEPC IN ACETONITRILE

Carboxylic acid	Eluent[a]	Detection limit (signal-to-noise ratio = 3) (fmol)
Indomethacin	1	3.9
Ibuprofen	1	4.3
Dehydrocholic acid	2	13
Ursodesoxycholic acid	2	13
Prednisolone succinate	3	12
Hydrocortisone succinate	3	14
Dinoprost	3	12
Prostaglandin E_1	3	14
Lauric acid ($C_{12:0}$)	4	3.9
Tridecanoic acid ($C_{13:0}$)	4	4.1
Myristic acid ($C_{14:0}$)	4	4.5
n-Pentadecanoic acid ($C_{15:0}$)	4	4.7
Palmitic acid ($C_{16:0}$)	4	4.1
Margaric acid ($C_{17:0}$)	4	4.3
Stearic acid ($C_{18:0}$)	4	3.8
Nonadecanoic acid ($C_{19:0}$)	4	3.9
Arachidic acid ($C_{20:0}$)	4	3.3
Heneicosanoic acid ($C_{21:0}$)	4	3.2
Behenic acid ($C_{22:0}$)	4	3.6
Tricosanoic acid ($C_{23:0}$)	4	3.2
Lignoceric acid ($C_{24:0}$)	4	3.8

[a] Eluent 1, acetonitrile–water (65:35), isocratic elution; eluent 2, acetonitrile–water (1:1), isocratic elution; eluent 3, acetonitrile–water (45:55), isocratic elution; eluent 4, gradient elution from acetonitrile–water (7:3) to acetonitrile–water (98:2) over 60 min and isocratic elution with acetonitrile–water (98:2) for 20 min.

tion of carboxylic acids if the unknown peak derived from Mukaiyama A does not interfere with the separation of the objective acids.

HPLC separations of drugs containing a COOH moiety in the structure were also performed after tagging with DBD-PZ in the presence of DEPC. Each chromatogram in Fig. 6 shows the separation of 5 pmol of each drug divided into four groups, antiinflammatory, bile acids, hormones and prostaglandins.

As listed in Table III, the detection limits (signal-to-noise ratio = 3) of FFAs and drugs tagged with DBD-PZ in the presence of DEPC were 3–14 fmol, and were lower than those with ABD-PZ and ABD-CD (10–50 fmol) [18]. The detection limits were low compared with those obtained by other methods (*e.g.*, 10 fmol by Br-Mac [6], 20–30 fmol by PDAM [14], 100 fmol by MDC [16], 9 pmol by Br-Mmc [3]). Moreover, the long maximum wavelengths of the adducts might be an advantage for the detection of carboxylic acids in biological samples. Among the proposed reagents. DBD-amine reagents (DBD-PZ and DBD-CD) are recommended for the detection of carboxylic acids which are activated with DEPC or Mukaiyama A in acetonitrile or DMF. The DBD moiety was also preferable for more sensitive detection by peroxyoxalate chemiluminescence [29], so that attomole detection limits could be achieved for carboxylic acids. As the proposed method including the activation step under mild conditions is useful for the determination not only of FFAs but also of drugs such as prostaglandins, it might be applicable to the determination of various carboxylic acids in biological specimens. Further studies are in progress.

ACKNOWLEDGEMENT

The authors thank Dr. C. K. Lim, Medical Research Council Laboratories, Surrey, UK, for his valuable suggestions on the manuscript.

REFERENCES

1 H. Lingeman, W. J. M. Underberg, A. Takadate and A. Hulshoff, *J. Liq. Chromatogr.*, 8 (1985) 789.
2 K. Imai and T. Toyo'oka, in R. W. Frei and K. Zech, (Editors), *Selective Sample Handling and Detection in High-Performance Liquid Chromatography*, Part A (*Journal of Chromatography Library*, Vol. 39A), Elsevier, Amsterdam, 1988, p. 209.
3 S. Lam and E. Grushka, *J. Chromatogr.*, 158 (1978) 207.
4 J. B. F. Lloyd. *J. Chromatogr.*, 178 (1979) 249.
5 W. Voelter, R. Huber and K. Zech, *J. Chromatogr.*, 217 (1981) 491.
6 H. Tsuchiya, T. Hayashi, H. Naruse and N. Takagi, *J. Chromatogr.*, 234 (1982) 121.
7 H. Tsuchiya, T. Hayashi, M. Sato, M. Tatsumi and N. Takagi, *J. Chromatogr.*, 309 (1984) 43.
8 M. Yamaguchi, S. Hara, R. Matsunaga, M. Nakamura and Y. Ohkura, *Anal. Sci.*, 1 (1985) 295.
9 M. Yamaguchi, S. Hara, R. Matsunaga, M. Nakamura and Y. Ohkura, *J. Chromatogr.*, 346 (1985) 227.
10 M. Yamaguchi, O. Takehiro, S. Hara, M. Nakamura and Y. Ohkura, *Chem. Pharm. Bull.*, 36 (1988) 2263.
11 W. D. Watkins and M. B. Peterson, *Anal. Biochem.*, 125 (1982) 30.
12 S. A. Barker J. A. Monti, S. T. Christian, F. Benington and R. D. Morin, *Anal. Biochem.*, 107 (1980) 116.
13 N. Nimura and T. Kinoshita, *Anal. Lett.*, 13 (1980) 191.
14 N. Nimura, T. Kinoshita, T. Yoshida, A. Uetake and C. Nakai, *Anal. Chem.*, 60 (1988) 2067.
15 I. Yanagisawa, M. Yamane and T. Urayama, *J. Chromatogr.*, 345 (1985) 229.
16 Y.-M. Lee, H. Nakamura and T. Nakajima, *Anal. Sci.*, 5 (1989) 681.
17 T. Iwata, M. Yamaguchi and M. Nakamura, *110th Annual Meeting of the Pharmaceutical Society of Japan, Sapporo, 1990*, Pharmaceutical Society of Japan, Vol. 3, 1990, p. 244.
18 T. Toyo'oka, M. Ishibashi, Y. Takeda and K. Imai, *Analyst (London)*, 116 (1991) 609.
19 T. Toyo'oka and K. Imai, *Analyst (London)*, 109 (1984) 1003.
20 T. Toyo'oka and K. Imai, *Anal. Chem.*, 56 (1984) 2461.
21 K. Imai and Y. Watanabe, *Anal. Chim. Acta*, 130 (1981) 377.
22 T. Toyo'oka, T. Suzuki, Y. Saito, S. Uzu and K. Imai, *Analyst (London)*, 114 (1989) 413.
23 T. Toyo'oka, T. Suzuki, Y. Saito, S. Uzu and K. Imai, *Analyst (London)*, 114 (1989) 1233.
24 T. Shioiri, *Yuki Gosei Kagaku Kyokai Shi*, 37 (1979) 856.
25 K. D. Kopple and D. E. Nitecki, *J. Am. Chem. Soc.*, 84 (1962) 4457.
26 T. Shioiri, K. Ninomiya and S. Yamada, *J. Am. Chem. Soc.*, 94 (1972) 6203.
27 T. Mukaiyama, R. Matsueda and M. Suzuki, *Tetrahedron Lett.*, (1970) 1901.
28 E. Bald, K. Saigo and T. Mukaiyama, *Chem. Lett.*, (1975) 1163.
29 S. Uzu, K. Imai, K. Nakashima and S. Akiyama, *Biomed. Chromatogr.*, 5 (1991) 184.

Journal of Chromatography, 588 (1991) 73–87
Elsevier Science Publishers B.V., Amsterdam

CHROM. 23 635

Reversed-phase liquid chromatography–mass spectrometry of complex mixtures of natural triacylglycerols with chloride-attachment negative chemical ionization

A. Kuksis*, L. Marai and J. J. Myher

Banting and Best Department of Medical Research, University of Toronto, Toronto M5G 1L6 (Canada)

(First received April 15th, 1991; revised manuscript received July 16th, 1991)

ABSTRACT

Short chain triacylglycerols of butteroil and long chain triacylglycerols of menhaden oil were resolved by conventional reversed-phase high-performance liquid chromatography (HPLC) using a linear gradient of 10–90% propionitrile in acetonitrile as the mobile phase. The triacylglycerol species were identified by positive chemical ionization mass spectrometry, which provided $[MH–RCOOH]^+$ and $[MH]^+$ ions and by negative chemical ionization mass spectrometry with chloride attachment, which yielded exclusively the pseudomolecular ions $[M + Cl]^-$. The negative ions were produced by the inclusion of 1% methylene chloride in the HPLC mobile phase, which did not affect the triacylglycerol elution profile. The restriction of ionization to the chloride-attachment pseudomolecular ions increased about 100-fold the sensitivity of detection of all molecular species and facilitated their quantitation by mass spectrometry. By combining the results of positive and negative chemical ionization mass spectrometry of the eluted peaks it was observed that the complex short chain triacylglycerols showed extensive resolution within isologous saturated carbon number while the polyunsaturated fish oil triacylglycerols showed readily detectable resolution within isologous carbon and double bond number*. These observations permit the identification and quantitation of molecular species of triacylglycerols in such complex mixtures as butterfat and fish oil, which have thus far proved difficult or impossible.

INTRODUCTION

Reversed-phase high-performance liquid chromatography (HPLC) of triacylglycerols has been extensively studied and the sequence of elution of the common molecular species well established [1]. Identification of molecular species is obtained by means of theoretical carbon numbers (TCN) that are determined from a plot of capacity factors k' *vs* carbon number of the corresponding saturated triacylglycerols [2,3]. The TCN is calculated as the equivalent carbon number (ECN) minus the sum of the emperical factors determined separately for each fatty acid. This method is adequate for oils and fats made up of the common medium and long chain fatty acids [1–3]. By changing the ratio of polar to non-polar solvents, it is possible to obtain a wider variety of mobile phase polarities, which affect the migration of the triacylglycerol species resulting in different retention times for different members of a given ECN [4]. It is therefore necessary to determine the exact retention times for each combination of saturated and unsaturated fatty acids in each solvent system, which may be impossible in the absence of standards. Furthermore, the more complex mixtures of natural triacylglycerols require HPLC with gradient elution [3,4] or temper-

* These are subsets of triacylglycerols: isologous saturated triacylglycerols contain same number of total acyl carbons but differ in their distribution among the fatty chains; isologous polyunsaturated triacylglycerols contain same number of total acyl carbons and number of double bonds, but differ in their distribution among the fatty chains.

0021-9673/91/$03.50

ature programming [5,6] which complicates the calculation of the TCN and peak identification. Since peak collection from poorly resolved profiles is impractical, HPLC with mass spectrometry (MS) appears to provide the only effective method of identification of the molecular species of the triacylglycerols. However, conventional LC–MS is not well suited for peak quantitation in absence of extensive calibration of the system because electron impact and positive chemical ionization (PCI) provide disproportional yields of the diacylglycerol fragment ions from mixed acid triacylglycerols, as well as little or no molecular ion [7,8].

In the present report we wish to describe the application of chloride attachment negative chemical ionization (NCI) mass spectrometry, which yields exclusively the pseudomolecular ions of triacylglycerols [9], as an aid in the identification and quantitation of triacylglycerol species in two complex natural fats by reversed-phase LC–MS.

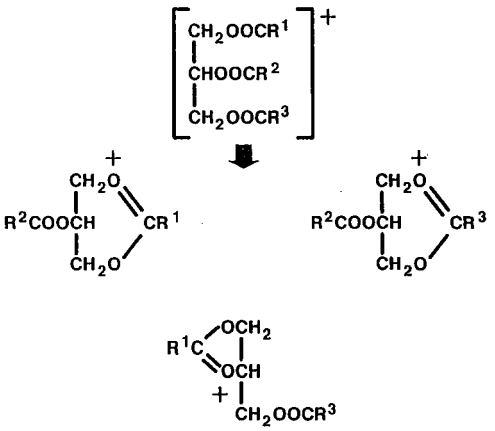

Scheme 1.

EXPERIMENTAL

Fats and oils

The third most volatile 2.5% distillate (R-3) of butteroil was available in the laboratory [10]. Menhaden oil triacylglycerols were obtained from Zapata Haynie (Reedville, VA, USA). Simple monoacid triacylglycerols were obtained from Serdary Research Laboratories (London, Ontario, Canada). Prior to LC–MS analysis the triacylglycerols were purified by normal-phase thin layer chromatography (TLC).

Reversed-phase HPLC and LC–MS

Reversed-phase C_{18} 5-μm columns (30 cm × 0.46 cm I.D.) were purchased from Supelco Canada (Mississauga, Ontario, Canada) and were installed in a Hewlett-Packard Model 1084B liquid chromatograph interfaced with a Hewlett-Packard Model 5895B quadrupole mass spectrometer via a direct liquid inlet interface as previously described [7]. The mobile phase consisted of a linear gradient of 10–90% propionitrile in acetonitrile for PCI and of a linear gradient of 10–90% propionitrile in acetonitrile containing 1% dichloromethane for NCI with chloride attachment. The columns were run at a flow-rate of 1.5 ml/min with 1% of the effluent being admitted to the mass spectrometer. The PCI and NCI spectra were recorded at 210 eV. The ion source temperature was 200 and 150°C for PCI and NCI, respectively. The mass spectrometer scans were restricted to masses above 200 and were taken at rates of one scan per 4–5 s (m/z 200–1000) over the entire elution profile. In some instances background subtractions were performed by the computer to compensate for impurities in the solvents. For detailed examination and quantitation, the data were recalled from the computer and displayed in a suitable manner. The limit of detection was defined as the lowest detectable concentration yielding a signal to noise ratio of at least two. The general pattern of fragmentation of triacylglycerols in LC–MS under PCI conditions may be represented as shown in Scheme 1 [7].

Polarizable capillary gas chromatography (GC)

This was performed with the R-3 distillate of butteroil as previously described for the R-4 distillate of butteroil [11].

RESULTS

R-3 distillate of butteroil

Fig. 1 shows the reversed-phase LC–MS profile of the third most volatile 2.5% molecular distillate in relation to that of whole butteroil triacylglycerols. The distillate represents the more complex part of the triacylglycerol mixture corresponding largely to that of the saturated short and medium chain species as shown elsewhere [12]. Peaks 27 to

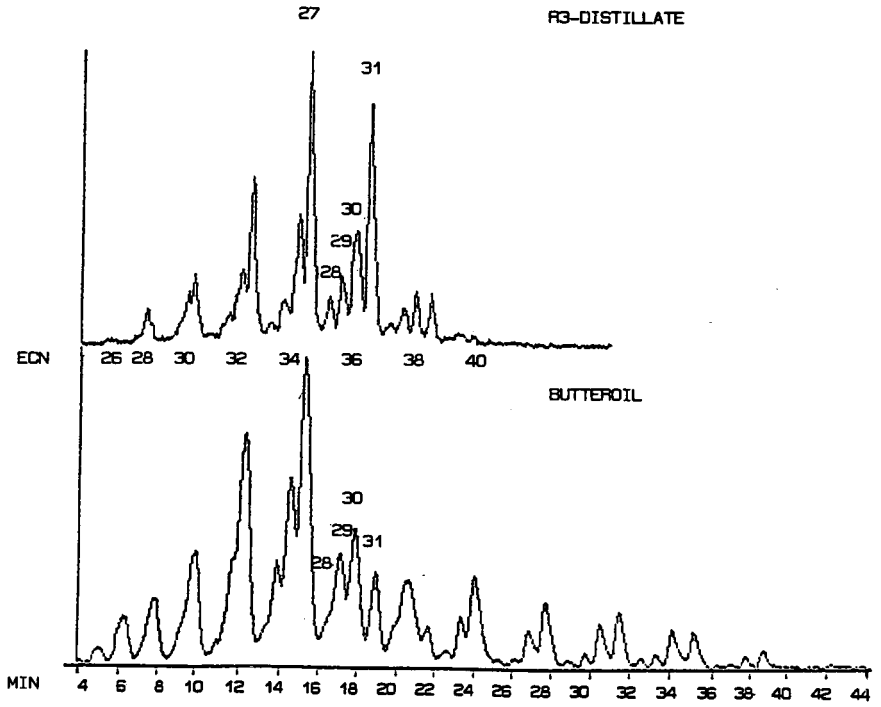

Fig. 1. Reversed-phase LC–MS profile of a butteroil distillate (R-3) and whole butteroil. HPLC conditions: C_{18} column (25 cm × 0.4 cm I.D. tube containing 5 μm packing); solvent system, 10–90% linear gradient of propionitrile in acetonitrile. Other LC–MS conditions as given in text. Peak detection by PCI. Mass range, 270–900 a.m.u.

31 represent triacylglycerols with ECNs 34 to 36, which are discussed in detail below Fig. 2 shows, on an expanded scale, the part of the chromatogram of interest along with the single ion plots for the major diacylglycerol ions detected in the different triacylglycerol peaks by PCI. Fig. 3 shows the corresponding total ion current profile along with the single pseudomolecular ion plots obtained by NCI with chloride attachment for the triacylglycerol species shown in Fig. 2. There were no diacylglycerol type ions seen in the NCI. PCI gave small and variable yields of molecular ions for the short chain triacylglycerols. By combining the data from diacylglycerol fragmentation and the formation of pseudomolecular ions in the NCI it was possible to obtain an unambiguous identification of all the major triacylglycerol species, which was consistent with the anticipated reversed-phase HPLC elution order of the molecules.

Thus, the major isologous triacylglycerols making up peak 31 are 16:0-16:0-4:0 (*m/z* 639, M + 1), as indicated by the presence in PCI (Fig. 2) of prominent diacylglycerol (DG) fragment ions ($[MH-RCOOH]^+$) corresponding to DG20:0 (*m/z* 383) and DG 32:0 (*m/z* 551), and much smaller amounts of 18:0-14:0-4:0 (*m/z* 639), as indicated by diacylglycerol fragment ions corresponding to DG18:0 (*m/z* 355), DG22:0 (*m/z* 411) and DG32:0 (*m/z* 551), as well as by the presence in NCI (Fig. 3) of the pseudomolecular ion $[M+35]^-$ at *m/z* 673. Peak 31 is preceded by peak 30, which is made up of two major triacylglycerols with pseudomolecular ions $[M+35]^-$, corresponding to TG38:1 (*m/z* 699), and $[M+35]^-$, corresponding to TG36:0 (*m/z* 673). The isologous triacylglycerols of the TG38:1 species were made up of 18:1-16:0-4:0, as indicated by the diacylglycerol fragment ions corresponding to DG20:0 (*m/z* 383), DG22:1 (*m/z* 409) and DG 34:1 (*m/z* 577), and very minor contribution of 18:0-16:1-4:0, as indicated by the diacylglycerol fragment ions corresponding to DG20:1 (*m/z* 381), DG22:1 (*m/z* 409) and DG34:1 (*m/z* 577). The 38:1 triacyl-

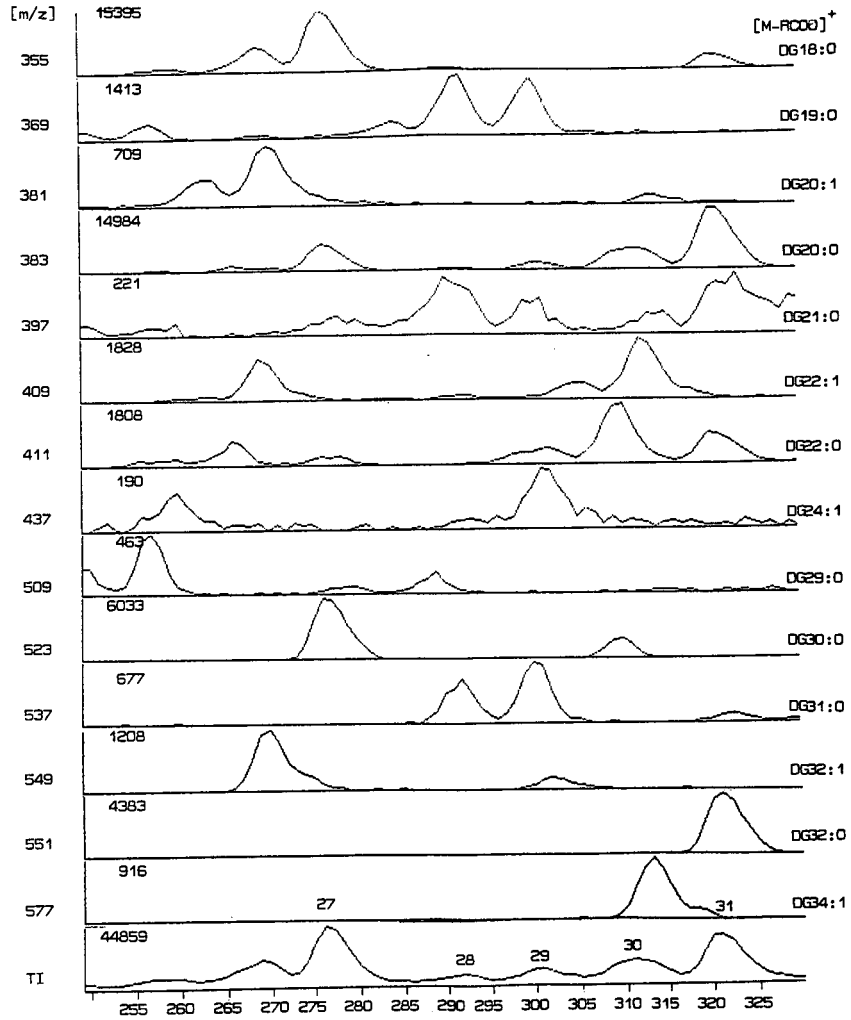

Fig. 2. Expanded scale representation of part of the LC–MS profile of R-3 in Fig. 1, along with single ion plots for major diacylglycerol fragments in PCI. TI, total PCI current; *m/z* values, $[M-RCOO]^+$ ions as identified by carbon number:double bond number; values inside panels, ion counts for each scan. Other LC–MS conditions as in Fig. 1.

glycerol species were preceded by another TG36:0 species, which was made up of 14:0-16:0-6:0, as indicated by the diacylglycerol fragment ions DG20:0 (*m/z* 383), DG22:0 (*m/z* 411) and DG30:0 (*m/z* 523), and smaller amounts of 18:0-12:0-6:0, as indicated by the appropriate diacylglycerol fragment ions. Peak 30 was preceded by peak 29 which was found to yield pseudomolecular ions $[M+35]^-$ at *m/z* 659, 673 and 699, corresponding to TG35:0, TG36:0 and TG38:1, with smaller amounts of TG37:1 and TG40:2, which were found to be eluted midway between peaks 29 and 30. The presence of the TG35:0 triacylglycerol was due to 15:0-16:0-4:0, as indicated by diacylglycerol fragment ions corresponding to DG19:0 (*m/z* 369), DG20:0 (*m/z* 383) and DG31:0 (*m/z* 537), while that of TG36:0 was due to 14:0-14:0-8:0, as indicated by diacylglycerol fragments DG22:0 (*m/z* 411) and DG28:0 (*m/z* 495), and that of TG38:1 due to 14:0-18:1-6:0, as indicated by the diacylglycerol fragment ions DG20:0 (*m/z* 383), DG24:1 (*m/z* 437) and DG32:1 (*m/z* 549). There were small amounts of other triacylglycerols in this

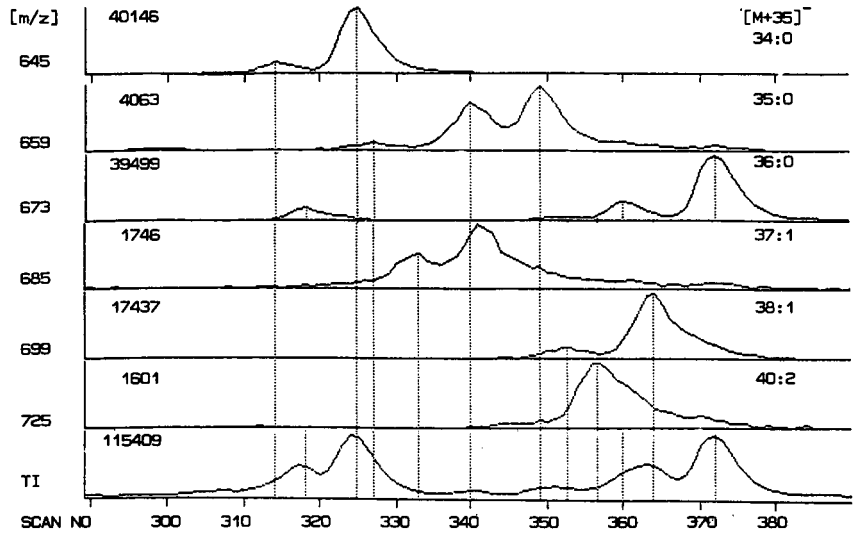

Fig. 3. Expanded scale representation of part of the LC–MS profile of R-3 in Fig. 3 as obtained by chloride attachment NCI. TI, total NCI current; *m/z* values, $[M+35]^-$ pseudomolecular ions as identified by carbon number:double bond number; values inside panels, ion counts for each scan. Solvent system: 10–90% linear gradient of propionitrile in acetonitrile containing 1% dichloromethane. Other LC–MS conditions as in Fig. 1. Peak detection by NCI.

minor peak either because of overlapping with other isologous triacylglycerols or because of the tailing of major triacylglycerols preceding the minor peaks. Peak 29 was preceded by peak 28, which also was made up of several triacylglycerols giving mainly pseudomolecular ions $[M+35]^-$ at *m/z* 645, 659 and 685 corresponding to TG34:0, TG35:0 and TG37:1, with smaller amounts of pseudomolecular ions of *m/z* 671 and 699 corresponding to TG36:1 and TG38:1. The 35:0 triacylglycerol was due to 15:0-14:0-6:0, as indicated by the presence of diacylglycerol fragment ions of DG20:0 (*m/z* 383), DG21:0 (*m/z* 397) and DG29:0 (*m/z* 509), while the presence of the TG37:1 was due to 15:0-16:1-6:0, as indicated by the diacylglycerol fragment ions DG21:0 (*m/z* 397), DG22:1 (*m/z* 409), and DG31:1 (*m/z* 535). Peak 28 also contained significant amounts of the 14:0-16:0-4:0 species due to tailing of the major peak 27, which contained this triacylglycerol species nearly exclusively. Fig. 4 compares the PCI and NCI spectra recorded for the center sections of peak 29, while Fig. 5 compares the PCI and NCI spectra for peak 28. As already explained, the short chain saturated and monounsaturated triacylglycerols give low yields of molecular ions and variable yields of diacylglycerol type of fragments in PCI. NCI with chloride attachment yields only the pseudomolecular ions from which the molecular weight of the triacylglycerol species can be reliably obtained.

Table I compares the quantitative estimates for the major triacylglycerols in the R-3 distillate as obtained from the negative pseudomolecular ions in LC–MS and from polarizable capillary GLC with flame ionization detection. The triacylglycerol species are matched on basis of total carbon and double bond number and include separate estimates for the major isologous species within each carbon and double bond number. The LC–MS data show good agreement with the data obtained by polar capillary GLC of the intact triacylglycerols of R-3 distillate. From the close agreement, it would appear that chloride attachment NCI yields quantitatively correct proportions for the component short chain length triacylglycerol when analyzed in a complex mixture.

Menhaden oil

Fig. 6 shows a three-dimensional reversed-phase LC–MS profile of menhaden oil triacylglycerols as obtained using PCI as a means of peak detection. This profile is similar to that reported for fish oil

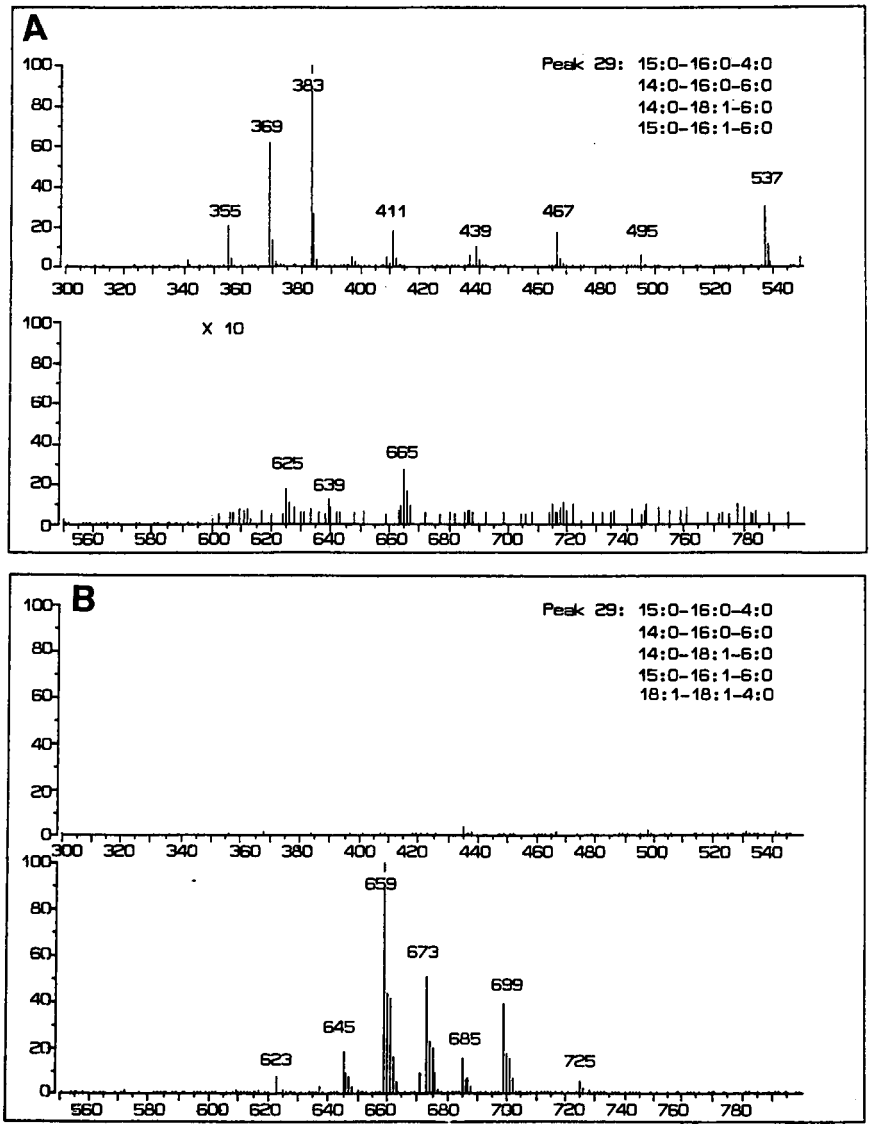

Fig. 4. Comparison of (A) PCI and (B) NCI mass spectra for the center cut of peak 29 (Fig. 2). LC–MS conditions as in Figs. 1 and 3 for the PCI and NCI, respectively. Major triacylglycerols identified by carbon number:double bond number. Ion identification as in Table I.

triacylglycerols by Wojtusik *et al.* [13]. The HPLC profile shows extensive peak overlapping and possible peak tailing. The ion plot which represents largely the distribution of the diacylglycerol type of fragments confirms the extensive peak overlapping and interdigitation but gives no evidence of peak tailing. The application of LC–MS to the identification and quantitation of the fish oil triacylglycerol peaks, all of which contain extremely complex mixtures of numerous molecular species [14], is illustrated by examining selected sections of the chromatographic profile.

Fig. 7 shows the PCI plots for the molecular ions of selected triacylglycerol species of ECN 42, 40 and 38, which are eluted over a wide range of the chromatographic profile due to differences in the con-

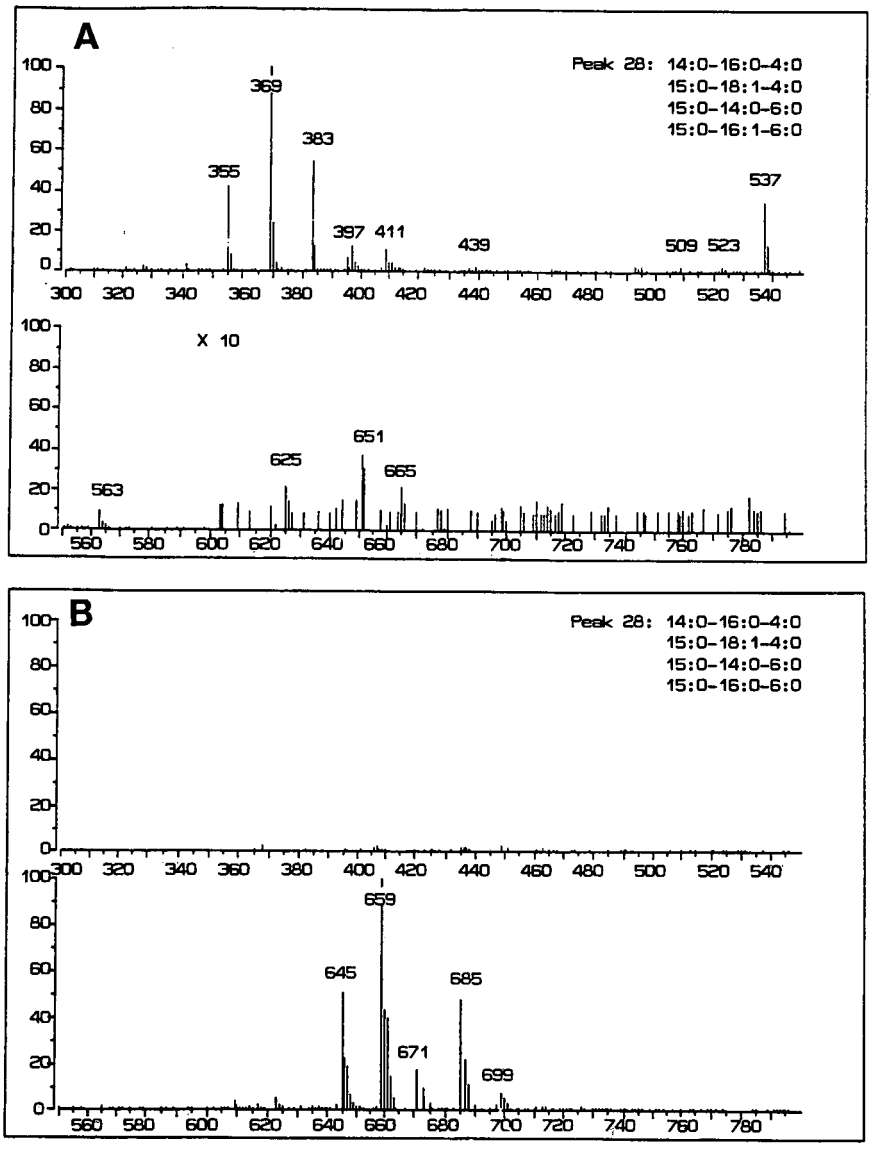

Fig. 5. Comparison of (A) PCI and (B) NCI mass spectra for a center cut of peak 28 (Fig. 2). LC–MS conditions as in Fig. 4. Major triacylglycerols identified by carbon number:double bond number. Ion identification as in Table I.

tent of acyl carbons and double bonds among the fatty chains. The molecular species have been selected to illustrate isologous triacylglycerol separation during reversed-phase HPLC of fish oil triacylglycerols, which makes peak identification based on theoretical carbon numbers difficult or impossible.

The positive ions corresponding to the diacylglycerol fragments in Fig. 8 show that the major isologous 52:5 triacylglycerols (*m/z* 853) in peak 4 are made up 16:0-16:0-20:5, as indicated by the presence of a prominent diacylglycerol fragment ion DG32:0 (*m/z* 551), although the corresponding DG36:5 ion (*m/z* 597) is seen in lesser abundance, along with a smaller amount of 18:0-14:0-20:5, as indicated by the presence of DG32:0 (*m/z* 551), DG34:5 (*m/z* 569) and still smaller amounts of

TABLE I

COMPOSITION OF TRIACYLGLYCEROLS IN R-3 DISTILLATE OF BOVINE MILK FAT AS ESTIMATED BY REVERSED-PHASE LC–MS WITH CHLORIDE-ATTACHMENT NEGATIVE CHEMICAL IONIZATION (AREA %)

Molecular species	NCI $[M+35]^-$	GC–FID[c]	Molecular species	NCI $[M+35]^-$	GC—FID
28:1	0.04 (11.65)[a]		36:0	4.53 (23.38)	6.46
30:1	0.46 (13.33)	0.63	38:1	7.66 (23.65)	6.24
32:1	0.21 (13.40)		39:1	0.14 (23.78)	0.48
28:0	0.31 (13.47)	0.75	41:2	0.09 (24.00)	n.d.
31:1	0.02 (14.45)	n.d.[b]	40:2	0.59 (24.03)	0.88
32:1	0.21 (14.97)	n.d.	36:0	15.91 (24.17)	15.22
30:0	0.27 (15.22)	0.37	37:0	1.36 (24.30)	1.12
32:1	1.53 (15.42)	1.58	39:1	0.27 (24.42)	n.d.
34:2	0.26 (15.48)	n.d.	37:0	2.39 (25:13)	1.18
30:0	1.26 (15.73)	2.16	39:1	0.27 (25.20)	0.48
33:1	0.07 (16.20)	n.d.	40:1	0.65 (25.33)	n.d.
31:0	0.20 (16.45)	0.40	42:2	0.27 (25.40)	n.d.
33:1	0.08 (16.72)	n.d.	37:0	2.39 (25.78)	1.22
31:1	0.02 (16.97)	n.d.	40:1	0.66 (25.92)	1.32
34:1	0.52 (17.37)	2.37	38:0	1.19 (25.98)	1.78
32:0	1.05 (17.62)	1.31	38:0	3.18 (26.57)	3.72
36:2	0.26 (17.75)	n.d.	40:1	0.66 (26.70)	0.75
34:1	3.03 (17.95)	2.37	41:1	0.14 (26.88)	n.d.
36:2	0.26 (18.13)	n.d.	38:0	3.32 (27.33)	4.45
32:0	4.43 (18.33)	6.11	39:0	0.33 (27.40)	n.d.
35:1	0.28 (18.72)	n.d.	44:2	– (27.98)	n.d.
33:0	0.55 (19.18)	0.99	39:0	0.22 (28.25)	n.d.
35:1	0.28 (19.30)	n.d.	42:1	0.15 (28.50)	n.d.
33:0	0.69 (19.70)	0.88	39:0	0.11 (28.90)	n.d.
40:3	0.12 (20.22)	n.d.	42:1	0.15 (28.97)	n.d.
34:0	2.57 (20.40)	3.13	40:0	0.68 (29.03)	1.38
38:2	0.06 (20.53)	n.d.	40:0	0.68 (29.67)	0.97
36:1	7.63 (20.67)	6.55	43:1	– (29.93)	n.d.
38:2	0.86 (21.05)	n.d.	41:0	0.14 (30.45)	n.d.
34:0	14.13 (21.12)	15.1	44:1	– (31.33)	n.d.
35:0	0.21 (21.25)	n.d.	42:0	– (31.88)	n.d.
37:1	0.82 (21.57)	n.d.	Other		
39:2	0.11 (21.70)	n.d.			
35:0	1.51 (22.10)	2.34			
37:1	1.40 (22.15)	0.97			
35:0	1.61 (22.68)	2.00			
38:1	1.24 (22.87)	n.d.			
40:2	0.11 (23.13)	n.d.			

[a] HPLC retention times (minutes) in brackets.
[b] n.d. = Not determined.
[c] FID = Flame ionization detection.

DG38:5 (*m/z* 625), and of 16:0-14:0-22:5, as indicated by the diacylglycerol fragment ions DG30:0 (*m/z* 523), DG36:5 (*m/z* 597) and DG38:5 (*m/z* 625). Peak 4 is preceded by peak 3, which is seen to be made up of 16:0-18:1-18:4 as indicated by the diacylglycerol fragment ions DG34:1 (*m/z* 577), DG34:4 (*m/z* 571) and DG36:5 (*m/z* 597), and of 14:0-18:1-20:4, as indicated by the diacylglycerol fragment ions corresponding to DG32:1 (*m/z* 549), DG34:4 (*m/z* 571) and DG38:5 (*m/z* 625). Peak 1 is due to the M + 2 ions from the 52:6 triacylglycerols (*m/z* 851), while peak 2 represents a complex mix-

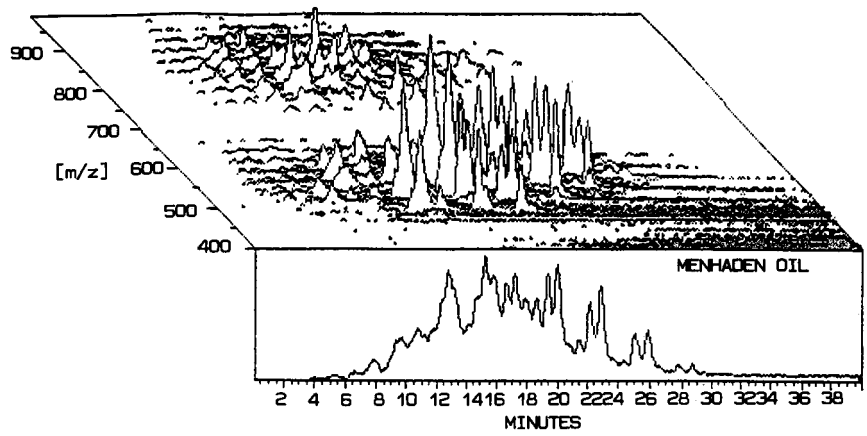

Fig. 6. Three-dimensional LC–PCI-MS profile of menhaden oil triacylglycerols. TI, total ion current; *m/z* 450–700, diacylglycerol fragment ions $[M-RCOO]^+$; *m/z* 700–1000, molecular ions of triacylglycerols $[M]^+$. HPLC solvent: 20–90% linear gradient of propionitrile in acetonitrile. Other LC–MS conditions as in Fig. 1.

ture of triacylglycerols of ECN 42 which contains very little of the isologous triacylglycerols (*m/z* 853) identified in peaks 3 and 4.

The diacylglycerol fragment ions in Fig. 9 show that the major isologous 54:6 triacylglycerols (*m/z* 879) in peak 3 are made up of 16:0-16:0-22:6, as indicated by the fragment ions DG32:0 (*m/z* 551) and DG38:6 (*m/z* 623), and 18:0-14:0-22:6, as indicated by the fragment ions DG32:0 (*m/z* 551), DG36:6 (*m/z* 595) and DG40:6 (*m/z* 651). Peak 3 is preceded by peak 2, which is made up of 16:0-18:1-20:5, as indicated by major fragment ions corresponding to DG34:1 (*m/z* 577), DG36:5 (*m/z* 597) and DG38:6 (*m/z* 623). Peak 1 contains 18:1-18:1-18:4, as indicated by major fragment ions corresponding to DG36:2 (*m/z* 603) and DG36:5 (*m/z* 597).

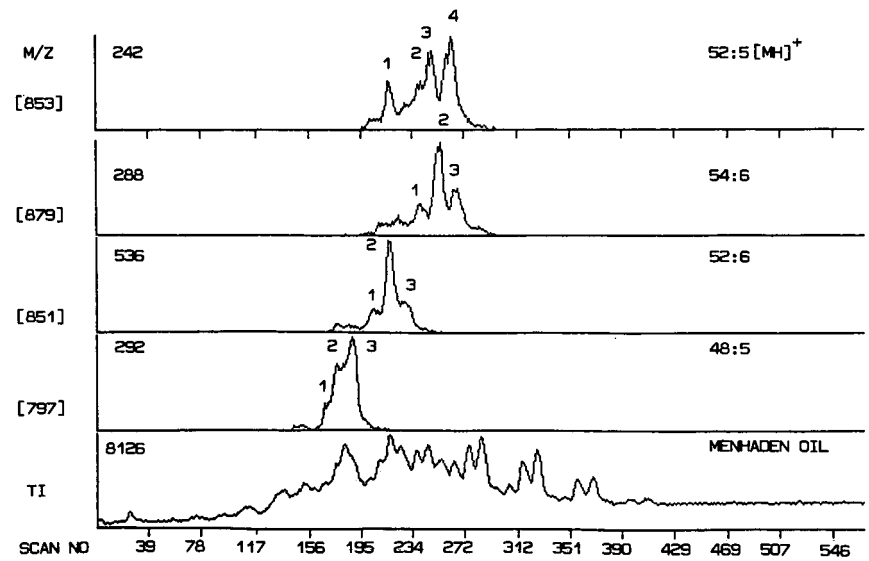

Fig. 7. Single ion plots in PCI for selected triacylglycerol (TG) species of ECN 38 (48:5), 40 (52:6) and 42 (52:5 and 54:6). TI, total PCI current; *m/z* values represent molecular ions $[M]^+$ of isologous triacylglycerol. Values inside panels, ion counts for each scan. LC–MS conditions as in Fig. 6.

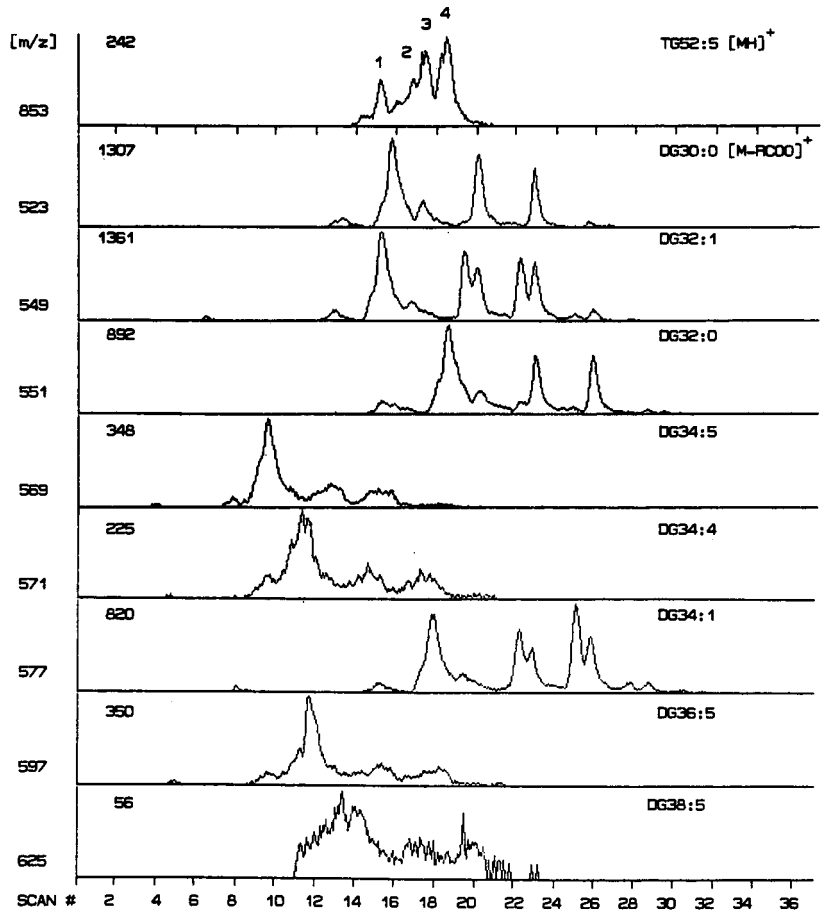

Fig. 8. Single ion plots in PCI for major diacylglycerol (DG) fragment ions $[M-RCOO]^+$ of isologous 52:5 triacylglycerols. TI, total PCI current; *m/z* values as identified by carbon number:double bond number. Values inside panels, ion counts for each scan. LC–MS conditions as in Fig. 6.

The major isologous 52:6 triacylglycerols (*m/z* 851) in Fig. 7 were made up of 16:1-18:1-18:4 (peak 1), as indicated by major fragment ions corresponding to DG34:2 (*m/z* 575), DG34:5 (*m/z* 569) and DG36:5 (*m/z* 597), along with 14:0-18:1-20:5 (peak 2), as indicated by major fragment ions corresponding to DG32:1 (*m/z* 549), DG34:5 (*m/z* 569), and DG38:6 (*m/z* 623) and 14:0-16:0-22:6 (peak 3), as indicated by the diacylglycerol fragment ions DG30:0 (*m/z* 523), DG36:6 (*m/z* 595) and DG38:6 (*m/z* 623), while the major isologous 48:5 triacylglycerols (*m/z* 797) could be identified as 16:1-16:1-16:3 (peak 1), as indicated by the major fragment ions corresponding to DG32:2 (*m/z* 547) and DG32:4 (*m/z* 543); 14:0-16:4-18:1 (peak 2), as indicated by fragment ions DG30:4 (*m/z* 515), DG32:1 (*m/z* 549) and DG34:5 (*m/z* 569), and 14:0-14:0-20:5 (peak 3), as indicated by the fragment ions corresponding to DG28:0 (*m/z* 495) and DG34:5 (*m/z* 569) (data not shown). It should be noted that in these instances the various isologous triacylglycerols were eluted in order of increasing content of saturated fatty chains. Those with two such chains were retained longer than those with one saturated fatty chain, while those containing three unsaturated fatty chains were eluted first within each isologous series. This elution order was confirmed for several other mixtures of isologous triacylglycerols, including 54:8 and 56:7 (data not shown).

In all instances the molecular weight distribution

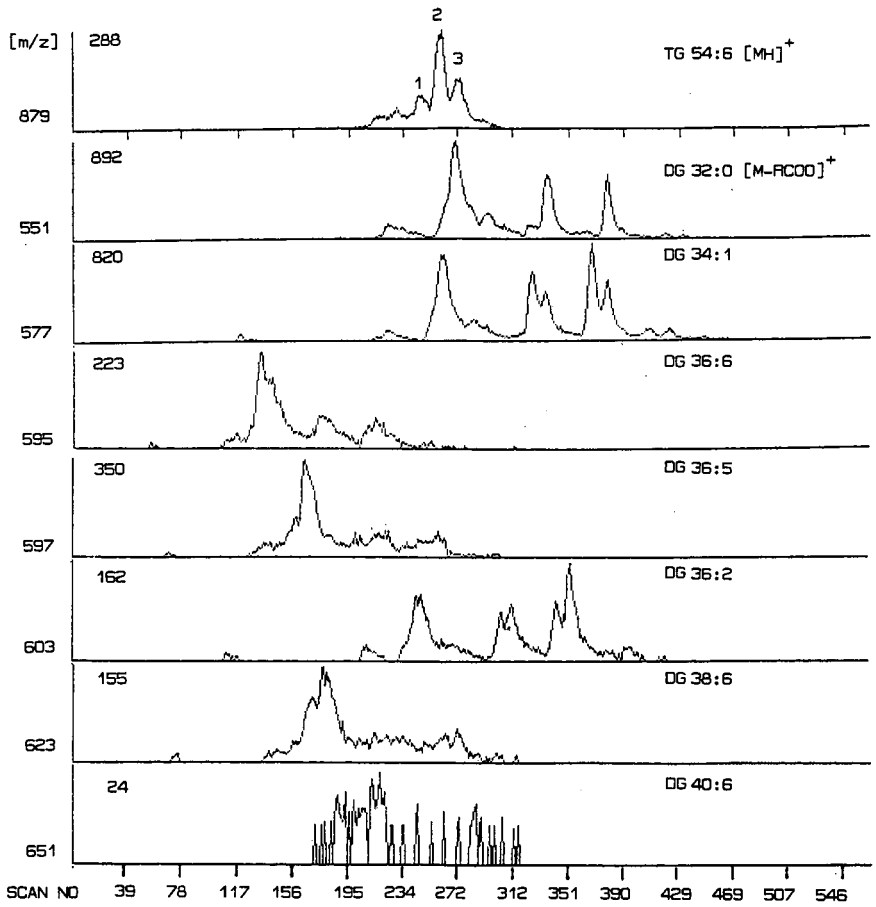

Fig. 9. Single ion plots in PCI for major diacylglycerol (DG) fragment ions $[M-RCOO]^+$ of isologous 54:6 triacylglycerols. TI, total PCI current; *m/z* values as identified by carbon number:double bond number. Values inside panels, ion counts for each scan. LC–MS conditions as in Fig. 6.

of the triacylglycerols was confirmed by NCI mass spectrometry with chloride attachment. Fig. 10 compares the full mass spectra obtained by PCI (panel A) and NCI (panel B) for the center section of the HPLC peak 4 (Fig. 7) corresponding to TG52:5. In addition to the molecular ions corresponding to triacylglycerols 50:4 (*m/z* 827), 52:5 (*m/z* 853), 54:6 (*m/z* 879), 56:7 (*m/z* 905), and 58:8 (*m/z* 931) seen in PCI, NCI reveals the presence of pseudomolecular ions for triacylglycerols 44:1 (*m/z* 783), 46:2 (*m/z* 809), 48:3 (*m/z* 835), 50:4 (*m/z* 861), 52:5 (*m/z* 887), 54:6 (*m/z* 913), 56:7 (*m/z* 939), 58:8 (*m/z* 965) and 60:9 (*m/z* 991). Fig. 11 compares the full mass spectra obtained by PCI (panel A) and NCI (panel B) for the center section of the HPLC peak 2 (Fig. 7) corresponding to the isologous TG54:6. The PCI spectrum yielded molecular ions only for the major polyunsaturated triacylglycerol species: TG48:3 (*m/z* 801); TG50:4 (*m/z* 827); TG52:5 (*m/z* 853); TG54:6 (*m/z* 879); TG56:7 (*m/z* 905); and TG58:8 (*m/z* 931), along with the corresponding diacylglycerol type of ions. From the NCI spectrum it is obvious that the triacylglycerol mixture is more complex and contains other species belonging to ECN 42: TG42:0 (*m/z* 757); TG44:1 (*m/z* 783); TG46:2 (*m/z* 809); TG48:3 (*m/z* 835); TG50:4 (*m/z* 861); TG52:5 (*m/z* 887); TG54:6 (*m/z* 913); TG56:7 (*m/z* 939); TG58:8 (*m/z* 965); and TG60:9

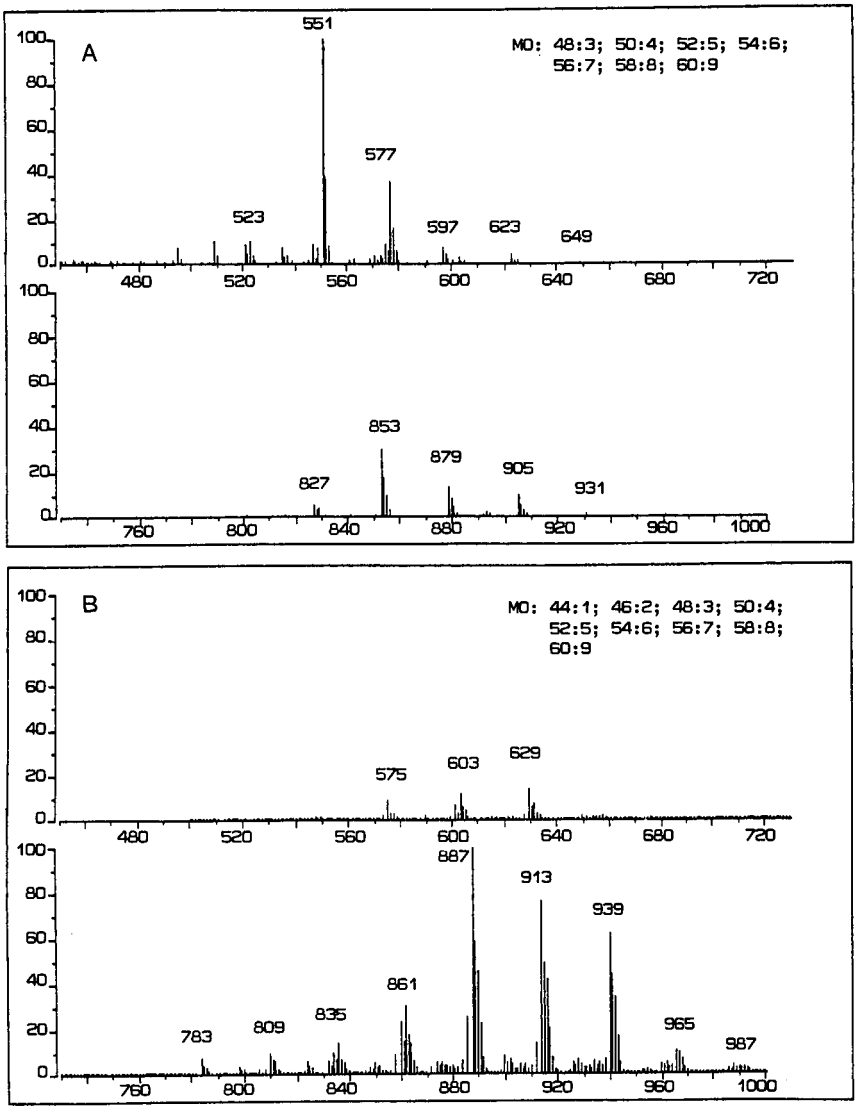

Fig. 10. Comparison of full mass spectra in (A) PCI and (B) NCI for the center sections of HPLC peak 4 (Fig. 7) corresponding to isologous 52:5 triacylglycerols. Solvent system: 20–90% linear gradient of propionitrile in acetonitrile containing 1% dichloromethane. Other LC–MS conditions as in Fig. 6.

(*m/z* 991). Only traces of diacylglycerol fragment ions were observed in the NCI spectrum obtained with chloride attachment.

Table II compares the recoveries of the different menhaden oil triacylglycerol species within ECN 36, 38 and 42 series as estimated by reversed-phase LC–MS with PCI and NCI and by calculation of the 1-random 2-random 3-random association based on the knowledge of the positional distribution of the fatty acids in menhaden oil triacylglycerols [14]. There is a reasonable agreement between the estimates from the PCI and NCI mass spectrometry, even though molecular species having more than 60 acyl carbons could not be estimated in the chloride attachment mode because the combined molecular weight exceeded the 1000 mass limit of the instrument. Furthermore, the measured values are reasonably close to the values calculated from the 1-random 2-random 3-random association of the fatty acids in the triacylglycerol species. This

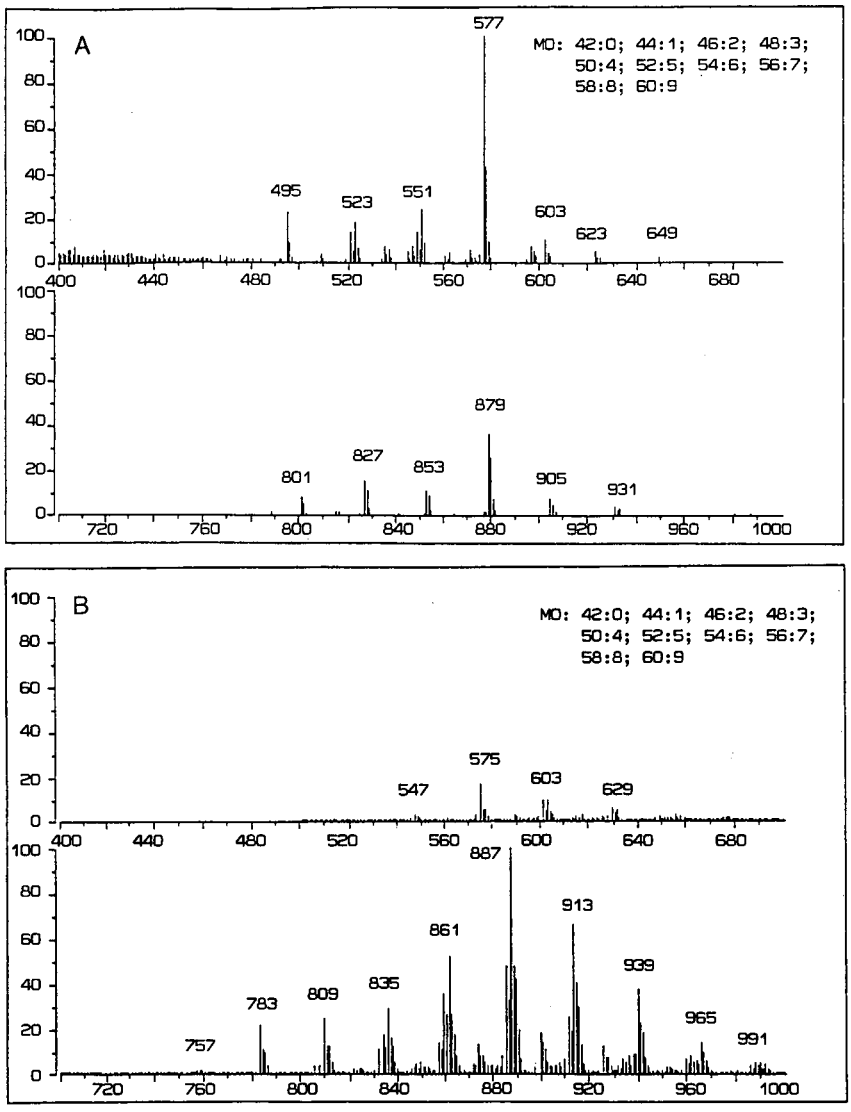

Fig. 11. Comparison of full mass spectra in (A) PCI and (B) NCI for the center section of HPLC peak 2 (Fig. 7) corresponding to a series of isologous 54:6 triacylglycerols. LC–MS conditions as in Fig. 10.

indicates that PCI of the polyunsaturated triacylglycerols yields nearly correct proportions of the molecular species, unlike the short and medium chain saturated fatty triacylglycerols, which gave low and variable yields of molecular ions in PCI. NCI with chloride attachment gave apparently correct proportions of molecular ions with both saturated and unsaturated triacylglycerols of short and long chain lengths.

DISCUSSION

The present study shows that a combination of HPLC with mass spectrometry is necessary for identification and quantitation of the molecular species of triacylglycerols in the more complex natural fats and oils. This is largely so because of the presence in the HPLC peaks of triacylglycerol species with closely similar or identical theoretical car-

TABLE II

COMPOSITION OF TRIACYLGLYCEROLS IN ECN 36, 38 AND ECN 42 OF MENHADEN OIL TRIACYLGLYCEROLS AS ESTIMATED BY REVERSED-PHASE LC–MS WITH POSITIVE AND NEGATIVE CHEMICAL IONIZATION (AREA %)

Molecular species	1-R-2-R-3-R[a] (Calculated)	PCI $[M]^+$	NCI $[M+35]^-$
ECN 36			
44:4	0.6	2.3	1.7
46:5	2.1	7.0	4.2
48:6	3.4	9.2	5.2
50:7	5.9	12.5	6.2
52:8	11.6	18.7	11.4
54:9	17.4	18.2	17.2
56:10	22.8	18.2	25.1
58:11	22.0	10.5	20.4
60:12	11.4	3.2	8.5
62:13	2.4	0.1	?[b]
ECN 38			
44:3	0.5	1.4	1.0
46:4	4.8	8.9	6.3
48:5	12.6	21.1	16.3
50:6	17.9	22.1	19.8
52:7	18.6	18.7	16.4
54:8	14.7	11.2	11.9
56:9	10.9	8.4	11.6
58:10	10.1	5.6	10.7
60:11	7.1	2.8	6.0
62:12	2.2	trace	?[b]
64:13	0.2	?[b]	?[b]
ECN 42			
44:1	3.7	2.1	3.0
46:2	5.6	3.8	5.5
48:3	8.6	12.6	8.4
50:4	12.1	20.0	12.8
52:5	21.6	26.8	24.0
54:6	26.2	22.8	27.7
56:7	16.4	9.9	13.6
58:8	4.9	1.8	3.9
60:9	0.6	trace	1.1

[a] 1-Random 2-random 3-random calculation.

[b] Combined molecular weight of ions $[M+Cl]^-$ exceeds the calibrated mass range of the instrument.

bon numbers. Furthermore, the elution of critical pairs of triacylglycerols over a wide range of theoretical ECN leads to increased overlapping and interdigitation of peaks. In the short chain triacylglycerols this additional resolution takes place within the saturated triacylglycerols. Since the butyrates, caproates and caprylates make up a high proportion of total triacylglycerols in the R-3 distillate of butteroil, they appear as prominent peaks in the HPLC profile. The order of elution is recognized in a modified form in the monoenoic and dienoic triacylglycerols, which occur in much smaller amounts in the distillate. This order of reversed-phase HPLC elution of the short chain saturated triacylglycerols is similar to that reported by Takamura *et al.* [15] for the acetates, butyrates and hexanoates when combined with palmitic and stearic acids in diacylglycerol acetates. It led to an effective separation of the butyrates, caproates and caprylates among the saturated triacylglycerols and the resolution of triacylglycerols with 0, 1, 2 or 3 saturated fatty acids per molecule of triacylglycerol within an equivalent carbon and double bond number. Surprisingly, the order of elution of the short-chain saturated triacylglycerols from the reversed-phase HPLC column is similar to that noted during polar capillary GC [11,16]. The butyrates would have been expected to be more polar than the corresponding caproates and caprylates and thus lead to an earlier elution from the reversed-phase column, which was not observed.

The LC–MS combination was equally effective in establishing the order of elution of the complex polyunsaturated triacylglycerols present in menhaden oil. In addition to resolution based on ECN and the separation of the critical pairs within each ECN as established for seed oils [2,3] we were able to recognize resolution within isologous series of triacylglycerol species. This resolution was based on the relative distribution of the carbon and double bond numbers among the fatty chains in the triacylglycerol molecules. The order of elution is similar to that observed for diacylglycerophospholipids [17,18] and the diacylglycerol dinitrobenzoates [19] where the saturated-polyunsaturated fatty acid combination is retained longer than the combination of two oligounsaturated fatty acids within the same equivalent carbon number (*e.g.* 18:2-18:2 eluted earlier than 16:0-20:4). This order of elution differs from that seen on polar capillary GC where the combination of the polyunsaturated and saturated fatty acid is eluted earlier than the combination of two oligounsaturated fatty acids (*e.g.* 16:0-20:4 eluted ahead of 18:2-18:2). Comparable pairs and triplets were found to result from the combination of other polyunsaturated fatty acids with saturated and oli-

gounsaturated fatty acids within an equivalent carbon and double bond number, which were eluted in a similar order of increasing retention time with increasing number of saturated fatty chains in the molecule.

The present study also shows that chloride attachment NCI mass spectrometry can greatly improve the identification and particularly the quantitation of the molecular species of complex triacylglycerols and yields nearly correct proportional response for the pseudomolecular ion. The increased sensitivity of detection of the ions eliminates the need for overloading the HPLC column in order to obtain sufficient number of ions for molecular weight determination. This extra sensitivity is especially important when using the direct liquid inlet interface which can admit only 1% of the total column effluent to the mass spectrometer. We have established that the increased sensitivity obtained by chloride attachment NCI of triacylglycerols is about 100 fold greater than that seen in PCI for total ion current and many more-fold higher when compared to the molecular ion yield obtained from the short-chain saturated triacylglycerols [9]. The high sensitivity and the proportionally correct ionization response allows the detection of both major and minor triacylglycerol species in a reversed-phase LC–MS run. Knowledge of the diacylglycerol fragment ions obtained by PCI, which is less sensitive and yields variable amounts of the ions, however, is necessary for the identification, although this requirement greatly reduces the overall sensitivity of determination of the molecular species of the triacylglycerols. The detection of diacylglycerols containing polyunsaturated fatty acids remains a problem in those instances where the specific polyunsaturated ions are absent from the PCI mass spectrum. On the basis of the relative retention time and the presence of the complementary saturated diacylglycerol ions, however, it is usually possible to establish the identity of the main molecular species of triacylglycerols in the major HPLC peaks also from PCI spectra. The improved triacylglycerol profiles resulting from the chloride attachment NCI permit the determination of the molecular weight and the order of elution of even minor molecular species in a complex triacylglycerol mixture.

Finally, this study confirms the universal applicability and high resolving power of the propionitrile–acetonitrile gradient as the mobile phase in HPLC of neutral lipids. Earlier Schulte [20] had demonstrated excellent resolution of seed oil triacylglycerols with propionitrile alone, while acetonitrile has been generally recognized as an excellent solvent for neutral lipids [1]. The propionitrile–acetonitrile gradient is also capable of accommodating up to 10% dichloromethane without loss of peak resolution. It is concluded, however, that even this reversed-phase HPLC system in combination with both PCI and NCI mass spectrometry cannot completely resolve and identify all fish oil triacylglycerols and some prefractionation [21] is clearly necessary.

ACKNOWLEDGEMENTS

These studies were supported by funds from the Heart and Stroke Foundation of Ontario, Toronto and the Medical Research Council of Canada, Ottawa, Canada.

REFERENCES

1 V. K. S. Shukla, *Progr. Lipid Res.*, 27 (1988) 5–38.
2 A. H. El Hamdy and E. G. Perkins, *J. Am. Oil Chem. Soc.*, 58 (1981) 867–872.
3 F. C. Phillips, W. L. Erdahl, J. D. Nadenicek, L. J. Nutter, J. Schmit and O. S. Privett, *Lipids*, 19 (1984) 142–150.
4 B. Herslof and G. Kindmark, *Lipids*, 20 (1985) 783–790.
5 L. R. Snyder, *J. Chromatogr. Sci.*, 8 (1970) 692.
6 E. Frede, *Chromatographia*, 21 (1986) 29–36.
7 L. Marai, J. J. Myher and A. Kuksis, *Can. J. Biochem. Cell Biol.*, 61 (1983) 840–849.
8 J. J. Myher, L. Marai, A. Kuksis and F. Manganaro, *J. Chromatogr.*, 283 (1984) 289–301.
9 A. Kuksis, L. Marai and J. J. Myher, *Lipids*, 26 (1991) 240–246.
10 M. J. McCarthy, A. Kuksis and J. M. R. Beveridge, *Can. J. Biochem.*, 10 (1962) 1693–1703.
11 J. J. Myher, A. Kuksis, L. Marai and P. Sandra, *J. Chromatogr.*, 452 (1988) 93–118.
12 A. Kuksis, L. Marai and J. J. Myher, *J. Am. Oil Chem. Soc.*, 66 (1989) 482, Abs. No. NN1.
13 M. J. Wojtusik, P. R. Brown and J. G. Turcotte, *Chem. Rev.*, 89 (1989) 397–406.
14 J.J. Myher, A. Kuksis and L-Y. Yang, *Biochem. Cell Biol.*, 68 (1990) 336–344.
15 A. Takamura, K. Takauchi, T. Asai, K. Kamiyasu, T. Ogawa and H. Tsukatani, *J. Lipid Res.*, 30 (1989) 219–224.
16 A. Kuksis, L. Marai and J. J. Myher, *J. Am. Oil Chem. Soc.*, 50 (1973) 193–201.
17 F. Hullin, H-Y. Kim and N. Salem, Jr., *J. Lipid Res.*, 30 (1989) 1963–1975.
18 A. Cantafora, M. Cardelli and R. Masella, *J. Chromatogr.*, 507 (1990) 339–349.
19 H. Takamura, H. Norita, R. Urade and M. Kito, *Lipids*, 21 (1986) 356–361.
20 E. Schulte, *Fette, Seifen, Anstrichm.*, 83 (1981) 289–291.
21 P. Laakso, W. W. Christie and J. Pettersen, *Lipids*, 25 (1990) 284–291.

Journal of Chromatography, 588 (1991) 89–98
Elsevier Science Publishers B.V., Amsterdam

CHROM. 23 533

General and selective isolation procedure for high-performance liquid chromatographic determination of anabolic steroids in tissues

Aldo Laganà*

Department of Industrial Chemistry, University of Bologna, Bologna (Italy)

Aldo Marino

Department of Chemistry, University "La Sapienza", Rome (Italy)

(First received March 14th, 1991; revised manuscript received May 21st, 1991)

ABSTRACT

A multi-residue method has been developed for the determination of anabolic steroids in animal tissue. The analytes are extracted from tissue with methanol and the extract is subjected to two solid-phase extractions, one using a non-specific adsorbing material, such as graphitized carbon black (Carbopack B), and the other Amberlite CG-400 I in the OH form. This procedure allowed the neutral anabolics (testosterone, trenbolone and progesterone) to be isolated and separated from the acidic type (phenolic group), such as diethylstilbestrol, oestradiol, zeranol/zearalenone and their respective metabolites. The determination was effected using high-performance liquid chromatography with different detectors (ultraviolet, fluorimetric and electrochemical). Several analytical parameters were studied: chromatographic conditions, recoveries, evaporation step, solvent flow-rate, cartridges reusability, interference of plastic cartridges. For all the anabolics investigated the recoveries were >83.6%.

INTRODUCTION

Anabolic compounds stimulate synthesis and thus increase the muscle size and strength in both humans and animals. Anabolic substances are used in animal production (cattle and sheep) to enhance rapid growth and to improve feed efficiency, resulting in economic benefits to both farmer and consumer. The compounds found to be effective in humans and animals are invariably steroids structurally related to the natural androgen testosterone, whereas in cattle either androgenic or oestrogenic agents or combinations of the two may be used. These compounds may be derived either from the natural steroids or from synthetic steroids, *e.g.*, oestradiol, testosterone, progesterone or trenbolone, or else may have a non steroid structure, *e.g.*, diethylstilbestrol, zeranol.

Improper use of these hormones or too short a withdrawal period between treatment and slaughter of the animals may result in high residual levels in the edible portion of the treated animals. The use of anabolics in animal feeds involves possible health risks if harmful residues remain in the meat products intended for human consumption [1].

At present, certain anabolic compounds can be legally given to farm animals in some countries but are banned in others. For example, the European Community (EEC) [2] has banned the use of all anabolic steroids because of their proven or alleged toxic and/or carcinogenic properties. Therefore the necessity to test for illegal use or to determine residue levels after legal use has led to a strong interest in methods for the detection of anabolizing agents in biological samples and in food products. Numerous techniques for determining these oestro-

0021-9673/91/$03.50

genic compounds and their metabolites have been reported.

The most frequently used techniques for the dosages concerned involve either chromatographic [thin-layer, high-performance liquid (HPLC) and gas chromatography (GC) and GC–mass spectrometry] [3–14] or immunochemical detection [15–18]. Many of these methods are tedious or comparatively insensitive. Immunoassays are highly sensitive, but analysis is limited to a single specific compound against which the antibody was raised and non-specific binding of a steroid antibody tends to produce false-positive results.

In analyses for single or multi-component anabolic compounds HPLC has proved to be an excellent separation, purification and detection technique. Ryan [19] reviewed its use in the analysis of hormone residues, including diethylstilbestrol (DES), oestradiol and zeranol. Other investigators have also reported the determination of zearalenone and α-zearalenol in porcine plasma, in chicken fat, heart and kidney and in animal feed. Groham *et al.* [20] developed a multi-residue analysis for anabolics (oestradiol, DES, zeranol, dienoestrol, hexoestrol and ethinyloestradiol) in meat. Medina and Sherman [21] described a multi-residue analysis for avian muscle tissue. Bagneris *et al.* [22] used liquid chromatography with fluorescence detection to determine zearalenone and zearalenol in animal feeds. Roybal *et al.* [23] described a method to determine zeranol, zearalenone and their metabolites in edible animal tissue. Frischkorn *et al.* [24] reported an LC system with voltammetric detection of several growth-promoting hormones.

The objectives of this study were to develop a method to resolve the anabolic steroids and their metabolites possessing high oestrogenic activities. The general procedure proposed consists of (i) a dual-column clean-up system for a methanol extract of from the tissue, one column containing a non-specific adsorbing material, such as graphitized carbon black (Carbopack B), and the other filled with Amberlite CG-400 I in the OH form; and (ii) the development of a reversed-phase HPLC method to separate the substances investigated followed by either UV detection or more sensitive and more highly specific fluorimetric or electrochemical detection.

EXPERIMENTAL

Reagents

Fig. 1 shows the structures of the compounds investigated. The anabolic compounds used as reference materials were obtained as follows: trenbolone (17β-hydroxy-4,9,11-estratien-3-one) from LabService (Bologna, Italy), DES [4,4′-(1,2-diethyl-1,2-ethenediyl)bisphenol], testosterone (17-β-hydroxy-4-androsten-3-one), progesterone (4-pregnen-3,20-dione) and 17β-oestradiol-[1,3,5-(10)-estratiene-3, 17-β-diol] from Sigma (St. Louis, MO, USA), taleranol [6-(6,10-dihydroxyundecyl)-β-resorcylic acid μ-lactone], zearalenol [6-(6,10-dihydroxyundecyl-*trans*-1)-β-resorcylic acid and zeranol [6-(6,10-dihydroxyundecyl)-β-resorcylic acid] from International Minerals and Chemical Corp. (Terre Haute, IN, USA). Standard solutions were prepared by dissolving accurately weighed 10-mg amounts of each reference standard in 100-ml volumetric flasks in methanolic solution. The solutions were then further diluted to obtain working standard solutions. The distilled water used was further purified by passing it through a Norganic cartridge (Millipore, Bedford, MA, USA). Acetonitrile of G Chromasolv grade (minimum transmittance 75% at 195 nm, 93% at 200 nm, 95% at 210 nm and 98% at 220 nm, path length 1 cm *vs.* water) was obtained from Riedel-de Haën (Hannover, Germany) and methanol, methylene chloride and tetrahydrofuran of HPLC grade from Carlo Erba (Milan, Italy). All other chemicals were of analytical-reagent grade (Carlo Erba) and were used as supplied.

Apparatus

Glass liquid–solid extraction columns (laboratory made) (6 cm × 8 mm I.D.) were filled with Carbopack B and columns (6 cm × 4 mm I.D.) were filled with Amberlite CG 400 I, both by a dry-packing technique. The columns were fitted with a Luer-type connection so that they could be inserted into the solid-phase extraction vacuum manifold (Supelco, Bellefonte, PA, USA). Carbopack B (200–400 mesh) was kindly supplied by Supelco. Amberlite CG-400 I (100–200 mesh) was obtained from Serva (Heidelberg, Germany). Small wads of quartz-wool were inserted in the head and tail of the glass columns.

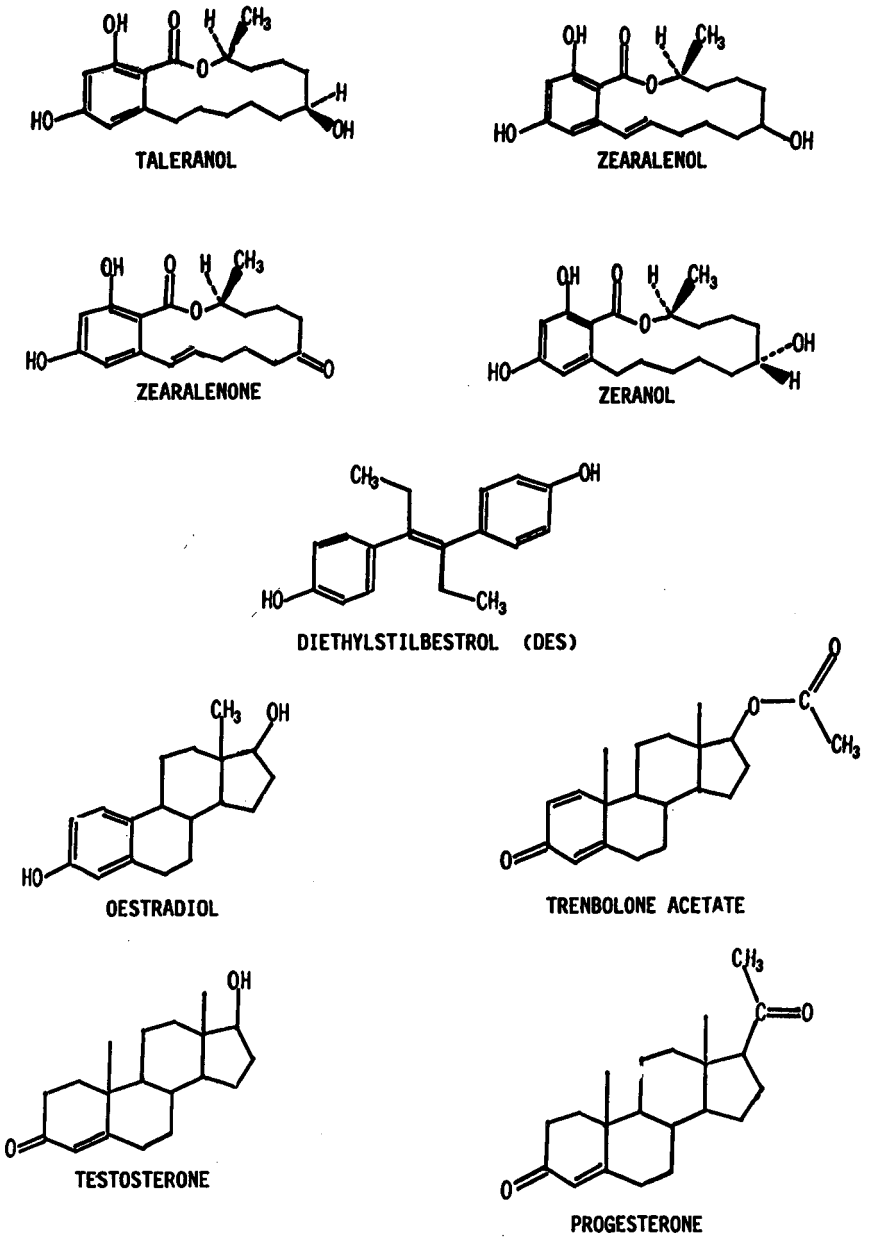

Fig. 1. Structures of compounds.

Instruments

A Series 410 liquid chromatograph (Perkin-Elmer, Norwalk, CT, USA) was used, equipped with a Rheodyne Model 7125 injection valve having a 100-μl loop, a Model LC 95 UV detector (Perkin-Elmer), a Model LS 3 spectrofluorimeter (Perkin-Elmer), and an electrochemical detector Model 5100A Coulochem (ESA, Bedford, MA, USA).

An LC-I 100 laboratory computing integrator (Perkin-Elmer) was used for peak-area measurements. A 25 cm × 4.6 mm I.D. column filled with 5-μm (average particle size) C_{18} reversed-phase

packing and a 2 cm × 4.6 mm I.D. Supelguard LC-18 (5 μm) column (both from Supelco) were used. A Polytron homogenizer (Kinematica, Kriens-LU, Switzerland) and a Uniset-ac ultrasonic bath (AGE Elettronica, Italy) were used.

Chromatographic conditions

The chromatographic conditions were selected according to the type of molecules involved and the detection technique. Acetonitrile–0.010 *M* KH_2PO_4 (pH adjusted to 3.0 with H_3PO_4) (48:52, v/v) was used for DES determination, with the electrochemical detectors set at 0.05 V (detector 1) and 0.30 V (detector 2), the flow-rate being 1.2 ml min^{-1}. The mobile phase for oestradiol determination was acetonitrile–0.010 *M* KH_2PO_4 (pH adjusted to 3.0 with H_3PO_4) (46:54, v/v). The fluorescence detector was set at λ_{ex} = 280 nm and λ_{em} = 308 nm, the flow-rate being 1.2 ml min^{-1}. For the determination of zeranol/zearalenone and their metabolites, 0.01 *M* KH_2PO_4 (pH adjusted to 3.0 with H_3PO_4)–acetonitrile–methanol–tetrahydrofuran (THF) (60:21:7:12, v/v) was used, the flow-rate being 1.5 ml min^{-1}. The electrochemical detectors were set at 0.05 V (detector 1) and 0.60 V (detector 2).

For testosterone, trenbolone and progesterone, an acetonitrile–water gradient was used, from 40% to 65% acetonitrile in 30 min, the flow-rate being 1.2 ml min^{-1}.

The absorbance of the effluent was monitored at 242 nm. In all experiments, the chromatographic column was operated at room temperature.

Quantitative data

The concentrations of anabolics in tissue samples were calculated by measuring the peak-area ratios of each oestrogenic compound to an internal standard and comparing peak-height ratios of the extracts with those of non-processed standards. The latter were prepared by adding an appropriate volume of anabolic working standard solution to an equal volume of the sample mixture used for the elution of anabolics from the clean-up column. To this solution were added 25 μl of solution containing the internal standard.

Pretreatment of column

Before use, the Carbopack B and resin columns were pretreated. The glass column was packed with 250 mg of Carbopack B and 5 ml of methanol, 15 ml of dichloromethane–methanol (70:30, v/v) and 10 ml of methanol–water (85:15, v/v) were successively passed through it. The glass columns used to be filled with resin were packed with 50 mg of Amberlite CG-400 I. The anion-exchange material was then purified and converted from the Cl^- to the OH^- form by treatment with 3 ml of 0.5 *M* sodium hydroxide solution and 8 ml of dichloromethane–methanol (70:30, v/v), then washed with 1 ml of water and finally deactived with 3 ml of 1 *M* HCl in methanol. This washing cycle was repeated four times, and finally the resin was converted into the OH^- form by passing through it 20 ml of 0.05 *M* sodium hydroxide solution and washed with 1 ml of water. When not in use, the column was kept in water.

Sample preparation, extraction and clean-up procedures

Portions of chicken (breast) muscle and ox muscle and liver were stored in a freezer. A 1-g amount of tissue was homogenized in 5 ml of methanol in the Polytron homogenizer and then sonicated for 5 min and centrifuged at 6000 rpm for 10 min (3956 *g*). Another 5 ml of methanol were added to the pellet and the extraction process was repeated and the supernates for each sample were pooled. To the remaining methanol solution, which had partially evaporated during the treatment, methanol was added to give a volume of 6.8 ml, then 1.2 ml of water were added in order to obtain 8 ml of a final solution of methanol–water (85:15, v/v). This mixture was allowed to percolate through the Carbopack B column and the eluate collected in a test-tube (I). The column was then washed with 2 ml of methanol–water (85:15, v/v), and the eluate again collected in the same test-tube (I). The column was washed with 2 ml of methanol, which was discarded.

Lastly, all the anabolizing agents except DES (already eluted into I) were eluted from the Carbopack column with 8 ml of dichloromethane–methanol (70:30, v/v) (test-tube II). The solution contained in test-tube I was allowed to percolate through one of the Amberlite columns, after which the column was washed with 1 ml of methanol and 1 ml of 1 *M* HCl (aspirating for 1 min in a vacuum after this last step). The DES was eluted into conical silanized tubes with 2 ml of 0.03 *M* HCl in acetoni-

trile–methanol (20:80, v/v). The eluate was evaporated to dryness using nitrogen at 40°C. The dried eluate was then immediately taken up with 100 μl of acetonitrile–0.010 *M* KH_2PO_4 (pH adjusted to 3.0 with H_3PO_4) (48:52, v/v) and a 50-μl portion was injected.

The solution contained in test-tube II was passed through the second resin-filled column, collecting the eluate in a silanized conical tube (III). The column was washed with 1 ml of methanol, added to tube III, and with 1 ml of 1 *M* HCl, which was discarded. The acidic anabolics (taleranol, zearalenol, zeranol, zearalenone and oestradiol) were eluted into silanized conical tube with 2 ml of 0.03 *M* HCl in acetonitrile–methanol (20:80, v/v). This eluate was evaporated to dryness with nitrogen at 40°C. A 100-μl portion of 0.010 *M* KH_2PO_4 (adjusted to pH 3.0 with H_3PO_4)–acetonitrile–methanol–THF (57:22:8:13, v/v) was added and a 50-μl portion was injected for the determination of zeranols. A 40-μl portion of the remaining amount was injected for the determination of oestradiol.

The solution of neutral anabolics contained in tube III was evaporated to dryness under nitrogen at 40°C, then taken up with 200 μl of methanol–water (50:50, v/v); 25 μl of *p*-chlorophenol (10 ng/μl) were added as internal standard (I.S.) and a 50-μl portion was injected.

RESULTS AND DISCUSSION

In biological fluids, anabolic steroids are present in a very complex matrix of other compounds, some of which are structurally very similar. Correct determinations of concentration can be achieved only by a combination of extensive purification of the sample and by using sensitive and specific detection systems. The main anabolizing agents are neutral or acidic compounds (phenolic group). Utilization of differences in functional groups may therefore considerably simplify the purification procedure needed for HPLC analysis.

Extraction of anabolic steroids from tissue

Extraction of anabolic steroids should be quantitative for all hormones at the ng/g level. The quantitative extraction of anabolic steroids from tissue without the formation of artefacts is extremely difficult, as isolation by means of solvents does not give a true picture of the extraction of the molecules present in the tissue. For this purpose, solvents must be used that have been shown to extract a wide range of lipids quantitatively and which are good solvents for anabolic steroids.

Methanol allows the complete removal of proteins [25] and quantitative extraction of hormones. Verbek [4] used a ternary system for the extraction of anabolics. Chloroform–methanol has been extensively used for the extraction of lipids from tissue [26], while Andersson and Sjovall [27] used *n*-hexane–isopropyl alcohol to isolate steroids from tissue. In comparative studies, Hara and Radim [28] also showed that most lipids can be quantitatively extracted with *n*-hexane–isopropyl alcohol.

As a preliminary measure, therefore, the extraction system must be selected on the basis of the solvent or solvent mixture which provides the highest relative extraction efficiency. For this purpose it is particularly important to use solvents that are capable of interacting with both the hydrophilic and hydrophobic components of the tissues. We investigated three solvent systems: methanol, methanol–chloroform and *n*-hexane–isopropyl alcohol (60:40, v/v). Comparative studies carried out on portions of animal tissues treated with the above substances showed that all three systems display comparable extraction percentages and therefore comparable extraction efficiencies. For our investigation we chose methanol, as it can be directly diluted with water in the ratio 85:15. This phase, which contains the extracted anabolic steroids, can then be percolated through the Carbopack B column, thus ensuring total adsorption of the dissolved substances. Because of their lower polarity, during Carbopack B adsorption the other two extraction systems allow only partial retention of these molecules. The problem can be solved by drying and dissolution in highly polar mixtures [methanol–water (85:15, v/v)], although the evaporation operation means a further loss of time. The main steps in the procedure during the analysis of anabolics from animal tissues are summarized in Fig. 2.

Adsorption of anabolic steroids on Carbopack B and Amberlite columns

The combination of an extraction trap containing a non-specific adsorbing material and the subsequent specific sorption of acidic compounds using a

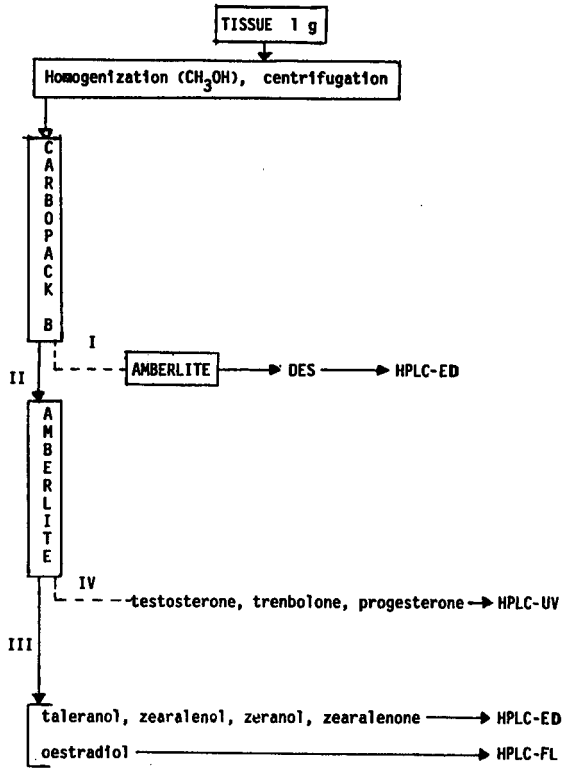

Fig. 2. Scheme of analytical procedure. Numbers I, II, III and IV relate to the various fractions eluted from extraction columns. ED = Electrochemical detection; FL = fluorimetric detection.

column filled with an anion exchanger allows us to simplify the isolation of the analytes and the subsequent identification of the anabolic steroids by means of multi-component analysis.

Acidic compounds display a typical behaviour on the Carbopack B surface. This effect can be explained by assuming that the Carbopack B surface is contaminated by certain positively charged chemical impurities, which may be a burnt-off residue left over from heating at 2700–3000°C of carbon black. Recently, we obtained experimental evidence [29,30] for the existence of a chromene-like structure in the surface framework of Carbopack B. This oxygen complex in the presence of oxygen and water can be rearranged to form a structure similar to benzopyran and benzopyrylium salts according to the following reaction:

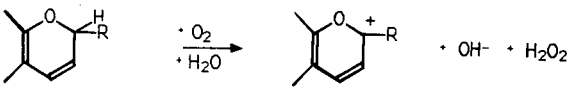

With acidic molecules, these salts are the cause of very strong interactions and so their elution requires solvent mixtures acidified with HCl [31,32]. However, recovery phases containing Cl^- ions are not compatible with our second extraction trap, because sorption is prevented from occurring as the Cl^- concentration has saturated the resin. Consequently, care has to be taken to avoid the formation of benzopyrylium salts.

Before use, the Carbopack B column is treated with non-aqueous solvents and solvent mixtures in order to avoid the formation of these salts. A partially aqueous solution [methanol–water (85:15, v/v)] does not allow these salts to be formed. All the anabolic steroids contained in the methanol–water (85:15, v/v) phase except DES are quantitatively adsorbed on the Carbopack B surface. Under conditions of percolation through the Carbopack B column the phenolic synthetic steroid (DES) is not adsorbed because its polarity exceeds that of the other anabolics. The solvent mixture dichloromethane–methanol (70:30, v/v) used to elute the anabolics quantitatively from the extraction column is also an ideal medium for their complete readsorption on the second isolation column (Amberlite).

Isolation of anabolics with specific functional groups on an exchanger converted to a suitable form is, in a sense, comparable to affinity chromatography. The only anabolics that can be sorbed on a resin in the OH^- form are those which can form complexes of the AOH^- type, where A indicates a generic acid molecule, whereas natural steroids (testosterone, trenbolone and progesterone) are not sorbed and therefore pass through the resin and can be analysed separately. Desorption of anabolic steroids from Amberlite was achieved by using acetonitrile–methanol (20:80, v/v), acidified with 0.03 *M* HCl.

The chloride ion has proved very effective in displacing the AOH^- complex from exchanger sites. It has been observed that if washing with 1 *M* HCl is omitted from the desorption operation, most of the non-exchanged resin sites will still be in the OH^- form. Therefore, these ions can enter into specific interactions with the phenol ions (hydrogen-type bond), thus extending the elution range. This behaviour has been tested experimentally by having the anabolic steroid mixture sorbed directly at the head of the Amberlite column.

In the procedure involving washing with 1 *M* HCl it was found that all the anabolics were eluted from the recovery mixture using only a 2-ml volume. On the other hand, in order to achieve quantitative recoveries, about 20 ml of acetonitrile–methanol (20:80, v/v) acidified with 0.03 *M* HCl were required.

Recoveries and reproducibility studies

Recoveries were initially performed on commercially available chicken breasts (muscle), ground beef (muscle) and ox liver. The samples were spiked with anabolics to a final concentration of 1–20 ppb (ng/g). Known amounts of hormones were added to the tissue solvent homogenate. The entire clean-up procedure and subsequent quantification were then performed. Recovery was calculated by subtracting the concentration of the endogenous steroid from the concentration of the steroid contained in the tissue to which it had been added; the difference was divided by the peak heights for the same spike dissolved in the final volume. The analytical recovery and the accuracy of the method at high (20 ng/g) and low (1 ng/g) muscle homogenate steroid contents were evaluated. In all instances the recoveries were at least 91.4 ± 4.1% for all substances except DES, for which it was at least 83.8 ± 4.0%. No difference in reproducibility was observed between samples prepared from different types of muscle tissue.

Chromatographic experiments

The chromatographic conditions were chosen on the basis of the function of the substances to be analysed and the detection technique used.

Optimum conditions for the separation of neutral compounds were found to be gradient elution from the acetonitrile–water (65:35, v/v) mobile phase in 30 min at a flow-rate of 1.2 ml min^{-1}; the peaks were detected at 242 nm. The chromatograms referring to the standard testosterone, trenbolone and progesterone mixture and a typical chromatogram referring to beef (muscle) to which the above anabolics had been added are shown in Fig. 3a and b. The type of acetonitrile used in the gradient elution is particularly important, because even when acetonitrile was used for HPLC the baseline was raised for high sensitivities. A gradient acetonitrile, "acetonitrile G", has recently come onto the market which minimizes this effect. For the separation of zeranol, zearalenone and their respective metabolites, iso-

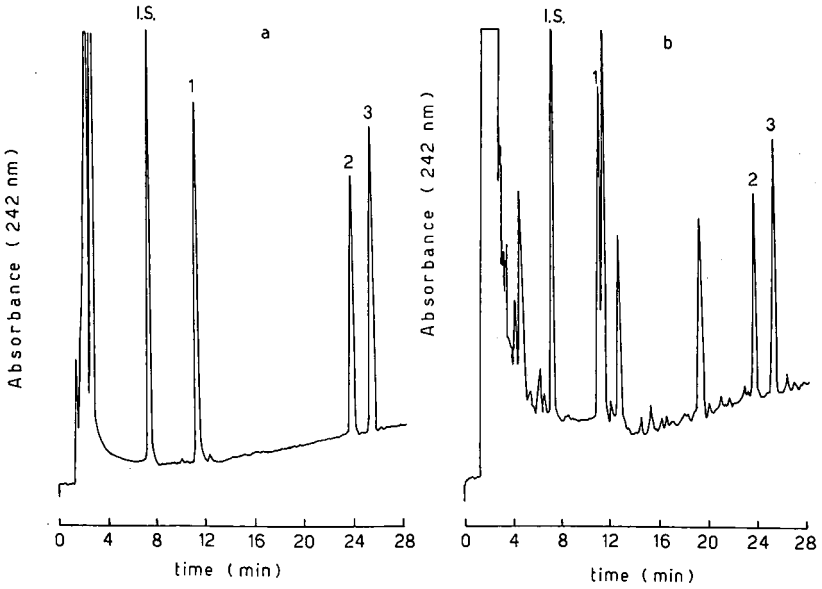

Fig. 3. HPLC separation of steroids with gradient elution and UV detection. Mobile phase, linear gradient of acetonitrile–water from 40% to 65% acetonitrile in 30 min; flow-rate, 1.2 ml min^{-1}; UV detection at 242 nm. (a) Standard mixture: I.S. = *p*-chlorophenol; 1 = testosterone; 2 = trenbolone; 3 = progesterone. (b) Chromatogram of extracted beef muscle spiked with (I.S.) *p*-chlorophenol, (1) testosterone (19 ng/g), (2) trenbolone (28 ng/g) and (3) progesterone (19 ng/g).

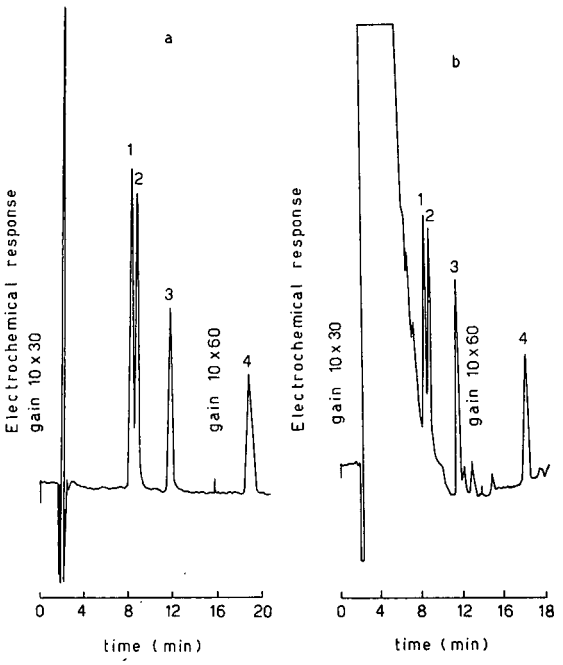

Fig. 4. HPLC of anabolics with isocratic elution and electrochemical detection. Mobile phase, 0.01 *M* KH_2PO_4 (adjusted to pH 3.0 with H_3PO_4)–acetonitrile–methanol–THF (60:21:7:12, v/v); flow-rate, 1.5 ml min^{-1}; electrochemical detection, detector 1 at 0.05 V, detector 2 at 0.60 V. (a) Standard mixture: 1 = taleranol; 2 = zearalenol; 3 = zeranol; 4 = zearalenone. (b) Chromatogram of extracted chicken muscle spiked with (1) taleranol (12 ng/g), (2) zearalenol (16 ng/g), (3) zeranol (13 ng/g) and (4) zearalenone (12 ng/g).

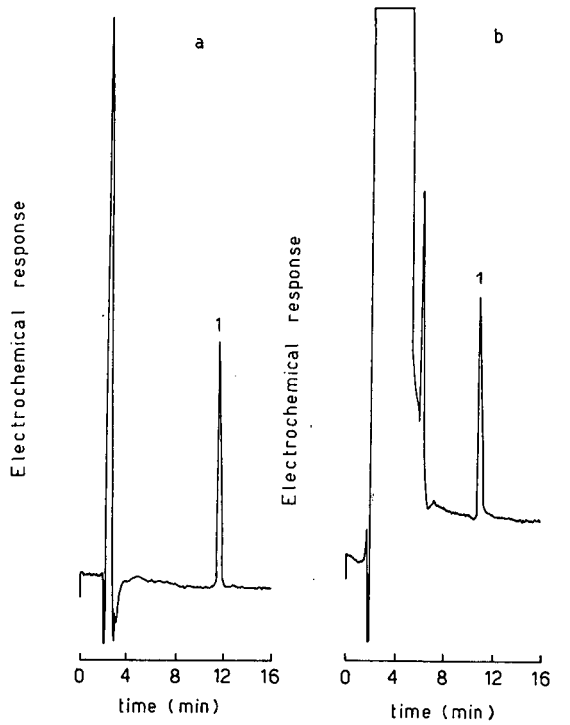

Fig. 5. HPLC of DES with isocratic elution and electrochemical detection. Mobile phase, 0.01 *M* KH_2PO_4 (adjusted to pH 3.0 with H_3PO_4)–acetonitrile (52:48, v/v); flow-rate, 1.2 ml min^{-1}; electrochemical detection, detector 1 at 0.05 V, detector 2 at 0.30 V. (a) Standard solution: 1 = DES. (b) Chromatogram of extracted beef muscle spiked with (1) DES (6 ng/g).

cratic elution with electrochemical detection is used.

Frischkorn *et al.* [24] used acetonitrile–water with LiCl and $LiClO_4$, which does not separate *cis*-zearalenone from *trans*-zearalenone. Roybal *et al.* [23] used methanol–sodium acetate, although this phase does not separate zearanol from taleranol. Our mixture completely separates taleranol from zeranol on the baseline and almost completely separates taleranol from zearalenol. The retention of these compounds is highly dependent on the acetonitrile and THF content. By maintaining the percentage of water constant and varying the percentage of organic solvents, the behaviour of these compounds was observed to vary. At higher percentages of tetrahydrofuran an enhanced separation between taleranol and zearalenol was obtained, although the zearalenone was eluted with a long retention time (> 30 min). An acceptable compromise was reached at higher acetonitrile percentages, although an unknown peak interfering with zeranol was found with tissue samples. The best mobile phase for separating the unknown substance from zeranol was found to be that reported under Experimental. The separation of a standard mixture of taleranol, zearalenol, zeranol and zearalenone is shown in Fig. 4a, and a chromatogram relating to the extract of a chicken tissue to which a mixture of zeranol and zearalenone and their respective metabolites had been added is shown in Fig. 4b.

For DES determination, isocratic elution with a low-potential electrochemical detector (detector 2, 0.30 V) was used. Frischkorn *et al.* [24] previously determined traces of oestrogenic growth-promoting hormones by HPLC with voltammetric detection by exploiting their different oxidation potentials. The use of a low oxidation potential allows greater

specificity to be achieved. Chromatograms relating to the standard DES solution and to an extract of beef muscle to which the latter had been added are shown in Fig. 5.

For the determination of oestradiol, its fluorescence emission was exploited. Oestradiol was eluted with the same fraction containing zeranol/zearalenone and their respective metabolites. Under the conditions of fluorescence detection, only oestradiol displays emission, which means that its determination is unaffected by other anabolic steroids. The chromatograms relating to the standard solution of oestradiol and an extract of bovine muscle spiked with this substance are shown in Fig. 6.

Evaporation

In all the methods in which samples are evaporated or concentrated in air or a nitrogen atmosphere, with or without heating, special care must be taken to avoid loss or structural modifications of the analytes. The significantly lower yields in the concentrated extracts are presumably due to partial adsorption of the anabolic steroid on the glass walls during evaporation of the extracts. This effect is observed in particular with DES, as its complete loss was observed during solvent removal. In order to reduce this problem and to obtain quantitative yields, silanized conical tubes were used in all operations involving concentration steps.

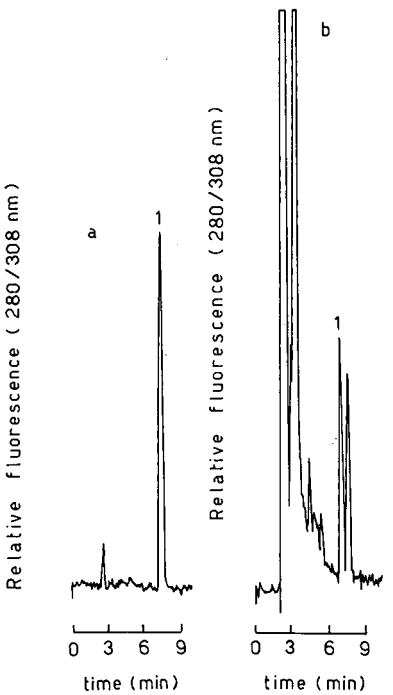

Fig. 6. HPLC of oestradiol with isocratic elution and fluorescence detection. Mobile phase, 0.01 *M* KH_2PO_4 (adjusted to pH 3.0 with H_3PO_4)–acetonitrile (54:46, v/v); flow-rate, 1.2 ml min^{-1}; fluorescence detection, λ_{ex} = 280 nm, λ_{em} = 308 nm. (a) Standard solution: 1 = oestradiol. (b) Chromatogram of extracted beef muscle spiked with (1) oestradiol (9 ng/g).

Solvent flow-rate

The solvent flow-rate through the column system was found to affect the recovery of anabolics from tissue extracts. With the Carbopack B column percolation flow-rates between 1 and 5 ml min^{-1} did not affect the recovery as Carbopack B has a surface area of 100 m^2 g^{-1} and interactions between the surface and analyte occur instantaneously.

The flow-rate through the resin column is more critical. Losses of zeranol/zearalenone and their respective metabolites, DES and oestradiol were observed when dichloromethane–methanol (70:30, v/v) was passed through the column at flow-rates higher than 1 ml min^{-1}.

Reusability

The reusability of both the Carbopack B and Amberlite columns was evaluated by performing repeated extractions of anabolics from homogenate tissue samples. After each use cycle the Carbopack B column was regenerated with 5 ml of dichloromethane followed by 5 ml of methanol. Resin regeneration was achieved using 20 ml of 0.05 *M* sodium hydroxide solution followed by 1 ml of water.

It was found that the entire solid-phase extraction system could be used only twice because, during the third cycle with homogenate tissue, the Carbopack B column became partially inefficient. This was probably due to the chemioadsorption of proteins on the carbon surface.

Plastic cartridges

As columns containing phases for solid-phase extraction have in recent years been made of plastic, experiments were carried out to see whether the cartridges could be packed with the phases used here. During the development of procedures to carry

out these analyses with plastic cartridges, the existence of a number of extraneous peaks was observed. These peaks varied according to the solvent used to elute the cartridges. A larger number of interferences were noted when mixtures containing dichloromethane were used. These interferents are present in the polypropylene of the cartridge and in the polyethylene of the frits. Repeated Soxhlet extraction with ethyl acetate and dichloromethane did not solve the problem of removing these interferences due to the commercial cartridges. For these reasons, plastic cartridges cannot be used, so that in the method proposed here, glass columns must be employed.

REFERENCES

1 *IARC Monograph on the Evolution of the Carcinogenic Risk of Chemicals to Humans*, International Agency for Research on Cancer, Lyon, 1979.
2 *Direttiva del Consiglio delle Comunità Europee*, G.U. CEE 21-5-1988, art. 7, 88/146/CEE.
3 P. L. Schuller, *J. Chromatogr.*, 31 (1967) 237.
4 R. Verbeke, *J. Chromatogr.*, 177 (1979) 69.
5 B. Boursier and M. Ledoux, *Analusis*, 9 (1981) 29.
6 M. B. Medina and D. P. Schwartz, *Food Additives Contam.*, 4 (1987) 415.
7 A. T. Rhys Williams, S. A. Winfield and R. C. Belloni, *J. Chromatogr.*, 235 (1982) 461.
8 W. G. de Ruig, T. D. B. van der Struijs and H. Hooyerink, *Fresenius' Z. Anal. Chem.*, 311 (1982) 405.
9 R. Verbeke and P. Vanhee, *J. Chromatogr.*, 265 (1983) 239.
10 E. H. J. M. Jansen, R. Both-Miedema, H. van Blitterswijk and R. W. Stephany, *J. Chromatogr.*, 299 (1984) 450.
11 E. H. J. M. Jansen, P. W. Zoontjes, H. van Blitterswijk, R. Both-Miedema and R. W. Stephany, *J. Chromatogr.*, 319 (1985) 436.
12 H. L. Trenholn and R. M. Warner, *J. Assoc. Off. Anal. Chem.*, 64 (1981) 302.
13 L. G. M. Tuinstra, W. A. Traag, H. J. Keukens and R. J. van Mazijk, *J. Chromatogr.*, 279 (1983) 533.
14 E. H. J. M. Jansen, J. Freudenthal, H. J. van Rossum, J. L. M. Litjens and R. W. Stephany, *Biomed. Environ. Mass Spectrom.*, 13 (1986) 245.
15 D. M. Henricks and A. K. Torrence, *J. Assoc. Off. Anal. Chem.*, 61 (1978) 1200.
16 E. H. J. M. Jansen, R. H. van den Berg, H. van Blitterswijk, R. Both-Miedema and R. W. Stephany, *Vet. Q.*, 6 (1984) 5.
17 E. H. J. M. Jansen, R. H. van den Berg, G. Zomer, R. Both-Miedema, C. Enkelaar-Willemsen and R. W. Stephany *Anal. Chim. Acta*, 170 (1985) 21.
18 E. H. J. M. Jansen, R. H. van den Berg, H. van Blitterswijk, R. Both-Miedema and R. W. Stephany, *Food Additives Contam.*, 2 (1985) 271.
19 J. J. Ryan, *J. Chromatogr.*, 127 (1976) 53.
20 H. G. Grohman, S. Jordan and H. J. Stan, *Fresenius' Z. Anal. Chem.*, 311 (1982) 399.
21 M. B. Medina and J. T. Sherman, *Food Additives Contam.*, 3 (1986) 263.
22 R. W. Bagneris, J. A. Gaul and G. M. Ware, *J. Assoc. Off. Anal. Chem.*, 69 (1986) 894.
23 J. E. Roybal, R. K. Munns, W. J. Morris, J. A. Hurlbut and W. Shimoda, *J. Assoc. Off. Anal. Chem.*, 71 (1988) 263.
24 C. G. B. Frischkorn, M. R. Smyth, H. E. Frischkorn and J. Golimowski, *Fresenius' Z. Anal. Chem.*, 300 (1980) 407.
25 H. F. De Brabander and R. Verbeke, *J. Chromatogr.*, 138 (1977) 131.
26 N. S. Radim, *Methods Enzymol.*, 14 (1969) 245.
27 S. H. G. Andersson and J. Sjovall, *Anal. Biochem.*, 134 (1983) 309.
28 A. Hara and N. S. Radim, *Anal. Biochem.*, 90 (1978) 420.
29 A. Di Corcia, R. Samperi, E. Sebastiani and C. Severini, *Anal. Chem.*, 52 (1980) 1345.
30 L. Campanella, A. Di Corcia, R. Samperi and A. Gambacorta, *Mater. Chem.*, 7 (1982) 429.
31 F. Andreolini, A. Di Corcia, A. Laganà, R. Samperi and G. Raponi, *Clin. Chem.*, 29 (1983) 2076.
32 F. Andreolini, C. Borra, A. Di Corcia, A. Laganà and R. Samperi, *Clin. Chem.*, 30 (1984) 742.

Journal of Chromatography, 588 (1991) 99–105
Elsevier Science Publishers B.V., Amsterdam

CHROM. 23 631

Determination of sterols and diterpenoids from brown algae (Cystoseiraceae)

Louis Piovetti* and Prosper Deffo

Laboratoire de Recherches de Chimie Marine des Organométalliques (RCMO), Université de Toulon et du Var, B.P. 132, F-83957 La Garde Cedex (France)

Robert Valls and Gilbert Peiffer

Laboratoire des Organo-Phosphorés, Université d'Aix-Marseille III, B.P. 552, F-13397 Marseille Cedex 13 (France)

(First received April 5th, 1991; revised manuscript received July 8th, 1991)

ABSTRACT

A high-performance liquid chromatographic method is described for the determination of secondary metabolites that belong to the brown algae of the Cystoseiraceae family. The study was focused on sterols, which are globally determined as fucosterol, and on the main structural families of diterpenes (mero- and linear diterpenes). An example is given of the analysis of three characteristic extracts from Atlantic and Mediterranean species.

INTRODUCTION

The lipidic extracts from the brown algae belonging to the Cystoseiraceae family have led to various studies on secondary metabolites [1–22]. They have permitted the identification of several sterols and diterpenes and the determination of the chemical structures of new compounds.

Gas chromatography and gas chromatography–mass spectrometry have often been used in order to identify sterols and determine their composition within the sterolic fraction [1,2,4,8]. The same holds for high-performance liquid chromatography (HPLC), which has been used to separate and purify the diterpenes [6,7,10–16,18–21]. However, we are not aware of any quantitative analysis that allows the precise evaluation of both the amount of sterols (the total amount of free sterols) and that of the main diterpenes from the studied algae. Therefore, such an investigation applied to all the seaweed species so far described could be useful for chemotaxonomic studies on the Cystoseiraceae family.

In this paper, we report a general method for the determination of secondary metabolites from brown seaweeds belonging to the Cystoseiraceae family using normal-phase HPLC. The study was focused on sterols, which are globally determined as fucosterol (**1**) and on the main structural families of diterpenes which have been isolated from Cystoseiraceae. These diterpenes include acyclic compounds with a geranylgeraniol skeleton (**2** and **3**) and meroditerpenes (diterpenes with mixed biogenesis) characterized by hydroquinonic methyl nucleus linked to a diterpenic chain. This chain might be either acyclic or cyclic (**4** and **6**) or even cyclically rearranged (**5A, B, C** and **D**).

EXPERIMENTAL

Instrumentation

Separations were carried out on an LDC liquid

0021-9673/91/$03.50

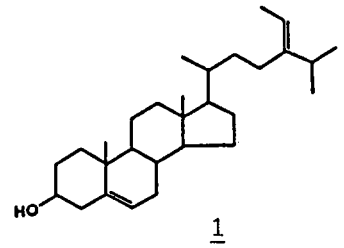

1

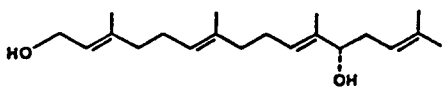

2

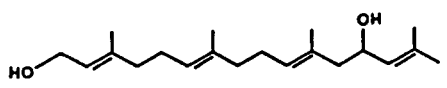

3

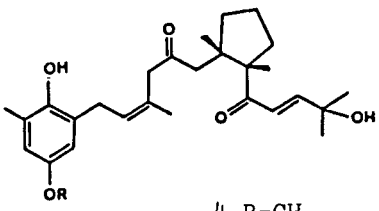

4 R=CH_3
6 R=H

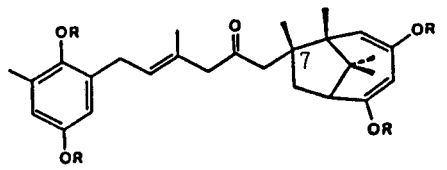

5 [A R=H; B R=H, C_7(S*)]

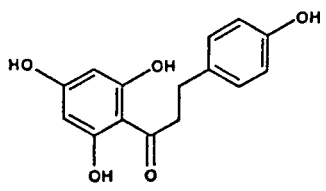

7

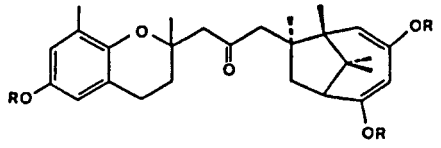

5 [C R=H; D R=H, C_7(R*)]

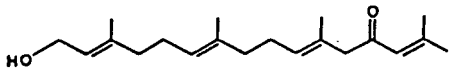

9

chromatograph (Milton Roy, Riviera Beach, FL, USA) equipped with a Constametric 3000 solvent-delivery system. A Spectromonitor 3100 X variable-wavelength UV detector set at 289 nm, with a 15-μl flow cell, was used for the analysis of meroditerpenes, whereas a Waters Assoc. Model R401 differential refractometer was used for the detection of sterols and linear diterpenes. Retention times and peak areas were obtained with a Shimadzu Chromatopac C-R6A integrator. The column (stainless steel, 250 × 4 mm I.D.) was packed with 5-μm silica (Partisil 5, Whatman, Clifton, NJ, USA). The flow-rate was 1 ml/min.

Solvents

The solvents used were ethyl acetate–isooctane (2,2,4-trimethylpentane) (2:3, v/v). They were freshly distilled and then filtered and degassed *in vacuo* through a sintered-glass filter.

Standards

Reference samples for the standardization were (1) Commercial fucosterol (**1**) (Sigma, St. Louis, MO, USA) for the analysis of the sterols; (2) bifurcadiol (**2**), eleganediol (**3**), methoxybifurcarenone (**4**) and a mixture of mediterraneols and bifurcarenone[a] (**5** and **6**) for the analysis of the diterpenes (compounds **2**, **3**, **4** and mixture **5–6** were previously isolated and identified from natural sources and purified by semi-preparative HPLC); and (3) commercial phloretin (**7**) (Sigma) and 2-methyl-2-butanol (**8**) (Carlo Erba, Milan, Italy), which can be used separately as an internal standard depending on the extract studied.

Sample preparation for HPLC analysis

Reference mixtures were obtained from stock solutions of each standard: 0.4–0.8 g/l in ethyl acetate for meroditerpenes (UV detection) and ten times more concentrated for sterols and linear diterpenes [refractive index (RI) detection]. Calibration was achieved using phloretin (**7**) as internal standard (stock solution at 0.5 g/l for UV detection and 2 g/l for RI detection) or using 2-methyl-2-butanol (**8**) as internal standard (stock solution at 5 g/l, only for RI detection). For the preparation of reference mixtures, 0.3 ml of internal standard solution was added to given volumes of each standard solution and diluted to 10 ml (UV detection) or 0.6 ml (RI detection) with ethyl acetate. Under identical conditions, a diethyl ether extract of the studied species (stock solution at 4 g/l for UV detection and 8 or 18 g/l for RI detection) was mixed with 0.3 ml of internal standard solution and diluted with ethyl acetate. This solution was injected directly into the HPLC apparatus.

[a] Compounds **5** and **6** are minor constituents of *Cystoseira stricta* which were isolated in very small amounts in order to effect their identification. Therefore, the mixture **5–6**, obtained from the extract studied, could be used for standardization purposes.

Standardization

Calibration graphs $w_i/w_{is} = f(A_i/A_{is})$, where w_i/w_{is} = sample weight per unit internal standard weight and A_i/A_{is} = sample peak area per unit internal standard peak area, were straight lines (regression lines were obtained from four points). Equations and correlation coefficients (r) are given in Table I for fucosterol and linear diterpene standards [RI detection; internal standard phloretin (**7**) or 2-methyl-2-butanol (**8**)] and in Table II for meroditerpene standards [UV detection at 289 nm; internal standard phloretin (**7**)].

RESULTS AND DISCUSSION

Compounds **1** to **6** were determined by normal-phase HPLC with isocratic elution with ethyl acetate–isooctane (2:3, v/v). Their retention times are given in Tables I and II and typical chromatograms of standard mixtures are shown in Figs. 1, 2.

Under these conditions, sterols are eluted together and globally determined as fucosterol (**1**), which is the main component of the sterolic fraction from the brown algae. The linear diterpenes (**2** and **3**) can only be detected by means of a differential refractometer. UV detection, which is more sensitive, could only be used for the linear diterpenes of the eleganolone (**9**) type, for which the conjugated ketone part of the molecule shows an absorption at 254 nm.For the meroditerpenes (**4–6**), which show a maximum wavelength at 289 nm, UV detection is more sensitive.

Ethyl acetate–isooctane has often been used as an eluent in thin-layer chromatography (TLC) or semi-preparative HPLC in order to separate the diterpenes from brown algae [6,7,16,18,19,21]. Isooctane is preferable to hexane because it is far less volatile and nearly as viscous (0.50 cP) as ethyl acetate. After several preliminary experiments, including gradient elution in combination with UV detection, we selected ethyl acetate–isooctane (2:3, v/v), which allows an optimum separation of the analyte compounds.

For the determination of these substances we used as an internal standard either phloretin (**7**) or the 2-methyl-2-butanol (**8**), depending on the extract studied. Phloretin (**7**), with its phenolic structure, is suitable for the determination of the meroditerpenes. It is eluted immediately after phlorogluci-

TABLE I

RETENTION TIMES AND EQUATIONS OF CALIBRATION GRAPHS FOR FUCOSTEROL AND LINEAR DITERPENE STANDARDS

Normal-phase column (silica, 5 μm) eluted with ethyl acetate–isooctane (2:3, v/v) at a flow-rate of 1 ml/min; RI detection; internal standard, (a) phloretin (**7**) or (b) 2-methyl-2-butanol.

No.	Compound	Retention time (min)	Equation	Correlation coefficient (r)	R.S.D.
1	Fucosterol	5.8	(a) $y = 2.12x - 0.02$	0.998	0.026
			(b) $y = 0.35x - 0.01$	0.999	0.003
2	Bifurcadiol	10.1	(a) $y = 1.71x + 0.005$	0.999	0.005
			(b) $y = 0.28x + 0.01$	0.999	0.012
3	Eleganediol	11.2	(a) $y = 1.77x + 0.02$	0.999	0.016
			(b) $y = 0.30x - 0.03$	0.999	0.022
7	Phloretin (I.S. 1)	15.8	–	–	–
8	2-Methyl-2-butanol (I.S. 2)	6.2	–	–	–

nol. Moreover, it allows the determination of sterols and linear diterpenes but not of eleganediol (**3**). By normal-phase HPLC this compound often leads to the formation of a small amount of an artifact which shows a retention time similar to that of **7**. In this instance, it is better to use the 2-methyl-2-butanol (**8**), which elutes between the sterols and the diterpenes. When a peak free of interferences is obtained, **8** is suitable as an internal standard for the determination of the sterols. Tables I and II give equations and correlation coefficients for the calibration graphs obtained with fucosterol and diterpene standards. The relative standard deviation (R.S.D.) of residues from the regression line of each standard is also given (calculated from four points).

The accuracy of the method is estimated, in the analysis range of each compound, by the difference ($d = w_i - \bar{w}_i$) between a known weight of the studied sample and the mean of the calculated value from the calibration graph (Table III). In this table, the value of the experimental coefficient ($t_{exp.}$) is lower than the corresponding Fischer coefficient (t) evaluated for a confidence level of 95%. On this basis, the method is not burdened with a systematic error.

The resuls obtained using this HPLC method are shown in Fig. 3 and Table IV. Three characteristic

TABLE II

RETENTION TIMES AND EQUATIONS OF CALIBRATION GRAPHS FOR MERODITERPENE STANDARDS

Normal-phase column (silica, 5 μm) eluted with ethyl acetate–isooctane (2:3, v/v) at a flow-rate of 1 ml/min; UV detection at 289 nm; internal standard, phloretin (**7**).

No.	Compound	Retention time (min)	Equation	Correlation coefficient (r)	R.S.D.
4	Methoxybifurcarenone	9.9	$y = 3.80x + 0.08$	0.999	0.024
5	Mediterraneols	12.7	$y = 20.50x + 0.73$	0.998	0.335
6	Bifurcarenone	14.0			
7	Phloretin (I.S)	15.8	–	–	–

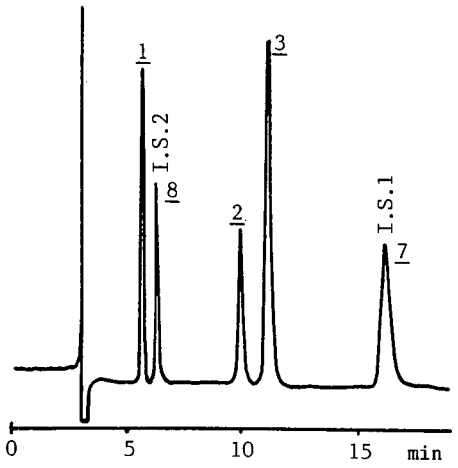

Fig. 1. Separation of standard mixtures of fucosterol and linear diterpenes. Experimental conditions as given in Table I. Fucosterol (**1**) (23.8 μg), bifurcadiol (**2**) (12 μg), eleganediol (**3**) (36 μg), phloretin (**7**) (20 μg) as internal standard 1,2-methyl-2-butanol (**8**) (49 μg) as internal standard 2.

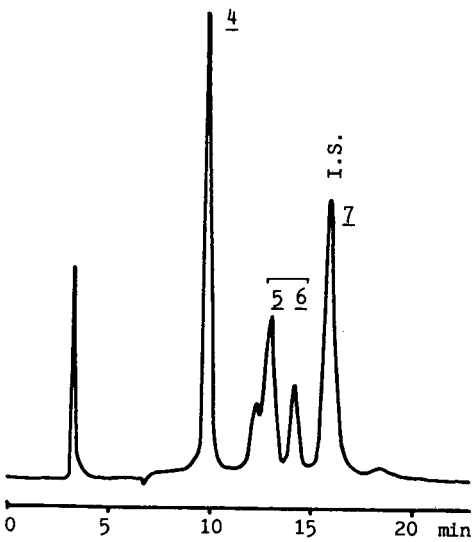

Fig. 2. Separation of a standard mixture of meroditerpenes. Experimental conditions as given in Table II. Methoxybifurcarenone (**4**) (1.2 μg), mediterraneols–bifurcarenone mixture (**5–6**) (5.9 μg), phloretin (**7**) (0.3 μg) as internal standard.

diethyl ether extracts from Atlantic and Mediterranean species were studied: *Bifurcaria bifurcata* from two different sources, (a) Atlantic coast, Cap Blanc, Morocco and (b) Atlantic coast, Casablanca, Morocco, and *Cystoseira stricta*, (c) from the Mediterranean coast, Saint Aygulf, Var, France. In Table IV, results are given in mg/g of dried seaweed. RI detection was used for sterols [globally determined as fucosterol (**1**)] and linear diterpenes **2** and **3**; UV detection was used for meroditerpenes **4** and **5–6**. Phloretin (**7**) was the internal standard in Fig. 3a and c′ and 2-methyl-2-butanol (**8**) in Fig. 3b and c.

The precision of the results is given as a percentage for a confidence level of 95% (Table IV). It was obtained from four measurements on the same sample.

TABLE III

COMPARISON OF A KNOWN WEIGHT OF STANDARDS WITH CALCULATED VALUE

$\bar{w}_i$ = Mean weight of sample calculated from the calibration graph; s = standard deviation from three measurements (n); w_i = known weight of sample; $t_{exp.} = d/s/\sqrt{n}$; t = corresponding Fischer coefficient for a confidence level of 95%.

No.	Compound	$\bar{w}_i$ (mg)	s (mg)	$d = w_i - \bar{w}_i$	$t_{exp.}$	t
1	Fucosterol	15.83	0.88	0.07	0.14	4.30
2	Bifurcadiol	24.03	1.46	0.03	0.04	4.30
3	Eleganediol	35.09	0.95	0.91	1.67	4.30
4	Methoxybifurcarenone[a]	0.374	0.008	0.007	1.62	4.30
5	Mediterraneols[a]	0.256	0.001	0.011	1.83	4.30
6	Bifurcarenone[a]					

[a] UV detection at 289 nm.

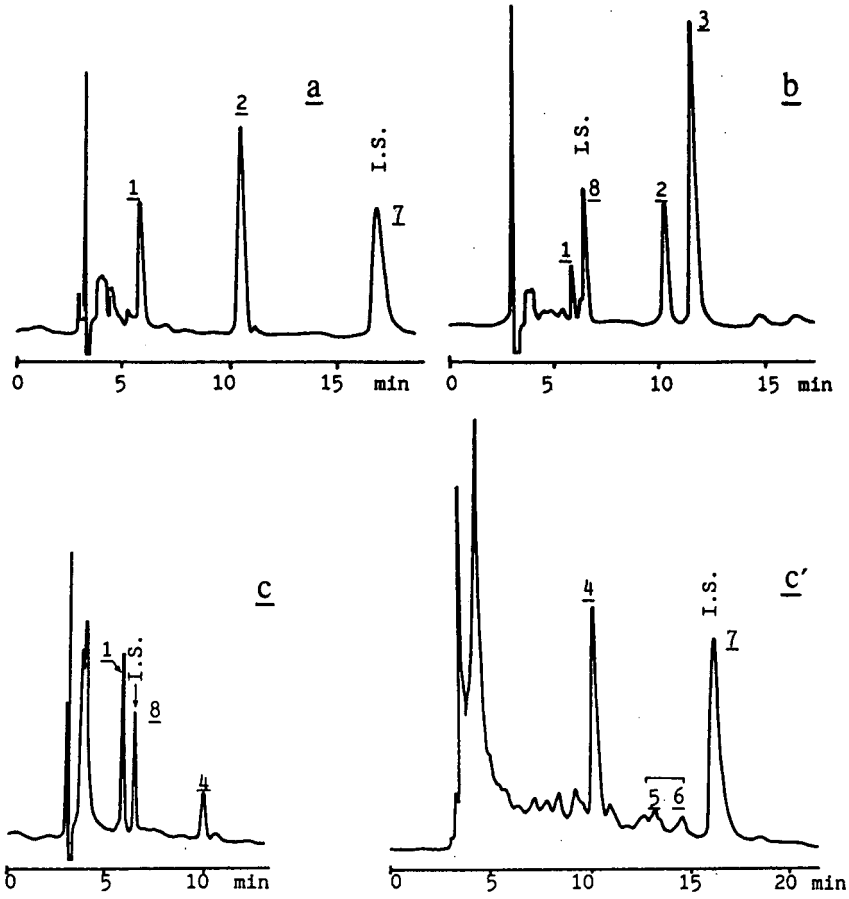

Fig. 3. Examples of HPLC analyses of diethyl ether extracts of (a) *Bifurcaria bifurcata* (Atlantic coast, Cap Blanc, Morocco) [experimental conditions as given in Table I (a)]; (b) *Bifurcaria bifurcata* (Atlantic coast, Casablanca, Morroco) [experimental conditions as given in Table I (b)]; (c) *Cystoseira stricta* (Mediterranean coast, Saint Aygulf, Var, France) [experimental conditions as given in Table I (b)]; (c') the same as (c), but experimental conditions as given in Table II.

The limit of detection was evaluated per gram of dried seaweed for each compound. The values were 0.20 mg/g (**7** as I.S.) and 0.01 mg/g (**8** as I.S.) for sterols; 0.24 mg/g (**7** as I.S.) and 0.57 mg/g (**8** as I.S.) for bifurcadiol (**2**); 0.44 mg/g (**8** as I.S.) for eleganediol (**3**); 0.015 mg/g (**7** as I.S.) for methoxybifurcarenone (**4**); and 0.22 mg/g (**7** as I.S.) for the mixture of mediterraneols and bifurcarenone (**5**–**6**).

CONCLUSIONS

This work, which was undertaken from a chemotaxonomic point of view, satisfies a double purpose: first, a rigorous phytochemical comparison between the species studied, and second, the evaluation of the geographic and seasonal evolution of their chemical components. This was achieved by means of a rapid, easy, reproducible method which could be applied to the determination of other secondary metabolites from different classes of seaweeds: (a) the sterols from red and green algae and (b) the diterpenoids eluted between sterols and phloretin (**7**) when using normal-phase HPLC for the determination.

TABLE IV

COMPOSITION OF EXTRACTS ORIGINATING FROM BROWN ALGAE BELONGING TO THE CYSTOSEIRACEAE FAMILY

(a) *Bifurcaria bifurcata* (Ross) (Atlantic coast, Cap Blanc, Morocco); (b) *Bifurcaria bifurcata* (Ross) (Atlantic coast, Casablanca, Morocco); (c) *Cystoseira stricta* (Mont.) Sauv. (Mediterranean coast, Saint Aygulf, Var, France). Results are given in mg/g of dried seaweed. Analyses were carried out in quadruplicate on the same sample.

No.	Compound	Amount (mg/g)					
		(a)	Precision (%)[a]	(b)	Precision (%)[a]	(c)	Precision (%)[a]
1	Fucosterol[b]	1.34	7.1	0.70	6.8	1.40	3.4
2	Bifurcadiol	4.41	2.5	3.97	10.8	–	–
3	Eleganediol	–	–	10.47	2.3	–	–
4	Methoxybifurcarenone[c]	–	–	–	–	0.29	5.5
5	Mediterraneols[c]	–	–	–	–	0.63	2.5
6	Bifurcarenone[c]						

[a] Precision for a confidence level of 95%.
[b] Total amount of free sterols.
[c] UV detection at 289 nm.

REFERENCES

1 G. Combaut, Y. Bruneau, G. Jeanty, C. Francisco, J. Teste and L. Codomier, *Phycologia*, 15 (1976) 275.
2 G. Combaut, L. Codomier and J. Teste, *Phytochemistry*, 20 (1981) 2036.
3 E. Fattorusso, S. Magno, L. Mayol, C. Santacroce, D. Sica, V. Amico, G. Oriente, M. Piatelli and C. Tringali, *Tetrahedron Lett.*, 12 (1976) 937.
4 C. Francisco, G. Combaut, J. Teste and B. F. Maume, *Biochim. Biosphys. Acta*, 487 (1977) 115.
5 C. Francisco, G. Combaut, J. Teste and M. Prost, *Phytochemistry*, 17 (1978) 1003.
6 C. Francisco, B. Banaigs, J. Teste and A. Cave, *J. Org. Chem.*, 51 (1986) 1115.
7 C. Francisco, B. Banaigs, M. Rakba, J. Teste and A. Cave, *J. Org. Chem.*, 51 (1986) 2707.
8 J. Artaud, M. C. Iatrides, C. Tisse, J. P. Zahra and J. Estienne, *Analusis*, 8 (1980) 277.
9 V. Amico, G. Oriente, M. Piatteli, O. Ruberto and C. Tringali, *Phytochemistry*, 19 (1980) 2759.
10 V. Amico, G. Oriente, M. Piattelli, G. Ruberto and C. Tringali, *Phytochemistry*, 20 (1981) 1085.
11 V. Amico, G. Oriente, M. Piattelli, G. Ruberto and C. Tringali, *Phytochemistry*, 21 (1982) 421.
12 V. Amico, P. Neri, M. Piattelli and G. Ruberto, *Phytochemistry*, 26 (1987) 2637.
13 V. Amico, M. Piattelli, F. Cunsolo, P. Neri and G. Ruberto, *Gazz. Chim. Ital.*, 118 (1988) 193.
14 V. Amico, M. Piattelli, F. Cunsolo, P. Neri and G. Ruberto, *J. Nat. Prod.*, 52 (1989) 962.
15 J. F. Biard, J. F. Verbist, R. Floch and Y. Letourneux, *Tetrahedron Lett.*, 21 (1980) 1849.
16 H. H. Sun, N. Ferrara, O. McConnel and W. Fenical, *Tetrahedron. Lett.*, 21 (1980) 3123.
17 M. Higgs and L. J. Mulheirn, *Tetrahedron*, 37 (1981) 3209.
18 B. Banaigs, C. Francisco, E. Gonzalez, L. Codemier and W. Fenical, *Tetrahedron Lett.*, 23 (1982) 3271.
19 B. Banaigs, C. Francisco, E. Gonzalez and W. Fenical, *Tetrahedron*, 39 (1983) 629.
20 G. Combaut and L. Piovetti, *Phytochemistry*, 22 (1983) 1787.
21 R. Valls, B. Banaigs, C. Franscisco, L. Codomier and A. Cave, *Phytochemistry*, 25 (1986) 751.
22 L. Semmak, A. Zerzouf, R. Valls, B. Banaigs, G. Jeanty and C. Francisco, *Phytochemistry*, 27 (1988) 2347.

Journal of Chromatography, 588 (1991) 107–114
Elsevier Science Publishers B.V., Amsterdam

CHROM. 23 614

Applications of automated amino acid analysis using 9-fluorenylmethyl chloroformate

Paul A. Haynes* and David Sheumack

School of Chemistry, Macquarie University, North Ryde, NSW 2109 (Australia)

Lisa G. Greig and Jeffrey Kibby

ICI Instruments, Dingley, Victoria 3172 (Australia)

John W. Redmond

School of Chemistry, Macquarie University, North Ryde, NSW 2109 (Australia)

(First received February 26th, 1991; revised manuscript received July 3rd, 1991)

ABSTRACT

A rapid and sensitive fully automated method for the determination of primary and secondary amino acids in different matrices is described. Amino acids are derivatized with 9-fluorenylmethyl chloroformate using an automated precolumn derivatization technique. Data are presented to show that the technique is both reproducible and highly sensitive. Applications of the technique are presented, including the analysis of peptide and protein hydrolysates and the profiling of free amino acids in physiological fluids.

INTRODUCTION

In recent years, the analysis of amino acids using precolumn derivatization and reversed-phase high-performance liquid chromatography (RP-HPLC) separation of the derivatives has become widely accepted. This approach requires much shorter analysis times and gives greater sensitivity than the traditional methods using ion-exchange chromatography and postcolumn derivatization [1].

A number of reagents have been used for precolumn derivatization, including phenyl isothiocyanate (PITC) [2–4], *o*-phthaldialdehyde (OPA) [5–8], 1-dimethylaminophthalene-5-sulphonyl (dansyl) chloride [9–11] and 9-fluorenylmethyl chloroformate (Fmoc-Cl) [12–16]. The development of increasingly sophisticated autosamplers has allowed several of these derivatization methods to be automated, with both the derivatization and analysis performed by the autosampler. There are a number of automated amino acid analysis systems available based on precolumn derivatization, such as those using Fmoc [17,18], dansyl-Cl [19], PITC [20,21] and a combination of OPA and Fmoc [22]. Automated procedures are desirable in situations where large numbers of samples are to be analysed, such as routine quality control testing or the screening of biological samples in the study of amino acid metabolism or acidopathies.

The currently available automated Fmoc methods [17,18] suffer from the same problems as the manual derivatization procedure: a solvent extraction to remove excess of reagent can cause errors in the quantification of the hydrophobic derivatives, and when a solvent extraction is not used, quantification of histidine is still problematic as it forms

0021-9673/91/$03.50

multiple derivatives. Derivatization with dansyl-Cl [19] is slow, and the quantification of histidine is also difficult as it again forms multiple derivatives. The major difficulty in automating the PITC procedure is that it is necessary to remove all traces of derivatizing reagent using high vacuum [23], although recent efforts [21] have avoided this problem by using solvent extraction to remove the excess of reagent. An automated procedure using a combination of OPA and Fmoc overcomes the problem of the instability of the OPA derivatives, but sophisticated detection is required to determine the two different derivatives.

In a previous paper [24] we described a method for derivatization using Fmoc which does not require a solvent extraction and which gives single stable derivatives for the common protein amino acids. We report here details of an automated amino acid analysis system, using the Fmoc reaction chemistry described previously, which is highly sensitive and reproducible and carries out derivatization and analysis in 30 min. The HPLC separation uses a phosphate buffer eluent rather than an acetate buffer as was used in the manual derivatization procedure [24]. This change gave an improved separation and a considerable increase in effective column lifetime. The system has been used for the analysis of amino acids in different matrices including protein hydrolysates and physiological fluids.

EXPERIMENTAL

Apparatus

The chromatographic system consisted of two LC1100 HPLC pumps controlled by a DP800 chromatography data station, a TC1900 column heater and an LC 1250 fluorescence detector (excitation wavelength 263 nm, emission wavelength 313 nm) or LC 1200 UV detector (absorbance wavelength 263 nm) (all from ICI Instruments). The column used was a 150 × 4.6 mm I.D. Spherisorb 3-μm ODS-2 coupled to a 15 × 3.2 mm I.D. Brownlee Newguard 7-μm ODS guard column. The DP800 chromatography data station was used to collect the data and to control an LC 1600 autosampler which was modified by ICI Instruments to prevent cross-contamination between samples and reagents. A continuous wash solution of 10% acetonitrile was drawn through the needle housing by a vacuum source, which was adjusted to give a flow-rate of the wash solution of *ca.* 10 ml/h.

Reagents and materials

All aqueous solutions were prepared with water purified with a Milli-Q purification system (Millipore). Fmoc-Cl (Sigma, St. Louis, MO, USA) was dissolved in acetonitrile (Mallinckrodt Australia, HPLC grade) as a 4.16 mg/ml solution (16 m*M*). Borate buffer was prepared from 200 m*M* boric acid (Ajax Chemicals, Sydney, Australia) solution adjusted to pH 8.5 with 5 *M* sodium hydroxide solution prepared from sodium hydroxide pellets (BDH, Poole, UK). The alkaline cleavage reagent was prepared daily in 250-μl batches by mixing 170 μl of 850 m*M* sodium hydroxide solution with 75 μl of 500 m*M* hydroxylamine hydrochloride (Aldrich, Milwaukee, WI, USA) solution and 5 μl of 2-(methylthio)ethanol (Aldrich). The quenching reagent was acetonitrile–water–acetic acid (20:3:2).

Ammonium dihydrogenorthophosphate (Merck, Darmstadt, Germany) stock solution (2.67 *M*), used for preparation of HPLC eluents, was adjusted to pH 6.5 with ammonia solution (Ajax AR Select). Sepramar amino acid calibration standard A was purchased from BDH and individual amino acid standards from Sigma, Angiotensin-II was from Auspep (South Melbourne, Australia), neurotensin, pepsin and chicken egg white lysozyme from Sigma and chymotrypsinogen-A from Boehringer (Mannheim, Germany).

Chromatographic separation

Separation of the Fmoc amino acid derivatives was carried out using a binary gradient. Eluent A was 20 m*M* ammonium dihydrogenorthophosphate (pH 6.5)–methanol (85:15) and eluent B was acetonitrile–water (90:10). The flow-rate was constant at 1.0 ml/min and the column was maintained at 35°C. The gradients used for protein hydrolysates and physiological samples are shown in Table I.

Hydrolysis procedure

Samples were placed in glass autosampler vials (ICI Instruments), dried in a Speed Vac vacuum centrifuge (Savant Instrument, Hicksville, NY, USA) for 1 h and then placed in a hydrolysis vessel (Pierce, Rockford, IL, USA). A 500-μl volume of 6 *M* hydrochloric acid (Pierce) was added to the

TABLE I

CHROMATOGRAPHIC GRADIENT CONDITIONS FOR Fmoc AMINO ACID ANALYSIS

Eluent A–B. A = 20 m*M* ammonium dihydrogenorthophosphate–methanol (85:15) (pH 6.5); B = acetonitrile–water (90:1). Flow-rate = 1.0 ml/min.

Protein hydrolysates		Physiological samples	
Time (min)	B (%)	Time (min)	B (%)
0	18	0	18
2	18	2	18
3	23	3	23
6	23	10	23
16	40	20	36
17	45	21	48
20	45	26	48
22	55	28	55
23	99	29	99

bottom of the vessel, which was then flushed with helium and evacuated. The hydrolysis was carried out at 110°C for 24 h, and the samples were then dried in the vacuum centrifuge. A 10-μl volume of triethylamine–ethanol–water (2:2:1) was added to each sample and evaporated to remove residual hydrochloric acid and the residues were then dissolved in 5 μl of the derivatization buffer.

Physiological sample preparation

Plasma samples were deproteinized by mixing vigorously with acetonitrile (1:3, v/v) and centrifuging at 12 000 *g* for 3 min [25]. Aliquots of the supernatant were evaporated to dryness in the vacuum centrifuge and reconstituted in derivatization buffer.

Derivatization procedure

The derivatization of amino acid samples dissolved in borate buffer (5 μl) was performed in the sample vial using an autosampler programme. An aliquot (5 μl) of each of the three derivatization reagents [24] was transferred to the sample vial in turn and mixed with the sample using an effective mixing procedure developed for the LC 1600 autosampler specifically for this application. A description of the full autosampler program is shown in Table II. The amounts of reagents used and sample injected can be adjusted as required.

RESULTS AND DISCUSSION

Stability of derivatives

The stability of the Fmoc derivatives at room temperature (21°C) was investigated by repeated injection of constant-volume aliquots, containing 100 pmol of each amino acid, from a single derivatization of an amino acid standard hourly for 24 h. All the amino acid derivatives were stable over this time, with relative standard deviations for normalized peak areas varying between 0.8 and 5.0% as shown in Table III. The monosubstituted histidine derivative gave a relative standard deviation of 0.9%, which indicates that it is far more stable than the disubstituted derivative, which has been reported previously [17] to show breakdown of 49.4% in

TABLE II

SEQUENCE OF STEPS INVOLVED IN AUTOMATED DERIVATIZATION PROCEDURE

Step	Description	Step	Description
1	Wash needle	9	Mix in sample vial
2	Collect Fmoc reagent	10	Wait for reaction time 2
3	Eject to sample vial	11	Collect quenching reagent
4	Mix in sample vial	12	Eject to sample vial
5	Wait for reaction time 1	13	Mix in sample vial
6	Wash needle	14	Wash needle
7	Collect cleavage reagent	15	Collect required quantity of derivatized sample
9	Eject to sample vial	16	Inject onto column

TABLE III

STABILITY OF Fmoc AMINO ACID DERIVATIVES

Values shown are relative standard deviations (R.S.D.) of normalized peak areas of Fmoc amino acids calculated from repeated injection of aliquots from a single derivatization of an amino acid standard hourly for 24 hours.

Amino acid	Peak-area R.S.D. (%) ($n = 24$)	Amino acid	Peak-area R.S.D. (%) ($n = 24$)
Asp	2.9	Tyr	1.0
Glu	2.4	Arg	0.9
Ser	1.9	Val	2.4
His	0.9	Met	1.8
Gly	2.1	Ile	3.5
Thr	1.7	Leu	4.1
Ala	0.8	Phe	5.0
Pro	0.8	Lys	3.1

similar stability trials. These results show that the amino acid derivatives are stable enough to allow for reanalysis of previously derivatized samples at any time within 24 h.

Limit of detection

The Fmoc derivatives of amino acids are highly fluorescent, and can be detected at very low levels [13,17,22]. The detection limit for hydroxyproline, chosen for this study as it was not present in reagent blank derivatizations, was 50 fmol at a signal-to-noise ratio of 3:1. In practice, the limit of detection for routine analysis is governed by the background levels of amino acids in both reagents and samples.

Reproducibility and linearity of derivatization

The reproducibility of the automated derivatization procedure was established at two different

TABLE IV

RELATIVE STANDARD DEVIATIONS FOR PEAK AREAS AND RETENTION TIMES OF Fmoc AMINO ACIDS PREPARED USING MANUAL AND AUTOMATED PROCEDURES

Values for peak areas and retention times for automated and manual derivatization procedures. Values for peak areas for manual procedure from Haynes *et al.* [24].

Amino acid	Peak-area R.S.D. (%), 100 pmol ($n = 20$)	Retention-time R.S.D. (%) ($n = 20$)	Peak-area R.S.D. (%), 5 pmol ($n = 10$)	Peak-area R.S.D. (%) (manual procedure), 500 pmol ($n = 10$)
Asp	0.6	1.1	2.5	1.5
Glu	0.8	1.0	1.5	1.7
Ser	1.8	0.5	2.3	1.5
His	1.5	0.5	3.8	1.1
Gly	1.3	0.5	2.6	0.5
Thr	2.2	0.5	1.6	1.5
Ala	1.0	0.5	3.3	0.8
Pro	0.5	0.5	2.2	0.3
Tyr	1.1	0.5	4.0	1.4
Arg	2.0	0.5	2.5	1.6
Val	0.9	0.5	2.1	1.0
Met	0.8	0.5	4.1	0.9
Ile	1.8	0.4	1.8	0.6
Leu	1.6	0.4	1.9	0.6
Phe	0.8	0.3	2.0	0.6
Lys	1.9	0.1	3.2	1.4

TABLE V

CORRELATION COEFFICIENTS FOR DERIVATIZATION OF AMINO ACID STANDARDS OVER A 200-FOLD RANGE

Calculated using five data points from amino acid standards containing 5, 100, 200, 500 and 100 pmol

Amino acid	r (n = 5)	Amino acid	r (n = 5)
Asp	0.9989	Tyr	0.9987
Glu	0.9984	Arg	0.9986
Ser	0.9989	Val	0.9987
His	0.9986	Met	0.9987
Gly	0.9989	Ile	0.9988
Thr	0.9990	Leu	0.9987
Ala	0.9988	Phe	0.9989
Pro	0.9989	Lys	0.9978

concentrations by analysing a series of twenty consecutive amino acid standards containing 100 pmol of each amino acid and a hydroxyproline internal standard, and a further series of ten amino acid standards containing 5 pmol of each amino acid and the internal standard. The relative standard deviations of normalized peak area for both series are shown in Table IV, together with retention time reproducibility data and reproducibility data for the manual derivatization procedure, from Haynes *et al.* [24]. The results show that the reproducibility of the automated derivatization is comparable to that of the manual procedure, with relative standard deviations for peak areas at the 100-pmol level varying between 0.5 and 2.2%. The relative standard deviations for peak areas at the 5-pmol level are higher, between 1.5 and 4.1%, but this is expected as the background levels of amino acids are a far more significant source of error.

The linearity of the automated derivatization procedure was established over a 200-fold concentration range, with the analysis of amino acid standards containing 5, 100, 200, 500 and 1000 pmol. All of the amino acids were found to give linear derivatization over this range, with the correlation coefficients greater than 0.997 as shown in Table V.

Analysis of peptide and protein hydrolysates

The chromatograms from the analysis of a typical protein hydrolysate amino acid standard by both fluorescence (10 pmol) and ultraviolet detection (500 pmol) are shown in Fig. 1. Ultraviolet detection is typically 25 times less sensitive than fluorescence detection, but it is useful for the analysis of tryptophan and cystine, which form non-fluorescent Fmoc derivatives.

A number of different peptide and protein hydrolysates have been successfully analysed using this procedure. A comparison of experimental results

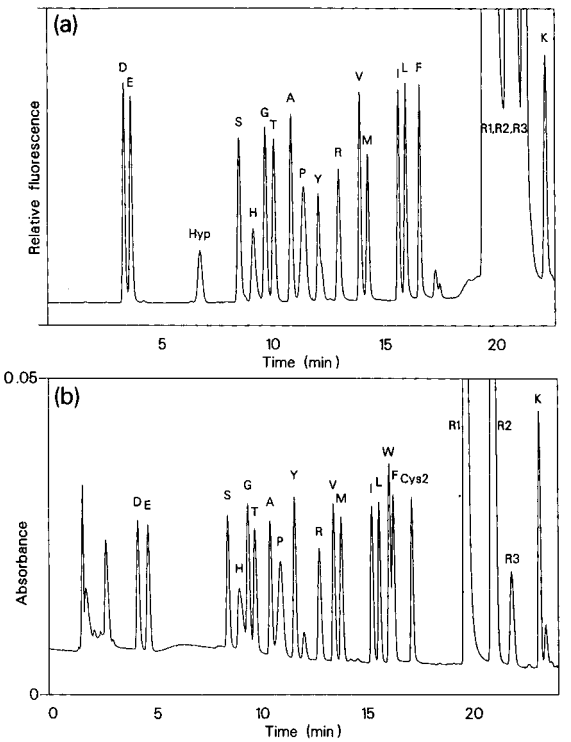

Fig. 1. (a) Chromatogram of a 10-pmol amino acid standard derivatized with Fmoc using automated protocol as in Experimental and detected by fluorescence (excitation wavelength 263 nm, emission wavelength 313 nm). Peaks are labelled with one-letter abbreviations for protein amino acids, and Hyp = hydroxyproline, R1 = Fmoc-hydroxylamine; R2 = Fmoc-OH, R3 = present in reagent blank derivatizations. Chromatographic conditions: column, 150 × 4.6 mm I.D. Spherisorb 3-μm ODS-2 with 15 × 3.2 mm I.D. Brownlee Newguard 7-μm ODS guard column; eluent A = 20 mM ammonium dihydrogenorthophosphate (pH 6.5)–methanol (85:15); eluent B = acetonitrile–water (90:10); flow-rate, 1.0 ml/min; column temperature, 35°C; gradient as for protein hydrolysates in Table I. (b) Chromatogram of a 500-pmol amino acid standard derivatized with Fmoc using automated protocol as in Experimental and detected by ultraviolet absorbance at 263 nm. Peaks are labelled as in (a), and W = tryptophan, Cys2 = cystine. Chromatographic conditions as in (a).

TABLE VI

AMINO ACID COMPOSITIONS OF ANGIOTENSIN-II, NEUROTENSIN, LYSOZYME, CHYMOTRYPSINOGEN-A AND PEPSIN

Comparison of automated Fmoc analysis data and literature values: peptide sequences from suppliers' data and protein compositions from Swiss protein data bank. Expected values given in parentheses. The molecular weights of the samples are angiotensin-II = 1047, neurotensin = 1673, lysozyme = 14 300, chymotrypsinogen-A = 26 400 and pepsin = 34 700.

Amino acid	Angiotensin-II	Neurotensin	Lysozyme	Chymotrypsinogen-A	Pepsin
Asx[a]	1.2 (1)	1.1 (1)	21.4 (21)	23.1 (23)	44.1 (42)
Glx[b]		2.0 (2)	5.2 (5)	14.4 (15)	26.9 (26)
Ser			9.3 (10)	23.2 (28)	40.7 (44)
His	0.8 (1)		0.8 (1)	2.0 (2)	1.0 (1)
Gly			11.8 (12)	21.7 (23)	34.9 (35)
Thr			7.0 (7)	21.9 (22)	26.4 (26)
Ala			12.6 (13)	22.3 (22)	17.2 (16)
Pro	1.1 (1)	2.0 (2)	2.1 (2)	8.9 (9)	14.8 (15)
Tyr	1.0 (1)	2.0 (2)	2.9 (3)	4.0 (4)	13.7 (16)
Arg	1.0 (1)	2.0 (2)	11.0 (11)	4.3 (4)	2.3 (2)
Val	0.9 (1)		5.6 (6)	20.4 (23)	19.9 (22)
Met			1.7 (2)	1.9 (2)	3.6 (4)
Ile	0.9 (1)	1.0 (1)	5.5 (6)	9.0 (10)	21.9 (26)
Leu		2.0 (2)	8.0 (8)	19.8 (19)	25.8 (26)
Phe	1.0 (1)		3.1 (3)	6.4 (6)	13.8 (14)
Lys		1.0 (1)	5.9 (6)	13.8 (14)	1.3 (1)
Trp			N.D.[c] (6)	N.D. (8)	N.D. (5)
Cys			N.D. (8)	N.D. (10)	N.D. (6)

[a] Aspartic acid + asparagine.
[b] Glutamic acid + glutamine.
[c] Not detected.

and literature values for the analysis of two synthetic peptides, angiotensin-II and neurotensin, and three proteins, lysozyme, chymotrypsinogen-A and pepsin, is presented in Table VI. Each derivatization was performed on 10 pmol of hydrolysate and 5 pmol of the derivatized samples were analysed. The results are in very good agreement with the expected values, including the determination of histidine at low levels in complex mixtures of amino acids. A chromatogram of the analysis of chymotrypsinogen-A is shown in Fig. 2.

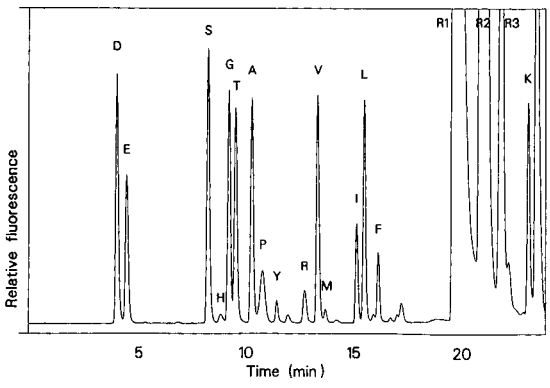

Fig. 2. Chromatogram of 5 pmol of chymotrypsinogen-A hydrolysate derivatized with Fmoc using automated protocol as in Experimental and detected by fluorescence (excitation wavelength 263 nm, emission wavelength 313 nm). Peaks are labelled as in Fig. 1a. Chromatographic conditions as in Fig. 1.

Analysis of physiological fluids

The analysis of amino acids in physiological fluids is important in the studies of disorders of amino acid metabolism and transport [26–34]. There are about 170 different physiological amino acids and at least 66 known disorders of amino acid metabolism

[26,27], most of which are detected by the accumulation of one or more amino acids in plasma, urine or cerebrospinal fluid [22]. The seven most frequently occurring amino acidopathies involve the protein amino acids Phe, Leu, Ile, Met, Val, Tyr and His, but even the most common disorder, phenylketonuria, occurs only in 1 in 10 000 people [28]. The number of samples involved in a screening programme for such disorders requires an analysis system that is both cost efficient and capable of detecting more than one disorder in a single analysis, unlike bacterial inhibition assays which were used prior to the advent of current HPLC technology [28].

The analysis of a standard containing 30 amino acids, including the major components of plasma and urine, is shown in Fig. 3. This is both considerably faster and more sensitive than analysis by conventional ion-exchange chromatography, and has the advantage of being able to detect secondary amino acids, which do not react in OPA derivatization systems [25,29].

Fig. 4 shows the amino acid profile of three deproteinized plasma samples: (a) normal adult human plasma; (b) from a subject with phenylalanine hydroxylase deficiency (phenylketonuria); and (c) from a 4-year-old male subject with tyrosine aminotransferase deficiency (tyrosinaemia type II).

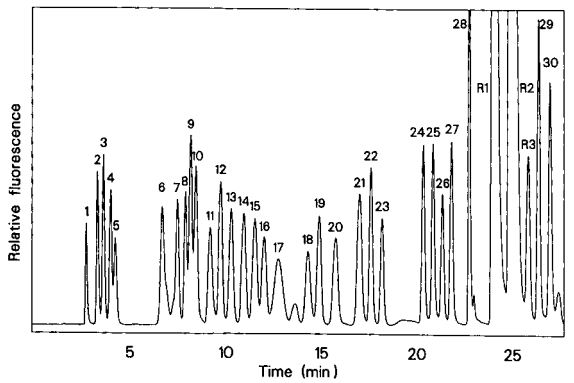

Fig. 3. Chromatogram of 100 pmol of an amino acid standard prepared with 30 amino acids, derivatized with Fmoc using automated protocol as in Experimental and detected by fluorescence (excitation wavelength 263 nm, emission wavelength 313 nm). Peaks: 1 = phosphoserine; 2 = aspartic acid; 3 = glutamic acid; 4 = α-aminoadipic acid; 5 = S-carboxymethylcysteine; 6 = hydroxyproline; 7 = asparagine; 8 = glutamine; 9 = citrulline; 10 = serine; 11 = histidine; 12 = glycine; 13 = threonine; 14 = β-alanine; 15 = alanine; 16 = taurine; 17 = proline; 18 = tyrosine; 19 = α-aminobutyric acid; 20 = arginine; 21 = homoarginine; 22 = valine; 23 = methionine; 24 = isoleucine; 25 = leucine; 26 = norleucine; 27 = phenylalanine; 28 = cystathionine; 29 = ornithine; 30 = lysine. Chromatographic conditions as in Fig. 1; gradient as for physiological samples in Table I.

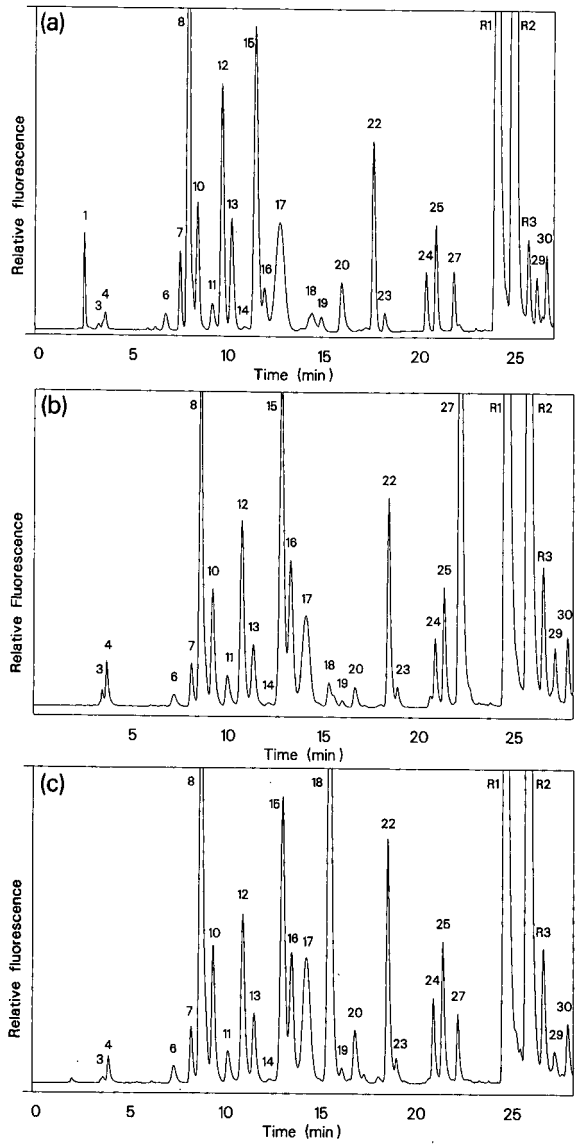

Fig. 4. Chromatograms of three deproteinized human plasma samples derivatized with Fmoc using automated protocol as in Experimental and detected by fluorescence (excitation wavelength 263 nm, emission wavelength 313 nm). (a) Normal adult human plasma; (b) Plasma from an adult patient with phenylketonuria; (c) Plasma from a 4-year-old male patient with tyrosinaemia type II. Peaks are labelled as in Fig. 3. Chromatographic conditions as in Fig. 3.

The greatly elevated levels of phenylalanine (Fig. 4b) and tyrosine (Fig. 4c) are immediately apparent, and show that the method could be used in a screening programme for the detection of the major amino acid metabolism disorders.

CONCLUSION

A method has been developed for the analysis of amino acids using an automated version of the reaction chemistry developed previously [24], which forms single stable derivatives of the protein amino acids. The method is highly sensitive and reproducible, and applicable to the analysis of amino acids in different matrices. These include the analysis of peptide and protein hydrolysates at low levels and the profiling of free amino acids in physiological fluids.

ACKNOWLEDGEMENTS

This work was carried out as a Teaching and Industry scheme project (awarded to J.W.R. and K. L. Williams) funded by ICI Instruments Australia and the NSW Government. The authors thank Andrew Gooley and Keith Williams (Macquarie University) for practical support and Robin Greenwood-Smith for continued encouragement and support. Normal plasma samples were supplied by Alex Babiy (Macquarie University) and other plasma samples were supplied by Judith Hammond (Oliver Latham Laboratory, New South Wales Department of Health).

REFERENCES

1 S. Moore and W. H. Stein, *J. Biol. Chem.*, 176 (1948) 367.
2 R. L. Heinrikson and S. C. Meredith, *Anal. Biochem.*, 136 (1984) 65.
3 B. A. Bidlingmeyer, S. A. Cohen and T. L. Tarvin, *J. Chromatogr.*, 336 (1984) 93.
4 G. E. Tarr, in J. E. Shively (Editor), *Methods of Protein Microcharacterisation*, Humana Press, Clifton, NJ, 1986, pp. 155–194.
5 M. Roth, *Anal. Chem.*, 43 (1971) 880.
6 P. Lindroth and K. Mopper, *Anal. Chem.*, 51 (1979) 1667.
7 D. W. Hill, F. H. Walters, T. D. Wilson and J. D. Stuart, *Anal. Chem.*, 51 (1979) 1338.
8 R. F. Chen, C. Scott and E. Trepman, *Biochim. Biophys. Acta*, 576 (1979) 440.
9 J. M. Wilkinson, *J. Chromatogr. Sci.*, 16 (1978) 547.
10 Y. Tapuhi, D. E. Schmidt, W. Lindner and B. L. Karger, *Anal. Biochem.*, 115 (1981) 123.
11 F. J. Marquez, A. R. Quesada, F. Sanchez-Jiminez and I. Nunez de Castro, *J. Chromatogr.*, 380 (1986) 275.
12 L. A. Carpino and G. Y. Han, *J. Org. Chem.*, 37 (1972) 3404.
13 S. Einarsson, B. Josefsson and S. Lagerkvist, *J. Chromatogr.*, 282 (1983) 609.
14 S. Einarrson, *J. Chromatogr.*, 348 (1985) 213.
15 S. Einarsson, S. Folestad, B. Josefsson and S. Lagerkvist, *Anal. Chem.*, 58 (1986) 1638.
16 I. Betner and P. Foldi, *Chromatographia*, 22 (1986) 381.
17 B. Gustavsson and I. Betner, *J. Chromatogr.*, 507 (1990) 67.
18 A. J. Smith, J. M. Presley and W. McIntire, in T. E. Hugli (Editor), *Techniques in Protein Chemistry*, Academic Press, San Diego, 1989, pp. 255–265.
19 M. Simmaco, D. De Biase, D. Barra and F. Bossa, *J. Chromatogr.*, 504 (1990) 129.
20 D. R. Dupont, A. H. Chui, P. S. Keim, M. Bozzini, R. S. Bello and K. J. Wilson, *J. Protein Chem.*, 7 (1988) 219.
21 R. S. Thoma and D. L. Crimmins, *J. Chromatogr.*, 537 (1991) 153.
22 R. Schuster, *J. Chromatogr.*, 431 (1988) 271.
23 P. Furst, L. Pollack, T. A. Graser, H. Godel and P. Stehle, *J. Chromatogr.*, 499 (1990) 557.
24 P. A. Haynes, D. Sheumack, J. Kibby and J. W. Redmond, *J. Chromatogr.*, 540 (1991) 177.
25 B. N. Jones and J. P. Gilligan, *J. Chromatogr.*, 266 (1983) 471.
26 Z. Deyl, J. Hyanek and M. Horakova, *J. Chromatogr.*, 379 (1986) 177.
27 W. L. Nyhan, *Heritable Disorders of Amino Acid Metabolism: Patterns of Clinical Expression and Genetic Variation*, Wiley, New York, 1974.
28 F. Moretti, M. Birarelli, C. Carducci, A. Pontecorvi and I. Antonozzi, *J. Chromatogr.*, 511 (1990) 131.
29 H. Godel, T. Graser, P. Foldi, P. Pfaender and P. Furst, *J. Chromatogr.*, 297 (1984) 49.
30 J. F. Davey and R. S. Ersser, *J. Chromatogr.*, 528 (1990) 9.
31 Y. Kamisaki, Y. Takao, T. Itoh, T. Shimomura, K. Takahashi, N. Uehara and Y. Yoshino, *J. Chromatogr.*, 529 (1990) 417.
32 S. Gunawan, N. Y. Walton and D. M. Treiman, *J. Chromatogr.*, 503 (1990) 177.
33 O. Ladron De Guevara, C. Cortinas De Nava, P. Padilla and J. Espinosa, *J. Chromatogr.*, 528 (1990) 35.
34 R. Sherwood, A. C. Titheradge and D. A. Richards, *J. Chromatogr.*, 528 (1990) 293.

Journal of Chromatography, 588 (1991) 115–123
Elsevier Science Publishers B.V., Amsterdam

CHROM. 23 627

Automated two-dimensional liquid chromatographic system for mapping proteins in highly complex mixtures

Toshiaki Isobe*, Kazuhisa Uchida, Masato Taoka, Fumiko Shinkai, Takashi Manabe and Tsuneo Okuyama

Department of Chemistry, Faculty of Science, Tokyo Metropolitan University, 1-1 Minami-Osawa, Hachioji-shi, Tokyo 192-03 (Japan)

(First received May 22nd, 1991; revised manuscript received July 12th, 1991)

ABSTRACT

An automated two-dimensional liquid chromatographic system was developed for systematic protein separations which could serve for analytical mapping and preparative separations of proteins. The system applies the principles of the column-switching technique, and consists of two different columns connected in tandem through an electrical column switching valve, two pumping systems to operate each column independently and a system controller to perform sequential chromatography on the two columns. A protein mixture is applied to the first-dimensional anion-exchange column and is separated by stepwise elution with an increasing sodium chloride concentration. The eluent is introduced directly to the second-dimensional reversed-phase column, and is further separated by gradient elution with an increasing acetonitrile concentration. The two elution stages are synchronized by a computer program. By this system, very complex protein mixtures such as crude cerebellar extracts were resolved reproducibly into *ca.* 200 peaks within 12 h. The method can be used for the total analysis of proteins in various tissues and cells without complicated premanupulation of samples, and allows the simultaneous analysis of a protein isolated by chromatography. The isolated protein is most suitable for use in the strategy of protein and gene sequence analysis.

INTRODUCTION

With recent advances in biochemical and gene cloning techniques, the need for rapid, systematic and universal methods for purifying and analysing proteins has become increasingly important. The development of such methods will serve, for instance, to reduce the time and labour of purifying proteins and to elucidate the molecular basis of various biological events accompanying qualitative or quantitative changes in proteins. Two-dimensional (2D) electrophoresis meets many of these requirements [1–3] and is widely used for both analytical and preparative purposes [4–6], but it has limitations in several respects: multi-step manual handling, small sample capacity, possible contamination of impurities from the gel matrix, etc.

In general, the purification of biological substances such as proteins has been achieved by multi-step chromatography operated manually, *e.g.*, the effluents from a first column are collected in a number of fractions, each fraction is desalted or/and concentrated when necessary and the concentrated fractions are applied to a second column of different specificity, and so on. Although such an approach has been extensively applied to the separation not only of proteins but also of peptides [7] and small urinary substances [8], a problem often encountered is low reproducibility through accumulation of experimental errors due to multi-step manual handling.

In the course of systematic studies of brain proteins, we have developed an automated two-dimensional high-performance liquid chromatographic (2D-HPLC) system that is applicable to systematic separations of complex protein mixtures such as crude tissue/cellular extracts. The system is an application of the column-switching technique, and is

0021-9673/91/$03.50

a modification of the system of Takahashi and coworkers [9,10] and its microscale version described by Matsuoka *et al.* [11], both of which were designed for the separation of complex mixtures of peptides. The modification includes the instrumentation of the system, where we employed one HPLC assembly with a valve control mechanism instead of two independent HPLC assemblies, and the utilization of polymer-based columns for both dimensional separations. The former modification simplified the apparatus and made the system more specific for the 2D-HPLC technique, and the latter approach was important in adapting the system for the separation of crude protein mixtures (described below). The system employs an ion-exchange and a reversed-phase column, and separates proteins first by charge [12] and second by hydrophobicity [13,14], which correlates with molecular weight [15]. These columns are connected in tandem through an electrical column-switching valve, and are eluted sequentially with a computer-assisted, time-dependent control of the flow system.

The automated 2D-HPLC technique shows reasonably high resolution and reproducibility, and has several advantages over the electrophoresis technique with respect to ease of sample handling, recovery, quantification and flexibility. A general feature of the 2D-HPLC technique has been described briefly [16,17]. This paper presents details of the protein separation system and its application to the separation of crude tissue/cellular extracts.

EXPERIMENTAL

Chemicals and proteins

Acetonitrile (chromatography grade) was obtained from Merck (Darmstadt, Germany) and trifluoroacetic acid (TFA) (Sequanal grade) from Wako (Tokyo, Japan). All other reagents were of analytical-reagent grade from Wako, unless mentioned otherwise. Water was distilled, passed through a mixed-bed ion-exchange resin and redistilled before use.

Bovine serum albumin was purchased from Seikagaku Kogyo (Tokyo, Japan). Haemoglobin was prepared from bovine erythrocyte lysate by repeated crystallization. Other proteins were purified from bovine brain essentially as described [18,19].

Apparatus

The system is illustrated in Fig. 1. It consists of two HPLC columns (C1 and C2) connected in tandem through an electrical column-switching valve (4WV; Mode EIE010, Senshu Kagaku, Tokyo, Japan) and two independent flow systems each equipped with a high-pressure pump (P1 and P2; Model LC6A, Shimadzu, Kyoto, Japan), two pairs of solenoid valves (V1/V2 and V3/V4; Model MTV2-M6, Takasago Electric, Tokyo, Japan) and a coil solvent mixer (M; 1.2 m × 0.25 mm I.D.). A system controller, composed of an eight-bit microcomputer (MC; Model PC-8801, NEC, Tokyo, Japan) connected to electrical relays through an interface, controls the pumps 1 and 2 (on/off), the column-switching valve (connect/disconnect C1 and C2) and the two pairs of solenoid valves to perform a series of stepwise elutions for C1 and to perform repetitive linear gradient elution for C2. Two wavelength-tunable UV detectors (DE; Model SPD-6A, Shimadzu, and Model UVIDEC-100E, Jasco, Tokyo, Japan), a recorder (RE; Model R-112, Shimadzu) and an integrator (INT; Model C-R6A, Shimadzu) are set to monitor the eluent and to quantify the peaks obtained by HPLC. The system is also equipped with a fraction collector (FC; Model 203, Gilson, Worthington, OH, USA) for peak collection. For our standard system focused on the separation of brain acidic proteins, we selected an anion-exchange TSK-gel DEAE-5PW column (7.5 cm × 0.75 cm I.D.) (Tosoh, Tokyo,

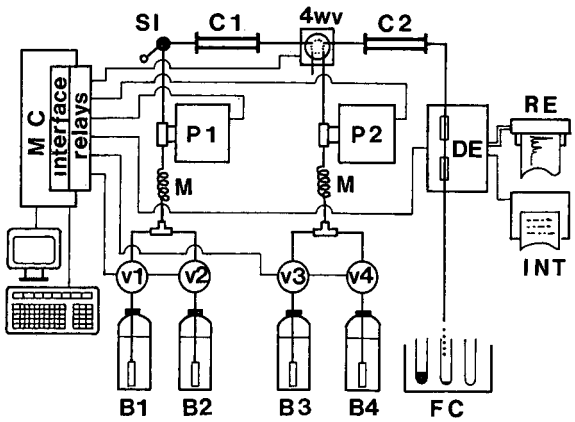

Fig. 1. Schematic diagram of the 2D-HPLC system for the separation of complex protein mixtures.

Japan) and a reversed-phase TSK-gel Phenyl 5PWRP column (7.5 × 0.46 cm I.D.) (Tosoh) for C1 and C2, respectively.

Performance of 2D-HPLC

On starting the program, columns C1 and C2 are equilibrated with B1 (25 m*M* Tris–HCl buffer, pH 7.5) and B3 (20% acetonitrile in 0.1% TFA), respectively, at a flow-rate of 1.0 ml/min. After 40 min, pump 2 is stopped and the column-switching valve (4WV) moves to connect C1 and C2. A sample mixture is applied to C1 through the sample injector (SI) and eluted with B1 for a time t_1 (20 min as standard) at a flow-rate of 1.0 ml/min. Pump 1 is stopped and, simultaneously, the second chromatography begins as pump 2 starts to pump at a flow-rate of 1.0 ml/min with a linear gradient from B3 to B4 (20 to 60% acetonitrile in 0.1% TFA) during the time t_2 (40 min as standard). Column C2 is equilibrated again with B3 for 15 min after the linear gradient elution is finished, then pump 2 is stopped. After this step, the first cycle of the 2D-HPLC is completed. Pump 1 then starts again to elute proteins stepwise from the anion-exchange column C1 by introducing and mixing a portion of buffer B2 (0.4 *M* NaCl in 25 m*M* Tris–HCl buffer, pH 7.5) into B1. After applying the eluent to C2, the second chromatography is repeated exactly as described above. These procedures are repeated for a number of cycles (n), changing the mixture ratio of B1 and B2 with time-dependent control of solenoid valves V1 and V2. In our standard procedure, the mixing ratio of B2 was increased as follows: 0, 5, 10, 15, 20, 25, 30, 40, 50 and 100% (n = 10). For versatility, however, the computer program has been made open for the elution times of C1 and C2 (t_1 and t_2), the cycle number (n) and the B1/B2 mixing ratio in each cycle for possible modification of these parameters depending on the complexity and ionic distribution of the sample mixture.

Preparation of soluble proteins from bovine cerebellum and from mouse myeloma cell

Bovine brain was obtained fresh from a slaughter house. The cerebellum was resected and was homogenized with a fourfold volume of 0.1 *M* potassium phosphate buffer (pH 7.1) containing 1.6 *M* ammonium sulphate and 1 m*M* EDTA. The homogenate was centrifuged at 10 000 *g* for 30 min and the soluble extracts were precipitated by addition of solid ammonium sulphate to 85% saturation at pH 4.7. After centrifugation, the precipitate was dissolved in 0.1 *M* potassium phosphate buffer (pH 7.1) containing 1 m*M* EDTA and dialysed against buffer B1 for 2D-HPLC. The preparation was divided into 0.5-ml portions and stored frozen at −80°C until use.

Mouse myeloma cells (P3U1) were cultivated in a 24-well plastic plate in RPMI-1640 medium (Nissui Pharmaceutical, Tokyo, Japan) containing 10% (v/v) of calf serum (Gibco Labs., Scotland, UK). The cells (*ca.* 10^6) were collected in a 1.5-ml plastic tube by centrifugation and washed twice with 10 m*M* sodium phosphate buffer (pH 6.8) containing 0.15 *M* NaCl. Soluble proteins were obtained by freezing and thawing the cells twice in distilled water, followed by centrifugation at 15 000 *g* for 5 min.

RESULTS AND DISCUSSION

Separation of standard proteins

The performance of the 2D-HPLC system was tested by applying a mixture of seven proteins puri-

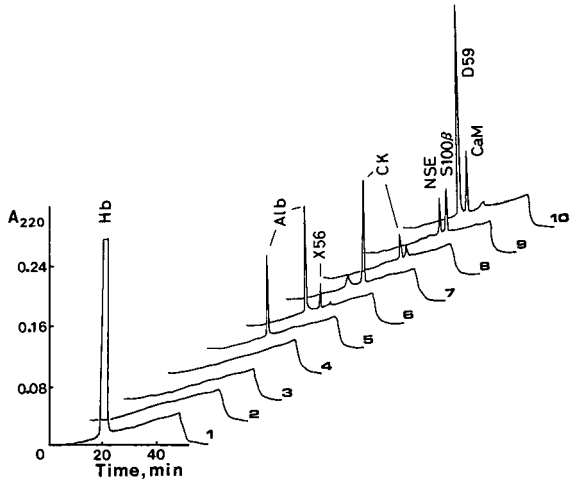

Fig. 2. Three-dimensonal representation of the 2D-HPLC of a mixture of haemogobin (Hb), serum albumin (Alb), X-56 protein (X-56), creatine kinase (CK), neuron-specific enolase (NSE), S100 protein β-chain (S100β), D59 protein (D59) and calmodulin (CaM). The chromatography was performed under the standard conditions described in the text. Each horizontal profile represents the result of the second reversed-phase chromatography of a protein fraction eluted from the first anion-exchange column. The cycle number is shown at the right of each profile.

fied in our laboratory or obtained from a commercial source (see legend to Fig. 2). Although a long, continuous elution profile was obtained as a result of the chromatography, the profile is represented in Fig. 2 by three-dimensional drawings of a series of elution profiles, each profile corresponding to one cycle in the chromatography. Thus, the separation cycle of the first anion-exchange and the second reversed-phase chromatography was repeated ten times, which required a total analysis time of 12 h.

Under these conditions, all of the tested proteins were separated from each other and were eluted at the positions indicated in Fig. 2. Here, five proteins appeared in a single peak, and two proteins, serum albumin and creatine kinase, were found in duplicated peaks eluted in the adjacent, first-dimensional chromatography. Because the elution profile was reproducible for these standard proteins and for the tissue extract as described below, we considered that the double peaks observed might be due to charge heterogeneity of the albumin and creatine kinase preparations used. It has been shown that commercial albumin exhibits charge heterogeneity during 2D-electrophoresis [2], probably because it contains several molecular species such as fatty acid-binding albumin and mercaptoalbumin, and microheterogeneity is known also for creatine kinase [20]. The profile also indicates that the proteins are eluted from the first-dimensional column in increasing order of acidity, as expected from the specificity of the anion-exchange column, and that those having similar acidities, such as neuron-specific enolase (pI = 4.7) and S100b protein (pI = 4.6), are eluted together from the first column and are subsequently separated on the second-dimensional, reversed-phase column.

Separation and analysis of bovine cerebellar extracts

To examine the resolution of the 2D-HPLC technique, the soluble extract of bovine cerebellum was injected directly into the system and eluted under the same conditions as in Fig. 2. The cerebellar extracts were resolved into *ca.* 200 peaks (Fig. 3) by applying 6 mg of proteins. Quantitative analysis indicated that each peak contained 0.5–60 μg of protein, suggesting that our system could detect proteins present at a level of more than 0.01% of total soluble proteins in bovine cerebellum with the detector sensitivity used (220 nm, 0.64 a.u.f.s.).

The number of peaks resolved by the separation of the cerebellar extracts increased to *ca.* 250 when the cycle number of the chromatography was increased to 20 and conversely decreased to *ca.* 75 with a cycle number of 4. A plot of the observed peak number *versus* the number of cycles (Fig. 4) suggests that the present system could separate the cerebellar extract into a maximum of about 280 peaks under the conditions employed. On the other hand, *ca.* 400 protein spots were detected by 2D electrophoresis of this preparation followed by Coomassie blue staining [21].

To test the purity of proteins separated by the 2D-HPLC technique, fourteen major peaks were collected as indicated in Fig. 3, and analysed by sodium dodecyl sulphate polyacrylamide gel electrophoresis (SDS-PAGE). In spite of the condition that these peaks were obtained directly from the crude tissue extracts, many of the peaks analysed contained proteins with sufficient purity for subsequent analysis, and several peaks contained a number of minor proteins or contained some impurities giving rise to a smeared band in the stained gel (Fig. 5). This demonstrates a reasonably high efficiency of the 2D-HPLC technique as a preparative method for proteins. In fact, most of these major cerebellar proteins were obtained in pure form by a single 2D-HPLC operation or by an additional reversed-phase chromatography with elution using a gentle gradient of acetonitrile or using 0.08% heptafluorobutyric acid in place of TFA. The purified proteins were characterized by one or more of the following analyses: (i) 2D electrophoresis, (ii) dot–blot immunochemical analysis, (iii) analysis of amino acid compoisition and (iv) analysis of amino-terminal sequence or internal amino acid sequence and, as a result of these analyses, we have so far identified fifteen brain proteins in the protein map of bovine cerebellum [16,17].

Reproducibility and stability

The reproducibility of the method is illustrated in Fig. 3. The profile was obtained by repeating the chromatography of the same extracts of bovine cerebellum. Between the analyses shown in Fig. 3a and b, the system was used twenty times mainly for separation of crude tissue extracts. In spite of these conditions and of the complexity of the protein mixture analysed, the separation patterns of the two

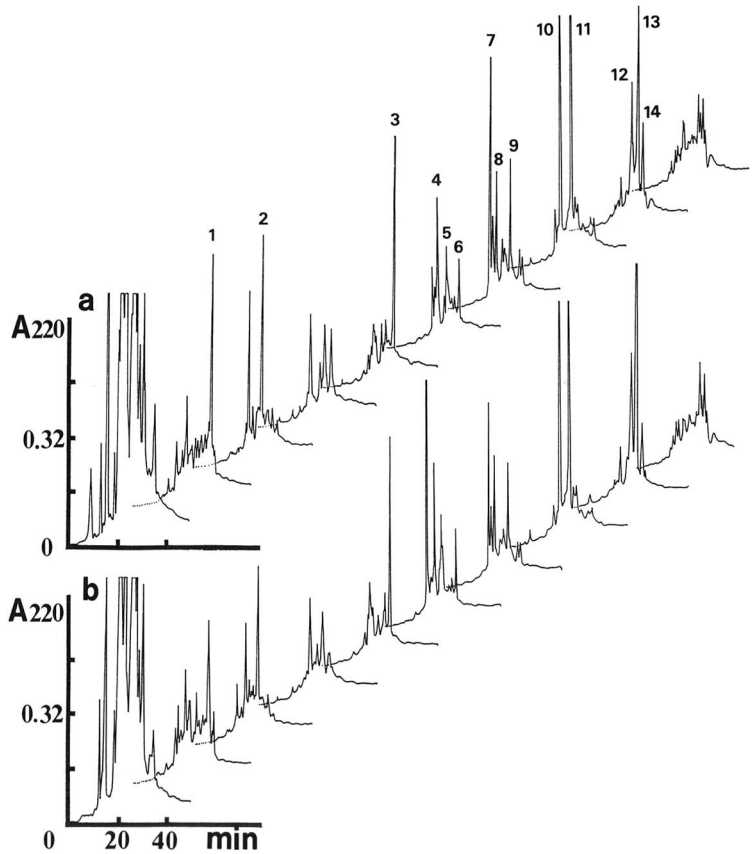

Fig. 3. Protein map of bovine cerebellum. The soluble extracts were applied to the 2D-HPLC system and eluted as described in the text; (a) and (b) are two separate experiments that illustrate the reproducibility of the method. The fourteen numbered peak were collected for SDS–PAGE.

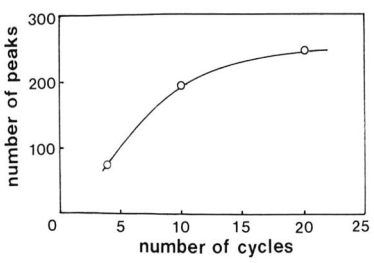

Fig. 4. Relationship between the number of stepwise elutions in the first anion-exchange chromatography, *i.e.*, the cycle number, and the number of peaks observed in the 2D-HPLC. The data were collected by applying crude cerebellar extracts (6 mg of protein).

chromatograms are highly reproducible, although there are small but noticeable changes in peak height for a number of peaks, including peaks 1, 4 and 7.

This 2D-HPLC system has currently been used more than 200 times for preparative and analytical protein separations. Repeated application of crude protein mixtures such as tissue extracts tended to increase the column pressure from 20 to more than 80 kg/cm^2, probably owing to the accumulation of lipids, nucleic acids and very large proteins of low solubility, etc., and this resulted in a gradual decrease in peak resolution. However, these columns could be regenerated by washing with 20 ml of 0.5

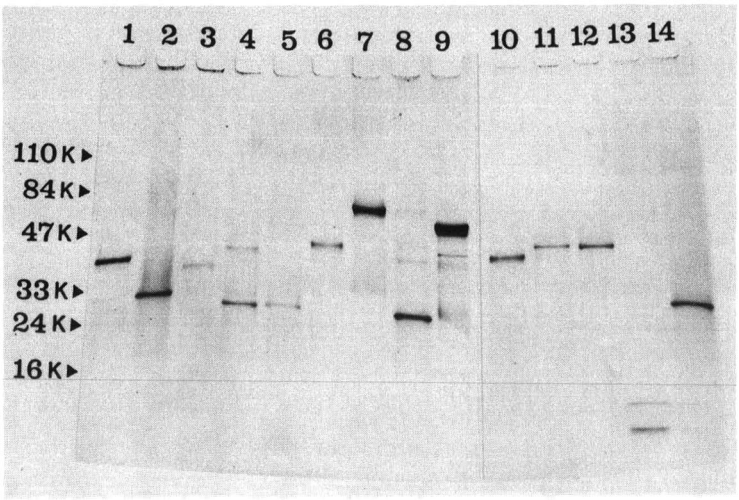

Fig. 5. SDS-PAGE of bovine cerebellar proteins collected from the 2D-HPLC. The numbers at the top of each lane correspond to the peak numbers in Fig. 3. A portion of the eluates was analysed in a 4–20% gradient of polyacrylamide gel containing 0.1% SDS (Coomassie blue staining). The molecular weight values indicated were measured with a prestained molecular weight standard mixture obtained from Bio-Rad Labs. (Richmond, CA, USA); K = kilodalton.

M sodium hydroxide solution without detectable deterioration in peak resolution. Hence the chemical stability of polymer-based columns is important for the maintenance of the system and to perform reproducible protein mapping.

Sensitivity

Our standard 2D-HPLC system equipped with a 7.5 mm I.D. anion-exchange column and a 4.6 mm I.D. reversed-phase column has a protein loading capacity of about 10 mg. Application of this

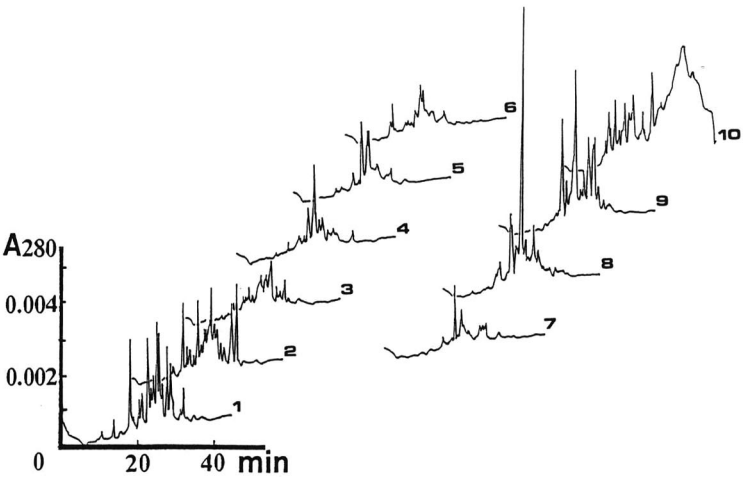

Fig. 6. Protein map of mouse myeloma cell, P3U1. Soluble proteins prepared from 10^6 cells (see Experimental) were analysed by the automated 2D-HPLC system. The detector sensitivity was set at 0.01 a.u.f.s. at 280 nm.

amount of the cerebellar extract enabled *ca.* 1–100 μg each of protein to be isolated by a single chromatography, and this sufficed for various biochemical and protein chemical analyses.

For analytical purposes, the sensitivity of this system could be increased 200-fold simply increasing the detector sensitivity without introducing a significant baseline problem. This allowed us to perform analytical protein mapping with 100 μg of extracts derived from 10 mg of bovine cerebellum and, likewise, to perform protein mapping of cells cultivated on an experimental scale. Fig. 6 shows the separation of soluble proteins in mouse myeloma cells (1×10^6 cells) grown in a single well of a conventional 24-well plastic plate. Here, *ca.* 210 peaks are detected in a clearly different pattern from that of the bovine cerebellum.

Applicability

Because of the high resolution and reproducibility, and because of the small amount of sample required, the method should be useful for analytical mapping of proteins in various tissues and cells. For instance, the system could detect differences in protein composition among various bovine tissues. Fig. 7 illustrates a partial comparison of the protein maps of (a) the cerebellum (b) the cerebrum and (c) the adrenal medulla, in which differences are apparent despite the close ontogenetic relationships among the tissues.

We have also applied this technique to the protein mapping of rat cerebellum at various developmental stages and searched for proteins that may be related to the maturation of this tissue. We analyzed the developmental profiles of more than 120 proteins resolved by the 2D-HPLC technique, and detected several proteins that were expressed transiently at an early stage of the postnatal development. One of these proteins, termed V-1, were isolated by HPLC and characterized in detail by direct protein sequence analysis and by cloning its complementary DNA [22]. In addition to such an application, the method should also be useful for the general purification of proteins that occur naturally or are produced by recombinant DNA techniques. Because the system is flexible, various types of separation are possible, depending on the purpose and the complexity of the protein mixture, *e.g.*, by modification of the elution conditions and number of cycles or by replacing the columns with larger or

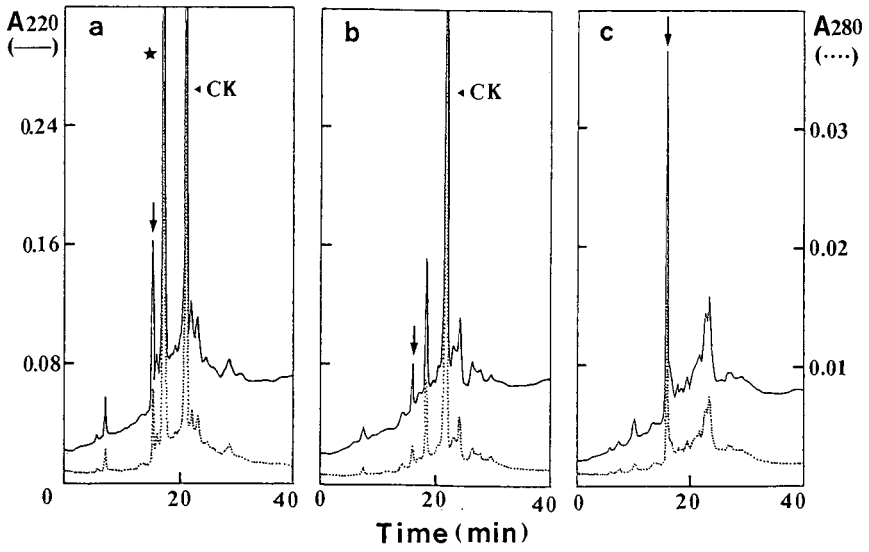

Fig. 7. Partial comparison of the protein maps of (a) bovine cerebellum, (b) cerebrum and (c) adrenal medulla. The profiles obtained at cycle 8, the reversed-phase separation of a protein fraction eluted from the first anion-exchange column with 40% B2, are shown. To facilitate comparison, a protein peak with a retention time of 17 min is indicated by an arrow. CK refers to the brain-type creatine kinase which is found abundantly in the cerebellum and the cerebrum, but is not detected in the adrenal medulla. A protein peak found in the cerebellum (indicated by an asterisk) is much less significant in the cerebrum and adrenal medulla.

smaller columns or columns having different specificities.

Limitations

Although the 2D-HPLC technique is useful for systematic protein separations, as could be demonstrated by the protein mapping of the bovine cerebellum and of the cultivated myeloma cells, it has some practical limitations, mainly due to the separation mode employed. We selected an anion-exchange column for the first separation, because our initial purpose in developing the 2D-HPLC system was the systematic separation of proteins in the brain, a tissue characterized by a high content of acidic proteins. Based on the analysis of a series of proteins with known acidity, this anion-exchange column adsorbs proteins having an isoelectric point below 6.5 under the solvent condition employed [12]. Thus, more basic proteins elute together in the first cycle of the chromatography. Complementary to the present system would be the use of a cation-exchange column, and in fact a cation-exchange TSK-gel CM-5PW column (Tosoh) or a ceramic hydroxyapatite column [23] was found to be more effective than the present system in separating basic proteins. It is advantageous, therefore, to select either an anion- or a cation-exchange column depending on the charge distribution of the protein mixture. Alternatively, the use of tandem anion- and cation-exchange columns or a mixed-bed ion-exchange column for the first-dimensional separation will decrease the number of proteins eluted in the first cycle.

The second reversed-phase separation introduces two limitations. First, very hydrophobic proteins will bind to the column too tightly and may be recovered in low yields, or may not be recovered during the chromatography. The reversed-phase column selected is the one which, in our experience, has the lowest hydrophobicity among the commercial columns tested and is able to separate relatively large proteins such as serum amine oxidase (subunit M_r = 95 000). However, we still cannot exclude the above possibility when the method is applied to very hydrophobic and poorly soluble proteins. Probably further optimization process of the chromatographic conditions, including column parameters such as the type of packing material and the size of column and also the mobile phase composition, as discussed by Burton and co-workers [24,25], will reduce this limitation. Second, the reversed-phase separation will reduce the biological activities of proteins which are labile at high acetonitrile concentrations and acidic pH. In general, small proteins can easily be renatured after the chromatography; however, the renaturation of large protein molecules may be relatively difficult. Therefore, as a tool for preparative purposes, the 2D-HPLC system presented here is thought to be most suitable for use in protein chemical studies such as microscale sequencing or the purification of a protein to produce a specific antibody. Such methods are needed in various biological studies, including the protein and gene analyses.

ACKNOWLEDGEMENTS

We thank Dr. F. W. Putnam (Indiana University, Bloomington, IN, USA) and Dr. N. Takahashi (Tonen, Saitama, Japan) for valuable discussions. This study was supported in part by a Grant-in-Aid for Scientific Research on Priority Areas (02220104) from the Ministry of Education, Science and Culture of Japan.

REFERENCES

1 P. H. O'Farell, *J. Biol. Chem.*, 250 (1975) 4007.
2 T. Manabe, K. Tachi, K. Kojima and T. Okuyama, *J. Biochem.*, 85 (1979) 649.
3 N. L. Anderson, R. P. Tracy and N. G. Anderson, in F. W. Putnam (Editor), *The Plasma Proteins*, Vol. IV, Academic Press, New York, 1982, p. 222.
4 M. W. Hunkapiller, E. Lujan, F. Ostrander and L. E. Hood, *Methods Enzymol.*, 91 (1983) 227.
5 P. Matsudaira, *J. Biol. Chem.*, 262 (1987) 10034.
6 R. H. Aebersold, J. Leavitt, R. A. Saavedra, L. E. Hood and S. B. H. Kent, *Proc. Natl. Acad. Sci. U.S.A.*, 84 (1987) 6970.
7 N. Takahashi, Y. Takahashi and F. W. Putnam, *J. Chromatogr.*, 266 (1983) 511.
8 E. L. Mattiuz, J. W. Webb and S. C. Gates, *J. Liq. Chromatogr.*, 5 (1982) 2343.
9 N. Takahashi, N. Ishioka, Y. Takahashi and F. W. Putnam, *J. Chromatogr.*, 326 (1985) 407.
10 N. Takahashi, Y. Takahashi, N. Ishioka, B. S. Blumberg and F. W. Putnam, *J. Chromatogr.*, 359 (1986) 181.
11 K. Matsuoka, M. Taoka, T. Isobe, T. Okuyama and Y. Kato, *J. Chromatogr.*, 515 (1990) 323.
12 T. Kadoya, T. Isobe, Y. Amano, Y. Kato, K. Nakamura and T. Okuyama, *J. Liq. Chromatogr.*, 8 (1985) 635.
13 T. Sasagawa, T. Okuyama and D. C. Teller, *J. Chromatogr.*, 240 (1982) 329.
14 C. A. Brown, H. P. Bennet and S. Solomon, in M. T. W.

Hearn, F. E. Regnier and C. T. Wehr (Editors), *High Performance Liquid Chromatography of Proteins and Peptides*, Academic Press, New York, 1983, p. 65.
15 T. Ichimura, Y. Amano, T. Isobe and T. Okuyama, *Bunseki Kagaku*, 34 (1985) 653.
16 T. Isobe, N. Takahashi and F. W. Putnam, in R. S. Hodges and C. Mant (Editors), *HPLC of Peptides and Proteins: Separation, Analysis and Conformation*, CRC Press, Boca Raton, FL, 1991, p. 835.
17 N. Takahashi, T. Isobe and F. W. Putnam, in M. T. W. Hearn (Editor), *HPLC of Proteins, Peptides, and Polynucleotides*, Verlag Chemie, New York, 1991, p. 307.
18 T. Isobe, T. Nakajima and T. Okuyama, *Biochim. Biophys. Acta*, 494 (1977) 222.
19 N. Ishioka, T. Isobe, T. Kadoya, T. Okuyama and T. Nakajima, *J. Biochem.*, 94(1984) 611.
20 D. Roman, J. Billadello, J. Gordon, A. Grace, B. Sobel and A. Straus, *Proc. Natl. Acad. Sci. U.S.A.*, 82 (1985) 8394.
21 T. Kadoya, Y. Takahashi, N. Ishioka, T. Manabe, T. Isobe and T. Okuyama, *Protides Biological Fluids, Proc. Colloq.*, 30 (1982) 591.
22 M. Taoka, T. Isobe, T. Okuyama, Y. Yamakawa, M. Watanabe, H. Kondo, F. Ozawa, F. Hishinuma, K. Noguchi, S.-Y. Song and T. Yamakuni, submitted for publication.
23 T. Kadoya, T. Isobe, M. Ebihara, T. Ogawa, M. Sumita, H. Kuwahara, A. Kobayashi, T. Ishikawa and T. Okuyama, *J. Liq. Chromatogr.*, 9 (1986) 3543.
24 W. G. Burton, K. D. Nugent, T. K. Slattery, B. R. Summers and L. R. Snyder, *J. Chromatogr.*, 443 (1988) 363.
25 K. D. Nugent, W. G. Burton, T. K. Slattery, B. F. Johnson and L. R. Snyder, *J. Chromatogr.*, 443 (1988) 381.

Journal of Chromatography, 588 (1991) 125–137
Elsevier Science Publishers B.V., Amsterdam

CHROM. 23 643

On-line characterization of polyethylene glycol-modified proteins

Michael Kunitani*, Gavin Dollinger, Deborah Johnson and Lilia Kresin

Analytical Chemistry Department, Cetus Corporation, 1400 Fifty-Third Street, Emeryville, CA 94608 (USA)

(First received March 8th, 1991; revised manuscript received July 16th, 1991)

ABSTRACT

An high-performance liquid chromatographic method has been developed which simultaneously determines three critical physical properties of polyethylene glycol (PEG)-modified proteins: molecular size, polymer distribution and weight composition. With both UV and refractive index (RI) detectors in series, size-exclusion chromatography (SEC) is used to separate the PEG–protein species according to size. The size analysis of these PEG–proteins is predicted to be accurately calibrated with the viscosity radius (universal calibration), which compensates for the shape differences between PEG and protein structures. The heterogeneity of the PEG–protein grafted copolymer is represented by the polymeric term "polydispersity", which describes the size distribution. Separate SEC calibrations of the PEG and the protein used for conjugation allow a determination of the weight composition of the PEG–protein (weight PEG/weight protein) by combining UV and RI chromatograms of a PEG–protein sample. This compositional analysis is validated through independent and direct measurement of the PEG on a PEG–protein via acid hydrolysis and quantitative SEC. Comparisons of compositional analysis of PEG–protein with sodium dodecyl sulfate polyacrylamide gel electrophoresis densitometry demonstrate that gel analysis of some proteins is misleading.

INTRODUCTION

Covalent conjugation of monomethoxy–polyethylene glycol (PEG) to proteins has recently become recognized as a method of dramatically altering a protein's pharmacology and immunogenicity. A number of enzymes, including superoxide dismutase, asparaginase and uricase, have been extensively modified with PEG, resulting in biologically active compounds with longer *in vivo* half-lives [1–5]. Investigators have conjugated PEG to lymphokines such as interleukin-2(IL-2), produced from *Escherichia coli*, in order to mimic some of the effects of native glycosylation [6]. PEG modification of IL-2 has led to increased protein solubility, decreased plasma clearance, increased antitumor potency in mice and reduced immunogenicity in rabbits and mice [7–9].

Many diverse approaches have been taken in the attempt to characterize PEG–proteins. The chemical reactivity of underivatized primary amino groups on lysine has been exploited in order to determine the degree of PEG conjugation [10,11]. This approach has had difficulty in accurately measuring low degrees of PEG modification. It relies upon differentiating between the derivatization of a native protein, which contains numerous lysine residues, and the PEG-modified protein. The result is a measurement of the difference between two relatively large numbers and, when that difference is small, the relative error can be considerable. Perhaps because of this limitation, rigorous validation of the method has been difficult [10]. Another approach to determining the degree of PEG conjugation has been through the densitometric analysis of sodium dodecyl sulfate (SDS) electrophoretic gels [7,11]. The resolution is sufficient to identify various gel band regions, but the gel bands are broad. Quantitative NMR has been used to determine the degree of PEG conjugation to ovalbumin [12]. Overlap of PEG and protein chemical shift resonances will limit the accuracy of this approach. Other approaches, in-

0021-9673/91/$03.50

cluding dynamic light scattering and size-exclusion chromatography, use the hydrodynamic size of the modified protein to infer the degree of PEG modification. With these methods, the relationship between hydrodynamic size and mass is not well defined owing to the difference in partial specific volume between the quasi-random coil configuration of PEG and the compact globular shape of native proteins.

Other chromatographic modes that have been used in characterizing PEG-proteins are reversed-phase, hydrophobic interaction, anion-exchange and cation-exchange high-performance liquid chromatography (HPLC) [11,12]. These four modes of absorptive chromatography all have demonstrated the ability to resolve clearly two or more peaks of PEG-conjugated superoxide dismutase (PEG–SOD) or PEG–ovalbumin. Common to these chromatographic separations are the broad HPLC peaks characteristic of polymeric mixtures. The identity and composition of these peaks are unknown. An approach to characterizing PEG–proteins without relying on surface interactions or molecular size is isoelectric focusing (IEF), which separates molecules on the basis of molecular charge. Presumably, higher degrees of PEG conjugation through lysine derivatization would be represented by bands of lower p*I*. IEF gels of PEG–SOD and PEG-conjugated IL-2 (PEG–IL-2) reveal either a continuous smear or a series of bands of lower p*I* than the native protein [7,11]. The complex array of IEF bands have been attributed to the degree of PEG conjugation and to conformational heterogeneity. Recently, capillary electrophoresis has shown promise in separating PEG–proteins, but is limited to those with relatively low degrees of PEG conjugation [13].

Native proteins, by virtue of a unique primary sequence, have well defined secondary and tertiary structures. In comparison, PEG is a linear polymer which always exists as a distribution of different lengths and random conformations. When PEG is conjugated to a protein, two additional dimensions of heterogeneity are introduced: the number of PEGs per protein molecule and their location. These three dimensions of heterogeneity (length of each PEG, number of PEGs and location of PEGs) all contribute to the effective hydrodynamic size of the PEG–protein conjugate. For example, PEGs may be on the same side or opposite sides of a small protein, resulting in vastly different hydrodynamic diameters for molecules of identical composition and molecular weight. Conversely, a narrow size range of a PEG–protein will contain many distinctly different PEG–protein molecules. Let us consider conjugating PEG to a relatively small protein, ribonuclease, which contains ten lysine residues and one reactive N-terminus. With a PEG of moderate distribution (molecular weight 7000–10 000), the number of combinations of ribonuclease conjugated with three PEGs is $5 \cdot 10^7$. With four PEGs it is $7 \cdot 10^9$. Owing to steric constraints and kinetic factors, not all of these combinations of PEG–proteins will occur. However, it is clear that the immense heterogeneity of PEG–proteins explains the limited resolution and broad peak width seen with the previously mentioned separation techniques.

Polymer chemists have previously characterized compounds such as PEG–proteins and have classified them as grafted copolymers, defined as "a polymer with a small number of long grafts attached to one backbone" [14]. As demonstrated by the previous calculation of theoretically possible PEG–protein heterogeneity, polymers exist as a large family of similar compounds exhibiting group characteristics. This perception diverges dramatically from that of protein chemists, for whom protein microheterogeneity is discrete and, at least in theory, resolvable. Examples of protein HPLC exist, such as that of recombinant IL-2, where variants differing by a single atom are readily resolved on reversed phase [15]. For grafted copolymers such as PEG–proteins, heterogeneity is not discrete, but is a semi-continuous distribution of molecules which can only be described through statistical measurements such as width, average, skew, etc. Analyte properties are not unique to a given mixture, since many other mixtures of similar compounds could have identical group properties and chromatographic behavior.

Sizing has been a traditional characterization of polymers, useful in determining group parameters which could be related to the physical chemical behavior of the PEG–protein mixture. For example, Knauf *et al.* [7] have established that the effective hydrodynamic size of a PEG–protein can be a critical pharmacological measurement. In their study, different numbers and lengths of PEG were conjugated to IL-2 to yield mixtures varying in their

effective hydrodynamic size, as measured by SEC. The pharmacokinetic behavior of the PEG-IL-2 species in rats showed a close correlation between clearance and PEG–IL-2 size. It was suggested that the abrupt reduction in clearance seen above 70 000 dalton was due to the permeability threshold of the kidney, which retains proteins larger than albumin in the plasma. However, the size-exclusion chromatographic (SEC) calibration used by Knauf *et al.* was derived with native protein molecular weight and did not account for the increased hydrodynamic volume of the PEG.

The difficulty in calibrating an SEC system for PEG–proteins lies in the inherent differences in shape between PEG and proteins. On aqueous SEC, PEG chromatographs as a random coil. However, viscometric, calorimetric and several spectroscopic approaches indicate that solutions of aqueous PEG retain a degree of helical character, probably in relatively short sections [16–18]. Further, the molar specific volume of aqueous PEG is smaller than that expected from a totally random coil. Thus the overall structure of aqueous PEG is most likely a quasi-random coil or partially random coil conformation with numerous helical sections. This is very different from the compact globular native conformation of a protein.

For years, many biochemists have assumed the relationship between SEC retention and the logarithm of molecular weight (log MW) to be linear, and have used commercially available protein standards to derive apparent molecular weights of analyte proteins. Under strongly denaturing conditions of high salt (*e.g.*, 6 *M* guanidine hydrochloride), this relationship holds true for most peptides and proteins [19]. Native proteins are defined by their characteristic secondary, tertiary and quaternary structures which may deviate from spherical geometry and thus represent exceptions to the SEC retention to log MW linearity. To account for the dependence of SEC retention on molecular shape and not molecular weight, some researchers have used the intrinsic viscosity-based radius (R_η) instead of the log MW term [20,21]. Called universal calibration, this method is a major improvement over molecular weight calibration and is generally more accurate than that of translational frictional-based Stokes radius (R_s) calibration. Previous researchers have shown that both globular proteins and random coil macromolecules such as pullulans and dextrans can be characterized through universal calibration techniques [22,23]. However, the absolute accuracy of universal SEC calibration for biological molecules is still an issue of debate in the literature, as exceptions have been found [22,24]. The calibration of the SEC system appropriate for PEG–proteins will be explored in this study.

The fundamental polymer characteristics obtained from SEC are the number–average molecular weight ($\bar{M}_n$), the weight–average molecular weight ($\bar{M}_w$) and polydispersity. The number-average molecular weight is traditionally defined as

$$\bar{M}_n = \frac{\sum N_i M_i}{\sum N_i} \tag{1}$$

where N_i is the number of molecules and M_i is the molecular weight of a given chromatographic increment. The number-average molecular weight is an arithmetic mean of the sizing distribution, and assumes that each molecule makes an equal contribution to the polymer property regardless of size or weight.

The weight-average molecular weight is defined as

$$\bar{M}_w = \frac{\sum N_i M_i^2}{\sum N_i M_i} \tag{2}$$

The weight-average molecular weight is a weighted average in which each molecule contributes in accordance with its weight.

The polydispersity is defined as

$$\text{polydispersity} = \frac{\bar{M}_w}{\bar{M}_n} \tag{3}$$

The polydispersity value is characteristic of a polymer distribution. For a Gaussian distribution the polydispersity is 1.0, although in practice its value is nearly always greater. $\bar{M}_n$ and $\bar{M}_w$ are normally calculated with commercially available data reduction programs and calibrated with narrow-range molecular weight standards. The size-exclusion chromatogram is divided into slices (*e.g.*, 0.1-min increments) for which the area (N_i) and molecular weight (M_i) are determined from the area and calibrated mass of each slice.

THEORY, PEG–PROTEIN COMPOSITION

The PEG composition (mass of PEG/mass of protein) can be determined using two different detectors in series: UV at 280 nm (A_{280}) for selectively measuring protein and refractive index (RI) for measuring both protein and PEG. Analysis of copolymer composition has been previously developed for traditional polymers using UV detection at different wavelengths and also the combined UV–RI detection employed here [25–27]. The weight of the protein portion of the PEG–protein, as derived from its UV absorbance, is used to determine the protein's contribution to the refractive index response of the PEG–protein. The remaining refractive index response of the PEG–protein is due to the PEG, and can be converted to a weight value through the appropriate calibrations. In the most general case where both copolymer components have UV and RI responses, the two unknown weights can be determined in a similar fashion from two independent concentration detectors.

The fundamental assumption of this analytical method is that the RI response of the PEG–protein is the sum of the RI responses of the PEG and the protein alone. The RI of a component is characteristic of the electron density of that component. As there is a single covalent bond between two large molecules, protein and PEG, the electron density of each should be essentially unchanged, and the approximation of their RI additivity should be accurate (eqn. 4) [14].

$$n = n_0 + \left(\frac{dn}{dc}\right)_p C_p + \left(\frac{dn}{dc}\right)_x C_x \tag{4}$$

where n_0 is the refractive index of the solvent, $(dn/dc)_p$ and $(dn/dc)_x$ are the specific RI increments for PEG and protein x, respectively, and C_p and C_x are the weight concentrations of the PEG and protein x per unit volume. Rearrangement of eqn. 4 yields

$$\frac{n - n_0}{C_x} \equiv \left(\frac{dn_{px}}{dc_x}\right) = \left(\frac{dn}{dc}\right)_p \frac{C_p}{C_x} + \left(\frac{dn}{dc}\right)_x \tag{5}$$

The left-hand part of eqn. 5 can be redefined as the RI increment for the PEG–protein as a function of the change in the protein portion of this copolymer (dn_{px}/dc_x). Eqn. 5 can be rearranged to give

$$\frac{C_p}{C_x} \equiv \frac{W_p}{W_x} = \frac{\left(\frac{dn_{px}}{dc_x}\right) - \left(\frac{dn}{dc}\right)_x}{\left(\frac{dn}{dc}\right)_p} \tag{6}$$

The volume dimension of the concentration terms, C_p and C_x, cancels to yield the mass ratio (composition) of PEG to protein (W_p/W_x).

Except for very short PEG polymers, the chemical composition per unit length of PEG is constant. Hence $(dn/dc)_p$ for PEG will also be constant over any practical weight range. For most proteins, the principal source of electron density is the amide peptide bond, which is proportional to the molecular weight of the protein. Hence most proteins will also have the same $(dn/dc)_x$ [14]. A protein having an unusual amino acid composition (*i.e.*, an unusually large number of aromatic residues) would have a slightly different $(dn/dc)_x$. However, it is not necessary to rely on literature values of dn/dc for PEG or protein because relative response factors for $(dn/dc)_p$ and $(dn/dc)_x$ can easily be determined experimentally.

Calibration graphs of the appropriate range are constructed both for the PEG alone and for the protein alone, both prior to conjugation. The slopes of these calibration graphs, in refractive index area/weight, will be proportional to the $(dn/dc)_p$ and $(dn/dc)_x$ values in eqn. 6. The (dn_{px}/dc_x) term is determined from the PEG–protein sample itself. The RI detector signal is proportional to the dn_{px} term for the PEG–protein, while the concentration of the protein in the PEG–protein, the dc_x term, is determined from the integrated UV detector area. During the calibration for the $(dn/dc)_x$ for protein alone, the UV response factor at 280 nm (protein UV area/weight) is established. Because the detectors are in series, the protein concentration of the PEG–protein can be determined from the identical injection used to determine the RI response of the PEG–protein sample (eqn. 7).

$$\left(\frac{dn_{px}}{dc_x}\right) = \frac{(\text{PEG–protein RI area})\,K}{\left(\frac{\text{PEG–protein UV area}}{\text{protein UV area/weight}}\right)} \tag{7}$$

where K is a proportionality constant for the RI increment. Therefore, once calibration graphs have been used to establish the RI response of PEG alone

and the UV and RI responses of the protein alone, a single injection of the PEG–protein sample can yield both UV and RI responses to calculate the weight composition of that sample (eqn. 8).

$$\frac{W_p}{W_x} = \frac{\dfrac{\text{PEG–protein RI area}}{\left(\dfrac{\text{PEG–protein UV area}}{\text{protein UV area/weight}}\right)} - \dfrac{\text{protein RI area}}{\text{weight}}}{\dfrac{\text{PEG RI area}}{\text{weight}}} \quad (8)$$

The proportionality constant, K, cancels out in the derivation of eqn. 8. The molar ratio of PEG per protein can be calculated from the weight composition and requires the number-average molecular weight of the PEG:

$$\frac{\text{mol PEG}}{\text{mol protein}} = \frac{(\text{weight composition})\,(\text{MW protein})}{\bar{M}_n(\text{PEG})} \quad (9)$$

Owing to impurities (*i.e.*, diol and elimination products) in the monomethyl-PEG normally used for conjugation, the $\bar{M}_n$ derived from calibrated SEC and end-group titration may differ from each other.

Previous approaches to the characterization of PEG–proteins usually did not consider the diverse nature of grafted copolymers and, as a result, they often suffered from a lack of accuracy. This paper presents data validating the accuracy of the determination of hydrodynamic size and weight composition for PEG–proteins.

EXPERIMENTAL

Apparatus

The semi-preparative SEC system consisted of an Altex Model 100A pump (Beckman, Fullerton, CA, USA), a WISP 710A autoinjector (Millipore–Waters, Milford, MA, USA), two Zorbax GF-250 columns in series, each 25 cm × 9.4 mm I.D. (DuPont, Wilmington, DE, USA), a Spectraflow 773 UV detector (Kratos, Ramsey, NJ, USA), an ERC-7510 RI detector (Erma, Tokyo, Japan) and a Nelson Analytical 6000-SEC/GPC data acquisition system and software (PE/Nelson, Cupertino, CA, USA). The SEC software calibration option used was a narrow standard peak position calibration method as described by Yau *et al.* [28]. It was employed to calculate $\bar{M}_n$ *and* $\bar{M}_w$ values for experimental PEG samples. Fractions were collected manually.

The analytical SEC system consisted of a Waters Model M6000 pump (Millipore–Waters), a Lo-Pulse LP-21 pulse damper (Scientific Systems, State College, PA, USA), a WISP 710A autoinjector, a Superose 12 column (Pharmacia–LKB, Piscataway, NJ, USA), an Eldex (Menlo Park, CA, USA) 725-101D column heater set at 25°C, a Waters Model 484 UV detector (Millipore–Waters), an ERC-7510 RI detector and a Nelson Analytical 6000-SEC/GPC data acquisition system and software. The eluent for both SEC systems, used at a flow-rate of 0.5 ml/min, consisted of 0.1 *M* sodium sulfate (Fluka, Ronkonkoma, NY, USA) and 0.01 *M* sodium phosphate (pH 7.0) in Type I water from a Technic (Seattle, WA, USA) water system. The hydrolysis equipment consisted of a Thermodyne heating block (Sybron/Thermolyne, Dubuque, IA, USA) and a Savant Speed Vac Concentrator (Savant Instruments, Farmingdale, NY, USA). A Camag TLC Scanner II (Wilmington, NC, USA) set at 590 nm was used to measure the gel bands.

Materials

IL-2 and PEG–IL-2 were obtained from Cetus (Emeryville, CA, USA) [29,30]. Monomethoxypolyethylene glycol used for the preparation of PEG–proteins was obtained from Union Carbide (S. Charleston, WV, USA). The number-average molecular weight of this polymer was *ca.* 6000. Narrow-range PEG and polyethylene oxide (PEO) standards were obtained from American Polymer (Mentor, OH, USA). Thyroglobulin and myoglobin were obtained from Bio-Rad Labs. (Richmond, CA, USA). β-Galactosidase, catalase, aldolase, transferrin, alkaline phosphatase, ribonuclease A, cytochrome *c* and N-(2-hydroxyethyl)piperazine-N′-(3-propanesulfonic acid) (EPPS) buffer were obtained from Sigma (St. Louis, MO, USA). Physical data for these PEG, PEO and protein calibrators are given in Table I. Glutaric anhydride and N-hydroxysuccinimide (NHS) were from Aldrich (Milwaukee, WI, USA). SDS-polyacrylamide gel electrophoresis (PAGE) Daiichi 10 × 10 cm precast, 4–20% gels were obtained from Enprotech (Hyde Park, MA, USA). Ester hydrolysis was performed using 6 *M*

TABLE I

CHARACTERISTICS OF SOLUTES USED FOR SEC CALIBRATION

Solute	MW	$\bar{M}_w/\bar{M}_n$	$[\eta]$ (dl/g)	R_η (Å)	R_s (Å)
PEG standards					
PEO 45000	45 000	1.07	0.610	76	
PEO 21000	21 000	1.12	0.360	49	
PEG 18000	18 000	1.18	0.282	43	
PEG 10750	10 750	1.04	0.202	33	
PEG 10665	10 665	1.05	0.201	32	
PEG 5050	5050	1.04	0.133	22	
PEG 4950	4950	1.10	0.127	22	
PEG 3410	3410	1.08	0.107	18	
PEG 2560	2560	1.08	0.090	15	
PEG 2065	2065	1.05	0.079	14	
PEG 1510	1510	1.06	0.067	12	
Protein standards					
Thyroglobulin	660 000				86
β-Galatosidase	465 000				69
Catalase	220 000				52
Aldolase	158 000				46
Immunoglobulin G	158 000				49[a]
Alkaline phosphatase	86 000				33
Transferrin	81 000				36
Myoglobin	16 900				19
Ribonuclease-A	13 700				18
Cytochrome *c*	13 400				17

[a] Determined by HPSEC as described under Experimental.

hydrochloric acid (J. T. Baker, Phillipsburg, NJ, USA).

Methods

PEG–protein conjugates were prepared using the method of Katre *et al.* [8] by first making an active ester of PEG, and then allowing it to react with protein in EPPS buffer (pH 8.5). Glutaric anhydride was used to make methoxy PEG–glutarate, and the active ester prepared from this was N-hydroxysuccinimide ester [5]. In order to achieve various degrees of protein conjugation, the activated PEG ester was added to the protein solutions at different molar excesses. The resulting solutions were chromatographed on the semi-preparative SEC system, two GF 250 columns in series, to isolate populations of PEG proteins enriched for certain compositions. This separation also excluded from further analysis the unconjugated protein and PEG. The mass of protein injected on the columns varied, but injection volume of the sample was $\leqslant 200$ μl. The polymeric nature of PEG–protein usually precluded the isolation of fractions containing a unique species. Fractions were collected manually. The analytical SEC system was then used to analyze PEG–proteins for weight composition. Although it provided lower resolution than the semi-preparative system, the Superose 12 column was chosen for the analytical system because it gave quantitative recoveries for the unconjugated proteins used in this study.

In order to make a direct measurement of the amount of PEG in each fraction, samples were hydrolyzed by incubation with an equal volume of 6 *M* hydrochloric acid at 85°C for 2 h. This step precipitated the protein fraction. It was followed by vacuum drying, extraction of the free PEG by reconstitution in eluent, centrifugation and removal of the supernatant. Hydrolyzed samples were injected onto the Superose 12 column in parallel with their non-hydrolyzed counterparts. The non-

hydrolyzed sample was used to determine the weight composition of the sample and the protein concentration; the hydrolyzed samples gave the amount of PEG.

Calibration graphs were obtained from analyses of standard solutions (in the range 0.1–1.5 mg/ml) of PEG alone and of protein alone in Type I water. Linear regression analysis of the composite, integrated peak areas in relation to mass for each calibrator yielded a slope (area/mg) which was used to calculate the weight composition using eqn. 8.

SDS-PAGE analyses of the PEG–proteins were loaded with an average protein load of 4.5 μg (15 μl load volume) per well and run at 30 mA constant current per gel. The running buffer was 0.025 *M* Tris–0.19 *M* glycine–0.1% SDS. The staining of the gel was done with a solution of 0.09% Coomassie Blue in 25% ethanol–8% glacial acetic acid in a microwave oven for 3 min. After cooling, the gels were destained in 25% ethanol–8% glacial acetic acid overnight.

RESULTS AND DISCUSSION

SEC calibration for PEG–proteins

As PEG is a homopolymer with a quasi-random structure, it would be expected to have an SEC calibration linear with log MW. Fig. 1a shows that, under the SEC conditions employed, calibration with narrow molecular weight range standards of PEG and PEO did yield a linear calibration for peak apex retention volume *vs.* log MW over a wide range of molecular weights. Protein standards covering a broad molecular weight range, chromatographed on the identical SEC system, gave the peak apex retentions plotted in Fig. 1a. This calibration demonstrates reasonable agreement with the retention volume *vs.* log MW calibration, but the deviations from linearity are greater than those for PEG and PEO. A dramatic difference is seen between the protein and the PEG or PEO calibration graphs in the displacement and dissimilarity of their respective slopes. The explanation for this difference is that the quasi-random coil conformation of aqueous PEG has a much larger effective volume than that of compact native proteins. Thus a commonly used calibration for the SEC of proteins, namely apparent molecular weight, will be unsatisfactory for PEG–proteins. In Fig. 1, a given retention volume indicates a protein molecular weight nearly ten times larger than that of a PEG of similar hydrodynamic volume. The calibration of a PEG–protein will lie between these two extremes and will vary as a function of the amount, length and placement of the

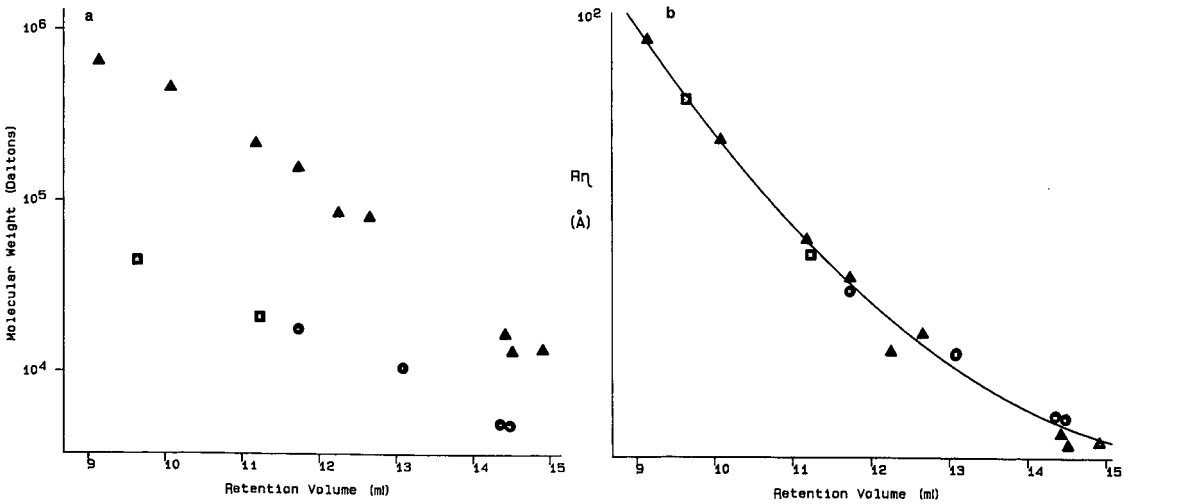

Fig. 1. (a) Peak apex retention volumes of (■) polyethylene oxides (MW 45 000 and 21 000), (●) polyethylene glycols (MW 18 000, 10 750, 10 665, 5050 and 4950) and (▲) proteins [thyroglobulin (660 000), β-galactosidase (465 000), catase (220 000), aldolase (158 000), alkaline phosphatase (86 000), transferrin (81 000), myoglobin (16 900), ribonuclease A (13 700) and cytochrome *c* (13 400)], plotted as a function of log (molecular weight). For conditions of SEC, see Experimental. (b) Chromatographic data identical with those in (a) plotted as a function of R_η.

PEGs conjugated to the protein.

The use of universal calibration is one way to address this calibration difference between PEG and proteins, and to provide a means of measuring the copolymeric species of PEG–proteins. Further, universal calibration of a PEG–protein yields a number or weight-averaged R_η which is a meaningful measure of its pharmacological behavior [7]. For the PEG and PEO calibrators, R_η was calculated from $[\eta]$ supplied by the vendor, using eqn. 10 as described in ref. 20.

$$R_\eta = \frac{30M[\eta]}{\pi N} \tag{10}$$

where R_η is the viscosity radius, M is the molecular weight, $[\eta]$ is the intrinsic viscosity of the molecule and N is Avogadro's number. These data are given in Table I and the results are plotted in Fig. 1b. For water-soluble, globular proteins, no systematic difference has been found between R_s (frictional-based) and R_η (viscosity-based radius) [20]. Thus, as a first approximation, literature values of R_s were used for the protein calibrators in Fig. 1a and substituted for R_η in Fig. 1b [21]. Fig. 1b is the universal calibration obtained for PEG, PEO and proteins. A third-degree polynomial fit shows a well behaved curve ($R^2 = 0.991$), with all of the calibrators sharing a common line. Although universal calibration for PEG–proteins is not rigorously validated in this paper, it is clearly an improvement over the erroneous native protein molecular weight calibration used by previous researchers [7,11]. As universal calibration utilizing both PEG and proteins is well behaved, universal calibration is likely also to be an accurate and pharmacologically relevant measure of PEG–protein size, as the viscosity radius, R_η, effectively compensates for the differences between aqueous PEG and globular protein structures.

The data in Fig. 1b show that proteins diverge from a common calibration more frequently than do PEGs, perhaps owing to residual secondary retention artifacts. It is also possible that the actual R_η values for these calibration proteins may vary from the values used for Fig. 1a, owing to a change in the protein tertiary structure when solubilized in an eluent differing from that used to determine the literature R_s value. Sensitive on-line HPLC viscometers, which have recently become commercially available, would be useful in establishing the R_η of protein and PEG calibrators and of analyte samples with the specific SEC system used. Use of an HPLC viscometric detector would also have allowed us to determine the actual R_η values for various PEG–proteins and thus validate the use of universal calibration for the SEC of PEG–proteins. Polydispersity is a unitless ratio of $\bar{M}_w/\bar{M}_n$ and is immune from issues of calibration accuracy.

Tables I and II list the R_η values for native and PEG conjugated versions of ribonuclease, myoglobin, and IgG. Using universal calibration, SEC analysis shows approximately a 2–3-fold increase in R_η on PEG conjugation of these proteins. The length of the PEG and the degree of conjugation can be controlled to provide PEG–proteins of a desired size range [1–5].

Weight composition

The determination of the weight of PEG per weight of protein as described in the theory section uses two detectors in series to provide sufficient information to solve for the two unknown values, PEG and protein weight concentration. The uncon-

TABLE II

VALIDATION OF WEIGHT COMPOSITION BY HYDROLYSIS FOR VARIOUS PEG–PROTEINS

PEG–protein	Weight composition	PEG expected (mg)	PEG found (mg)	% of expected	R_η (Å)
PEG–ribonuclease	1.69	0.35	0.33	94	58
PEG–myoglobin	0.45	0.17	0.16	90	39
	1.29	0.49	0.44	94	57
PEG–IgG	0.25	0.13	0.12	92	102

jugated PEG and protein used in the construction of the PEG–protein are chromatographed separately over the appropriate concentration ranges as independent calibration graphs. Peak symmetry, quantitative recovery and linearity of the calibration graphs assure that the PEG and the protein are not chemically interacting with the column support and are being retained only through sizing mechanisms. For proteins, this type of calibration graph also establishes the lack of chromatographic artifact from concentration-dependent aggregates. Calibration graphs for the PEG are monitored only with RI detection, as underivatized PEG has no useful UV absorbance at 280 nm. Both UV and RI detectors are used in series to monitor protein calibration graphs. From the calibration graphs, the response factors in RI area/weight is calculated for PEG and for protein. The slopes of these calibration graphs, in RI area/weight, will be proportional to the dn/dc values for the particular SEC set-up. The arbitrary area units are specific for the data system used and also for the column, eluent and detector combination used. Changes in eluent should be monitored for changes in the dn/dc proportionality constant for both PEG and protein. For the four proteins used in this study, the RI calibration graph slopes were similar to one another with a relative standard deviation (R.S.D.) of 6%. This result supports the expectation that protein dn/dc values will be similar. These protein calibration graphs were also highly linear, with R^2 ranging from 0.9984 to 0.9999, and averaging 0.9995 for the UV and RI calibration graphs. Determination of protein concentrations from absorbance at 280 nm will be more accurate than weighing if an accurate molar absorptivity (ε'_{280}) is available, owing to possible errors from salt and hydration.

In this study, experiments were designed to establish that the RI detector was accurately measuring polymer mass. To validate this aspect of the analysis, calibration graphs for five of the PEG and PEO narrow range molecular weight calibrators were chromatographed and the resulting RI areas plotted *versus* weight of polymer injected (Fig. 2). All five calibration graphs are highly linear (R^2 = 0.999), and have virtually identical slopes. This shows that PEGs of any length can be used for RI calibration and that the PEG dn/dc is constant. However, calibrating with the PEG used for PEG–protein conjugation has the advantage of establishing the

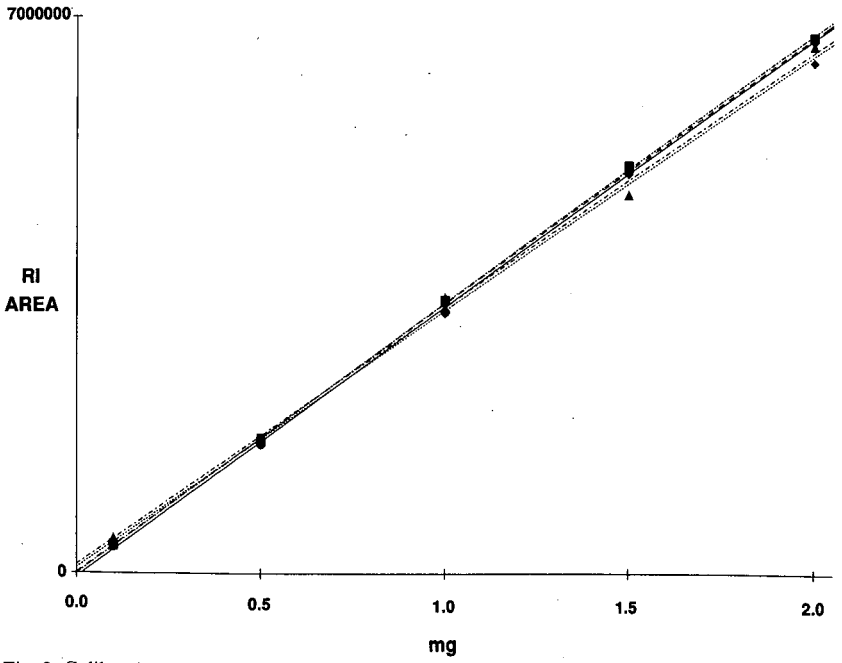

Fig. 2. Calibration graphs of peak area *versus* weight injected for various size PEG and PEO standards (■ = 45 000; ◆ = 21 000) and PEG standards (▲ = 10 750, □ = 3410).

distribution ($\bar{M}_n$,$\bar{M}_w$ and polydispersity) of the PEG actually employed.

The weight composition of a PEG–protein sample is calculated from the three slopes derived from the calibration graphs obtained when protein UV, protein RI and PEG RI responses are measured. Using the identical SEC system, a sample of PEG–protein whose mass is consistent with the PEG and protein calibration graphs is chromatographed, and the resulting area values are used to calculate the weight composition using eqn. 8. Linearity can be checked by constructing calibration graphs of the appropriate range, or it can be assumed, and the slope calculated from a one-point standard calibration passing through zero concentration. The mass of protein injected is calculated on-line with the use of the UV detector area so that a knowledge of the actual protein concentration in the amount injected is not critical.

Another aim of this study was to establish the accuracy of this approach to weight compositional analysis by independently measuring the mass of the PEG and protein moieties. Various PEG–proteins were prepared and semipreparatively fractionated to yield samples conjugated to different extents. For the examples presented here, glutaric acid was used as a linker, providing an easily hydrolyzable ester bond between the PEG and the protein. Acid hydrolysis was used to cleave the conjugated PEG from the corresponding protein. The protein concentration in the PEG–protein conjugate was determined from a calibration graph for the PEG–protein, which was calibrated off-line by UV absorbance of the standards at 280 nm. Literature molar absorptivities were then used to calculate the protein concentrations of the standards. Non-hydrolyzed aliquots of the PEG–protein samples were analyzed by the UV–RI method to establish their weight composition. The expected amount of PEG in a given volume was calculated for each sample. After acid hydrolysis, the free PEG was measured by SEC with RI detection. The PEG recovery was calculated by dividing the amount of PEG found by the amount expected and multiplying by 100. The results for PEG–ribonuclease, PEG–myoglobin and PEG–IgG are given in Table II. The uniformly high recoveries of hydrolyzed PEG for the various PEG–protein samples establish the validity and general utility of this approach.

As the glutaric acid linker is not hydrolyzed off the protein but is measured as PEG–protein mass prior to hydrolysis, one expects the recovery to be 2% low, the ratio of glutaric acid molecular weight to the PEG number-average molecular weight. Errors in the protein molar absorptivities will lead to proportional errors in the weight composition as it will affect the protein calibration graphs. However, when calculating the recovery of hydrolyzed PEG, inaccuracy in molar absorptivity will be inversely compensated for by the calculation of the expected mass of PEG. Thus, errors in molar absorptivities are immaterial to the calculation of PEG recovery. As a check on chromatographic artifacts, acid hydrolysis of a PEG sample was performed in parallel, and no effect on the PEG was seen. However, base hydrolysis of PEG–proteins did yield chromatographic artifacts, perhaps from base–catalyzed protein reactions.

Calculation of the molar composition is a useful PEG–protein characterization and is easily done with eqn. 9. Accurate determination of $\bar{M}_n$ requires some additional analysis. During the process of conjugating PEG to a protein, the PEG undergoes several chemical and purification steps. There are many opportunities to alter the size distribution of the PEG through kinetic or physical chemical differences. Thus, $\bar{M}_n$ should be determined for the acid-hydrolyzed PEG to establish precisely the PEG size distribution on the PEG–protein itself. In this study, the PEG that was hydrolyzed from the IL-2 protein was compared with the starting material PEG and was found to have the same size distribution.

In order to characterize further a PEG–protein population by weight composition, preparations of PEG–IL-2 were sequentially fractionated (preparatively and analytically) by SEC to yield samples which were enriched in species of a given weight composition. Analysis of all the fractions revealed that their weight compositions varied over a broad range (Table III). Nearly quantitative recoveries of hydrolyzed PEG were seen for all of these samples. This establishes that weight composition analysis is valid over any practical PEG to protein ratio, provided that the sample size and peak resolution are sufficient for accurate baseline integration. Because the PEG–protein mixture is essentially a continuous distribution of conformers, baseline

TABLE III

VALIDATION OF WEIGHT COMPOSITION BY HYDROLYSIS FOR PEG–IL-2 FRACTIONS ISOLATED BY SEMI-PREPARATIVE SEC

PEG–IL-2 sample	Weight composition	PEG expected (mg)	PEG found (mg)	% of expected
A	0.53	0.44	0.44	100
B	0.85	0.79	0.77	98
C	1.01	0.22	0.21	94
D	1.16	0.29	0.28	95
E	1.20	0.43	0.42	98
F	1.32	1.64	1.60	97
G	1.36	1.05	0.99	95
H	1.41	1.68	1.70	101
I	1.70	4.59	4.41	96
J	1.70	10.27	9.96	97
K	1.82	2.28	2.22	97
L	2.18	2.59	2.44	94
M	2.35	2.23	2.23	100
N	26.50	15.92	15.76	99

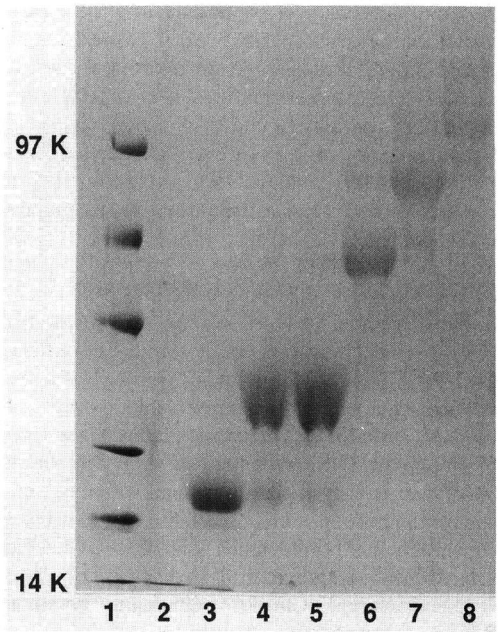

Fig. 3. Coomassie Blue-stained SDS-PAGE gel of PEG–IL-2 samples isolated by semi-preparative SEC. Molar composition (mol PEG/mol IL-2): lane 1 = MW standards; lane 2 = 0 PEG; lane 3 = 1.0 PEG; lane 4 = 2.0 PEG; lane 5 = 3.1 PEG; lane 6 = 4.1 PEG; lane 7 = 4.9 PEG; lane 8 = 6.0 PEG. K = kilodalton.

drops between fused peaks represent arbitrary divisions of related mixtures and may not be equally reflected in both the RI and UV chromatograms. Compositional accuracy of a sample will be assured only if the entire chromatographic peak area is integrated.

Comparison with gels

SDS-PAGE has been a popular method to characterize PEG–protein distributions [7,11]. The assumptions made were that the higher molecular weight gel band ladders represented one molar incremental additions of PEG to the protein, and that the staining density was proportional to protein concentration in each of the bands. In this study, the validity of these assumptions was tested using UV–RI SEC methodology.

Some of the PEG–IL-2 samples used for the hydrolysis validation were also analyzed by SDS-PAGE (Fig. 3). As the weight composition increased, the gel lanes generally increased in apparent hydrodynamic size. However, the 2.0 and 3.1 molar composition PEG–IL-2 samples were not resolved, but co-migrated in a broad band. An investigator without the aid of compositional analysis would incorrectly identify the SDS-PAGE bands of PEG–IL-2 based purely on the one molar ladder assumptions. This anomalous PAGE migration of the PEG–IL-2 samples was also observed in the SEC analysis of similar samples (Fig. 4). Comparison of the molar composition with retention time and observed R_η of these samples shows a similar pattern; the 2.1 and 3.0 molar PEG–IL-2 species were not resolved, whereas other samples followed the expected retention trend.

The lack of resolution between the 2.1 and 3.0 molar composition PEG–IL-2 species is not a general phenomenon, as the other proteins used in this study, ribonuclease, myoglobin and IgG, did not display similar behavior. One explanation is that conjugation of the third PEG–NHS molecule to IL-2 might occur close to either the first or the second PEG molecule in the IL-2 tertiary structure, presenting a minimum increase in effective hydrodynamic size. Another possibility is that the 2-PEG–

IL-2 molecules might have an altered tertiary protein structure, resulting in a larger hydrodynamic size. Although these PEG conjugations are statistical and yield complex mixtures of molecular combinations, there may be enough kinetic variation in lysine reactivity in IL-2 to direct a selective PEG conjugation. The kinetics of PEG–NHS conjugation coupled with the lysine locations and reactivities within the tertiary structure for IL-2 apparently lead to PEG–IL-2 species varying in composition but having similar PAGE migrations and SEC retentions. The exact location and distribution of the PEG–lysine conjugations is not well established. This PAGE and SEC anomaly demonstrates the importance of recognizing the polymeric nature of PEG–IL-2. PEG–protein samples which are relatively pure by SDS-PAGE, having similar apparent molecular weights (hydrodynamic volumes), are actually composed of millions of different molecules which vary in all three dimensions of PEG–protein heterogeneity, including molar composition.

The gel lanes in Fig. 3 were scanned with a densitometer and the results are shown in Fig. 5. The amount of protein applied to each lane was calculated from A_{280} of the in-solution samples, and the gel band response factors were expressed as scan area per milligram of IL-2 protein. As the degree of PEG conjugation increased, the response factor dramatically decreased to approximately one tenth of its original value. It is thought that the PEG molecules shield the IL-2 molecules from dye adsorption. Studies with other PEG–proteins have shown this trend to vary widely from protein to protein. Some proteins, such as myoglobin, do not display decreases in gel response factor with increasing degree of PEG conjugation (data not shown). The PEG–IL-2 SDS-PAGE is therefore an example showing the potential for error in both gel band identification and in estimating PEG distribution.

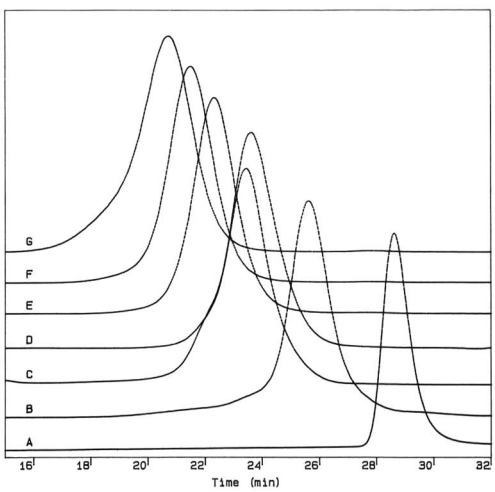

Fig. 4. SE-HPLC traces for PEG–IL-2 samples. Molar compositions and (in parentheses) R_η in Å for trace (A) 0 PEG (18); (B) 1.0 PEG (35); (C) 2.1 PEG (49); (D) 3.0 PEG (44); (E) 4.1 PEG (53); (F) 4.9 PEG (59); (G) 6.0 PEG (67).

CONCLUSIONS

Conjugation of a monomethoxy-PEG polymer to a protein does not create a unique species, but a family of compounds called grafted copolymers which are highly heterogeneous. The normal definition of purity used by protein biochemists is therefore inappropriate for the description of PEG–proteins, as are the methods normally used to characterize them. An SEC analysis based on the premise of polymeric heterogeneity has been developed and validated for PEG–proteins. This method quantitatively describes a PEG–protein mixture in statistical, non-unique terms, thus taking into account its heterogeneous nature. By using UV and RI detectors in series, three characteristics of PEG–proteins can be measured from a single chromatographic run: molecular size (R_η), polydispersity and weight composition. The viscosity-based universal SEC calibration compensates for the difference in

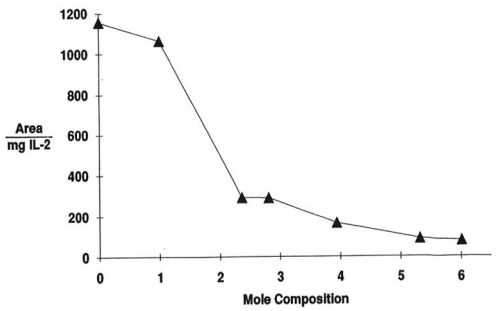

Fig. 5. Densitometric analysis of the SDS-PAGE gel in Fig. 3. Normalized response factors (integrated area per weight protein) as a function of molar composition as determined by UV–RI SEC.

partial specific volume of aqueous PEG and native, globular proteins, allowing meaningful SEC calibration of the PEG–protein hybrid. Both the PEG and PEO standards and the protein standards follow universal calibration for SEC, suggesting that the PEG–protein copolymer will also be accurately calibrated by this method. The width of the polymeric distribution is described by the traditional polymer term, polydispersity. The weight (or molar) composition is obtained through UV and RI detector calibration of the SEC system with the PEG and protein separately, before conjugation. Comparison of the SEC analysis with traditional biochemical analysis by SDS-PAGE shows that the latter can produce errors in band identification and quantification. To prevent erroneous gel interpretation, investigators are advised to calibrate their particular PEG–protein for SDS-PAGE or replace it with the UV–RI SEC compositional analysis.

ACKNOWLEDGEMENT

We thank Heatherbell Fong for her editorial aid in the preparation of the manuscript.

REFERENCES

1 F. F. Davis, A. Abuchowski, T. Van Es, N. C. Palczuk, K. Savoca, R. H.-L. Chen and P. Pyatak, *Biomedical Polymers*, Academic Press, New York, 1980.
2 K. Y. Park, A. Abuchowski, S. Davis and F. Davis, *Anticancer Res.*, 1 (1981) 373.
3 R. H.-L. Chen, A. Abuchowski, T. Van Es, N. C. Palczuk and F. F. Davis, *Biochim. Biophys. Acta*, 660 (1981) 293.
4 C. O. Beauchamp, S. L. Gonias, D. P. Menapace and S. V. Pizzo, *Anal. Biochem.*, 131 (1983) 25.
5 A. Abuchowski, G. M. Kazo, C. R. Verhoest, T. Van Es, D. Kafkewitz, M. L. Nucci, A. T. Viau and F. F. Davis, *Cancer Biochem. Biophys.*, 7 (1984) 175.
6 R. J. Goodson and N. V. Katre, *Biotechnology*, 8 (1990) 343.
7 M. J. Knauf, D. P. Bell, P. Hirtzer, Z.-P. Luo, J. D. Young and N. V. Katre, *J. Biol. Chem.*, 263 (1988) 15064.
8 N. V. Katre, M. J. Knauf and W. J. Laird, *Proc. Natl. Acad. Sci. U.S.A.*, 84 (1987) 1487.
9 N. V. Katre, *J. Immunol.*, 144 (1990) 209.
10 S. J. Stocks, A. J. M. Jones, C. W. Ramsey and D. E. Brooks, *Anal. Biochem.*, 154 (1986) 232.
11 P. McGoff, A. Baziotis and R. Maskiewicz, *Chem. Pharm. Bull.*, 36 (1988) 3079.
12 C.-J. Jackson, J. Charlton, K. Kuzminski, G. Lang and A. Sehon, *Anal. Biochem.*, 165 (1987) 114.
13 R. Cunico, V. Gruhn, L. Kresin, D. Nitecki and J. Wiktorowicz, *J. Chromatogr.*, 555 (1991) 467.
14 P. Kratochvil, *Classical Light Scattering from Polymer Solutions*, Elsevier, Amsterdam, 1987, pp. 209 and 314.
15 M. Kunitani, P. Hirtzer, D. Johnson, R. Halenbeck, A. Boosman and K. Koths, *J. Chromatogr.*, 359 (1986) 391.
16 E. A. Bekturov and Z. K. Bakauova, *Synthetic Water-Soluble Polymers in Solution*, Hüthig & Wepf, Basle, 1981, p. 142.
17 P. Molyneux, *Water-Soluble Synthetic Polymers: Properties and Behavior*, Vol. 1, CRC Press, Boca Raton, FL, 1983, p. 19–45.
18 W. Melander, A. Nahum and Cs. Horváth, *J. Chromatogr.*, 185 (1979) 129.
19 W. O. Richter, B. Jacob and P. Schwandt, *Anal. Biochem.*, 133 (1983) 288.
20 K. Horiike, H. Tojo, T. Yamano and M. Nozaki, *J. Biochem.*, 93 (1983) 99.
21 M. Potschka, *Anal. Biochem.*, 162 (1987) 47.
22 P. Dubin and J. Principi, *Macromolecules*, 22 (1989) 1891.
23 R. Frigon, J. Leypoldt, S. Uyeji and L. Henderson, *Anal. Chem.*, 55 (1983) 1349.
24 M. le Marie, A. Viel and J. Moller, *Anal. Biochem.*, 177 (1989) 50.
25 S. Mori and T. Suzuki, *J. Liq. Chromatogr.*, 4 (1981) 1685.
26 J. R. Runyon, D. E. Barnes, J. F. Rudd and L. H. Tung, *J. Appl. Polym. Sci.*, 13 (1969) 2359.
27 X. Zhonge, Y. Ping, Z. Jingguo, J. Erfang, W. Meiyan and L. J. Fetters, *J. Appl. Polym. Sci.*, 37 (1989) 3195.
28 W. W. Yau, J. S. Kirkland and D. D. Bly, *Modern Size Exclusion Chromatography*, Wiley-Interscience, New York, 1979, pp. 289 and 317.
29 S. Wolfe, G. Dorin, F. Smith and A. Lim, *Eur. Pat. Appl.*, WO88/08849 (1988).
30 K. Koths, J. Thomson, M. Kunitani, K. Wilson and W. Hanisch, *US Pat.*, 4 569 790 (1986).

Journal of Chromatography, 588 (1991) 139–145
Elsevier Science Publishers B.V., Amsterdam

CHROM. 23 638

Rapid ion-exchange chromatography for preparative separation of proteins

IV. Application to bovine carbonic anhydrase III from skeletal muscle

Kristina Borén*, Marie Larsson, Nils Bergenhem and Uno Carlsson

IFM/Department of Chemistry, Linköping University, S-581 83 Linköping (Sweden)

(Received July 4th, 1991)

ABSTRACT

Bovine muscle carbonic anhydrase III was purified to homogeneity by the strategy of rapid ion-exchange chromatography. The ionic exchanger used was CM-cellulose, and this is the first application of this technique on a cation exchanger. Nitrogen gas was used to pressurize the chromatographic column to accelerate the elution. The results show that proteins with high isoelectric points can also be purified in this way. The procedure is very time-saving compared with conventional chromatography, reducing the elution time five- to ten-fold. The proteins are in addition protected against oxidation by air.

INTRODUCTION

Carbonic anhydrase (CA) III (EC 4.2.1.1) is the most abundant soluble protein in red fibres of skeletal muscle [1]. The physiological function of this enzyme is to facilitate the diffusion of carbon dioxide from the muscle cells to the blood capillaries [2]. CA III can be isolated from mammalian muscle by conventional techniques, including cation-exchange and gel-filtration chromatography [3]. These purification procedures are, however, time-consuming (they take *ca.* 2 weeks to perform), and the high cysteine content of the enzyme makes it susceptible to air oxidation. These problems were overcome by applying nitrogen gas pressure to the column during both the sample application and the chromatographic procedure. The resulting rapid ion-exchange chromatography approach, with an anion exchanger (DEAE-cellulose), has previously been found to be a successful method for preparing porcine and bovine CA from blood [4]; the technique has also been used to purify ribulose-1,5-bisphosphate carboxylase from spinach leaves [5] and coagulation factors from blood [6]. In these cases, the chromatographic times were reduced by about a factor of ten. By introducing a cation-exchange resin (CM-cellulose), this technique can also be used to purify proteins with high isoelectric points, such as CA III.

EXPERIMENTAL

Calcium phosphate gel used for batch-wise adsorption chromatography

The gel was prepared mainly according to the method of Keilin and Hartree [7], as described by Colowick [8]. Using a magnetic stirrer, 0.60 l of 2.2 *M* $CaCl_2$ and 0.64 l of distilled water were mixed with 0.60 l of 14 m*M* Na_3PO_4. The pH was adjusted to 7.4 with 1 *M* acetic acid, and the suspension was stirred for 1 h. The slurry was centrifuged (3200 *g*,

10 min), and the precipitate was carefully mixed with distilled water and centrifuged as before. The washing procedure was repeated until the conductivity was the same as in 20 m*M* sodium phosphate (pH 7.5). The gel was finally suspended in 0.60 l of the same buffer.

Chromatographic resins

CM-Cellulose CM-23 (Whatman), a fibrous resin that allows high flow-rates and resists moderate pressures, and Sephadex G-100 (Pharmacia) were used.

Rapid ion-exchange chromatography equipment

The equipment used for rapid ion-exchange chromatography is very simple and has previously been depicted (see Fig. 1 in ref. 4). In the present application, a nitrogen gas cylinder was used to pressurize the chromatographic equipment. Two 2.5-l plastic bottles with screw-caps were connected to the nitrogen cylinder and, by means of a siphon, to each other. A glass column was joined to one of the bottles, and a clamp was placed above the column stopper to keep it in position. All connections were made with poly(vinyl chloride) tubing. This chromatographic set-up was used for gradient elutions. One of the bottles and the siphon were omitted during packing of the column, equilibration, sample application and isocratic elution. After the column had been packed the surface of the gel was covered with a filter paper. All chromatographic steps mentioned above were run at the same flow-rate.

Crude enzyme purification

Fresh, lean skeletal muscle from cattle (*e.g.*, from the flank) was obtained at a local slaughterhouse. The muscle was freed from fat and connective tissue, 1.5 kg were minced, and 3 l of 20 m*M* sodium phosphate buffer (pH 7.5), containing 0.5 m*M* EDTA and 1 m*M* dithiothreitol (DTT), were added. The suspension was homogenized in a commercial Waring blender for five 1-min intervals. The suspension was carefully chilled and exposed to a powerful stream of nitrogen, when the blender was off. The homogenate was then centrifuged (3200 *g*, 1 h), and any fat floating on top of the supernatant was discarded. A volume of 170 ml of calcium phosphate gel containing 0.5 m*M* EDTA and 1 m*M* DTT was added to each litre of solution, and this mixture was stirred under nitrogen for 30 min. The gel was removed by centrifugation (3200 *g*, 20 min), and the supernatant was dialysed overnight against 3 m*M* sodium phosphate buffer (pH 6.8), containing 0.5 m*M* EDTA and 1 m*M* DTT, in a weak flow of nitrogen gas. The purification was performed in a cold room (+4 to +8°C).

First rapid ion-exchange chromatography

The crude enzyme extract (2.9 l, 14.4 g of protein) was chromatographed on a CM-cellulose gel (38 × 4.0 cm I.D.) eluted with a linear gradient (10–30 m*M*) of two 2.5-l volumes of sodium phosphate buffer (pH 6.8), containing 0.5 m*M* EDTA and 1 m*M* DTT. Prior to the chromatography, the enzyme extract and the cellulose gel were equilibrated to the same ionic strength and pH as the 10 m*M* buffer. The flow-rate was *ca.* 20 ml/min, and the volume of the fractions was 25 ml. The fractions with enzyme activity were pooled and concentrated under nitrogen (Amicon Diaflo ultra-filters, PM 10).

Gel filtration

A column was filled with Sephadex G-100 (85 × 7.5 cm I.D.), and the concentrated enzyme solution (190 ml, 1.7 g of protein) from the rapid ion-exchange chromatography was applied. Elution was achieved with 3 l of 6 m*M* Tris–H_2SO_4 (pH 7.5), containing 0.5 m*M* EDTA and 1 m*M* DTT. The flow-rate was 2 ml/min, and the fraction volumes were 20 ml. The fractions with enzyme activity were pooled.

Second rapid ion-exchange chromatography

The pooled enzym sample (800 ml, 880 mg of protein) from the gel filtration was rechromatographed on the CM-23 resin in the same column as before. Prior to chromatography, the enzyme sample and the cellulose gel were equilibrated to the same ionic strength and pH as 6 m*M* Tris–H_2SO_4 (pH 7.5), containing 0.5 m*M* EDTA and 1 m*M* DTT. The elution was started with 1 l of the equilibration buffer, and this was followed by a linear gradient elution step with 6–15 m*M* of the same buffer (two 2.5-l volumes). Finally, an isocratic elution step was applied (1.5 l of the 15 m*M* buffer). The flow-rate and the fraction volumes were the same as during the first rapid ion-exchange chroma-

tography. The fractions with activity were pooled and concentrated.

Extra purification step

An extra ion-exchange chromatographic purification step was included when extremely pure preparations were needed. This chromatography was performed without applying any extra pressure to the column. A fraction of the concentrate (35 ml, 102 mg of protein) from the second rapid ion-exchange chromatography was then applied to a CM-23 column (33 × 1.1 cm I.D.). The enzyme sample and the column were equilibrated to the same ionic strength and pH as 6 m*M* Tris–H_2SO_4 (pH 7.5), containing 0.5 m*M* EDTA and 1 m*M* DTT. Elution was first performed with 70 ml of the equilibration buffer, followed by a linear gradient (two 50-ml volumes) of 6–15 m*M* of the same buffer and terminated with 200 ml of 15 m*M* buffer. The flow-rate was 2 ml/min, and the volume of the fractions was 1.4 ml. Fractions with activity were pooled and stored under nitrogen.

Activity measurements

The carbon dioxide hydration activity was determined by the colourimetric method of Rickli *et al.* [9]. The number of activity units (AU) was defined as $5 \times (t_0/t - 1)/V_e$, where t and t_0 are the times for change of indicator colour with and without enzyme, respectively, and V_e is the volume (ml) of enzyme solution added to the total assay solution of 5 ml.

Protein concentration determination

Protein concentrations were estimated spectrophotometrically using an $A_{280\,nm}$ of 2.07 for a 1 mg/ml solution of CA III [3].

Determination of isoelectric points

The p*I* values of bovine CA III and of myoglobin were determined with the aid of the PhastSystem (Pharmacia). A standard containing eleven proteins with p*I* values from 3.75 to 9.30 was used.

Sodium dodecyl sulphate–polyacrylamide gel electrophoresis (SDS–PAGE)

Electrophoresis was carried out in a Mini-PROTEAN II dual slab cell (Bio-Rad). The concentrations of the spacer gel and the separation gel were 4% and 15%, respectively. Separation of the proteins was performed for 40 min at 180 V. A 0.025 *M* Tris–glycine buffer (pH 8.3), containing 3.5 m*M* SDS, was used as electrode buffer. An electrophoresis calibration kit for molecular mass determination of low-molecular-weight proteins (Pharmacia) was used as a reference. The protein bands were stained with 0.1% Coomassie blue R-250 in methanol–acetic acid.

RESULTS

By using the strategy of rapid ion-exchange chromatography, a yield of 331 mg of bovine CA III was obtained from 1.5 kg of muscle in a considerably shorter time than with conventional techniques. The various purification steps are summarized in Table I.

TABLE I

PURIFICATION OF BOVINE MUSCLE CARBONIC ANHYDRASE[a]

Purification step	A_{280} (cm^{-1})	A_{420}/A_{280}	Spec. act.[b] (AU/A_{280})	Yield of activity (%)	Purity
First centrifugation	36.6	0.54	2.9	100	1
First rapid ion-exchange chromatography	18.9	1.06	31.1	45	11
Gel filtration chromatography	2.4	1.25	45.8	36	16
Second rapid ion-exchange chromatography	6.0	0.023	105	30[c]	37

[a] Starting material was 1.5 kg of fresh skeletal muscle.
[b] Specific activities were calculated as the number of activity units (AU) in the assay solution divided by A_{280}.
[c] The yield of purified enzyme was 331 mg.

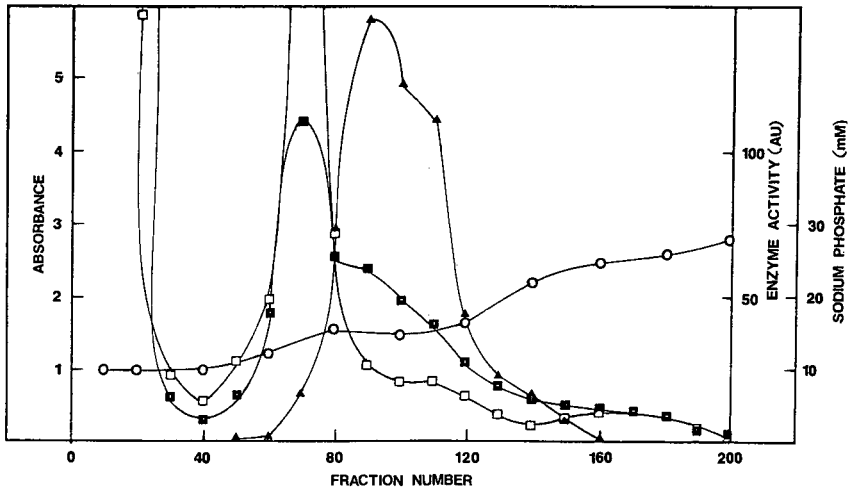

Fig. 1. First rapid ion-exchange chromatography of crude bovine CA III on a CM-cellulose CM-23 column. Gel bed dimensions, 38 × 4.0 cm I.D.; flow-rate, 20 ml/min (96 ml/h · cm^2); applied pressure, 0.2–0.3 kg/cm^2; volume of fractions, 25 ml; temperature, +4 to +8°C. Fractions 65–150 were pooled and concentrated. ■ = $A_{280\,nm}$; □ = $A_{420\,nm}$; ▲ = carbon dioxide hydration activity; ○ = buffer concentration. For further details, see Experimental.

Initial purification

To obtain an enzyme preparation in high yield, it is important that the bovine muscle tissue is not more than 2 days old: the older the tissue is, the more carbonic anhydrase seems to be associated to the muscle protein myoglobin, leading to separation problems and reduced yield of active enzyme. Furthermore, the oxidized fraction of the cysteines in the enzyme increases with time. To avoid oxidation by air, nitrogen gas was used in the initial purifica-

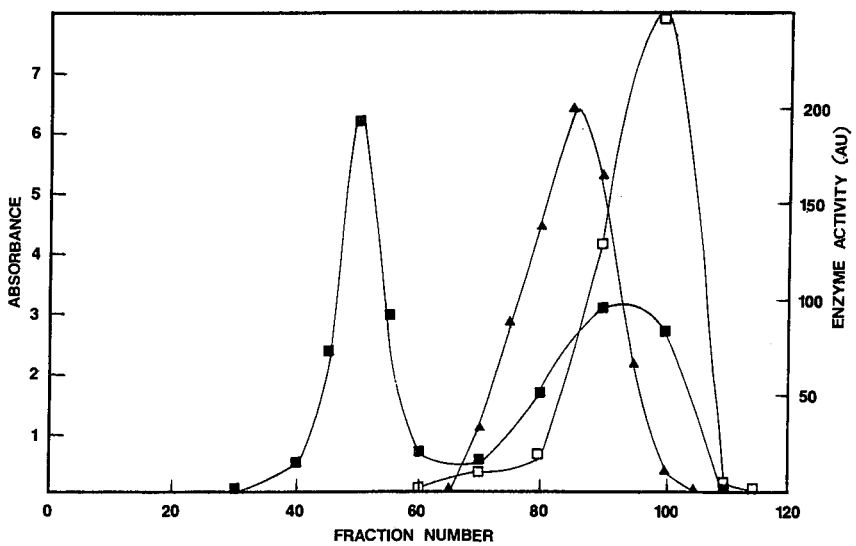

Fig. 2. Gel filtration chromatography of the concentrated bovine CA III solution from the first rapid ion-exchange chromatography on a Sephadex G-100 column. Gel bed dimensions, 85 × 7.5 cm I.D.; flow-rate, 2 ml/min (2.7 ml/h · cm^2); volume of fractions, 23.5 ml; temperature, +4 to +8°C. Fractions 65–98 were pooled. ■ = $A_{280\,nm}$; □ = $A_{420\,nm}$; ▲ = carbon dioxide hydration activity. For further details, see Experimental.

tion, as well as in several steps throughout the preparation. To further decrease the oxidation potential, DTT and EDTA were added to all solutions. The DTT-containing solutions should be as fresh as possible.

It is essential that all visible fat is discarded, otherwise the flow properties of the first ion-exchange column will be impaired owing to increased back-pressure.

First rapid ion-exchange chromatography

The first ion-exchange chromatography (Fig. 1) was completed in less than 4 h; this can be compared with conventional chromatography, which takes more than 24 h to perform [3]. During this step, CA III was separated from a large amount of contaminating substances. To facilitate the elution of myoglobin, with a determined p*I* of 7.0, the pH of the buffer was increased from 6.6 in the original preparation [3] to 6.8.

Gel filtration

Gel filtration (Fig. 2) was the most time-consuming preparation step. During this procedure CA III should be separated from proteins with higher molecular weights. However, CA and myoglobin (with molecular weights of 29 300[3] and 16 900[10], respectively, both calculated from amino acid sequence) cochromatographed to a great extent. The phosphate buffer (pH 6.6) previously used during this step [3] was replaced by a Tris buffer (pH 7.5), to avoid the need for a buffer change for the second rapid ion-exchange chromatography.

Second rapid ion-exchange chromatography

The p*I* value of bovine CA III was determined to be 9.0. During the second rapid ion-exchange chromatography (Fig. 3), a pH value of 7.5 was chosen between the p*I* values of CA III and the contaminating myoglobin. At low ionic strength, CA III was bound to the cation exchanger, whereas the negatively charged myoglobin was eluted during the first isocratic elution step.

The purity of the enzyme

To analyse the purity of bovine CA III in the various purification steps, SDS–PAGE was used (Fig. 4). Some minor bands, in addition to the predominant CA III band, appeared after the second rapid ion-exchange chromatography (Fig. 4, lane 5), indicating the presence of a small amount of contaminating proteins, probably mainly myoglobin. This protein has an absorbance maximum at 420 nm, hence the A_{420}/A_{280} ratio can be used as an

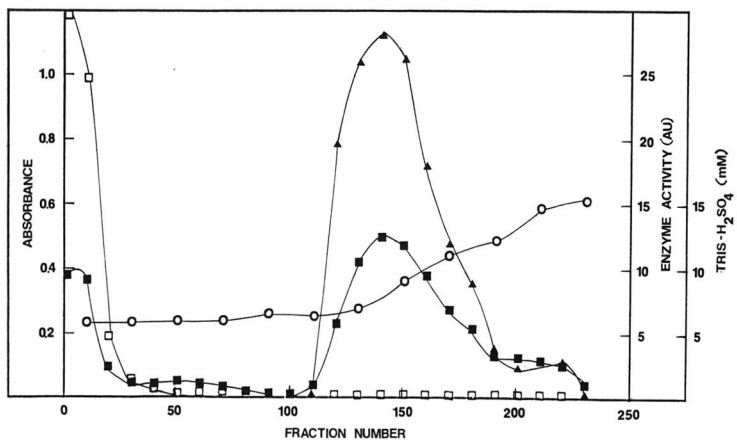

Fig. 3. Second rapid ion-exchange chromatography of the pooled fractions from the gel filtration chromatography. The resin, the bed dimensions, the flow-rate and the temperature were the same as in Fig. 1. Volume of fractions, 23 ml. Fractions 110–228 were pooled and concentrated. ■ = $A_{280\ nm}$; □ = $A_{420\ nm}$; ▲ = carbon dioxide hydration activity; ○ = buffer concentration. For further details, see Experimental.

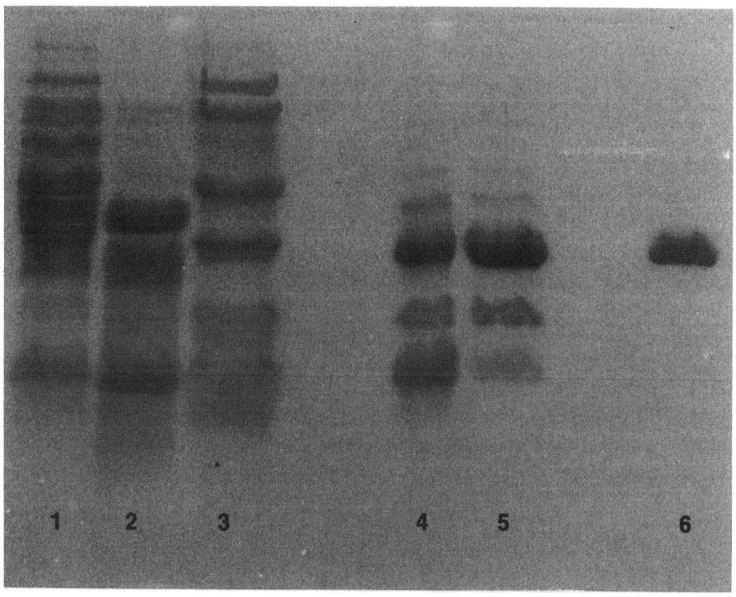

Fig. 4. SDS–PAGE. The samples in the respective lanes, with the amount of protein applied given within parentheses, are from: 1 = the centrifuged homogenate (20.5 μg); 2 = first rapid ion-exchange chromatography (20.9 μg); 3 = the reference calibration kit (30.0 μg); 4 = gel filtration chromatography (11.8 μg); 5 = second rapid ion-exchange chromatography (5.2 μg); 6 = the extra ion-exchange chromatography (5.8 μg). For further details, see Experimental.

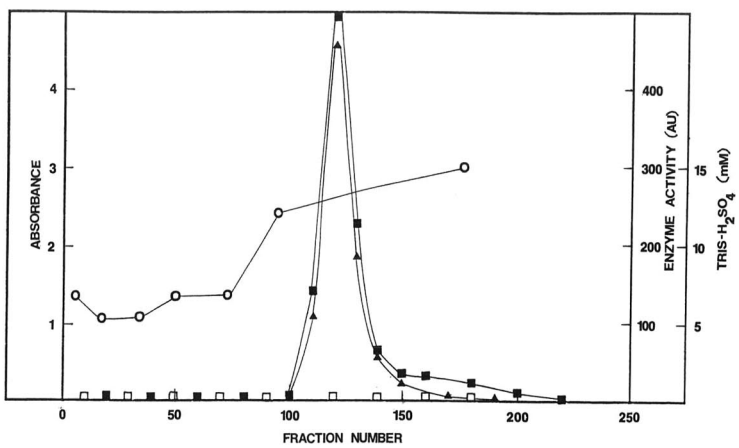

Fig. 5. Extra purification step of the bovine CA III from the second rapid ion-exchange chromatography on a CM-cellulose CM-23 column. Gel dimensions, 35 × 1.1 cm I.D.; flow-rate, 2 ml/min (126 ml/h · cm^2); no pressure applied; volume of fractions, 1.4 ml; temperature, +4 to +8°C. Fractions 110–130 were pooled. ■ = $A_{280\,nm}$; □ = $A_{420\,nm}$; ▲ = carbon dioxide hydration activity; ○ = buffer concentration. For further details, see Experimental.

index of myoglobin contamination of the CA III samples. A somewhat elevated A_{420}/A_{280} ratio was obtained for the enzyme solution from the second rapid ion-exchange chromatography, confirming the presence of some myoglobin impurities at this stage of the preparation.

If, for some purpose, an extremely pure enzyme is required, some of the protein solution from the second rapid ion-exchange chromatography can be rechromatographed on a CM-cellulose CM-23 resin (Fig. 5). The A_{420}/A_{280} ratio was decreased from 0.023 to 0.002 by this extra chromatographic step, and the SDS–PAGE analysis showed no contaminating bands, indicating that this treatment removed the last traces of myoglobin (Fig. 4, lane 6).

DISCUSSION

The results indicate the successful purification of bovine CA III by rapid ion-exchange chromatography performed on a CM-cellulose resin. This means that, in addition to anion exchangers [4–6], the "flush chromatography" technique can be used with a cation exchanger. Thus, the pH interval for using rapid ion-exchange chromatography has been considerably increased, and the method can therefore be applied even to proteins with high isoelectric points.

The nitrogen gas used to produce the rapid elution also protects the cysteine-containing bovine CA III from oxidation by air. The total preparation time, including all steps, is decreased from 2 weeks with conventional chromatography to only 5 days. If an ultra-pure enzyme is to be prepared, an extra ion-exchange step can be added, which will take another day.

Myoglobin can be difficult to separate from the CA III solution, since the two proteins seem to associate to each other. A similar phenomenon has also been noted for the closely related protein haemoglobin, which has been shown to associate to human CA I and II [11,12]. This problem is diminished by the shortened preparation time and by using very fresh muscle tissue. The purified enzyme is homogeneous, as judged by SDS–PAGE (Fig. 4), and the recovery of active enzyme is similar to that obtained using conventional methods.

ACKNOWLEDGEMENTS

This work was financially supported by grants from Carl Tryggers Fond and the Per Eckerbergs Stiftelse.

REFERENCES

1 A. M. Register, M. K. Koester and E. A. Noltmann, *J. Biol. Chem.*, 253 (1978) 4143–4152.
2 G. Gros and S. J. Dodgson, *Ann. Rev. Physiol.*, 50 (1988) 669–694.
3 P. Engberg, E. Millqvist, G. Pohl and S. Lindskog, *Arch. Biochem. Biophys.*, 241 (1985) 628–638.
4 N. Bergenhem, U. Carlsson and K. Klasson, *J. Chromatogr.*, 319 (1985) 59–65.
5 N. Bergenhem and U. Carlsson, *J. Chromatogr.*, 360 (1986) 279–281.
6 N. Bergenhem, U. Carlsson, L. E. Ellow and S. Rosén, *J. Chromatogr.*, 403 (1987) 383–387.
7 D. Keilin and E. F. Hartree, *Proc. Royal Soc. (London)*, B 124 (1938) 397–405.
8 S. P. Colowick, *Methods Enzymol.*, 1 (1955) 90–98.
9 E. E. Rickli, S. A. S. Ghazanfar, B. H. Gibbons and J. T. Edsall, *J. Biol. Chem.*, 239 (1964) 1066–1078.
10 K. K. Han, M. Dautrevaux, X. Chaila and G. Biserte, *Eur. J. Biochem.*, 16 (1970) 465–471.
11 L. Backman, *Eur. J. Biochem.*, 120 (1981) 257–261.
12 N. Bergenhem, U. Carlsson and C. Hansson, *Anal. Biochem.*, 134 (1983) 259–263.

Journal of Chromatography, 588 (1991) 147–155
Elsevier Science Publishers B.V., Amsterdam

CHROM. 23 615

High-performance liquid chromatographic study of some biologically active analogues of arabinosylcytosine

V. Reichelová and L. Novotný*

Department of Experimental Therapy, Cancer Research Institute, Slovak Academy of Sciences, Čsl. armády 21, 812 32 Bratislava (Czechoslovakia)

D. Zima

Computing Centre, Slovak Academy of Sciences, Dúbravská 9, 842 31 Bratislava (Czechoslovakia)

(First received March 12th, 1991; revised manuscript received July 1st, 1991)

ABSTRACT

The effects of methanol concentration, pH and flow-rate of the mobile phase and column temperature on the retention of two cytidine deaminase-resistant analogues (cyclocytidine hydrochloride and 5′-chloro-5′-deoxyarabinosylcytosine) of the antineoplastic agent arabinosylcytosine (araC) and their metabolites in a reversed-phase system were examined. Cyclocytidine hydrochloride (pK_a 6.60) changed its retention significantly in the pH range 6–7 and when the methanol concentration increased from 3 to 5% comparing to other compounds. The greatest changes in the capacity factors were observed for 5′-chloro-araC (pK_a = 3.84) in mobile phases with low methanol concentrations (up to 5%, v/v). The effect of temperature was most significant in the case of 5′-chloro-araC. Its retention decreased the most when the temperature was changed from ambient to 30°C. The relationship between capacity factors and hydrophobicity (logarithm of partition coefficients) of the studied compounds was also studied.

INTRODUCTION

Arabinosylcytosine (araC) is a cell cycle (S-phase) specific antitumour agent widely used in the treatment of leukaemias and lymphomas [1]. Its clinical utility is severely limited by its rapid deamination to a biologically inactive compound, arabinosyluracil (araU) [2].

Drug research has been focused on araC analogues resistant to deamination in order to improve the stability of araC. For example, O^2,2′-cyclocytidine hydrochloride, an anhydride derivative of araC, has been found to be biologically active against a variety of tumours [1,3] and it is not deaminated by cytidine deaminase. It is more effective and less toxic than araC. It is hydrolysed to araC and therefore it can serve as an araC pro-drug.

Studies of structure–activity relationships for nucleoside analogues [4] indicate that 5′-chloro-5′-deoxyderivatives of nucleosides, especially of araC, are a potentially interesting new group of biologically active compounds. The results show that 5′-haloderivatives of araC are superior in their transport rate and metabolic stability to the clinically used compound araC [5,6]. The results have stimulated further investigation of the mechanism of action and biological activity of the 5′-chloro derivative of araC. As high-performance liquid chromatography (HPLC) has often been used for the determination of araC nucleosides and nucleotides in physiological fluids, we report in this paper an HPLC study of the effects of mobile phase methanol concentration, pH, column temperature and flow-rate on the retention of 5′-chloro-araC, cyclocytidine, araC and their possible metabolites and related compounds 2′,5′-anhydro-araC, 2′,5′-anhydro-araU, araU, cyclouridine and the natural nucleosides cytidine and uridine in reversed-phase systems.

0021-9673/91/$03.50

We have also investigated the relationship between lipophilicity expressed as the logarithm of partition coefficients (log P) and capacity factors of the compounds in reversed-phase LC; although no correlation was found between lipophilicity and transport rate but there was a good correlation between lipophilicity and metabolic transformation [5].

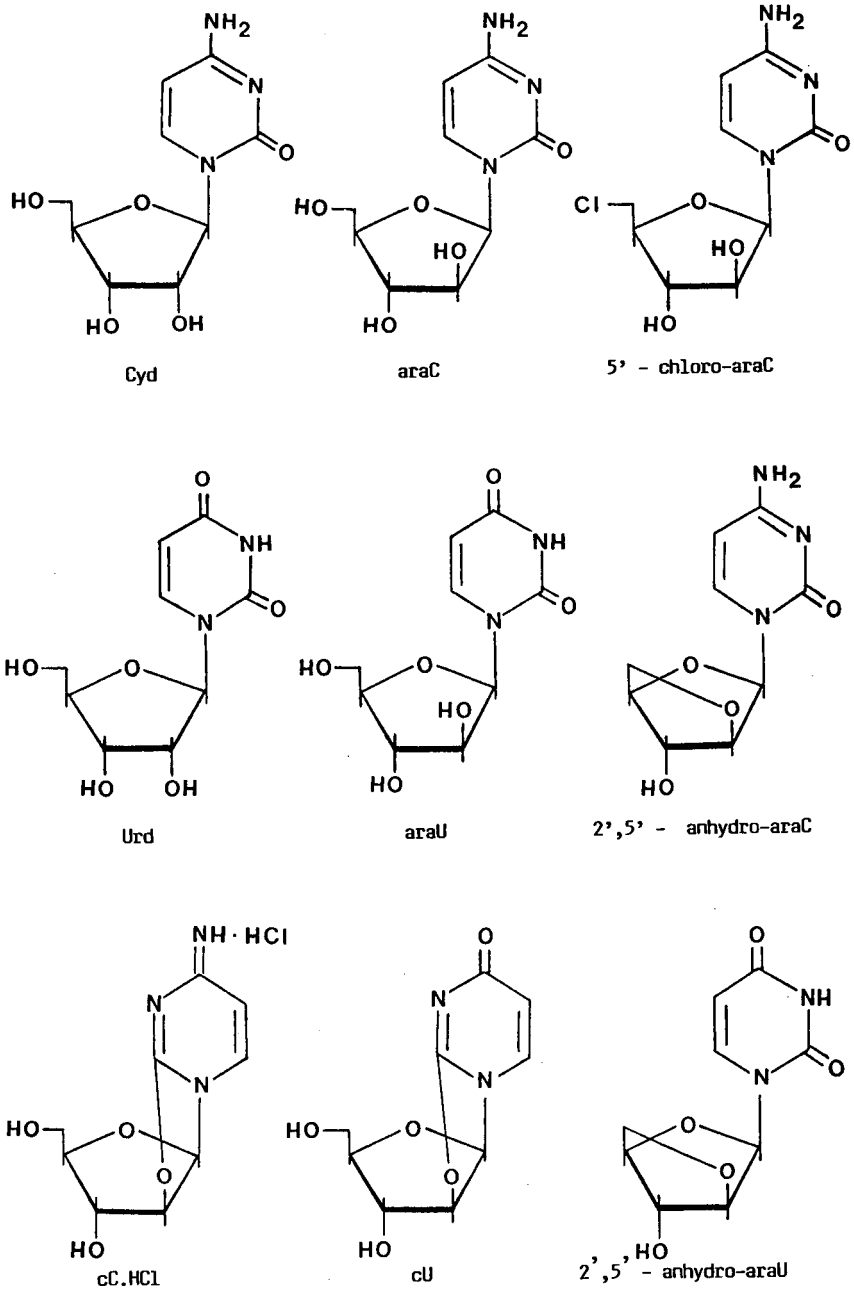

Fig. 1. Structural formulae of the compounds studied.

EXPERIMENTAL

Materials

The studied compounds (Fig. 1) were synthesized according to the references indicated in Table I.

Cytidine and uridine were obtained from Pharma-Waldhof (Mannheim, Germany), potassium dihydrogenphosphate from Merck (Darmstadt, Germany) and methanol and potassium hydroxide of the highest purity available from Lachema (Brno, Czechoslovakia). Doubly-distilled, deionized water was purified using an Elgastat Spectrum SC 20 system (Elga, High Wycombe, UK).

Single-compound stock solutions of nucleosides were prepared to give concentrations of about 0.4 m*M* (Urd, cC · HCl, 5′-Cl-araC, 2′,5′-An-araC and 2′,5′-An-araU), 0.27 m*M* (Cyd and araC) or 0.5 m*M* (araU and cU). Working standard solutions were prepared by diluting the stock solutions tenfold with doubly distilled, deionized water. The working standard solutions were diluted to a final volume of 50 ml containing 7 ml of cU and 5 ml of other nucleosides. All stock and working standard solutions were stored at −4°C.

Chromatography

The HPLC equipment consisted of a Pye Unicam PU 4003 gradient elution high-performance liquid chromatograph equipped with a Rheodyne Model 7125 injector (20-μl sample loop), PU 4030 controller, PU 4031 column oven and PU 4020 variable-wavelength UV detector (Philips Scientific, Cambridge, UK). Peak recording was achieved using a dual-channel SP 4200 computing integrator (Spectra-Physics, Darmstadt, Germany).

Separon SGX C_{18} (150 × 3 mm I.D.; 7 μm) analytical columns were obtained from Tessek (Prague, Czechoslovakia).

The isocratic mobile phases consisted of 0.01 *M* potassium dihydrogenphosphate solutions containing various concentrations of methanol by volume. The pH was adjusted with a few drops of either potassium hydroxide or orthophosphoric acid. The eluents were filtered through 0.45-μm nylon 66 membranes (Supelco, Bellefonte, PA, USA) and vacuum degassed prior to the analysis. The flow-rate was 0.45 ml/min. UV detection was performed at 275 nm (1.28 a.u.f.s.).

RESULTS AND DISCUSSION

Effect of pH and methanol concentration

It is known that the solute retention in a reversed-phase system can be decreased by the addition of an organic modifier (such as methanol) to an aqueous mobile phase [14,15]. We studied the effect of various methanol concentrations in 0.01 *M* KH_2PO_4 mobile phase at pH 4.5, 5.0, 5.5, 6.0, 6.5 and 7.0. Similarly to the results for purine nucleosides, inosine and guanosine compounds [15], we also observed that the retention times of all the compounds studied decreased with increasing percentage of methanol in the mobile phase.

Except for cC · HCl and 5′-chloro-araC, the ca-

TABLE I

COMPOUNDS STUDIED AND THEIR ABBREVIATIONS

Compounds are listed according to increasing log *P* values

Compound	Abbreviation	Ref.	pK_a [ref.]
Cyclocytidine	cC · HCl	7	6.60[11]
Cyclouridine	cU	8	
Cytidine	Cyd	–	4.22[12]
Arabinosylcytosine	araC	9	4.15[11]
Uridine	Urd	–	9.17[12]
Arabinosyluracil	araU	9	9.20[13]
2′,5′-Anhydroarabinosylcytosine	2′,5′-An-araC	10	
2′,5′-Anhydroarabinosyluracil	2′,5′-An-araU	10	
5′-Chloroarabinosylcytosine	5′-Cl-araC	10	3.84[a]

[a] Unpublished result.

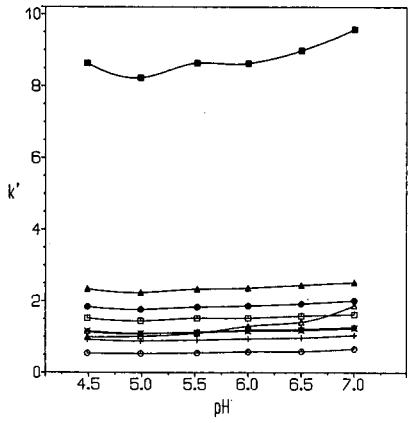

Fig. 2. Effect of pH of the mobile phase on capacity factors (k') in the isocratic reversed-phase LC separation of (○) cU, (△) cC · HCl, (+) Cyd, (×) araC, (◇) Urd, (□) araU, (●) 2′,5′-An-araC, (▲) 2′,5′-An-araU and (■) 5′-Cl-araC. Column, Separon SGX C_{18} (150 × 3 mm I.D.; 7 μm); mobile phase, 0.01 *M* KH_2PO_4 containing 8% of methanol; flow-rate, 0.45 ml/min; detection, 275 nm, 1.28 a.u.f.s.; temperature, 23°C.

pacity factors (k') of the compounds did not change significantly when the pH of the mobile phase changed from 4.5 to 7.0 (Fig. 2). At all methanol concentrations (0–10%), the k' of cC · HCl increased with increasing pH of the mobile phase (Fig. 3). The k' of 5′-chloro-araC increased noticeably with increasing pH of the mobile phase only at less than 3% of methanol (Fig. 4). cC · HCl was the only solute studied that showed a reversed elution

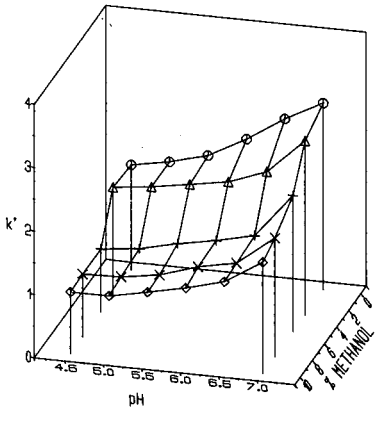

Fig. 3. Effect of pH of the mobile phase on capacity factor (k') of cC · HCl in a mobile phase containing (◇) 10%, (×) 8%, (+) 5%, (△) 3%, and (○) no methanol. Other chromatographic conditions as in Fig. 2.

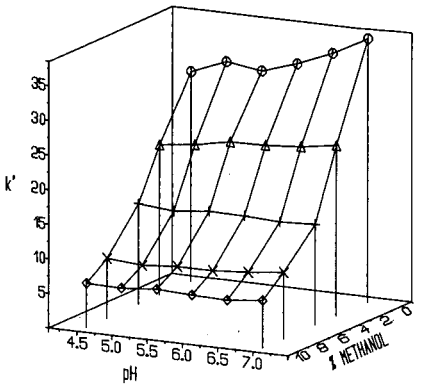

Fig. 4. Effect of pH of the mobile phase on capacity factor (k') of 5′-chloro-araC in a mobile phase containing (◇) 10% (×) 8%, (+) 5%, (△) 3% and (○) no methanol. Other conditions as in Fig. 2.

order in mobile phases containing more than 5% of methanol at pH 6.0–7.0 (data not shown). We assume that cC · HCl (pK_a 6.60) can undergo ionization at pH 6.0–7.0 and its ionized form can participate in non-hydrophobic interactions that influence the retention of cC · HCl in the reversed-phase LC system. 5′-Chloro-araC, the least polar analogue of araC, is the most retained of studied nucle-

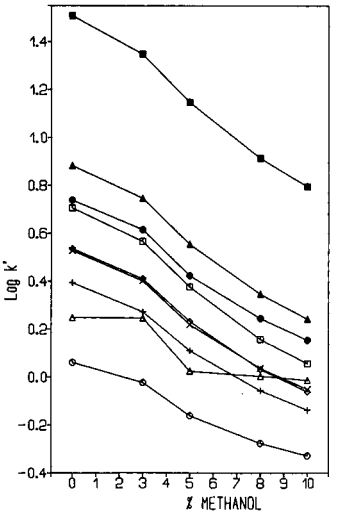

Fig. 5. Effect of the concentration of methanol in the mobile phase (pH 5.5) on logarithm of capacity factor (log k') in reversed-phase systems for (○) cU, (△) cC · HCl, (+) Cyd, (×) araC, (◇) Urd, (□) araU, (●) 2′,5′-An-araC, (▲) 2′,5′-An-araU and (■) 5′-chloro-araC. Other conditions as in Fig. 2.

osides on the hydrophobic ligand. This can provide a possible explanation for the variations of the retention times of 5′-chloro-araC.

A remarkable change in the retention of cC · HCl was observed when the methanol concentration in the mobile phase was changed from 3 to 5% (v/v), as can be seen from the log k' *vs.* methanol concentration plot in Fig. 5. Unlike purine nucleosides, for which the plot of log k' vs. methanol concentration was linear at pH 5.5 and non-linear at pH 6.5 [15], the plots for the present compounds were non-linear at all pH values studied.

According to theory, if the solvophobic mechanism is operative, the plots of log k' *vs.* methanol concentration at different pH values should be linear [15]. However, it was observed that log k' *vs.* methanol concentration plot was non-linear when k' was measured over a wide range of organic modifier (methanol) concentrations. Log–log plots of k' *vs.* 1/(concentration of organic modifier in aqueous mobile phase) have been attempted to describe the non-linearity of the log k' *vs.* methanol plot concentration [16].

The requirement of four premises was reported for the linearity of the log k' *vs.* 1/[methanol] plot based on the displacement model [17]. First, an intermediate concentration of organic modifier (methanol) of about 30–80% [18] or 45–80% [19] was reported for the hydrophobic (solvophobic) retention mechanism on an ODS ligand. However, for nucleosides the amount of methanol in the mobile phase is usually less than 10% [20]. This also interferes with the second premise that the solvation and the conformation of the ligand should be unchanged. At lower methanol concentrations the amount of methanol adsorbed on the ligand will be decreased and the ligand conformation will be changed as, for example, alkyl ligands can contact each other. As for the third premise, that non-hydrophobic interactions can be negligible, at relatively low methanol concentrations a hydrophilic solute may suffer from non-hydrophobic interactions with the stationary phase, such as silanophilic interactions with residual silanols [21] and from the interaction with the organic modifier adsorbed on the ligand [22]. The solute–solvent interaction, called the mobile phase effect, involved in the fourth premise should be negligible. However, hydrogen bonding between the polar functional groups of a solute and the mobile phase solvent (especially water) leads to a negative contribution to the hydrophobic interaction with the stationary ligand [19].

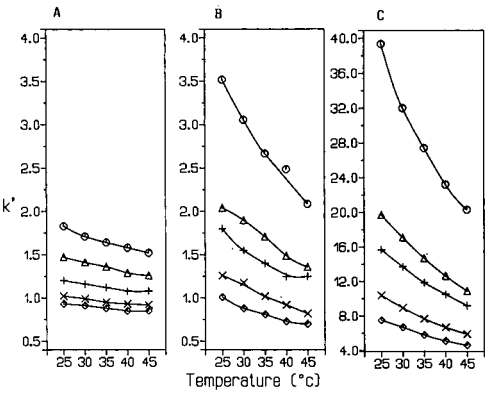

Fig. 6. Effect of temperature on capacity factors (k') of (A) cC · HCl, (B) araC and (C) 5′-chloro-araC in mobile phase of pH 5.5 containing (◇) 10%, (×) 8%, (+) 5%, (△) 3% and (○) no methanol. Other conditions as in Fig. 2.

As the plots of log k' *vs.* methanol concentration for cC · HCl for all the mobile phases used differed substantially from the non-linear plots for the other compounds (Fig. 5), we assume that the retention mechanism of cC · HCl is the most affected by processes other than solvophobic.

Effect of temperature

We also investigated the effect of temperature from 25 to 45°C on the retention of araC and its polar derivative cC · HCl and the less polar derivative 5′-chloro-araC (Fig. 6). Although the values decreased with increasing temperature, the differences among capacity factors (at different temperatures) were found to be negligible for cC · HCl. The greatest changes in the k' values were observed for 5′-chloro-araC in mobile phases with low methanol concentrations (up to 5%) and especially when the temperature was changed from ambient to 30°C. Relative retention (α) values for cC · HCl and araC of nearly 1.00 (when the peaks merged) were observed at higher methanol concentrations (from 8 to 10%) and at higher temperatures (Table II).

From a temperature study for purine compounds [15], the conclusion was made that if faster separations are necessary, it is preferable to increase the flow-rate rather than temperature, because temperature affects not only the mass transfer terms, both

TABLE II

CAPACITY FACTORS (k') AND RELATIVE RETENTIONS (α) OF CYCLOCYTIDINE (cC · HCl) AND ARABINOSYLCYTOSINE (araC)

Sample, 20 μl of a standard solution; column, Separon SGX C_{18} (150 × 3 mm I.D.; 7 μm); mobile phase, 0.01 M KH_2PO_4; pH, 5.5; flow-rate, 0.45 ml/min; detection, 275 nm, 1.28 a.u.f.s.

Methanol concentration (%)	25°C			30°C			35°C			40°C			45°C		
	k'		α	k'		α	k'		α	k'		α	k'		α
	cC·HCl	araC		cC·HCl	araC		cC·HCl	araC		cC·HCl	araC		cC·HCl	araC	
0	1.83	3.52	1.92	1.71	3.06	1.79	1.64	2.67	1.63	1.58	2.38	1.51	1.52	2.09	1.38
3	1.47	2.04	1.39	1.41	1.90	1.35	1.36	1.71	1.26	1.29	1.49	1.16	1.26	1.36	1.08
5	1.20	1.80	1.50	1.16	1.55	1.34	1.12	1.40	1.25	1.08	1.25	1.15	1.08	1.25	1.16
8	1.02	1.26	1.24	0.99	1.18	1.19	0.95	1.02	1.07	0.93	0.92	0.99	0.92	0.82	0.89
10	0.93	1.01	1.09	0.91	0.88	0.97	0.88	0.81	0.92	0.85	0.73	0.86	0.85	0.70	0.82

in the mobile and stationary phases, but also solute–solvent and solute–stationary phase interactions.

In our experiments we confirmed the widely accepted fact that capacity factors are independent of flow-rate of the mobile phase (Fig. 7). Therefore, we assume that an increase in temperature could have a more significant effect than an increase in flow-rate on accelerating the separation of the present compounds.

The optimized separation of all the nucleosides studied is shown in Fig. 8. The chromatographic

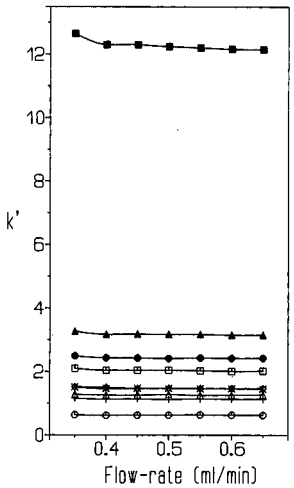

Fig. 7. Effect of flow-rate on capacity factors (k') of (○) cU, (△) cC · HCl, (+) Cyd, (×) araC, (◇) Urd, (□) araU, (●) 2′,5′-An-araC, (▲) 2′,5′-An-araU and (■) 5′-chloro-araC. Mobile phase, 0.01 M KH_2PO_4 containing 8% of methanol (pH 5.5); other conditions as in Fig. 2.

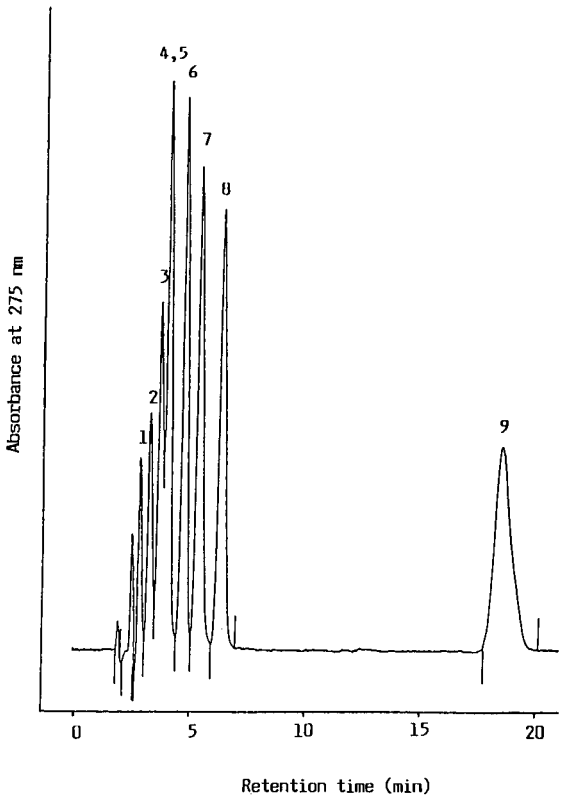

Fig. 8. Reversed-phase isocratic HPLC separation of the nucleosides (1) cU, (2) Cyd, (3) cC · HCl, (4) araC, (5) Urd, (6) araU, (7) 2′,5′-An-araC (8) 2′,5′-An-araU and (9) 5′-chloro-araC. Sample, 20 μl of a standard solution; column. Separon SGX C_{18} (150 × 3 mm I.D.; 7 μm); mobile phase, 0.01 M KH_2PO_4 containing 8% of methanol; pH, 5.5; flow-rate, 0.45 ml/min; detection, 275 nm, 1.28 a.u.f.s.; temperature, 23°C.

conditions were as follows: eluent, 0.01 *M* potassium dihydrogenphosphate solution containing 8% of methanol; pH, 4.5–5.5; column, Separon SGX C_{18} (150 × 3 mm I.D.; 7 μm); flow-rate, 0.45 ml/min; and detection at 275 nm (1.28 a.u.f.s.).

Correlation between hydrophobicity and retention in reversed-phase LC

The ability of a chemotherapeutic agent to be effective depends on the drug hydrophobicity. Hydrophobicity, one of the most important physicochemical properties that affect a drug's biological activity, is commonly expressed as the logarithm of the partition coefficients (log *P*) of the compound between *n*-octanol and an aqueous phase.

Cheung and Kenney [20] reported a linear correlation between log *P* and log *k'* values of diverse nucleoside analogues. They used monocratic LC to obtain log *k'* values, although the major weakness of the method is that the Collander relationship between log *k'* and log *P* [23]:

$$\log k' = a \log P + b$$

has been shown to be valid for congeners only [24,25]. From their data, it is evident that the hydrophobicities of nucleoside analogues can be calculated from their log *k'* values. However, the LC system should closely resemble the octanol–aqueous partition system and the analytes should be kept in the neutral form.

TABLE III

PARTITION COEFFICIENTS AND CAPACITY FACTORS OF SOME NUCLEOSIDE ANALOGUES

Log *P* values were determined by the traditional shake-flask method and *k'* values by HPLC. Sample, 20 μl of a standard solution; column, Separon SGX C_{18} (150 × 3 mm I.D.; 7 μm); mobile phase, 0.01 *M* KH_2PO_4 containing 3% of methanol; pH, 7.0; flow-rate, 0.45 ml/min; detection, 275 nm, 1.28 a.u.f.s.

Compound	Log *P*	*k'*	Log *k'*
5'-Cl-araC	−0.71	24.56	1.390
2',5'-An-araC	−1.64	4.45	0.648
araU	−1.71	3.82	0.582
Urd	−1.98	2.65	0.423
araC	−2.05	2.63	0.420
cU	−2.85	1.05	0.021
cC · HCl[a]	−4.03	2.74	0.438

[a] Data for cC · HCl were not included in regression analysis.

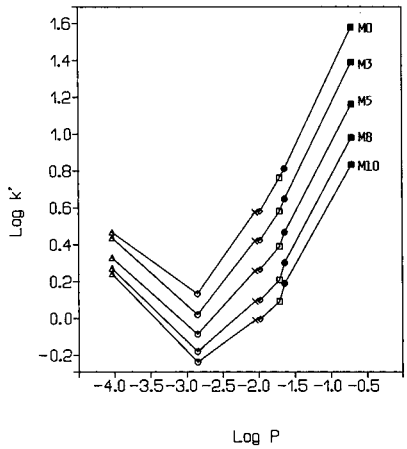

Fig. 9. Relationship between log *k'* and log *P* for (△) cC · HCl, (○) cU, (×) araC, (◇) Urd, (□) araU, (●) 2',5'-An-araC and (■) 5'-chloro-araC in mobile phases of 0.01 *M* KH_2PO_4 (pH 7.0) containing (M10) 10%, (M8) 8%, (M5) 5%, (M3) 3% and (M0) no methanol. Other conditions as in Fig. 2.

We tried to find a correlation between log *P* determined by the traditional shake-flask method in octanol–water [26] and log *k'* obtained from reversed-phase LC at different mobile phase compositions for seven nucleosides. Plots of log *k'* *vs.* log *P* in mobile phases of pH 7.0 with different methanol concentrations are shown in Fig. 9. For simplicity, we tried to analyse the relationship between log *k'* and log *P* (Table III) excluding cC · HCl. Although a correction for the degree of ionization in octanol–water was made and cC · HCl should have been eluted as the first of the studied compounds according to its log *P*, its retention in a reversed-phase system differed considerably from that expected. We do not suppose that it is the effect of the already mentioned possible ionization of cC · HCl in a mobile phase of pH 7.0, because the plots of log *k'* *vs.* log *P* for cC · HCl in mobile phases of pH 4.5–7.0 (data not shown) were very similar.

We assume that this can possibly be explained by the fact that naturally the log *P* value is affected by the non-hydrophobic nature of a solute, especially by solute–solvent complex formation, owing to hydrogen bonding [17]. This effect is obviously different from the effect on the hydrophobic retention of a solute in an aqueous–methanolic mobile phase. The difference in relative solvation effects through the hydrogen bonding between the stationary

TABLE IV

LINEAR REGRESSION ANALYSIS OF LOG k' *VS.* LOG P

Log k' = Slog P + I; S = slope, I = intercept, S.D. = standard deviation, r = correlation coefficient, n = number of compounds studied

Compounds[a]	$S \pm$ S.D.	$I \pm$ S.D.	r	n
Group I	0.737 ± 0.045	1.900 ± 0.070	0.997	3
Group II	0.485 ± 0.028	1.399 ± 0.062	0.999	3
Group I + II	0.641 ± 0.071	1.750 ± 0.138	0.985	6

[a] See text.

phase–mobile phase and octanol–water systems is expected to be increased with decrease in the methanol concentration in the eluent [27].

Linear plots and linear regression analyses between log P and log k' values in a mobile phase containing 3% of methanol (pH 7.0) were performed for group I (araC derivatives including 5′-chloro-araC, its metabolite 2′,5′-anhydro-araC and araC) and group II (uracil nucleosides, araU, cU and Urd). The results are summarized in Table IV and the linear plots are presented in Fig. 10. The linear correlation coefficient for group I, except for cC · HCl, was r = 0.997. An even better correlation coefficient r = 0.999 was obtained for group II.

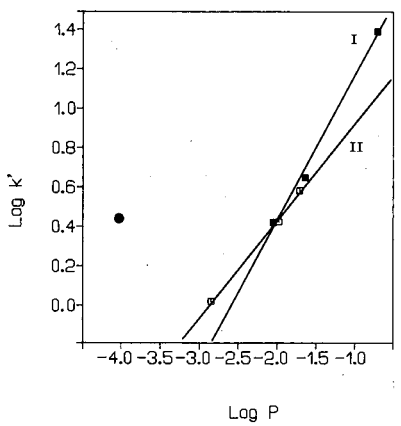

Fig. 10. Linear plot of log k' *vs.* log P for the araC analogues. Group I (■) fits the equation log k' = 0.737log P + 1.900 and group II(□) log k' = 0.485log P + 1.399. cC · HCl (●) was not included in the regression analysis. Mobile phase, 0.01 M KH_2PO_4 containing 3% of methanol (pH 7.0); other conditions as in Fig. 2.

When all six nucleosides were considered as a whole, the correlation coefficient between log P and log k' was only r = 0.985.

In conclusion, this work has shown that the polar derivative cC · HCl of araC, changed its behaviour in a reversed-phase system depending on the pH and the concentration of methanol in the mobile phase. On the other hand, the retention of the less polar araC derivative 5′-chloro-araC was the most influenced by the concentration of methanol in the mobile phase and the temperature.

ACKNOWLEDGEMENT

We thank Mrs. Mária Benesová for technical assistance.

REFERENCES

1 B. A. Chabner, *Pharmacologic Principles of Cancer Treatment*, Saunders, Philadelphia, 1982, p. 387.
2 R. K. Y. Zee-Cheng and C. C. Cheng, *Methods Findings Exp. Clin. Pharmacol.*, 11 (1989) 439.
3 D. H. W. Ho, V. Rodriques, T. L. Loo, G. P. Bodey and E. J. Freireich, *Clin. Pharmcol. Ther.*, 17 (1975) 66.
4 J. Beránek, *Drugs Exp. Clin. Res.*, 12 (1986) 355.
5 L. Novotný, H. Farghali, M. Ryba, I. Janků and J. Beránek, *Chemother. Pharmacol.*, 13 (1984) 195.
6 G. I. Birnbaum, M. Buděšinský and J. Beránek, *Can. J. Chem.*, 66 (1988) 1203.
7 J. Beránek, J. Brokeš and H. Hřebabecký, *Czech. Pat.*, 1501 (1977).
8 J. P. H. Verheyden, D. Wagner and J. G. Moffatt, *J. Org. Chem.*, 36 (1971) 250.
9 J. Brokeš and J. Beránek, *Collect. Czech. Chem. Commun.*, 39 (1974) 3100.
10 H. Hřebabecký, J. Brokeš and J. Beránek, *Collect. Czech. Chem. Commun.*, 45 (1980) 599.
11 L. Novotný, V. Reichelová, E. Balážová and V. Ujházy, *Neoplasma*, 37 (1990) 1.
12 *Properties of the Nucleic Acid Derivatives*, California Corporation for Biochemical Research, Los Angeles, 4th revision 1961.
13 M. Tuncel, R. E. Notari and L. Malpeis, *J. Liq. Chromatogr.*, 4 (1981) 887.
14 A. M. Krstulovic and P. R. Brown, *Reversed-Phase High Performance Liquid Chromatography, the Theory, Practice and Biomedical Applications*, Wiley, New York, 1982, p. 9.
15 Ch. Yi, J. L. Fasching and P. R. Brown, *J. Chromatogr.*, 339 (1985) 75.
16 F. Muramaki, *J. Chromatogr.*, 178 (1979) 393.
17 A. Kaibara, C. Hohda, N. Hirahata, M. Hirose and T. Nakagawa, *Chromatographia*, 29 (1990) 275.
18 E. H. Slaats, W. Markovski, J. Fekete and H. Poppe, *J. Chromatogr.*, 207 (1981) 299.

19 A. Kaibara, M. Hirose and T. Nakagawa, *Chromatographia*, 29 (1990) 551.
20 A. P. Cheung and D. Kenney, *J. Chromatogr.*, 506 (1990) 119.
21 K. E. Bij, Cs. Horvath, W. R. Melander and A. Nahum, *J. Chromatogr.*, 203 (1981) 65.
22 W. E. Hammers, G. J. Meurs and C. L. de Ligny, *J. Chromatogr.*, 246 (1982) 169.
23 R. Collander, *Acta Chem. Scand.*, 5 (1951) 774.
24 K. Miyake, F. Kitawa, N. Mizuno and H. Terada, *Chem. Pharm. Bull.*, 35 (1987) 377.
25 V. D. Biasi and W. J. Lough, *J. Chromatogr.*, 353 (1986) 279.
26 H. Farghali, L. Novotný, M. Ryba, J. Beránek and I. Janků *Biochem. Pharmacol.*, 33 (1984) 655.
27 C. Yamagami, T. Ogura and N. Takao, *J. Chromatogr.*, 514 (1990) 123.

Journal of Chromatography, 588 (1991) 157–164
Elsevier Science Publishers B.V., Amsterdam

CHROM. 23 652

High-performance affinity chromatography of messenger RNA

Thomas A. Goss and Martin Bard

Department of Biology, Purdue University School of Science, 1125 E. 38th Street, Indianapolis, IN 46205 (USA)

Harry W. Jarrett*

Department of Biochemistry, 800 Madison Avenue, University of Tennessee, Memphis, TN 38168 (USA)

(First received April 3rd, 1991; revised manuscript received July 23rd, 1991)

ABSTRACT

A 50-mer of thymidylic acid, $(dT)_{50}$, was coupled to silica inside prepacked columns using the N-hydroxysuccinimide chemistry. The resulting $(dT)_{50}$-silica columns were used to resolve oligomers of adenylic acid, $(dA)_{19-24}$, and to separate poly(A) mRNA (messenger RNA) from *Saccharomyces*. Oligomers which differed in length by a single nucleotide base were readily resolved. Using either $(dT)_{50}$- or $(dT)_{18}$-silica, poly(A) mRNA could be purified in as little as 8 min. The poly(A) mRNA isolated appeared to be full length and could be used directly for T_4 RNA ligase and RNAse A and T_1 enzymatic reactions. The $(dT)_{50}$-silica column was used to fractionate total poly(A) mRNA by tail length. While the separation was primarily due to poly(A) tail length, most fractions appeared to contain multiple tail lengths. Whether this represents an intrinsic feature of the RNA or a limitation of the method is discussed. These studies show that polynucleotides in the kilobase size range can be separated rapidly and with good resolution on DNA-silica.

INTRODUCTION

Recently, we reported experiments to determine the usefulness of high-performance affinity chromatography (HPAC) of DNA [1]. In the method, an octadecamer of thymidylate, $(dT)_{18}$, tethered by way of the 5'-terminus to macroporous silica was shown to hybridize with and allow the separation of $(dA)_{6-18}$. Differences of a single base pair were sufficient to resolve samples using either temperature or salt gradients. Here, we extend these studies to the fractionation of polydenylated messenger RNA [poly(A) mRNA] from *Saccharomyces cervisiae*.

The first affinity chromatography of polynucleotides used oligothymidylate-cellulose synthesized by Gilham [2]. Today, poly(A) mRNA is routinely isolated by affinity chromatography on polythymidylic acid or polyuridylic acid covalently attached to cellulose, agarose, or Sepharose supports. Most established procedures use abrupt changes from loading buffer to elution buffer and require rechromatography to obtained sufficient purity [3,4]. Higher resolution with high-performance liquid chromatography (HPLC) could improve the purity obtained and increase the speed of isolation. Since degradation of RNA by ubiquitous RNAses is a source of concern [4], rapid isolation which lessens exposure to digestion should produce more intact mRNA. Thus, the higher speed and resolution of HPAC on DNA-silica should prove useful for the preparation of mRNA. There may also be important analytical uses for this support in the analysis of poly(a) tail length polymorphism.

Poly(A) mRNA from the yeast *Saccharomyces cerevisiae* has an average 3'-poly(A) tail length of about fifty [5,6]. Poly(A) tail lengths are thought to be important to mRNA turnover and translational efficiency [7–9]. Other investigators have used poly (U)-Sepharose to crudely fractionate by tail length and have observed that factors such as types of cell

0021-9673/91/$03.50

strain, growth phase, transcription inhibition with actinomycin [10], translation inhibition with cycloheximide and other antibiotics [11], and the osmotic state of the cell [12] affect tail length. After synthesis, some poly(A) tails are progressively shortened with time. The mechanism is unknown but one component may involve the poly(A) binding protein(s) [7,8,13]. There is thus considerable interest in tail length and a facile method for the analysis of tail length could have important potential. Since we have previously shown that $(dT)_{18}$-silica cannot resolve lengths longer than 18, a new silica would be needed for tail length analysis.

Here we report on the synthesis $(dT)_{50}$-silica and its use to fractionate total mRNA by poly(A) tail length. Methods for selective elution using temperature, formamide, and salt gradients are also described.

METHODS

DNA synthesis

5'-Aminoethylphosphoryl-$(dT)_{50}$ was synthesized using standard phosphoramidite chemistry and was purified by reversed-phase chromatography using volatile triethylamine–acetonitrile gradients as previously described [1]. This purified polynucleotide will be referred to as amino-$(dT)_{50}$.

DNA–silica column preparation

N-Hydroxysuccinylimidyl ester–silica (NHS–silica) was prepared immediately prior to use from Macrosphere-WCX (Alltech) as previously described [14]. The activation chemistry was performed inside prepacked 30 × 4.6 mm I.D. cartridge columns. Amino-$(dT)_{50}$ was coupled to NHS-activated silica using two different protocols. In one, the amino-$(dT)_{50}$ was recirculated through the activated column as previously described [1]; 8.6 units of amino-$(dT)_{50}$ was recirculated for an hour at pH 7.5 and 2.7 units (31%) coupled to the column. Another column was made by a stopped-flow procedure at pH 5.0. In this case, the column was activated and washed with 2-propanol as previously described [1] and then rapidly flushed with 1 ml of water at 10 ml/min. Then 85 μl of 0.2 *M* sodium phosphate, pH 5.0 containing 6 units of amino-$(dT)_{50}$ was injected and the flow stopped with the DNA inside the column. The column was removed, the ends sealed, and the column was then incubated at 50°C for 3 h. This procedure resulted in 4.4 units (73%) coupled to the column.

RNA isolation from Saccharomyces

RNA was prepared essentially as described by Sherman *et al.* [15]. Briefly, yeast (*Saccharomyces cervisiae* strain A184D Mat α) were grown in yeast extract–peptone–dextrose medium at 30°C to between 50 and 115 Klett units. After adding 10 mg cycloheximide per liter, the cultures were mixed for 10 min at 5°C and then centrifuged (Sorvall GLC-2B) for 5 min at 6500 rpm (5400 *g*). The pellet was resuspended in 2.5 ml of LETS buffer [0.1 *M* LiCl, 0.01 *M* EDTA, 0.01 *M* Tris–HCl, pH 7.4, 0.2% sodium dodecyl sulphate (SDS), 0.1% diethylpyrocarbonate]. Phenol equilibrated with LETS buffer (3 ml) was added and the cells were homogenized by vortexing with 1/4 volume glass beads (0.4 mm) for 7.5 min. An aliquot of 5 ml LETS buffer was added and the mixture was centrifuged (8000 rpm, 10 min, 8200 *g*) and the aqeuous layer was recovered and extracted twice with phenol–chloroform–isoamyl alcohol. The final aqeuous layer was made 0.5 *M* LiCl and the RNA precipitated. The RNA was collected by centrifugation and washed with 70% ethanol.

^{32}P-Labeling

RNA fractions were 3'-labeled by the method of Cobianchi and Wilson [16] using 5'-^{32}P-3',5'-cytidine bisphosphate (^{32}P-pCp) and T_4 RNA ligase. $(dA)_{12-18}$ and $(dA)_{40-60}$ size markers were 5'-labeled when necessary using γ-^{32}P-ATP and T_4 polynucleotide kinase [4].

Poly(A) tail length analysis

Poly(A) tail length of RNA from various fractions was determined by first removing non-tail RNA by digestion with RNAses T_1 and A and determining the size of the tails on acrylamide gels. The method used was similar to Nichols and Welder [17]. Briefly, mRNA fractions obtained from chromatography were made 8 *M* LiCl and precipitated at −70°C. The precipitated RNA was washed once with 70% ethanol and redissolved in 20 m*M* Tris–HCl, pH 7.5, 2 m*M* EDTA. NaCl was then added to 0.2 *M* and RNAse A and T_1 were added to a final concentration of 0.003 and 0.1

units/μl, respectively. The final reaction volume was typically 10 μl and digestions were for 30 min at 37°C. The samples were then diluted with an equal volume of formamide and applied to 10% acrylamide gels and electrophoresed [4].

Electrophoresis and autoradiography

The gels were 10% acrylamide, 0.3% bisacrylamide, and 8 *M* urea as described by Sambrook *et al.* [4]. Electrophoresis was at 20°C and 50 to 100 V for 4–8 h. $(dA)_{12-18}$ and $(dA)_{40-60}$ mixtures were run as size markers. For autoradiography experiments, 3'-labeled mRNA and 5'-kinased markers were used. After electrophoresis, the unfixed gels were sealed in seal-a-meal bags. Autoradiography was at −70°C using DuPont Chronex film and Chronex intensifying screens.

Chromatography

The chromatograph was a Varian 5000 ternary gradient instrument outfitted with a Varichrome detector. Mobile phase composition and the solvent and temperature gradients used were optimized for each separation and are given in the legends to the figures. Column temperature was maintained by immersion in a Lauda RM-20 refrigerated water bath (Brinkman Instruments); since heating rates were dependent upon the bath volume, this was kept at 15 l of water. For most experiments, the heater and circulator in the Lauda bath were used to raise the bath temperature with refrigeration turned off; this combination allowed a temperature change of about 1.1°C min. For one experiment (Fig. 5) a slower heating rate was obtained by using the circulating pump with both refrigeration and heating turned off and using a small immersion heater and a Variac variable transformer set at 60% of line voltage (120 V). The immersion heater is 200 W and is of the type sold in department stores to heat individual cups of water for tea or coffee.

Two precautions were taken to prevent degradation of RNA during chromatography: (1) The chromatograph was cleaned monthly by pumping 10% nitric acid through the system (without a column) for 30 min. (2) All mobile phases and samples were prepared using water that had been treated with 0.1% diethylpyrocarbonate and autoclaved.

Sample preparation is also important. Before injection onto a column, ethanol precipitated RNA (either crude or previously purified Saccharomyces mRNA) is redissolved in either diethylpyrocarbonate treated water or TE buffer (10 m*M* Tris, 1 m*M* EDTA, pH 7.5), heated to 80°C, and rapidly cooled in an ice-water bath. Immediately prior to injection, sufficient 2 *M* or 5 *M* NaCl is added to the sample to give a final concentration of 1 *M* NaCl.

RESULTS

When $(dT)_{50}$ was coupled by either the pH 7.5 recycling protocol or the pH 5 stopped-flow procedure, columns with good chromatographic performance were obtained. At room temperature in mobile phases containing 1 *M* Na^+, either column quantitatively bound 0.5 unit injections of either an oligoadenylic acid mixture (lengths 19–24) or polyadenylic acid (average length, 5000) that had been sonicated. Neither was bound when the column was equilibrated at 40°C in water or 0.005 *M* Na^+ containing mobile phases, demonstrating that low ionic strengths and moderate temepratures can be used to completely elute the columns. Since the length of poly(A) tails (average length is 50 bases for *Saccharomyces* [5,6]) is small relative to the length of mRNA (greater than one kilobase), a column that binds 0.5 units of $(dA)_{24}$ would be expected to bind at least 10 units ($\approx$0.3 mg) of poly(A) mRNA.

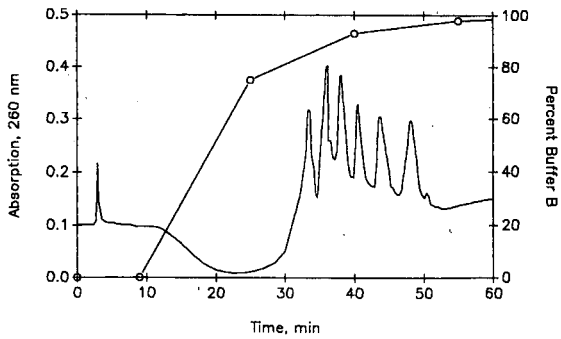

Fig. 1. Formamide gradient separation of adenylic acid oligomers on DNA-silica. An aliquot of 20 μl of 0.025 unit/μl of the $(dA)_{19-24}$ mixture was injected at zero time. Buffer A was 1 *M* NaCl, 57 μ*M* thymidylic acid (TMP), 50 m*M* Tris/phosphate, pH 7 and buffer B was 50% (v/v) formamide, 0.5 *M* Tris/phosphate, pH 7. The flow-rate was 0.2 ml/min and the temperature was 27°C throughout, and the gradient (open circles) was 0 min, 0% B; 9 min, 0% B; 25 min, 75% B; 40 min, 93% B; 55 min, 98% B; 70 min, 99% B. From left to right, the peaks eluting after 30 min are $(dA)_{19}$ to $(dA)_{24}$, respectively.

Since the experiments here required capacities of less than ≈ 3 units of mRNA, these columns had adequate capacity.

More selective methods for eluting the columns using salt, temperature, (data not shown) or formamide gradients were developed using oligoadenylate mixtures. Since we have previously demonstrated the use of salt and temperature gradients for separating oligomers [1], here we show only the formamide based separation. The separation of a $(dA)_{19-24}$ mixture using a formamide gradient is illustrated in Fig. 1. All six components of the oligoadenylic acid mixture, $(dA)_{19-24}$, were readily resolved (Fig. 1). The most challenging aspect of this separation was to develop a gradient in which the high UV absorption of formamide in buffer B would not interfere. This was accomplished by adding a small amount of thymidylic acid (TMP) to buffer A just sufficient to obtain the same absorption at 260 nm for both mobile phase buffers as specified in the figure legend. Even with this refinement, the baseline was still not ideal (Fig. 1). Since equivalent or better separations were also obtained with either salt or temperature gradients similar to those previously described with considerably less baseline problems [1], we used salt and temperature gradients to carry out all other separations presented here.

Fig. 1 shows that all six of the different length oligoadenylic acids present in the mixture could be separated. Previously, we had shown that a $(dT)_{18}$ column could separate a $(dA)_{12-18}$ mixture but could not fractionate oligomers longer than 18 from one another [1]. Fig. 1 shows that by increasing the length of the column bound DNA to $(dT)_{50}$, longer oligomers such as the $(dA)_{19-24}$ mixture can be resolved.

The separation of crude, LiCl-precipitated mRNA from *Saccharomyces* was then investigated as shown in Fig. 2. For these experiments, a $(dT)_{18}$-silica column previously described was used [1]. Similar separations were found with the $(dT)_{50}$-silica columns. The individual peaks and the starting material were also investigated using polyacrylamide gel electrophoresis (data not shown). LiCl-precipitated RNA is known to contain other RNAs (*e.g.*, ribosomal RNA) in addition to mRNA. These other RNAs and nonpolyadenylated mRNA elute in the flow-through peak (peak 1). mRNAs that contain only short stretches of oligoadenylic acid elute next (peak 2) when the column temperature was abruptly increased by immersion in a 40°C water bath. This was confirmed by determining the poly(A) tail length using RNAses A and T_1. Peak 3, representing 28% of the LiCl precipitated cellular RNA, represents the bulk of the poly(A) mRNA. It elutes in this experiment when the salt in the mobile phase was rapidly decreased to 0.005 *M*. Notice that this fraction was obtained in about 7 min and peak 3 in Fig. 2 represents about 2.2 units of mRNA collected in a total volume of 2 ml. Thus, the $(dT)_{18}$-silica is capable of very rapid isolation of mRNA in amounts adequate for most experiments and in a more concentrated form than is typically obtained by low-pressure chromatography. Peak 4 (which elutes when the column is placed in a 55°C bath) represents the longest poly(A) tail mRNAs (lengths of about 80).

The poly(A) mRNA (peak 3) obtained from the rapid chromatography in Fig. 2 showed no evidence of degradation. Degradation could occur by either

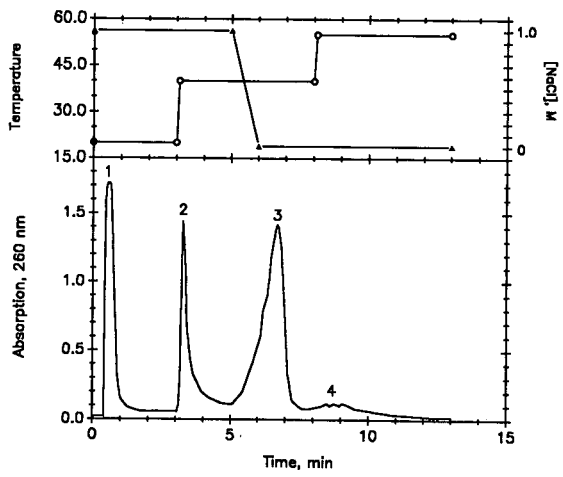

Fig. 2. Rapid isolation of messenger RNA. An aliquot of 100 μl of 1 *M* NaCl containing 6.7 units of LiCl-precipitated Saccharomyces RNA was injected onto a $(dT)_{18}$-silica column (30 × 4.6 mm I.D.) prepared as previously described [1]. Buffer A was 1 *M* NaCl, 10 m*M* sodium phosphate, pH 7, buffer B was 5 m*M* sodium phosphate, pH 7, and the flow-rate was 1 ml/min throughout. Initially, the column was equilibrated in buffer A at 20°C. Temperature (circles) was that of the water bath and was changed abruptly at 3 min and at 8 min by immersing the column in 40 and 55°C water baths, respectively. The salt gradient (triangles) was 0 min, 0% B; 5 min, 0% B; 6 min, 100% B; 15 min, 100% B.

the shear forces expected during chromatography or by RNAses contaminating the apparatus. That the RNA was not degraded was shown in two ways (data not shown): (1) the poly(A) mRNA obtained by HPLC (Fig. 2) was shown to be the expected length by comparison on acrylamide gels to λ phage Hind III digest and ϕX174 DNA length markers and (2) the size distribution of HPLC purified poly (A) mRNA does not change upon rechromatography. Degradation by RNAses was of special concern since RNAses are frequently found to contaminate laboratory apparatus and a chromatograph is a particularly complex piece of apparatus. Evidently, monthly cleaning of the chromatograph, the treatment of water with diethylpyrocarbonate, and the rapid separation performed are adequate precautions to ensure that the RNA is isolated intact. On autoradiograms of gels, the mRNA appeared as a diffuse band in the 1–2 kilobase size range. Previous studies [1] with DNA-silica had used only short oligonucleotides. Fig. 2 demonstrates that 300 Å pore DNA silica can be used to fractionate polynucleotides in the kilobase size range.

The poly(A) mRNA purified as in peak 3 of Fig. 2 was used for all subsequent experiments. This mRNA was 3′-labeled with ^{32}P-pCp and the complete labeling reaction mixture was applied to the $(dT)_{50}$-silica column for further fractionation as shown in Fig. 3.

As stated above most of the length of mRNA is not contained in the poly(A) tail; an average mRNA is 1–2 kilobase while an average tail length is 50 [5,6]. The previous fractionation [1] of $(dA)_{12\text{-}18}$ and $(dA)_{19\text{-}24}$ (Fig. 1) leaves little doubt that isolated tails could be readily fractionated. However, except for the poly(A) tail, most of the polynucleotide sequence of mRNA will not hybridize to the column and represent a heterogeneous mixture of sequences which test the selectivity of the column. This challenging separation should test polynucleotide HPAC resolution. Such a separation was carried out in Fig. 3 using increasing temperature and decreasing salt gradients.

Most of the radioactivity and absorption contained in the flow through peak (Fig. 3) comes from unincorporated pCp and other components of the labeling reaction; unlabeled poly(A) or poly(A) mRNA was shown to be quantitatively retained by the column (data not shown). The fractionation appears to show an unequal distribution of tail lengths in *Saccharomyces*. For DNA-RNA hybrids [such as between the column and the poly(A) mRNA], an empirical equation describing the influence of length, temperature, salt and formamide concentration on hybrid melting temperature has been described [18]. From this equation and the elution conditions, the main peak eluting at 78 min corresponds to a hybrid with a predicted $(A)_{25}$ length tail. The presence of large amounts of mRNA with $(A)_{21}$ tails has been previously reported for *Saccha-*

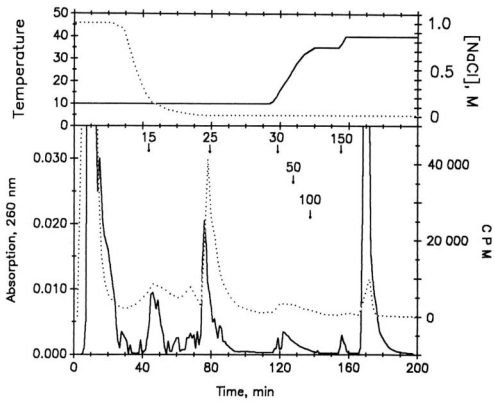

Fig. 3. Fractionation of polyadenylated messenger RNA on DNA-silica. The mRNA was purified as shown in Fig. 2 (peak 3), 3′-labeled with 5′-^{32}P-pCp, and 500 μl (0.025 units, $1.5 \cdot 10^6$ cpm) was applied to the $(dT)_{50}$-silica column [30 × 4.6 mm I.D., containing 4.4 units $(dT)_{50}$]. The flow-rate was 0.085 ml/min and 1-min fractions were collected for further analysis. The lower part of the figure shows the absorption (solid line, from the flow detector) or the counts per min ("C.P.M.", dotted line, measured for the fractions). The arrows show where the indicated length of poly(A) was calculated to elute using the gradient conditions and an equation [18] for predicting hybrid melting behavior. Gradient: buffer A was the same as in Fig. 2, buffer B was 0.1 *M* NaCl, 10 m*M* sodium phosphate, pH 7, and buffer C was water titrated to pH 7. The solvent gradient was 0 min, 100% A; 5 min, 100% A; 20 min, 10% A, 90% B; 40 min, 100% B; 80 min, 50% B, 50% C; 120 min, 10% B, 90% C; 130 min, 100% C. At 165 min, 500 μl formamide was injected to further elute the column. The upper part of the figure shows the measured NaCl concentration (dotted line, measured by conductivity of the fractions) or temperature (solid line, measured using a J-type thermocouple) of the water bath during the separation. The temperature gradient shown was obtained by immersing the column in the Lauda RM-water bath cooled to 10°C. At 114 min, the refrigeration was turned off and the bath set temperature was changed to 35°C. At 154 min, the set temperature was changed to 40°C. The temperature gradient shown simply represents the intrinsic heating rate of the water bath used.

romyces [6] and perhaps this is the peak at 78 min. The conditions used to elute the column would have eluted tail lengths up to about length 200 and yet clearly some possible lengths are not observed. For example, calculated tail lengths in the 15–25 range are quite common and abundant and another somewhat less abundant cluster of tail lengths between 30 and about 80 is also seen, but tail lengths between 25–30 and greater than 80 appear to be uncommon.

Since the above analysis is based on lengths calculated from an equation rather than actual lengths, we further investigated the individual fractions using RNAse A and T_1 to recover the poly(A) tails which were sized on acrylamide gels. The results are shown in Fig. 4. Before RNAse digestion, the fractions contain kilobase size RNA (Fig. 4A). After RNAse A and T_1 digestion, the densitometry scans of the gel autoradiographs (Fig. 4B) show that only poly(A) tails between about 15 and 60 in length are recovered. These densitometry scans are of long exposure (3 days) autoradiographic films which increases the apparent broadness of bands and thus underestimates the resolution obtained.

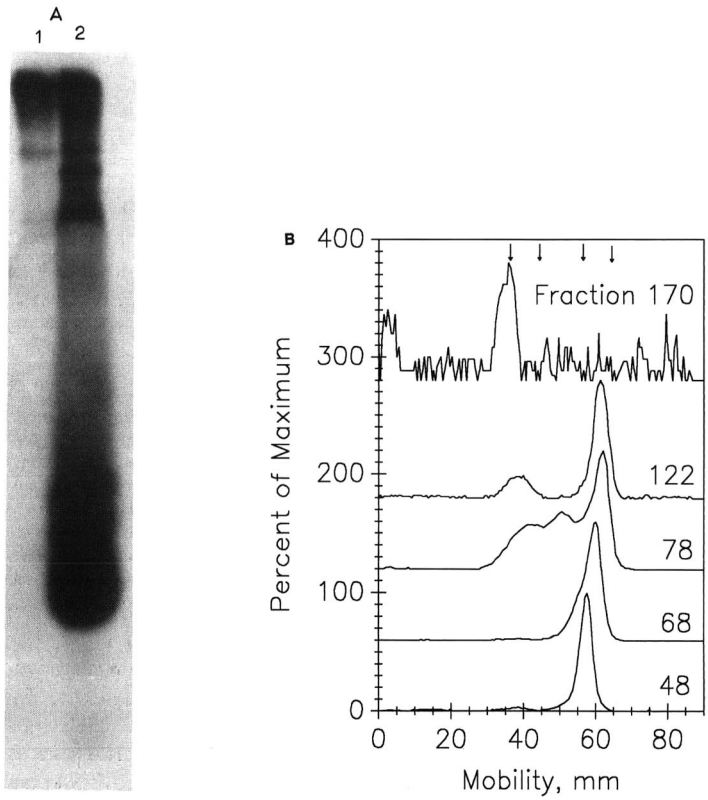

Fig. 4. Analysis of fractionated messenger RNA and its tail lengths. The autoradiography is of a 10% acrylamide, 8 *M* urea gel. (A) Lane 1: the sample was from the fraction eluting at 78 min, Fig. 5, showing intact mRNA (*i.e.*, before RNAse digestion). Lane 2: mRNA isolated as in peak 3 of Fig. 2 and 3′-labeled with pCp. The entire, unfractionated labeling reaction was applied to the gel. (B) Fractions (1 min, 0.085 ml) from the experiment in Fig. 3 were precipitated, digested with RNA A and T_1, and electrophoresed. The gel was then sealed in a plastic bag and used to expose X-ray film for 3 days at −70°C and the film was then scanned for densitometry. The results of the densitometry scans for fractions (Fig. 3) eluting at 48, 68, 78, 122, and 170 min, are shown as indicated in the figure. The tracings were all scaled so that the largest peak represents 100% which results in larger amounts of noise in weakly detected fractions (*e.g.*, fraction 170). The arrows at the top of the figure shows (from right to left) the position of $(dA)_{12}$, $(dA)_{18}$, $(dA)_{40}$, and $(dA)_{60}$ size markers, respectively.

The digests of all the column fractions contained radiotracer at a position corresponding to a tail length in the $(dA)_{12-18}$ range (the most rapidly migrating band in each sample) What this represents will be discussed further below. Also, salt carried over from the early eluting HPAC fractions is retarding their mobility on the gel (notice how the most rapidly migrating peak is retarded in fractions 48 and 68). In spite of these factors, the result is still readily seen: fractions eluting early during chromatography contain short poly(A) tails while those eluting later contain longer tail lengths. Thus, fraction 48 contains only the rapidly migrating $(A)_{12-18}$ peak. Since the average size determined was a length of 15, we will refer to this band as $(A)_{15}$. Fraction 68 shows an additional band represented as a shoulder on the $(A)_{15}$ peak, fraction 78 contains additional tail lengths in the $(A)_{20-50}$ size range, and fraction 122 contains primarily $(A)_{50}$. Fraction 170, eluted by a formamide injection (which should elute even very long tails) in fact elutes very little (notice the low cpm in Fig. 3 and the baseline noise in Fig. 4B resulting from densitometry scanning of a faint band) and that is of length $\approx(A)_{60}$. However, it is also clear that more than one tail length is present in some of the fractions. Whether this is due to a limitation of the chromatography or due to an intrinsic feature of the mRNA will be discussed below.

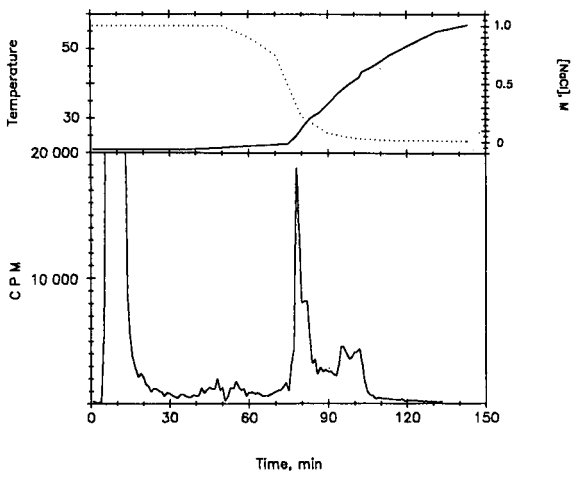

Fig. 5. Alternative gradients for fractionating mRNA by tail length gave similar results. The experiment is similar to that in Fig. 3 except that an alternative gradient was used (shown in the upper part of the figure) in which temperature and salt were varied simultaneously. In this case, the Lauda water bath was used with only the circulating pump running (initial temperature, 21°C). The temperature increase up to 75 min (to 22.8°C) was due to heating by the pump alone. At 75 min, a 200 W immersion heater and a variable transformer set at 60% was turned on and used to obtain a slow rate of heating. The sample load ($1.5 \cdot 10^6$ cpm) and the mobile phase buffers were the same as in Fig. 3.

A somewhat different elution protocol in which salt and temperature were varied simultaneously gave similar results as shown in Fig. 5. The largest peak (at 81 min, Fig. 5) has a calculated poly(A) tail length of about 25. Again the length of the poly(A) tails present in various column fractions was investigated using the RNAse method (gel not shown) with results similar to those already discussed for Fig. 4.

DISCUSSION

Here, we were primilarly interested in DNA-silica chromatography and used mRNA fractionation to test the usefulness of these columns. The experiment in Fig. 2 leaves little doubt that DNA-silica can be used for the rapid purification of poly(A) mRNA. This alone would be a powerful use of DNA-silica, but for that $(dT)_{18}$-silica would be sufficient (Fig. 2) and perhaps preferred because of its lower cost of preparation. For the analysis of poly(A) tail length polymorphism though, columns such as $(dT)_{50}$-silica would be needed. Here we show that such columns can be made and are capable of high resolution of oligomers (Fig. 1); however, their usefulness in the study of polymorphism requires further discussion.

Fractionating mRNA by tail length using low-pressure supports [6,10,19] shows lower resolution than our HPLC fractionation (Figs. 3 and 4B); HPLC thus represents a significant improvement over the previously used techniques. However, Fig. 4B also shows that after fractionation, most fractions contain at least two different lengths of poly (A). One poly(A) stretch is about 15 in length and is present in almost every fraction examined (except for fraction 170). The other poly(A) stretches are longer and the length increases in later column fractions. This may result from mRNA containing more than one stretch of poly(A) of different origins [6,19]. In *Dictyostelium*, two different stretches of poly(A) are present in the mRNA; one of about $(A)_{25}$ in length is apparently coded in the genome,

while another of variable length is added post-transcriptionally [19]. Both tail lengths are observed in poly(U)-Sepharose fractionated mRNA, even those eluted at high stringency [10]. *Saccharomyces* mRNA is similar is some respects [6]. Here, the genome coded, constant length stretch is apparently $(A)_{21}$ [6] which is somewhat longer than that estimated from Fig. 4B ($\approx$15 long), but this could be accounted for by differences in the procedures used for RNAse A and T_1 digestion and the ways length was determined in the two experiments. This short, constant tail length was found in most fractions from fractionated mRNA (in this case using oligo (dT)-cellulose) and is apparently at the 3'-terminus of some of the mRNA [6]. Thus, our results are consistent with previous studies [6,10,19] with two different organisms in that we also find a short, constant length poly(A) as well as a longer, variable length poly(A) in fractionated mRNA. However, the presence of two kind of poly(A) tail indicated by this (Fig. 4) and previous studies [6,10,19] complicates the use of chromatography to estimate tail length. Thus, while DNA-silica can be used to improve upon the fractionation of mRNA by tail length, the analytical uses of such separation should be approached with caution.

The studies presented here show that polynucleotides of kilobase lengths can be fractionated by HPAC. The mRNA recovered is apparently full length and shows no evidence of short fragments being produced by either shear forces or RNAse digestion during the chromatography experiment. The mRNA recovered is equivalent to mRNA isolated by more traditional techniques in size and that it can be ligated and specifically digested by enzymes (*e.g.*, T_4 RNA ligase, RNAse A and T_1). It could presumably also be used directly for the various other enzymatic manipulations commonly used in molecular biology. When kilobase size mRNA was fractionated (Fig. 3 and 5), the fractionation is again clearly based on the length of the poly(A) tail (Fig. 4) and is of higher resolution than that obtained in similar low-pressure applications. Using DNA-silica preparatively, poly(A) mRNA can be isolated from crude RNA in as little as 8 min (Fig. 2). DNA-silica can separate oligonucleotides which differ by a single base in length (Fig. 1 and ref. 1).

Thus, DNA-silica, because it is a fast, high-resolution method for fractionating polynucleotides, represents a significant improvement over existing low-pressure chromatographic supports.

ACKNOWLEDGEMENTS

This work was supported by grants from the NIH (GM 43609) and NSF (DMB 8996229). We thank William Foster of Alltech/Applied Science for the kind gift of the Macrosphere-WCX cartridges, Ms. Jo Akhavan for RNA isolation, and Dr. Steve Larsen for synthesizing the 5'-aminoethyl-$(dT)_{50}$. T.A.G. is a recipient of the Alltech Fellowship in Chromatography whose support is gratefully acknowledged.

REFERENCES

1 T. A. Goss, M. Bard and H. W. Jarrett, *J. Chromatogr.*, 508 (1990) 279–287.
2 P. T. Gilham, *J. Am. Chem. Soc.*, 86 (1964) 4982–4989.
3 N. Tanner, *Methods Enzymol.*, 180 (1989) 25–41.
4 J. Sambrook, E. Fritch and T. Maniatis, *Molecular Cloning—A Laboratory Manual*, Cold Spring Harbor Laboratory Press, Cold Spring Harbor, NY, 2nd ed., 1989 pp. 7.1–7.77.
5 C. S. McLaughlin, J. R. Warner, M. Edmonds, H. Nakazato and M. H. Vaughan, *J. Biol. Chem.*, 248 (1973) 1466–1471.
6 S. L. Phillips, C. Tse, I. Serventi, and N. Hynes, *J. Bacteriol.*, 138 (1979) 542–551.
7 A. J. P. Brown, *Yeast*, 5 (1989) 239–257.
8 P. Bernstein, S. W. Pelz and J. Ross, *Mol. Cell. Biol.*, 9 (1989) 659–670.
9 D. Monroe and A. Jacobson, *Gene*, 91 (1990) 151–158.
10 C. Palatnic, R. Storti, A. Capone and A. Jacobson, *J. Mol. Biol.*, 141 (1980) 99–118.
11 H. Rubin and M. Halim, *Biochem. Biophys. Res. Commun.*, 144 (1987) 269–271.
12 D. Carter and D. Murphy, *Neurosci. Lett.*, 109 (1990) 180–185.
13 J. M. Kelly and R. A. Cox, *Nucleic Acids Res.*, 10 (1982) 4173–4179.
14 H. W. Jarrett, *J. Chromatogr.*, 405 (1987) 179–189.
15 F. Sherman, G. R. Fink and J. B. Hicks, *Laboratory Course Manual for Methods in Yeast Genetics*, Cold Spring Harbor Laboratory Press, Cold Spring Harbor, NY, 1986, pp. 143–144.
16 F. Cobianchi and S. Wilson, *Methods. Enzymol.*, 152 (1987) 103–110.
17 J. L. Nichols and L. Welder, *Biochim. Biophys. Acta*, 652 (1981) 99–108.
18 G. M. Wahl, S. L. Berger and A. R. Kimmel, *Methods Enzymol.*, 152 (1987) 399–407.
19 A. Jacobson, R. A. Firtel, and H. L. Lodish, *Proc. Natl. Acad. Sci. USA*, 71 (1974) 1607–1611.

Journal of Chromatography, 588 (1991) 165–170
Elsevier Science Publishers B.V., Amsterdam

CHROM. 23 623

Selective and sensitive determination of lactone and hydroxy acid forms of camptothecin and two derivatives (CPT-11 and SN-38) by high-performance liquid chromatography with fluorescence detection

Katsuya Akimoto*, Akiko Goto and Kazumi Ohya

Pharmaceutical Formulation Research Centre, Research Institute, Daiichi Pharmaceutical Co. Ltd., 1–16–13 Kita-kasai, Edogawa-ku, Tokyo 134 (Japan)

(First received April 12th, 1991; revised manuscript received July 12th, 1991)

ABSTRACT

A simple and rapid ion-pair high-performance liquid chromatographic (HPLC) method for the simultaneous determination of the lactone and hydroxy acid forms of camptothecin and its derivatives CPT-11 and SN-38 was developed. The method allows the hydroxy acid form to be eluted before the lactone form for each compound. The application of this method is limited by the minimum interval between subsequent injections and the void time for starting a measurement. However, it is possible to determine the lactone and hydroxy acid forms in aqueous solutions at the pH and the temperature near to biological conditions.

INTRODUCTION

Camptothecin is widely known as an antitumour alkaloid isolated from *Camptotheca acuminata* [1]. Recently, several derivatives of camptothecin were synthesized by Yakult (Tokyo, Japan) for medical application [2] and have been evaluated from the biological, physico-chemical and pharmaceutical standpoints [3]. The results indicated that a derivative of camptothecin, CPT-11 (I), was the most effective compound for antitumour purposes, and that SN-38 (II) was the main biologically active metabolite of I (Fig. 1) [3].

The molecules of camptothecin, I and II all contain an α-hydroxy δ-lactone ring which is essential for their antitumour activity [4,5]. In general, the lactone ring is stable in acidic media but hydrolyses in neutral and/or alkaline media to form a hydroxy acid, and it is therefore important to clarify the effects of pH and temperature on the hydrolysis and lactonization of these compounds. Several kinetic studies of their hydrolysis and lactonization by means of acid–base titration [6,7], potentiometry [8], conductometry [7], spectrometry [9,10], high-performance liquid chromatography (HPLC) [11], etc., have been reported. However, these methods are insufficiently selective and insensitive for the purposes of our study.

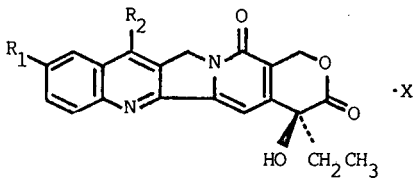

Fig. 1. Structures of camptothecin, CPT-11 (I) and SN-38 (II). Camptothecin: $R_1 = R_2 = H$, X = none. CPT-11: $R_1 = OCONC_5H_9NC_5H_{10}$, $R_2 = C_2H_5$, $X = HCl \cdot 3H_2O$. SN-38: $R_1 = OH$, $R_2 = C_2H_5$, $X = H_2O$.

This paper describes a rapid, selective and sensitive ion-pair HPLC method for the determination

0021-9673/91/$03.50

of the lactone and hydroxy acid forms of camptothecin, I and II in aqueous solutions.

EXPERIMENTAL

Materials and reagents

Camptothecin, I and II were obtained from Yakult. Sodium 1-heptanesulphonate for ion-pair HPLC was purchased from Tokyo Kasei Kogyo (Tokyo, Japan). Water was distilled and all other chemicals were of analytical-reagent grade. Britton–Robinson buffer solutions [12] (pH 4.0, 7.0 and 10.0) were used.

The HPLC column was a YMC (Kyoto, Japan) prepacked AM-312 C_{18} reversed-phase column (150 mm × 6 mm I.D., 5 μm). The mobile phase was a 1:1 mixture of methanol and pH 4.0, 0.1 *M* K_2HPO_4–H_3PO_4 buffer solution containing 3 m*M* (for I) or 6 m*M* (for camptothecin and II) sodium 1-heptanesulphonate.

Apparatus

A Hitachi Model 655 liquid chromatograph equipped with a JASCO (Tokyo, Japan) Model 820-FP intelligent spectrofluorometer and a Rheodyne (Cotati, CA, USA) Model 7125 injector with a 20-μl sampling loop was used. A Shimadzu (Kyoto, Japan) Chromatopac CR-4A integrator was used.

Analytical procedure

Samples were dissolved in the mobile phase to prepare solutions from about 20 to 1000 ng ml^{-1}. The solutions were subjected to HPLC at ambient temperature. The flow-rates of the mobile phase were 1.4 ml min^{-1} for I and 1.6 ml min^{-1} for camptothecin and II. The spectrofluorometer was automatically maintained at the maximum wavelength of each compounds, which are listed in Table I. The concentrations of the lactone and hydroxy acid were determined from the calibration graphs obtained by the peak-area method. The calibration

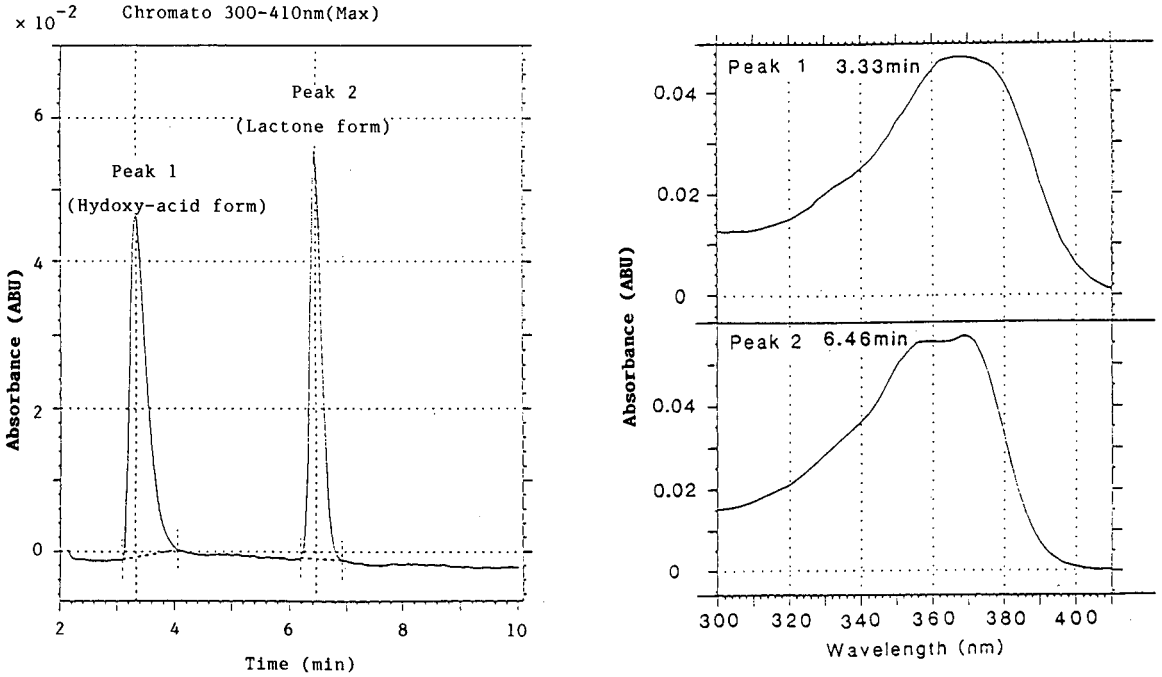

Fig. 2. Chromatogram of lactone and hydroxy acid forms of I and UV–VIS spectra of each peak measured with a multi-channel photodiode-array detector for HPLC. The sample was prepared from a 0.1% aqueous solution of I by dilution 20-fold with pH 7.0 Britton–Robinson buffer, and was stored at 35°C. HPLC was performed 1 h after diluting the sample. HPLC conditions: column, YMC AM-312 (ODS) (150 mm × 6 mm I.D.); temperature, ambient; eluent, methanol–0.1 *M*, pH 4.0 buffer solution containing 3 m*M* sodium 1-heptanesulphonate (50:50); flow-rate, 1.4 ml/min.

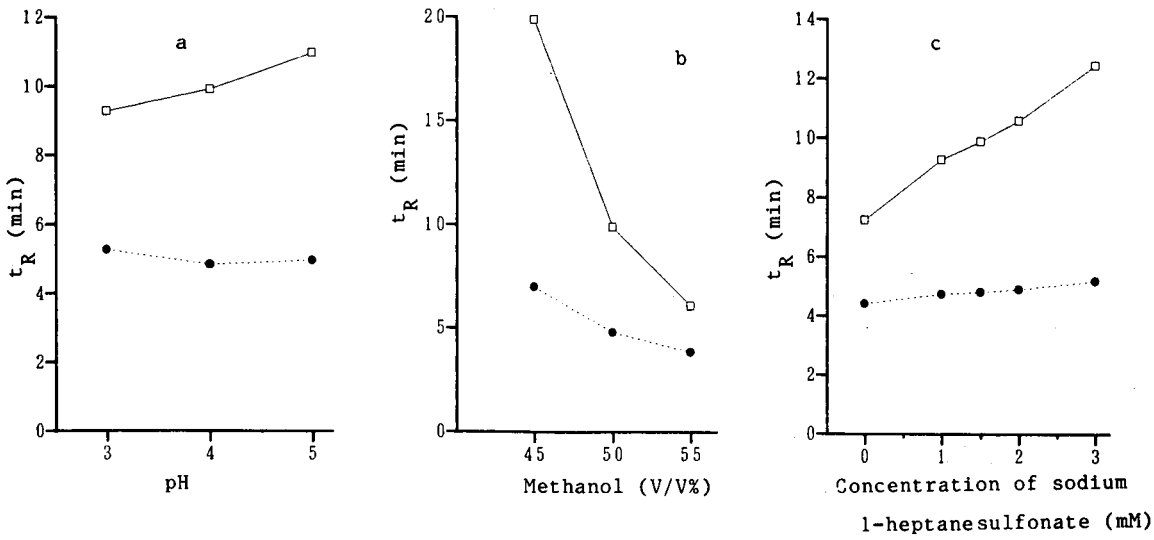

Fig. 3. Effects of (a) the pH of the aqueous phase, (b) the percentage (by volume) of methanol and (c) the concentration of sodium 1-heptanesulphonate in the mobile phase on the retention times of the hydroxy acid and lactone forms of I. HPLC conditions as in Fig. 2, except for the parameters evaluated and flow-rate (1.0 ml/min). □ = Lactone form; ● = hydroxy acid form.

graphs were obtained from standard sample solutions prepared by dissolving camptothecin, I or II in both pH 4.0 and pH 10.0 buffer solutions.

RESULTS AND DISCUSSION

Assignment of elution peaks

A preliminary HPLC separation of the lactone and hydroxy acid forms of I was carried out with a UV photodiode-array detector. Fig. 2 shows chromatograms and the UV spectra of the two elution peaks.

The two peaks eluting at 3.3 and 6.5 min were thought to represent the hydroxy acid and lactone, respectively. In order to confirm this, the UV spectra of the peaks were measured with a photodiode-array detector and were compared with those of the authentic samples. The results confirmed that the retention time of the hydroxy acid form was shorter than that of the lactone form.

Choice of mobile phase

In order to determine the optimum separation conditions, the mobile phase was examined. Fig. 3 shows the effects of pH, percentage (by volume) of methanol and concentration of sodium 1-heptanesulphonate in the mobile phase on the retention time (t_R).

The t_R of the hydroxy acid was slightly affected by these parameters, but that of the lactone was greatly affected by both the percentage of methanol and the concentration of sodium 1-heptanesulphonate. Similar elution patterns were found for camptothecin and II. The optimum HPLC conditions presented under Experimental were determined

TABLE I

MAXIMUM WAVELENGTHS OF EXCITATION AND EMISSION SPECTRA IN THE HPLC ELUENTS OF THE LACTONE AND HYDROXY ACID FORMS OF CAMPTOTHECIN, I AND II

Compound	Form	Maximum wavelength (nm)	
		Excitation	Emission
Camptothecin	Lactone	371	432
	Hydroxy acid	364	450
I	Lactone	372	431
	Hydroxy acid	374	444
II	Lactone	381	556
	Hydroxy acid	385	544

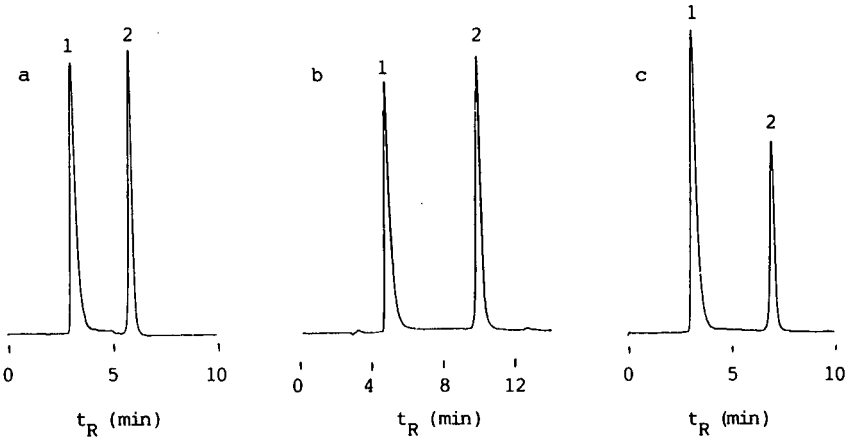

Fig. 4. Typical separation of the lactone and hydroxy acid forms of (a) camptothecin, (b) I and (c) II. For HPLC conditions, see Experimental. 1 = Hydroxy acid form; 2 = lactone form.

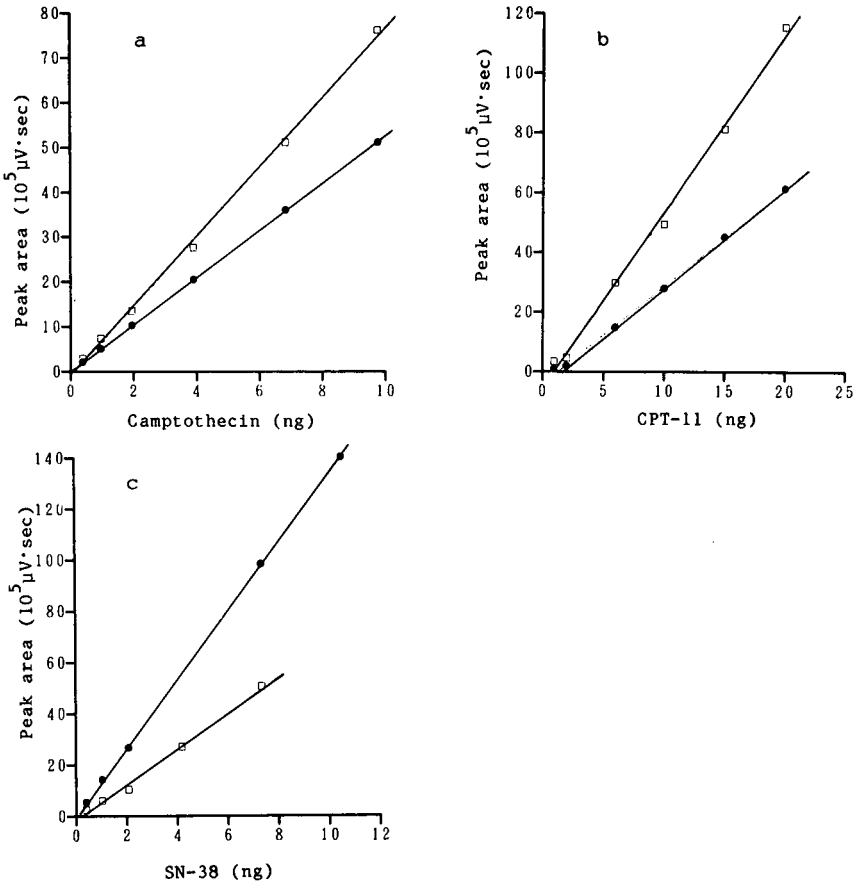

Fig. 5. Calibration graphs for the lactone and hydroxy acid forms of (a) camptothecin, (b) I and (c) II. Each peak area is the mean of two measurements. □ = Lactone form; ● = hydroxy acid form.

TABLE II

LIMIT OF DETECTION, LINEARITY RANGE AND PRECISION FOR THE LACTONE AND HYDROXY ACID FORMS OF CAMPTOTHECIN, I AND II

Compound	Form	Charged amount (ng)		Relative standard deviation (%)[a]	
		Limit of detection	Linearity range	Intra-assay	Inter-assay
Camptothecin	Lactone	0.05	0.4–10	1.0	1.8
	Hydroxy acid	0.1	0.4–10	0.6	2.0
I	Lactone	0.1	1–20	0.9	1.6
	Hydroxy acid	0.1	1–20	1.0	1.8
II	Lactone	0.1	0.4–7	1.0	2.0
	Hydroxy acid	0.2	0.4–10	0.7	1.7

[a] The intra- and inter-assay relative standard deviations were calculated from ten determinations and determinations on six different days, respectively.

from the analytical viewpoint, that is, from the peak shape, t_R and the separation factor.

Monitoring wavelength

Fluorescence detection was used for highly sensitive analysis. The maximum wavelenghts of the emission spectra and the excitation spectra were different from compound to compound, as shown in Table I.

The monitoring wavelengths for each compound were selected at the maximum emission and excitation wavelengths by programmed controlled switching.

Calibration graphs and precision

Fig. 4 shows typical chromatograms of the lactone and hydroxy acid forms for camptothecin, I and II, and Fig. 5 shows their calibration graphs.

The chromatograms showed sharp, symmetrical peaks for each compound, and the calibration graphs were linear. The results are summarized in Table II. The reproducibility among runs in one day was about 1% or less (relative standard deviation).

Application

The method was employed succesfully for kinetic studies of the hydrolysis and lactonization of camptothecin, I and II in aqueous solutions. Fig. 6 shows an example. The details will be presented in a later paper.

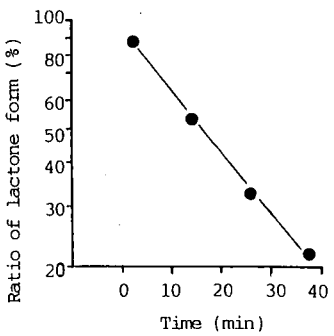

Fig. 6. Progress of the conversion reaction of the lactone form of I to the hydroxy acid form in an aqueous solution of pH 7.4 at 37°C.

REFERENCES

1 M. E. Wall, M. C. Wani, C. E. Cook, K. H. Palmer, A. T. McPhail and G. A. Sim, *J. Am. Chem. Soc.*, 88 (1966) 3888.
2 S. Sawada, S. Okajima, R. Aiyama, T. Yokokura, K. Yamaguchi and T. Miyasaka, *Chem. Pharm. Bull.*, 39 (1991) 1446.
3 Y. Kawato, M. Aonuma, Y. Hirota, H. Kuga and K. Sato, *Cancer Res.*, 51 (1991) 4187.
4 R. P. Hertzberg, M. J. Caranfa, K. G. Holden, D. R. Jakas, G. Gallagher, M. R. Mattern, S. M. Mong, J. O. Bartus, R. K. Johnson and W. D. Kingsbury, *J. Med. Chem.*, 32 (1989) 715.
5 M. C. Wani, P. E. Ronman, J. T. Lindly and M. E. Wall, *J. Med. Chem.*, 23 (1980) 554.
6 J. Grace and M. C. R. Symons, *J. Chem. Soc.*, (1961) 47.
7 M. L. Bender, H. Matsui, R. J. Thomas and S. W. Tobey, *J. Am. Chem. Soc.*, 83 (1961) 4193.
8 C. Galli, G. Illuminati, L. Mandolini and P. Tamborra, *J. Am. Chem. Soc.*, 99 (1977) 2591.
9 D. R. Storm and D. K. Koshland, Jr., *J. Am. Chem. Soc.*, 94 (1972) 5815.

10 M. C. Caswell and G. L. Schmir, *J. Am. Chem. Soc.*, 102 (1980) 4815.
11 J. H. Beijnen, J. J. M. Holthuis, H. G. Kerkdijk, O. A. G. J. van der Houwen, A. C. A. Paalman, A. Bult and W. J. M. Underberg, *Int. J. Pharm.*, 41 (1988) 169.
12 H. T. S. Britton and R. A. Robinson, *J. Chem. Soc.*, 458 (1931) 1456.

Journal of Chromatography, 588 (1991) 171–175
Elsevier Science Publishers B.V., Amsterdam

CHROM. 23 634

Determination of a small amount of niacin in foodstuffs by high-performance liquid chromatography

Shuji Hirayama

Laboratory of Q.P. Corporation, Sumiyoshi, Fuchu-shi, Tokyo 183 (Japan)

Masao Maruyama*

Faculty of Science and Engineering, Chuo University, Kasuga, Bunkyo-ku, Tokyo 112 (Japan)

(First received March 5th, 1991; revised manuscript received June 18th, 1991)

ABSTRACT

A high-performance liquid chromatographic method for the determination of a small amount of niacin in foodstuffs is described. This method is based on hydrolysis of sample, extraction, clean-up (anion-exchange and cation-exchange columns) and separation from interferences by chromatography on an amino phase column. The detection limit of niacin in foodstuff is about 0.01 mg per 100 g. The results of analysis of foodstuffs by this method are in good agreement with those obtained by the microbiological method.

INTRODUCTION

Determination of niacin in foodstuffs is generally performed by the chemical method [1] or the microbiological method [2]. In these methods, the sample is treated with strong acid or alkali to free niacin before quantitation because niacin is usually bonded with nucleotides or proteins in its natural form. Therefore many hydrolysis interferences are contained in the extracted solution and some separation procedures are needed before colorimetric measurement.

Today, the microbiological method is generally better than the above chemical method and therefore is widely accepted as the official method. There are two microbiological methods. One method is quantitation by titration after a 72 h incubation period. The other method is analysis by turbidimetric measurement after 16–22 h incubation. These procedures are very time-consuming, and culture of test organisms and their handling are troublesome. This method is also not able to determine levels of niacin below 0.1 mg per 100 g. High-performance liquid chromatography (HPLC) has been suggested to offer a good approach to the precise determination of niacin in foodstuffs [3–6] at the mg per 100 g level. However, in the case of many foodstuffs, notably those containing a small amount, niacin cannot be completely separated from interferences and therefore a good result with high sensitivity cannot be obtained. This situation is the same as in the Association of Official Analytical Chemists chemical method.

The purpose of this paper is to develop a simple, efficient and highly sensitive method for determination of a small amount of niacin in foodstuffs by means of hydrolysis of sample, clean-up (anion-exchange column and disposable cation cartridge column) and liquid chromatographic determination.

EXPERIMENTAL

Apparatus

The HPCL system (Waters, Division of Millipore, Milford, MA, USA) consisted of a Model 590 pump, a U6K injector, a Model 490 UV–VIS detec-

0021-9673/91/$03.50

tor and a Model 840 data system. The column was a 250 mm × 4.6 mm I.D. Asahipak NH2P-50 column, 5 μm particle size, preceded by an NH2P 50 mm × 4.6 mm I.D. guard column supplied by Asahi Kasei (Tokyo, Japan). The chromatographic column used for clean-up was a 150 mm × 27 mm I.D. glass column, equipped with a stopcock.

Reagents

Standard niacin was purchased from Wako (Osaka, Japan). The AGI-X8 anion-exchange resin (acetate$^-$, 100–200 mesh) was purchased from Bio-Rad (Tokyo, Japan) and the Toyopack IC-SP M cartridge column was purchased from Toso (Tokyo, Japan). This column is a cation-exchange gel and its exchange capacity is 0.4 mequiv. Acetonitrile used was HPLC grade. All other chemicals and solvents were reagent grade and were used without purification.

Chromatographic conditions

The mobile phase consisted of acetonitrile–water (60:40, v/v) containing 0.075 *M* sodium acetate. The flow-rate was 0.5 ml/min. Separation was carried out at ambient temperature. The eluate was monitored by UV–VIS detection at a wavelength of 261 nm.

Procedure

Extraction and hydrolysis. The sample (5–10 g) was accurately weighed into a 100-ml beaker. A 4-ml aliquot of 40% sodium hydroxide solution and approximately the same volume of water were added and the beaker was covered with a watch-glass. The mixture was heated on a steam bath for 30 min. After cooling to room temperature, the solution was neutralized with 25% hydrochloric acid and the same volume of methanol added. This solution was filtered through Toyo No. 5 filter paper into a 100-ml volumetric flask. The residues were rinsed with 50% methanol and passed into the same flask. Then the flask was filled up to 100 ml with 50% methanol. A 30-ml aliquot of this solution was transferred into a 200-ml round-bottom flask and methanol was added. The solution was evaporated to dryness using a rotary evaporator. The residues were taken up in 20 ml of water.

Clean-up. A 9-g portion of anion-exchange resin was packed in a glass tube (mentioned in the Experimental section) and washed with 50 ml of water. Aliquots of 20 ml of sample extracts were added to the column and passed through at a flow-rate of about 1 ml/min. After being washed with 50 ml of water, the niacin was eluted from the column with 50 ml of 13% acetic acid into a 50-ml volumetric flask. A 30-ml aliquot of the above fractionated solution was transferred in a 200-ml round-bottom flask, 50 ml of methanol was added and the solution was evaporated to dryness using a rotary evaporator. The residues were taken up in 5 ml of water. This solution was passed through a Toyopak cation cartridge column which was previously conditioned with 4 ml of 1 *M* hydrochloric acid and rinsed with 10 ml of water. Then niacin was eluted from cartridge with 15 ml of 1 *M* hydrochloric acid. This fraction was collected in a 100-ml round-bottom flask. After adding methanol, the solution was evaporatred to dryness with a rotary evaporator until free from chloride odor. Then the residues were taken up in 2 ml of water accurately.

Analysis. This solution was passed through a membrane filter (0.45 μm) and 5–20 μl of sample solution were injected into the chromatograph. The eluate was monitored by UV–VIS detection at a wavelength of 261 nm. A standard stock solution was prepared by weighing out 10.0 mg of niacin, dissolving it in water and diluting it to 100 ml accurately. The working standards used for the normalization as well as for the fortification of recovery samples were prepared by pipetting the stock solution.

RESULTS AND DISCUSSION

Extraction

Samples of foodstuff may be of many kinds, for example with high fat or protein contents and liquid or solid, etc. It is generally very difficult to extract niacin from samples without interferences. In this study, we attempted to find a general procedure that can be used for many kinds of sample and the following one is given as an example. Samples were hydrolyzed in the presence of alkali, neutralized with acid, and the same volume of methanol was added to the neutralized solution. After hydrolysis, filtration from the solution can be performed effectively, especially for high-protein or carbohydrate-rich samples, when methanol is added to the neutralized solution.

Elution from AGI-X8 anion-exchange column

If the methanolic solution is applied to the top of AGI-X8 column, niacin cannot be sufficiently retained on the column unless the column has previously been conditioned with 50% methanol solution for equilibration. In this experiment, the sample solution was evaporated to dryness by a rotary evaporator and residues were taken up in 20 ml of water. The solution so obtained was applied to the top of column.

Fig. 1 shows the elution pattern of niacin from AGI-X8 with the eluate of 13% acetic acid. Of the niacian, 89% was eluted with the first 20 ml and 98% with 50 ml. In this case, since no salt existed, niacin could not be eluted from the AGI-X8 column with 50 ml of acetic acid. Therefore elution in the above experiment was carried out int he presence of a 0.4 *M* sodium chloride solution, about the same amount as in the practical samples.

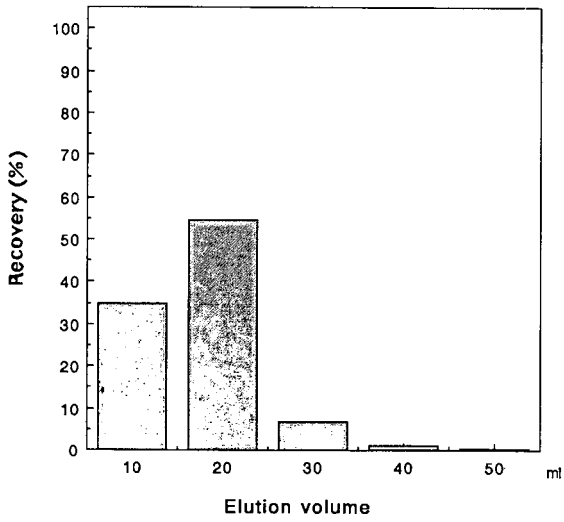

Fig. 1. Elution pattern of niacin from an AG1-X8 column. Eluent, 13% acetic acid; niacin, 100 μg.

Additional clean-up with an IC-SP M cation-exchange column.

It is difficult to determine a small amount of niacin with high sensitivity by utilizing only a one-step clean-up with an anion-exchange column. It is effective to carry out additional clean-up with a cation-exchange column with which the pyridine nucleus in a niacin molecule interacts.

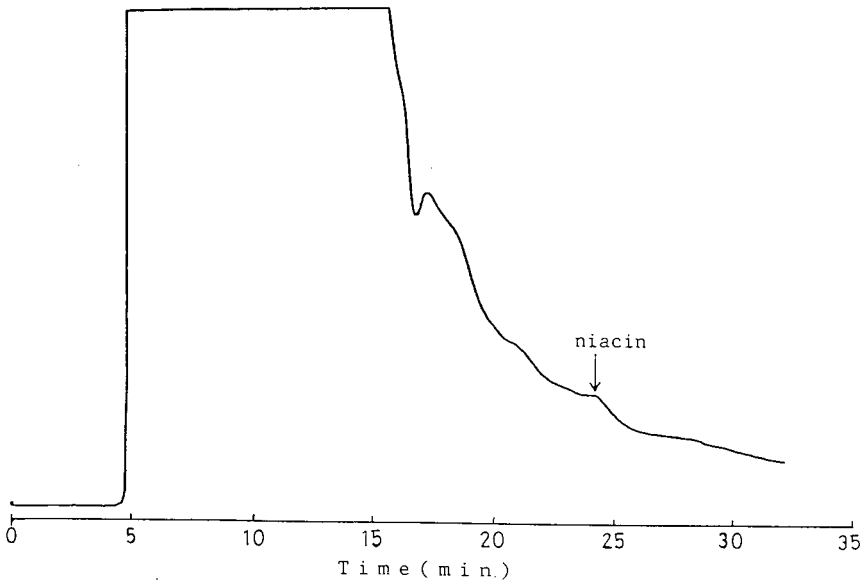

Fig. 2. Chromatogram of niacin in strawberry jam (niacin content: 0.07 mg per 100 g), after clean-up by anion-exchange resin only. Column: Hitachi gel 3014N, 300 mm × 4 mm; column temperature, 40°C; mobile phase, 0.1 *M* ammonium chloride + 0.025 *M* potassium dihydrogenphosphate + 0.0125 *M* dipotassium hydrogenphosphate, butyl alcohol (97:3); flow-rate, 0.6 ml/min.

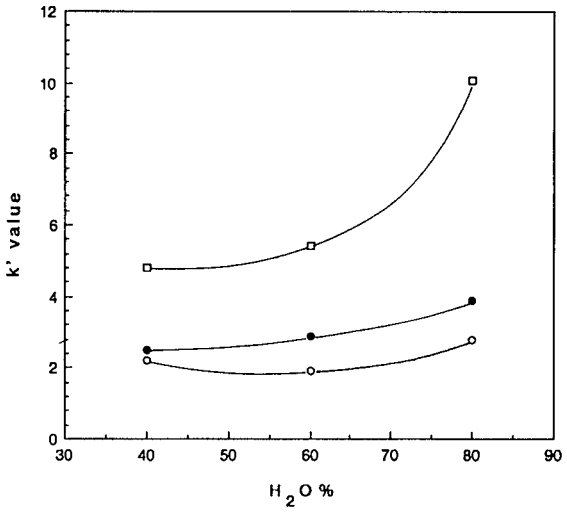

Fig. 3. Variation of k' value with mobile phase composition. (□) 0.02 M, (●) 0.05 M and (○) 0.075 M sodium acetate.

HPLC separation of niacin

Several types of column were tried to separate niacin from interferences in foodstuff. Niacin was eluted very rapidly at near-void volume in the C_{18} stationary phase using methanol–water or acetonitrile–water mixtures as the mobile phase, because in this case niacin interacts weakly with the octadecyl group in the stationary phase. By using an ion-exchange column (Hitachi gel, 3014N) niacin can be interferences with phosphate buffer solution as eluent. Fig. 2 shows a typical chromatogram obtained from strawberry jam (niacin content: 0.07 mg per 100 g) after clean-up by anion exchange resin only. However, in the case of the carbohydrate-rich sample, niacin is hindered by the impurities arising from the hydrolysis process and cannot be separated from interferences. For this reason, the detection limit of niacin is only about 0.3 mg per 100 g. However, this column may be used for determination of a small amount of niacin in foodstuffs by adding more clean-up steps. On the other hand, niacin strongly interacts with amino groups and may be separated by an amino phase column. Niacin is not eluted using an acetonitrile–water mixture only as the mobile phase but can be eluted quickly by increasing the salt concentration in the mobile phase. Fig. 3 shows a few examples of the variation of capacity factor, k', with the mobile phase composition. Niacin is eluted faster with increasing salt concentration.

This mechanism of bonded-phase chromatography is very complex, but in this case the retention behavior may be affected by the interaction of oxygen in the carbonyl group of a niacin molecule with the hydrogen of the amino group in the stationary phase. In the practical analysis, acetonitrile–water (60:40, v/v) containing 0.075 M sodium acetate was used as the mobile phase to avoid precipitation of salt. A typical chromatogram of niacin obtained from strawberry jam (the same sample as used in Fig. 2) after clean-up is shown in Fig. 4.

Quantitation of niacin

The calibration curve for niacin was linear over the concentration range 10–100 ng. The minimum detectable amount of niacin was found to be approximately 1 ng.

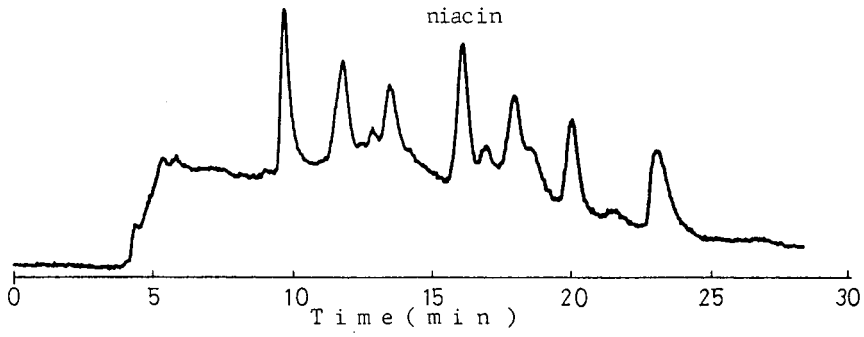

Fig. 4. Chromatogram of niacin extracted from strawberry jam (niacin content: 0.07 mg per 100 g) after clean-up.

TABLE I

RECOVERY AND REPRODUCIBILITY TEST

Experiment No.	Recovery (μg)	Recovery (%)
Fortification level of 60 μg per 10 g		
1	58.4	97.3
2	56.0	93.3
3	57.1	95.2
4	55.5	92.5
5	56.6	94.3
Mean	56.7	94.5
S.D.	1.1	1.9
Fortification level of 5 μg per 10 g		
1	4.90	98.0
2	4.25	85.0
3	4.50	90.0
4	4.46	89.2
5	4.60	92.0
Mean	4.54	90.8
S.D.	0.24	4.7

The recovery and reproducibility of the method were measured with vinegar samples fortified with a standard niacin. Niacin was added at a concentration of 60 and 5 μg per 10 g in five experiments and subjected to analysis as described in the Experimental section. The standard deviation of this method was found to be 1.9 and 4.7%, respectively (Table I).

Comparison of the HPLC method with the microbiological method

Niacin in a several kinds of vinegar and jam was determined using the HPLC method mentioned above (Table II). Niacin in the same sample was also determined by the microbiological method. The titration technique was used in the determination because this procedure is more precise than turbidimetric measurement. But it is not easy to determine correctly a small amount of niacin in these samples using the microbiological method. The results obtained by the HPLC method were in reasonable agreement with the microbiological data.

TABLE II

DETERMINATION OF NIACIN IN FOODSTUFFS

Sample	Concentration (mg per 100 g)	
	HPLC	Microbiological method
Rice vinegar	0.13	0.1
Grain vinegar	0.02	Trace
Strawberry jam	0.07	0.1
Orange jam	0.07	0.1
Apple jam	0.02	Not detected

CONCLUSION

The microbiological method has been widely used but it is difficult to determine correctly a small amount of niacin in foodstuffs. The HPLC method described here has been used for the analysis of niacin at concentrations as low as 0.1 mg per 100 g or less in foodstuffs simply and with high sensitivity. In this study, most of work was carried out using vinegar or jam as samples, but other foodstuffs can be handled similarly. The method described here can be adopted as a routine method.

REFERENCES

1 *Official Methods of Analysis*, Association of Official Analytical Chemists, Washington, DC, 15th ed., 1990, Section 961. 14.
2 *Official Methods of Analysis*, Association of Official Analytical Chemists, Washington, DC, 15th ed., 1990, Section 960.46.
3 T. A. Tyler and R. R. Shrago, *J. Liq. Chromatogr.*, 3 (1980) 26.
4 P. J. Niekerk, S. C. C. Smit, E. S. P. Strydom and G. Armbruster, *J. Agric. Food Chem.*, 32 (1984) 304.
5 K. Takatsuki, S. Suzuki, M. Sato, K. Sakai and J. Ushizawa, *J. Assoc. Off. Anal. Chem.*, 70 (1987) 698.
6 T. Hamano, Y. Mitsuhashi, N. Aoki, S. Yamamoto and Y. Oji, *J. Chromatogr.*, 457 (1988) 403.

Journal of Chromatography, 588 (1991) 177–180
Elsevier Science Publishers B.V., Amsterdam

CHROM. 23 654

Reversal of elution order during direct enantiomeric separation of pyriproxyfen on a cellulose-based chiral stationary phase

Masahiko Okamoto* and Hiroshi Nakazawa

Environmental Health Science Laboratory, Sumitomo Chemical Co., Ltd., 1-98, 3-chome, Kasugade-naka, Konohana-ku, Osaka 554 (Japan)

(First received July 2nd, 1991; revised manuscript received July 26th, 1991)

ABSTRACT

The enantiomeric separation of pyriproxyfen (Sumilarv), a new insect growth regulator, was investigated on several commercially available chiral stationary phases consisting of cellulose esters coated on silica. The mobile phases were composed of *n*-hexane and alcohols. Resolution was achieved only by using a cellulose tris-(4-methylbenzoate)-coated silica gel. The enantiomeric elution order changed according to the steric bulk of the alcohols. The possible mechanisms of the reversal of elution order are discussed.

INTRODUCTION

Pyriproxyfen (Sumilarv, Fig. 1), newly synthesized in our company, has a high juvenile hormone mimic activity, and its high efficacy as a control agent for flies, mosquitoes, and cockroaches has recently been reported [1–5]. Pyriproxyfen has a chiral centre, and the (*S*)-(−)-enantiomer is the more active [6]. A detailed investigation of both its biological activity and metabolic fate could require a knowledge of the individual behaviour of each enantiomer under a variety of biological environment.

As a first step towards establishing this, a method should be developed that would allow the direct chromatographic separation of the optical isomers, preferably without derivatization. We report here the direct chromatographic resolution of the enantiomers of pyriproxyfen on a cellulose tris-(4-methylbenzoate)-coated silica gel. During this investigation we found that the elution order of the enantiomers changed according to the steric bulk of the alcohol in the mobile phase. This is the first example to be reported of a reversal of elution order, on a modified cellulose column, associated with changes in mobile phase modifiers, although only a few studies have been performed on the inversion of the enantiomeric elution order on chiral stationary phases [7–10]. The possible mechanisms of this reversal are discussed.

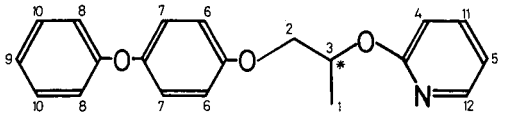

Fig. 1. Molecular structure of pyriproxyfen (Sumilarv).

EXPERIMENTAL

Apparatus

The chromatography was performed with a Hitachi (Tokyo, Japan) L-6000 pump and a Hitachi L-4000 variable-wavelength spectromeric detector. The column was stainless steel (25 cm × 4.6 mm

0021-9673/91/$03.50

I.D.), packed with cellulose tris-(4-methylbenzoate) absorbed on microporous silica (Chiralcel OJ column; Daicel, Tokyo, Japan).

Chemicals

The (*R*)-(+)- and (*S*)-(−)-enantiomers and the racemic mixture of pyriproxyfen were obtained from Takarazuka Research Center, Sumitomo, Hyogo, Japan. The mobile phase tested were composed of UV grade *n*-hexane and various alcohols, which were purchased from Wako (Osaka, Japan). The deuterated solvents for nuclear Overhauser effect (NOE) difference experiments were bought from Aldrich (Milwaukee, WI, USA).

Chromatographic conditions

The solute was dissolved in *n*-hexane–2-propanol (1:1) at a concentration of 1 mg/ml and injected onto the column via a 20-μl loop (Rheodyne injector). The injection volume was 5 μl. The column was operated at ambient temperature and solutes were detected at 254 nm. A flow-rate of 1 ml/min was maintained throughout the study.

Order of enantiomeric elution

To determine the order of elution of the (*S*)- and (*R*)-isomers, a 3:1 mixture [(*S*):(*R*)] of the two isomers was chromatographed. The mixture was prepared by using known amounts of the pure (*S*)-enantiomer and the racemic mixture.

NOE experiments

The $^1H\{^1H\}$ NOE difference spectra were recorded on a JEOL (Tokyo, Japan) JNM-GSX 270J spectrometer with tetramethylsilane as an internal standard. NOE experiments were performed with the irradiation of all the protons of pyriproxyfen in both $[^2H_{14}]$*n*-hexane–$[^2H_8]$2-propanol (9:1) and $[^2H_{14}]$*n*-hexane–$[^2H_{10}]$1-butanol (9:1).

Some connectivities established by NOE difference experiments in both *n*-hexane–2-propanol (9:1) and *n*-hexane–1-butanol (9:1) are listed in Table I.

Circular dichroism spectra

Circular dichroism (CD) measurements were carried out with a JASCO (Tokyo, Japan) J-500 spectrometer, using a 10-mm pathlength cell thermostatted at 23°C. The CD spectra of (*S*)-(−)-pyriproxyfen (4.2 mg/ml) in both *n*-hexane–2-propanol (9:1) and *n*-hexane–1-butanol (9:1) were recorded from 350 to 200 nm. The CD spectra obtained in both solvent systems were almost the same as those of the solvent blank.

TABLE I

RESULTS OF NOE DIFFERENCE EXPERIMENTS

Proton(s) irradiated	Proton(s) affected
1-CH_3 (δ 1.48)	3-H, 2-H
2-H (δ 4.10)	1-CH_3, 3-H, 6,7,8-H
3-H (δ 5.61)	1-CH_3, 2-H
4-H (δ 6.74)	11-H
5-H (δ 6.85)	–
6,7,8-H (δ 6.96)	2-H, 10-H
9-H (δ 7.04)	–
10-H (δ 7.29)	6,7,8-H
11-H (δ 7.55)	4-H
12-H (δ 8.15)	–

RESULTS AND DISCUSSION

The chromatographic resolution of the optical isomer of pyriproxyfen is shown in Fig. 2, using a Chiralcel OJ column and *n*-hexane–1-hexanol (9:1) as eluent. The column was the only one that gave excellent separation of the enantiomers. No resolution was observed using a variety of modified cellulose columns, such a Chiralcel OB, OC, OD, OF, OK or OG. The capacity factors (k'_1 and k'_2) were

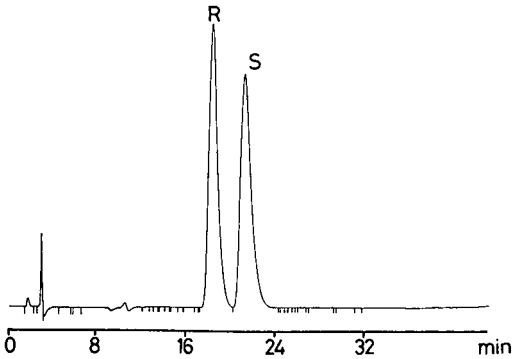

Fig. 2. Enantioseparation profile of racemic pyriproxyfen. Eluent, *n*-hexane–1-hexanol (9:1); for other analytical conditions, see text.

5.15 and 6.18, respectively. The separation factor (α) and the resolution (R_s) were determined to be 1.20 and 1.80, respectively.

We examined the mobile phase effects on the retention and stereoselectivity. A variety of the alcohols were used as the mobile phase modifiers. In general, mobile phases containing 10% alcohol were used, except for methanol and ethanol as with 10% methanol or ethanol the enantiomers were eluted too fast. The separation factor decreased with an increase in the methanol or ethanol concentration, but the elution order did not change. The chromatographic results are presented in Table II. No clear relationship between the capacity factors and the molecular weight and steric bulk of the mobile phase modifier could be identified. Measurable separation was observed in all cases, except for *n*-hexane–2-butanol. This observation does not appear to be affected by the chirality of 2-butanol, because pyriproxyfen could not be resolved using (*S*)-(+)-2-butanol as the mobile phase modifier, and the observed k' was identical with that obtained using the racemic alcohol. The maximum resolution was obtained with 1-hexanol as the mobile phase modifier (α = 1.20), and the minimum resolution with ethanol (α = 1.05).

During this study, we found a unique reversal of elution order on changing the mobile phase modifiers, as shown Table II. Two explanations for this abnormal behaviour are possible: (i) the solvation or the conformation of either pyriproxyfen or the chiral stationary phase is affected by the change in the nature of the modifier; (ii) an alteration in the steric environment of chiral cavity on the stationary phase could be induced by changing the modifier.

We performed extensive NOE and CD experiments to confirm whether a conformational change of the solute occurred depending on the mobile phase used. The $^1H\{^1H\}$ NOE difference and CD spectra of pyriproxyfen in *n*-hexane–2-propanol (9:1) were identical with those in *n*-hexane–1-butanol (9:1). These results show that the conformation of pyriproxyfen did not alter during the separation process. The conformation of the chiral stationary phase (cellulose) is not likely to be changed easily since it is supposed to be rigid [11]. The possibility that solvation occurs could not be ruled out, but Wainer *et al.* [12] have reported that solvation may play only a minor role in the chromatographic process on the cellulose ester derivative chiral stationary phase. Thus we consider that alteration of the conformation of both the solute and the chiral stationary phase does not play an important part in the inversion with a fair degree of certainty.

The observed reversal in the enantiomeric elution order can be explained by the difference of the steric bulk around the hydroxyl moiety of the mobile phase modifier. The enantiomeric elution order was

TABLE II

CHROMATOGRAPHIC RESULTS OBTAINED ON CHIRALCEL OJ

Mobile phase: *n*-hexane–alcohol (v/v).

Alcohol in mobile phase	k'_1	α	R_s	Elution order
Methanol (95:5)	2.53	1.14	1.41	*S*/*R*
Ethanol (95:5)	3.99	1.05	0.48	*S*/*R*
1-Propanol (9:1)	3.80	1.08	0.75	*R*/*S*
2-Propanol (9:1)	3.36	1.13	1.14	*S*/*R*
1-Butanol (9:1)	4.67	1.10	0.98	*R*/*S*
2-Butanol (9:1)	4.16	1.00	–	–
(*S*)-(+)-2-Butanol (9:1)	4.16	1.00	–	–
Isobutanol (9:1)	4.83	1.09	0.83	*R*/*S*
tert.-Butanol (9:1)	6.01	1.06	0.44	*S*/*R*
1-Pentanol (9:1)	5.67	1.10	1.00	*R*/*S*
2-Pentanol (9:1)	4.92	1.10	0.91	*R*/*S*
3-Pentanol (9:1)	4.64	1.06	0.40	*R*/*S*
1-Hexanol (9:1)	5.15	1.20	1.80	*R*/*S*
2-Hexanol (9:1)	6.51	1.19	1.91	*R*/*S*

S/*R* with 2-propanol as the mobile phase modifier, and the elution order was *R*/*S* with 1-propanol, although the solvent polarity parameter (p') values for 1- and 2-propanol are virtually the same, 4.0 and 3.9, respectively [13]. When methanol, ethanol, 2-propanol, or *tert.*-butanol was used as the mobile phase modifier, the (*S*)-(−)-enantiomer eluted before the (*R*)-(+)-enantiomer. The (*R*)-(+)-isomer eluted first with 1-propanol, 1-butanol, isobutanol, pentanols or hexanols. This shows that diastereomeric complex(es) between the chiral stationary phase and the (*R*)-isomer may be more stable with less bulky alcohols, methanol, ethanol, 2-propanol, or *tert.*-butanol, as the mobile phase modifier, and that with more bulky alcohols, 1-propanol, 1-butanol, isobutanol, pentanols, or hexanols, diastereomeric complex(es) between the chiral stationary phase and the (*S*)-isomer may be more stabilized.

It has been reported that the chiral cavity (or ravine) of the stationary phase plays an important role in the chiral recognition on cellulose-based chiral stationary phase [12]. The less bulky alcohols could be inserted into the cavity of the chiral stationary phase more easily than the more bulky alcohols. The insertion of the mobile phase modifier into the chiral cavities of the chiral stationary phase could induce changes in the dominant chiral recognition mechanism, leading eventually to inversion of the elution order of enantiomers. The observation noted above suggests that at least two chiral binding- or recognition-sites are present in this chiral stationary phase.

In this instance, the enantioselectivity and enantiomeric elution order of pyriproxyfen on a cellulose tris-(4-methylbenzoate) depend on the mobile phase modifier used. It will be essential to take into account the contribution of mobile phase modifier to the enantioseparation of racemic compounds.

ACKNOWLEDGEMENTS

We thank Mr. Masayuki Nagase of Organic Synthesis Research Laboratory, Sumitomo Chemical Co. Ltd., for the CD spectra measurements, and Mr. Akio Kawamoto of our Laboratory for the NOE experiments. We are indebted to Ms. Sanae Sakaguchi of our laboratory for her excellent technical assistance. The gifts of (*R*)-(+)- and (*S*)-(−)-enantiomers and the racemic mixture of pyriproxyfen from Dr. Makoto Hatakoshi of Takarazuka Research Center, Sumitomo Chemical Co. Ltd. are gratefully acknowledged.

REFERENCES

1 J. G. Estrada and M. S. Mulla, *J. Am. Mosq. Control. Assoc.*, 2 (1986) 57.
2 M. Hatakoshi, H. Kawada, S. Nishida, H. Kishida and I. Nakayama, *Jpn. J.Saint Zool.*, 38 (1987) 271.
3 H. Kawada, K. Dohara and G. Shinjo, *Jpn. J. Saint Zool.*, 38 (1987) 317.
4 H. Kawada, K. Dohara and G. Shinjo, *Jpn. J. Saint Zool.*, 39 (1988) 339.
5 H. Kawada, I. Kojima and G. Shinjo, *Jpn. J. Saint Zool.*, 40 (1989) 195.
6 N. Itaya, *J. Synth. Org. Chem., Jpn.*, 45 (1987) 36.
7 T. D. Doyle and I. W. Wainer, *J. High Res. Chromatogr. Chromatogr. Commun.*, 7 (1984) 38.
8 P. Macaudière, M. Lienne, M. Caude, R. Rosset and A. Tambuté, *J. Chromatogr.*, 467 (1989) 357.
9 A. M. Dyas, A. F. Fell and M. L. Robinson, *Chirality*, 2 (1990) 20.
10 J. Haginaka, J. Wakai, K. Takahashi, H. Yasuda and T. Katagi, *Chromatographia*, 29 (1990) 587.
11 J. F. Kennedy, G. O. Phillips and P. A. Williams, *Cellulose: Structural and Functional Aspects*, Ellis Horwood, Chichester, UK, 1989.
12 I. W. Wainer, R. M. Stiffin and T. Shibata, *J. Chromatogr.*, 411 (1987) 139.
13 L. R. Snyder and J. J. Kirkland, *Introduction to Modern Liquid Chromatography*, John Wiley, New York, 2nd ed., 1979, pp. 246–266.

Journal of Chromatography, 588 (1991) 181–186
Elsevier Science Publishers B.V., Amsterdam

CHROM. 23 624

High-performance liquid chromatographic analysis of oxytetracycline in chinook salmon following administration of medicated feed

Ron G. Aoyama, Keith M. McErlane and Hildegard Erber

Faculty of Pharmaceutical Sciences, 2146 East Mall, Vancouver, B.C. V6T 1Z3 (Canada)

David D. Kitts

Department of Food Science, Faculty of Agricultural Sciences, 6650 N.W. Marine Drive, Vancouver, B.C. V6T 1Z4 (Canada)

Helen M. Burt*

Faculty of Pharmaceutical Sciences, 2146 East Mall, Vancouver, B.C. V6T 1Z3 (Canada)

(Received July 12th, 1991)

ABSTRACT

A high-performance liquid chromatographic assay was developed to detect oxytetracycline (OTC) in chinook salmon muscle tissue. A solid-phase extraction protocol was used to recover OTC and the internal standard, epitetracycline hydrochloride, from the salmon tissue samples. OTC was analyzed using a mobile phase of methanol–0.02 *M* phosphate buffer, pH 2.25 (60:190), an ultraviolet detection wavelength of 365 nm and a 250 mm × 4.6 mm I.D. Ultrasphere ODS column. A linear calibration curve ($r^2 = 0.999$) of OTC in salmon muscle tissue from 0.05 to 3.0 ppm was obtained. Using a signal-to-noise ratio of 5:1, the OTC detection limit was 0.05 ppm in salmon muscle tissue. OTC recovery (74.4%) and intra-assay variability (2.3%) were optimized for salmon muscle tissue. An *in vivo* feeding study was performed by administrating OTC-medicated feed for a period of 10 days, followed by a 42-day sampling period. The half-life for the elimination of OTC in chinook salmon muscle tissue was found to be 5.4 days.

INTRODUCTION

The raising of farmed salmon is an established, growing industry. Frequently antibiotics are used to treat diseases in salmon and the possible health risk to humans, presented by traces of antibiotics in salmon tissue, has generated considerable concern.

To ensure that levels of antibiotics in salmon tissue are within acceptable limits, monitoring of drug residues is an essential aspect of aquaculture. Thus, there is a demand for development of techniques which are specific and sensitive for the quantitative detection of antibiotic residues in salmon tissue and the determination of antibiotic wash-out times from tissue.

Oxytetracycline (OTC) is a widely used antibiotic in the aquaculture industry. It is used to treat a variety of diseases including coldwater disease, columnaris, enteric redmouth, fin rot, furunculosis, gill disease and vibriosis [1,2].

Previously reported methods for the analysis of OTC in fish include microbiological studies which investigated the clearance times of OTC from rainbow trout (*Salmo gairdneri*) [3–5] and another study which used a microbiological assay to determine the pharmacokinetics and tissue distribution of OTC in

0021-9673/91/$03.50

carp (*Cyprinus carpio*) [6]. However, chromatographic methods are generally preferred for their greater selectivity and sensitivity for antibiotic analysis. Many high-performance liquid chromatographic (HPLC) methods have been reported for the analysis of OTC in fish. The OTC concentrations of spiked serum, liver and muscle of rainbow trout and other fish species have been measured using HPLC analysis [7,8].

Rainbow trout have been used for studies of the absorption, elimination and tissue distribution of OTC. In one study, trout were fed medicated feed every day for 10 days and muscle and liver tissue were analyzed by HPLC for OTC [9]. In another study, trout were fed medicated freed every day for 8 days and OTC concentrations were determined for blood, kidney, muscle, skin and gutted trout using HPLC techniques [10].

This study employed an HPLC assay to measure the concentrations of OTC in muscle tissue of salmon administered medicated feed. To date, there have been no published reports of HPLC analysis of OTC in salmon. The wash-out time for OTC from salmon muscle tissue was also determined.

EXPERIMENTAL

Materials

Oxytetracycline dihydrate and trichloroacetic acid (TCA) were obtained from Sigma (St. Louis, MO, USA). The internal standard, epitetracycline hydrochloride, was obtained from the European Pharmacopeia (Strasbourg, France). HPLC-grade methanol was obtained from Fisher Chemicals (Vancouver, Canada). Disodium hydrogen orthophosphate dihydrate ($Na_2HPO_4 \cdot 2H_2O$) and analytical-grade phosphoric acid (H_3PO_4; 85%) were obtained from BDH Chemicals (Toronto, Canada). HPLC-grade water was produced using a Milli-Q water purification system [Millipore (Canada) Mississauga, Canada].

Apparatus

The HPLC system consisted of a Beckman Model 110A pump, a Model 210 sample injection valve fitted with a 20-μl loop, a Beckman Model 160 fixed-wavelength detector with a 365-nm filter, a mercury lamp and a Shimadzu C-R3 integrator. The column was a 250 mm × 4.6 mm I.D. Ultrasphere octadecylsilane (ODS) phase with a particle size of 5 μm. The mobile phase consisted of methanol–0.02 *M* phosphate buffer, pH 2.25 (60:190) and was delivered isocratically at a flow-rate of 1.0 ml/min. The mobile phase was filtered prior to use with a Millipore HPLC solvent filtration system and FP Vericel 47-mm, 0.45-μm membrane filters (Gelman Sciences, Ann Arbor, MI, USA).

Preparation of standard solutions and reagents

All OTC solutions were prepared immediately before use. A 500 μg/ml OTC stock solution was prepared by dissolving 5 mg in 10.0 ml of methanol. Varying volumes of stock solution were diluted with methanol to give concentrations of 0.5, 1.0, 4.0, 10, 20 and 30 μg/ml.

The internal standard, epitetracycline hydrochloride, was used for the calibration curve samples and the treated fish samples. A 200 μg/ml stock solution was prepared by dissolving 2.0 mg of epitetracycline hydrochloride in 10.0 ml of methanol. The 10 μg/ml working solution was prepared by diluting 0.5 ml of epitetracycline hydrochloride stock solution to a final volume of 10.0 ml with methanol. To each 5-g tissue sample, 0.5 ml of the internal standard working solution were added, resulting in a final concentration of 1.0 μg/g of tissue.

Extraction procedure

In a 50-ml polypropylene centrifuge tube, 15 ml of 0.02 *M* phosphate buffer, pH 2.0, 0.5 ml of the internal standard solution and 1.0 ml of 50% (w/v) TCA were added to 5.0 g of salmon muscle tissue. Each sample was homogenized three times for 30-s intervals at medium speed using a Brinkman Polytron Model PT 10/35 homogenizer (Brinkman Instruments, Rexdale, Canada). The samples were centrifuged for 20 min at 30 000 *g* at 4°C (JA-17 rotor, r_{avg}) in a Beckman Model J2-21 centrifuge (Beckman Instruments). The supernatant was transferred to a 50-ml erlenmeyer flask and stored in the dark at 4°C. An aliquot of 15 ml of phosphate buffer and 1.0 ml of TCA was added to the salmon muscle residue and the homogenization was repeated as before. The supernatants were combined and filtered through a Bakerbond solid-phase extraction (SPE) Sephadex G-25 gel disposable 6-ml column (J. T. Baker, Phillipsburg, NJ, USA). Three 2-ml

aliquots of phosphate buffer were used to rinse the supernatant onto the column. The Sephadex column was conditioned before use by adding 5 ml of phosphate buffer, pH 2.0, shaking well and drawing off the liquid under gentle vacuum until a 2-mm layer remained above the surface of the gel. The salmon tissue extract was collected in another 50-ml erlenmeyer flask and then passed through an activated Bakersbond SPE octadecyl (C_{18}) disposable 6-ml column (J. T. Baker) fitted with an adaptor and a 60-ml reservoir. The C_{18} column was activated by passing through 4 ml of 50% (v/v) methanol and then 4 ml of buffer. The OTC and internal standard were then eluted off the column with 7 ml of methanol into a 10-ml culture tube. The samples were evaporated under nitrogen in a 40°C water bath to dryness and reconstituted to 1.0 ml with methanol. The samples were vortex-mixed for 15 s and stored at −20°C until required for analysis. A 50-μl aliquot was injected onto the HPLC column. Since the sampling loop used had a volume of 20 μl, this excess volume of sample removed any residue from the previous analysis.

Calibration curve, assay precision and recovery

A calibration curve was prepared from salmon muscle tissue samples (5 g) to which 0.5 ml of the internal standard solution (1.0 μg/g of tissue) and 0.5 ml of the appropriate OTC standard solutions were added to give final concentrations of 0.05, 0.1, 0.4, 1, 2 and 3 ppm of tissue. The calibration curve was constructed by plotting the ratios of the peak areas of OTC to the peak areas of the internal standard against the known concentrations of OTC.

The recovery study was performed by adding 0.5 ml of 1.0, 10.0 and 20.0 μg/ml OTC solution to 5-g samples of salmon muscle tissue. One sample was prepared at each concentration. The samples were processed as described above, however, no internal standard solution was added to the samples. The area of the OTC peak was compared to the area of the peaks for identical amounts of the unextracted standard solutions.

Feeding study

Approximately 80 chinook salmon varying in weight from 222 to 1044 g were kept in a circular (4′ deep × 8′ diameter) flowing seawater tank at the West Vancouver Laboratory of the Department of Fisheries and Oceans (West Vancouver, Canada). The tank capacity was 3600 l and the flow-rate of seawater was 40–60 l/min. The water temperature varied from a minimum of 7.8°C to a maximum of 10.3°C during the 52-day study period. Prior to the start of the feeding study, three fish were removed and analyzed to confirm the absence of OTC as these fish were also used as control samples for the calibration curves, assay precision and recovery studies. The fish were fed medicated feed, Extruded New Age Salmon feed, 3.5 mm pellets (Moore-Clark, Vancouver, Canada) containing OTC at a concentration of 10 kg oxytetracycline per tonne of feed. The actual dosage of OTC was 80 mg per kg of biomass per day. Feeding was done twice daily until satiation, or until the 500-g aliquot of feed was consumed. The medication period was 10 days after which the fish were then fed a non-medicated feed formulation (Moore-Clark). Prior to the morning feeding, four fish were removed on days 2, 4, 6, 8, 11, 12, 14, 17, 20, 24, 28, 31, 34, 38, 45 and 52. The fish were sacrificed by a blow to the head, tagged and stored at −20°C. For analysis, three 5-g samples were removed from each fish at evenly spaced sites along the length of the fish.

RESULTS AND DISCUSSION

Fig. 1 shows representative chromatograms of a blank salmon extract and a salmon extract containing OTC and the internal standard. Epitetracycline hydrochloride was selected due to its elution properties and ultraviolet absorption characteristics. Other tetracycline analogues such as doxycycline and minocycline had unsuitable retention times, while chlorocycline and demeclocycline had impurities which eluted at the same retention time as OTC, thus precluding their use as internal standards.

The calibration curve for OTC extracted from salmon muscle tissue is shown in Fig. 2. A linear relationship was established over the concentration range 0.05–3.0 ppm of OTC ($r^2 = 0.999$).

OTC was recovered from salmon muscle tissue using the SPE procedure described. The mean recovery of OTC was found to be 74.4% over the concentration range 0.1–2.0 ppm. (Table I).

Protein precipitation with TCA and extraction into a buffer was found to be the most efficient method of recovering OTC from the salmon muscle

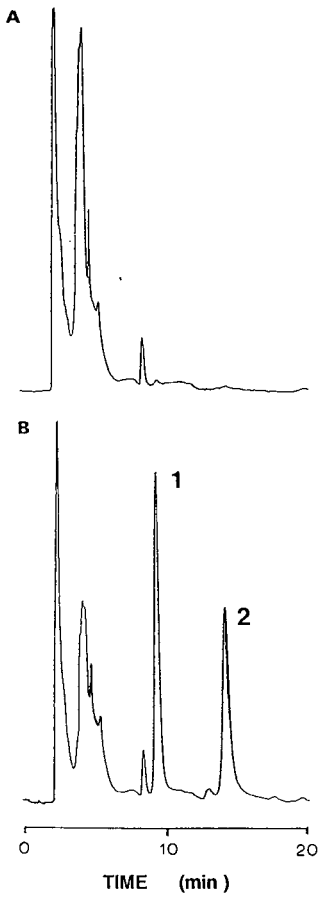

Fig. 1. Representative chromatograms from (A) a blank salmon muscle tissue extract and (B) salmon muscle tissue extract to which 2.0 ppm of OTC had been added. Chromatographic conditions: Ultrasphere ODS 5-μm (250 mm × 4.6 mm I.D.) column; mobile phase, methanol–0.02 *M* phosphate buffer, pH 2.25 (60:190); HPLC flow-rate, 1.0 ml/min; ultraviolet detection wavelength, 365 nm. Peaks: 1 = epitetracycline; 2 = OTC.

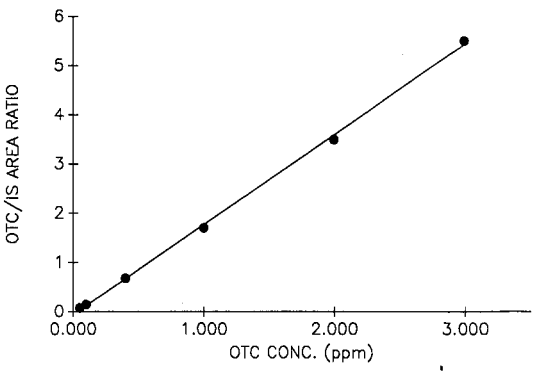

Fig. 2. Calibration curve for OTC extracted from salmon muscle tissue over the concentration range 0.05–3.0 ppm. r^2 = 0.999; *y*-intercept = −0.056; slope = 0.364. I.S. = internal standard.

tissue. The double-extraction procedure improved recoveries over a single-extraction method. Using a signal-to-noise ratio of 5:1, the detection limit was 0.05 ppm. The quantitation limit was 0.1 ppm. The recovery of OTC compares favorably with a recovery of 69.9% in fish muscle reported by Rogstad *et al.* [8] and 61.3% in rainbow trout by Norlander *et al.* [9]. Other studies performed with rainbow trout muscle tissue [7] and yellow-tail and porgy [11] reported higher OTC recoveries. These differences may be explained by the high level of cholesterol and carotenoids found in salmon muscle tissue. Sheridan [12] found that cholesterol levels in coho salmon muscle tissue were two times higher than for muscle tissue from rainbow trout. Salmon tissue also has high levels of carotenoids. The high levels of carotenoids and cholesterol may contribute to the high total lipid content in the salmon muscle. These factors appeared to affect the efficiency of antibiotic extraction for chinook salmon muscle tissue. The intra-assay coefficient of variation was found to be 2.3% and is shown in Table II. A 0.4-ppm salmon extract was injected five times. The average calculated concentration was 0.410 ppm.

The feeding study was used in conjunction with the HPLC assay method to determine the wash-out time for OTC in salmon muscle tissue. The protocol for the administration of medication was the same as that used on a commercial salmon farm. The fish appeared to eat all of the feed aliquot. The flow-rate

TABLE I

RECOVERY OF OXYTETRACYCLINE FROM CHINOOK SALMON MUSCLE TISSUE

Each value represents a single determination at each sample concentration.

Sample concentration (ppm)	Recovery (%)
0.1	62.4
1.0	81.8
2.0	77.9
Mean	74.4

TABLE II

INTRA-ASSAY VARIABILITY OF OXYTETRACYCLINE IN CHINOOK SALMON MUSCLE TISSUE

Injection No.	Sample concentration (ppm)	OTC internal standard area ratio	Calculated concentration (ppm)
1	0.4	0.717	0.425
2	0.4	0.683	0.403
3	0.4	0.698	0.414
4	0.4	0.678	0.406
5	0.4	0.676	0.402
Mean		0.691	0.410
Standard deviation		0.017	0.009
Coefficient of variation (%)		2.30	2.30

of seawater resulted in a complete exchange in the tank in 60 to 90 min. The relatively low initial levels and short duration of OTC in seawater would suggest that the possibility of OTC uptake by the fish from the seawater was minimal.

There was some variation in concentration between different fish sampled on the same day. For samples from different sites of the same fish, the variation was only slightly above that of experimental error. There also appeared to be no correlation between the weight of the salmon and tissue concentrations of OTC. Fig. 3 shows the uptake and decline for OTC in salmon muscle tissue. The OTC concentrations are also given in Table III. Peak concentrations of 1.36 ppm were observed at day 14. The concentration of OTC then declined from day 17 to day 38. OTC could not be detected from day 45 to day 52 in any of the samples. Data points from the last eight sampling periods derived in Fig. 3 were used in the computer program Non-lin [13] to calculate a half-life of 5.4 days for OTC in salmon muscle tissue. Under the conditions of this study, the data show that OTC levels are below the detection limit of 0.05 ppm, 35 days after the last administration of medicated feed. Nordlander *et al.* [9] found that the levels of OTC in rainbow trout

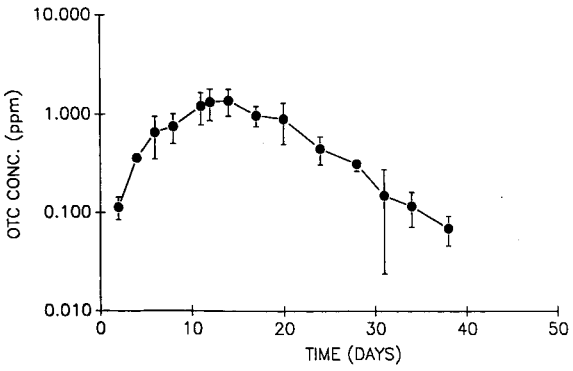

Fig. 3. Uptake and decline of OTC is muscle tissue from chinook salmon after administration of medicated feed. Each data point represents the average concentration of the samples assayed from four salmon on the sampling day ± standard error.

TABLE III

CONCENTRATION OF OXYTETRACYCLINE IN CHINOOK SALMON MUSCLE TISSUE OVER TIME

Day	OTC concentration (ppm)	Standard deviation (ppm) ($n=12$)[a]
2	0.050	0.020
4	0.359	0.024
6	0.650	0.300
8	0.752	0.252
11	1.203	0.432
12	1.317	0.463
14	1.360	0.411
17	0.959	0.221
20	0.885	0.396
24	0.444	0.140
28	0.311	0.048
31	0.148	0.124
34	0.116	0.045
38	0.069	0.023

[a] Four fish were sampled and triplicate analyses were performed for each day.

muscle tissue was 0.041 ppm, 23 days after last administration of medicated feed. Jacobsen [10] found that OTC could be detected in rainbow trout at the level of 0.05 ppm 22 days after the last dose of drug.

ACKNOWLEDGEMENTS

This research was supported by the Science Council of British Columbia, the Department of Fisheries and Oceans, and the Ministry of Agriculture, B.C. The authors would like to acknowledge the technical assistance of Mr. Andy Lamb and Ms. Jacqueline Walisser during the feeding study. The authors would also like to thank Dr. Ed Donaldson, Department of Fisheries and Oceans, for providing tank space for housing the salmon.

REFERENCES

1 B. Austin, *Proceedings Aquaculture International Congress and Exposition, Vancouver, Sept. 6–9, 1988*, Aquaculture International Congress, Vancouver, 1988, p. 597.
2 C. J. Sinderman and D. V. Lightner (Editors), *Disease Diagnosis and Control in North American Marine Aquaculture*, 2nd. ed., 1988.
3 L. Silver, N. Johansson and O. Ljungberg, *Bull. Off. Int. Epizoot.*, 69 (1968) 1465–1474.
4 R. Salle and K. Lieslol, *Acta Vet. Scand.*, 24 (1983) 418–430.
5 A. McCracken, S. Fidgeon, J. J. O'Brien and D. Anderson, *J. Appl. Bactericol.*, 40 (1976) 61–66.
6 J. J. Groudel, J. F. M. Nousiv, M. Dejong, A. R. Schutte and F. Driessens, *J. Fish Dis.*, 10 (1987) 153–163.
7 H. Bjorklund, *J. Chromatogr.*, 432 (1988) 381–387.
8 A. Rogstad, V. Hormazabal and M. Yndestad, *J. Liq. Chromatogr.*, 11 (1987) 2337–2347.
9 I. Nordlander, H. Johnsson and B. Osterdahl, *Food Addit. Contam.*, 4 (1987) 291–296.
10 M. D. Jacobsen, *J. Fish Dis.*, 12 (1989) 29–36.
11 Y. Onji, M. Uno and K. Tanigawa, *J. Assoc. Off. Anal. Chem.*, 67 (1984) 1135–1137.
12 M. A. Sheridan, *Comp. Biochem. Physiol.*, 90B (1988) 679.
13 A. J. Sedman and J. G. Wagner, *Non-lin: A Decision-Making Pharmacokinetic Computer Program*, Michigan Publication Distribution Services, Ann Arbor, MI, 1976.

Journal of Chromatography, 588 (1991) 187–193
Elsevier Science Publishers B.V., Amsterdam

CHROM. 23 647

Ion-pairing high-performance liquid chromatographic method for the determination of 5-aminosalicylic acid and related impurities in bulk chemical

Brian S. Kersten*, Tom Catalano and Yury Rozenman

Searle Research and Development, 4901 Searle Parkway, Skokie, IL 60077 (USA)

(First received April 2nd, 1991; revised manuscript received July 22nd, 1991)

ABSTRACT

An ion-pairing high-performance liquid chromatographic method has been developed for the determination of 5-aminosalicylic acid (5-ASA) bulk chemical in the presence of thirteen potential synthetic process impurities. In addition, the method is suitable for the determination of the in-process intermediate, 5-nitrosalicylic acid. A selective method was achieved on a Hypersil-BDS reversed-phase column using 1-heptanesulfonic acid sodium salt as the ion-pairing reagent in a 0.08 *M* sodium phosphate buffer (pH 2) containing 0.005 *M* 1-heptanesulfonic acid sodium salt and 0.07 *M* sodium chloride–methanol–tetrahydrofuran (85:11:4, v/v/v) isocratic mobile phase. The method was validated using a multi-day, intra-laboratory protocol. The validation addressed linearity, accuracy, precision, sensitivity, and ruggedness of the method. The validated method characterizes the purity of 5-ASA bulk chemical.

INTRODUCTION

Over the last decade, high-performance liquid chromatography (HPLC) has established itself as the analytical method of choice in the pharmaceutical industry. More specifically, HPLC methods have been developed for the analysis of bulk chemicals, dosage forms, and biological samples. However, HPLC of polar, ionizable compounds often exhibit poor resolution, retention, and/or peak shape under reversed-phase conditions. These problems can be solved using ion-pairing reagents to improve the chromatographic separation. The selectivity that is often attainable along with its wide applicability to many pharmaceutical compounds has made ion-pairing chromatography a powerful analytical tool.

5-Aminosalicylic acid (5-ASA) has been shown to be an effective drug for the treatment of inflammatory bowel disease, ulcerative colitis, and Crohn's disease [1–3]. Several methods describe the determination of 5-ASA in biological samples [4–11] and dosage forms [12,13] utilizing HPLC with various methods of detection (*i.e.*, UV, fluorescence, and electrochemical detection). However, no method describes the purity determination of 5-ASA bulk chemical. The proprietary synthesis of 5-ASA can potentially produce thirteen synthetic process impurities in the final product. Purity testing would require the determination of these potential impurities in 5-ASA as well as the characterization of its in-process intermediate, 5-nitrosalicylic acid (5-NSA). To achieve the high degree of selectivity needed for the analysis of a wide polarity range of compounds, an ion-pairing method was developed and validated for the determination of 5-ASA.

EXPERIMENTAL

Materials

5-ASA and 5-NSA were synthesized at Searle Chemical (Augusta, GA, USA). Authentic samples of the impurities were purchased from the following vendors: 4-aminophenol (4-AP), 2,4-diaminophe-

0021-9673/91/$03.50

nol (2,4-DAP), 2,4-dinitrophenol (2,4-DNP), 2-aminophenol (2-AP), 2,5-dihydroxybenzoic acid (2,5-DHBA), phenol, 3,5-dinitrosalicylic acid (3,5-DNSA), 4-nitrophenol (4-NP), and 2-nitrophenol (2-NP), Aldrich (Milwaukee, WI, USA); salicylic acid (SA), Monsanto (St. Louis, MO, USA); 3-aminosalicylic acid (3-ASA), Sigma (St. Louis, MO, USA); 3-nitrosalicylic acid (3-NSA), Custom (Elmwood Park, NJ, USA). Mobile phase and diluting solvent constituents were obtained from the following vendors: HPLC-grade water, J. T. Baker (Phillipsburg, NJ, USA); methanol and tetrahydrofuran, Burdick & Jackson (Muskegon, MI, USA); 85% phosphoric acid, hydrochloric acid, glacial acetic acid, 50% (w/w) sodium hydroxide solution and sodium chloride, Mallinckrodt (St. Louis, MO, USA); 1-heptanesulfonic acid sodium salt, Sigma; sodium phosphate monobasic monohydrate, 98+%, Aldrich.

Apparatus

Development and validation of the method was conducted utilizing the following chromatographic systems: a Beckman Model 421 controller/Model 100A pump (Fullerton, CA, USA) with a Waters Model 710B WISP autosampler (Milford, MA, USA) connected to a Kratos Model 757 UV detector (Foster City, CA, USA) in series with a Waters Model 481 UV detector. The column was a Hypersil-BDS C_{18} (250 mm × 4.6 mm I.D., 5 μm particle size) obtained from Keystone Scientific (Bellefonte, PA, USA) and heated using FIAtron Model TC-50 controller/Model CH-30 column heater (Milwaukee, WI, USA). The exact temperature of the column was measured with a Digi-Sense type K thermocouple obtained from Cole-Palmer (Chicago, IL, USA). Optimization of the method was performed on a Hewlett-Packard Model 1090 liquid chromatograph equipped with a 1040 diode-array detector (Palo Alto, CA, USA). Hewlett-Packard's optimization software package [*i.e.*, interactive computer optimization of HPLC separations (ICOS)] was utilized for the final optimization of the method. Chromatographic measurements (*i.e.*, retention times, peak areas, etc.) and statistical calculations were made with an in-house chromatographic and statistical data management system.

Chromatographic conditions

The aqueous portion of the mobile phase was prepared by accurately weighing 8.6 g (± 0.1 g) of sodium phosphate, 8.2 g (± 0.1 g) of sodium chloride, and 2.2 g (± 0.1 g) of 1-heptanesulfonic acid sodium salt into a suitable 3-l Erlenmeyer flask. HPLC water (2 l) and 5.75 ml of 85% phosphoric acid were added. The buffer solution (pH 2) was mixed well and filtered through a 0.45-μm Nylon filter. Appropriate amounts of methanol and tetrahydrofuran were added for a mobile phase composition of 0.08 *M* sodium phosphate buffer (pH 2) containing 0.005 *M* 1-heptanesulfonic acid sodium salt and 0.07 *M* sodium chloride–methanol–tetrahydrofuran (85:11:4, v/v/v) which was degassed before use. Other pertinent HPLC parameters were as follows: column, Hypersil-BDS C_{18}, 5 μm particle size; flow-rate, 1.5 ml/min; injection volume, 20 μl; column temperature, 35°C; detection, assay, UV at 300 nm and 0.1 a.u.f.s., impurities, UV at 215 nm and 0.1 a.u.f.s.; total run time, 45 min.

Sample preparation

5-ASA samples were prepared by dissolving the desired amount in acidified water (pH 2 using concentrated hydrochloric acid). Dissolution of 5-ASA in the diluting solvent required sonication especially for the more concentrated samples ($\geq$ 0.8 mg/ml).

5-NSA samples were prepared by dissolving the desired amount in a 0.1 *M* acetate buffer at pH 5. Dissolution of the 5-NSA at 1 mg/ml also required sonication.

RESULTS AND DISCUSSION

The HPLC method was developed for the purity testing of 5-ASA bulk chemical. The HPLC method had to ideally resolve thirteen potential synthetic process impurities of different polarity from 5-ASA with the condition that the system be isocratic and able to quantitate 0.1% of each impurity. Due to the wide polarity range of the impurities, an ion-pairing HPLC method was developed. Method development consisted of the selection of an ion-pairing reagent, buffer system, and organic modifiers. Once the selectivity of the method was optimized, performance characteristics were determined through a validation study. Validation addressed

method linearity, accuracy, precision, sensitivity, and ruggedness.

Development/optimization of the HPLC method

The potential synthetic process impurities to be resolved from 5-ASA are shown in Fig. 1. The following ion-pairing reagents were evaluated: 1-hexanesulfonic acid, 1-heptanesulfonic acid, 1-octanesulfonic acid, and 1-dodecylsulfonic acid sodium salt. A plot of the capacity factor as a function of the alkyl chain length of the sulfonic acid sodium salt for 5-ASA, selected potential impurities, and selected nitro compounds are shown in Figs. 2 and 3, respectively. As the alkyl chain of the ion-pairing reagent increased, 5-ASA and its potential impurities retained longer on the column while the nitro compounds retained less. It is conjectured that the ion-pairing reagent causes an ion-exclusion mechanism to occur which decreases the retention of the nitro compounds. 1-Heptanesulfonic acid sodium salt provided a reasonable retention of 5-ASA and its potential impurities; therefore, it was selected as the ion-pairing reagent.

During the initial method development process, a

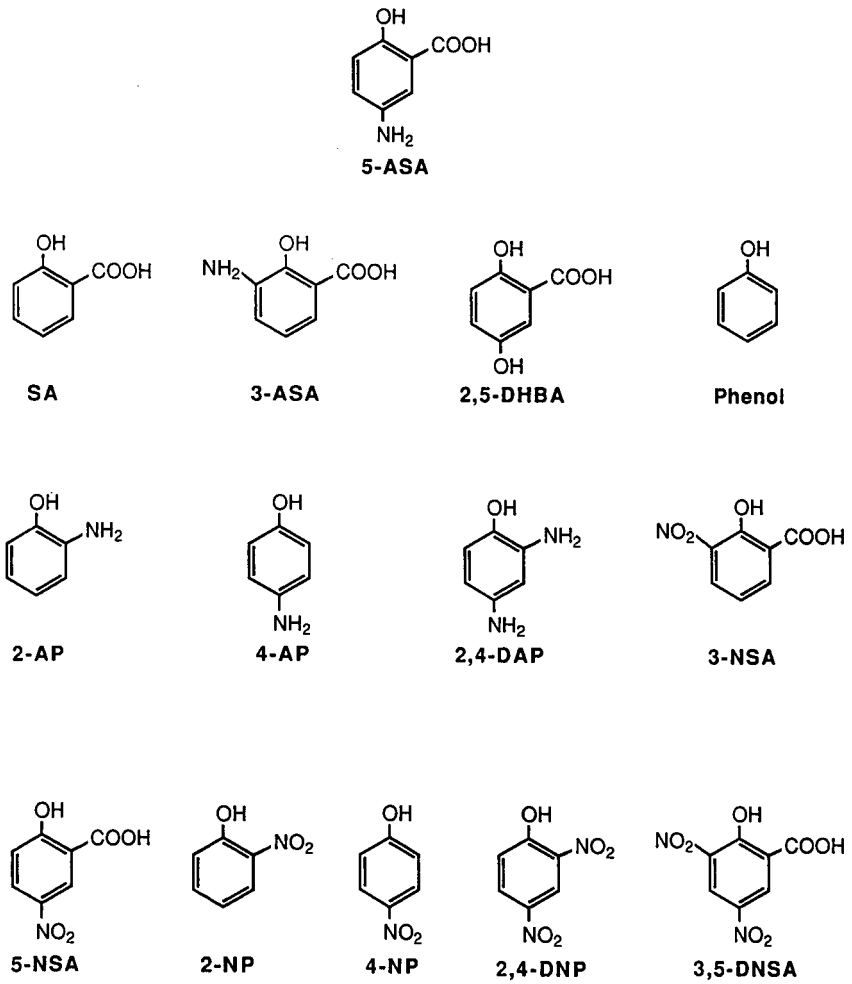

Fig. 1. Structures of 5-aminosalicylic acid (5-ASA) and potential synthetic process impurities: salicylic acid (SA), 3-aminosalicylic acid (3-ASA), 2,5-dihydroxybenzoic acid (2,5-DHBA), phenol, 2-aminophenol (2-AP), 4-aminophenol (4-AP), 2,4-diaminophenol (2,4-DAP), 3-nitrosalicylic acid (3-NSA), 5-nitrosalicylic acid (5-NSA), 2-nitrophenol (2-NP), 4-nitrophenol (4-NP), 2,4-dinitrophenol (2,4-DNP), and 3,5-dinitrosalicylic acid (3,5-DNSA).

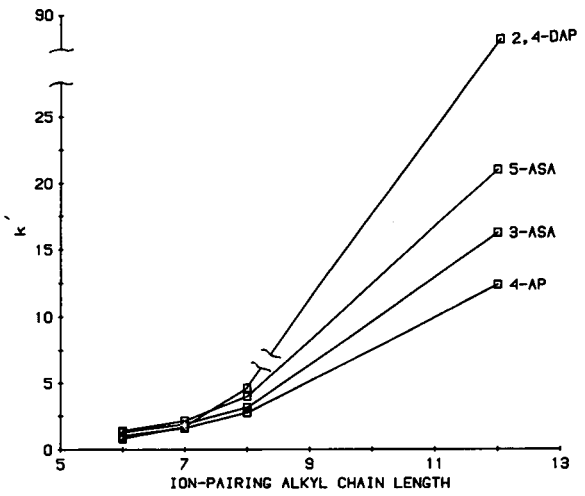

Fig. 2. Capacity factor (k') as a function of the alkyl chain length of the sulfonic acid sodium salt for 5-ASA and selected related impurities.

0.03 *M* sodium acetate buffer system at pH 3 was utilized. Due to the lack of retention of 5-ASA and several impurities at pH 3, the buffer system was adjusted to pH 2 with 85% phosphoric acid. At a sodium phosphate buffer concentration of 0.08 *M* (pH 2), adequate retention of 5-ASA and its potential impurities was obtained; however, the selectivity was not reproducible. It was determined that the phosphate ion plays a role in the selectivity of the method. Therefore, preparation of the buffer system required that the phosphoric acid be added

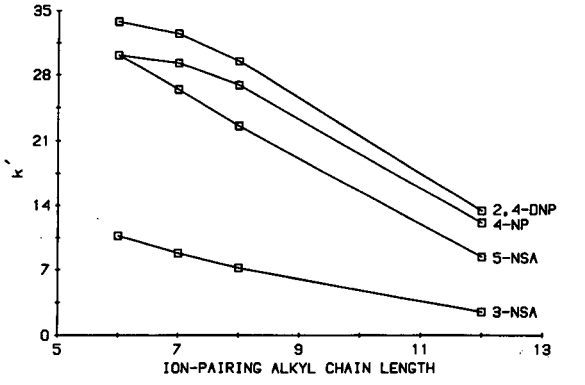

Fig. 3. Capacity factor (k') as a function of the alkyl chain length of the sulfonic acid sodium salt for selected nitro compounds.

quantitatively to obtain the desired selectivity of the method. Ionic strength was investigated as playing a role in the reproducibility of the method by adding sodium chloride to the buffer system. As a result of these investigations, a 0.08 *M* sodium phosphate buffer (pH 2) containing 0.07 *M* sodium chloride yielded reproducible selectivity.

Optimization of the organic modifier was performed on a HP 1090 equipped with Hewlett-Packard's optimization software package, ICOS. ICOS utilizes a solvent selectivity triangle and retention mapping as a means of optimizing the separation. Basically, three steps are involved in the program. First, the ratio of buffer to organic modifier for each corner of the triangle is determined so that a similar retention time of 5-ASA is achieved. For this study, methanol, acetonitrile, and tetrahydrofuran were selected as the organic modifiers. Next, the program runs selective percentage combinations of the three corners so selectivity throughout the triangle is fully investigated. Finally, the data are reduced and retention mapping allows the prediction of separations for potential solvent combinations. From the program, several combinations of buffer and organic modifier were selected and experimentally tested. The predicted separations were in excellent agreement with the experimental results. A mixture of 0.08 *M* sodium phosphate buffer (pH 2) containing 0.005 *M* 1-heptanesulfonic acid sodium salt and 0.07 *M* sodium chloride–methanol–tetrahydrofuran (85:11:4, v/v/v) gave the best selectivity of the thirteen potential synthetic impurities in the presence of 5-ASA. The selectivity of the method along with a typical lot of 5-ASA are illustrated in Figs. 4 and 5.

Utilizing the same chromatographic conditions, 5-NSA, an in-process intermediate to 5-ASA, can be profiled. The method's selectivity along with a typical lot of 5-NSA are shown in Fig. 6. The detection of 3-NSA, 3-NP, 2,4-DNP, SA and two unknowns in a lot of 5-NSA chemical demonstrates the method's suitability for the determination of this in-process intermediate. In addition, spectral analyses were performed on 5-ASA and 5-NSA chemical lots utilizing a photodiode-array detector to support further the selectivity of the method.

Validation of the HPLC method

The chromatographic profile of a typical lot of 5-ASA indicated the presence of the impurity 3-

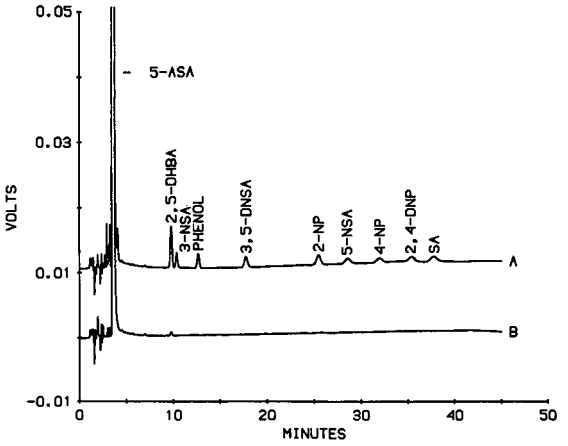

Fig. 4. HPLC of 5-ASA and potential synthetic process impurities at approximately the 0.1% level (A) and a typical lot of 5-ASA (B). Conditions: column, Hypersil-BDS C_{18}, 250 mm × 4.6 mm I.D., 5 μm particle size; mobile phase, 0.08 *M* sodium phosphate buffer (pH 2) containing 0.005 *M* 1-heptanesulfonic acid sodium salt and 0.07 *M* sodium chloride–methanol–tetrahydrofuran (85:11:4, v/v/v); column temperature, 35°C; flow-rate, 1.5 ml/min; injection volume, 20 μl; detection, UV at 215 nm.

ASA at a level of < 0.1%. Therefore, 3-ASA was selected as the impurity for the validation along with 5-ASA. The validation addressed method linearity, accuracy, precision, sensitivity, and ruggedness. The experimental design of the validation consisted of a two run/one analyst/three replicates per

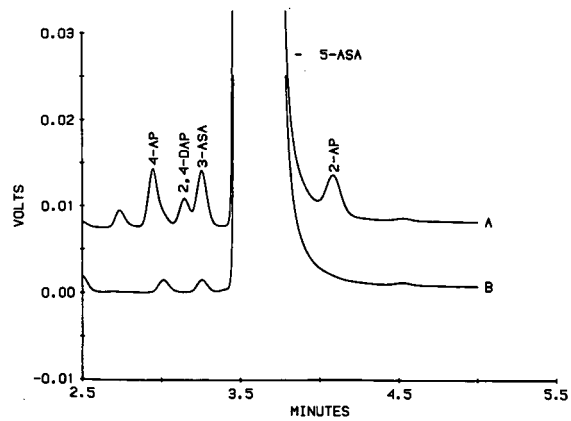

Fig. 5. HPLC from Fig. 4 illustrating the selectivity of the method between 2.5 min and 5.5 min.

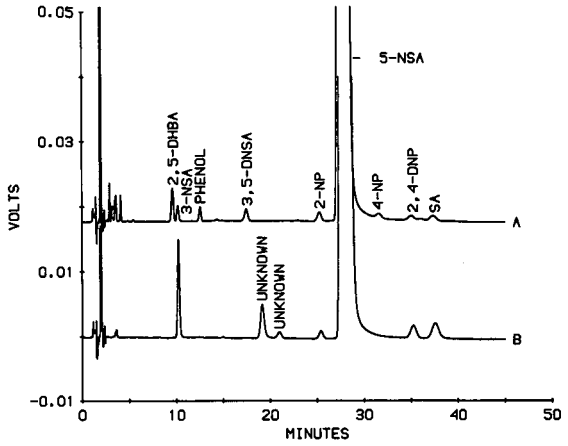

Fig. 6. HPLC of 5-NSA with spiked impurities at approximately the 0.1% level (A) and a typical lot of 5-NSA (B). Conditions as in Fig. 4.

run. For each run of the validation, a system suitability sample was evaluated. The system suitability mixture contains 5-ASA (1 mg/ml), 3-ASA (0.1%), and 2-AP (0.1%). Three parameters from the chromatogram are calculated to ensure that the system is suitable for performing the analyses. At 215 nm, the relative standard deviation (R.S.D.) of the 3-ASA peak-area response recorded for six injections of the system suitability mixture must be less than or equal to 2%. Also, the resolution factors for 3-ASA/5-ASA and for 5-ASA/2-AP must be greater than 2 and 3, respectively. The values of the resolution factors are calculated using the plate count determined from the 3-ASA peak. The linear range investigated for 5-ASA was from 40% to 120% of the target concentration of 1 mg/ml, while at the impurity level, 0.05–1.5% was investigated for 3-ASA. Since linearity of a bulk chemical is being evaluated, three replicates per concentration point were prepared so that accuracy and precision could be addressed at each concentration, concurrently. Data were collected at 215 and 300 nm for 5-ASA, whereas data for 3-ASA were collected only at 215 nm. At 215 nm, the method is sufficiently sensitive to detect 0.1% of each impurity as shown in Figs. 4 and 5. The performance characteristics, based on a single-point standard of the peak areas, for 5-ASA and 3-ASA are given in Tables I and II, respectively. Utilizing a single-point standard at 1 mg/ml for 5-ASA, mean bias recoveries at 215 nm for the

TABLE I

PERFORMANCE CHARACTERISTICS FOR 5-ASA AT 215 nm AND 300 nm UTILIZING A SINGLE-POINT STANDARD AT 1 mg/ml (n = 3)

Concentration level (mg/ml)	Mean bias recovery (%)		Within-run R.S.D. (%)		Between-run R.S.D. (%)		Total R.S.D. (%)	
	215 nm	300 nm	215 nm	300 nm	215 nm	300 nm	215 nm	300 nm
0.4	132.1	100.8	2.2	0.2	0.0	0.4	2.2	0.4
0.6	120.9	100.6	0.5	0.2	1.4	0.3	1.5	0.3
0.8	109.7	100.2	0.6	0.4	0.0	0.0	0.6	0.4
1.0	100.0	100.0	0.3	0.1	0.0	0.0	0.3	0.1
1.2	92.8	99.6	0.5	0.3	0.0	0.4	0.5	0.5

assay concentrations (0.4–1.2 mg/ml) suggest significant error in their determinations. This error, due to the high absorptivity of 5-ASA at 215 nm, causes non-linearity over this concentration range. However, at 300 nm the results show that over the assay concentration range of 0.4–1.2 ml/ml, mean bias recoveries of 99–101% are obtained with excellent precision (total R.S.D.s < 1%). Based on these performance characteristics, 300 nm was selected as the assay wavelength for 5-ASA. Correlation coefficients of 0.9935 and 0.9999 were obtained for 5-ASA at 215 and 300 nm, respectively. The analysis of 3-ASA at 215 nm demonstrated mean bias recoveries of 97–103% and total R.S.D.s less than 1.2% over the range of 0.05–1.5% of the target concentration of 1 mg/ml when utilizing a single-point standard at 0.1%. A correlation coefficient of 0.9997 was obtained for 3-ASA at 215 nm. Therefore, a solution of 5-ASA at 1 mg/ml would be assayed at 300 nm with impurities determined at 215 nm. This would require either a dual-wavelength detector, diode-array detector, or two detectors in series so both wavelengths could be monitored simultaneously and thus allow one injection per sample for both assay and impurity determination.

Finally, method ruggedness was evaluated. This involved investigating columns of different batches and different HPLC instrumentation during the validation. The experimental design of the validation consisted of two runs with a column from a different batch employed for each run. As shown in Tables I and II, the between-run R.S.D.s at the assay (300 nm) and impurity (215 nm) concentrations are less than 0.5% indicating that the method is reproducible when going from column to column. However, when going from one HPLC system to another, two observations were made. First, the temperature setting of the block heaters is not consistent with the actual temperature of the column. A thermocouple connected to the column showed that the

TABLE II

PERFORMANCE CHARACTERISTICS FOR 3-ASA AT 215 nm UTILIZING A SINGLE-POINT STANDARD AT 1 μg/ml (n = 3)

Concentration level (mg/ml)	Mean bias recovery (%)	Within-run R.S.D. (%)	Between-run R.S.D. (%)	Total R.S.D. (%)
0.0005	97.3	0.7	0.0	0.7
0.001	100.0	0.5	0.0	0.5
0.005	102.4	0.8	0.0	0.8
0.01	102.8	0.6	0.0	0.6
0.015	103.1	1.1	0.0	1.1

actual temperature of the column can vary among column heaters. Second, and what is more important, is the temperature of the column needs adjusting to approximately 35°C so the resolution of 5-ASA from 3-ASA and 2-AP is achieved. Although the column temperature can vary from one HPLC system to another, the method is very reproducible once the temperature of the column is adjusted to approximately 35°C and set for that particular HPLC system.

ACKNOWLEDGEMENTS

The authors thank Mr. John Goetz of Searle Chemical (Augusta, GA, USA) for preparation of the 5-ASA and 5-NSA samples and for his cooperation throughout the study. The authors also thank Bob Dillard of the Pre-Clinical Statistics Department and Rob Faulstich of Product Development Analytical Department of Searle Research and Development.

REFERENCES

1 M. A. Peppercorn, *J. Clin. Pharmacol.*, 27 (1987) 260.
2 A. K. A. Khan, D. T. Howes, J. Piris and S. C. Truelove, *Gut*, 21 (1980) 232.
3 R. W. Summers, O. M. Switz, J. T. Sessions, J. M. Beckel, W. R. Best, F. Kern and J. W. Singleton, *Gastroenterology*, 77 (1979) 847.
4 V. S. Chungi, G. S. Rekhi and L. Shargel, *J. Pharm. Sci.*, 78 (1989) 235.
5 E. Brendel, I. Meineke, D. Witsch and M. Zschunke, *J. Chromatogr.*, 385 (1987) 299.
6 K. Rona, V. Winkler, T. Riesz and B. Gachalyi, *Chromatographia*, 24 (1987) 720.
7 C. Fischer, K. Maier and U. Klotz, *J. Chromatogr.*, 225 (1981) 498.
8 E. J. D. Lee and S. B. Ang, *J. Chromatogr.*, 413 (1987) 300.
9 S. H. Hansen, *J. Chromatogr.*, 491 (1989) 175.
10 E. Nagy, I. Csipo, I. Degrell and G. Szabó, *J. Chromatogr.*, 425 (1988) 214.
11 R. Verbesselt, T. B. Tjandra-Maga and P. J. De Schepper, *Eur. J. Pharmacol.*, 183 (1990) 2384.
12 I. Cendrowska, M. Drewnoska, A. Grzeszkiewicz and K. Butkiewicz, *J. Chromatogr.*, 509 (1990) 195.
13 D. E. Hughes and A. M. Bramer, *J. Chromatogr.*, 408 (1987) 296.

Journal of Chromatography, 588 (1991) 195–200
Elsevier Science Publishers B.V., Amsterdam

CHROM. 23 653

Elution behaviour of polyamic acid and polyamide–imide in size-exclusion chromatography

Yoshiyuki Mukoyama

Goi Works, Hitachi Chemical Co., Ltd., Goi-minami Kaigan, Ichihara, Chiba 290 (Japan)

Naoto Shimizu and To-Ichi Sakata

Ibaraki Research Laboratory, Hitachi Chemical Co., Ltd., Higashi-cho, Hitachi, Ibaraki 317 (Japan)

Sadao Mori*

Faculty of Engineering, Mie University, Tsu, Mie 514 (Japan)

(First received May 22nd, 1991; revised manuscript received July 25th, 1991)

ABSTRACT

The causes of the peculiarities of the elution behaviour of thermoresistant resins, when N,N-dimethylformamide (DMF) is used as the mobile phase were investigated. In order to establish whether the peculiarities are caused by the properties of DMF, by the interactions between the stationary phase and DMF, or by the generation of specific properties of the solutes in DMF, tetrahydrofuran (THF)-soluble polyamic and polyamide–imide resins were prepared. Two stationary phases, hydrophobic polystyrene gel and hydrophilic polymer gel, were used and DMF, THF and a mixture of DMF and THF with or without H_3PO_4 and LiBr were used as the mobile phases. The peculiarities are discussed from the point of dissociation of carboxylic groups of the solutes and of the hydrophilic stationary phase. Adsorption of the resins on the columns or early elution from the columns were prevented by the addition of H_3PO_4 and early elution of the neutral polyamide–imide from the column was prevented by the addition of LiBr. The early elution of the resins was not due to the intramolecular chain expansion of the resins in DMF, but to the interactions between carboxylic groups of the resins and of the hydrophilic polymer gels. The addition of H_3PO_4 suppressed the dissociation of carboxylic groups of the resins. DMF partially controls the dissociation of the carboxylic groups.

INTRODUCTION

Polyamic acid (PAA), which is a precursor of aromatic polyimides, has high heat resistance and is widely used for electronic materials, especially for the surface protection membrane in the production process of integrated circuit (IC). Aromatic polyamide–imide (PAI) is employed as an electrical insulator or in special engineering plastics. These resins are heat resistant and have good film-forming properties. These distinct features are dependent on the monomer type, the composition and the types of end groups and also the molecular weights and molecular weight distributions. However, the determination of molecular weights and molecular weight distributions of these resins by size-exclusion chromatography (SEC) is usually difficult.

As most PAA and PAI are insoluble in tetrahydrofuran (THF), which is widely used in SEC, N,N-dimethylformamide (DMF) and N,N-dimethylacetamide (DMAc) [1], DMF with 0.01 *M* LiBr [2], 0.03 *M* LiBr–0.03 *M* H_3PO_4–1 vol% THF in DMF [3] and 0.03 *M* LiBr–0.03 *M* H_3PO_4–1 vol% THF in DMAc [4] have been reported as mobile phases for the SEC of these resins. Several peculiarities of the elution behaviour of these resins have been observed when DMF or related solvents were used as the mobile phases in SEC.

0021-9673/91/$03.50

The objective of this work was to clarify the causes of these peculiarities. In order to establish whether the peculiarities of the elution behaviour of PAA and PAI resins are caused by the properties of DMF itself, by interactions between the stationary phases and DMF, or by the generation of specific properties of the solutes in DMF, THF-soluble PAA and PAI were prepared and the elution behaviour of PAA and PAI resins on two types of stationary phases, hydrophobic polystyrene (PS) gel and hydrophilic polymer gel, was investigated with THF, DMF and a mixture of THF and DMF (1:1) as mobile phases. A column packed with a hydrophilic polymer gel has recently been found to be compatible with several organic solvents such as THF and DMF, in addition to aqueous solvents [5].

EXPERIMENTAL

Samples

PAA was prepared by polycondensation of 2,2-bis[4-(4-aminophenoxy)phenol]propane (BAP) and pyromellitic dianhydride in DMAc. The reaction was continued for 8 h at 25°C and then a portion of water was added to the reaction mixture to precipitate PAA. PAA has two carboxylic groups capable of dissociation and two amide groups in a repeating unit with the following structural formula:

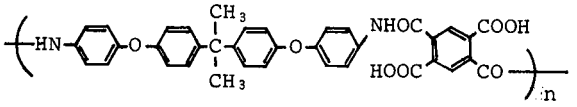

PAI with an acid value of 0 (PAI-A) was prepared by the following procedure. A DMAc solution containing trimellitic anhydride chloride was added dropwise to a DMAc solution containing BAP and triethylamine at 0°C. After 3 h at 0°C, the temperature of the reaction mixture was raised to 20°C, an excess of a mixture of acetic anhydride and pyridine (2:1, v/v) was added, the reaction was continued for 12 h at 20°C and then a portion of water was added to the reaction mixture.

PAI with an acid value of 11 (PAI-B) was obtained by reaction of BAP and trimellitic anhydride with phosphoric acid in N-methyl-2-pyrrolidone (NMP) at 140°C, followed by adding methanol to the reaction mixture to obtain solid PAI-B. The structure of PAI is

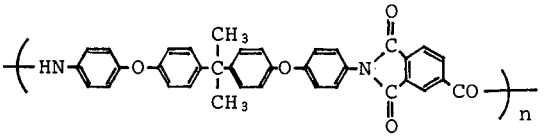

Both PAI-A and PAI-B contain imide and amide groups. PAI-B may contain a certain amount of free carboxylic groups in the chain.

The acid value of PAI was determined by the following procedure. PAI and triethylamine were dissolved in NMP and the solution was titrated with a 0.05 *M* solution of potassium hydroxide in ethanol. The volume of the titrant (ml) minus the blank was divided by the amount of sample (g) and this ratio (ml/g) is defined as the acid value.

Apparatus

High-performance liquid chromatography (HPLC) was performed with a Hitachi (Tokyo, Japan) Model L6000 liquid chromatograph equipped with a Model L-4000 UV–VIS spectrophotometer. Solvents used as the mobile phase were THF, DMF and a mixture of DMF and THF (1:1, v/v), with and without 0.06 *M* orthophosphoric acid (H_3PO_4) and 0.03 *M* lithium bromide (LiBr). The flow-rate of the mobile phase was 1.0 ml/min and the wavelength of the UV detector was 270 nm. The sample concentration was 0.5% (w/v) and a portion of 5 μl of the solution was injected.

Three different types of columns were used. Column A was Gelpack GL-A100MX (30 cm × 7.8 mm I.D.) (Hitachi) packed with PS gel having an exclusion limit of 2×10^8 PS molecular weight. This column was used with THF and two columns were connected in series. Column B was Gelpack GL-S300MTDT-5 (30 cm × 7.8 mm I.D.) packed with the same PS gel. This column contained DMF–THF (1:1, v/v) and was used exclusively with this mixture and DMF alone. Two columns were used in series. Column C was Gelpack GL-W550 (30 cm × 10.7 mm I.D.) packed with hydrophilic polymer gel (polyglyceryl methacrylate gel) with an exclusion limit of 2×10^6 PS molecular weight. The column was filled with water, but it can be used interchangeably with organic solvents such as DMF, THF–

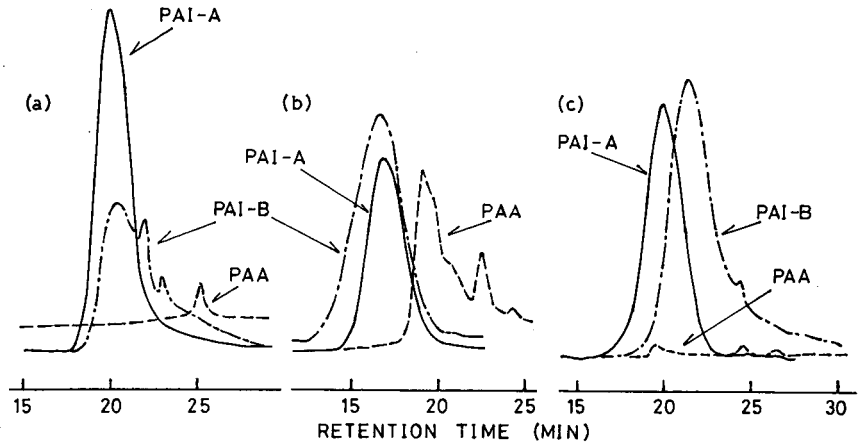

Fig. 1. Chromatograms of PAA and PAI on polystyrene gel columns. Mobile phase and column: (a) THF, column A; (b) DMF, column B; (c) DMF–THF (1:1, v/v), column B.

DMF and alcohols and with aqueous solvents. A single column was used.

RESULTS AND DISCUSSION

Typical chromatograms of PAA, PAI-A and PAI-B in three mobile phases without additives on columns A and B are shown in Fig. 1 and those on column C are shown in Fig. 2. PAI-A which had no free carboxylic groups in the chain showed similar shapes of the chromatograms irrespective of the mobile phase and column. The only difference was in the retention volumes in the different systems of mobile phases and columns: PAI-A eluted at the exclusion limit of the column in the DMF–column C system (Fig. 2a), whereas it eluted at the normal position of retention volume in other systems. On the other hand, PAA and PAI-B, with free carboxylic groups in the chain, showed different elution profiles in different mobile phases and on different columns. The addition of 0.06 *M* H_3PO_4 and 0.03 *M* LiBr to the mobile phases led to dramatic changes in the elution profiles for these resins and the chromatograms of PAA and PAI-B were almost the same and symmetrical, irrespective of the mobile phase and column. Examples are shown in Fig. 3.

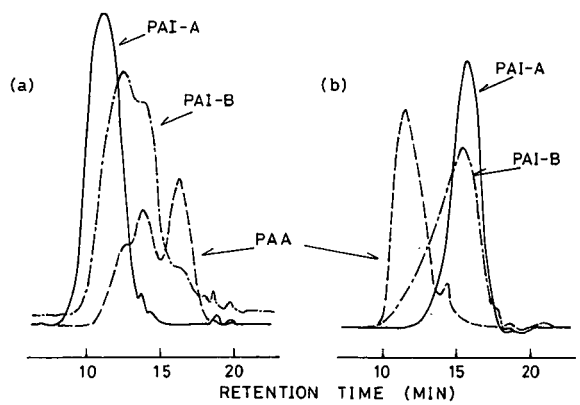

Fig. 2. Chromatograms of PAA and PAI on column C packed with hydrophilic polymer gel. Mobile phase: (a) DMF; (b) DMF–THF (1:1, v/v).

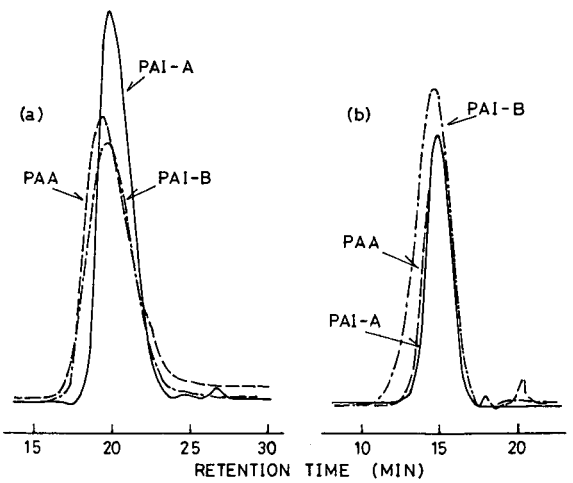

Fig. 3. Chromatograms of PAA and PAI with mobile phases containing H_3PO_4 and LiBr. Mobile phase and column: (a) DMF with 0.06 *M* H_3PO_4 + 0.03 *M* LiBr, column B; (b) DMF–THF with 0.06 *M* H_3PO_4 + 0.03 *M* LiBr, column C.

The elution behaviour of these resins is summarized in Table I. Cha [2] has shown that the elution behaviour of polyacids is profoundly affected by the addition of LiBr to a DMF mobile phase. The chromatogram of polyacid in a 0.1 *M* LiBr–DMF solution had a symmetrical shape and eluted at much higher retention volume than in pure DMF. Nefedov [3] reported the SEC of polyamic acid with a mobile phase consisting of 0.03 *M* LiBr–0.03 *M* H_3PO_4–1 vol% THF in DMF on porous glass and Sephadex columns. He noted that LiBr suppressed polyelectrolyte effects and that the addition of H_3PO_4 improved the solubility of polyamic acid. He also mentioned that the only possible explanation for the anomalous elution behaviour of polyelectrolytes in pure DMF was the expansion of the polyelectrolytes [3].

Although it is possible to consider that the addition of LiBr is effective in suppressing the expansion of polyelectrolytes and in eluting them at the appropriate retention volume [6], it is not sufficient for the elucidation of the elution behaviour of the resins in our work. PAI (A and B) eluted at the normal retention volumes in the DMF–PS gel system (Fig. 1b), but at the exclusion limit in the DMF–column C system (Fig. 2a).

In order to interpret the elution behaviour by taking into account the chromatograms and the summary in Table I, the following factors were considered:

(1) The solubility parameters of gels and solvents are as follows: PS gel 18.6, hydrophilic polymer gel such as polyhydroxy methacrylate gel 18.4, THF 18.6 and DMF 24.8 $(J/m^3)^{1/2} \times 10^{-3}$; those with similar solubility parameters were considered to have a greater affinity between them [7].

(2) It is estimated that PS gels have no residual free carboxylic groups, whereas the hydrophilic polymer gels do; the charge of the surface of the hydrophilic polymer gels was negative.

(3) The pH of a 0.5 *M* DMF solution in water is 6.5 [8].

(4) The addition of a small amount of H_3PO_4 to the mobile phase improved the recovery of PAA

TABLE I

ELUTION BEHAVIOUR OF PAA AND PAI IN DIFFERENT MOBILE PHASES

Conditions			Resin		
Column	Mobile phase	Additive[a]	PAA	PAI-A	PAA-B
A	THF	Without	Not eluted	Normal elution	Broad and tailing
		With	Normal elution	Normal elution	Normal elution
B	DMF	Without	Broad and tailing, retardation	Normal elution	Normal elution
		With	Normal elution	Normal elution	Normal elution
B	DMF–THF	Without	Not eluted	Normal elution	Broad and tailing, retardation
		With	Normal elution	Normal elution	Normal elution
C	DMF	Without	Split into two and retardation	Eluted at the exclusion limit with normal shape	Broad and early elution
		With	Normal elution	Normal elution	Normal elution
C	DMF–THF	Without	Eluted at the exclusion limit with normal shape	Normal elution	Leading
		With	Normal elution	Normal elution	Normal elution

[a] 0.06 *M* H_3PO_4 + 0.03 *M* LiBr.

from column A or B, but the addition of LiBr did not improve the recovery.

(5) LiBr is a neutral electrolyte and has two main effects: it reduces the electric double layer on the gel surface to minimize the ion-exclusion or the electrostatic repulsion effects [9], and it decreases the expansion of the resin to elute them at the expected retention volume.

(6) H_3PO_4 is a weak acid and suppresses the dissociation of weakly acidic substances. H_3PO_4 also acts as an electrolyte.

In this paper, the role of H_3PO_4 is mainly discussed from the point of view of the dissociation of the carboxylic groups in the chain of the resins.

Elution behaviour of PAI-A

PAI-A had an acid value of zero and was considered not to have free carboxylic groups in the structure. Only amide and imide groups may interact with gels. The elution of PAI was normal on PS columns, irrespective of the mobile phase with or without the LiBr and H_3PO_4 additives. On the other hand, it eluted at the exclusion limit on column C with DMF (Fig. 2a), and the addition of the additives or THF (Fig. 2b) was effective in eluting it at the expected retention volume. These results suggest that the expansion of PAI-A in DMF, which was pointed out by Nefedov *et al.* [1], was not observed in the DMF–PS gel system (Fig. 1b) and the elution at the exclusion limit in the DMF–column C system is due to the interaction of PAI-A with the stationary phase. It is important to note that the interrelation between the mobile phase and the stationary phase must be taken into account when the elution behaviour of solutes is discussed.

The anomalous elution behaviour of PAI-A in pure DMF on column C is explained as follows. Although DMF has a high basicity parameter [10], the pH of a DMF solution in water is below 7.0 [8]. Therefore, the dissociation of the residual carboxylic groups on the surface of the hydrophilic polymer gel may be substantially suppressed. The surface of the gel is negatively charged owing to a small extent of the dissociation or to the non-dissociated carboxylic groups. The solubility parameter of DMF is far from that of the gel and the solute molecules can approach close to the gel surface, resulting in an electrostatic repulsion between the gel surface and the solute molecules. PAI-A may have a negative charge on the surface due to *n* electrons on oxygen and nitrogen atoms on the surface. The addition of LiBr to DMF reduces the electric double layer in the pores of the gel, resulting in the facile approach of the solute molecules to the inside of the gel pores. The addition of THF prevents the access of the solute molecules to the surface of the gel, because the solubility parameter of THF is close to that of the gel and THF molecules are assembled on the surface of the gel much more than DMF molecules.

Elution of PAA

PAA contained two carboxylic groups in a repeating unit and the interaction with the stationary phase is assumed to be higher than that with PAI-A. In the THF–PS gel system (Fig. 1a), the retardation of carboxylic acids is well known because of the adsorption on the gel surface. The situation is similar to PAA molecules and PAA retained in the column in the THF–PS gel system, because of the adsorption of PAA on the gel surface. The addition of H_3PO_4 suppressed the dissociation of the carboxylic groups of PAA and eluted PAA from the column. Although DMF suppressed the dissociation of the carboxylic groups, a small amount of dissociation still caused the adsorption of PAA on the surface of the gel to some extent (Fig. 1b). The addition of THF to DMF (Fig. 1c) increased the dissociation of carboxylic groups due to the decrease in the acidity of the mobile phase, resulting in an increase in adsorption.

The elution behaviour in the DMF–column C system (Fig. 2a) is considered to be the same as that in the DMF–PS gel system. The addition of THF (Fig. 2b) accelerated the dissociation of the carboxylic groups of both PAA and of the gel, and the access of PAA molecules to the gel surface was prevented because of the superior access of THF molecules to the gel surface, resulting in an ion-exclusion effect between them. The addition of H_3PO_4 suppressed the dissociation of the carboxylic groups of both PAA and of the gel and the addition of LiBr reduced the electric double layer of the gel pore.

Elution behaviour of PAI-B

PAI-B has one free carboxylic group per three repeating units, and thus it must have an intermediate behaviour between PAA and PAI-A. A typical

example is shown in chromatograms obtained in the THF–PS gel system (Fig. 1a). In the DMF–PS gel system (Fig. 1b), the dissociation of PAI-B was suppressed and the normal elution behaviour was observed. The addition of THF to the DMF–PS gel system (Fig. 1a) partially accelerated the dissociation of PAI-B and peak broadening was observed as a result of the adsorption effects.

In the DMF–column C system, early elution of PAI-B was observed because of the ion-exclusion effect. The addition of THF caused the chromatogram of PAI-B to be asymmetric. The peak shape indicates that the interphase distribution is characterized by a concave sorption isotherm which is formed as a result of the electrostatic exclusion [1]. The roles of the additives are the same as those for PAA.

CONCLUSIONS

In this paper, the elution behaviour of PAA and PAI has been discussed from the point of view of the dissociation of the carboxylic groups in the chain of the resins and those in the stationary phase of the hydrophilic polymer gel. The addition of H_3PO_4 to the mobile phase suppressed the dissociation of the carboxylic groups and was very effective in preventing the adsorption of the resins to the gel surface or the ion-exclusion effect between them.

DMF controls the dissociation of carboxylic groups of the resins. The early elution of the resins was not due to the intramolecular chain expansion of the resin in DMF, but to the interactions between carboxylic groups of the resins and of the hydrophilic polymer gels. Although potentiometric titration of the hydrophilic polymer gels showed that the acid value of the gels was zero, it was assumed that the gels have a small amount of the residual carboxylic groups.

The addition of LiBr may be effective in preventing the association of the resins and in eluting them at much higher retention volumes than in pure DMF. It can be concluded that H_3PO_4 acts to suppress the dissociation of the carboxylic groups of the resins and of the hydrophilic polymer gel, and LiBr acts to prevent the association of the non-dissociated resins.

The optimum system for the SEC of these resins was DMF with H_3PO_4 + LiBr and column B or DMF–THF (1:1, v/v) with H_3PO_4 + LiBr and column C. For PAI-A, the system can be used without the additives.

REFERENCES

1 P. P. Nefedov, M. A. Lazareva, B. G. Belenkii, S. Ya. Frenkel and M. M. Koton, *J. Chromatogr.*, 170 (1979) 11.
2 C. Y. Cha, *J. Polym. Sci., Part B*, 7 (1969) 343.
3 P. P. Nefedov, *Polym. Sci. USSR*, 23 (1981) 1055.
4 C. C. Walker, *J. Polym. Sci., Part A: Polym. Chem.*, 26 (1988) 1649.
5 Y. Mukoyama and S. Mori, *J. Liq. Chromatogr.*, 12 (1989) 1417.
6 S. Mori, *Anal. Chem.*, 55 (1983) 2414.
7 S. Mori, *Anal. Chem.*, 50 (1978) 745.
8 *Merck Index*, Merck, Rahway, NJ, 9th ed., 1976, No. 3233.
9 S. Mori, *Anal. Chem.*, 61 (1989) 530.
10 A. D. Headley, *J. Org. Chem.*, 56 (1991) 3688.

Journal of Chromatography, 588 (1991) 201–210
Elsevier Science Publishers B.V., Amsterdam

CHROM. 23 673

Chromatographic behaviour of the *closo*-$[B_{12}H_{12}]^{2-}$ derivatives on hydroxyethylmethacrylate gels

B. Grüner* and Z. Plzák

Institute of Inorganic Chemistry, Czechoslovak Academy of Sciences, 250 68 Řež, near Prague (Czechoslovakia)

Ivan Vinš

Tessek Ltd., Křižovnická 3, 101 00 Prague 1 (Czechoslovakia)

(First received April 19th, 1991; revised manuscript received August 7th, 1991)

ABSTRACT

Halo derivatives (Cl, Br, I) of the *closo*-dodecahydro-dodecaborate anion, $[B_{12}H_{12}]^{2-}$, and their positional isomers were separated on Separon HEMA hydroxyethylmetacrylate sorbents. Different effects on the separation process, including cations and anions in the mobile phase, the electrolyte concentration in the eluent, pH, addition of organic modifier and separation temperature, were studied. Optimum conditions for the separation were accomplished with Separon HEMA BIO 300 and 1000 sorbents using 0.1–0.5 *M* sodium perchlorate solutions in 0.01 *M* phosphate buffer (pH 8.5) as the mobile phase. The separated compounds were detected using direct UV detection in the range 200–210 nm.

INTRODUCTION

Over the last two decades, high-performance liquid chromatography has become an invaluable tool for the separation of non-ionic cage borane compounds [1–3]. However, an adequate chromatographic method for the separation of complex reaction mixtures produced from reactions of boron cage anionic species and purity assay of individual compounds has still been lacking. This especially applies to the family of polyhedral *closo*-hydroborate cage anions $[B_{10}H_{10}]^{2-}$ and $[B_{12}H_{12}]^{2-}$ and their derivatives, where a major difficulty lies in obtaining uncontaminated crystals [4].

Salts of the $[B_{12}H_{12}]^{2-}$ anion are non-volatile compounds of reasonable chemical and thermal stability. Taking the symmetrical structure of this anion (point group *Ih*), as depicted in Fig. 1, into account, the possibility of producing an extensive range of derivatives and positional isomers via substitution reactions is evident [5]. Substitution reactions proceeding via an electrophilic or radical mechanism usually produce complex mixtures of various derivatives and their positional isomers, *e.g.*, in halogenation reactions [6].

The main factors controlling the behaviour of these anions are derived from the properties of relatively highly charged small particles (dimensions comparable to the benzene molecule). The *closo*-hydroborate anions exhibit strange solution beha-

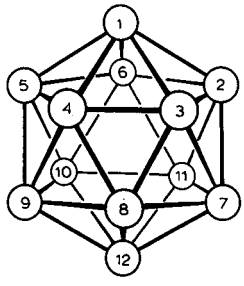

Fig. 1. Structure of the boron framework of the *closo*-$[B_{12}H_{12}]^{2-}$ anion.

0021-9673/91/$03.50

viour, and seem to be borderline between inorganic and organic compounds. They behave simultaneously as strong electrolytes (a high degree of dissociation; the free acids have pK_a values comparable to those of the strongest inorganic acids), but they exhibit also hydrophobic properties comparable to those of organic aromatic molecules. The solubility of such compounds in water is therefore caused by the relatively high anionic charge. For comparison, the isostructural and isoelectronic, but uncharged, compounds of the *closo*-dicarbadodecaborane series, $C_2B_{10}H_{12}$, exhibit sufficient solubility only in non-polar solvents. The combination of both controversial properties of the *closo*-hydroborates mentioned above makes mixtures of such compounds unseparable by ordinary separation methods (crystallization, extraction and conventional adsorption and partition chromatography). The separation difficulties outlined above are the main reason for the still limited number of papers dealing with syntheses and properties of pure $[B_{12}H_{12}]^{2-}$ derivatives.

Several separation methods that have so far been developed to separate the latter derivatives are based on thin-layer chromatography [4] and ion-exchange chromatography on DEAE-cellulose [7] or on electromigration methods [8,9]. Only one high-performance liquid chromatographic (HPLC) method has been reported in this area [10], which is based on partition chromatography on silica to allow the separation of the unsubstituted anions $[B_{10}H_{10}]^{2-}$ and $[B_{12}H_{12}]^{2-}$. This method seems not to be sufficiently powerful for the separation of complex mixtures of isomers produced by substitution reactions.

The purpose of this study was to employ hydroxyethylmethacrylate-based sorbents to effect the separation of polyhedral *closo*-dodecaborate analytes to investigate the range of separation conditions that could permit a more effective separation of these species.

Based on the ionic character of the compounds under study and their strong hydrophobic behaviour, two approaches can principally be considered to provide routine separations, as follows.

(1) Ion-pair and ion-exchange chromatography [11] can be considered. In ion-pair chromatography, the selection of ion-pairing agents is difficult owing to the limited solubility of alkylammonium salts of the $[B_{12}H_{12}]^{2-}$ anion and its derivatives in water. A more suitable method seems to be ion-exchange chromatography [11], which is a powerful analytical tool for the simple and rapid determination of a wide variety of common inorganic and organic anions. However, only a comparatively small number of such methods have been developed to separate inorganic anions of higher hydrophobicity. Both of these methods are characterized by a decrease in retention with increasing ionic strength of the eluent.

(2) Ion-exclusion chromatography [11] and hydrophobic interaction chromatography [12,13] have been used effectively to separate mixtures of hydrophobic organic anions. In this type of chromatography, the solute retention is enhanced with increasing mobile phase ionic strength.

The broad range of Separon HEMA hydroxyethylmethacrylate sorbents available enabled us to study both types of separation mechanisms on one type of material. The Separon HEMA sorbents have been extensively used for the separation of biochemicals and organic molecules by hydrophobic interaction chromatography [14–16]. They can be modified for ion-exchange chromatographic purposes by including appropriate ion-exchange groups [17–19]. As already demonstrated, unmodified hydroxyethylmethacrylate gels can also serve as a support for the separation of small inorganic anions [20].

For both ion-exchange and hydrophobic interaction chromatographic methods, UV detection should be preferred because of the expected need for a high electrolyte concentration in the eluent, associated with a very high background conductivity preventing conductivity detection. The use of electrochemical detection is also restricted owing to the high effective oxidation potentials of $[B_{12}H_{12}]^{2-}$-type anions. The $[B_{12}H_{12}]^{2-}$ anion absorbs in the UV region below 210 nm, thus limiting separations with direct UV detection to the use of eluents that are sufficiently transparent in this range (aqueous solutions of salts, *e.g.*, perchlorates, sulphates, phosphates and chlorides).

EXPERIMENTAL

Columns

A wide range of CGC (cartridge glass columns)

TABLE I

SURFACE PROPERTIES (FUNCTIONALITY) AND RETENTION MODES OF THE COLUMNS USED

Stationary phase	Particle size (μm)	Functional groups	Ion-exchange capacity (mequiv./g)	Mode[a]
Separon HEMA-S 1000 Q-L	10,12	Quaternary ammonium	0.03–0.1	IEC
Separon HEMA-BIO 1000 CM	7	Carboxy	0.05	IE
Separon HEMA-S 1000	10,12	None	–	HIC
Separon HEMA-BIO 300[b]	10,12,15	None	–	HIC
Separon HEMA-BIO 1000[b]	10	None	–	HIC
Separon SIX C_{18}	5	Octadecyl	–	HIC
Separon SIX CN	5	Cyanopropyl	–	HIC

[a] IEC = ion-exchange, IE = ion-exclusion, HIC = hydrophobic interaction chromatography.

[b] Separon HEMA-BIO 300 and 1000 materials differ in pore size; exclusion limits for dextran are 250 000–800 000 and 800 000–$2 \cdot 10^6$ dalton, respectively. The Separon HEMA-BIO and -S materials differ in the surface content of hydroxy groups.

(150 × 3.3 mm I.D.) packed with Separon HEMA hydroxyethylmethacrylate supports (provided by Tessek, Prague, Czechoslovakia) were used. The columns were packed with (1) low-capacity (0.03–0.1 mequiv./g) sorbents for ion-exchange or ion-exclusion chromatography, including Separon HEMA-S 1000 Q-L (quaternary ammonium groups) and HEMA-BIO 1000 CM (carboxy groups), and (2) supports for hydrophobic interaction chromatography or for the separation of biomolecules of the Separon HEMA-S 1000, HEMA-BIO 300 and HEMA-BIO 1000 types.

Commercial cartridge CGC columns packed with the silica-based materials Separon SIX-CN and Spheron SIX-C_{18}, both 5 μm (supplied by Laboratory Instruments, Prague, Czechoslovakia), were also used.

The surface characteristics and retention modes of the columns used are summarized in Table I.

Eluents

Deionized water was used throughout. HPLC-grade acetonitrile was obtained from Fluka (Buchs, Switzerland); and all other reagents were of analytical-reagent grade from Lachema (Brno, Czechoslovakia); and Laborchemie (Apolda, Germany). The mobile phase was prepared by dissolving the calculated amount of the electrolyte either in water or in 0.01 *M* phosphate buffer with the pH adjusted with aqueous NaOH, or alternatively in a mixed acetonitrile–water solvent prepared in the required volume ratios. Eluents were filtered through a 0.45-μm filter and degassed under vacuum before use.

Apparatus

A simple isocratic HPLC system was used. The chromatographic equipment consisted of a VCR 40 pulseless dual-piston high-pressure pump, a K 1 six-port sampling valve (with 20- or 50-μl loops) (Development Workshops of the Czechoslovak Academy of Sciences, Prague, Czechoslovakia), an LCD 2040 variable-wavelength (190–360 nm) UV spectrophotometric detector (Laboratory Instruments), a PKS-1 column holder (Tessek) equipped with a heating glass jacket with circulating water from a thermostated bath, a Servogor 2s line recorder (Brown Boveri, Germany) and a CI 100 integrator (Laboratory Instruments).

Sample preparation

Pure derivatives and positional isomers of substituted *closo*-dodecaborate anions were prepared by published methods [7,21,22]. Salts of the unsubstituted $[B_{12}H_{12}]^{2-}$ and $[B_{10}H_{10}]^{2-}$ anions were prepared by conventional methods [23,24]. Free acids or sufficiently water-soluble salts of the $[B_{12}H_{12}]^{2-}$ derivatives, *e.g.*, salts with Li^+, Na^+, K^+, Rb^+, Cs^+, NH_4^+ and $N(CH_3)_4^+$ counter cations, were directly injected as aqueous solutions at concentrations ranging from 0.01 to 7 μmol/ml. Sparingly soluble compounds, such as salts with bulky cations, were converted into sufficiently solu-

ble forms by standard ion-exchange techniques or by suitable metathetical reactions before injection. All samples were filtered through a 0.45-μm nylon microfilter (Tessek) before injection.

RESULTS AND DISCUSSION

To optimize the chromatographic procedures, we investigated the effects of the following factors that might affect the separation: (1) surface properties of the supports used; (2) dependence of retention on the concentration of strong electrolytes in the mobile phase; (3) influence of cations and anions present in the mobile phase on the retention of solutes and the separation selectivity of the isomeric dihalo derivatives; (4) influence of pH; (5) effect of the organic modifier (acetonitrile) in the mobile phase; and (6) influence of the separation temperature.

We found that the retentions of the *closo*-borate anions $[B_{10}H_{10}]^{2-}$ and $[B_{12}H_{12}]^{2-}$ and their derivatives on differently surface modified sorbents under identical conditions increased in the order Separon HEMA-BIO 1000 CM $\ll$ HEMA-S 1000 $<$ HEMA-BIO 300 $\leqslant$ HEMA-BIO 1000 $\ll$ HEMA-S 1000 Q-L. The very weak retention on Separon HEMA-BIO 1000 CM was apparently affected by electrostatic exclusion of *closo*-borate anions by the carboxy group of the same charge from the polymer surface. The very strong retention was observed on materials with quaternary ammonium group, indicating that an ion-exchange mechanism plays an important role in this particular instance.

The best column efficiency and separation selectivity for the disubstituted 1,2- and 1,7-isomers of the *closo*-$[B_{12}H_{12}]^{2-}$ anion was achieved on Separon HEMA-BIO 300 and 1000. The use of these types of materials enabled us to separate, under appropriately selected conditions, a wide variety of $[B_{12}H_{12}]^{2-}$ derivatives. The separation of a model mixture of monosubstituted species (Fig. 2) demonstrates the efficiency and scope of the method.

The capacity factors of various *closo*-$[B_{12}H_{12}]^{2-}$ derivatives for a series of materials employed for the separation either in pure water or in the presence of different strong electrolytes were also measured and are discussed below.

Except for the material for ion-exchange chromatography (Separon HEMA-S 1000 Q-L), the retention of the *closo*-$[B_{12}H_{12}]^{2-}$ derivatives in pure water is slightly higher than the column void volume. Nevertheless, the addition of a strong electrolyte to the mobile phase significantly increases the retention of both substituted and unsubstituted $[B_{12}H_{12}]^{2-}$ anions to make their separation possible. The retention of individual derivatives also increases in the order of increasing hydrophobicity of the substituent groups. The retention of $[B_{10}H_{10}]^{2-}$ and $[B_{12}H_{12}]^{2-}$ anions and their chloro derivatives increased in the following order of salts used for the preparation of the eluent: perchlorate $<$ chloride $<$ sulphate $<$ sulphosalicylate; $Na^+ <$

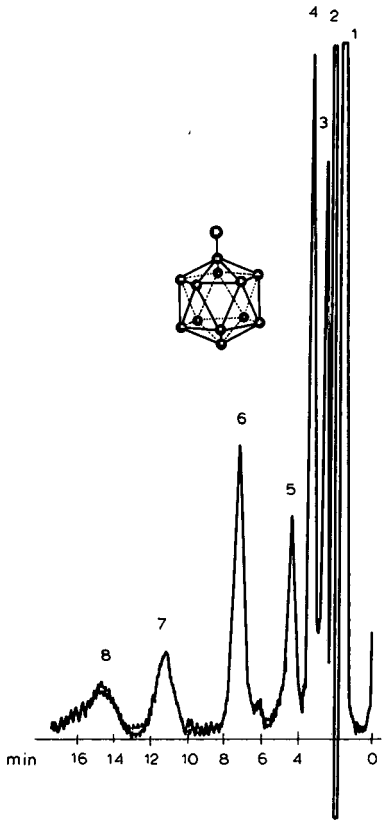

Fig. 2. Separation of *closo*-$[B_{12}H_{12}]^{2-}$ and its monosubstituted derivatives. Column, CGC (150 × 3.3 mm I.D.), Separon HEMA-BIO 300 (12 μm); mobile phase, 0.1 *M* $NaClO_4$ in acetonitrile–water (10:90); flow-rate, 0.5 ml/min; detection, UV at 205 nm; sensitivity, 0.16 a.u.f.s.; injection volume, 20 μl; temperature of separation, 55°C. Peaks: 1 = $[B_{12}H_{11}OH]^{2-}$; 2 = $[B_{12}H_{12}]^{2-}$; 3 = $[B_{12}H_{11}SH]^{2-}$; 4 = $[B_{12}H_{11}Cl]^{2-}$; 5 = $[B_{12}H_{11}Br]^{2-}$; 6 = $[B_{12}H_{11}I]^{2-}$; 7 = $[B_{12}H_{11}SCN]^{2-}$; 8 = $[B_{12}H_{11}SMe_2]^{-}$.

TABLE II

CAPACITY FACTORS (k') FOR SOME *closo*-$[B_{12}H_{12}]^{2-}$ DERIVATIVES IN THE PRESENCE OF LOW CONCENTRATIONS OF ELECTROLYTES IN AQUEOUS MOBILE PHASES

Column, Separon HEMA-BIO 300 (12 μm); detection, UV at 200 nm (indirect at 289 nm for sulphosalicylate).

Anion	Electrolyte concentration (mmol/l)													
	NaCl				KCl		NH_4Cl				Na_2SO_4		NaSul[a]	
	5	10	20	100	5	10	1	2.5	5	10	2.5	5	2.5	5
$[B_{12}H_{12}]^{2-}$	0.88	1.33	2.50	5.50	1.33	1.60	2.17	5.50	5.83	7.33	1.17	1.30	1.08	1.16
$[B_{12}H_{11}Cl]^{2-}$	2.08	3.66	8.83	–	4.50	6.67	8.00	12.7	–	–	2.67	3.50	2.50	3.66
$[B_{12}H_{11}Br]^{2-}$	5.33	8.67	–	–	–	–								
$[B_{12}H_{10}Cl_2]^{2-}$	9.0	23.5	–	–	13.0	–	15.0	–	–	–	8.17	20.5	9.33	16.0

[a] Sodium sulphosalicylate.

TABLE III

CAPACITY FACTORS (k') OF *closo*-BORATE ANIONS $[B_{10}H_{10}]^{2-}$ AND $[B_{12}H_{12}]^{2-}$ AND HALOGENO DERIVATIVES WITH VARIOUS CONCENTRATIONS OF SODIUM PERCHLORATE IN THE MOBILE PHASE

Column, Separon HEMA-BIO 300 (12 μm); detection, UV at 200 nm.

Anion	Concentration of $NaClO_4$ (mmol/l)							
	0	5	10	20	50	100	250	500
$[B_{10}H_{10}]^{2-}$	0.17	0.17	0.17	0.17	0.25	0.33	0.25	0.25
$[B_{12}H_{12}]^{2-}$	0.58	0.75	1.17	1.38	1.62	1.66	–	1.17
$[B_{12}H_{11}Cl]^{2-}$	1.00	1.83	4.33	4.83	5.16	5.25	–	3.33
$[B_{12}H_{11}Br]^{2-}$	1.33	3.16	6.33	7.66	8.45	8.63	–	4.38
1,7-$[B_{12}H_{10}Cl_2]^{2-}$	2.00	8.83	14.5	21.2	24.7	22.3	21.0	10.54
1,7-$[B_{12}H_{10}Br_2]^{2-}$	2.66	21.0	–	–	–	–	–	29.6

TABLE IV

CAPACITY FACTORS (k') OF *closo*-BORATE ANIONS $[B_{10}H_{10}]^{2-}$ AND $[B_{12}H_{12}]^{2-}$ AND CHLORO DERIVATIVES FOR VARIOUS CONCENTRATIONS OF SODIUM PERCHLORATE IN THE MOBILE PHASE

Column, Separon HEMA-S 1000 Q-L (12 μm), capacity 0.05 mequiv./g; pH of the eluent, adjusted to 6.1 with 0.01 *M* phosphate buffer; detection, UV at 200 nm.

Anion	Concentration of $NaClO_4$ (mmol/l)				
	5	50	250	500	750
$[B_{10}H_{10}]^{2-}$	2.43	1.10	1.00	0.29	0.29
$[B_{12}H_{12}]^{2-}$	7.28	2.57	1.29	0.71	0.71
$[B_{12}H_{11}Cl]^{2-}$	–	9.00	3.60	1.57	1.43
1,7-$[B_{12}H_{10}Cl_2]^{2-}$	–	–	7.00	4.57	4.43

$K^+ < NH_4^+$. It was also found that sodium salts generally tend to exhibit a better selectivity than potassium and ammonium salts. The capacity factors of some solutes for low-concentration electrolytes (except for $NaClO_4$) for the Separon HEMA-BIO 300 column are summarized in Table II. It should be noted that concentrations of electrolytes below 0.1 *M* caused the peaks to be highly asymmetric.

The best separation selectivity for the 1,2- and 1,7-positional isomers of $[B_{12}H_{10}X_2]^{2-}$ (X = halogen) on all the materials used was achieved with $NaClO_4$ in the mobile phase. The capacity factors measured in mobile phases containing different molarities of this salt on Separon HEMA-BIO 300 and HEMA-S 1000 Q-L columns are shown in Tables III and IV. As already outlined above, concentrations below *ca.* 0.1 *M* caused an asymmetric shape of the peaks. The retention on Separon HEMA-BIO 300, 1000 and HEMA-S 1000, which were not modified by ion-exchange groups, increased with increasing concentration of $NaClO_4$ in the mobile phase in the approximate range 0.15–0.20 *M*. Further increases in the concentration caused only a slight decrease in retention and a slight increase in column efficiency.

The capacity factors on Separon HEMA S 1000 Q-L decreased monotonously as the $NaClO_4$ concentration in the eluent increased. However, the decrease in retention was unexpectedly small enough to be explained by an ion-exchange mechanism alone. From this fact together with the above-mentioned retention behaviour on the parent material Separon HEMA-S 1000 having no ion-exchange capacity, it was concluded that a mixed ion-exchange and hydrophobic interaction mechanism is probably involved in the separation on Separon HEMA S 1000 Q-L; the electrolyte concentration of *ca.* 0.1 *M* represents a boundary for a predominant ion-exchange mechanism.

Changes in the eluent pH in the range 2–10 had only a slight effect on the retention of *closo*-$[B_{12}H_{12}]^{2-}$ derivatives.

Mobile phases containing $NaClO_4$ at a constant concentration of 0.1 *M* were used to study the influence of the acetonitrile concentration in the mobile phase on the capacity factors of *closo*-$[B_{12}H_{12}]^{2-}$ derivatives on Separon HEMA-BIO 300. As shown in Fig. 3, the log *k'* values decrease approximately

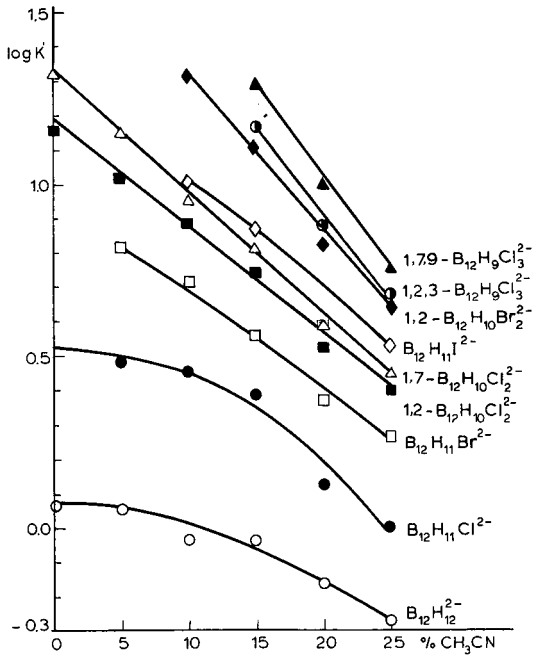

Fig. 3. Dependence of the capacity factors of the anions on the content of the organic modifier (acetonitrile) in the mobile phase (0.1 *M* $NaClO_4$). Column, Separon HEMA-BIO 300 (12 μm); detection, UV at 205 nm.

linearly with increasing acetonitrile concentration in the mobile phase, except for some species with log *k'* values below *ca.* 0.5. A significant decrease in *k'* values was observed for strongly retained species. Higher acetonitrile contents cause a slight decrease in the resolution of positional isomers, namely of the isomeric chlorinated anions $[B_{12}H_{10}Cl_2]^{2-}$ and $[B_{12}H_9Cl_3]^{2-}$. On the other hand, the presence of this organic modifier increased the peak symmetry for strongly retained species.

Plots of log *k' versus* $1/T$ in the temperature range of 25–80°C on colums packed with Separon HEMA-S 1000 Q-L and HEMA-BIO 300 are depicted in Figs. 4 and 5. The results suggest an apparent decrease in the retention of solutes with increase in temperature. Temperature has a negative effect on the resolution of isomers; at elevated temperatures, however, the increase in column efficiency due to the lower mobile phase viscosity competes with this effect. The appropriate *k'* values for the most strongly retained *closo*-$[B_{12}H_{12}]^{2-}$ anion derivatives, *e.g.*, iodo and rhodano derivatives, or deriv-

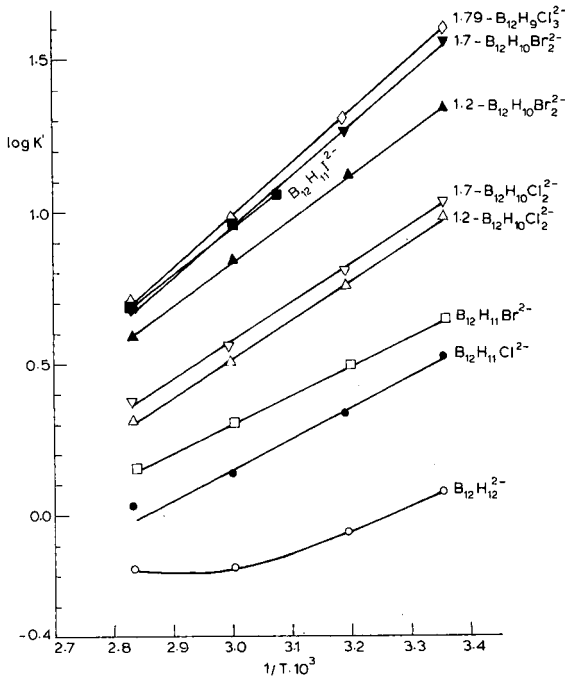

Fig. 4. Plots of the capacity factors (k') of the *closo*-$[B_{12}H_{12}]^{2-}$ derivatives as a function of $1/T$. Column, Separon HEMA-BIO 300 (12 μm); mobile phase, 0.5 *M* $NaClO_4$ in 0.01 *M* phosphate buffer (pH 8.5); detection, UV at 205 nm.

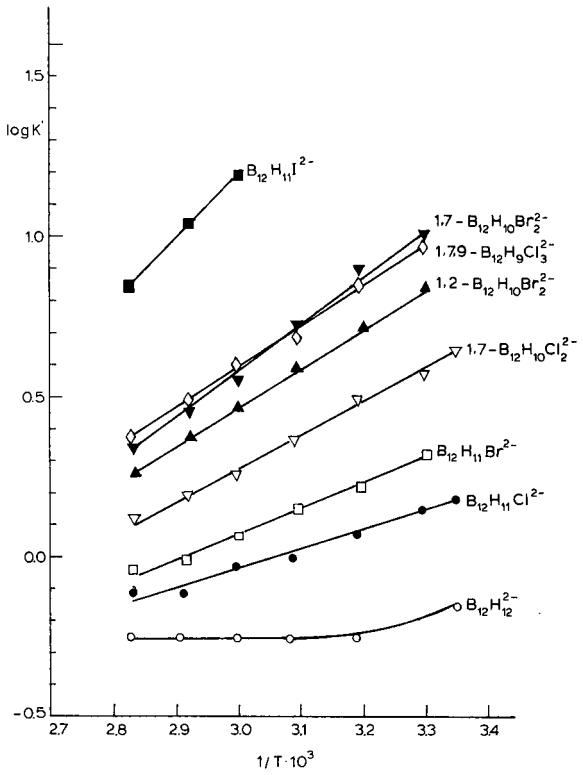

Fig. 5. Plots of the capacity factors (k') of the *closo*-$[B_{12}H_{12}]^{2-}$ derivatives as a function of $1/T$. Column, Separon HEMA-S 1000 Q-L (12 μm); mobile phase, 0.5 *M* $NaClO_4$ in 0.01 *M* phosphate buffer (pH 8.5); detection, UV at 205 nm.

atives with a greater number of substituents, can be adjusted either by increasing the temperature or by adding an organic modifier.

The results of the study of the dependence of the retention properties of the $[B_{12}H_{12}]^{2-}$-type anions on Separon HEMA materials on both the concentration of salts and the organic modifier in the mobile phase, together with the temperature dependence of the capacity factors, suggest that the separations on materials that do not contain ion-exchange groups were controlled by hydrophobic interactions of the solutes with the polymer surface. This behaviour seems to parallel, to some extent, that of aromatic sulphonic acids in chromatography on octadecylsilica in the presence of an electrolyte in aqueous or aqueous–organic mobile phases [12,13]. In contrast, both the retention and the selectivity are strongly dependent on the nature of the electrolyte used.

In order to understand this factor better, a study of the retention behaviour of the *closo*-$[B_{12}H_{12}]^{2-}$ derivatives on the ordinary revesed-phase silica-based Spheron SIX-C_{18} and SIX-CN was also performed. A similar influence of the nature of the electrolyte in the eluent was also observed. However, in contrast to Separon HEMA sorbents, concentrations of $NaClO_4$ in the range 0.1–0.5 *M* are low enough to effect a sufficient retention of hydroborate anions on this type of material. A mobile phase consisting of 0.1–0.5 *M* Na_2SO_4 with a higher salting-out effect must be used to achieve appropriate values of the capacity factors and a higher resolution of positional isomers. However, poor selectivity and peak shapes were observed on the octadecylsilica material. The selectivity achieved on the cyanopropylsilica with Na_2SO_4 solutions as eluent for mixtures of positional isomers exhibiting similar properties (such as positional isomers of chloro derivatives) is better but still poorer than that obtained using Separon HEMA systems with $NaClO_4$ as eluent.

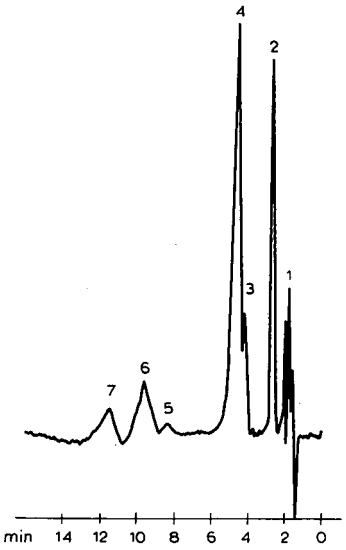

Fig. 6. Separation of the products of the chlorination of $Na_2B_{12}H_{12}$ in aqueous solution with chlorine–nitrogen mixture (2 vol.% of chlorine). Column, CGC (150 × 3.3 mm I.D.), Separon HEMA-BIO 300 (12 μm); mobile phase, 0.5 *M* $NaClO_4$ in 0.01 *M* phosphate buffer (pH 8.5); detection, UV at 205 nm; sensitivity, 0.16 a.u.f.s.; flow-rate, 0.5 ml/min; injection volume, 20 μl; temperature of separation, 60°C. Peaks: 1 = $[B_{12}H_{12}]^{2-}$; 2 = $[B_{12}H_{11}Cl]^{2-}$; 3 = 1,2-$[B_{12}H_{10}Cl_2]^{2-}$; 4 = 1,7-$[B_{12}H_{10}Cl_2]^{2-}$; 5 = isomer of $[B_{12}H_9Cl_3]^{2-}$, unknown structure; 6 = 1,2,3-$[B_{12}H_9Cl_3]^{2-}$; 7 = 1,7,9-$[B_{12}H_9Cl_3]^{2-}$.

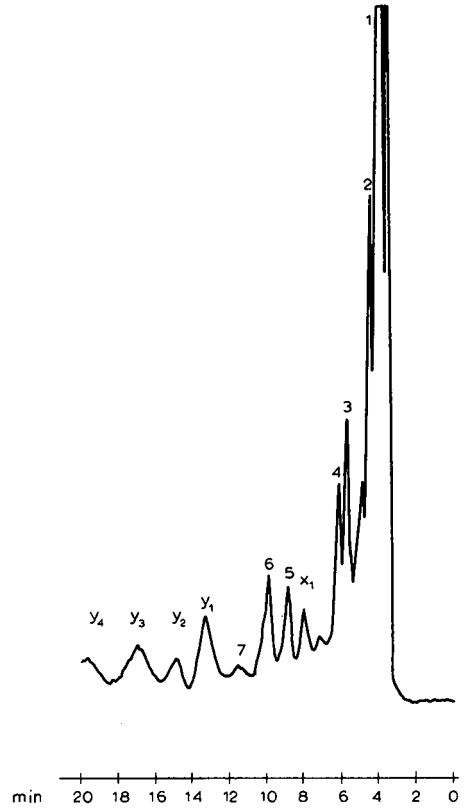

Fig. 7. Separation of the products of the high-temperature chlorination of solid $Na_2B_{12}H_{12}$ with gaseous BCl_3–H_2. Chromatographic conditions as in Fig. 6, except temperature of separation (80°C). Peaks: 1 = $[B_{12}H_{12}]^{2-}$; 2 = $[B_{12}H_{11}Cl]^{2-}$; 3 = 1,2-$[B_{12}H_{10}Cl_2]^{2-}$; 4 = 1,7-$[B_{12}H_{10}Cl_2]^{2-}$; 6 = 1,2,3-$[B_{12}H_9Cl_3]^{2-}$; 7 = 1,7,9-$[B_{12}H_9Cl_3]^{2-}$; 5, x_1 = $[B_{12}H_9Cl_3]^{2-}$, undetermined structure; y_1–y_4 = anions of formula $[B_{12}H_{12-n}Cl_n]^{2-}$ with $n > 3$.

The selectivity of the system with Separon HEMA-BIO 300 using 0.1–0.5 *M* $NaClO_4$ is sufficient to achieve the separation of a number of *closo* derivatives of the general formula $[B_{12}H_{12-n}X_n]^{2-}$ (for the halo derivatives, $n \doteq$ 1–6 for chloro, 1–4 for bromo and 1–3 for iodo derivatives). The separation efficiency of the method described is sufficient, at least for resolving the positional isomers of di- and trisubstituted derivatives of the $[B_{12}H_{12}]^{2-}$ anion.

Figs. 6–8 summarize practical examples of the separation of real mixtures of isomeric halo derivatives of the *closo*-$[B_{12}H_{12}]^{2-}$ anion resulting from various substitution reactions. Fig. 6 shows the separation of a mixture of derivatives and positional isomers of di- and trisubstituted anions prepared by electrophilic chlorination under mild conditions. Fig. 7 is a chromatogram of a mixture that is more abundant in positional isomers of chloro derivatives arising from the high-temperature reaction of solid $Na_2B_{12}H_{12}$ with boron trichloride–hydrogen mixture. Fig. 8 exemplifies a separation of a mixture of iodo derivatives, the retention of which is considerably higher than that of chloroderivatives. This can be, simply separated, however, with an acetonitrile-containing mobile phase. The chromatograms in Figs. 2 and 6–8 demonstrate that both the separation efficiency and peak symmetry are acceptable.

CONCLUSIONS

The chromatographic separation of a wide range of *closo*-$[B_{12}H_{12}]^{2-}$ derivatives can be performed

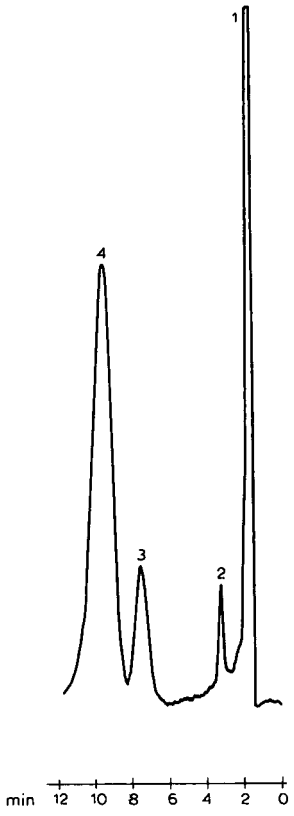

Fig. 8. Separation of the mixture of products of iodination of $Na_2B_{12}H_{12}$ in aqueous solution with iodine in CCl_4. Chromatographic conditions as in Fig. 2, except acetonitrile content in the mobile phase (25 vol.%) and temperature of separation (45°C). Peaks: 1 = I^-; 2 = $[B_{12}H_{11}I]^{2-}$; 3 = 1,2-$[B_{12}H_{10}I_2]^{2-}$; 4 = 1,7-$[B_{12}H_{10}I_2]^{2-}$.

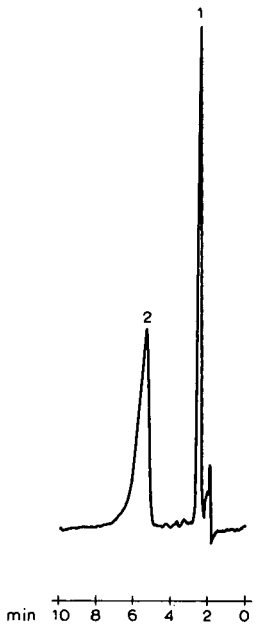

Fig. 9. Separation of the the *closo*-hydroborate anions $[B_{10}H_{10}]^{2-}$ and $[B_{12}H_{12}]^{2-}$. Column, Separon HEMA-S 1000 Q-L (12 μm) (capacity 0.1 mequiv./g); mobile phase, 0.1 *M* $NaClO_4$ in 0.01 *M* phosphate buffer (pH 8.5); flow-rate, 0.55 ml/min; detection, UV at 205 nm; sensitivity, 0.32 a.u.f.s.; injection volume, 20 μl. Peaks: 1 = $[B_{10}H_{10}]^{2-}$; 2 = $[B_{12}H_{12}]^{2-}$.

using Separon HEMA-BIO 300 hydroxyethylmethacrylate material and aqueous solutions of sodium perchlorate as the mobile phase. The retention and selectivity can be controlled to some extent by adjusting the concentration of the salt, separation temperature and, in some instances, the acetonitrile content in the mobile phase. The mechanism of separation is governed by the hydrophobic interaction of the *closo*-$[B_{12}H_{12}]^{2-}$ framework and its substituted groups with the polymer surface when a strong electrolyte is present in the mobile phase. The influence of the nature of the electrolyte used was observed.

Ion-exchange chromatography on materials modified with quaternary ammonium groups (Separon HEMA-S 1000 Q-L) was found to be less suitable for the separation of halo derivatives because of their very strong retention and the involvement of a mixed separation mechanism causing peak tailing. In contrast, such a method seems to be more suitable than hydrophobic interaction chromatography for the separation of less hydrophobic anions, *e.g.*, the unsubstituted anions $[B_{12}H_{12}]^{2-}$ and $[B_{10}H_{10}]^{2-}$ (Fig. 9) and hydroxy and fluoro derivatives of the $[B_{12}H_{12}]^{2-}$ anion. The method presented seems to offer a very simple and powerful tool for the analysis of a number of the mixtures of *closo*-hydroborate anions arising from synthetic work, and for purity assay of *closo*-hydroborate species.

REFERENCES

1 W. J. Evans and M. F. Hawthorne, *J. Chromatogr.*, 88 (1974) 187.
2 Z. Plzák, and B. Štíbr, *J. Chromatogr.*, 151 (1978) 363.
3 Z. Plzák, J. Plešek and B. Štíbr, *J. Chromatogr.*, 168 (1979) 280.

4 G. R. Wellum, E. I. Tolpin, L. P. Andersen and R. Sneath, *J. Chromatogr.*, 103 (1975) 153.
5 T. E. Haas, *Inorg. Chem.*, 3 (1964) 1053.
6 E. L. Muetterties, W. H. Knoth, *Polyhedral Boranes*, Marcel Dekker, New York, 1968.
7 W. Preetz, M. G. Srebny and H. C. Marsmann, *Z. Naturforsch., Teil B*, 39 (1984) 189.
8 I. Ikeuchi and T. Amano, *J. Chromatogr.*, 396 (1987) 273.
9 K. G. Bührens and W. Preetz, *J. Chromatogr.*, 139 (1977) 291.
10 M. Columbier, B. Bonnetot and H. Mongeot, *Bull. Soc. Chim. Fr.*, (1988) 844.
11 P. R. Haddad and P. E. Jacson, *Ion Chromatography—Principles and Applications* (*Journal of Chromatography Library*, Vol. 46), Elsevier, Amsterdam, 1990.
12 P. Jandera, J. Churáček and J. Bartošová, *Chromatographia*, 13 (1980) 485.
13 K. Šlais, *J. Chromatogr.*, 469 (1989) 223.
14 J. Borák and M. Smrž, *J. Chromatogr.*, 133 (1977) 127.
15 M. Macek, Z. Deyl, J. Čoupek and J. Sanitrák, *J. Chromatogr.*, 222 (1981) 284.
16 P. Šmídl, I. Kleinmann, J. Plicha and V. Svoboda, *J. Chromatogr.*, 523 (1990) 131.
17 F. Vláčil, I. Vinš and J. Čoupek, *J. Chromatogr.*, 391 (1987) 119.
18 F. Vláčil and I. Vinš, *J. Chromatogr.*, 391 (1987) 133.
19 V. Pacáková, K. Štulík and M. J. Wu, *J. Chromatogr.*, 520 (1990) 349.
20 J. Borák, *J. Chromatogr.*, 155 (1978) 69.
21 B. Grüner, *Thesis*, Institute of Inorganic Chemistry, Czechoslovak Academy of Sciences, Prague, 1990.
22 B. Grüner, S. Heřmánek, Z. Plzák, *International Meeting on Boron Chemistry, IMEBORON VII, Torun, Poland, July 30–August 3, 1990*, Nicolai Copernicus University, Torun, 1990, Abstracts, Poster 5.
23 E. L. Muetterties, *Inorg. Synth.*, 10 (1967) 81.
24 M. F. Hawthorne and R. L. Pilling, *Inorg. Synth.*, 9 (1967) 16.

Journal of Chromatography, 588 (1991) 211–216
Elsevier Science Publishers B.V., Amsterdam

CHROM. 23 662

Ion chromatographic analysis of the purity and synthesis of sulfonium and selenonium ions

Jerald L. Hoffman

Department of Biochemistry, School of Medicine, University of Louisville, Louisville, KY 40292 (USA)

(Received June 3rd, 1991)

ABSTRACT

The use of single-column ion chromatography with conductometric detection was shown to be useful for the analysis of sulfonium and selenonium ions. A Hamilton PRP X-200 cation column was eluted with either solvent A (5 m*M* nitric acid in 30% methanol) or solvent B (4 m*M* nitric acid). With solvent B, trimethylsulfonium ion was separated from trimethylselenonium ion. With solvent A, amounts of trimethylsulfonium ion from 2 to 250 nmol were detected with a linear response. The retention times and response factors for a series of sulfonium ions with various organic groups were determined. In general the ions with more hydrophobic groups eluted later, but all had similar response factors. The method was shown to be useful for optimizing conditions for the synthesis of methylsulfonium ions, specifically the reaction of methyl iodide with diallyl sulfide.

INTRODUCTION

In the course of studies on the enzyme thioether methyltransferase which methylates thioethers or selenoethers to form the corresponding methylonium ions [1] it was necessary for this laboratory to chemically synthesize and characterize various sulfonium ions for use as chromatographic standards [2]. It became apparent that a facile method was needed to monitor the purity of these compounds, particularly in view of the multiple products possible from the reaction of methyl iodide with a thioether [3]. This problem is illustrated specifically in Fig. 1 which shows that the nominal synthesis of DAMS (see Table I for abbreviations) from diallyl sulfide and methyl iodide can result in three additional sulfonium ions by various cycles of dealkylation by I^- and subsequent realkylation. A similar outcome may result starting with other thioethers.

In previous studies the sulfonium and selenonium ions of interest were radioactively labeled either chemically or metabolically, separated by conventional cation-exchange high-performance liquid chromatography (HPLC), and detected by liquid scintillation counting of collected fractions [1,2]. However, a method of analysis not requiring radioactive detection was desired for two reasons. First, during the chemical synthesis of methylsulfonium ions using [^{14}C]methyl iodide a non-radioactive product, exemplified by TAS in Fig. 1, can be

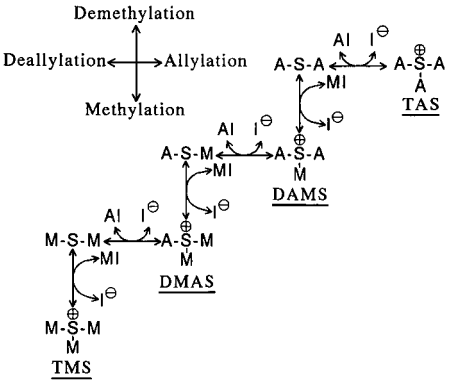

Fig. 1. Potential sulfonium ion products starting with diallyl sulfide and methyl iodide. M = Methyl group; A = allyl group. Abbreviations of sulfonium ions are underlined.

0021-9673/91/$03.50

obtained and would not be detected by the above method. Second, further studies of synthesis and excretion of methylsulfonium ions in intact animals would be facilitated by a direct detection method, and would be required in the case of human studies since the use of radioactivity would be precluded.

Most of the sulfonium and selenonium compounds of interest lack chromophores or fluorophores which prevents their detection by flow monitors sensitive to such groups. The ion chromatographic fractionation of triethylsulfonium and TMS and their detection by conductivity with the use of a suppressor column have been reported [4]. Therefore we investigated the analysis of sulfonium and selenonium ions with the simpler system of column ion chromatography with conductometric detection. This paper describes the use of the simplest trialkylsulfonium ion, TMS, to determine the sensitivity and dynamic range of single-column ion chromatography for analysis of this class of compounds. The effects on retention time of replacing the sulfur of TMS with selenium, and of varying the structures of the organic groups of sulfonium ions, are demonstrated. Finally the utility of this method of analysis in monitoring the temporal appearance of sulfonium ions produced by varying the ratio of methyl iodide/thioether is illustrated using diallyl sulfide.

EXPERIMENTAL

Apparatus

The HPLC system consisted of a Wescan Model 315 conductivity detector and Spectra-Physics 8800 pump, 8780 autosampler and 4290 integrator. System control and data capture were provided by Spectra-Physics Chromstation/2 software run with an IBM PS/2 Model 50 computer. The column used was a 15 × 0.46 cm I.D. Hamilton PRP X-200 cation column obtained from Rainin Instrument (Woburn, MA, USA).

Reagents

Methyl iodide, TMS iodide, thioethers and dimethyl selenide were obtained from Aldrich (Milwaukee, WI, USA). All other chemicals were generally of the highest grade obtainable.

Onium ion synthesis and characterization

The synthesis and characterization by low-resolution fast atom bombardment mass spectrometry (FAB-MS) has been described for all the sulfonium ions used here [2] except those containing allyl groups. The latter were prepared in 5-ml batches under conditions yielding a mixture of TAS, DAMS and DMAS (19 h, equimolar diallyl sulfide and methyl iodide; see Results). When this mixture was extracted into water as below for TMSe and then subjected to low-resolution FAB-MS, it showed m/z of 155, 129 and 103 corresponding, respectively, to TAS, DAMS and DMAS in the proportions found in the mixture by ion chromatography. TMSe was synthesized by reaction for 24 h in a total volume of 5 ml containing 1 *M* methyl iodide and 1 *M* dimethyl selenide in methanol. At the end of this time 5 ml each of water and diethyl ether were added, and the suspension was shaken and allowed to settle in a separatory funnel. The resulting aqueous phase was similarly extracted twice more with 5 ml of ether, and the final aqueous phase containing TMSe iodide was lyophilized to dryness. This product was used without further characterization.

Time course of the reaction of diallyl sulfide and methyl iodide

Reaction mixtures with total volumes of 1 ml in methanol contained 0.5 *M* diallyl sulfide and either 0.5 or 2.5 *M* methyl iodide at room temperature. Sampling was accomplished by placing reaction mixtures in vials in the autosampler with the HPLC system programmed to inject a sample of 3 μl from each vial at hourly intervals over a 10-h period. Additional samples were run at 18–19 h. Solvent A was used to elute all samples.

Chromatography

Solvent A contained 5 m*M* nitric acid in methanol–water (30:70) and was used for all analyses other than the separation of TMS and TMSe shown in Fig. 2, which utilized solvent B consisting of 4 m*M* nitric acid in water. Both solvents were run at a flow-rate of 2 ml/min. Injection volumes varied depending on the sample but were in the range from 3 to 100 μl. The detector range was set at 0.1 μS per 10 mV with the integrator attenuation set from 32 to 256 mV full scale depending on the anticipated peak sizes. Before use each day the column was regener-

ated by injection of 100 μl of 4 *M* nitric acid and equilibrated with the appropriate solvent.

RESULTS AND DISCUSSION

The initial experiments utilized commercially available TMS and chemically synthesized TMSe to establish the applicability of ion chromatography in the analysis of this type of compound. Typical elution profiles using solvent B for TMS, TMSe and a mixture of the two are shown in Fig. 2. The ability to separate these two closely related ions encouraged further exploration of the sensitivity and dynamic range of the method for TMS.

Amounts of TMS ranging from 2 to 250 nmol were next analyzed using solvent A, and the results are shown in Fig. 3. Panel A shows the integrator peak area *versus* amount of TMS. Linearity was observed over the entire range tested with a response factor (slope) of 42 300 μV · s/nmol. Amounts of TMS greater than 250 nmol exceeded the capacity of the detector at the 0.1 μS per 10 mV range. Less sensitive (higher capacity) settings are available, but some peak distortion was evident at sample loads greater than 250 nmol. The data at lower TMS levels are shown in the inset, which reveals the limit of detection to be 2 nmol. Thus at a single-detector range setting the dynamic range is greater than 100-fold. More sensitive detector range settings of 0.05 and 0.01 μS per 10 mV were available, but much higher noise levels prevented their use. The 2-nmol sensitivity may be sufficient for further biochemical studies of thioether methylation since this would correspond to 100 μl of a 20 μM solution of sulfonium ion. Such concentrations might be expected in urine of animals treated with doses of thioethers up to 1 mmol/kg. However, a sensitivity of 2 nmol would not be sufficient to detect the quantities of TMSe excreted in urine by rats or humans under conditions of normal selenium intake without extensive concentration by sample processing [5].

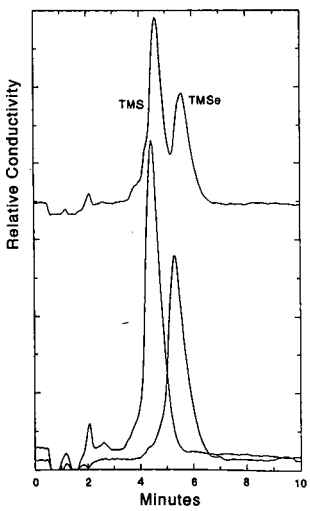

Fig. 2. Ion chromatographic separation of TMS and TMSe. Individual samples of 50 nmol of TMS and 40 nmol of TMSe (lower curves) and a mixture of 25 nmol of TMS and 20 nmol of TMSe (upper curve) were eluted with solvent B.

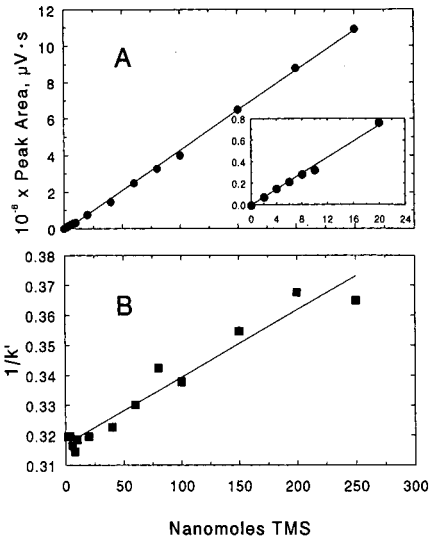

Fig. 3. Sensitivity, range and capacity factor for ion chromatography of TMS. Amounts of TMS from 2 to 250 nmol were eluted with solvent A. Panel A shows the linear range and detection limit for TMS. The inset is an expanded view of the lower end of the sample range. Panel B shows the linear dependence of the inverse of the capacity factor (k') on sample amount.

Fig. 3B shows that the inverse of the capacity factor (k') for TMS on the PRP X-200 column varies linearly with the sample load, which is predicted by the dual-retention model of ion chromatography [6]. In more practical terms the retention time of TMS varied from 4.17 min at 2 nmol to 3.74 min at 250 nmol. With biological samples having high total cation content, it may be difficult to identify peaks by comparison of retention times to those of exter-

TABLE I

RETENTION TIMES AND RESPONSE FACTORS OBTAINED DURING ION CHROMATOGRAPHY OF SULFONIUM AND SELENONIUM IONS

Cation[a]	Retention time[b] (min)	Response factor[b] (μV · s/nmol)
Potassium	3.54	36 800
Trimethyl (TMS)	3.97 (4.54)	42 300
Dimethyl-2-hydroxyethyl (DMHES)	4.00	50 500
Trimethylselenonium (TMSe)	4.25 (5.67)	48 400
2-Hydroxyethylethylmethyl (HEEMS)	4.34	42 300
Diethylmethyl (DEMS)	4.74	43 300
Tetramethylenemethyl (TMMS)	4.76	42 700
Dimethylpropyl (DMPS)	5.38	50 100
Dimethylallyl (DMAS)	5.50	N.D.
2-Chloroethylethylmethyl (CEEMS)	7.68	41 600
Diallylmethyl (DAMS)	7.80	N.D.
Triallyl (TAS)	11.52	N.D.

[a] Abbreviations in parentheses are used in the text. All cations other than K^+ and TMSe are sulfonium ions.

[b] Data given were obtained with solvent A, except for those retention times in parentheses which were obtained with solvent B. Samples contained no more than 50 nmol of each ion. N.D. means not determined.

nal standards. Duplicate runs with one sample containing an added internal standard would provide more definitive peak identification.

The next feature examined was the dependence of retention time on the structure of the onium ion, and the results are shown in Table I arranged in order of increasing retention time. An inorganic cation, K^+, was included for comparison. Samples contained no more than 50 nmol to minimize load effects on retention times. All of the organic cations eluted later than K^+, apparently due to hydrophobic interaction with the poly(styrene–divinylbenzene) resin. This interaction necessitated the inclusion of the organic modifier in solvent A (5 m*M* nitric acid in 30% methanol), since the sulfonium ions with higher carbon content eluted late and in broad peaks in solvent B (4 m*M* nitric acid). TMSe eluted later than TMS in both solvents consistent with the greater electronegativity of the selenium atom imparting more basicity to its onium ion.

Comparison of the retention times of the various sulfonium ions gives greater insight into the separation mechanism. In general, higher carbon content led to stronger retention. An interesting comparison is between DEMS and DMPS which have identical compositions, $(CH_3)_3(CH_2)_2S$; however, DMPS with the longest hydrocarbon chain eluted later. Another 5-carbon sulfonium ion, TMMS (S-methyltetrahydrothiophene), of slightly lower hydrogen content, $CH_3(CH_2)_4S$, had essentially the same retention time as DEMS. Substitution with a polar group such as hydroxyl decreased retention (DEMS *versus* HEEMS), while halide substitution greatly increased retention (DEMS *versus* CEEMS). Finally, unsaturation slightly increased retention (DMPS *versus* DMAS).

All of the organic ions gave response factors similar to each other and not greatly different from that of K^+. The most reliable response factors in Table I are those for TMS, TMSe and TMMS which were obtained as dry solids. All the other sulfonium ions gave oils or pastes upon drying which made accurate weighing difficult. Response factors were not obtained for the allylsulfonium ions, DMAS, DAMS and TAS, because they tended to decompose and rearrange when concentrated as halide salts. However, it appears safe to assume that they, like most other sulfonium and selenonium ions, would have response factors of approximately 45 000 μV s/nmol in this HPLC system.

The synthesis of methylsulfonium ions by reaction of thioethers and methyl iodide can lead to

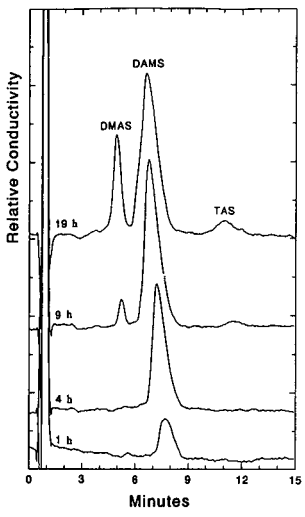

Fig. 4. Representative elution profiles of samples taken during the reaction of methyl iodide and diallyl sulfide. Samples of 3 μl from reaction mixtures containing 0.5 *M* each of methyl iodide and diallyl sulfide were run at the times indicated using solvent A.

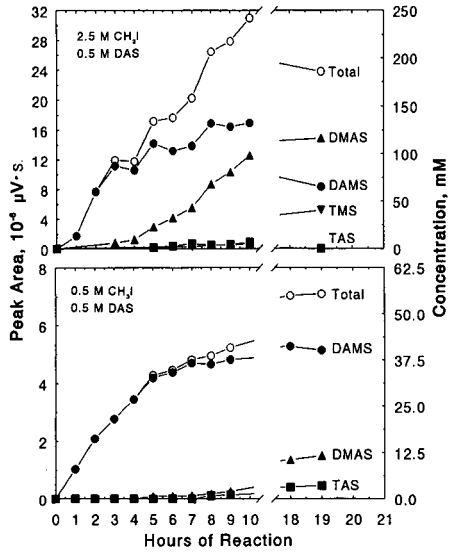

Fig. 5. Rates of appearance of sulfonium ions during the reaction of methyl iodide and diallyl sulfide. Samples of 3 μl were analyzed at the times indicated as in Fig. 4. The ordinates on the left are the integrated peak areas for sulfonium ions in the 3-μl samples. The concentration scales on the ordinates on the right assume a response factor of 44 000 μV · s/nmol for sulfonium ions. The concentrations of the two reactants are shown on each panel with diallyl sulfide abbreviated as DAS.

several undesired products as illustrated in Fig. 1. Ion chromatography proved to be very useful in obtaining optimal yield and purity. Representative elution profiles of samples obtained at various times during the reaction of 0.5 *M* each of methyl iodide and diallyl sulfide are shown in Fig. 4. For the first 4 h, only the desired product DAMS was evident. By 9 h DMAS and TAS appeared and were major contaminants after 19 h. A more quantitative summary of these data is shown in the lower panel of Fig. 5. At this equimolar ratio of methyl iodide and diallyl sulfide, DAMS was the major product after 19 h, and no TMS was synthesized. At 4 h, when DAMS was the only sulfonium product, its concentration of 27 m*M* corresponded to 5.4% conversion of the 500 m*M* diallyl sulfide. Increasing the ratio of methyl iodide/diallyl sulfide to 5:1 gave a more rapid initial rate of DAMS synthesis, as shown in the top panel, but extended reaction time led to the major product being DMAS with heavy contamination by TMS. Because of the high total methyl group concentration only a trace of TAS was detectable midway through the reaction period which disappeared by 19 h. At 3 h, when DAMS was the only sulfonium product, its concentration of 90 m*M* corresponded to 18% conversion of the 500 m*M* diallyl sulfide. Thus one could conclude that use of the higher methyl iodide concentration for 3 h would give the highest yield of pure DAMS. An additional advantage of this method is that the ion chromatographic analysis takes a relatively short time compared to the rate of methylation, permitting reactions to be stopped when the first trace of undesired product appears. More thorough studies may reveal conditions giving even higher yields of DAMS, but the above results establish the utility of ion chromatography in monitoring sulfonium ion synthesis.

In summary, ion chromatography with conductometric detection is shown to be a facile and sensitive method for the detection of sulfonium and selenonium ions. The technique should be useful in further studies of the chemistry and biochemistry of these compounds.

ACKNOWLEDGEMENTS

This work was supported by Grant No. ES04887 from the National Institute of Environmental Health Sciences, US Public Health Service. Expert technical

assistance was provided by Jane Williams. Mass spectral analyses were performed by the Midwest Center for Mass Spectrometry, University of Nebraska-Lincoln, Department of Chemistry (Lincoln, NE, USA), a National Science Foundation Regional Instrument Facility.

REFERENCES

1 N. M. Mozier, K. P. McConnell and J. L. Hoffman, *J. Biol. Chem.*, 263 (1988) 4527.
2 N. M. Mozier and J. L. Hoffman, *FASEB J.*, 4 (1990) 3329.
3 P. A. Lowe, in C. J. M. Stirling (Editor), *The Chemistry of the Sulfonium Group*, Part 1, Wiley, New York, 1981, Ch. 11.
4 R. J. Williams, *J. Chromatogr. Sci.*, 20 (1982) 560.
5 H. E. Ganther, R. J. Kraus and S. J. Foster, *Methods Enzymol.*, 143 (1987) 195.
6 S. Afrashtehfar and F. Cantwell, *Anal. Chem.*, 54 (1982) 2422.

Journal of Chromatography, 588 (1991) 217–224
Elsevier Science Publishers B.V., Amsterdam

CHROM. 23 621

GCSIM: a gas–liquid chromatography simulator for educational purposes

J. C. Reijenga

Laboratory of Instrumental Analysis, Eindhoven University of Technology, P.O. Box 513, 5600 MB Eindhoven (Netherlands)

(First received May 22nd, 1991; revised manuscript received July 11th, 1991)

ABSTRACT

A gas–liquid chromatography simulation program was written for personal computers. A graphic display of a chromatogram is shown by the simulator. The program can be used to illustrate various effects in gas chromatography for demonstrations or lectures. In addition, it can be used as an advanced supplemental instrument simulator in a practical course. Variables include column length, inlet pressure, phase ratio, temperature (both isothermal and linear programming) and detector attenuation. Additional parameters offer a choice between packed and capillary columns, two different detectors, two stationary phases and two carrier gases. The sample composition can be changed to include any solvent and up to six components from a library of 75 at different concentrations.

INTRODUCTION

Teaching chromatography implies the description of a number of phenomena occurring at the interface of the mobile and stationary phases: phase equilibria, concentration distributions and other effects that can all be put into equations. This latter aspect provides a sound basis of the principles of chromatography. Attractive though this may seem, a lot of imagination is necessary to really understand what is happening in a column. For this reason, at the Faculty of Chemical Engineering of the Eindhoven University of Technology, we have decided to introduce chromatography in a practical course for first-year students. First, column chromatography and thin-layer chromatography (TLC) of dyes are dealt with in a qualitative manner. Subsequently, a gas chromatography (GC) course is given. In this case, with the TLC results in mind, GC is more readily understood. A minimum of theory, however, is required before the use of a microsyringe can be considered.

A gas chromatography simulator was written for personal computers. The aim of the program is twofold. First, it can be used, in an introductory lecture, to visualize various effects associated with the variables that are at our disposal on a modern gas chromatograph. Second, the simulator can be used as an additional instrument in a practical course.

A number of simulators of chromatographic separations have been described [1,2]. The high-performance liquid chromatography simulator from the SERAPHIM project is attractive, especially for a practical course on reversed-phase liquid chromatography. Another program is aimed at solving a specific separation problem (PROTEINS; IRL Press, Eynsham, Oxford, UK). This simulator combines a number of pretreatment, separation and identification techniques with the purpose of isolating a protein from a mixture.

Of the GC simulators available, GLCSIM (A. B. de Vries, Werkgroep BOS, Zuidhorn, Netherlands) contains a limited number of sample components, a considerable number of stationary phases and variable retention times. Its limitation is that it only works with packed columns, under isothermal conditions, with a single detector. Another GC simulator, distributed in the SERAPHIM project, seems restricted to the evaluation of column packings (J. K. Hardy, University of Akron, Akron,

0021-9673/91/$03.50

OH, USA). A severe drawback of the SERAPHIM products is that they are distributed as ASCII sources for GWBASIC, a programming tool unsuitable for structured programming.

Our aim was therefore to write a simulator with relatively advanced features, as a stand-alone, compiled EXE file. Also, the program should not be too choosy regarding the hardware required. As usual while programming, specifications grew as time went by. One requirement, however, was adhered to: a simulator for educational purposes and not an accurate predictor of experimental results. We are aware of the existence of simulators that claim to be in compliance with present state-of-the art in GC retention modelling [3], mostly for optimization purposes [4]. In those instances, the simulator is used as a research tool. This paper describes GCSIM, a teaching tool.

EXPERIMENTAL

Hardware and software

The program runs on any IBM-compatible personal computer of the PC, XT or AT type, operating under DOS operating system version 3.2 or higher with 640 kbyte of memory. A single disk drive of 3.5 or 5.25 in. is sufficient. A graphics adapter and monitor are required, either monochrome or colour. The program does not use colours and automatically adapts to any of the following graphics cards: EGA, CGA, AT&T 6300 and Hercules. If a mathematical coprocessor is present, this greatly improves the calculation speed; otherwise the coprocessor is emulated. An XT-type PC with a coprocessor is preferred over an AT type without. There is no mouse support. An IBM graphics printer is optional, with the restriction that not all graphics cards allow screen dumps to be printed.

The program was written in Microsoft Quickbasic version 4.5 and compiled into a stand-alone EXE file which can be run independently from the Quickbasic programming environment. Details of the availability of the program can be obtained form the author.

In addition to the program GCSIM, the program diskette contains six help files that can be accessed from the program. Finally, there is a data file with retention data for 75 sample components on two stationary phases as a function of temperature. The program is self-explanatory. The available course manual contains a description and a number of experiments.

The model

The chromatographic model on which the simulator is based is simplified but straightforward [5]. Values of constants in the equations are mostly derived from experimental data. The gas compressibility factor j is assumed to be unity throughout the model. The gas velocity u is calculated from the pressure gauge reading P and the column length L:

$$u = c_1 P/L \tag{1}$$

In which the constant c_1 depends on the carrier gas and the type of column. The retention time of the unretained component t_0 is then calculated with

$$t_0 = L/u \tag{2}$$

The velocity dependence of the plate height H is described by a three-parameter model:

$$H = c_2 + c_3 u + c_4/u \tag{3}$$

Constants in this equation depend on the column type and carrier gas. The temperature dependence of the net retention volume V_N is approximated by a two-parameter model [2]:

$$\ln V_N/\beta = c_5/T + c_6 \tag{4}$$

where β represents the phase ratio V_m/V_s.

Neglecting gas compressibility, the net retention volume V_N can be rewritten as:

$$V_N = kV_m \tag{5}$$

Combination of eqns. 4 and 5 gives

$$\ln(kV_m) = c_5/T + c_7 \tag{6}$$

where k is the capacity factor. From the literature we obtained tabulated values of V_g, the specific retention volume, at different temperatures and for two stationary phases [6]. The specific retention volume is defined as the net retention volume per unit mass of stationary phase W_s:

$$V_g = V_N \cdot 273/T/W_s \tag{7}$$

where T is the absolute temperature.

Combination of eqns. 5 and 7, with $W_s = \rho_s V_s$, yields

$$V_s = k\beta 273/\rho_s/T \tag{8}$$

This relationship is now approximated by

$$k = V_g(T)/\beta \quad (9)$$

thus simplifying subsequent calculations to a considerable extent. Accurate prediction of experimental retention times, which is not the aim of the simulator, is not possible, mainly owing to this last approximation which introduces a slight systematic error because $273/\rho_s/T$ is usually less than unity. Finally, it is assumed that k fits a two-parameter model similar to that of eqn. 4:

$$k = \exp(c_8/T + c_9) \quad (10)$$

The retention time t_R is then calculated using

$$t_R = t_0(1 + k) \quad (11)$$

The peak width σ is obtained from

$$\sigma = t_R/\sqrt{N} \quad (12)$$

The detector sensitivity and selectivity are modelled as follows: the thermal conductivity detection (TCD) response is the same for all sample components and in addition depends on the carrier gas. The flame ionization detection (FID) response is proportional to the molecular weight of the sample component and the gas velocity u.

The algorithm

In the algorithm for the calculation of retention, values of k at two reference temperatures are first calculated from V_g using eqn. 9, then values of c_8 and c_9 are calculated using eqn. 10, which is finally used to calculate k at the desired temperature.

For temperature programming, retention times are calculated by summation of time increments (and corresponding temperature and column length increments) of 5 s until the column outlet is reached. The peak width in temperature programming is approximated by the width of the peak if it were to have eluted isothermally at the programmed elution temperature.

The algorithm for the calculation of chromatograms consists of the following procedures. On start-up of the simulator, a baseline with random white noise is generated once. During a session with the simulator this baseline is used throughout, because random generation is time consuming, especially for normally distributed noise. In order to maintain the random character of the noise, the noisy baseline is randomly shifted with respect to the resulting chromatogram each time a new chromatogram is calculated. For each component in the sample, k, t_R and σ are first calculated as described in the previous section. For each sample component, the corresponding peak is now added to the baseline if t_R is within the time interval displayed. Of each of these peaks only a width of 8σ units around the top is considered, thus reducing the calculation time to a considerable extent. The resulting chromatogram is now displayed in the graphics window, using the detector attenuation as a scaling factor.

Performance of the simulator

The gas chromatography siumulator contains a large number of instrumental parameters. For educational purposes a choice was made for two distinctly different stationary phases in terms of polarity. Also, comparison of capillary and packed columns was considered an important feature. The latter are especially useful for illustrating peak broadening in a graphic presentation. Table I lists the operational range of all experimental parameters.

The simulator screen (Fig. 1) consists of graphical and numerical information, with a main menu command line at the top of the screen. The chromatogram displayed is limited to a time interval of *ca.* 21 min (23 min for Hercules graphics), the time resolution of one screen pixel corresponding to 2 s. This resolution seems poor for capillary GC, but was found to represent an attractive compromise between calculation time and amount of information contained in one graphics screen. In addition to the sample component peaks, a solvent peak and the unretained peak are shown. Recalculation and display of a new chromatogram is immediately executed, following a change in any of the instrumental or sample parameters.

The lower left-hand corner of the screen gives information on instrumental parameters such as column, detector and carrier gas. Sample information is given at the lower right-hand corner: component name, k, concentration and peak area are given. In between these two blocks, some additional information on instrument performance is given: retention time of the unretained component, gas velocity, plate number and resolution if there are two sample components.

TABLE I

OPERATIONAL RANGE OF EXPERIMENTAL PARAMETERS OF THE SIMULATOR

Parameter	Operational range
Packed column	Length 1–5 m in 1-m increments
	I.D. 2 mm
	Phase ratio 8–20 in increments of 1
Capillary column	Length 10–30 m in 10-m increments
	I.D. 0.35 mm
	Phase ratio 80–400 in increments of 10
	Injection splitting ratio 50–200 in increments of 10
Carrier gas	Nitrogen or helium
Detection	FID or TCD (packed only)
	Attenuation 1–8192 in increments of a factor of 2
	Linear or logarithmic display
	Rectangular noise filter width 1, 3, 5, 7, 9 screen resolution units
Temperature	50–200°C in increments of 2°C
	Isothermal hold time 0–9 min in increments of 1 min
	Programme 0–9°C/min in increments of 1°C/min
Injection	Choice of any sample component as solvent
	Concentration of sample components 0–10 000 ppm
	Volume 0–2 μl in 0.1-μl increments
Retention time	0–21 min (23 min for Hercules)

The main menu, always visible in line 1, gives access to a number of pull-down submenus by means of the key corresponding to the first capital letter of the main menu item. Cursor (arrow) keys can be used in the pull-down menus in addition to the capital letter keys.

Table II lists all submenus, some of which are again followed by a further submenu, etc.; for instance, SLC (System Load Chromatogram) loads a chromatogram previously stored.

Registration of operation

When used in a practical course, information on how the simulator is used by the student can be valuable to the teacher. To this end, GCSIM stores all information on commands used in a sequential ASCII file with extension .REG. This may be especially useful in optimizing studies, as will be shown in the next section. The contents of the .REG file will look like this

90_TG:9
12_SLS:butanols

In this example the user has decided after 90 s to change temperature programming to a gradient of 9°C/min and 12 s later decided to load a sample called "butanols".

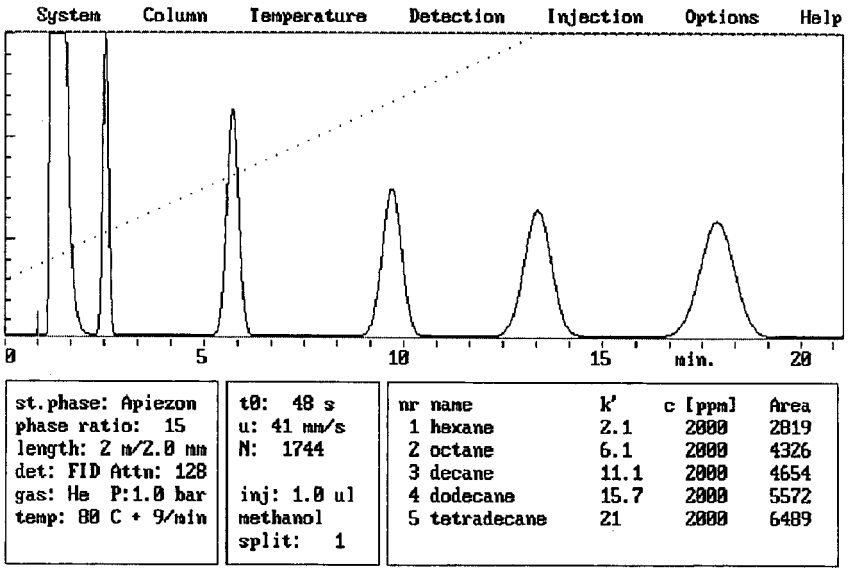

Fig. 1. A typical GCSIM screen with the main menu on the top line. Instrumental and sample parameters are given below the chromatogram. See text for details.

TABLE II

SUBMENUS TO THE MAIN MENU OF THE SIMULATOR

Further submenus are denoted by three periods.

System	Column	Temperature	Detection	Injection	Options	Help
Load ...	column Type...	Temperature	Type	Components...	Disturbance.	Main
Save ...	column Length.	Isothermal	Attenuation	coNcentrations	Variance...	Options
Dos shell	Phase type...	Gradient	Filtering	Solvent...	Quality	Score
Quit...	phase Ratio			Volume	Scaling ...	sPecs.
	Gas type ...			splitting Ratio	Inject...	sImul.
	gaS pressure			Delete all	Erase...	
					sCore...	
					options Help	

Any text editor can be used to page through the registration files. When upon start-up of the simulator an identification number is given, the registration filename contains this identification number, so that individual results can be stored separately.

What is not simulated and why

Computer simulation of instumental analysis offers the possibility of changing parameters that are normally not variables: noise, drift, tailing and spikes can be changed at will (Fig. 2). This does not imply that an instrument simulator should always have better specifications than the original instrument.

A number of features were considered and omitted for two reasons: their effect was of minor influence and they would not additionally contribute to the aim of the simulator. These features include dependence of the plate height equation on k, additional selective detectors, mutual interference of sample components, detector non-linearity, injection errors, stationary phase bleeding, sample component condensation and more stationary phases.

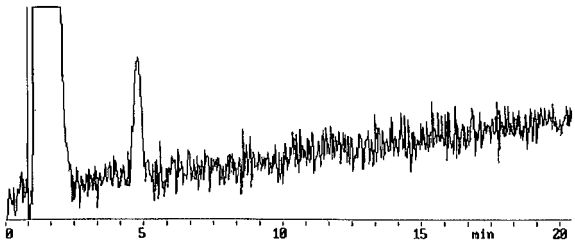

Fig. 2. A number of optional parameters, such as noise, drift, spikes and tailing, can produce complicated looking chromatograms that can be used to illustrate aspects of detection limits.

Concerning the range allowed for different variables, values can in principle be chosen that would in practice lead to unsatisfactory performance. Consider, for instance, the possibility of heavily overloading a capillary column with tetradecane at 50°C. This has not been prohibited by the simulator as good use should be made of the possibility to make mistakes, an obvious advantage over a real instrument. The intelligence required by the program to prohibit such actions by the user is considerable and should be thoroughly tested. Otherwise it would severely limit the flexibility of the program.

RESULTS AND DISCUSSION

Use of GCSIM in lectures and demonstrations

Some features of the simulator were incorporated with the purpose of speeding up the demonstration of various effects in GC. Load and Save options enable the user to prepare examples to illustrate these effects. The quickest way to show previously prepared results is by means of Save Chromatogram and Load Chromatogram as no calculation is necessary. A chromatogram thus stored takes up less than 3 kbyte of memory. Details on how the chromatogram was obtained are not saved, however, except in the .REG file.

In the case of Save/Load of Parameters or Samples, however, these details are included but recalculation prior to display is necessary. When using a coprocessor this takes only a few seconds. Without a coprocessor and calculating temperature pro-

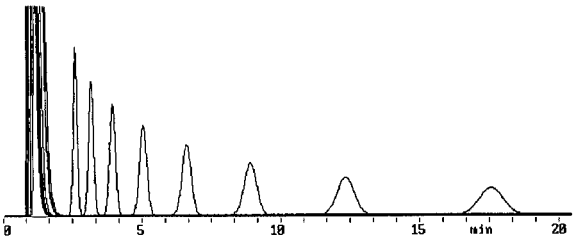

Fig. 3. With the Option Erase off, chromatograms can be superimposed. The example shows the influence of temperature in 10°C increments on the retention of octane on a packed Apiezon column of 2 m length, with helium at 1 bar inlet pressure.

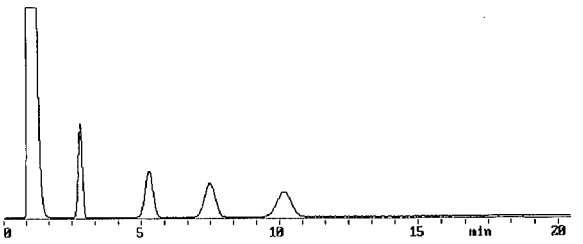

Fig. 5. As Fig. 4, with the same elution order but higher selectivity using Carbowax as a stationary phase under otherwise identical conditions.

gramming, calculation times of up to 20 s can be a problem in an otherwise rapid demonstration. Saving instrumental parameters or sample compositions requires less than 1 kbyte of memory each. A collection of most commonly used examples can therefore be included on the GCSIM diskette.

For comparison of chromatograms, the option Erase may be useful. In this instance, the previously shown chromatogram is not erased. Fig. 3 shows an example of the non-linear dependence of k on T. In this example octane is analysed at different temperatures. Also illustrated by Fig. 3 is the principle of peak broadening and decreasing peak height at increasing retention times. At low concentrations, the detector attenuation can be decreased to visualize the disappearance of the peak into the noise on decreasing the temperature. The application of a simple rectangular moving average noise filter can be shown to give some improvement of the signal-to-noise ratio.

A third example is shown in Figs. 4 and 5 where, at the touch of a key, the selectivity of the stationary phase is illustrated by the analysis of butanols. The elution order is the same (it would have required a number of experiments to verify this in reality), but the selectivity is greatly improved when switching to a polar stationary phase.

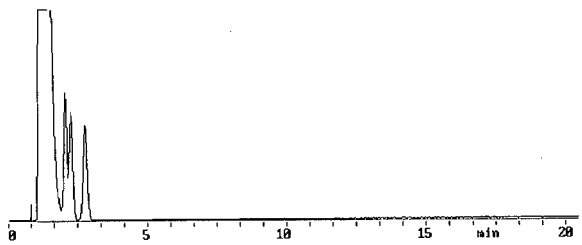

Fig. 4. Analysis of *tert.-*, *sec.-*, iso- and *n*-butanol on a 2-m packed Apiezon column at 90°C, with helium at 1 bar inlet pressure and FID.

A comparison of packed and capillary columns easily shows the effect of plate number and phase ratio on the elution profile of a mixture. In this instance, the other instrumental parameters switch to their default values, which are different for packed and capillary columns.

Use of GCSIM in a practical course

This computer program is not intended to replace all gas chromatographs in the instruction laboratory by PC's, although this would certainly be cheaper. It will be shown, however, that the simulator as a supplemental tool can provide experimental results in a very short time. In a try-out at the Eindhoven University of Technology, fifteen students in their second year first attended a 6-h series of lectures on GC theory, followed by a practical course using the simulator for a total of 7 h during two afternoons.

The practical course consisted of a number of experiments with GCSIM. The procedure was as follows. A course manual contains short descriptions of certain phenomena in GC and corresponding experiments to be carried out. First, instrumental parameters for that experiment are loaded, then a sample composition is chosen. The actual experiment consisted of changing certain instrumental and sample parameters. The values obtained are then put in a graph, using forms provided. The results are interpreted by answering a few questions on the subject.

The following experiments were included: (1) de-

pendence of k on T; (2) calibration, dynamic range, detection limit; (3) effect of phase ratio on retention; (4) effect of plate number on resolution; (5) effect of stationary phase type on selectivity; (6) analysing homologous series; (7) specific detector response for FID and TCD; (8) effect of linear gas velocity on plate height; (9) optimizing separation with and without temperature programming; and (10) comparison of packed and capillary columns. These are only some of the possibilities for practical course subjects. Tables I and II can be used to design additional subjects.

As an example, a description of experiment 4 from the course manual is given below:

"As indicated in the lecture, a difficult separation requires more plates than an easy one. The concept of Resolution was introduced to quantify the separation of two peaks at given k values (Selectivity). Load parameter file 4 (this is a short packed column) and choose a sample consisting of 10 ppm each of 3-hexanol and 2-hexanol dissolved in acetone. The resolution will now be measured as a function of the plate number. The plate number depends on the column length and the linear gas velocity. Change the column length and gas inlet pressure in such a range that plate numbers between 500 and 2000 are obtained.

Plot the results of resolution and plate number on sheet no. 4, which has double log scales (see Fig. 6).

Answer the following questions:

—which two parameter exponential relation describes this dependence?

—what plate number would be required for unit resolution?"

The resulting graph fits a straight line that can be extrapolated to unit resolution. Linear curve fitting yields a value of *ca.* 0.5 for the slope of the line, which means resolution improves with the square root of the plate number, as expected.

As a second example of a practical course subject, an optimization experiment is presented. Here, the sequence of loading parameters first, sample next is important. The underlying idea is that the initial conditions are to be identical for all students and of course far from optimized. The registration files are used here for two purposes: (1) it can be checked if the course manual instructions were adhered to and (2) exact reconstruction of the actions by the students is possible.

As a first optimizing experiment, only a limited number of parameters were allowed to be changed. The reason was that otherwise most students would very soon switch to a 30-m capillary with temperature programming, thus short-cutting the optimization process. In most instances, this would also lead to an over-specified instrument.

In the initial chromatogram, some peaks are outside the time window displayed and others overlap. At this stage, additional information on sample component properties could be given. In our try-

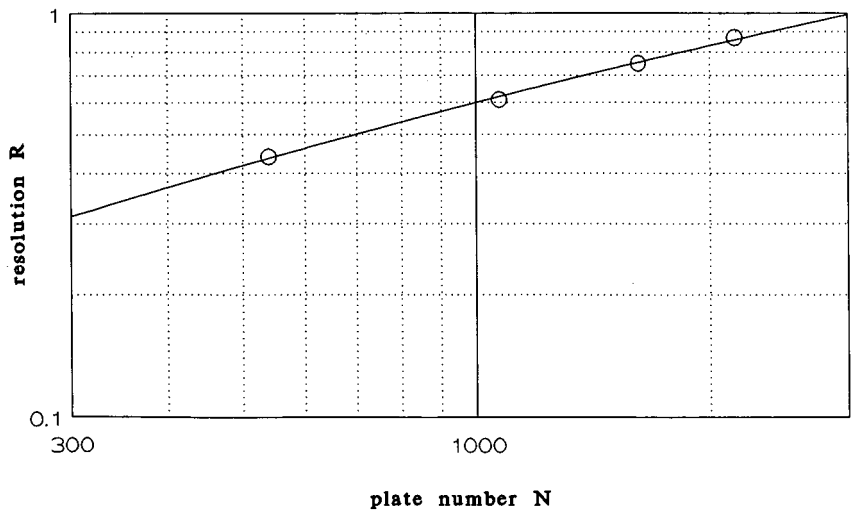

Fig. 6. Resolution of 3- and 2-hexanol on a packed Carbowax column as a function of plate number.

out, we decided not to do this, resulting in a more or less trial-and-error approach. The choice of the parameters changed was shown to give a good indication of whether the concept of GC selectivity was understood.

Good first guesses were (if allowed): a stationary phase change and a steep temperature gradient, provided the initial linear velocity was not too low. Less smart students were seen playing with parameters of minor importance instead. In this context, one additional option should be mentioned, namely the scoring facility, which permits the introduction of a game element in optimizing experiments. With the scoring option turned on, each change in a parameter results in a change in the score variable, shown at the lower left-hand corner of the screen. Some changes, however, are more expensive than others. Evidently, selecting a capillary column is more expensive than doubling the length of a packed column. If, in addition to a good separation, a minimum score is required, students are forced to think before acting.

CONCLUSIONS

It was shown that the instrument simulator GCSIM can provide graphic illustrations of numerous phenomena in GC, for both lectures and demonstrations but also for written course material. A large number of experiments can be simulated in a very short time when used in a practical course. However, we advise against replacing all gas chromatographs in the instruction laboratory. As a first acquaintance with instrumentation, we recommend that the students perform a few syringe injections into a simple gas chromatograph, and wait for peaks to appear ("Sir, is this the last one?"). Waiting for the end of chromatograms takes a lot of practical course time, a problem largely eliminated by additional use of GCSIM in such a course.

ACKNOWLEDGEMENT

The author is indebted to P. A. Leclercq, Eindhoven University of Technology, for reading the manuscript.

REFERENCES

1 J. W. Moore, *J. Chem. Educ.*, 65 (1988) 1051.
2 A. Ghosh, D. S. Morison and R. J. Anderegg, *J. Chem. Educ.*, 65 (1988) A154.
3 E. V. Dose, *Anal. Chem.*, 59 (1987) 2414, and references cited therein.
4 D. E. Bautz, J. W. Dolan, W. D. Raddatz and L. R. Snyder, *Anal. Chem.*, 62 (1990) 1560.
5 E. Heftmann (Editor), *Chromatography, Part A (Journal of Chromatography Library,* Vol. 22A), Elsevier, Amsterdam, 1983.
6 W. O. McReynolds, *Gas Chromatographic Retention Data,* Preston Technical Abstracts, Evanston, IL, 1966.

Journal of Chromatography, 588 (1991) 225–230
Elsevier Science Publishers B.V., Amsterdam

CHROM. 23 669

Gas chromatographic properties of immobilized poly(ethylene glycol) stationary phases

Miroslav Cigánek*, Milan Dressler and Jiří Teplý

Institute of Analytical Chemistry, Czechoslovak Academy of Sciences, Veveří 97, 611 42 Brno (Czechoslovakia)

(First received September 24th, 1990; revised manuscript received July 26th, 1991)

ABSTRACT

Optimization of the preparation of immobilized poly(ethylene glycol) on Chromosorb W AW was carried out. The optimum concentration ratio of Carbowax 20M and Desmodur L75 in moles lies in the range 1:8 to 1:14. The effect of three different procedures of Chromosorb W AW treatment on the chromatographic properties of the packing material was investigated. Conditioning under a nitrogen stream at 240°C for 4 h appears to be the best. Carbowax 20M immobilized on the support prepared in this way also showed the best stability towards washing with different solvents. A new procedure was used for testing the thermal stability of the stationary phase, which also takes into consideration the extent of the phase immobilization on the support.

INTRODUCTION

Poly(ethylene glycol) (PEG) phases are used in gas chromatography (GC) for their selectivity, permitting separation of polar compounds with similar boiling points which cannot be separated on silicone phases [1]. Owing to their chemical structure, PEG phases have low thermal stability (about 220°C). However, their degradation occurs in chromatographic columns at substantially lower temperatures [2,3]. A high minimum working temperature (about 70°C) and a low oxidation stability are other disadvantages which result in a short service life of the stationary phases in the chromatographic column. These drawbacks can be eliminated by immobilizing PEG phases.

In capillary columns PEG phases have been immobilized by radical cross-linking with organic peroxides [4–6] or dibutyltin dilaurate [7] and by chemical reaction between the terminal OH groups of Carbowax 20M and NCO groups of isocyanates, producing urethane bonds [8,9]. The last reaction was also used by us to prepare immobilized Carbowax 20M on the chromatographic support.

In the present work the optimization of the preparation of immobilized Carbowax 20M on the chromatographic support is described. The influence of the concentration of the cross-linking agent, various procedures for the support surface treatment, extractability of the immobilized phase film with different solvents and thermal stability of the packing material depending on washing with solvents were studied.

EXPERIMENTAL

Chemicals and materials

The following major chemicals were used: Carbowax 20M (Carlo Erba, Italy), γ-glycidoxypropyltrimethoxysilane (Union Carbide, USA), Desmodur L75 (Plurisocyanate based on toluene diisocyanate, Bayer, Germany) and DABCO R-8020 [1,4-diazobicyclo-(2,2,2)-octane, Air Products, Chemical Group, Paulsboro, NJ, USA]. Other chemicals of analytical reagent grade were supplied by Lachema (Brno, Czechoslovakia). Acid-washed Chromosorb W (80–100 mesh) was supplied by Becker (Delft, Netherlands). The measurements were carried out with glass columns of 1.2 m × 3 mm I.D., using a Chrom 5 gas chromatograph (Laboratory Instruments, Prague, Czechoslovakia).

0021-9673/91/$03.50

Procedure

Chromosorb W AW was always first heated at 200°C for 4 h. Three procedures were used for the modification of the support surface.

AW: the chromatographic support (Chromosorb) was conditioned at 240°C under a nitrogen stream for 4 h.

AUE: the support was modified with a non-extractable layer of PEG film using the procedure described by Aue *et al.* [10].

S: the support was silylated with γ-glycidoxypropyltrimethoxysilane [11].

The S-type support was coated with solutions of various concentrations of Carbowax 20M, Desmodur L75 and DABCO R-8020 in dichloromethane to investigate the effects of the concentration of the cross-linking agent on the degree of immobilization. To study the influence of the modification of the support surface on the extractability of the immobilized PEG film with solvents, AW, AUE and S supports were coated with solutions containing 10% (w/w) Carbowax 20M, 3% (w/w) Desmodur L75 and DABCO R-8020 in dichloromethane (percentages relative to the mass of the support). The immobilization was performed using the procedure previously described [12].

The extractability of the stationary phase film was checked as follows. The packed column was gradually washed with a given volume of an organic solvent. After washing the column with distilled water the column was washed with 5 ml of acetone. After each column washing the remaining solvent was removed from the column by nitrogen flow and the column was conditioned at 200°C for 1 h at a nitrogen flow-rate of 25 ml/min. Changes in the capacity factors of solutes and in column efficiencies were followed.

The thermal stability test of the packing material was performed as follows. The capacity factors of the test solutes and the column efficiencies were measured first. The packed column was then heated at 200°C for 1 h and the capacity factors and the column efficiencies were again measured at a column temperature of 100°C. The column packing was then washed with 30 ml of dichloromethane, the column was conditioned at 200°C for 1 h and the capacity factors and the column efficiencies were again measured at a column temperature of 100°C. The same procedure was repeated at temperature intervals of 20°C up to 320°C.

n-Tridecane, *n*-tetradecane (evaluation of dispersion interactions), 1-heptanol and 1-nonanol (evaluation of interactions with etheric and hydroxyl groups of PEG) were used to test the chromatographic properties of the packing material.

RESULTS AND DISCUSSION

Effect of the cross-linking agent

In earlier work [12] we showed that it is possible to prepare column packings with immobilized PEG. The stoichiometric ratio of Carbowax 20M to Desmodur L75 cross-linking agent is 1:0.5 mol (or 1:0.02 g for the cross-linking reaction.

TABLE I

EFFECT OF CROSS-LINKING AGENT CONCENTRATION

n/m = efficiency per 1 m of the column; k' = capacity factor.

Column packing	Ratio Carbowax 20M/Desmodur		*n*-Tetradecane		1-Heptanol	
	w/w (%)	mol/mol	k'	n/m	k'	n/m
1	6:4	1:18	13.6	1870	17.2	1120
2	7:3	1:12	15.8	2460	20.8	1900
3	8:2	1:7	14.3	2240	19.2	1840
4	9:1	1:3	15.0	1460	18.4	1540
5	10:3	1:8	17.5	2600	21.1	2080
6	10:5	1:14	18.5	2450	25.9	1960
7	10:10	1:27	18.3	1720	26.3	370

The capacity factors (k') and the column efficiencies are listed in Table I for the packings prepared from solutions of different concentrations of Carbowax 20M and cross-linking agent (packing 1–4) and from solutions containing a constant concentration of Carbowax 20M (10%, w/w) and different concentrations of the cross-linking agent (packing 5–7). The ratios of the solution concentrations expressed in weight per cent relative to the mass of support are listed in the second column. The same data expressed in moles are listed in the third column (the value 1800 was taken as an average molecular weight of Carbowax 20M). It follows that the optimum ratio of the components of the liquid phase expressed in moles ranges from 1:8 to 1:14. The concentration of the cross-linking agent is about twenty-fold that given by the stoichiometric ratio. A large excess of the cross-linking agent, packings 1 and 7 in Table I, results in a decrease in the column efficiency, particularly for 1-heptanol. An almost six-fold decrease in the column efficiency was observed for packing 7. It is interesting that the optimum concentration ratio of only about 1:6.6 mol [9] was found for similar immobilization in the capillary column.

Column packings 1, 2, 5 and 6 are the most stable against washing. If a large decrease in the capacity factors occurs after washing, the column efficiency usually increases (compare packing materials 3 and 4). A larger decrease in the capacity factors and the column efficiencies occurs with 1-heptanol. On packing material 7 the alcohol peak is asymmetric and broad (already the efficiency of the column which was not washed is very low —see Table I).

Effect of support surface modification

The properties of the support before being coated with the liquid stationary phase substantially affect the chromatographic properties of the obtained packing material.

The capacity factors, the column efficiencies and asymmetry factors (TF) for our three different types of support treatment are listed in Table II. *n*-Tetradecane shows the lowest retention on Chromosorb W AW that was only thermally conditioned (type AW) and the highest on the silylated surface (Type S). At 100°C 1-heptanol does not elute from support AW even within 1 h. At higher temperatures the alcohol peak tails and retention times of peak maxima depend on the amount of alcohol injected. This is because of interaction between the alcohol molecules and the active sites on the support surface. If the support surface is treated with PEG at a high temperature (Type AUE), deactivation of its surface occurs. 1-Heptanol therefore elutes from the column as a narrow peak (compare the column efficiencies and TF). Silylation of the support surface (type S) leads to higher 1-heptanol retentions (more than two-fold) in comparison with the AUE-type support. *n*-Tetradecane retention is similar. The peak tailing intensified and the efficiency decreased. This is obviously because of poorer deactivation of the support surface.

The best deactivation of the support surface is achieved with the AUE support. This agrees with previous observations that a homogeneous inextractable film of PEG decomposition products [10] is created. It was however found that the film formed in this way is not stable at temperatures

TABLE II

EFFECT OF SUPPORT SURFACE MODIFICATION

For AW, AUE, S see text; TF = asymmetry factor (calculated from front and rear halves of the tailing peak, both halves measured at 10% of the peak height above the baseline); x = does not elute (see text).

Support type	*n*-Tetradecane			1-Heptanol		
	k'	n/m	TF	k'	n/m	TF
AW	4.3	1220	123	x	x	x
AUE	6.4	1710	139	7.2	1110	161
S	7.4	730	262	16.7	460	475

TABLE III

EFFECT OF SUPPORT SURFACE MODIFICATION ON EXTRACTABILITY OF IMMOBILIZED CARBOWAX 20M

Solvent: dichloromethane; for CW-AW, CW-AUE, CW-S, see text.

Column packing	Solvent volume (ml)	*n*-Tetradecane		1-Heptanol	
		k'	n/m	k'	n/m
CW-AW	0	18.3	2620	23.2	1960
	30	18.8	2460	23.5	2130
	60	18.7	2510	23.9	2130
	90	18.6	2470	23.1	2120
	120	18.4	2500	22.9	2240
CW-AUE	0	20.8	1260	29.5	1130
	30	20.6	1380	28.1	910
	60	20.1	1700	27.5	960
	90	21.1	1370	29.8	1060
	120	18.8	1620	26.3	1440
CW-S	0	18.0	2500	25.0	1840
	30	18.2	2780	23.3	1530
	60	17.2	2430	22.9	1630
	90	17.2	2630	23.3	1580
	120	16.2	2510	21.6	1340

above 300°C and is very sensitive to oxygen traces in both carrier gas and injected sample [13].

The influence of support surface modification on the extractability with dichloromethane of the immobilized PEG is obvious from Table III. A simultaneous decrease in retention and column efficiency does not occur only on the CA-AW packing. Reduction in the retention of 1-heptanol and *n*-tetradecane to 90% occurs on the CW-AUE packing only after washing with 120 ml of dichloromethane. The column efficiencies remain unchanged. On the CW-S packing, the k' value for *n*-tetradecane decreases to 90% and the efficiency remains unchanged; for 1-heptanol k' decreases to 86% and the efficiency to 70%. The best column efficiency is achieved for 1-heptanol on the CW-AW packing and the worst on CW-AUE. Hence the modifed AW- and S-types supports seem to be suitable for the preparation of the packing with the polar phase. The stabilities of the immobilized phase films towards washing with different solvents are listed in Table IV. The packings were gradually washed with 30 ml of each solvent. Neither retention nor efficiency decreased significantly for CW-AW type (except for acetone and ethanol for *n*-tetradecane). With the CW-S-type support the k' value decreases for *n*-tetradecane to 87% and the efficiency remains unchanged: for 1-heptanol the k' value decreases to 80% and the efficiency to 64% of the original value. The CW-AW packing again seems to be the best.

Thermal stability

Immobilization of the liquid stationary phase contributes significantly to the increase in the thermal stability of the packing. The thermal stability of the stationary phase is usually evaluated with the aid of the so-called maximum operating temperature limit (MAOT) [14]. This procedure has also been used in all known procedures for the evaluation of thermal stabilities of immobilized phases. However, the described procedure does not consider the changes in the phase cross-linking during the time when the column temperature is increased. That is why we have used for the evaluation of the thermal stability the procedure which also takes into account the changes in the immobilization due to thermal stress. We found that the immobilized PEG phases can withstand relatively high temperatures

TABLE IV

EXTRACTABILITY OF IMMOBILIZED CARBOWAX 20M WITH DIFFERENT SOLVENTS

For CW-S, CW-AW, see text.

Solvent	Solvent volume (ml)	*n*-Tetradecane		1-Heptanol	
		CW-S	CW-AW	CW-S	CW-AW
Capacity factors					
Dichloromethane	0	18.0	18.3	25.0	23.2
	30	18.2	18.8	23.3	23.5
	60	17.2	18.7	22.9	23.9
	90	17.2	18.6	23.3	23.1
	120	16.2	18.4	21.6	22.9
Acetone	30	16.3	18.3	21.4	23.3
	60	16.8	18.9	21.9	24.6
Ethanol	30	16.8	18.5	22.1	23.6
	60	16.8	19.11	20.4	24.5
Water	30	16.0	17.8	19.8	22.6
	60	15.6	18.3	19.9	22.6
Column efficiency					
Dichloromethane	0	2500	2620	1840	1960
	30	2780	2460	1530	2130
	60	2430	2510	1630	2130
	90	2630	2470	1580	2120
	120	2510	2500	1340	2240
Acetone	30	2250	2350	1350	1850
	60	2680	2310	1590	1780
Ethanol	30	2540	2160	1310	2050
	60	2440	2300	1390	2430
Water	30	2220	2860	1210	2300
	60	2510	2610	1180	2060

without significant changes in the values of k' and the column efficiencies, but, after washing with the solvent, some phase destruction occurs. This fact is demonstrated by Table V. After heating the packing at 310°C for 30 min, the value of k' did not change for *n*-tridecane and 1-nonanol, and the efficiencies even increased. However, after washing the column with the solvent, the value of k' for *n*-tridecane decreased to 80% and the efficiency remained unchanged. For 1-nonanol the k' value decreased to 75% and the efficiency to 60%. After heating the column at 330°C for the next 30 min the situation was similar. Further decrease in the k' value and in the column efficiency only occurred after washing with solvent. The column efficiency decreased to 32% of the original value for 1-nonanol.

TABLE V

THERMAL STABILITY

Packing: CW-S.

Treatment	*n*-Tridecane		1-Nonanol	
	k'	n/m	k'	n/m
–	7.5	2170	51.0	1800
310°C	8.0	2550	50.5	2230
20 ml	6.5	2600	38.7	1320
330°C	5.8	2700	24.0	1310
20 ml	5.5	1250	30.9	570

Based on the above findings, the test of thermal stability of the immobilized phase was performed as follows. After heating the column at the given temperature and after testing its chromatographic properties, the column was washed with 30 ml of dichloromethane and retested. The results of the test are illustrated in Fig. 1 for all packings. The values of k' decrease with increasing test temper-

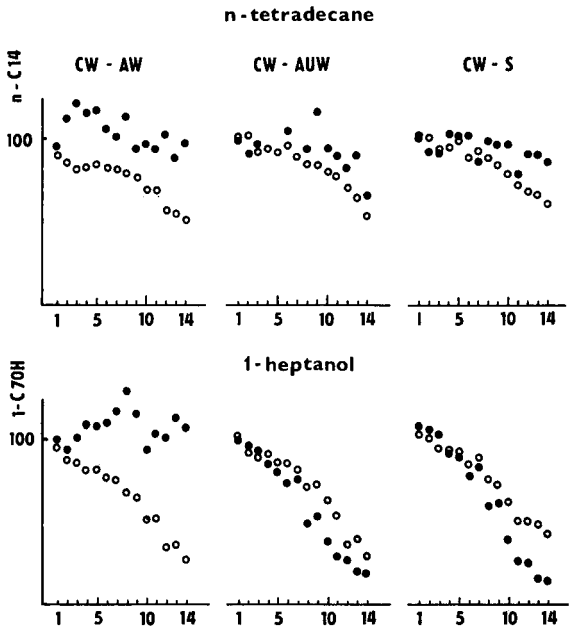

Fig. 1. Stationary phase thermal stability. (○) z_k and (●) z_n designated the ratio (%; of, respectively, the capacity factors and column efficiencies for solutes after washing with dichloromethane to their values before the washing (for *n*-tetradecane and 1-heptanol). 1 = 200°C; 2 = 200°C and 30 ml of dichloromethane; 3 = 220°C; 4 = 220°C and 30 ml; 5 = 240°C; 6 = 240°C and 30 ml; 7 = 260°C; 8 = 260°C and 30 ml; 9 = 280°C; 10 = 280°C and 30 ml; 11 = 300°C; 12 = 300°C and 30 ml; 13 = 320°C; 14 = 320°C and 30 ml.

ature for all packing types. The decrease occurs at temperatures between 260 and 280°C. The decrease in the k' value for 1-heptanol is greater than for *n*-tetradecane. With the packings of CW-AUE and CW-S types there is also a decrease in efficiency. This is obvious first of all from the comparison of z_n values for 1-heptanol. While the efficiency decreased to 14 and 18% of the original value at the end of the test for CW-S and CW-AUE, respectively, it remained unchanged for the CW-AW packing. The results of the thermal stability test of the immobilized PEG suggest that, under given chromatographic conditions, the maximum temperature at which no destruction of immobilized PEG occurs with this packing is 260–280°C. It follows from the above experiments that it is necessary to differentiate two types of thermal stability test of the column packing. One evaluates the packing by the phase bleeding only. The other simultaneously also evaluates the state of the phase immobilization on the support.

CONCLUSIONS

The procedure by which Chromosorb W AW is thermally treated at 240°C for 4 h and then coated with a mixture of 10% (w/w) of Carbowax 20M, 3% of Desmodur 75L and 0.02% (w/w) DABCO R-8020 in dichloromethane is the optimum technique for the preparation of immobilized PEG on the support. This fact is confirmed by the results of the tests of the thermal stability of the phase and its extractability with a solvent.

REFERENCES

1 I. A. Yancey, *J. Chromatogr. Sci.*, 23 (1985) 370.
2 R. A. Keller, R. Bate, B. Costa and P. Forman, *J. Chromatogr.*, 8 (1962) 157.
3 J. R. Conder, N. A. Fruitwala and M. K. Shingari, *J. Chromatogr.*, 269 (1983) 171.
4 V. Martinez de la Gandara, J. Danz and I. Martinez-Castro, *J. High Resolut. Chromatogr. Chromatogr. Commun.*, 7 (1984) 44.
5 J. Buijten, L. Blomberg, K. Markides and T. Wännman, *J. Chromatogr.*, 268 (1983) 387.
6 M. V. Russo, G. C. Goretti and A. Liberti, *J. High Resolut. Chromatrogr. Chromatogr. Commun.*, 8 (1985) 535.
7 H. Traitler, L. Kolarovic and A. Sorio, *J. Chromatogr.*, 279 (1983) 69.
8 M. Horká, V. Kahle, K. Janák and K. Tesařík, *J. High Resolut. Chromatogr. Chromatogr. Commun.*, 8 (1985) 259.
9 M. Horká, V. Kahle, K. Janák and K. Tesařík, *Chromatographia*, 21 (1986) 454.
10 W. A. Aue, C. R. Hastings and S. Kapila, *J. Chromatogr.*, 77 (1973) 299.
11 M. Horká, K. Janák, V. Kahle and K. Tesařík, *Chem. Listy*, 79 (1986) 1309.
12 M. Cigánek, M. Dressler and J. Teplý, *Chromatographia*, 27 (1989) 109.
13 M. M. Daniewski and W. A. Aue, *J. Chromatogr.*, 147 (1978) 119.
14 Z. Juvancz, M. A. Pulsipher, B. J. Tarbet, M. M. Schirmer, R. S. Johnson, K. E. Markides, J. S. Bradshaw and M. L. Lee, *J. Microcolumn Sep.*, 1 (1989) 142.

Journal of Chromatography, 588 (1991) 231–237
Elsevier Science Publishers B.V., Amsterdam

CHROM. 23 620

Comparison of four liquid crystal stationary phases used above and below their melting point temperatures for the gas chromatography of some volatile oil constituents

T. J. Betts

School of Pharmacy, Curtin University of Technology, G.P.O. Box U1987, Perth, Western Australia 6001 (Australia)

(First received May 24th, 1991; revised manuscript received July 6th, 1991)

ABSTRACT

All four liquid crystal stationary phases used for the gas chromatography of volatile oil constituents function below their melting points, but the azoxydiphenetole (ADP)-packed column does not exhibit reliable supercooling. Safrole always preceding anethole provides an identifying test for these liquid crystal phases. Various distinctive shifts in solute sequence were noted for each phase. An "MPMS" polysiloxane capillary gave the highest relative retention times of the four phases and is required for satisfactory peaks of monoterpenes with a terminal polar group, like geraniol. It is also good for polar aromatics like thymol, although bis(methoxybenzylidineanil-chloroaniline) in a packed column is an alternative. Linear ether aromatics like estragole can be studied on all four phases, which have this structure themselves. Whilst ADP may be best for terpene hydrocarbons, especially caryophyllene, bis(methoxybenzylidineanil-bi-toluidine) is the best general purpose liquid crystal for packed columns.

INTRODUCTION

We have reported on the use of liquid crystal stationary phases for the gas chromatography (GC) of some constituents of volatile oils. Their organised nematic fluid state may offer separation advantages by retaining molecules of particular shapes. Bis-(methoxybenzylidineanil-chloroaniline) [$(MBCA)_2$; Fig. 1] was chosen for initial studies [1] as it has a moderate melting point around 150°C. The long nematic range of this substance (190°C) before it changed to a true isotropic liquid was an attraction, but decomposition of the $(MBCA)_2$ severely limits its use to below 190°C. This first work did not reveal the complexity of the response of some liquid crystals, which was appreciated only during detailed work with another anil, bis(methoxybenzylidine-anil-bi-toluidine) [$(MBT)_2$], which has a higher melting point around 180°C (Fig. 1). This second study [2] revealed that $(MBT)_2$, when heated from cold for the first time, had a "naive" condition giving low relative retention times to linalol which sharply increased as the melting point of the $(MBT)_2$ was passed. With further increase of temperature, these values gradually decreased, but could be increased (or maintained) by supercooling the liquid crystal. Cooling to room temperature or below restored a lower value state, which gave higher relative retention times than the naive column, but below the supercooled results. A changing unmelted *versus* melted/supercooled condition exists.

It seemed of interest to check whether these changes of liquid crystal state as a stationary phase applied to $(MBCA)_2$ and to other liquid crystals, for example with a lower melting point and a short nematic span [azoxydiphenetole (ADP) with only a 30°C range (Fig. 1)] and with a polysiloxane liquid crystal commercially available in capillaries. This "MPMS" (Fig. 1) represents a modern liquid crystal, with side-chains attached to a polysiloxane backbone, whilst ADP is like the first azoxy liquid crystals employed by Dewar and Schroeder [3] for

0021-9673/91/$03.50

Acronym of liquid cryst. & abbreviation		Chemical formula	Chemical feature	Melting point (L) and transition temp.°C	
$(MBCA)_2$	C	$(CH_3O—C_6H_4—CH=N—C_6H_3Cl—)_2$	anil dimer	154	344
$(MBT)_2$	T	$(CH_3O—C_6H_4—CH=N—C_6H_4—CH_2—)_2$	anil dimer	181	320
ADP	D	$(C_2H_5O—C_6H_4—N=)_2\rightarrow O$	azoxy	138	168
'MPMS'	S	$(CH_3O—(C_6H_4)_2\text{-}O\text{-}CO—C_6H_4—O—(CH_2)_3—SiO—CH_3)_n$	ester polymer	145?	320

Fig. 1. Details of liquid crystal stationary phases used. The abbreviations are used in Figs. 2 and 3. These substances function as GC stationary phases below their melting points. The two anils decompose before they reach their transition points to give normal liquids. MPMS details are from ref. 10.

the GC of disubstituted benzenes. Finkelmann and Laub [4] first synthesised a mesogenic polymeric methyl siloxane in 1982, and MPMS has recently been used to separate polycyclic aromatics [5]. It has already been shown [2] that supercooled $(MBT)_2$ can be used advantageously for volatile oil studies, so this condition was investigated with the other three phases. ADP also allowed observations when it was a true liquid and no longer a liquid crystal.

EXPERIMENTAL

Apparatus

A Hewlett-Packard 3380A integrator/recorder was used with (a) the MPMS capillary in a Hewlett-Packard 5790A gas chromatograph fitted with a flame ionisation detector, capillary control unit and splitter injection port in split mode or (b) the packed columns in a Pye GCD gas chromatograph fitted with a flame ionisation detector.

An MPMS Heliflex fused-silica capillary (Alltech Assoc., Deerfield, IL, USA), 25 m × 0.25 mm I.D., was used. Test conditions imply it had been checked at 265°C.

Two 3% ADP-packed columns were used, 1.5 m × 4 or 2 mm I.D. The weighed ADP was dissolved in dichloromethane and taken to dryness in a rotary evaporator with weighed Chromosorb W AW 80–100 mesh for packing. No preheating was used before the first results were obtained, but subsequent behaviour of the columns depended on their history of heating.

Four 3% $(MBCA)_2$-packed columns were used, all 1.5 × 4 mm I.D., prepared as for ADP. These showed substantial changes in behaviour with use.

One 3% $(MBT)_2$-packed column was used, no longer naive as it has been used previously [2].

Operating conditions are given in Tables I–IV, observing the GCD oven temperatures with a Technoterm 7300 probe.

Materials and methods

ADP was obtained from TCI (Tokyo, Japan). As were $(MBCA)_2$ and $(MBT)_2$, see refs. 1 and 2, respectively. Formulae details are shown in Fig. 1.

Anethole, cineole, estragole (4-allylanisole), geraniol, linalol and thymol were from Sigma. Also used were α-terpineol (TCI), caryophyllene (Koch-Light), limonene (BDH), safrole (Fritzsche) and cuminal (*p*-isopropylbenzaldehyde, Eastman). Repeated injections were made from a microsyringe which had been filled then "emptied" of these solutes.

RESULTS AND DISCUSSION

Results are presented in the tables and in Figs. 2 and 3. $(MBCA)_2$ and $(MBT)_2$ observations are best made on a column heated above the melting point of the liquid crystal and cooled to the desired temperature (supercooling). However, values on heating a naive (never used before) column of $(MBCA)_2$ and for heating a mature $(MBT)_2$ column are given. These supplement results previously published in refs. 1 and 2. In contrast, ADP is best used by heating from cold, as it does not supercool reliably. Owing to the design of the 5790A gas chromatograph the MPMS capillary could not be cooled slowly (less than 5°C/min is recommended) so it could only be observed in the heating mode, rising to the desired temperature at 4.5°C/min.

TABLE I

RELATIVE RETENTION TIMES (LINALOL = 1.00) ON A PACKED COLUMN OF 3% ADP HEATED TO ISOTHERMAL OPERATING CONDITIONS

Mobile phase, nitrogen at a flow-rate of 20–27 ml/min at the flame ionisation detector outlet. Values are averages of two or more observations. Values in italics are "out of sequence" (descending) at the temperature given and indicate a solute "shift" in relation to subsequent solutes.

Solute	Nominal column temperature (°C) *heated* from lower temperature											
	111	120	125	130	135 *m*	140	150[a]	165 *t*	170[b]	174[b]	186[b]	
Anethole			*1.11*	*1.28*		6.17		5.28	4.50			
Cuminal			2.71	2.81		4.64		4.20				
Safrole	0.63	*0.87*	3.37[c] / *0.94*	*1.09*	2.34	4.22	4.21	3.83		3.52	3.08	
α-Terpineol			2.46	2.41		2.59	2.50	*2.31*	2.27			
Caryophyllene		0.99		1.47		*2.22*	2.52	3.00				
Estragole	0.38	0.52	2.15[c] / 0.57	0.86	1.41	2.50	2.50	2.26		2.06	1.86	
Cineole		*0.30*[c] / 0.24										
Limonene		0.34[c] / 0.18										

[a] Typical holdup time 0.33 min; linalol retention time 0.50 min.
[b] Temperatures above the transition temperature (*t*) of ADP to a normal liquid are not recommended as column deterioration may result.
[c] Values only obtained on slow cooling (4°C/min) from above the melting point of ADP (*m*).

TABLE II

RELATIVE RETENTION TIMES (LINALOL = 1.00) ON A PACKED COLUMN OF 3% $(MBCA)_2$ COOLED TO ISOTHERMAL OPERATING CONDITIONS

Mobile phase, nitrogen at a flow-rate of 6–10 ml/min at the flame ionisation detector outlet. Values are averages of two or more observations. Values in italics are "out of sequence" (descending) at the temperature given and indicate a solute "shift" in relation to subsequent solutes.

Solute	Nominal column temperature (°C) *cooled* from above the melting point (*m*)											
	122	125	130	135	140	145	150 *m*	160[a]	170	175	180	190[e]
Thymol							3.72[b]	3.62		*3.24*		*3.02*
Cuminal		3.65 / 3.22[c]		3.38[c]	3.60	3.61	3.52	3.48[b]	3.35	*3.25*[b]	*3.20*	3.64
Anethole	3.73	3.64	3.60 / 2.27[c]	3.57[b]	3.53 / 2.55[c]	3.51 / 3.04[c]	3.54[b,d] / 3.22[c]	3.44[b]		3.41	3.30	3.58
Safrole	2.76	2.69	*1.69*[c]	2.67 / *1.78*[c]	2.64		2.57	2.54	2.55	2.52	2.42	2.62
Caryophyllene						2.53		2.51		2.43		
α-Terpineol			2.29 / 2.11[c]	2.32	2.32	2.31	2.29	2.21	2.19		2.06	
Estragole	1.56		1.53 / 1.00[c]	1.57	1.55 / 1.14[c]	1.20[c]	1.57 / 1.43[c]	1.57[b]		1.56	1.52	1.80
Cineole			0.38 / 0.38[c]	0.39			0.41[b]	0.48		0.48		0.56
Limonene			0.27 / 0.27[c]				0.30			0.36		

[a] Typical holdup time 0.90 min; linalol retention time 0.65 min.
[b] Results not within previously published ranges [1], probably the consequence of not overheating $(MBCA)_2$ here, see footnote *e*.
[c] Values only obtained on initial heating of a naive column.
[d] Unusually high value of 3.64 sometimes observed for anethole at 150°C.
[e] Temperature not recommended as sharp increases in values suggest decomposition of the liquid crystal.

TABLE III

RELATIVE RETENTION TIMES (LINALOL 1.00) ON A CAPILLARY OF MPMS HEATED TO ISOTHERMAL OPERATING CONDITIONS

Mobile phase, helium at a flow-rate of about 0.75 ml/min at the flame ionisation detector outlet. Values are averages of two or more observations. Values in italics are "out of sequence" (descending) at the temperature given and indicate a solute "shift" in relation to subsequent solutes. *m*? = Approximate melting point of the liquid crystal.

Solute	Nominal capillary temperature (°C) *heated* from lower temperature					
	100	120	140[a]	145 *m*?	150	160
Anethole		9.83	8.61		7.60	
Thymol					6.20	
Safrole	6.44	6.32	5.64	5.48	5.21	*4.86*
Cuminal		5.91	5.50	5.48	5.21	4.97
Caryophyllene		3.82	3.47	3.44	3.26	3.12
Estragole	*3.49*	*3.36*	3.18	3.13	3.03	2.95
Geraniol	3.92	3.45	3.06	2.88	2.58	2.68
α-Terpineol	2.86	2.76	2.68	2.61	2.54	2.36
Limonene		0.60				0.75
Cineole		0.53				0.75

[a] Typical holdup time 1.40 min; linalol retention time 0.20 min.

TABLE IV

RELATIVE RETENTION TIMES (LINALOL = 1.00) ON A PACKED COLUMN OF 3% $(MBT)_2$ HEATED TO ISOTHERMAL OPERATING CONDITIONS

Mobile phase, nitrogen at a flow-rate of 7–10 ml/min at the flame ionisation detector outlet. Values are averages of two or more observations. For more results see ref. 2. Values in italics are "out of sequence" (descending) at the temperature given and indicate a solute "shift" in relation to subsequent solutes.

Solute	Nominal column temperature (°C) *heating mature column* from lower temperature				
	150	160[a]	175 *m*	185	200
Safrole [2]	4.58[b] *2.67*	4.46[b] 2.93	4.24[b]		4.10
Geraniol	4.27[b] 3.85		3.29	3.38	
Estragole [2]	2.83[b] *1.70*	2.80[b] *1.79*	2.75[b]		2.61
Caryophyllene	2.18[b,c] 2.87	2.33[b,c] 2.80	2.41	2.28	2.22
Cineole	*0.35*[b,c] 0.41	*0.43*[b] 0.43		0.49	
Limonene	0.42[b] 0.34	0.49[b] 0.39			

[a] Typical holdup time 0.60 min; linalol retention time 0.20 min.
[b] Values only obtained on cooling from above the melting point (*m*) of $(MBT)_2$.
[c] Values lower than when column is heated, a phenomenon not previously observed.

This discussion draws on comments made earlier when studying packed columns of $(MBT)_2$. The previously recorded [2] sequence of the aromatics estragole (quickest)–safrole–cuminal can be seen on all four liquid crystal phases, although only on MPMS at high temperatures (160°C or more) (see Table III). On the MPMS capillary safrole and cuminal are close together, but with cuminal ahead of safrole below 145°C. This safrole–cuminal shift (see Fig. 3) is not shown by the three packed columns. Thymol gives no results on ADP but it comes after cuminal on the other liquid crystals (see Tables II and III and ref. 2).

Fig. 2 (plot D^1) shows that the solute estragole, on a packed ADP column heated up to 125°C from room temperature, gives relative retention times to linalol quite close to those on $(MBT)_2$, around 0.5 (plot T^1). These values then rise quite sharply as the melting point of this liquid crystal (138°C) is approached, and are about 2.5 at 140°C, which is almost the value on supercooled $(MBT)_2$ at this temperature [2]. ADP exhibits the most rapid large increase in relative retention times seen on a packed liquid crystal column. With temperature further increasing above 150°C (plot D) the values fall away to below 2 more rapidly than on $(MBT)_2$ (plot T) and without any change to the plot as ADP passes its transition point (168°C) when it changes from a liquid crystalline state to a normal isotropic liquid. The supercooled condition, which is easily obtained on $(MBT)_2$, can only be seen on ADP if it is slowly cooled (at 4°C/min) to 125°C. Even then, supercooled ADP gives lower values than in its true liquid crystal condition [unlike $(MBT)_2$ or $(MBCA)_2$, plots T and C, respectively] and tends to revert to the naive low retention times seen on unmelted ADP. It is unwise to take this liquid crystal above its transition point, as on cooling a "gummed up" inferior column may result and there are no advantages in using it as a true liquid. Transition points

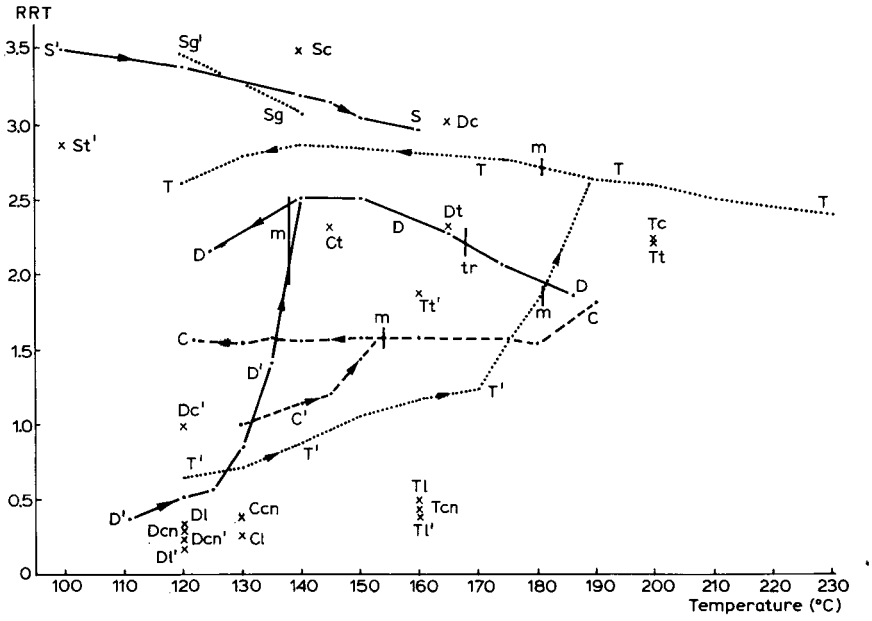

Fig. 2. Plots (connected points) at various temperatures (°C) of relative retention times for estragole against linalol (1.00) on the four liquid crystal columns. Crosses (unconnected) are selected values for some other solutes against linalol. C = dashes connecting estragole results on $(MBCA)_2$; D = lines connecting estragole results on ADP; S = lines connecting estragole results on MPMS capillary; T = dots connecting estragole results on $(MBT)_2$ taken from ref. 2. Suffix ′ = results on unmelted liquid crystal (C′ and T′ being naive). c = Caryophyllene; cn = cineole; g = geraniol; l = limonene; m = melting point of the liquid crystal; t = α-terpineol; tr = transition point of the liquid crystal to normal liquid (only D). Sc is thus the caryophyllene result on MPMS, etc.

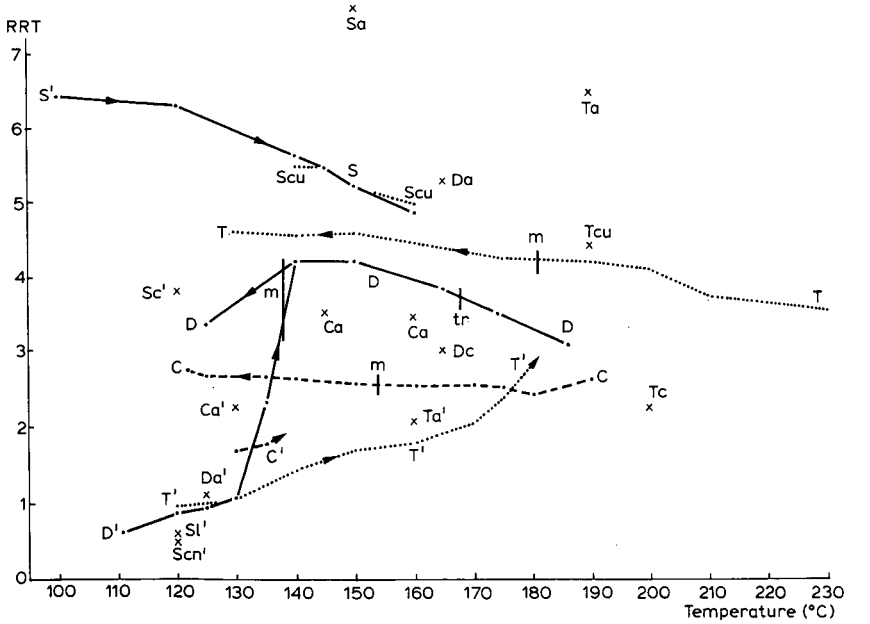

Fig. 3. Plots (connected points) at various temperatures (°C) of relative retention times for safrole against linalol (1.00) on the four liquid crystal columns. C = dashes connecting safrole results on $(MBCA)_2$; D = lines connecting safrole results on ADP; S = lines connecting safrole results on MPMS capillary; T = dots connecting safrole results on $(MBT)_2$ taken from ref. 2. Otherwise, as for Fig. 2. a = Anethole; cu = cuminal. Ta is thus the anethole result on $(MBT)_2$, and Dc′ is the caryophyllene result on unmelted ADP.

were not passed with $(MBT)_2$, $(MBCA)_2$ or MPMS.

Safrole (3,4-methylenedioxyallylbenzene) gives a similar pattern (Fig. 3, plot D^1) on ADP to estragole, with larger relative retention times. These remain below 1 up to 125°C, but rapidly climb to about 4.2 by 140°C, falling away to near 3 past the transition point. Safrole, on this and the other three liquid crystals studied, whether "unmelted", melted or supercooled, is always ahead of anethole (4-propenylanisole), which is the reverse of normal GC phases, and so provides an identifying test for liquid crystals (see Fig. 3, safrole plots and anethole points).

Fig. 2 (plot C) also shows that $(MBCA)_2$, with the solute estragole, gives a greatly contracted version of the situation previously recorded [2] with $(MBT)_2$ (plot T). On naive unmelted $(MBCA)_2$ relative retention times to linalol (C^1) start to rise from unity and level off past the liquid crystal melting point at just under 1.6. These are maintained (plot C) on rapid supercooling, as with $(MBT)_2$ but unlike ADP. Also as with $(MBT)_2$, on cooling down, the $(MBCA)_2$ naive-condition low values are not fully recovered. The only reason for using $(MBCA)_2$ is that it is suitable for some of the more polar aromatic solutes like cinnamal [1]. It is unwise to heat $(MBCA)_2$ above 180°C as an increase in relative retention times (Fig. 2), seen before [1], suggests decomposition has started.

From Figs. 2 and 3, the MPMS capillary plots S show the highest relative retention times for estragole and safrole, respectively, of the four liquid crystals. This capillary gives satisfactory peaks at a lower temperature than the packed columns, and shows, as the temperature increases towards its melting point, a fairly steady decline (not rise) in values towards those given by supercooled $(MBT)_2$ (plots T). MPMS revealed a solute shift involving estragole, not shown by any of the other liquid crystals. Above 130°C geraniol is faster than estragole, but there is a "shift" (see Fig. 2) at lower temperatures to the normal sequence seen on other liquid crystals, even though they yield variable retentions with geraniol which are not given in some tables. Unlike the other three phases, geraniol is always ahead of the sesquiterpene caryophyllene on MPMS (Table III).

The shift terpineol–estragole previously [2] detected on $(MBT)_2$ and indicated by points Tt on Fig. 2 seems exclusive to this. On $(MBCA)_2$ estragole is always ahead of α-terpineol (Table II), whilst the reverse holds for MPMS (Table III). These two solutes have about the same retention on melted ADP (point Dt on Fig. 2), but estragole is well ahead on umelted ADP as the terpenoid α-terpineol keeps a reasonably "constant" retention relative to linalol of about 2.4. The anethole–thymol shift also seen before [2] on $(MBT)_2$ could be detected on $(MBCA)_2$ too (see Table II), but not on the other two liquid crystals, and occurs well above its melting point, unlike on $(MBT)_2$.

Four new shifts of limited occurrence were noted. (a) Limonene typically is faster than cineole on normal GC phases [6], a lyotropic (mixed) liquid crystal [7] and $(MBCA)_2$ (Table II); but the reverse holds after melting and supercooling ADP and $(MBT)_2$ (Tables I and IV and Fig. 2) and is always true for MPMS at low temperatures (Table III and Fig. 3). (b) On MPMS caryophyllene is always faster than safrole (point Sc′ in Fig. 3), but this only applies to $(MBT)_2$ and ADP on melting (Tc and Dc in Fig. 3). Their values are very close on $(MBCA)_2$ (Table II). On normal polar GC phases, caryophyllene is ahead of safrole, although the reverse holds for non-polar phases [8]. (c) An anethole–cuminal shift can be seen on melting ADP and on naive $(MBT)_2$ (see Table I and ref. 2). (d) The fourth shift is another practically unique to $(MBT)_2$ if melted or supercooled, when caryophyllene (Tc, Fig. 2) is ahead of estragole, otherwise their values are close. The reverse applies (see Dc and Sc, Fig. 2) on the other liquid crystals (apart from ADP near 140°C) and on normal GC phases. Both caryophyllene and cineole anomalously show lower relative retention times on supercooling than they do on unmelted $(MBT)_2$ (Table IV).

Like $(MBT)_2$, $(MBCA)_2$ can be used below its melting point, either supercooled or "unmelted". It exhibits the anethole–thymol but not the anethole–terpineol shift [2]; the latter is seen on ADP. However, ADP does not give reliable supercooling and is best used just above its melting point at 140–150°C. MPMS is also best below its "recommended" lower limit of 150°C (just below which temperature it melts) except for polar aromatics like eugenol. Retentions of solutes tend to be variable on MPMS at 150°C or more. It has recently been claimed [9] that polyethyleneglycol 20M can be used

as a stationary phase at 30°C, below its melting point (about 60°C), so this phenomenon may not be peculiar to liquid crystals.

Acyclic monoterpenoids with terminal polar (oxygen function) groups like citral and geraniol do not fit very well into the three non-polymeric liquid crystals, tending to "tail", and should be studied on MPMS. Monoterpenoids with more central (concealed) polar groups like linalol and cyclic α-terpineol give a better liquid crystal "fit" and respond with narrower peaks unless a low temperature is used like 120°C or less on ADP, or 135°C on $(MBCA)_2$. At higher temperatures, the cyclic monoterpenoid perillal with a protruding polar group at one end gives satisfactory peaks. The non-polar, relatively large bicyclic sesquiterpene caryophyllene, however, shows an unusual rapid increase in relative retention times with temperature rise on ADP and can even fit into it at 120°C, possibly better than on MPMS at the same temperature. MPMS is also poor at resolving the pinenes (bicyclic monoterpene hydrocarbons).

All the liquid crystals are well suited to resolving some linear aromatic substances like estragole, safrole and anethole, as might be expected from their linear multi-aromatic structures (Fig. 1). However, thymol and eugenol, with protruding polar oxygen-containing groups are not always handled well; MPMS and $(MBCA)_2$ are the phases of choice here.

ACKNOWLEDGEMENT

Thanks are due to Mr. B. Mackinnon, who prepared the various packed columns.

REFERENCES

1 T. J. Betts, *J. Chromatogr.*, 513 (1990) 311.
2 T. J. Betts, C. A. Moir and A. I. Tassone, *J. Chromatogr.*, 547 (1991) 335.
3 M. J. S. Dewar and J. P. Schroeder, *J. Org. Chem.*, 30 (1965) 3485.
4 H. Finkelmann and R. J. Laub, *Report DOE/ER/10554-25*, Ohio State University, Columbus, OH, 1982; *C.A.*, 98 (1983) 78 678.
5 P. Fernandez and J. M. Bayona, *J. High Resolut. Chromatogr.*, 12 (1989) 802.
6 P. N. Breckler and T. J. Betts, *J. Chromatogr.*, 53 (1970) 163.
7 T. J. Betts, *J. Chromatogr.*, 467 (1989) 272.
8 T. J. Betts, *J. Chromatogr.*, 449 (1988) 312.
9 K. Surowiec and J. Rayss, *Chromatographia*, 30 (1990) 630.
10 Alltech Associates, State College, PA, personal communication, 1990.

Journal of Chromatography, 588 (1991) 239–249
Elsevier Science Publishers B.V., Amsterdam

CHROM. 23 645

Photoemissive ionisation source for ion mobility detectors

P. Begley, R. Corbin, B. E. Foulger* and P. G. Simmonds

Admiralty Research Establishment, Holton Heath, Poole, Dorset BH16 6JU (UK)

(First received April 17th, 1991; revised manuscript received July 19th, 1991)

ABSTRACT

A combination of a photoemissive ionisation source coupled to an ion mobility detector has been developed which utilises a pulsed light source thereby eliminating the need for an ion injection gate. Factors influencing the performance of this negative ion detector have been investigated. With air as the sample and drift gas streams, the performance of the detector is comparable to conventional designs employing radioactive ionisers.

INTRODUCTION

Recently, there has been renewed interest in the ion mobility spectrometer [1], both as a stand-alone detector [2–9] and as a detector for use with a range of separation techniques including gas chromatography [10–14], supercritical fluid chromatography [15,16], high-performance liquid chromatography [17], and capillary electrophoresis [18]. In a conventional ion mobility spectrometer, ionisation is produced using a ^{63}Ni radioactive foil, which emits a steady current of electrons of energies up to 67 keV [19]. As alternatives to radioactive ionisation, other workers have used photoionisation [20–23], non-resonant laser photoionisation [24], resonant two-photon laser ionisation [25,26], corona [27], and coronaspray ionisation [28]. The work presented here has concentrated on the investigation of a photoemissive source based on ultraviolet irradiation of a thin gold layer with a work function of *ca.* 4.5 eV [29]. This photoemissive source has several potential advantages. Firstly, it is unipolar, generating an initial population of only gaseous low-energy electrons, so eliminating possible loss mechanisms involving both positive ion–negative ion or positive ion–electron recombination. Secondly, it is free from constraints associated with the safe handling of radioactive materials, and thirdly, the initial electron concentration can be controlled, in principle, over a wide range simply by changing the incident light intensity. Furthermore, when combined with a pulsed light source it offers the attractive design option of eliminating the shutter grid at the entrance to the drift tube and its associated gating electronics, so reducing signal losses. Photoemission electron sources have been used in low-pressure drift tubes [30–35], in negative ion detectors [36–40] and as a source of thermal electrons in an electron-capture detector [41,42]. The combination of a photoemissive source with an ion mobility spectrometer as described in this paper is, to our knowledge, the first practical demonstration of such a device for trace analysis at atmospheric pressure.

EXPERIMENTAL

The design of the detector is shown in Fig. 1. The drift tube (Welwyn Electronics, Bedlington, UK) is composed of a 10 mm I.D. × 12 mm O.D. ceramic cylinder which has been internally coated with a low-conductivity ink to produce a nominally uniform resistance of *ca.* 2 MΩ cm^{-1}, whilst a high-conductivity ink was applied to the ends to facilitate electrical connections. The tubes used were 3.7 cm long, but by selecting a well matched pair (8.0 ± 0.1 MΩ),

0021-9673/91/$03.50

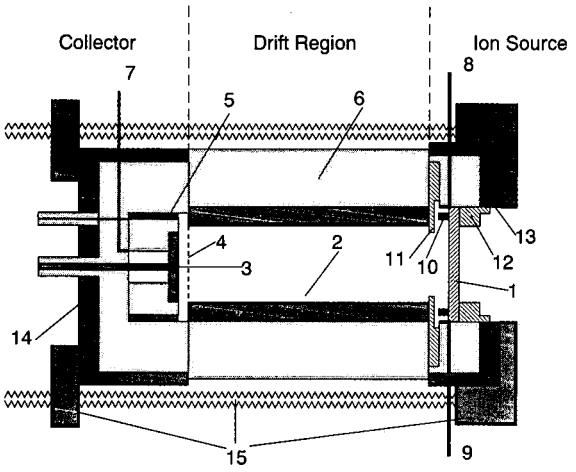

Fig. 1. Photoemissive ion mobility cell. Key: 1 = gold-coated photoemissive window; 2 = drift tube; 3 = perforated collector; 4 = screen grid; 5 = annular guard electrode; 6 = PTFE body; 7 = drift gas inlet; 8 = sample gas inlet; 9 = exhaust gas outlet; 10 = graphite "O"-ring; 11 = gas access plate; 12 = threaded vespel plug; 13, 14 = brass end caps; 15 = clamping (× 3).

two tubes could be used in tandem to give a drift length of 7.4 cm with correspondingly increased ion resolution. In the work reported here, both 3.7 cm and 7.4 cm drift lengths were evaluated experimentally. The photoemissive window was produced by placing 11 mm O.D. × 1.5 mm thick high-purity fused-silica discs (TSL Group, Wallsend, UK) in a sputter coater (Model S150B; Edwards High Vacuum, Crawley, UK), followed by coating with gold for *ca.* 2 min. The performance of the photoemitters was found to be only slightly dependent on the sputter coating time over the range 45 s to 2.5 min. Once the window is assembled in the detector the effective photoemissive window diameter is 9 mm. The screen grid was purchased from Graseby Ionics (Watford, UK) and consisted of a gold-plate photoetched mesh, mounted upon a ceramic former. As the detector was operated with a drift voltage of *ca.* 2000 V on the collector, a guard ring held at the same potential as the collector was incorporated to reduce leakage currents. This configuration whereby the collector is operated at high potential, as opposed to the more conventional arrangement with the collector grounded, was adopted to facilitate studies in which fields within the ion source field could be pulsed. The machining of the various detector components was carried out without the use of cutting fluids to minimise problems arising from contamination.

The signal from the collector was taken to an optically isolated voltage-to-current convertor and head amplifier, which was designed and manufactured in-house, and was mounted within a screened enclosure attached to the drift tube assembly. The main drift field (*ca.* 240 V cm^{-1}) was supplied from an EMI PM28B photomultiplier power supply, which was also used as the current source for high-voltage operation of the detector electronics. A second power supply was developed in-house to supply the lens polarising voltage. This power supply also contained appropriate driver circuitry to allow it to be used with a gating grid.

For the majority of this work, a pulsed xenon lamp (Hamamatsu, type L2415 or L2439) with its associated power supply (Hamamatsu, type C2190-01) was used as the illumination source. The pulse repetition rate was operated as high as possible while still ensuring that the product ions from each flash reached the detector before the next flash. This corresponded to a repetition rate of *ca.* 50 Hz for the short tube, and *ca.* 30 Hz for the long tube. A series of experiments were also conducted with continuous output low-pressure mercury lamps ("Pen-Ray" Ultra-Violet Products, San Gabriel, CA, USA) operated in a pulsed mode using a laboratory constructed pulsed power supply driven by a Hewlett-Packard Model 214B pulse generator.

The signal from the detector amplifier was displayed on a Nicolet Model 4094A digital storage oscilloscope which allowed signal averaging, integration, etc., to be undertaken. To study the effect of different wavelengths of incident light, measurements were carried out using an Oriel Model 7185 photodiode and a Nicolet 430E digital storage oscilloscope. The latter had a higher sampling rate than the 4094A oscilloscope and so was more appropriate for monitoring the light pulses of width at half height of *ca.* 10 μs. A Spectral Energy GM100-3 monochromator was used with 1 mm entrance and exit slit widths in conjunction with the Hamamatsu lamps to provide monochromatic illumination. The results were not corrected for variation in the spectral response of the photodiode since the response variation was minimal over the wavelength range studied. The VU-POINT software

package (S-CUBED; Maxwell Labs., La Jolla, CA, USA) was used to transfer data stored on the Nicolet 4094A's discs directly into an IBM PC-compatible computer.

In operation, a high drift gas flow was maintained through the inlet in the collector region, while the sample gas flow entered through one of two ports in the ion source, the other port forming the exhaust. Drift gas, either air, or for some experiments, "oxygen-free" [<8 vpm (ppm, v/v) oxygen] nitrogen, was supplied through two stage regulators (Model 11 or 11A; Scott Environmental Technology, Plumsteadville, PA, USA) fitted with stainless-steel diaphragms and passed through a trap containing a mixture of charcoal, 5A and 13X molecular sieves to precision gas-pressure regulators (Porter Model 8286) fitted with stainless-steel bodies and diaphragms. Gas flows were controlled by needle valves (Nupro Model SS-SS1) and were measured using digital mass flowmeters (Teledyne-Hastings-Raydist). To perform quantitative measurements, a simple gas manifold was built which allowed compounds of known vapour pressure to be continuously diluted in one or two stages with dry air to a known concentration, which could then be admitted to the detector for long periods. A gas blender (Model 850; Signal Instrument Co., Camberly, UK) was used in experiments in which the oxygen content of both drift and sample gas streams was varied in the range 0 to 20% (v/v). In normal operation, 50–100 ml/min of gas was maintained through the sample inlet port with a drift gas flow of 250–300 ml/min. The system was operated at ambient temperature and pressure for all experiments. In some experiments, the sample inlet was sealed off and a flow of 300–400 ml/min of gas, which included a target chemical at a known concentration, was admitted through the drift gas inlet. When not in use, a small purge gas flow of 10–20 ml/min was always maintained through the detector.

RESULTS AND DISCUSSION

Initially a series of experiments were conducted to investigate the influence of a number of design aspects on the detector performance, which was assessed by measuring the size and width of the $O_2^-(H_2O)_n$ reactant ion peak. Two methods of illuminating the ioniser were evaluated. In the first method, a xenon flashlamp with fixed pulse length but adjustable intensity was used. For comparison, a low-pressure mercury lamp was operated at constant intensity but with variable pulse length. Unfortunately the design of this lamp did not permit any variation in the intensity. It was found that the light output from the mercury lamp was disproportionately low at short pulse lengths as the lamp was not reaching its correct operating temperature resulting in the mercury vapour pressure within the lamp not being sufficiently high. This was corrected by wrapping the bulb in heating wire and maintaining the outside of the silica envelope at a temperature of *ca.* 75°C. With this system, the total light input was controlled by varying the pulse width. Fig. 2 compares the reactant ion characteristic across the accessible range of light intensities for this light source and the xenon lamp for a 3.7 cm drift cell. In this and subsequent figures, resolution has been defined as the drift time divided by the peak width at half height. Clearly the major drawback with the mercury lamp is its low output, leading to unacceptable losses in resolution when the pulse width was increased to give an acceptable signal size. However, the variable pulse width from the mercury lamp did allow the experimental resolution to be compared with values calculated from Spangler and Collins' theoretical derivation [43] by substituting the lamp pulse length for the gate width. Although Fig. 3 shows the experimental data qualitatively followed

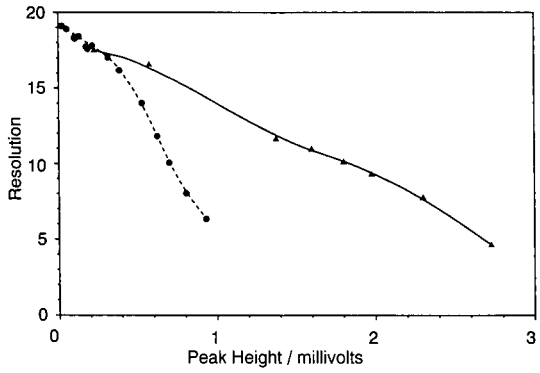

Fig. 2. Effect of the light source on the detector performance. Circles: illuminated by low-pressure mercury lamp. Triangles: illuminated by xenon flash lamp. Conditions: 3.7 cm drift tube, 920 V drift field, photoemissive lens 80 V, sample flow 50 ml/min, drift flow 300 ml/min, temperature 292–297 K.

the theory, the experiments yielded resolutions which are consistently lower than those predicted. The variation in peak height with lamp pulse width is also shown in Fig. 3. No variation was observed in the baseline noise as the pulse width was altered, and signal to noise ratios would have been proportional to the peak heights.

The subsequent study of the effect of the illumination wavelength, as shown in Fig. 4, indicates that illumination at 254 nm, which constitutes the bulk of the output from the mercury lamp, is relatively inefficient. In Fig. 4, the efficiency is defined as the detector output per unit intensity input relative to 220 nm. In contrast, the xenon lamp has strong emission lines in the 200–250 nm region, and its overall output power is also much greater. The emission spectrum measured here is in good qualitative agreement with results previously reported for similar lamps [44]. As a result, the xenon lamp was adopted as the preferred light source for this study.

A series of photoemissive windows were prepared using masks of different diameters and exposing the windows to extended sputter coating times of 5 min. This produced a series of windows with a opaque conductive outer rim and a central transparent region. After removal of the mask, each window was then coated for 2 min to the usual density. These windows were then installed in turn in a 7.4 cm drift length detector, and the peak widths, heights and areas measured for the oxygen reactant ion peak as the input light intensity was varied. The results of these experiments are summarised in Fig. 5. Several aspects of this work are of relevance to future designs. Firstly, the resolution increases as the window area decreases, which presumably reflects the greater uniformity of the drift field near the centre of the tube. However, the resolution of the

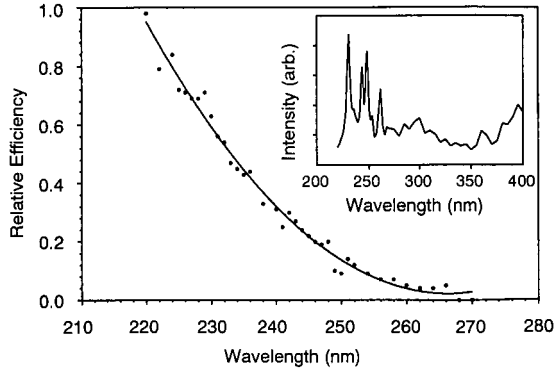

Fig. 4. Relative photoemission efficiency as a function of wavelength. Inset: emission spectrum of the xenon flash lamp.

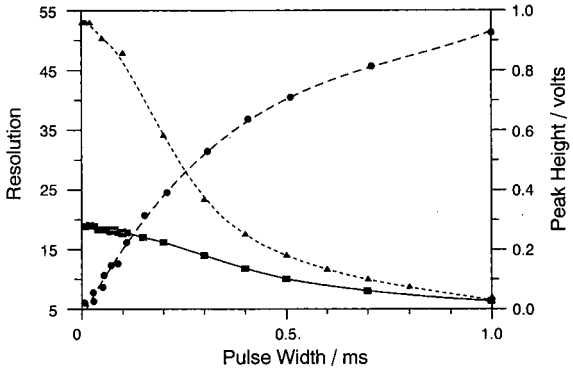

Fig. 3. Comparison of the calculated and experimental resolution for a 3.7 cm drift tube. Triangles: theoretical resolution values. Squares: experimental resolution values. Circles: experimental peak heights. Conditions as in Fig. 2.

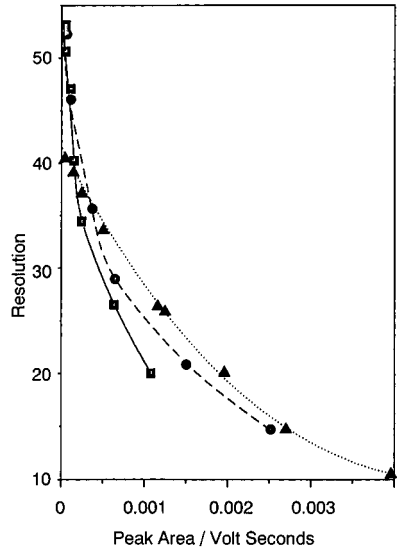

Fig. 5. Effect of the photoemissive window diameter on the detector's performance. Solid line: 2 mm diameter. Dashed line: 3 mm diameter. Dotted line: 9 mm diameter. Conditions: 7.4 cm drift tube, 1900 V drift field, photoemissive lens 80 V, sample flow 70 ml/min, drift flow 260 ml/min, temperature 292–297 K.

smaller windows degrades much more rapidly as the peak area increases than does that for the larger window diameters. This strongly suggests that mutual ion repulsion is a significant factor at the ion densities generated and any attempt to improve the detector's sensitivity by further increasing the input light intensity, and hence the reactant ion density, would be counter-productive, as the increased yield of ions would be offset by degraded resolution. A better approach, which will be the subject of future research, is to design detectors which operate at similar light intensities to those currently used, but with a larger tube diameter and greater active photoemissive area.

There are several factors that contribute to the observed resolution for gridless systems that are not relevant with a conventional gated source. In the gated source, processes occurring in front of the entrance gate do not contribute to the observed resolution, which is determined by the shape and duration of the gate pulse, diffusional broadening, ion molecule reactions within the drift tube and other factors which have been identified by previous workers in the field [45]. All of these factors are also present in the gridless system but in addition, resolution can also be affected by processes occurring within the ionisation region. In addition to mutual ion repulsion described above, any steps occurring within the ionisation region on timescales comparable with the peak widths could degrade the resolution. Clearly, as shown in Fig. 3, the lamp pulse width can affect the resolution. However, the xenon lamp used in the majority of our studies has a pulse half-width of only 0.01 ms which will not significantly increase the ion peak width. Also, the finite distance the electrons travel prior to conversion to O_2^- reactant ions must be considered. Using a three-body attachment rate constant of $2 \cdot 10^{-30}$ cm^6 s^{-1} at *ca.* 290–300 K for the reaction $e^- + O_2 + M \rightarrow O_2^- + M$ (where $M = O_2$) [46], the electrons will have a lifetime in air of *ca.* $2 \cdot 10^{-8}$ s. Since, at room temperature, the rate constant for the reverse reaction is negligible and the three-body rate constant for O_2^- formation with nitrogen as the third body is at least an order of magnitude less [46], the contribution of these two processes to the lifetime of the electron in air have been ignored. At a E/N value of *ca.* 10^{-17} V cm^2 the drift velocities of electrons in nitrogen and oxygen at 293 K are $5 \cdot 10^5$ and 10^6 cm s^{-1}, respectively [47] (E is the electric field intensity and N the gas number density, and their ratio is commonly used to characterise the average energy which an ion acquires from an applied electric field). Therefore, assuming an electron drift velocity in air of *ca.* $6 \cdot 10^5$ cm s^{-1}, the electrons will only penetrate *ca.* $1.2 \cdot 10^{-2}$ cm along drift tube prior to conversion to O_2^- reactant ion. For a reactant ion drift velocity of *ca.* $5 \cdot 10^2$ cm s^{-1}, this means the half peak width of the reactant ion peak will be increased by *ca.* 0.02 ms as a result of the electron drift in air. The observed half peak widths at the lowest light levels are 0.34 ms for our standard photoemissive window. Therefore, the electron drift in air is not an important factor in determining the system resolution. However, this argument is only valid at low electron concentrations since, as we have observed, mutual charge repulsion will degrade resolution at higher concentrations of electrons or ions. In practice (see later) the most important processes are the sequence of ion molecule reactions leading to the observed product ions.

In order to direct the design changes within the photoemissive source into potentially useful areas, a series of kinetic model simulations were made using rate constants from the literature, and concentrations equivalent to those encountered in testing the prototype gridless detectors. The primary motivation was to derive information about the timescales required for the product formation reaction, and to compare these with the detectors' characteristics. For this purpose, the model was constructed to simulate reactions occurring in a closed, homogeneous gas mixture in the absence of applied electric fields. In this way, the equilibration times required for the reactions could be determined, and compared with the species lifetimes implied by the detector designs. The simulations were implemented using the simulation program CHEKMAT (AERE, Harwell, UK) [48] which is specifically designed to produce numerical solutions to problems involving systems of chemical reactions and simultaneous diffusion, although the latter capability was not required in this case. A series of runs were made, simulating the following system of reactions, where P represents the target compound:

$$e^- + O_2 \rightarrow O_2^-$$

$$O_2^- + P \rightarrow P^- + O_2$$

$$P^- \rightarrow P + e^-$$

Although the equations above imply charge transfer from the oxygen ion, attachment of the oxygen ion to form an adduct, or second order nucleophilic substitution, is mathematically equivalent, and so conclusions about reaction timescales can be applied to any of these reaction mechanisms. The oxygen concentration was that derived assuming standard temperature, pressure and composition. The concentration of the target compound P was assumed to be 70 ppb[a] at standard temperature and pressure in most cases, but was varied to 7 ppb for a few comparative runs. The number of electrons was measured directly on the gridless photoemission cell with nitrogen drift gas using a Kiethley Model 617 electrometer connected to the collector, and light intensities identical to those used in normal operation. No correction was applied for losses to the wall of the drift tube. By measuring peak widths on the oxygen ion, a maximum reaction volume was derived ignoring the effect of diffusional broadening, and so tending to overestimate the volume. The electron concentration was then calculated assuming that it was homogeneous throughout this volume.

The electron attachment to oxygen was modelled using the treatment developed by Shimamori and Hatano [49], which uses a Bloch–Bradbury mechanism, modified for the effect of third-body stabilisation, by both oxygen and nitrogen, using measured rate constants [50–52] from the literature. The lifetime of the oxygen ion was taken as that measured by Shimamori and Hatano, which is in reasonable agreement with theoretical calculations [53,54]. In accordance with the rate constants measured by workers using flowing afterglow techniques, a range of values were assumed for charge transfer from, or attachment of, the oxygen anion, covering the values found for fast reactions (10^{-10} – $3 \cdot 10^{-9}$ cm^3 molecule^{-1} s^{-1}). No measured rate constants for the decay or further reaction of the product anions have been found in the literature. Autodetachment lifetimes, which are the lifetimes of the excited ions formed by capture of a free electron, have been measured for perfluorotoluene and perfluoromethylcyclohexane [55], so simulation runs have been made covering the range of possible autodetachment rates implied by these lifetimes. The rate of consumption of the product ion implied by these lifetimes is equivalent to that which would be observed if it was consumed in a second-order process proceeding at the collision limit with a second species present at 15–100 ppb levels. Fig. 6 shows some typical results.

A wide range of simulation runs were conducted covering the range of conditions described above. By eliminating the reactions of the target compound P, and modelling only the capture of electrons by oxygen, good agreement was found with the calculations of Grimsrud and Stebbins [56] after allowing for differences in concentrations. The following salient conclusions can be made from our simulations:

(a) While the electron transfer reaction to oxygen was extremely fast (10–100 ns), equilibration times for the target compound P ion formation were much longer (10–1000 μs). The free electron concentration was negligible within a period of 1 μs.

(b) The equilibration time was critically dependent upon the lifetime of the product ion. In the case of perfluorotoluene the system reaches equilibrium within 40 μs, whilst for an extremely long-lived ion such as perfluoromethylcyclohexane, significant further product formation is continuing even after 1 ms.

(c) For a given reaction time, the number of product ions formed increases as the postulated lifetime increases.

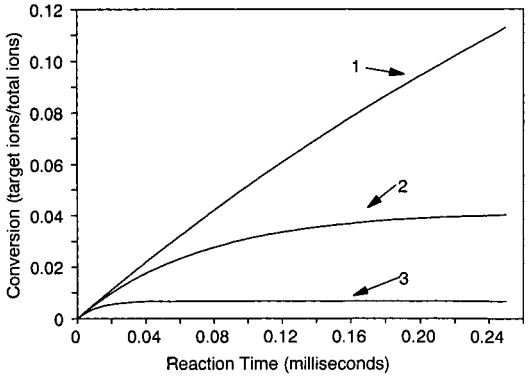

Fig. 6. Simulation runs for a formation rate of $3.0 \cdot 10^{-10}$ cm^3 molecule^{-1} s^{-1} and decay rates of (1) $1.3 \cdot 10^3$ s^{-1}, (2) $1.3 \cdot 10^4$ s^{-1} and (3) $8.3 \cdot 10^4$ s^{-1}.

[a] Throughout this article, the American billion (10^9) is meant.

(d) The formation rate has a direct influence on the number of ions after a given reaction time, but has no apparent effect upon the equilibration time.

(e) When direct electron capture by the target compound P was included in the simulation using a rate constant typical of perfluorocarbons, there was a significant increase in the initial rate of product formation, but this was rapidly dwarfed by the contribution through charge transfer, and was an insignificant contribution to the total at reaction times greater than 25 μs.

(f) Simulations at concentrations of target compound P of 70 ppb and 7 ppb showed no difference in equilibration time, but there appeared to be a small increase in overall ionisation efficiency at 7 ppb. If this accurately reflects the real behaviour, then departure from a linear concentration/signal relationship will occur at 70 ppb levels.

In the context of detector design, the most relevant aspect of these simulations was the prediction of reaction times of the order of milliseconds for optimal product ion yield, and hence sensitivity. Since the gridless photoemission detector was estimated to allow reaction times of no more than 0.2–0.3 ms based on the observed peak widths of the reactant ion, this strongly suggests that improved performance could be achieved if the reaction time could be increased without compromising the detector's resolution.

One advantage which was predicted for the photoemissive devices was that the absence of signal losses through positive ion–negative ion neutralisation reactions would result in improved product ion yields, and hence sensitivities, when compared to the bipolar radioactive source. In order to assess the likely importance of this advantage, the reaction system described above was modified to include positive ions at the same concentration as electrons. These were then permitted to undergo neutralisation reactions with both the reactant oxygen ion and the product anion, with a rate constant of $2.0 \cdot 10^{-6}$ cm^3 ion^{-1} s^{-1}, which is the upper limit suggested by both theoretical and experimental studies [57,58]. Other candidate loss mechanisms such as radiative and dissociative electron-ion recombination have been excluded from consideration since the predicted electron concentration within the source is negligible except at very short times. Fig. 7 demonstrates the effect of these processes on the predicted ion yield, with the equivalent unipolar case included for comparison. The particular set of conditions used in these simulation runs are for a very long-lived product ion at low concentrations. While the absence of recombination pathways is a significant advantage at long reaction times, giving an increased yield by approximately a factor of two, very little advantage (10–20%) is gained over the 0.2–0.3 ms timescales estimated for reaction in the gridless photoemission system. This has provided further motivation for attempts to increase the available reaction time in the photoemission source designs.

A series of determinations were made on the 3.7 cm drift length detector cell in which the oxygen content of both the drift and sample gas streams was varied in the range 0 to 20% (v/v). A further series of experiments was conducted in which the sample gas stream was varied in oxygen composition, while the drift stream was pure nitrogen. These results are presented in Fig. 8. This series of experiments highlights several important features of the gridless photoemissive system. Where oxygen is present in both the sample and drift streams, the resolution is effectively unchanged at oxygen concentrations in excess of 6% (v/v). Furthermore, the resolution declined as the oxygen content decreased, which strongly suggests that electrons were able to travel substantial distances along the drift tube before attachment to oxygen molecules. The peak shapes confirmed this interpretation, as a progressively

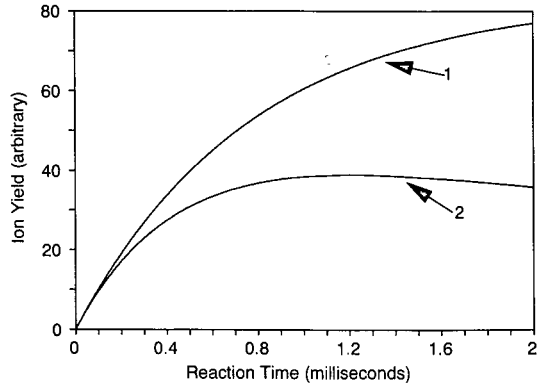

Fig. 7. Simulation including ion–ion recombination. (1) No recombination. (2) Recombination rate of $2.0 \cdot 10^{-6}$ cm^3 molecule^{-1} s^{-1}.

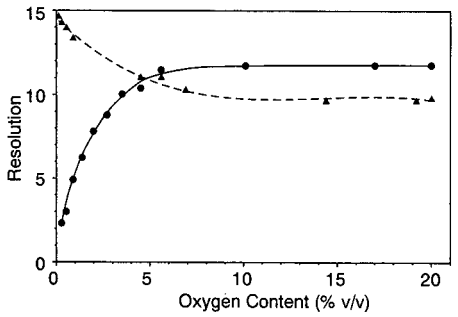

Fig. 8. Effect of the gas composition on the reactant ion resolution. Solid curve: both the sample and drift streams contained the indicated oxygen level. Dashed curve: oxygen was present only in the sample gas stream. The balance was nitrogen in both cases. Conditions as in Fig. 2, except sample flow 45 ml/min, drift flow 220 ml/min.

more conspicuous leading edge "shoulder" developed on the reactant ion as the oxygen content was reduced. For the situation with nitrogen drift gas and where a varying oxygen content is admitted into the sample stream, the peak resolution improves as the oxygen content of the sample gas is reduced. Since the nitrogen drift flow is approximately five times greater than the sample inlet flow this leads to the complication that the effective oxygen concentration in the reaction zone will be reduced by one fifth, assuming complete mixing. Therefore because relatively few oxygen molecules are available for electron attachment, the concentration of oxygen anions will not reach a sufficiently high density for mutual ion repulsion to significantly degrade resolution, while many electrons will simply escape capture altogether. The observation that with oxygen present in the drift gas the overall resolution is greater in the plateau region may be due to the increased rate constant for the electron attachment reaction when oxygen acts as the third body [46]. A smaller reaction volume is associated with this faster rate constant, therefore accounting for the improved resolution.

The detector response was measured for some representative target compounds in each of two flow configurations. In the "conventional flow" configuration, pure drift gas was introduced at the collector inlet on the cell and the gas stream containing the target chemical was introduced at the inlet immediately adjacent to the photoemissive window. In this configuration the bulk of the cell drift volume does not contain the unionised target chemical. For comparison, measurements were also carried out with the sample inlet port sealed off and the target chemical introduced into the drift gas stream, so producing a uniform target chemical concentration throughout the drift volume.

Fig. 9 shows the observed response for concentrations of benzoquinone up to 200 ppb. Furthermore, Fig. 9 illustrates that when the sample is introduced into the drift flow increased sensitivity is observed at the lower concentrations. Similar results were observed for methyl salicylate and 4-chloronitrobenzene. The observed sensitivity enhancement, defined as the ratio of the peak height in the "sample in drift" mode to the peak height in the "conventional flow" mode, and measured at low concentrations, was calculated as 18.7 for benzoquinone, 4.8 for 4-chloronitrobenzene, and 2.9 for methyl salicylate. These response enhancements suggest that in the conventional flow configuration, the oxygen ion reactant peak is not present in a region of significant target neutral concentration for a sufficient time to allow the reaction to reach equilibrium. In the "conventional flow" configuration, the concentration is that which was delivered in the sample gas line, and has not been adjusted for dilution by the drift gas, as it has not proved possible to calculate

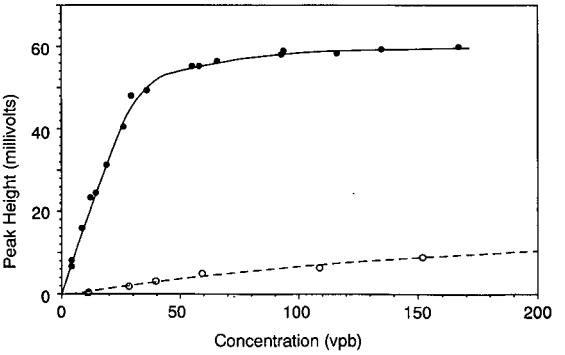

Fig. 9. Response of the detector to benzoquinone (BQ). Dashed curve: "conventional" flow pattern (BQ present only in the sample gas stream). Solid curve: sample inlet blanked off and sample of BQ introduced through the drift gas inlet. Conditions as in Fig. 5, except in "conventional" mode sample flow 50–80 ml/min, drift flow 200–230 ml/min, in "sample in drift" mode, drift flow 280–320 ml/min.

the actual concentration in the reaction zone. It could be argued that the inlet concentration is the more relevant quantity to help assess the detector's applicability in real-world applications. However, this uncertainty in the concentration in the reaction zone makes the comparison of the two flow configurations less clear-cut than we would wish, although the results for benzoquinone cannot be completely explained by a simple dilution effect since for the sample and drift flow-rates used in this work the maximum envisaged relative enhancement would be *ca.* 6, while 18.7 was observed. Such a maximum enhancement could only arise if complete mixing of the sample and drift flows occurred at the sample inlet while in the "conventional flow" configuration, whereas we believe that a more or less well-defined plume of sample gas, which is progressively diluted by the drift gas as the exhaust outlet is approached, is generated across the face of the photoemissive window. In contrast, when the target compound is present throughout the drift region, longer reaction times are available and so the equilibrium distribution is more closely approached. The wide variation in the enhancement ratio for the different compounds is believed to reflect differences in the formation rates and stabilities of the ions formed. Unfortunately, we were unable to find any appropriate kinetic data in the literature to support this view. When the system was operated in the "sample in drift" mode, the product ion peaks were wider than those observed in the "conventional flow" mode, and, at lower concentrations, a leading edge "shoulder" appeared. For benzoquinone at concentrations of *ca.* 15 ppb, the measured resolution was 33 in the conventional flow mode, but only 18 when the sample was introduced in the drift gas. Again this is consistent with the reaction continuing after the oxygen ions had moved a significant distance down the drift tube. As a consequence, the sensitivity enhancement quoted above is not fully realised as an improved limit of detection. In the current experiments, 256 spectra were averaged for each determination, and the detection limits were estimated to lie in the range 0.2–5 ppb. Sensitivities of this order are broadly comparable with those claimed for radioactive ion mobility detectors [59], although the large variation in sensitivity to different chemicals complicates the comparison. A more comprehensive study is currently underway to quantify the limits of detection of the gridless photoemissive and ^{63}Ni radioactive sources on a test assembly in which the source assemblies are interchangeable. As illustrated in Fig. 10, when the system was operated in the conventional flow configuration, the reactant ion peak dominates the ion mobility spectrum. As the target chemicals are reduced in concentration, poor resolution from the reactant ion peak becomes the controlling factor in defining their detection limits. Fig. 8 also demonstrates that the product ion peaks could, for some compounds, achieve higher resolution than did the reactant peak.

A series of experiments were also conducted in which the flash rate of the Hamamatsu lamp was varied while low levels of target chemicals were introduced into the gridless 7.4 cm detector. This was accomplished by disconnecting the trigger signal supplied from the ion mobility electronics, so producing a lamp pulse every 30 ms, and using the lamp power supply's internal trigger, which is variable over the range 10–120 ms. The oscilloscope was synchronised with the flash lamp by monitoring the lamp with an Oriel 7185 photodiode and using the photodiode output as the external trigger for the oscilloscope. In air, in all cases, a precursor to the main reactant peak was found that increased in magnitude as the flash repetition rate was increased. This precursor was observed in other experiments, particularly when a given photoemissive window had been in use for several weeks, and has been tentatively ascribed to O_3^-, on the basis of its relative mobility [60] and since it was found to increase in size if the sample gas stream was subjected to intense

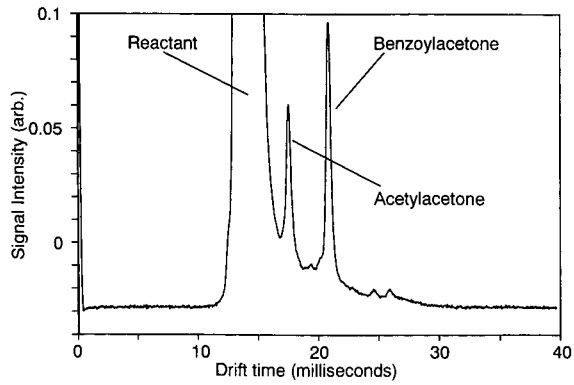

Fig. 10. Ion mobility spectrum for acetylacetone and benzoylacetone at trace levels. On the *y*-axis scale shown, the full height of the reactant peak is *ca.* 1. Conditions as in Fig. 5.

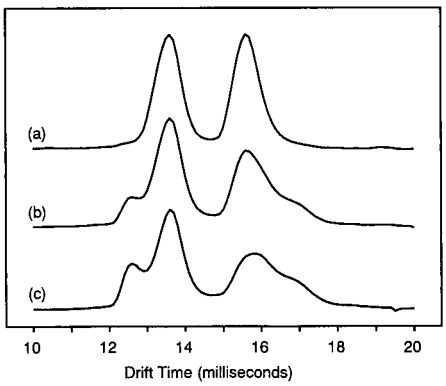

Fig. 11. Effect of the flash repetition rate on the benzoquinone mobility spectrum (reactant peak drift time *ca.* 13.5 ms, BQ product peak drift time *ca.* 15.7 ms). (a) Lamp flashes at 110-ms intervals. (b) Lamp flashed at 22-ms intervals. (c) Lamp flashed at 11-ms intervals. Conditions as in Fig. 5.

short-wave ultraviolet radiation before admission to the detector cell. The principal O_2^- reaction ion peak was observed to decrease in magnitude in an approximate inverse proportion. In the presence of target chemicals such as acetylacetone, methyl salicylate and benzoquinone, the expected product ion peak was reduced in magnitude to a greater degree than the reactant peak, and in the case of benzoquinone a trailing edge shoulder developed on the peak, suggesting that another product ion was being formed. For perfluorodimethyladamantane, the observed effects were much smaller, with no major reduction in product ion intensity accompanying higher flash rates. However, a small trailing edge shoulder which was present on the product ion peak at low repetition rates diminished as the flash rate increased. No conclusive explanation can be offered for this contrasting behaviour, but it may reflect differences in the ionisation mechanisms for the various compounds used. Typical results, in this case for benzoquinone, are summarised in Fig. 11. It was noted that these above effects became more severe if the total flow of gas through the detector was reduced, which suggests that they might be caused by the production of photoexcited neutral species from the target molecule, or by the photochemical production of ozone within the ionisation region. Either of these products, being neutral, would be cleared from the detector only by ventilation in the cell exhaust. This ventilation would be expected to have a half lifetime of 5–10 ms and is therefore on a comparable timescale to the flash repetition rate. Once formed, such photochemical products could participate in a range of reactions with either the reactant ions or the desired product ions. Such reactions need not lead to the production of observable peaks in the ion mobility spectrum, if the reaction products were unstable with lifetimes less than their drift times. Ideally, these effects should be studied in greater detail using spectroscopic or mass spectral techniques.

CONCLUSIONS

This work has demonstrated that photoemission can be exploited as a viable ionisation technique for use in ion mobility detectors. Several factors have been investigated that influence the performance of a photoemissive ion mobility detector. For the gridless design investigated here, the evidence suggests that the ion–molecule chemistry which leads to the characteristic product ions may not be proceeding to equilibrium under the conditions attainable, and that the sensitivity of the detector may be reduced as a result. Further work is now in progress using a photoemissive detector in which a conventional drift tube entrance grid is also employed, so that, by delaying operation of the gating grid with respect to the light pulse, longer reaction times can be tolerated in the ion source without degrading the resolution of the detector in the manner described here. Furthermore the performance of the photoemissive source is currently constrained by mutual ion repulsion degrading the ion resolution and studies are in hand using wider bore systems to reduce the ion densities.

ACKNOWLEDGEMENTS

The authors would like to thank Dr. J. Lovelock for advocating the use of a photoemissive ionisation source and for useful discussions on aspects of this work. We also thank Mr. F. Norris and Mr. P. Hunter for fabrication of the prototype detectors.

REFERENCES

1 H. H. Hill, Jr., W. F. Siems, R. H. St. Louis and D. G. McMinn, *Anal. Chem.*, 62 (1990) 1201A.

2 J. P. Carrico, A. W. Davis, D. N. Campbell, J. E. Roehl, G. R. Sims, G. E. Spangler, K. N. Vora and R. J. White, *Am. Lab.*, 152 (1986) 155.
3 C. J. Proctor and J. F. Todd, *Anal. Chem.*, 56 (1984) 1794.
4 A. H. Lawrence and P. Neudorfl, *Anal. Chem.*, 60 (1988) 104.
5 G. E. Spangler, J. P. Carrico and D. N. Campbell, *J. Test. Eval.*, 13 (1985) 234.
6 S. H. Kim and F. W. Karasek, *Anal. Chem.*, 50 (1977) 152.
7 G. E. Spangler and J. P. Carrico, *Int. J. Mass Spectrom. Ion Phys.*, 52 (1983) 267.
8 G. E. Spangler, K. N. Vora and U. P. Carrico, *J. Phys. E: Sci. Instrum.*, 19 (1986) 191.
9 G. E. Spangler, D. E. Campbell and J. P. Carrico, *US Pat.*, 4 551 624 (1985).
10 F. W. Karasek, H. H. Hill, Jr., S. H. Kim and S. Rokushika, *J. Chromatogr.*, 135 (1977) 329.
11 M. A. Baim and H. H. Hill, Jr., *J. Chromatogr.*, 299 (1984) 309.
12 M. A. Baim and H. H. Hill, Jr., *J. High Resolut. Chromatogr. Chromatogr. Commun.*, 6 (1983) 4.
13 R. H. St. Louis, W. F. Siems and H. H. Hill, Jr., *J. Microcolumn Sep.*, 2 (1990) 138.
14 R. H. St. Louis, W. F. Siems and H. H. Hill, Jr., *J. Chromatogr.*, 479 (1989) 221.
15 H. H. Hill, Jr. and M. A. Morrissey, in C. M. White (Editor), *Modern Supercritical Fluid Chromatography*, Hüthig, Heidelberg, 1988, p. 95.
16 R. L. Eatherton, M. A. Morrissey, W. F. Siems and H. H. Hill, Jr., *J. High Resolut. Chromatogr. Chromatogr. Commun.*, 9 (1986) 154.
17 D. G. McMinn, J. Kinzer, C. B. Shumate, W. F. Siems and H. H. Hill, Jr., *J. Microcolumn Sep.*, 2 (1990) 188.
18 R. W. Hallen, C. B. Shumate, W. F. Siems, T. Tsuda and H. H. Hill, Jr., *J. Chromatogr.*, 480 (1989) 233.
19 F. W. Karasek, *Res. Develop.*, 21 (1970) 34.
20 C. S. Leasure, *Ph.D. Thesis*, New Mexico State University, Las Cruces, NM, May 1986.
21 R. L. Eatherton, *Ph.D. Thesis*, Washington State University, Pullman, WA, December 1987.
22 M. A. Baim, R. L. Eatherton and H. H. Hill, Jr., *Anal. Chem.*, 55 (1983) 1761.
23 G. A. Eiceman and V. J. Vandiver, *Anal. Chem.*, 58 (1986) 2335.
24 D. M. Lubman and M. L. Kronick, *Anal. Chem.*, 54 (1982) 1546.
25 D. M. Lubman and M. L. Kronick, *Anal. Chem.*, 54 (1982) 2289.
26 D. M. Lubman and M. L. Kronick, *Anal. Chem.*, 55 (1983) 1486.
27 R. F. D. Bradshaw, *UK Pat.*, 1 606 926 (1978).
28 C. B. Shumate and H. H. Hill, Jr., *Anal. Chem.*, 61 (1989) 601.
29 L. M. Rangarajan and G. K. Bhide, *Vacuum*, 30 (1980) 515.
30 G. S. Hurst, L. B. O'Kelly, E. B. Wagner and J. A. Stockdale, *J. Chem. Phys.*, 39 (1963) 1341.
31 J. L. Pack and A. V. Phelps, *Phys. Rev.*, 121 (1961) 798.
32 J. L. Moruzzi and A. V. Phelps, *Rev. Sci. Instr.*, 40 (1969) 461.
33 J. L. Moruzzi, *Rev. Sci. Instr.*, 38 (1967) 1284.
34 J. L. Moruzzi, J. W. Ekin, Jr. and A. V. Phelps, *J. Chem. Phys.*, 48 (1968) 3070.
35 J. Dutton, A. Goodings, A. L. K. Lucas and A. W. Williams, *J. Phys. E: Sci. Instrum.*, 21 (1988) 264.
36 Y. Gosho and A. Harada, *J. Phys. D: Appl. Phys.*, 16 (1983) 1159.
37 R. Fox and A. V. Phelps, *US Pat.*, 3 211 996 (1965).
38 J. E. Lovelock and A. Jenkins, *UK Pat.*, 1 553 071 (1975).
39 R. J. Wernlund, *US Pat.*, 3 626 181 (1971).
40 M. J. Cohen and R. W. Crowe, *US Pat.*, 3 742 213 (1973).
41 P. G. Simmonds, *J. Chromatogr.*, 399 (1987) 149.
42 J. C. Sternberg and D. T. L. Jones, *US Pat.*, 3 238 367 (1966).
43 G. E. Spangler and C. E. Collins, *Anal. Chem.*, 47 (1975) 403.
44 R. Phillips, *Sources and Applications of Ultraviolet Radiation*, Academic Press, London, 1983.
45 E. A. Mason, in T. Carr (Editor), *Plasma Chromatography*, Plenum Press, New York, 1984, p. 84.
46 L. G. Christophorou, *Electron Molecule Interaction and Their Applications*, Academic Press, London, 1984, p. 583.
47 L. G. Christophorou, *Electron Molecule Interaction and Their Applications*, Academic Press, London, 1984, p. 133.
48 A. R. Curtis and W. P. Sweetenham, *Facsimile/CHEKMAT User's Manual*, AERE Harwell, Report R12805, February 1988.
49 H. Shimamori and Y. Hatano, *J. Chem. Phys.*, 21 (1977) 187.
50 H. Shimamori and Y. Hatano, *J. Chem. Phys.*, 12 (1976) 439.
51 B. G. Young, A. W. Johnson and J. A. Garruthors, *Can. J. Phys.*, 41 (1963) 625.
52 J. L. Pack and A. V. Phelps, *J. Chem. Phys.*, 44 (1966) 1870.
53 F. Koike, *J. Phys. Soc. Jpn.*, 35 (1973) 1166.
54 F. Koike, *J. Phys. Soc. Jpn.*, 39 (1975) 1590.
55 W. T. Naff, C. D. Cooper and R. N. Compton, *J. Chem. Phys.*, 49 (1968) 2784.
56 E. P. Grimsrud and R. G. Stebbins, *J. Chromatogr.*, 155 (1978) 19.
57 D. R. Bates, *Adv. Atom. Mol. Phys.*, 20 (1985) 1.
58 B. H. Mahan, *Adv. Chem. Phys.*, 23 (1973) 1.
59 V. J. Vandiver, *Ph.D. Thesis*, New Mexico State University, Las Cruces, NM, May 1987.
60 R. N. Snuggs, D. J. Volz, J. E. Schummers, C. W. Martin and E. W. McDaniel, *Phys. Rev.*, A3 (1971) 477.

Journal of Chromatography, 588 (1991) 251–258
Elsevier Science Publishers B.V., Amsterdam

CHROM. 23 626

Isotope effect in gas–liquid chromatography of labelled compounds

M. Matucha*

Institute of Nuclear Biology and Radiochemistry, Czechoslovak Academy of Sciences, Vídeňská 1083, 142 20 Prague (Czechoslovakia)

W. Jockisch

Central Institute of Isotope and Radiation Research, Permoserstr. 15, O-0705 Leipzig (Germany)

P. Verner

Diagnostic Centre for Inherited Metabolic Disorders, Charles University, Karlovo nám. 32, 120 00 Prague 2 (Czechoslovakia)

G. Anders

Central Institute of Organic Chemistry, Permoserstr. 15, O-0705 Leipzig (Germany)

(First received February 14th, 1991; revised manuscript received June 11th, 1991)

ABSTRACT

The isotope effect in the gas–liquid chromatography (GLC) of ^{14}C- and ^{2}H-labelled compounds was examined experimentally and theoretically. Capillary column gas chromatographic–mass spectrometric (GC–MS) data indicated that the isotope effect was very small for ^{14}C-labelled higher fatty acids and large for perdeuterated *n*-alkanes. Measurement of the temperature dependence of the corrected retention volumes and separation factors of C_{15}–C_{17} *n*-alkanes and their perdeuterated analogues yielded a relationship between the molar volume, enthalpy change and chromatographic retention: heavier isotopomers having lower molar volumes are eluted earlier when Van der Waals dispersion forces plays a dominant role in the solute–stationary phase interaction. The effect is proportional to the number of heavier atoms in the molecule and should be taken into account in the GLC and GC–MS of isotopically substituted compounds on efficient capillary columns.

INTRODUCTION

Labelled (isotopically modified) compounds are often used in organic and analytical chemistry and in biochemistry and other life sciences as a powerful tool to trace the path of compounds of interest and/or to investigate their behaviour and transformations. One of important analytical methods used in applications of labelled compounds is gas chromatography: radio-gas chromatography (RGC) for radioactively labelled compounds and gas chromatography–mass spectrometry (GC–MS) for compounds substituted with stable isotopes. Relatively little attention has been paid to the theory of isotope effects in the gas–liquid chromatography (GLC) of labelled compounds, but based on earlier studies by others on chromatographic solute–stationary phase interactions [1,2] we have considered further the chromatographic behaviour of isotopic species.

In GC, the retention volumes of organic compounds labelled with deuterium or tritium have often been found to differ from those of isotopically unmodified substances [3–17]; the separation of

0021-9673/91/$03.50

^{12}C-, ^{13}C- and ^{14}C-isotopomers of methane by means of capillary gas–solid chromatography (GSC) was found to be low [16], whereas in GLC no isotope effect of ^{14}C-labelled compounds has so far been reported. In the RGC of tritium-labelled compounds, "radioactivity was detected earlier than mass" [12,13]. Isotope effects in GC have been well studied in the past, but the data obtained were mostly evaluated according to the thermodynamics of the chromatographic process only and no clear theoretical conclusions were made [8–10].

A situation when lighter isotopomers are eluted earlier (in GSC at lower temperatures) is called the normal isotope effect. The "inverse" isotope effect was mostly found in GLC [3–17]; it was explained several years ago as being due to shorter internuclear carbon –hydrogen distances resulting in slightly lower molar volumes and boiling points of perdeuterated compounds [17]. The size and shape of the solute molecules, not mass differences as such, played a significant role [18].

In the GC–MS literature an inverse effect is often reported [19,20] and it is sometimes denoted a "chromatographic isotope effect" [20]. The introduction of several deuterium atoms into a small molecule usually results in a significantly decreased retention time in GC [21]. A recent report concerns the isotope effect in the "chromato-mass spectrometry" of deuterium-substituted amino acids [22] and also in the GC of low-boiling isotopic molecules on PLOT columns [23].

A very small isotope effect was observed in the GLC of methyl esters of [G-^{14}C]fatty acids obtained by biosynthesis, in contrast to that of perdeuterated *n*-alkanes of the same mass difference with respect to their isotopically unmodified analogues [18]. We confirmed the earlier hypothesis that the peak broadening of methyl esters of [G-^{14}C]fatty acids on highly efficient capillary columns is caused by overlapping of their isotopomers [24] using GC–MS. However, the method used did not permit us to determine the magnitude of the isotope effect.

Much attention has recently been paid to the relationship between structure and chromatographic retention [1,2]. One of the results is the linear relationship between the enthalpy change (heat of solution in the stationary phase) and the molar volume of the solute [2], which in our opinion can also be extended to isotopic species. The conclusions in recent papers on isotope effects in GC are that heavier isotopomers have smaller sizes or volumes [16,23]. Many years ago, GLC was suggested as a method for investigating isotope effects in solution to gain a fuller understanding of the intermolecular forces in solution [7], which is in accord with the new approaches [1,2]. However, also in older studies of isotope effects on thermodynamic properties of isotopic molecules in condensed systems the influence of isotopic substitution, molecular structure and geometry, molar volume and also polarizability were noticed [25,26]. Hence all factors of the chromatographic solute–stationary phase interaction should be considered.

EXPERIMENTAL

Chemicals

Methyl palmitate and *n*-hexane (analytical-reagent grade) were purchased from Merck (Darmstadt, Germany), [G-^{14}C]palmitic acid with a specific acitivity of 720 mCi/mmol (71,9% ^{14}C) from the Institute for Research, Production and Application of Radioisotopes (Prague, Czechoslovakia), a mixture of C_{15}–C_{17} *n*-alkanes, fully substituted with deuterium, from the Zentralinstitut für Isotopen- und Strahlungsforschung (Leipzig, Germany) and unsubstituted *n*-alkanes from Supelco (Bellefonte, PA, USA).

GC–MS analysis

A Model 1020 B mass spectrometer (Finnigan, San Jose, CA, USA) coupled with a Sigma 3B gas chromatograph (Perkin-Elmer, Norwalk, CT, USA) was used under the following conditions: 12 m × 0.10 mm I.D. fused-silica open tubular (FSOT) column coated with BP-1 polydimethylsiloxane stationary phase (crosslinked and bonded, film thickness 0.1 μm) (SGE, Victoria, Australia), injector in the split mode, splitting ratio 1:100, operated at 230°C, oven temperature 165°C, helium as carrier gas, flow-rate 50 cm s^{-1}, GC–MS interface direct inlet at 260°C, manifold temperature 70°C and electron energy 70 eV.

GC of *n*-alkanes was performed on a Hewlett-Packard Model 5890 gas chromatograph on a 50 m × 0.25 mm I.D. FSOT column coated with PS-255 polydimethylsiloxane phase (cross-linked), film

thickness 0.2 μm, injector in the split mode, splitting ratio 1:100, carrier gas (hydrogen) linear velocity 40–50 cm s^{-1}, in the isothermal mode at temperatures between 120 and 200°C.

RESULTS AND DISCUSSION

The peak broadening of methyl esters of [G-^{14}C]palmitic and oleic acid on highly efficient capillary column [24] and the knowledge of the mechanism of fatty acid biosynthesis [27–29] led us to investigate the causes of this effect by GC–MS; the putative cause was overlapping of the peaks of individual isotopomers contained in the [G-^{14}C]palmitic acid preparation. Because of the low intensity of molecular ions in the electron impact (EI) mass spectra of the methyl ester of [G-^{14}C]palmitic acid of high specific activity (the isotopic abundance of ^{14}C was higher than 70%, *i.e.*, the preparation represented a rich mixture of isotopomers formed during biosynthesis), the isotope effect was not completely distinct [18]. The situation is clear from Fig. 1. A molecular ion of the non-radioactive methyl ester of palmitic acid having its origin in the non-radioactive inoculum is found at *m/z* 270, and the cluster of molecular ions of heavier radioactive isotopomers lies in the region *m/z* 280–302 with a maximum at *m/z* 298. The intensities were found to correspond to the specific acitivity determined by liquid scintillation counting and GC.

Mass chromatograms of molecular ions belonging to individual isotopomers were, however, of low intensity, showing only that the heavier isotopom-

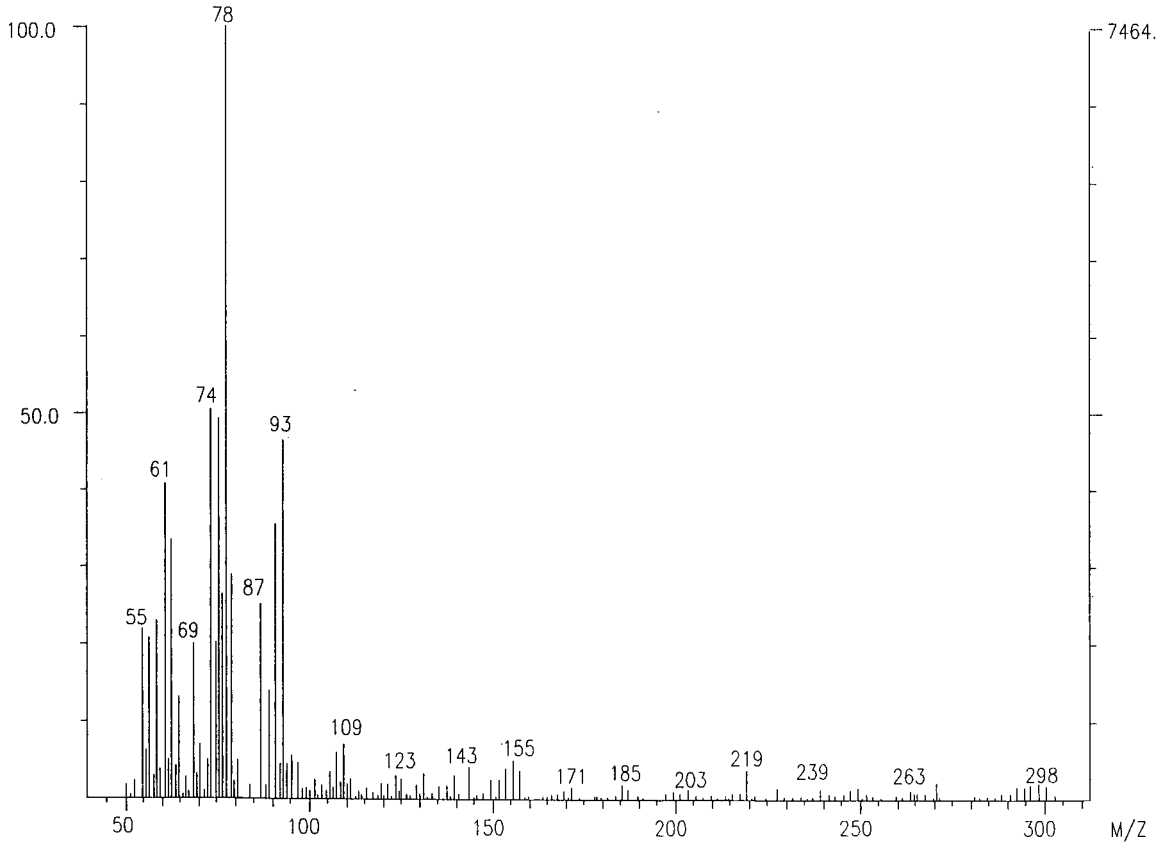

Fig. 1. EI mass spectrum of methyl ester of [G-^{14}C]palmitic acid at its peak maximum during GC–MS on a non-polar stationary phase. The molecular ions of *m/z* 270–302 confirm the presence of isotopomers; the mass peak at *m/z* 302 corresponds to palmitic acid containing only ^{14}C atoms. The highest intensities belong to the ^{14}C-fragments at *m/z* 78 and 93.

ers are eluted earlier [18]. The intensity of methylated C_2- and C_3-fragments of palmitic acid at *m/z* 74 and 87 is substantially higher than that of the other mass peaks in the spectrum. This can be also seen in Fig. 1, where the peaks at *m/z* 78 and 93 correspond to the ^{14}C fragments. The isotope effect in GLC on the capillary column used is then clear from the mass chromatograms of the fragments shown in Figs. 2 and 3, its magnitude being about 3 s. We must consider, however, that the fragments recorded in Figs. 2 and 3 do not originate from one isotopomer only, but that the position of the maxima agree relatively well with the position of the maxima of isotopomers of the highest content, *i.e.*, of [$^{12}C_{16}$]- and [$^{14}C_{14}$]palmitic acid methyl ester of molecular weights 270 and 298, respectively. At any rate, the isotope effect of larger molecules substituted with ^{14}C in GLC was confirmed; the heavier isotopomers are eluted earlier, which corresponds to their lower molar volumes [1,2] (and to the smaller size of the ^{14}C atom), as is apparent from the mass chromatograms in Figs. 2 and 3. Hence the advances of capillary GC are evident in the light of the older prediction about the impossibility of the GC separation of ^{14}C-labelled species from the corresponding non-radioactive standards [30].

Also, because of very small differences in the chemical and chromatographic behaviour of ^{14}C-labelled compounds and their unlabelled analogues, these compounds can be well recommended for chemical and biological research.

The isotope effect was also studied in more detail on perdeuterated *n*-alkanes in GLC on a capillary column with an efficiency higher than 200 000 plates for every species. An example of the separation of the isotopic species is shown in Fig. 4. All the data obtained on a capillary with a cross-linked polydimethylsiloxane stationary phase are given in

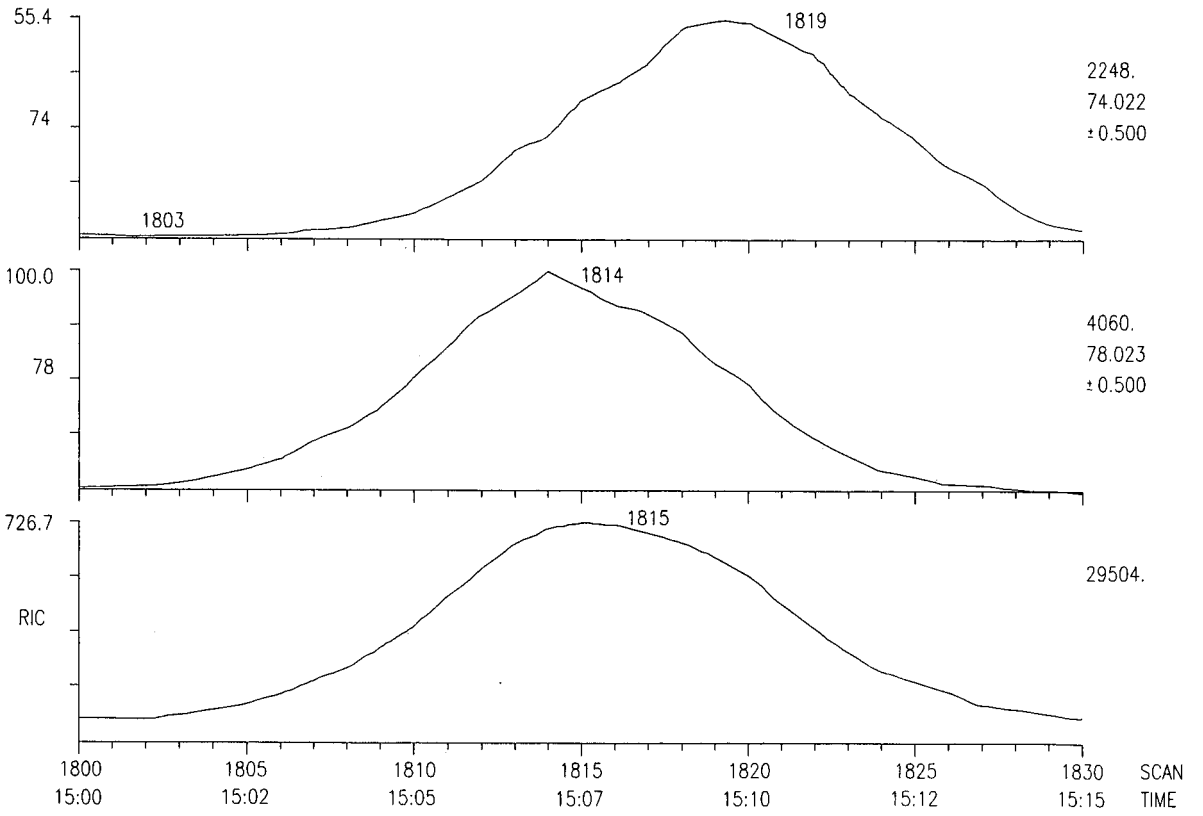

Fig. 2. Total ion and mass chromatograms at *m/z* 74 and 78 of isotopically unmodified and ^{14}C-fragments $CH_2 = C(OH)OCH_3^+$ of the methyl ester of [G-^{14}C]palmitic acid. Time in min:s.

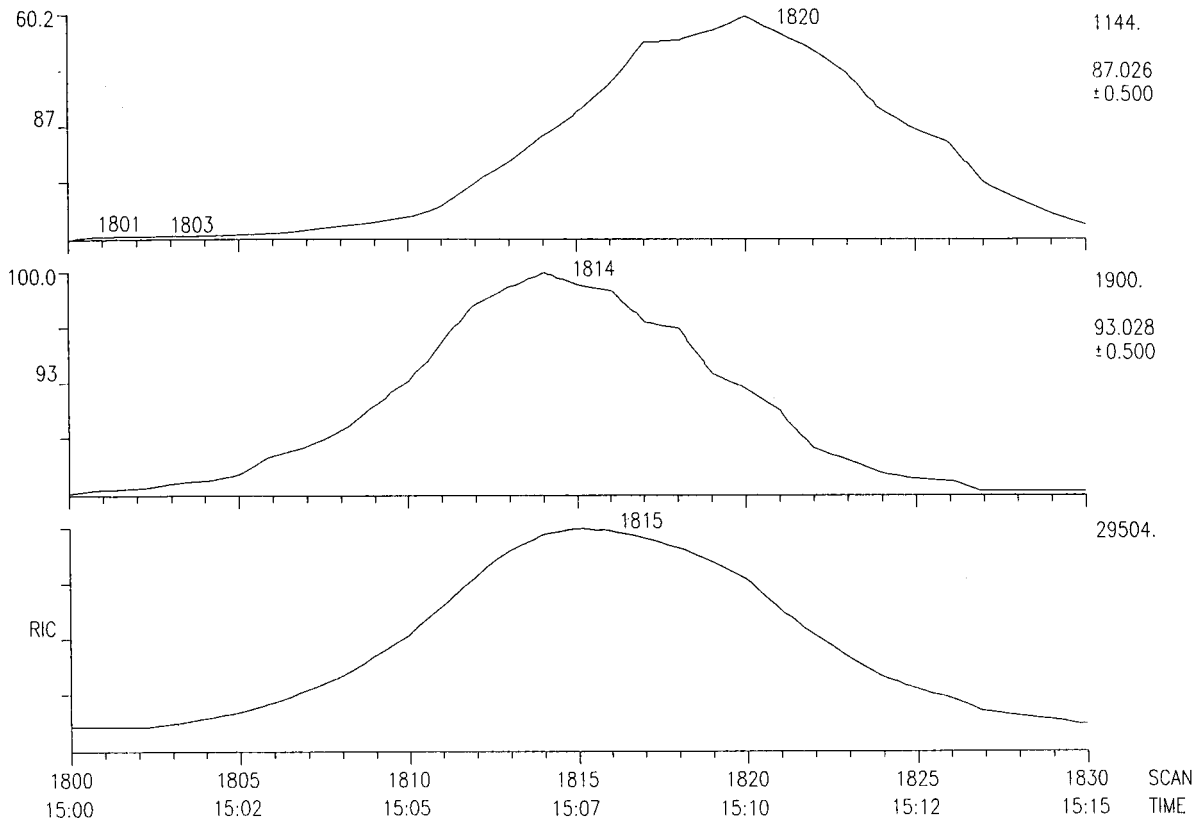

Fig. 3. Total ion and mass chromatograms at m/z 87 and 93 of isotopically unmodified and ^{14}C-fragments $CH_3OC(OH) = CHCH_2^+$ of the methyl ester of [G-^{14}C]palmitic acid. Time in min:s.

Table I. From these values one may calculate the differences in the enthalpy and entropy changes of the isotopomers (see Table II). The differences in enthalpy changes, $\Delta(\Delta H)$, are considerable and show a lower interaction of perdeuterated species with the stationary phase (owing to a larger number of deuterium atoms in C_{15}–C_{17} *n*-alkane molecules) in comparison with the values of about -60 cal mol^{-1} for molecules with a smaller number of deuterium atoms [8]. Also, the values of $(r_{12}-1)/N_D$ in Table I are interesting and confirm the earlier statements that the contribution to the value $r_{12}-1$ is approximately proportional to the number of ^2H atoms in the molecule [6,14]. In agreement with the results of Bermejo *et al.* [17], the separation factors depend on molar volumes, *i.e.*, on internuclear distances, as it was already claimed by Krumbiegel [15].

The "inverse" isotope effect was also found during a GC–MS investigation of the catalytic exchange of hydrogen with deuterium in desipramine [31], a compound with methylaminopropyl group ($C_{18}H_{22}N_2$); five isotopomers ($^2H_0$, $^2H_1$, $^2H_2$, $^2H_3$ and $^2H_4$) were determined in the mixture, which formed also a broader peak than the isotopically unmodified standard. Similarly to [G-^{14}C]palmitic acid, the mass chromatograms in Fig. 5 show that the heavier species are again eluted earlier (the relatively large peak broadening was probably caused by the relatively low temperature of the ion source of the mass spectrometer).

A comparison of the isotope effect in the GLC of isotopically substituted compounds suggests a *ca.* 30-fold higher separation factors for perdeuterated C_{15}–C_{17} *n*-alkanes as compared with [^{14}C]palmitic acid methyl ester with the same mass difference.

TABLE I

GLC DATA FOR PERDEUTERATED C_{15}–C_{17} *n*-ALKANES WITH ISOTOPICALLY UNMODIFIED C_{14}–C_{17} STANDARDS USING A 50 m × 0.25 mm I.D. FSOT COLUMN COATED WITH PS-255 CROSS-LINKED POLYDIMETHYLSILOXANE OF d_f 0.2 μm

t_r = Uncorrected retention time; r_{12} = separation factor; $w_{1/2}$ = peak width at half-heigth; R = resolution; I = Kováts retention index; N_D = number of deuterium atoms in molecule.

Conditions	*n*-Alkane	t_r	$w_{1/2}$	r_{12}	Log r_{12}	R	I	$\frac{r_{12}-1}{N_D}$
120°C, t_d = 1.354 min	$[^1H]C_{14}$	15.338	0.089					
	$[^2H]C_{15}$	22.793	0.154	1.1256	0.0514	10.23	1478.3	0.00393
	$[^1H]C_{15}$	25.486	0.156					
	$[^2H]C_{16}$	38.326	0.291	1.1314	0.0536	10.14	1577.6	0.00386
	$[^1H]C_{16}$	43.185	0.273					
	$[^2H]C_{17}$	64.721	0.453	1.1443	0.0585	14.07	1680,2	0.00401
	$[^1H]C_{17}$	73.865	0.312					
140°C, t_d = 1.699 min	$[^1H]C_{14}$	8.134	0.044					
	$[^2H]C_{15}$	11.104	0.068	1.1154	0.0474	9.25	1477.7	0.00361
	$[^1H]C_{15}$	12.189	0.070					
	$[^2H]C_{16}$	17.026	0.126	1.1203	0.0493	8.93	1576.9	0.00354
	$[^1H]C_{16}$	18.870	0.117					
	$[^2H]C_{17}$	26.509	0.181	1.1329	0.0542	10.49	1674.7	0.00369
	$[^1H]C_{17}$	29.806	0.189					
160°C, t_d = 1.877 min	$[^1H]C_{14}$	5.173	0.028					
	$[^2H]C_{15}$	6.489	0.039	1.1045	0.0432	7.27	1477.2	0.00327
	$[^1H]C_{15}$	6.971	0.039					
	$[^2H]C_{16}$	9.009	0.059	1.1095	0.0451	7.99	1576.4	0.00322
	$[^1H]C_{16}$	9.790	0.056					
	$[^2H]C_{17}$	12.840	0.081	1.1212	0.0497	9.42	1674.0	0.00337
	$[^1H]C_{17}$	14.169	0.085					
180°C, t_d = 2.032 min	$[^1H]C_{14}$	3.838	0.020					
	$[^2H]C_{15}$	4.472	0.024	1.0959	0.0398	5.74	1476.7	0.00300
	$[^1H]C_{15}$	4.706	0.024					
	$[^2H]C_{16}$	5.640	0.032	1.1012	0.0419	6.82	1575.7	0.00300
	$[^1H]C_{16}$	6.005	0.031					
	$[^2H]C_{17}$	7.350	0.042	1.1100	0.0453	8.20	1673.6	0.00310
	$[^1H]C_{17}$	7.935	0.042					
200°C, t_d = 2.124 min	$[^1H]C_{14}$	3.184	0.016					
	$[^2H]C_{15}$	3.515	0.019	1.0897	0.0373	3.87	1476.0	0.00280
	$[^1H]C_{15}$	3.640	0.019					
	$[^2H]C_{16}$	4.110	0.023	1.0932	0.0387	4.73	1575.2	0.00274
	$[^1H]C_{16}$	4.295	0.023					
	$[^2H]C_{17}$	4.946	0.028	1.1017	0.0421	6.03	1673.0	0.00283
	$[^1H]C_{17}$	5.233	0.028					

This is caused by the substantially lower molar volumes of compounds with peripheral deuterium atoms relative to the molar volume of compounds with skeletal ^{14}C atoms; the latter compounds exhibit a smaller decrease in their size compared with the hydrogen isotopes.

The interactions encountered in GLC differ from those appearing in GSC; they include Van der

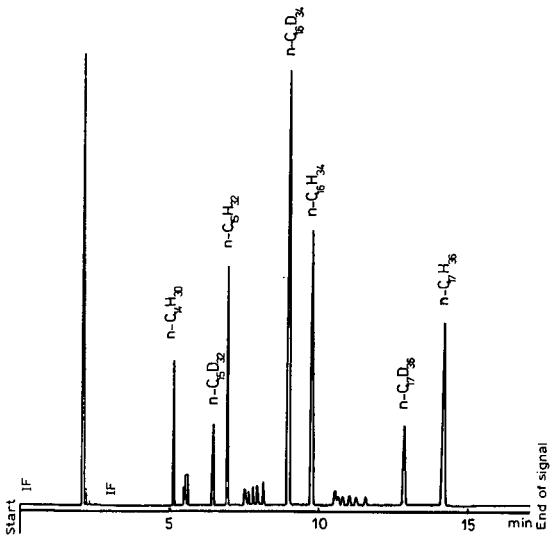

Fig. 4. Gas chromatogram of perdeuterated C_{15}–C_{17} *n*-alkanes with isotopically unmodified C_{14}–C_{17} standards on a FSOT column coated with PS-255 cross-linked polydimethylsiloxane (50 m × 0.25 mm I.D., d_f 0.20 μm) at 160°C and carrier gas (hydrogen) linear flow-rate 44 cm s^{-1}.

Waals dispersion forces, dipole–dipole interactions, influence of hydrogen bonds and polarizability [1], and therefore also isotope effects have a different character. In accordance with the enthalpy–molar volume–chromatographic retention relationship [2], the heavier isotopomers were found to have lower retentions, especially when dispersion forces played a dominant role.

CONCLUSIONS

The isotope effect in the GLC of ^{14}C-labelled compounds has been confirmed; it is small but measurable on highly efficient capillary columns.

Deuterated compounds, in comparison with ^{14}C-labelled species, exhibit much larger effects, which are caused by substantially lower molar volumes, and are proportional to the number of deuterium atoms in the molecules.

The isotope effects in the GLC of labelled compounds should be taken into account in RGC and in GC–MS; heavier isotopomers are eluted earlier,

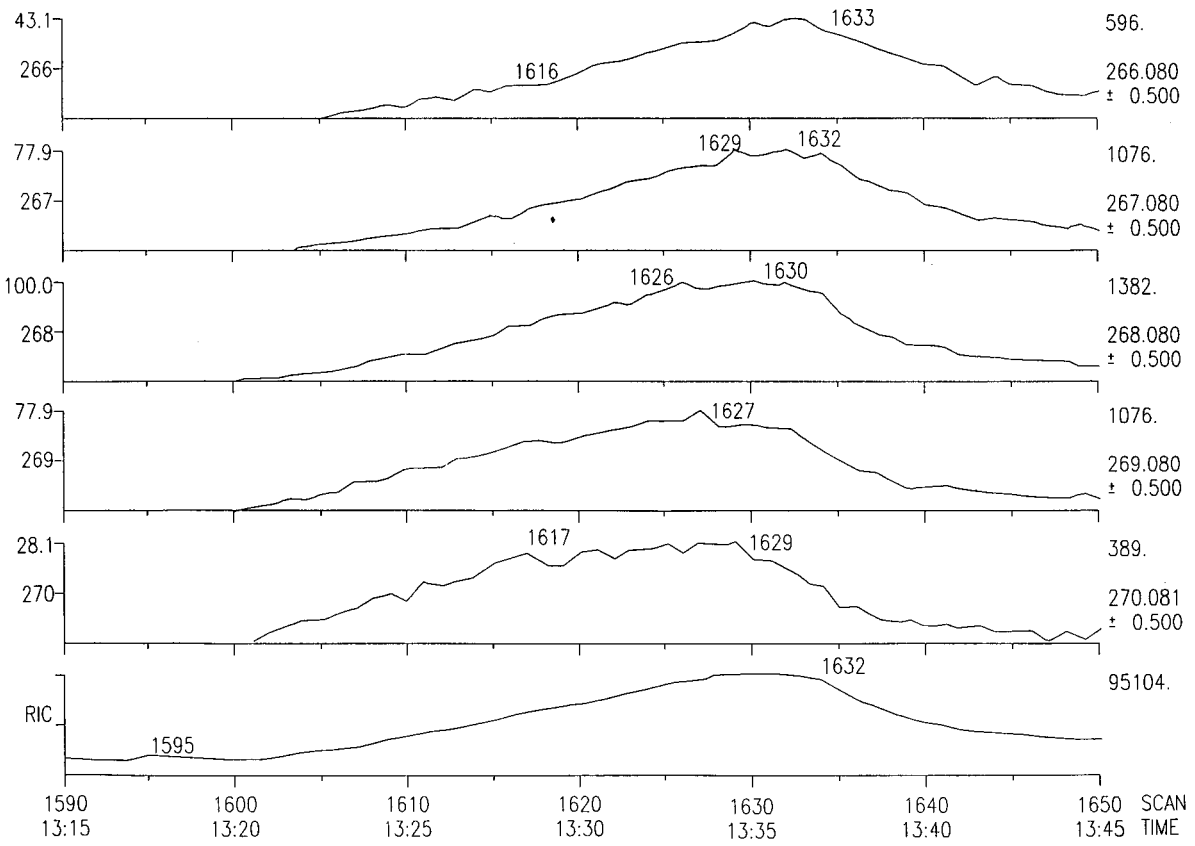

Fig. 5. Total and molecular ion chromatograms of catalytically deuterated desipramine, *i.e.*, of its $^2H_0$, $^2H_1$, $^2H_2$, $^2H_3$ and $^2H_4$ isotopomers. Time in min:s.

TABLE II

DIFFERENCES IN THE ENTHALPY AND ENTROPY CHANGES BETWEEN *n*-ALKANES AND THEIR PERDEUTERATED ANALOGUES CORRESPONDING TO THE CHROMATOGRAPHIC INTERACTION WITH POLYDIMETHYLSILOXANE PS-255

R = Correlation coefficient.

n-Alkane pair	$\Delta(\Delta H)$ (cal mol^{-1})	$\Delta(\Delta S)$ (cal K^{-1} mol^{-1})	R
n-C_{15}	−152.6	−0.1534	0.9974
n-C_{16}	−158.5	−0.1583	0.9992
n-C_{17}	−177.4	−0.1827	0.9984

predominantly when the solute–stationary phase interaction is due to dispersion forces.

REFERENCES

1 R. Kaliszan, *Quantitative Structure Chromatographic Retention Relationship*, Wiley, New York, 1987.
2 T. Hanai, *J. High Resol. Chromatogr.*, 13 (1990) 178.
3 K. E. Wilzabach and P. Riesz, *Science*, 126 (1957) 748.
4 A. F. Thomas, *Deuterium Labelling in Organic Chemistry*, Appleton-Century-Crofts, New York, 1971, p. 402.
5 E. A. Evans, *Tritium and Its Compounds*, Butterworths, London, 2nd ed., 1974.
6 W. E. Falconer and R. J. Cvetanovič, *Anal. Chem.*, 34 (1962) 1064.
7 W. A. Van Hook and M. E. Kelly, *Anal. Chem.*, 37 (1965) 508.
8 F. Bruner, G. P. Cartoni and A. Liberti, *Anal. Chem.*, 38 (1966) 298.
9 G. P. Cartoni, A. Liberti and A. Pela, *Anal. Chem.*, 38 (1966) 1618.
10 A. Liberti and L. Zeccolillo, *J. Chromatogr.*, 49 (1970) 18.
11 M. Matucha and E. Smolková, *J. Chromatogr.*, 127 (1976) 163.
12 B. E. Gordon, J. W. Otvos, W. R. Erwin and R. M. Lemmon, *Int. J. Appl. Radiat. Isot.*, 33 (1982) 721.
13 W. Jockisch, unpublished results, 1983.
14 G. Müller, K. Mauersberger and H. Sprinz, *Analyse Stabiler Isotope durch Spezielle Methoden*, Akademie-Verlag, Berlin, 1969, p. 257.
15 P. Krumbiegel, *Isotopieeffekte*, Akademie-Verlag, Berlin, 1970, p. 135.
16 F. Bruner, G. P. Cartoni and M. Possanzini, *Anal. Chem.*, 41 (1969) 1123.
17 J. Bermejo, C. G. Bianco and M. D. Guillén, *J. Chromatogr.*, 351 (1986) 425.
18 M. Matucha, *Chromatographia*, 27 (1989) 552.
19 B. F. Maume, P. Bournot, J. C. Lhuguenot, C. Baron, F. Barbier, G. Maume, M. Prost and P. Padieu, *Anal. Chem.*, 45 (1973) 1073.
20 Y. Cherrah, J. B. Falconnet, M. Desage, J. L. Brazler, R. Zini and J. P. Tillement, *Biomed. Environ. Mass Spectrom.*, 14 (1987) 653.
21 A. M. Lawson (Editor), *Mass Spectrometry*, Walter de Gruyter, Berlin, New York, 1989, p. 650.
22 Yu. A. Zolotarev, D. A. Zaitsev, M. Ju. Lubnin, V. Yu. Tatur and N. F. Myasoyedov, *Appl. Radiat. Isot.*, 39 (1988) 619.
23 M. Mohnke and J. Heybey, *J. Chromatogr.*, 471 (1989) 37.
24 M. Matucha, *Radioisotopy*, 29 (1988) 144.
25 J. Bigeleisen, *J. Chem. Phys.*, 34 (1961) 1485.
26 W. A. Van Hook, *J. Chem. Phys.*, 44 (1966) 234.
27 F. Lynen, *Angew. Chem.*, 67 (1955) 463.
28 P. Harris and A. T. James, *Biochem. J.*, 112 (1969) 325.
29 P. W. Majerus and P. R. Vagelos, *Adv. Lipid Res.*, 5 (1967) 1.
30 J. R. Catch, *Carbon-14 Compounds*, Butterworths, London, 1961, p. 68.
31 K. Fuksová and M. Matucha, presented at the *12th Radiochemical Conference, Mariánské Lázně, Czechoslovakia, May 7–10, 1990.*

Journal of Chromatography, 588 (1991) 259–264
Elsevier Science Publishers B.V., Amsterdam

CHROM. 23 640

Quality control procedure for the gas chromatographic determination of light hydrocarbons in petroleum liquid

G. P. Cooles*, A. P. O'Brien and J. J. Watt

B.P. International Limited, Sunbury Research Centre, Chertsey Road, Sunbury-on-Thames, Middlesex TW16 7LN (UK)

(Received April 15th, 1991)

ABSTRACT

The accurate determination of light hydrocarbons by gas chromatography is crucial to the petroleum industry. In production operations, it helps determine engineering applications at the wellsite and the refinery and assists in formulating production negotiations with business partners. This paper describes the steps taken to control the quality of gas chromatographic determination of C_2–C_{12} hydrocarbons in samples of petroleum liquid.

INTRODUCTION

Analysis and design of petroleum production facilities and schemes require thorough knowledge of the thermodynamic and physical properties of hydrocarbon fluids. It would, naturally, be best if knowledge of the physical properties was available from experimental observations. Those are, however, impossible to measure for all hydrocarbon fluids in all relevant conditions. Thermodynamic equations of state are therefore used to simulate and predict the phase and physical behaviour of fluids.

For oil and gas mixtures, the phase behaviour and physical properties, such as density and viscosity, are uniquely defined by the state of the system, *i.e.* the temperature (T), pressure (p) and the composition of the fluid. In simulating phase behaviour and physical properties of complex hydrocarbon mixtures accurately, it is a prerequisite to have detailed and accurate compositional information for each mixture.

The compositional description of production fluids at specific reservoir conditions of high p and T is usually achieved by analysis of separate gas and liquid phases after it has been flashed to ambient p and T (Fig. 1). When these analyses are combined in the correct gas-to-liquid ratio, the result is the total composition of the original pressurised fluid.

The analysis of the petroleum liquid can be performed in two steps: a simulated distillation (packed column) technique is used to determine integral C_1 to C_9 components and individual C_{10} to C_{39} pseudo-components*. The individual C_1 to C_9 hydrocarbons are determined by a capillary column technique, and the distribution is scaled to the C_1 to C_9 integral from the simulated distillation analysis. The methods employed to quality control the front end analysis of petroleum liquids is the subject of this paper.

EXPERIMENTAL

The gas chromatography system is conventional and comprises a nominal 100 m × 0.25 mm I.D. fused-silica wall-coated open tubular (WCOT) analytical column internally coated with OV-1 cross-linked stationary phase. Upstream of the analytical column is a short pre-column (150 × 6.35 mm)

* A pseudo-component is the sum of all individual components that elute from the chromatographic column after one *n*-alkane up to and including the next *n*-alkane. For example, the C_{12} pseudo-component is the sum of all components that elute after *n*-C_{11} up to and including *n*-C_{12}.

0021-9673/91/$03.50

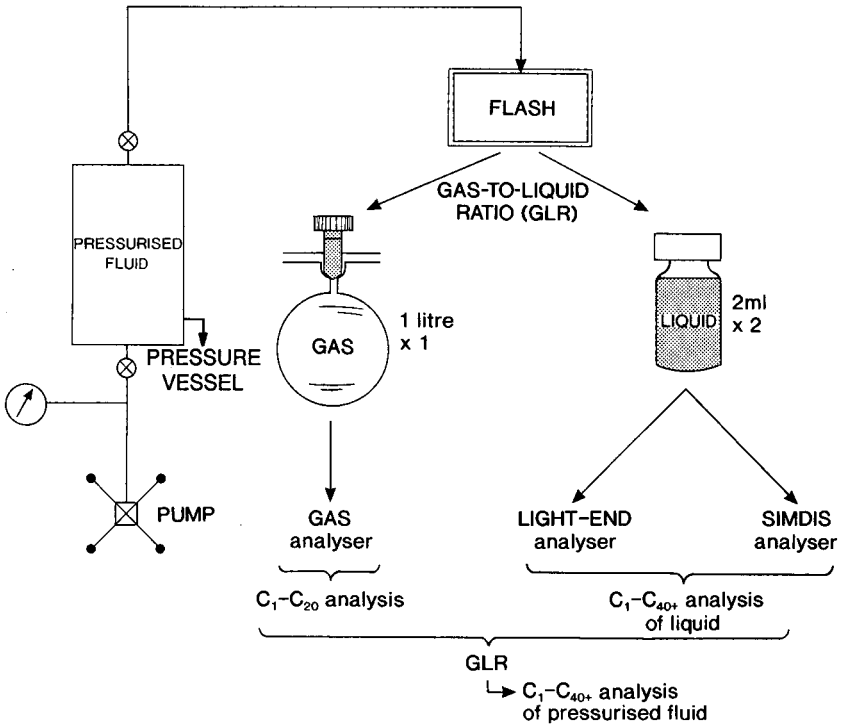

Fig. 1. Single flash separation and analysis (schematic).

packed with Chromosorb W coated with 5% OV-101. Backflush of the pre-column after a predetermined time (*ca.* 1 min) after sample injection, prevents heavy hydrocarbons reaching and degrading the analytical column. The pre-column is kept isothermal at 200°C, whilst the analytical column is programmed from 25°C (hold for 20 min) to 180°C (hold for 10 min) at 3°C min^{-1}. A schematic of the gas chromatography system is shown in Fig. 2.

Samples

Petroleum samples at ambient pressure and temperature are generated from flash separation of pressurised fluids at temperatures and pressures that are commonly encountered during production operations. The samples are presented for analysis in 2-cm^3 septum-capped glass vials with a small ullage space. They are analysed by gas chromatography as soon as possible after generation.

Quality control

It is vital to verify that compositional analyses by a chromatography system meet precision and accuracy criteria required by the end-user of the data. It is therefore imperative to have quality control procedures in place to be assured of the relevance and value of analytical data being produced.

Daily maintenance includes leak tests, "blank" runs and analyses of natural and synthetic standards of known and accepted composition. Failure to reach a desired performance results in remedial action being taken and satisfactory re-verification of the chromatographic system before samples are analysed.

The traditional method for verifying the performance of gas chromatographs for determining light hydrocarbons in liquid samples was by the analysis of a synthetically prepared blend of C_5–C_{20} *n*-alkanes and benzene, toluene, ethylbenzene and *o*-xylene diluted in CS_2. The drawbacks of using a C_5–C_{20} hydrocarbon blend to quality control a

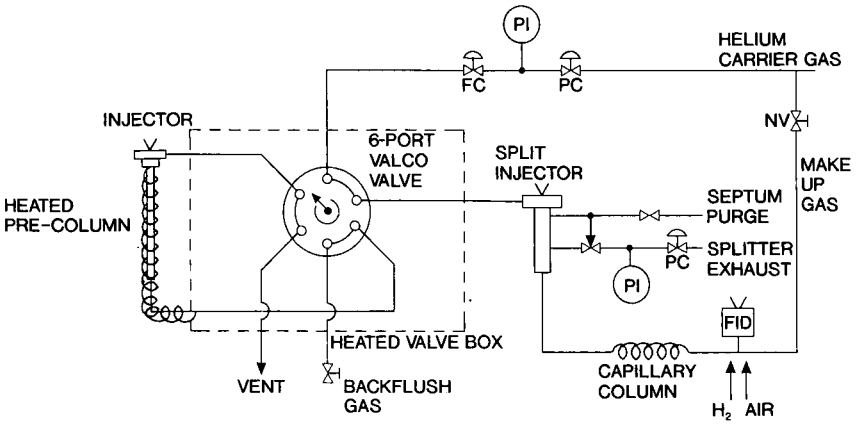

Fig. 2. Flow diagram of gas chromatography system. FC = Flow controller; FID = flame ionization detector; PC = pressure controller; PI = pressure indicator; NV = needle valve.

C_1–C_9 analysis method are obvious: (i) this blend can only quality control the analysis down to C_5; (ii) sample light-ends may be rapidly lost; and (iii) the verification procedure can only be rigorously applied when a fresh batch of standard is prepared.

A standard for the quality control of gas chromatographic determinations of C_1–C_9 hydrocarbons in liquid samples need to fulfil several stringent criteria. A standard needs to be: (i) a representative example of the majority of sample compositions encountered; (ii) homogeneous; (iii) available in sufficient quantities to last a significant period of time (preferably > 1 year); (iv) stable in long-term storage; and (v) stored as a single phase.

A representative stabilised condensate sample from a producing field gave a C_1–C_{12} composition given in Table I. With the exception of the ethane content, this analysis provides a useful target composition for a synthetic gravimetrically blended standard. In order to make the standard easier and more accurate to prepare, a higher concentration of ethane was used in the preparation of the standard.

Predicted phase behaviour

A most important consideration for the preparation of a standard is for it to be stored and sampled as a single homogeneous phase. The phase behaviour of the target composition was determined as a function of temperature and pressure using a cubic equation of state based on that of Peng and Robinson [1].

The resultant phase envelope that describes the predicted phase behaviour of the standard composition is given in Fig. 3. The area inside the curve describes the temperature and pressure conditions in which the standard would exist as two discrete phases. Outside of this region the blend occurs as a single phase; to the left of the critical point as a single

TABLE I

PETROLEUM LIGHT HYDROCARBON ANALYSIS

Component/ pseudo-component	Representative analysis (%, w/w)	Composition of standard (%, w/w)
Methane	0.000	0.000
Ethane	0.011	0.204
Propane	1.363	1.331
2-Methylpropane	1.774	1.861
Butane	6.766	6.927
2-Methylbutane	3.824	3.786
Pentane	6.051	7.081
Hexanes	10.260	10.248
Heptanes	15.167	15.278
Octanes	15.313	15.026
Nonanes	8.500	8.508
Decanes	9.733	8.141
Undecanes	7.032	7.025
Dodecanes	5.413	5.421
Benzene	1.600	1.588
Toluene	3.168	3.256
Ethylbenzene	0.850	1.031
o-Xylene	3.175	3.286

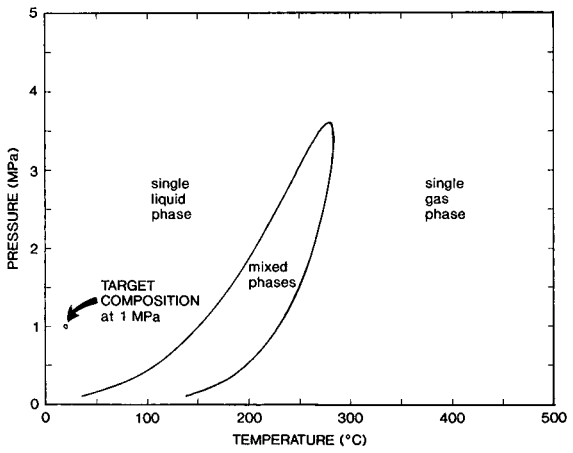

Fig. 3. Predicted phase diagram for C_2–C_{12} gravimetric blend.

liquid phase and to the right as a single gas phase. At *ca.* 1 MPa (10 bar) and ambient temperature, the blend is expected to be well within the desired single liquid phase region.

Preparation of the standard

The most common type of pressure vessel used for petroleum phase studies employs metallic mercury as the pressuring medium. The requirement of a gas ullage space in a mercury-containing vessel also prevent these type of vessel being used. As a consequence, hydrocarbons were blended within mercury-containing pressure vessels and then transferred to a mercury-free piston vessel for storage and dispensation.

The light hydrocarbon standard was prepared in two parts: a gas fraction (ethane to pentane) and a liquid fraction (hexane to dodecane). This allowed the minor components to be weighed in acceptable masses to help minimise any weighing errors.

The mercury pressure vessel which was used to prepare the gas fraction had no seals exposed to the fluid. The vessel was evacuated and then weighed on a double pan swing balance before ethane, the component destined to have the lowest concentration in the blend, was introduced. The vessel was reweighed to give the mass of ethane.

A second vessel was filled with propane and pressurised to *ca.* 7 MPa (70 bar) with mercury. This second vessel was then connected to the first vessel using 3.175 mm O.D. stainless-steel tubing. All the pipework and valves were purged with propane. With a knowledge of the density of propane at these conditions, the volume required to give the desired mass was calculated and introduced into the first vessel. This vessel was then reweighed to determine the exact mass of propane transferred. This procedure was repeated for all the hydrocarbons up to pentane.

For each weighing the barometric pressure, humidity and laboratory temperature were recorded so that buoyancy corrections for the weighed masses could be determined. All weights used were traceable to national standards.

The liquid fraction (C_6–C_{12} and aromatics) was prepared in a 250-cm^3 volumetric flask. The highest molecular mass (*i.e.*, lowest vapour pressure) hydrocarbons were weighed in first, using a single pan electronic balance. This blend was then transferred to an evacuated and preweighed pressure vessel.

The two fractions were combined by first pressuring the gas fraction to *ca.* 7 MPa with mercury, and then inverting the vessel several times to ensure homogeneity of the fluid. After ensuring that the valves were free of residual mercury the required mass of gas was then added to the liquid fraction. The resultant blend was finally pressured to 7 MPa and inverted several times to ensure homogeneity.

The blend was transferred to a mercury-free piston vessel (500 cm^3 capacity) for long-term storage. Aliquots of the blend were sampled into a smaller (30 cm^3 capacity) piston vessel and diluted to *ca.* 10% in hexadecane. Both piston vessels were pressurised with nitrogen, the diluted blend is used as the quality control standard as the neat blend is too concentrated to use directly.

Analysis technique

The sampling pipework on the piston vessel between the valve and septum is removed and cleaned with acetone and vacuum dried before each sample is taken. The hydrocarbon blend is thoroughly mixed with an internal mixing rod prior to a sample being taken.

The phase envelope of the gravimetric mixture shows that the bubble pressure is *ca.* 0.1 MPa absolute (1 bar a) at room temperature (Fig. 3). In order to keep the blend single phase when sampling, it was expected that gas- and liquid-tight syringes

needed to be used. However, it was found that the conventional 5- or 10-μl syringes were suitable. The sampling technique withdraws 5 μl of liquid (the pressure of the blend pushes sample into the syringe) of which 4 μl is ejected immediately prior to manual injection.

RESULTS

The light-hydrocarbon blend was analysed on two different instruments at different laboratories and with different operators. The instruments were given designations GC1 and GC2. Analytical results from GC1 (8 analyses) were taken over a two-week period, whilst those for GC2 (7 analyses) were taken over a 4-week period subsequent to the former. All component recoveries are taken relative to *n*-octane = 100% (Table II). Detector response factors for all alkanes was taken to be unity; those for the aromatic components are specified in Table II.

The recovery of normal and branched alkane components fall within a narrow 98–102% range, with the exception of the lighter ($<C_4$) components recovered from GC1 (Fig. 4). The loss of these components was attributed to the use of an unchilled syringe in this laboratory. When the syringe was chilled in a refrigerator at 4°C for at least 5 min before sampling (as with GC2), the C_2–C_4 component recoveries are greatly improved.

The other outliers from the 98–102% recovery interval are the aromatic components, where the component recoveries are generally greater than expected. Both instruments tested show this behaviour for toluene and *o*-xylene (103–105% recovery), although for benzene there is a difference between the two instruments (100% and 103%). Ethylbenzene has a recovery of *ca.* 100% in both instruments.

It is difficult to reconcile these apparent discrepancies from "expected" behaviour in a consistent way. Aromatic species exhibit a different flame ionisation detector response than aliphatic species. The response factors applied for this study were originally derived experimentally [2]. However,

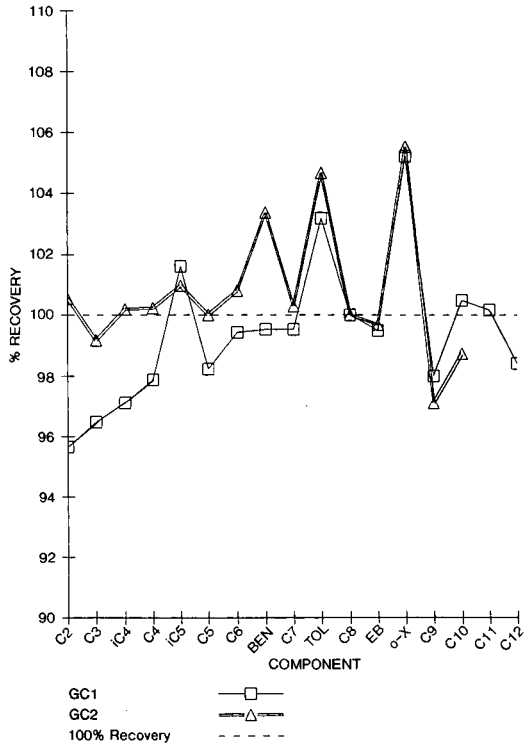

Fig. 4. Results summary.

TABLE II

LIGHT-HYDROCARBON ANALYSIS OF GRAVIMETRIC STANDARD

Relative response factor $(RRF)_{benzene} = 0.89$; $RRF_{toluene} = 0.94$; $RRF_{EB/X} = 0.97$. EB = ethylbenzene, X = xylenes.

Component	Mean recovery (%)	S.D.		
	GC1		GC2	
Ethane	95.7	1.84	100.6	0.96
Propane	96.5	1.38	99.2	1.95
2-Methylpropane	97.1	0.98	100.2	1.50
n-Butane	97.9	1.15	100.2	1.26
2-Methylbutane	101.6	1.10	101.0	1.07
n-Pentane	98.3	1.07	100.0	1.17
n-Hexane	99.5	0.81	100.8	0.94
Benzene	99.5	0.80	103.4	0.88
n-Heptane	99.5	0.45	100.3	0.50
Toluene	103.2	0.31	104.7	0.38
n-Octane	100.0	0.00	100.0	0.00
Ethylbenzene	99.5	1.63	99.7	0.64
o-Xylene	105.2	0.41	105.5	0.46
n-Nonane	98.0	0.43	97.1	0.64
n-Decane	100.5	1.88	98.7	1.07
n-Undecane	100.2	0.33	[a]	
n-Dodecane	98.4	0.64	[a]	

[a] Data collection stopped after *n*-decane.

these response factors may depend on such factors as detector design or gas flow into it.

The aromatic hydrocarbons are also present in much lower concentrations compared to most components in the blend: this makes the examination of aromatic hydrocarbon recoveries a very stringent test of the system.

The analytical performance of the gas chromatographs are considered excellent for the analysis of C_2–C_9 hydrocarbons in liquid petroleum samples. The apparent loss of some of the lightest alkanes in GC1 is practically insignificant in view of the small amounts of these components in most liquid samples, which is further reduced when the analytical results from both gas and liquid samples are combined to yield compositional analyses of total petroleums.

Response factors

Dietz's classical work on the experimental determination of weight relative response factors [2] suggests that response factors of between 0.92 and 1.00 should be applied to aliphatic species between C_2 and n-C_9, and that the response factors between these end members vary in an unsystematic way. Our findings, however, demonstrate that it is satisfactory for response factors of 1.00 to be applied to all alkanes between C_2 and C_{12}, which is widespread practice with flame ionisation detectors.

SUMMARY

In summary, the synthesis and routine analysis of a pressurised blend of hydrocarbons between ethane and dodecane verifies our standard operation procedures for the determination of light hydrocarbons in liquid samples. The determinations validate precision (<2% relative standard deviation) and accuracy (generally 98–102% component recovery). With contentious production issues providing the most stringent analytical quality requirements, it is believed that only with such a quality control procedure are such analyses fit for purpose.

ACKNOWLEDGEMENTS

The authors wish to thank Mr. D. G. Young and Mrs. K. J. Roberts for chromatographic separations, and British Petroleum plc for permission to publish.

REFERENCES

1 D.-Y. Peng and D. B. Robinson, *Ind. Eng. Chem. Fundam.*, 15 (1976) 59–64.
2 W. A. Dietz, *J. Gas Chromatogr.*, 5 (1967) 68–71.

Journal of Chromatography, 588 (1991) 265–272
Elsevier Science Publishers B.V., Amsterdam

CHROM. 23 636

Gas chromatographic analysis of fatty acid methyl esters: avoiding discrimination by programmed temperature vaporizing injection

K. Eder, A. M. Reichlmayr-Lais and M. Kirchgessner*

Institut für Ernährungsphysiologie, Technische Universität München, 8050 Freising 12 (Germany)

(First received April 19th, 1991; revised manuscript received July 9th, 1991)

ABSTRACT

The programmed temperature vaporizing injection technique was used in its three operation modes (split injection, splitless injection and solvent elimination injection) for injection of fatty acid methyl esters into a gas chromatographic system. The relative response factors of standard fatty acid methyl esters and their coefficients of variation were determined. Using programmed temperature vaporizing injection, discrimination between high- and low-boiling-point fatty acid methyl esters can be avoided and also high precision can be achieved by injecting small amounts of fatty acid methyl esters. High precision was also demonstrated by the injection of small amounts of fatty acid methyl esters from rat red blood cell membrane phosphatidylcholine and phosphatidylethanolamine. Contrary to the programmed temperature vaporizing injection technique, sample discrimination occurred when classical split injection with the usual injection conditions was used for injection of standard fatty acid methyl esters.

INTRODUCTION

In high-resolution gas chromatography (GC) sample injection is the most critical step for achieving high accuracy and precision [1–4]. For injection of samples into a GC system the classical split and splitless injection techniques, the on-column injection technique and the programmed temperature vaporizing (PTV) injection technique are used. The classical split injection, introducing the sample into the hot injection chamber, is the most widely used techique for injection of fatty acid methyl esters (FAMEs) [5–10]. However, controversy exists about the accuracy and precision of results obtained by GC analysis of FAMEs with classical split injection. While many studies have shown that this technique may cause discrimination between acids with low and high boiling points [5,10] because of the high temperature of the injection chamber, others [6,9] have shown that using the same technique it is possible to obtain excellent results. The problems of the classical split injection resulting from the high temperature of the injection chamber can be avoided by cold injection of the sample using the on-column or PTV injection technique. Some authors have shown that, using cold injection techniques, excellent accuracy and precision of GC determination of hydrocarbons [11–18] can be achieved. In spite of this, cold injection has been applied by only a few authors for the determination of FAMEs [19,20].

In the present work standard FAMEs were injected using PTV injection in its three operation modes, namely cold split and splitless injection and solvent elimination injection for injection of standard FAMEs into a GC system. The accuracy and precision of the results were checked by measuring the relative response factors of standard FAMEs and their coefficients of variation. Moreover, as an example for practical application, FAMEs of rat red blood cell phospholipid classes were injected. Besides the PTV technique classical split injection technique was also used for injection of standard

0021-9673/91/$03.50

FAMEs in order to compare the suitability of both injection techniques for injection of FAMEs.

EXPERIMENTAL

Reagents, samples and chromatographic equipment

Fatty acid standards were procured from Sigma (Taufkirchen, Germany). The purity of all fatty acid standards was at least 99%. A standard solution was prepared which contained $C_{8:0}$–$C_{24:1}$ fatty acids in concentrations of 10–100 mg/l [in dichloroethane, butylated hydroxytoluene (BHT) as an antioxidant; the composition is shown in Table I]. Preparation of standard FAMEs was carried out with methanolic boron trifluoride according to Morrison and Smith [21].

Blood samples were taken from male Sprague–Dawley rats. GC analysis of FAMEs was performed on a Sichromat 2 GC system (Siemens, Karlsruhe, Germany) equipped with a 50 m × 0.25 mm I.D. CP-Sil 88 wall-coated (film thickness 0.25 μm) fused-silica column (Chrompack, Middelburg, Netherlands) and a flame ionization detector (300°C). For injection either a PTV injection system or a classical split injection system was used. Hydrogen was used as the carrier gas. Peak areas were measured using a Merck-Hitachi (Darmstadt, Germany) D-2500 integrator. Separation of rat red blood cell phospholipid classes was performed on a Merck-Hitachi high-performance liquid chromatographic (HPLC) system consisting of a gradient pump (L-6200), a diode array (L-3000), an integrator (D-2000), a Merck Si-60 (5 μm) column and a fraction collector (Gilson, Model 201, Villiers-le-Bel, France).

TABLE I

COMPOSITION OF THE FATTY ACID STANDARD SOLUTION USED IN THE PRESENT EXPERIMENTS

FAME	Concentration (mg per 100 ml)
8:0	10.65
10:0	7.98
11:0	8.06
12.0	6.57
14:0	10.94
14:1	6.50
16:0	6.78
16:1	12.56
17:0	6.63
18:0	11.24
18:1	6.41
18:2	10.37
18:3	6.68
20:0	10.26
20:1	5.89
20:2	1.59
20:3	2.71
20:4	7.27
21:0	7.59
22:0	9.57
22:1	7.79
22:2	2.54
22:3	4.76
22:6	8.48
24:0	9.30
24:1	2.60

Preparation of FAMEs from rat red blood cell membrane phospholipid classes

Red blood cell membranes were prepared according to ref. 22. Phospholipids were extracted from red blood cell membranes with isopropanol [23]. Extracted phospholipid classes were separated using normal-phase HPLC according to ref. 24 and collected with a fraction collector. Transesterification of separated phospholipid classes was carried out with sodium methoxide [25].

Chromatographic conditions

Classical split injection. A 2.0-μl aliquot of standard FAME solution was manually fast-injected with a 2-μl Hamilton syringe into the injection chamber (temperature 300°C). The carrier gas flow-rate was 2.0 ml/min; the split ratio was 1:25. The injection insert consisted of a plain tube packed with silanized glass wool. The oven temperature program was: 120°C held for 3 min, 30°C/min to 160°C, 15°C/min to 200°C, 200°C held for 1.5 min, 10°C/min to 225°C, 225°C held for 15 min. The relative response factors (RRFs) of FAMEs were calculated in relation to either one ($C_{17:0}$) or three ($C_{11:0}$, $C_{17:0}$, $C_{21:0}$) internal standards.

PTV injection. The PTV injection program was: 25°C held for 1 min after injection, 800°C/min to 300°C, 300°C held for 10 min, then the PTV injector was cooled. The oven temperature program was: 50°C held for 1 min, 30°C/min to 160°C, 15°C/min to 200°C, 200°C held for 1.5 min, 10°C/min to

225°C, 225°C held for 15 min. Note that the oven temperature was initially low in order to avoid peak splitting. A typical chromatogram is shown in Fig. 1.

Injection of standard FAMEs. For cold splitless injection the split vent was closed for the first 5 min to allow total entrance of the vaporized sample into the column and was then opened to allow purging of the vaporizer. A 2.0-μl sample of the standard FAME solution (diluted 1:36) was injected.

For cold split injection the split vent was opened during the whole analysis. Split ratios were 1:25, 1:6 and 1:2. A 2.0-μl sample of the standard FAME solution (undiluted for a split ratio of 1:25, 1:6 diluted for a split ratio of 1:6, and 1:36 diluted for a split ratio of 1:2) was injected.

For solvent elimination injection a 2.0-μl aliquot of FAME standard solution (1:36 diluted) was injected. The split vent (split ratio 1:100) was opened for the first 6 s after injection in order to allow elimination of the solvent by passage through the split exit and was then closed in order to allow complete entrance of the sample vapors from the injector to the column after heating the vaporizer.

Injection of FAMEs from red blood cell membrane

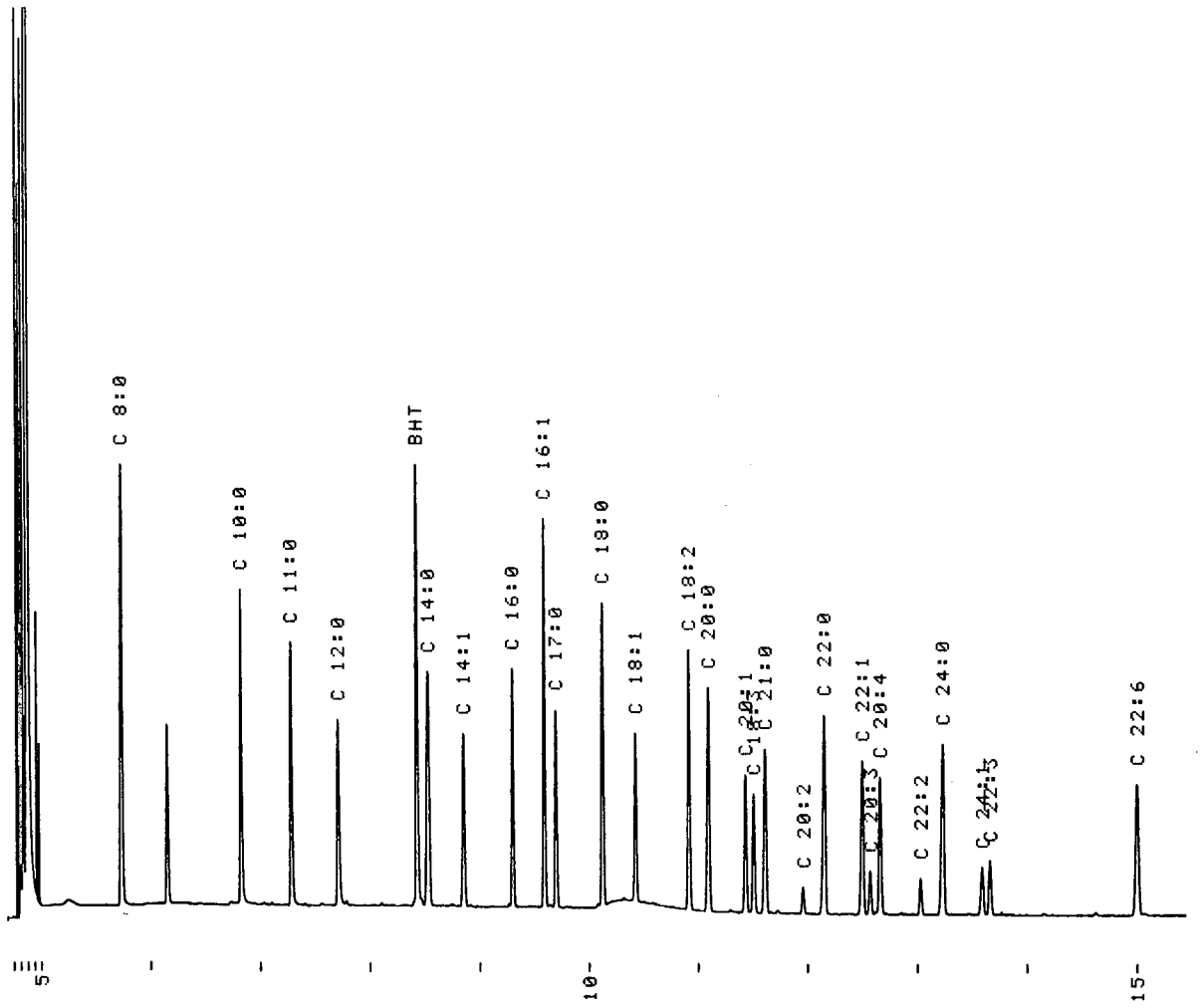

Fig. 1. Separation of standard FAMEs using PTV split injection. Split ratio was 1:25; the amounts of FAMEs injected into the injection chamber were between 32 and 252 ng. Time scale in min.

phospholipid classes. A 2.0-μl sample of the FAME extract was injected using the cold split injection technique with a split ratio of 1:2. Other chromatographic conditions were as described above.

RESULTS AND DISCUSSION

The aim of the present study was to check the accuracy and precision of the GC analysis of FAMEs with either PTV or classical split injection. For the investigation of accuracy, response factors of standard FAMEs were determined. Ackman and Sipos [26] proposed theoretical response factors for all FAMEs depending on the weight percentage in the molecule of "active" carbon atoms, including all carbon atoms except that of the carbonyl group. Bannon and co-workers [27–30] and Albertyn *et al.* [31] have shown in experiments that these theoretical response factors are highly accurate for all FAMEs. Therefore the occurrence of sample discrimination can be recognized by the deviation of determined response factors from the theoretical values.

The classical split injection technique is the most widely used technique for injection of FAMEs. In the present study the classical split injection technique was used for injection of standard FAMEs with injection conditions similar to those used by many authors [5–8,10,32,33] with the exception of a higher injector temperature (300°C), which has been reported to be useful in order to avoid discrimination between acids with high- and low-boiling points [9]. The results of the present study (Table II) show that determination of FAMEs using the classical split injection and the conditions chosen gives results with low accuracy and precision. Determined RRFs of FAMEs deviated from theoretical RRFs with an increase in their chain length. This means that there occurred discrimination of FAMEs which was highest for high-boiling-point FAMEs. The high coefficients of variation show that the precision of the results was also low when $C_{17:0}$ was used as the internal standard. The use of additional internal standards for calculation reduced the coefficients of variation somewhat, but the precision achieved by this method was also unacceptable. Similar results were obtained by other authors using the classical split injection technique with similar conditions. Their results also showed differences between determined and theoretical RRFs of FAMEs [32,33], and coefficients of variation were similar to those obtained in the present study [5,10]. However, besides these studies demonstrating that the classical split injection technique causes problems due to discrimination effects, a few authors [6,9] have shown that if all injection parameters (injector temperature, split vent flow-rate, volume injected, speed of injection, injector insert design, etc.) are optimized

TABLE II

RRFs OF STANDARD FAMEs RELATED TO EITHER ONE ($C_{17:0}$) OR THREE ($C_{11:0}$, $C_{17:0}$, $C_{21:0}$) INTERNAL STANDARDS DETERMINED USING CLASSICAL SPLIT INJECTION TECHNIQUE

Coefficients of variation (%) are stated in parentheses.

FAME[a]	RRF (n = 5)	
	$C_{17:0}$[b]	$C_{11:0}$, $C_{17:0}$, $C_{21:0}$[c]
8:0	0.91 (24.0)	1.35 (16.5)
10:0	0.71 (13.9)	1.06 (3.0)
11:0	0.67 (13.8)	1.00
12:0	0.72 (12.3)	1.06 (2.9)
14:0	0.76 (9.3)	1.13 (5.6)
14:1	0.78 (9.7)	1.16 (5.2)
16:0	0.86 (3.7)	0.86 (3.7)
16:1	0.88 (4.6)	0.88 (4.6)
17:0	1.00	1.00
18:0	1.12 (5.0)	1.12 (5.0)
18:0	1.08 (3.2)	1.08 (3.2)
18:2	1.12 (3.8)	1.12 (3.8)
18:3	1.28 (3.9)	1.28 (3.9)
20:0	1.48 (15.3)	0.88 (8.0)
20:1	1.33 (13.9)	0.79 (8.9)
20:2	1.58 (15.3)	0.92 (2.3)
20:3	1.65 (14.4)	0.99 (9.6)
20:4	1.56 (11.5)	0.93 (10.8)
21:0	1.71 (24.0)	1.00
22:0	1.72 (26.3)	1.00 (5.3)
22:1	1.85 (25.1)	1.07 (4.8)
22:2	1.86 (22.0)	1.08 (5.7)
22:3	2.20 (25.5)	1.28 (4.5)
22:6	3.58 (22.6)	2.09 (3.6)
24:0	2.08 (35.3)	1.19 (12.8)
24:1	2.14 (33.1)	1.23 (10.1)

[a] Amounts of FAMEs injected into the injection chamber were between 32 and 252 ng.

[b] $C_{17:0}$ was used as internal standard for calculation of all FAMEs.

[c] $C_{11:0}$ was used as internal standard for calculation of C_8 to C_{14}, $C_{17:0}$ for calculation of C_{16} to C_{18} and $C_{21:0}$ for calculation of C_{20} to C_{24}.

discrimination of FAMEs can be totally eliminated and thus high accuracy and precision in GC determination of FAMEs with classical split injection can be achieved. This means that it is possible to achieve results with high accuracy and precision using classical split injection. However, it seems that achieving high accuracy and precision is not easy and the injection conditions used by many authors, including those of our classical split injection technique, might not allow it.

The PTV injection technique was introduced by Vogt and co-workers [34–36] in order to inject very large sample volumes using the solvent elimination mode. However, other authors [14–18] have shown that PTV injection is also able, like the on-column injection, to avoid sample discrimination during injection, a problem often demonstrated with classical split injection because of the high temperature of the injection chamber. In spite of the excellent results of GC determination of hydrocarbons [14–

TABLE III

RRFs (RELATING TO $C_{17:0}$) OF FAMEs DETERMINED BY PTV INJECTION IN DIFFERENT OPERATION MODES IN COMPARISON WITH THEORETICAL RRF

Coefficients of variation (%) of RRFs are stated in parentheses.

FAME	Theoretical RRF[a]	RRF determined				
		Split injection			Splitless injection ($n = 5$) (0.9–7 ng)	Solvent elimination injection ($n = 6$) (0.9–7 ng)
		Split ratio				
		1:2 ($n = 5$) (0.9–7 ng)[b]	1:6 ($n = 5$) (5.4–42 ng)	1:25 ($n = 8$) (32–252 ng)		
8:0	1.18		0.98 (4.51)	0.78 (8.95)		
10:0	1.12	0.74 (3.57)	0.83 (2.99)	0.69 (8.67)	2.19 (14.22)	
11:0	1.09	0.72 (4.12)	0.92 (4.59)	0.73 (6.58)	2.40 (7.20)	
12:0	1.07	0.81 (11.33)	0.92 (6.01)	0.94 (4.39)	1.12 (13.48)	
14:0	1.04	0.90 (3.21)	0.98 (1.15)	1.00 (2.26)	0.99 (9.19)	1.12 (14.78)
14:1	1.03	0.98 (5.11)	1.00 (1.86)	1.02 (2.42)	1.03 (2.35)	1.29 (16.33)
16:0	1.02	0.98 (2.27)	1.01 (1.08)	0.99 (0.83)	1.01 (1.06)	0.98 (2.30)
16:1	1.01	1.00 (1.67)	1.00 (0.96)	1.00 (0.53)	0.97 (0.40)	1.00 (2.40)
17:0	1.00	1.00	1.00	1.00	1.00	1.00
18:0	1.00	1.00 (1.95)	1.01 (1.31)	1.00 (1.07)	0.95 (5.68)	1.02 (0.74)
18:1	0.99	1.02 (2.39)	1.01 (2.80)	1.01 (0.52)	1.00 (1.23)	1.02 (0.24)
18:2	0.99	1.01 (1.38)	1.01 (1.17)	1.02 (0.19)	1.01 (0.47)	1.02 (0.56)
18:3	0.98	1.04 (1.74)	1.02 (2.30)	1.03 (0.44)	1.02 (1.36)	1.02 (0.57)
20:0	0.98	1.01 (2.36)	1.02 (1.36)	1.00 (0.41)	0.97 (2.48)	1.01 (3.07)
20:1	0.98	0.97 (2.07)	0.99 (1.18)	1.01 (0.43)	1.02 (0.68)	1.02 (0.44)
20:2	0.97	1.02 (1.19)	1.04 (3.87)	1.02 (0.69)	1.03 (1.02)	1.03 (1.07)
20:3	0.97	1.03 (4.80)	1.03 (3.51)	1.02 (1.23)	1.04 (5.22)	1.04 (2.82)
20:4	0.96	1.06 (5.55)	1.04 (4.20)	1.05 (0.96)	1.03 (0.66)	1.05 (0.94)
21:0	0.98	1.00 (1.95)	0.98 (1.38)	1.04 (0.66)	0.99 (0.60)	1.01 (3.43)
22:0	0.97	0.95 (1.49)	0.95 (1.61)	1.01 (0.53)	0.99 (2.03)	0.98 (0.83)
22:1	0.97	0.96 (0.83)	0.97 (1.45)	1.04 (0.53)	1.02 (1.63)	0.99 (0.40)
22:2	0.96	1.01 (4.39)	1.01 (2.39)	1.02 (2.75)	1.08 (2.02)	1.03 (3.65)
22:3	0.96	1.03 (3.14)	1.02 (1.31)	1.03 (0.95)	1.06 (9.27)	1.05 (0.84)
22:6	0.94	1.06 (1.76)	1.03 (1.43)	1.06 (0.91)	1.06 (0.94)	1.07 (1.21)
24:0	0.96	1.02 (2.25)	1.00 (1.70)	0.98 (0.58)	1.01 (2.88)	1.01 (1.47)
24:1	0.96	1.02 (3.43)	0.99 (2.35)	1.00 (0.82)	1.01 (3.60)	1.02 (0.65)

[a] As proposed by Ackman and SIPOS [26].
[b] FAME amounts injected into the injector chamber.

18] achieved by injection with PTV, this injection technique is very seldom used for injection of FAMEs.

Table III shows that determined RRFs of $C_{12:0}$ and higher deviated only slightly from their theoretical RRFs when PTV injection was used. Moreover, RRFs of FAMEs were similar for all PTV injection techniques used. This indicates that discrimination of high-boiling-point FAMEs during injection did not occur. The precision of the results was good even for small amounts of FAMEs. The RRFs of polyunsaturated FAMEs were somewhat higher than those of saturated FAMEs. The reason for this might be that the purity of available polyunsaturated FAME standards is lower because of possible autoxidation of these FAMEs during storage, methylation or injection. The RRFs of the low-boiling-point FAMEs deviated more from their theoretical RRFs. The coefficients of variation were also higher for these FAMEs. When the solvent elimination technique was used the recovery of the low-boiling-point FAMEs was far below 100% (below 10% for $C_{8:0}$ and $C_{10:0}$, 18% for $C_{11:0}$, 23% for $C_{12:0}$, 88 and 92% for $C_{14:0}$ and $C_{14:1}$ and between 99 and 101% for the higher boiling acids) because they are lost at the same time as the solvent through the split exit.

Figs. 2 and 3 show the separation of FAMEs from rat red blood cell membrane phosphatidylcholine (PC) and phosphatidylethanolamine (PE). The amount of FAMEs injected into the injector chamber was for PC in the range from 0.26 ng ($C_{20:0}$) to 52.16 ng ($C_{16:0}$) and for PE in the range from 0.08 ($C_{16:1}$) to 8.14 ng ($C_{20:4}$). The amount of internal standard injected ($C_{17:0}$) was in both cases 11.8 ng.

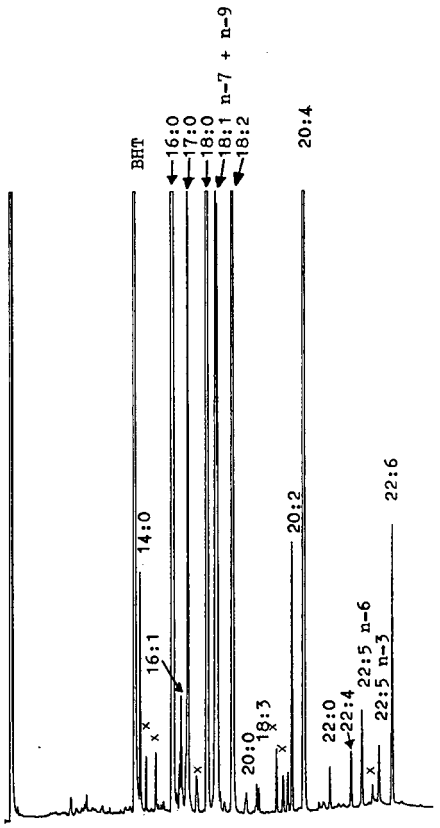

Fig. 2. Separation of FAMEs from rat red cell blood cell phosphatidylcholine ($C_{17:0}$ = internal standard, x = non-identified peaks).

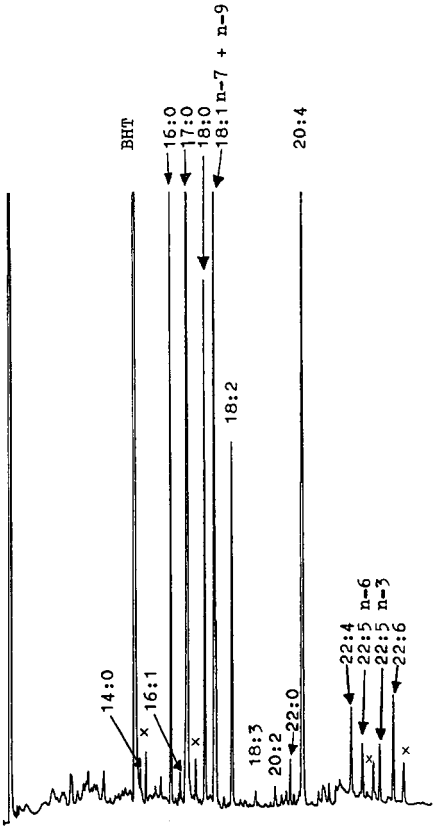

Fig. 3. Separation of FAMEs from rat red cell blood cell phosphatidylethanolamine ($C_{17:0}$ = internal standard, x = non-identified peaks).

TABLE IV

PRECISION OF GAS CHROMATOGRAPHIC DETERMINATION OF FAMEs FROM RAT RED BLOOD CELL MEMBRANE PC AND PE

C.V. = coefficient of variation. Each FAME extract was injected three times.

FAME	PC		PE	
	Amount (ng)[a]	C.V. (%)	Amount (ng)	C.V. (%)
14:0	1.08	2.83	–	
16:0	52.16	0.13	2.52	3.45
16:1	0.80	3.56	0.32	5.91
18:0	24.68	0.46	2.02	2.12
18:1	16.60	0.65	4.61	2.82
18:2	16.58	0.38	1.84	2.09
20:0	0.26	4.34	–	
20:2	2.24	1.98	0.14	4.56
20:4	20.16	0.76	8.14	0.58
22:0	0.36	1.64	0.24	3.89
22:4	0.58	1.67	0.36	3.87
22:5 n-3	0.56	1.95	0.30	4.64
22:5 n-6	1.06	2.08	0.32	4.34
22:6	2.96	0.88	0.54	3.32

[a] Amounts of FAMEs injected into the injector chamber.

Although the injected amounts of FAMEs were small, precise results were achieved. The coefficients of variation when the same FAME extract was injected three times were between 0.13 and 4.34% for FAMEs from PC and between 0.58 and 5.91% for FAMEs from PE (Table IV).

These results show that although the determined RRFs of low-boiling-point FAMEs differed from their theoretical RRFs, PTV might be useful for injection of FAMEs from most lipids, because most lipids contain few or no fatty acids with ten or fewer carbon atoms. Thus it seems that with PTV accurate and precise results can be achieved more easily than with classical split injection. Moreover, injection of FAMEs with PTV in most cases might be a good alternative to on-column injection, which is considered to be the optimal technique for injection of FAMEs with high accuracy and precision [37]. Compared with on-column injection, PTV injection offers the advantage that it can be used in various operation modes. Using the split injection mode, samples containing very different amounts can be determined without the risk of exceeding the capacity of the capillary column; using the splitless injection mode compounds of very diluted samples can be determined. PTV solvent elimination injection is useful for injection of large sample volumes. However, the solvent elimination technique is restricted to determination of fatty acids containing sixteen or more carbon atoms.

REFERENCES

1 G. Schomburg, H. Behlau, R. Dielmann, F. Weeke and H. Husmann, *J. Chromatogr.*, 142 (1977) 87.
2 K. Grob, Jr. and H. P. Neukom, *J. High Resolut. Chromatogr. Chromatogr. Commun.*, 2 (1979) 15.
3 W. Jennings and M. F. Mehran, *J. Chromatogr. Sci.*, 24 (1986) 34.
4 K. Grob, *Classical Split and Splitless Injection in Capillary Gas Chromatography*, Huethig, Heidelberg, Basel, New York, 1988.
5 G. van der Steege, F. A. J. Muskiet, I. A. Martini, N. H. Hutter and E. R. Boersma, *J. Chromatogr.*, 415 (1987) 1.
6 M. Volmer, G. Meiborg and F. A. J. Muskiet, *J. Chromatogr.*, 434 (1988) 385.
7 W. Welz, W. Sattler, H.-J. Leis and E. Malle, *J. Chromatogr.*, 526 (1990) 319.
8 N. C. Shantha and R. G. Ackman, *J. Chromatogr.*, 533 (1990) 1.
9 C. D. Bannon, J. D. Craske, D. L. Felder, I. J. Garland and L. M. Norman, *J. Chromatogr.*, 407 (1987) 231.
10 F. A. J. Muskiet, J. J. van Doormaal, I. A. Martini, B. G. Wolthers and W. van der Slik, *J. Chromatogr.*, 278 (1983) 231.
11 K. Grob and K. Grob, Jr., *J. Chromatogr.*, 151 (1978) 311.
12 K. Grob, *J. High Resolut. Chromatogr. Chromatogr. Commun.*, 1 (1978) 263.
13 G. Schomburg, H. Husmann and R. Rittmann, *J. Chromatogr.*, 204 (1981) 85.
14 F. Poy, S. Visani and F. Terrosi, *J. Chromatogr.*, 217 (1981) 81.
15 F. Poy, S. Visani and F. Terrosi, *J. High Resolut. Chromatogr. Chromatogr. Commun.*, 5 (1982) 355.
16 F. Poy and L. Cobelli, *J. Chromatogr.*, 279 (1983) 689.
17 G. Schomburg, H. Husmann, F. Schulz, G. Teller and M. Bender, *J. Chromatogr.*, 279 (1983) 259.
18 G. Schomburg, H. Husmann, H. Behlau and F. Schulz, *J. Chromatogr.*, 279 (1983) 251.
19 H. T. Badings and C. De Jong, *J. Chromatogr.*, 279 (1983) 493.
20 B. D. Beaumelle and H. J. Vial, *J. Chromatogr.*, 356 (1986) 187.
21 W. R. Morrison and L. M. Smith, *J. Lipid Res.*, 5 (1964) 600.
22 D. J. Hanahan and J. E. Eckholm, *Methods Enzymol.*, 31 (1974) 168.
23 E. Peuchant, R. Wolff, C. Salles and R. Jensen, *Anal. Biochem.*, 181 (1989) 341.
24 M. Seewald and H. M. Eichinger, *J. Chromatogr.*, 469 (1989) 271.
25 R. Olegard and L. Svennerholm, *Acta Paediat. Scand.*, 59 (1970) 637.

26 R. G. Ackman and J. C. Sipos, *J. Am. Oil Chem. Soc.*, 41 (1964) 377.
27 C. D. Bannon, J. D. Craske, N. T. Hai, N. L. Harper and K. L. O'Rourke, *J. Chromatogr.*, 247 (1982) 63.
28 C. D. Bannon, G. J. Breen, J. D. Craske, N. T. Hai, N. L. Harper and K. L. O'Rourke, *J. Chromatogr.*, 247 (1982) 71.
29 C. D. Bannon, J. D. Craske and A. E. Hilliker, *J. Am. Oil. Chem. Soc.*, 62 (1985) 1501.
30 C. D. Bannon, J. D. Craske and A. E. Hilliker, *J. Am. Oil. Chem. Soc.*, 63 (1985) 105.
31 D. E. Albertyn, C. D. Bannon, J. D. Craske, N. T. Hai, K. L. O'Rourke and C. Szonyi, *J. Chromatogr.*, 247 (1982) 47.
32 P. Bohov, V. Balaz and J. Hrivnak, *J. Chromatogr.*, 286 (1984) 247.
33 S. A. Makdessi, J.-L. Andrieu and A. Bacconin, *J. Chromatogr.*, 339 (1985) 25.
34 W. Vogt, K. Jacob and H. W. Obwexer, *J. Chromatogr.*, 174 (1979) 437.
35 W. Vogt, K. Jacob, A. B. Ohnesorg and H. W. Obwexer, *J. Chromatogr.*, 186 (1979) 197.
36 W. Vogt, K. Jacob, A. B. Ohnesorg and G. Schwertfeger, *J. Chromatogr.*, 217 (1981) 91.
37 J. D. Craske and C. D. Bannon, *J. Am. Oil Chem. Soc.*, 64 (1987) 1413.

Journal of Chromatography, 588 (1991) 273–280
Elsevier Science Publishers B.V., Amsterdam

CHROM. 23 619

Superoxide chemical transformation of diolepoxide polyaromatic hydrocarbon DNA adducts

Determination of benzo[*a*]pyrene-*r*-7,*t*-8,9,*c*-10-tetrahydrotetrol by gas chromatography☆

Wenni Li, Chariklia Sotiriou-Leventis, Samy Abdel-Baky, Daniel H. Fisher and Roger W. Giese*

Department of Pharmaceutical Sciences in the College of Pharmacy and Allied Health Professions, and Barnett Institute of Chemical Analysis and Materials Science, Northeastern University, Boston, MA 02115 (USA)

(First received May 14th, 1991; revised manuscript received July 12th, 1991)

ABSTRACT

Benzo[*a*]pyrene-*r*-7,*t*-8,9,*c*-10-tetrahydrotetrol (100 pg, 342 fmol) was measured using the following sequence of steps: (1) chemical transformation with potassium superoxide to 2,3-pyrenedicarboxylic acid; (2) electrophore derivatization with pentafluorobenzyl bromide; (3) sample clean-up by high-performance liquid chromatography and (4) measurement by gas chromatography with electron-capture detection and by gas chromatography with electron-capture negative-ion mass spectrometry. The overall, absolute yields obtained by the two procedures were 69% and 60%, respectively. This work completes the first stage towards the establishment of a general method for detecting diolepoxide polyaromatic hydrocarbon DNA adducts by gas chromatography.

INTRODUCTION

Many polyaromatic compounds have been found to be carcinogenic or mutagenic in animal exposure studies, including bacterial testing. It is generally considered, and there is much evidence, that many of these compounds exert their toxicity by chemically damaging DNA, producing so-called "DNA adducts" [1]. One important class of such adducts arises from the metabolic activation of polynuclear aromatic hydrocarbons (PAHs) to corresponding diolepoxide intermediates [2]. The latter electrophilic compounds can react with nucleophilic sites on the DNA bases, such as the N-2 position of guanine. Hence there is interest in the detection of diolepoxide PAH DNA adducts in biological samples.

Principally three kinds of methods have been employed to date for the measurement of PAH DNA adducts in biological samples: ^{32}P post-labeling, immunoassays and fluorescence. Examples of the effectiveness of these methods, and their shortcomings for the detection of PAH DNA adducts, have been summarized recently [3].

Gas chromatography (GC) is a useful analytical technique, especially when coupled with detection by mass spectrometry (MS). High sensitivity can be achieved by introducing strongly electrophoric analytes into a system comprising GC with detection by electron-capture negative-ion MS (GC–ECNI-MS). Attomole amounts of analytes can be measured in this way [3]. In order to subject diolepoxide PAH DNA to such detection, they first need to be

☆ *r* = Reference, *t* = trans and *c* = cis.

0021-9673/91/$03.50

chemically transformed and electrophore derivatized. Inherently they are not strong electrophores, nor can they become so by derivatization alone. In part, this is because of the large size of these adducts, including a diversity of functional, thermally labile groups.

In this paper, we present a novel chemical transformation technique for diolepoxide PAH DNA adducts. The technique was applied to femtomole amounts of the model analyte benzo[*a*]pyrene-*r*-7, *t*-8,9,*c*-10-tetrahydrotetrol. This compound is oxidized by potassium superoxide, the chemical transformation reagent, to a corresponding dicarboxylic acid, which in turn is electrophore derivatized and detected by GC. Both GC with electron-capture detection (GC–ECD) and GC–ECNI-MS were used, allowing them to be compared.

Recently we introduced methodology similar in concept to that here, in which an amino-PAH DNA adduct was chemically transformed by hydrazinolysis [3].

EXPERIMENTAL

Chemicals and reagents

Potassium superoxide (KO_2), 18-crown-6 (a crown ether; CE), 9,10-dihydrobenzo[*a*]pyren-7 (8*H*)-one, pentafluorobenzyl bromide, triethylamine, succinic anhydride (99%), aluminum chloride (anhydrous, 99.99%), zinc (20 mesh), mercury (II) chloride (99.5%), phosphorus pentachloride, tin(IV) chloride, high-performance liquid chromatographic (HPLC)-grade dichloromethane, HPLC-grade benzene, nitrobenzene (99 + %), HPLC-grade *p*-xylene, HPLC-grade N,N-dimethylformamide (DMF) and HPLC-grade glacial acetic acid were purchased from Aldrich (Milwaukee, WI, USA). 2,3,5,6-Tetrafluorobenzyl bromide was obtained from Alfa Products (Danvers, MA, USA), benzo[*a*]pyrene-*r*-7,*t*-8,9,*c*-10-tetrahydrotetrol (Tetrol) from the NCI Chemical Carcinogen Repository (Kansas City, MO, USA), [$^2H_{10}$]pyrene from Icon Services (Summit, NJ, USA) and acetonitrile (UV) and hexane (GC^2) from American Burdick and Jackson (American Scientific Products, Boston, MA, USA). Distilled water was purified to HPLC grade with a Nanopure/Organicpure system (Barnstead, Boston, MA, USA). For the reactions, DMF and benzene were dried with type 4Å molecular sieves (Aldrich). The molecular sieves were washed with hexane three times followed by activation overnight at 250°C before use. USP-grade carbon dioxide (99.9%), ultra-high-purity helium (99.999%), high-purity helium, ultra-high-purity nitrogen (99.999%), high-purity nitrogen. C.P.-grade methane (99.998%) and Oxisorb-LP cartridges were purchased from Medical Technical Gases (Medford, MA, USA).

Equipment

High-performance liquid chromatography. The HPLC system consisted of a Series-4 liquid chromatograph from Perkin-Elmer (Norwalk, CT, USA), a Rheodyne Model 7125 injector from Rainin (Woburn, MA, USA), a Spectroflow 773 UV detector from Kratos (Ramsey, NJ, USA) and a SP-4270 integrator (Spectra-Physics, Piscataway, NJ, USA). The solvents were degassed and the solvent chamber pressurized to 7 p.s.i. with helium. The analytical HPLC clean-up was carried out on a Microsorb C_{18} column (150 × 4.6 mm I.D., 5-μm diameter particles; Rainin) fitted with a Microsorb C_{18} guard column (15 × 4.6 mm I.D., 5-μm diameter particles; Rainin). Detection was at 263 nm for 2,3-bis(pentafluorobenzyl)pyrenedicarboxylate.

Gas chromatography with electron-capture detection. A Model 3740 gas chromatograph from Varian (Walnut Creek, CA, USA), was fitted with a ^{63}Ni electron-capture detector, a Model 1095 on-column capillary injector and a Waters Model 840 data system (Millipore–Waters, Milford, MA, USA). The determination of 2,3-bis(pentafluorobenzyl)-pyrenedicarboxylate was carried out on an HP-1 (cross-linked methylsilicone gum) capillary column (10 m × 0.32 mm I.D., 0.17-μm film thickness; Hewlett-Packard, Palo Alto, CA, USA). The flow-rate of the carrier gas (helium) was 4 ml/min at 250°C and that of the make-up gas (nitrogen) was 26 ml/min at 250°C. The initial injector and column temperatures in the GC–ECD were 90 and 120°C, respectively. Immediately after injection, the injector temperature was programmed to 280°C at 180°C/min. The column, after a 3-min hold, was programmed to 290°C at 10°C/min. The detector temperature was kept constant at 340°C.

Gas chromatography–mass spectrometry. The equipment consisted of a Hewlett-Packard Model 5988A mass spectrometer equipped with an HP-5890 gas chromatograph. The mass spectrometer

was interfaced to an HP 59970C (Rev. 3.2) MS ChemStation computer and an HP-7957B disc drive (the formatted storage capacity of the disc is 81 Mbyte). The GC separations were carried out on an Ultra-1 (cross-linked methylsilicone) capillary column (12 m × 0.20 mm I.D., 0.11-μm film thickness) (Hewlett-Packard). The column was interfaced directly to the mass spectrometer, using an interface temperature of 290°C. Helium (UHP) at a column head pressure of 20 p.s.i. was used as the carrier gas. Methane (UHP) was used as the reagent gas with a source temperature of 250°C and a source pressure of 2.0 Torr. The instrument was manually tuned daily for maximum sensitivity. For the determination of 2,3-bis(pentafluorobenzyl)pyrenedicarboxylate, the oven was programmed from 160 to 290°C at 70°C/min.

Other techniques. Fluorescent indicator plates for analytical and preparative separations by thin-layer chromatography (TLC) were obtained from Analtech. ^{1}H and ^{13}C NMR spectra were recorded on a Varian XL-300 spectrometer. All the glassware was cleaned according to a previously described procedure [4].

Syntheses

2,3-Pyrenedicarboxylic acid. Finely powdered potassium superoxide (657 mg, 9.2 mmol), 18-crown-6 (611 mg, 2.3 mmol) and 9,10-dihydrobenzo[*a*]pyrene-7(8*H*)-one (50 mg, 0.18 mmol) were suspended in dry benzene (20 ml). The mixture was stirred vigorously for 20 h at room temperature, in the dark, then 40 ml of water were added. The benzene layer was separated and the water layer was filtered through a filter-paper (Whatman). The filtrate was acidified to *ca.* pH 2 (pH paper) with concentrated hydrochloric acid under stirring, and extracted with ethyl acetate. After the ethyl acetate had been evaporated on a rotary evaporator, the product was purified on a Dynamax C_{18} semi-preparative HPLC column (Rainin Microsorb, 250 mm × 10 mm I.D., 5-μm particles) with a Rainin C_{18} guard column (50 mm × 10 mm I.D., 5-μm particles). Detection was effected at 264 nm, and the mobile phase program was (1) a 15-min equilibrium period with acetonitrile–0.1 *M* acetic acid (50:50) at a flow-rate of 5 ml/min; (2) a linear increase in the proportion of acetonitrile to 58:42 over a 8-min period; (3) a linear increase over 1 min to 100% acetonitrile, which was maintained for 10 min; and (4) a linear change in 10 min back to the initial composition (50:50). The time window for peak collection was 5.7–6.7 min. After the evaporation, the product gave ^{1}H NMR ([$^2H_6$]acetone), δ 8.21–8.45 (m, 7H, Ar), 8.90 (s, 1H, H_1), 11.94 (br s, 2H, COOH); MS[electron impact (EI)], *m/z* 290 (M, 4%), 272 (M − H_2O, 50%), 200 (M − $2CO_2H$, 100%). Analysis: calculated for $C_{18}H_{10}O_4$, C 74.47, H 3.47; found, C 74.37, H 3.41%.

2,3-Bis(pentafluorobenzyl)pyrenedicarboxylate. Finely powdered potassium carbonate (210 mg, 1.52 mmol, dried at 250°C) in 20 ml of acetonitrile was stirred at room temperature overnight. 2,3-Pyrenedicarboxylic acid (32 mg, 0.11 mmol) and pentafluorobenzyl bromide (1.4 ml, 9.27 mmol) were added. Derivatization was performed at 60°C (water condenser) with stirring until no more starting material could be seen on silica TLC [hexane–ethyl acetate (9:1)]. The reaction mixture was filtered and the acetonitrile was evaporated with a rotary evaporator. The product was purified twice by preparative silica TLC (20 × 20 cm plate, 1000-μm layer) with hexane–ethyl acetate (9:1). This led to a light yellow powder which gave a single peak on analytical HPLC. ^{1}H NMR (C^2HCl_3), δ 5.53, 5.64 (s, 2H each, CH_2), 8.05–8.26 (m, 7H, Ar), 8.67 (s, 1H, H_1); MS (EI), *m/z* 650 (M, 11%), 181 ($C_6F_5CH_2$, 100%).

2,3-Bis(tetrafluorobenzyl)pyrenedicarboxylate. This compound was synthesized and purified using the same procedure as for 2,3-bis(pentafluorobenzyl)pyrenedicarboxylate except that 2,3,5,6-tetrafluorobenzyl bromide was used instead of pentafluorobenzyl bromide. ^{1}H NMR (C^2HCl_3), δ 5.58, 5.67 (s, 2H each, CH_2), 7.08–7.14 (m, 2H, C_6F_4H), 8.03–8.23 (m, 7H, Ar), 8.67 (s, 1H, H_1); MS (EI), *m/z* 614 (M, 13%), 163 ($C_6F_4HCH_2$, 100%).

β-3-[$^2H_9$]Pyrenoylpropanoic acid [5]. Anhydrous aluminum chloride (1.20 g, 9 mmol) was added slowly, with cooling (ice-bath) and stirring, to a solution of succinic anhydride (0.48 g, 4.8 mmol) in nitrobenzene (20 ml). [$^2H_{10}$]Pyrene (1 g, 4.7 mmol) was then gradually introduced, and the color of the solution (yellow) immediately turned deep red. The mixture was stirred at 0°C for 3 h, then hydrolyzed by careful addition of dilute hydrochloric acid (3 ml of concentrated hydrochloric acid in 9 ml of water). The yellow precipitate was filtered and washed with water. The filter cake was then dis-

solved in hot aqueous sodium carbonate (12 g of sodium carbonate in 100 ml of water) and filtered immediately in order to remove aluminum hydroxide. The filtrate, on cooling to room temperature, gave a solid, the sodium salt of β-3-[$^2H_9$]pyrenoylpropanoic acid, which was filtered and recrystallized from acetic acid to yield yellow needles (1.12 g, 82%). ^1H NMR [dimethyl sulfoxide (DMSO)], δ 2.77, 3.49 (t, 2H each, CH_2), 12.26 (br s, 1H, CO_2H).

γ-3-[$^2H_9$]Pyrenylbutanoic acid [5]. Zinc (10 g, 20 mesh) was cleaned by stirring in 10% hydrochloric acid (2.6 ml of concentrated hydrochloric acid in 7.4 ml of water) for 2 min followed by washing with water (3 × 10 ml). It was then amalgamated with mercury(II)chloride (1 g). The amalgamated zinc was placed in a 100-ml round-bottom flask, followed by the addition of 7.5 ml of water, 10 ml of concentrated hydrochloric acid, 10 ml of *p*-xylene and 1 g of β-3-[$^2H_9$]pyrenoylpropanoic acid. The mixture was refluxed for 6 h, during which period concentrated hydrochloric acid (2 × 5 ml) was added. The reaction mixture was allowed to cool until crystallization was completed. The crystals, together with the zinc, were filtered, washed with water and dried under vacuum. The product, with the zinc, was digested with hot sodium hydroxide solution (3 g of sodium hydroxide in 150 ml of water) to separate the reduced acid from the insoluble colorless by-product and zinc. On acidifying the alkaline solution with concentrated hydrochloric acid, the product was obtained as a chalk-white solid (0.87 g, 91%) which was washed (water, then a small amount of benzene) and dried under vacuum. ^1H NMR ([$^2H_6$]DMSO), δ 2.02 (m, 2H, CH_2), 2.40, 3.34 (t, 2H each, CH_2), 12.10 (br s, 1H, CO_2H).

[1,2,3,4,5,6,11,12-$^2H_8$]9,10-Dihydrobenzo[a]-pyren-7(8H)-one [5]. Phosphorus pentachloride (460 mg, 2.20 mmol) was added in portions to a stirred solution of γ-3-[$^2H_9$]pyrenylbutanoic acid (600 mg, 2.02 mmol) in 50 ml of dry benzene. The mixture was stirred at room temperature under nitrogen for 1.5 h. To the clear, dark-yellow solution, 0.3 ml (2.55 mmol) of tin(II)chloride was added and the mixture was stirred at room temperature under nitrogen for 8 h. The purple complex was decomposed by adding ice and concentrated hydrochloric acid with vigorous stirring until a clear, yellow, two-phase solution was formed. The benzene layer was separated, washed twice with water, dried with anhydrous sodium sulfate and the solvent was removed under vacuum. The residual solid was recrystallized from dichloromethane–methanol to give a yellow product (260 mg, 46%). ^1H NMR (C^2HCl_3), δ 2.24 (m, 2H, CH_2), 2.74, 3.30 ppm (t, 2H each, CH_2); ^{13}C NMR (C^2HCl_3), δ 22.9, 25.8, 38.7, 122.8, 124.0, 124.8, 125.0, 126.7, 128.0, 128.9, 129.3, 131.1, 137.3, 199.0 (CO).

2,3-[$^2H_8$]Bis(pentafluorobenzyl)pyrenedicarboxylate. A solution of [1,2,3,4,5,6,11,12-$^2H_8$]9,10-dihydrobenzo[*a*]pyren-7(8*H*)-one (100 mg, 0.36 mmol) in 10 ml of dimethylformamide was added to a suspension of potassium superoxide (767 mg, 10.80 mmol) and 18-crown-6 (1.14 g, 4.30 mmol) in 10 ml of dimethylformamide in a 100-ml round-bottomed flask. The oxidation was conducted at room temperature, in the dark, with stirring. The reaction was stopped after 24 h by adding water (5 ml) and carefully acidified with concentrated hydrochloric acid until a precipitate formed. The reaction mixture was then extracted with 3 × 20 ml of ethyl acetate, dried over sodium sulfate and evaporated to dryness. The crude product was esterified directly with pentafluorobenzyl bromide (1 ml) and triethylamine (0.5 ml) in acetonitrile (20 ml) at 60°C for 4 h. The product was purified by preparative TLC using hexane–dichloromethane (1:1) and recrystallized from dichloromethane–methanol to give white crystals {144 mg, overall yield of 61% from [1,2,3,4,5,6,11,12-$^2H_8$]9,10-dihydrobenzo[*a*]pyren-7(8*H*)-one}. ^1H NMR (C^2HCl_3), δ 5.53 (s, 2H each, CH_2).

Analytical procedure

Oxidation. In triplicate, 70 μl of a Tetrol stock solution (1.56 pg/μl in methanol) were added to a 1-ml clear silanized Micro-V vial (American Scientific Products). The sample was dried at 40°C under nitrogen, followed by addition of 25 μl of DMF containing 200 μg of potassium superoxide and 190 μg of 18-crown-6. The vial was capped with a PTFE-lined screw-cap and kept at room temperature, in the dark, for 20 h, with vortex mixing for 30 s every 30 min for the first 6 h. Water (25 μl) was added, followed by two drops of acetic acid and removal of solvent at 70°C under nitrogen.

Derivatization. The 2,3-pyrenedicarboxylic acid formed was derivatized in the same vial by adding 30 μl of acetonitrile containing 0.8 μl of pentafluoro-

benzyl bromide and 0.15 μl of triethylamine. The vial was capped and kept at 60°C for 6 h with vortex mixing for 30 s every 30 min. After cooling and addition of 70 μl of acetonitrile, the sample was kept at 4°C overnight prior to post-derivatization clean-up by HPLC.

HPLC clean-up. The mobile phase program for the determination of 2,3-bis(pentafluorobenzyl)pyrenedicarboxylate was (1) a 10-min equilibrium period with water–acetonitrile (15:85) at 1 ml/min and (2) on injection, a linear change of water–acetonitrile to 5:95 in 10 min, followed by a 5-min hold at this composition. A 100-μl volume of 2,3-bis(pentafluorobenzyl)pyrenedicarboxylate standard (36.05 pg/μl in acetonitrile) was injected to establish the retention time. The injector was washed with 2 × 1 ml of hot acetonitrile. Three 100-μl volumes of acetonitrile were then injected. The fraction from 10.4 to 11.6 min was collected from the third acetonitrile injection, evaporated and analyzed by GC–ECD to assure that the HPLC system was clean.

The sample was removed from the refrigerator, left at room temperature for 30 min, vortex mixed well and allowed to stand for 5–10 min. The entire volume was then injected into the HPLC column. Three blanks were injected first, followed by three samples. The fraction from 10.4 to 11.6 min for each was collected in a 2-ml silanized Reacti-Vial. The injector was washed with 2 × 1 ml of hot acetonitrile after each injection. After evaporation at 60°C under nitrogen, the residue was dissolved in 100 μl of acetonitrile, and the entire volume was again purified as before on the same HPLC column. A 30-μl volume of GC internal standard, 2,3-bis (tetrafluorobenzyl)pyrenedicarboxylate, was added to each of the second collection vials prior to evaporation.

GC–ECD. A calibration graph was established by injecting 1 μl of three GC standards containing 1.2–12.1 fmol/μl of 2,3-bis(pentafluorobenzyl)pyrenedicarboxylate (A) and 6.6 fmol/μl each of 2,3-bis(tetrafluorobenzyl)pyrenedicarboxylate (B) in isooctane. The ratio of the concentration of A to that of B was plotted *versus* the ratio of the peak areas, using the least-squares quantitation equation (Waters 840 data system), along with the correlation coefficient. Isooctane was injected before and after each standard injection.

After evaporation of the HPLC solvent at 60°C under nitrogen, the residue was dissolved in 30 μl of isooctane, followed by vortex mixing, and 1 μl of each sample was injected into the GC–ECD system. The peak area was obtained by manual integration using the Model 840 data system.

GC–ECNI-MS. After GC–ECD analysis, 100 μl of a 524.6 fg/μl solution of deuterated internal standard in acetonitrile were added to both blanks and samples, followed by evaporation at 60°C under nitrogen. The residue was dissolved in 100 μl of isooctane and 1 μl was injected into the GC–ECNI-MS system.

RESULTS AND DISCUSSION

Our long-term aim is to establish a general assay, based on MS, for diolepoxide PAH DNA adducts. One such adduct, as a prototype, has been studied previously by several investigators [2]. This adduct arises from the reaction of *r*-7,*t*-8-dihydroxy-*t*-9,10-epoxy-7,8,9,10-tetrahydrobenzo[*a*]pyrene with the N-2 position of guanine residues in DNA. The resulting adduct, no doubt like related adducts at this site, can be hydrolyzed by mild acid hydrolysis of the DNA [6]. For the prototype, this releases a corresponding benzo[*a*]pyrenetetrahydrotetrol (Tetrol). Thus, as a first step towards our long-term aim, we set up an assay for the latter compound, as reported here.

It is known that carboxylic acids can be converted by reaction with pentafluorobenzyl bromide into corresponding esters that are sensitive for detection by GC–ECD [7] and GC–ECNI-MS [8]. Importantly, these esters undergo dissociative electron capture to form a structurally characteristic carboxylate anion in high yield; hence the detection of such esters by GC–ECNI-MS can be specific. This makes it potentially attractive to oxidize the Tetrol to 2,3-pyrenedicarboxylic acid. We demonstrated previously that this can be achieved in high yield not only for the Tetrol, but also for a variety of related compounds by reaction with potassium superoxide [9]. This prior work was performed on milligram amounts of the PAHs. Here we extended this approach for analytical purposes by applying it to a trace amount of Tetrol, and conducted subsequent steps leading to the detection of the Tetrol, as a corresponding pentafluorobenzyl diester (Diester), by GC–ECD and GC–ECNI-MS.

In this procedure, Tetrol is first oxidized by potassium superoxide to 2,3-pyrenedicarboxylic acid (Diacid) which, in turn, is converted by pentafluorobenzyl bromide into Diester, followed by purificatio n by HPLC and determination by GC. This procedu re is a consequence of previous work in which we first determined microgram and then nanogram amounts of the Tetrol. The Diacid and the Diester could be determined by HPLC down to the low nanogram level (data not shown). This prior work helped us to optimize the conditions for the overall procedure.

Superoxide oxidation

The Tetrol is oxidized with potassium superoxide in the presence of 18-crown-6 in dimethylformamide at room temperature in the dark for 20 h (Fig. 1, step 1). On acidic aqueous work-up, 2,3-pyrenedicarboxylic acid is formed. It is attractive that one obtains the product dissolved in a clear, aqueous solution, which is simply evaporated prior to the next step. This is an advantage of using potassium superoxide for the oxidation.

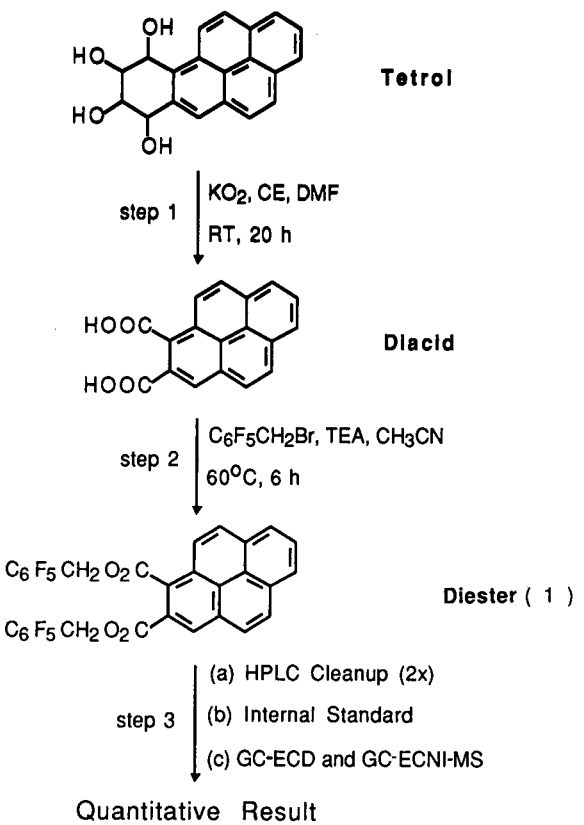

Fig. 1. Scheme for the measurement of benzo[*a*]pyrene-*r*-7,*t*-8,9,*c*-10 tetrahydrotetrol (Tetrol) by KO_2 chemical transformation, electrophore derivatization, GC–ECD and GC–ECNI-MS. CE = 18-Crown-6 (a crown ether); TEA = triethylamine.

Derivatization

The 2,3-pyrenedicarboxylic acid is derivatized with pentafluorobenzyl bromide in the presence of triethylamine in acetonitrile at 60°C for 6 h (Figure 1, step 2). The reaction volume is only 30 μl in order to allow the entire sample to be simply diluted with acetonitrile (70 μl) and injected into an HPLC column for post-derivatization clean-up. Vortex mixing instead of magnetic stirring is done as a PTFE-coated stirring bar causes an adsorption loss of the analyte and a glass-coated stirring bar is too fragile.

HPLC clean-up

Post-derivatization sample clean-up by HPLC is attractive because it can be reproducible and convenient and give a high recovery. For example, a quantitative recovery was obtained when 602 fg (in duplicate) of standard Diester was injected onto the

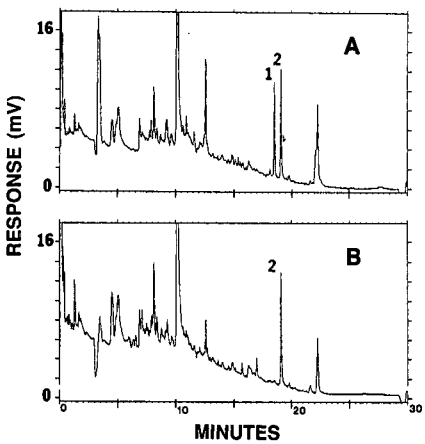

Fig. 2. GC–ECD for the oxidation and derivatization of 100 pg of Tetrol. After the second HPLC clean-up, 30 μl of internal standard solution of **2** (6.6 fmol/μl in acetonitrile) were added to blanks and samples, followed by evaporation at 60°C under nitrogen. The residue was dissolved in 30 μl of isooctane and 1 μl was injected. (A) Reaction mixture; (B) reaction blank. Peaks: 1 = 2,3-bis(pentafluorobenzyl)pyrenedicarboxylate; 2 = 2,3-bis(tetrafluorobenzyl)pyrenedicarboxylate.

HPLC column, followed by collection, evaporation, dissolution and GC–ECNI-MS (data not shown). The potential to automate the HPLC separation in the future for this method is also important. As interferences are encountered in the subsequent GC–ECD step after a single passage of the sample through the HPLC column, the HPLC purification is done twice (step 3a in Fig. 1). The same column is used twice for each sample, and the column is carefully washed between the injections to prevent analyte carryover.

GC–ECD

After the second HPLC separation, the first internal standard, compound **2** (for GC–ECD purposes; see below) is added to each sample (step 3b in Figure 1), followed by evaporation. The sample is dissolved in 30 μl of isooctane and 1 μl is injected into the GC–ECD system (step 3c in Fig. 1). This results in the chromatograms shown in Fig. 2, where A represents the reaction mixture (starting from 100 pg of Tetrol) and B is the blank (entire procedure starting from 0 pg of Tetrol). As shown in Figure 2, the chromatogram for the reaction blank is reasonably clean at this level of sensitivity in the elution region of interest. The overall, absolute yield for the triplicate sample is 69% (77, 68 and 62%), based on a calibration graph constructed by measuring samples containing increasing amounts of the analyte and a constant amount of **2**.

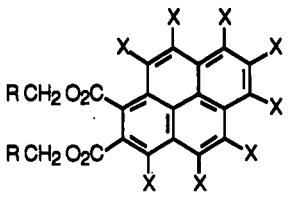

Internal Standards

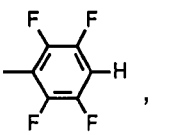

2: R = , X = H (for GC-ECD)

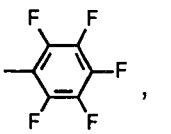

3: R = , X = D (for GC-ECNI-MS)

GC–ECNI-MS

After GC–ECD, the second internal standard, compound **3**, is added to all of the same samples followed by GC–ECNI-MS, giving the chromatograms shown in Fig. 3. Chromatogram A represents the reaction mixture and B the blank. In this instance the yield is 60% (80, 50 and 49%), which agrees with the GC–ECD value.

In future work, we shall extend the method to lower Tetrol levels and to related tetrols, and apply it to biological samples. As is apparent from comparing Figs. 2 (GC–ECD) and 3 (GC–ECNI-MS), only the latter method can be trusted at lower analyte levels. This reaffirms our earlier observation that GC–ECD tends to be useful in procedures such as this only down to about the picogram level [4]. We plan to use the [1,2,3,4,5,6,11,12-$^2H_8$]9,10-dihydrobenzo[*a*]pyren-7(8*H*)-one that we synthesized as the internal standard for future work. This compound can be added early in the procedure, prior to the superoxide oxidation step. Like the Tetrol, this compound is oxidized by potassium superoxide into the corresponding dicarboxylic acid [9]. As GC–

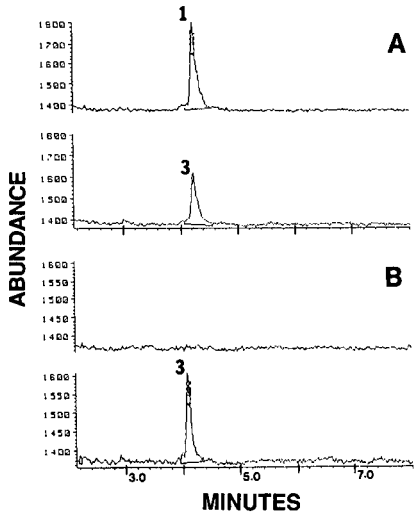

Fig. 3. GC–ECNI-MS for the oxidation and derivatization of 100 pg of Tetrol. After GC–ECD, 100 μl of an internal standard solution of **3** (524.6 fg/μl in isooctane) were added to both blanks and samples, followed by evaporation at 60°C under nitrogen. The residue was dissolved in 100 μl of isooctane and 1 μl was injected. (A) Reaction mixture; (B) reaction blank. Peaks: 1 = 2,3-bis(pentafluorobenzyl)pyrenedicarboxylate; 3 = [$^2H_8$]2,3-bis(pentafluorobenzyl)pyrene-dicarboxylate.

ECD was compared with GC–ECNI-MS in this study, internal standards **2** and **3** were added late in the current procedure just to monitor the GC step.

CONCLUSION

A novel procedure relying on superoxide oxidation shows promise for the general measurement of diolepoxide PAH DNA adducts. While both GC–ECD and GC–ECNI-MS can be used to detect as little as 100 pg of the model analyte, benzo[*a*]pyrene-*r*-7,*t*-8,9,*c*-10-tetrahydrotetrol, only the latter technique gives a clean baseline that encourages its further application to lower analyte levels including, eventually, a diversity of such analytes present in biological samples.

ACKNOWLEDGEMENTS

This research was conducted in part under contract to the Health Effects Institute (HEI), an organization jointly funded by the US Environmental Protection Agency (EPA) (Assistance Agreement X-812059) and automative manufacturers. The specific grant was HEI Research Agreement 86-82. The contents of this paper do not necessarily reflect the views of the HEI, nor do they necessarily reflect the policies of the EPA or automotive manufacturers. Contribution No. 494 from the Barnett Institute.

REFERENCES

1 H. Bartsch, K. Hemminki and J. K. O'Neill, *Methods for Detecting DNA Damaging Agents in Humans: Applications in Cancer Epidemiology and Prevention (IARC Scientific Publications*, No. 89), International Agency for Research on Cancer, Lyon, 1988.
2 B. Singer and D. Grunberger, *Molecular Biology of Mutagens and Carcinogens*, Plenum Press, New York, 1983.
3 J. Bakthavachalam, S. Abdel-Baky and R. W. Giese, *J. Chromatogr.*, 538 (1990) 447.
4 D. H. Fisher and R. W. Giese, *J. Chromatogr.*, 452 (1988) 51.
5 W. E. Bachmann, M. Carmack and S. R. Safir, *J. Am. Chem. Soc.*, 63 (1941) 1682.
6 K. Vahakangas, A. Haugen and C. C. Harris, *Carcinogenesis*, 6 (1985) 1109.
7 O. Gyllenhaal, H. Brotell and P. Hartvig, *J. Chromatogr.*, 129 (1976) 295.
8 U. Hofmann, S. Holzer and C. O. Meese, *J. Chromatogr.*, 508 (1990) 349.
9 C. Sotiriou, W. Li and R. W. Giese, *J. Org. Chem.*, 55 (1990) 2159.

Journal of Chromatography, 588 (1991) 281–287
Elsevier Science Publishers B.V., Amsterdam

CHROM. 23 661

Gas chromatographic–mass spectrometric analysis of ginkgolides produced by *Ginkgo biloba* cell culture

Nathalie Chauret*

Department of Medicinal Chemistry, Merck Frosst Canada, C.P. 1005, Pointe-Claire-Dorval, Quebec H4R 4P8 (Canada)

Julie Carrier

Department of Chemical Engineering, McGill University, 3480 University Street, Montreal, Quebec H3A 2A7 (Canada)

Michael Mancini

Biotechnology Research Institute, National Research Council Canada, 6100 Royalmount Avenue, Montreal, Quebec H4P 2R2 (Canada)

Ronald Neufeld and Martin Weber

Department of Chemical Engineering, McGill University, 3480 University Street, Montreal, Quebec H3A 2A7 (Canada)

Jean Archambault

Biotechnology Research Institute, National Research Council Canada, 6100 Royalmount Avenue, Montreal, Quebec H4P 2R2 (Canada)

(First received May 13th, 1991; revised manuscript received July 29th, 1991)

ABSTRACT

An analytical method was developed to confirm the production of ginkgolides by *Ginkgo biloba* cells cultured *in vitro*. Biomass samples were extracted for 16 h with acetone. This extract was loaded onto a silica gel column and purified by differential elution using a cyclohexane–ethyl acetate solvent system. The recoveries of ginkgolide A and ginkgolide B were × ei90% and × ei35%, respectively. Subsequently, this purified extract was trimethylsilylated for gas chromatographic separation of ginkgolide A and ginkgolide B. Flame-ionization detection was not selective enough for identification of ginkgolides A and B in the extracts. The ginkgolides were detected by coupling the gas chromatograph to a high-resolution mass spectrometer operated in the selected-ion monitoring mode. The concentration of ginkgolides A and B in culture extracts was determined by gas chromatography–mass spectrometry using deutero-trimethylsilylated ginkgolides as internal standards. This technique permitted detection of ginkgolides A and B at concentrations as low as 10^{-1} pmol/μl of injected purified extract.

INTRODUCTION

Ginkgolides are potent and specific platelet antagonist factors (PAF) that are presently undergoing clinical trial in Europe to treat asthma and allergy [1]. The synthesis of these phytochemicals (Fig. 1) is complex, making large-scale production difficult [2]. The main source of ginkgolides is the leaves of the slow-growing tree *Ginkgo biloba* L. [3].

Lobstein-Guth *et al.* [4] have developed an extensive purification method using liquid–liquid extraction and preparative chromatography to prepurify

0021-9673/91/$03.50

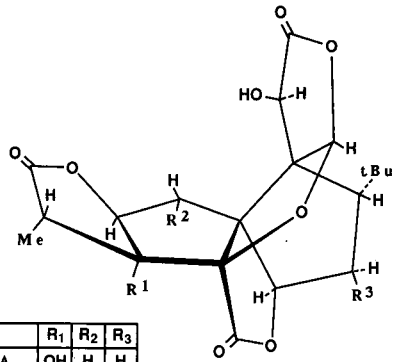

	R_1	R_2	R_3
GA	OH	H	H
GB	OH	OH	H

Fig. 1. Chemical structures of ginkgolides.

ginkgolides obtained from leaf extracts and have used high-performance liquid chromatography (HPLC) and ultraviolet (UV) detection at 220 nm for analysis. The low UV absorption coefficient of ginkgolides resulted in a detection limit of ~ 70 nmol [4]. Van Beek *et al.* [5] reduced this detection limit to 7 nmol using refractive index detection after HPLC separation, which is similar to that obtained by Tallevi and Kurz [6] using thin-layer chromatography (TLC) and UV visualisation of ginkgolides obtained from commercial plant extracts.

G. biloba cell culture is an alternative to agricultural supply of ginkgolides. However, Nakanishi and Habaguchi [7] could not detect ginkgolides in cultured cells using HPLC. These results suggested that cultured cells were not producing ginkgolides or were producing them at concentrations lower than the detection limit of their analytical technique.

In order to confirm the presence of ginkgolides in cultured *G. biloba* cells, a detection method that is more sensitive and selective than those used previously is required. Mass spectrometry (MS) was found to be suitable for this purpose. The analysis of ginkgolides by MS has not been extensively documented. Nakanishi [8] seems to be the only one who has reported on the lactone structure of ginkgolide A (GA) derivatized as a dimethyl ether using MS.

First experiments conducted in our laboratory have shown the usefulness of gas chromatography (GC) combined with electron-impact (EI) MS for identification and quantification of trimethylsylilated GA in crude cultured cell extracts [9]. These analyses, which were performed on resinous crude extracts, resulted in numerous GC–MS problems (contamination of the injector, column and MS source). This method could not be used routinely. This work describes a procedure to purify biomass extracts using a silica gel column and GC–MS protocols for proper characterization and analysis of ginkgolides A and B.

EXPERIMENTAL

Chemicals

Ginkgolide standards A and B were kindly provided by Dr. P. Braquet (Institut Henri Beaufour, Les Ulis, France). Stock solutions of these standards (~ 120 pmol μl^{-1}) were prepared monthly in methanol and stored at 4°C. All solvents (methanol, acetone, ethyl acetate and cyclohexane) were HPLC grade (Caledon, Georgetown, Canada). *G. biloba* cells, cultured as described elsewhere [9,10], were the experimental source of ginkgolides.

Sample preparation

Lyophilized *G. biloba* cells (20 g) were extracted with acetone (1 l) for 16 h at ambient temperature with gentle mixing. The suspension was filtered (0.45-μm HVLP filter, Millipore, Bedford, MA, USA) by vacuum. The acetone extract was evaporated to dryness on a Rotavap (Brinkman, Westbury, NY, USA). The residue was redissolved in ~ 5 ml of cyclohexane–ethyl acetate (50:50, v/v), yielding a dark-brown syrup (fraction I).

For GC–flame-ionization detection (FID) analysis, all the volume of fraction I was enriched with GA and GB (~ 60 nmol) prior to purification (fraction IE). For GC–MS analysis, fraction I was divided in two equal volumes (fractions Ia and Ib). Before purification on silica gel, fraction Ia was enriched with 5 nmol of GA and 5 nmol of GB (fraction IaE). No ginkgolide was added to fraction Ib.

Biomass extract purification

The purification of fraction IE was done using a silica gel column (Kieselgel, 230–400 mesh, Merck, Darmstadt, Germany) as suggested by Lobstein-Guth *et al.* [4] for purification of leaf extracts. The column (11 cm × 2.5 cm I.D.) was prepared from a slurry of silica gel (20 g) in ~ 75 ml of cyclohexane–

ethyl acetate (50:50, v/v). The column was conditioned with ~ 200 ml of cyclohexane–ethyl acetate (50:50, v/v) at a flow-rate of ~ 1 ml min^{-1} 16–24 h before use. Fraction IE was loaded on the column, which was washed with 60 ml of cyclohexane–ethyl acetate (50:50, v/v) at ~ 1 ml min^{-1}. This first fraction (green) was discarded. Thereafter, the column was eluted with 80 ml of cyclohexane–ethyl acetate (20:80, v/v) at ~ 1 ml min^{-1}. This second fraction (yellow) was collected and evaporated to ~ 5 ml (fraction IIE). Fractions IaE and Ib for GC–MS analysis were purified simultaneously with two silica columns similarly. The resulting fractions were designated IIaE and IIb.

Derivatization

Purified fractions (~ 5 ml) were transferred to a test vial, evaporated to dryness under a stream of nitrogen at 38°C and trimethylsilylated by adding 100 μl of N,O-bis(trimethylsilyl)acetamide (BSA) (Trisil BSA DMF, Pierce Chemicals, Rockford, IL, USA). This mixture was vortexed and heated for 1 h at 75°C.

Standards for GC–FID analysis were prepared by combining 100-μl volumes of GA and GB stock solutions, which were evaporated to dryness and trimethylsilylated wtih 200 μl of BSA as above. This yielded a standard solution of ~ 60 pmol μl^{-1} GA and GB.

For GC–MS standards, appropriate volumes of GA and GB stock solutions were combined, evaporated to dryness and trimethylsilylated with 100 μl of BSA to yield five standards of concentrations of 0.25, 2.5, 25, 60 and 120 pmol μl^{-1} GA and GB.

GC analysis

Analyses by GC–FID were performed with a Perkin-Elmer Sigma 2000 gas chromatograph (Norwalk, CT, USA) equipped with a 30 m × 0.25 mm I.D. DB1 WCOT capillary column (J&W Scientific, Folsom, CA, USA). Helium was used as the carrier gas at a head pressure of 2 bar. The temperatures of the injector, column and detector were 295°C, 270°C and 345°C, respectively. Injections (2 μl) were made in the splitless mode. Retention times of GA and GB were 6.7 and 7.7 min, respectively.

Analyses by GC–MS were performed with a Varian 6000 gas chromatograph (Sunnyvale, CA, USA) equipped with the same capillary column as above and an on-column injector (J&W Scientific). The gas chromatograph was interfaced directly to a VG ZAB-HF mass spectrometer (Middlewich, UK). Helium was the carrier gas at a head pressure of 1 bar. The temperature was increased from 250°C to 275°C at a rate of 5°C min^{-1}, and then to 285°C at a rate of 1°C min^{-1}, and finally to 300°C at a rate of 15°C min^{-1}. This temperature was maintained for 5 min.

The MS conditions were: electron-impact ionization, −70 eV; trap current, 100 μA; source temperature, 275°C. All re-entrants and transfer lines were maintained at 250°C. Resolution was 7500 (10% valley definition). Chromatograms were acquired in the selected-ion monitoring (SIM) mode using accelerating voltage switching with a dwell time of 120 ms each and a 10-ms switching delay between the eight ions monitored with m/z ranging from 537 to 667. Perfluorokerosene (PFK) was used as a lock-mass compound.

Internal standards were required for quantification of GA and GB by GC–MS. The internal standards chosen were deutero-trimethylsilylated GA and GB, which were prepared by adding 100 μl of deutero-regisil (Regis, Morton Grove, IL, USA) and 250 μl of dimethylformamide (DMF; Regis) to 20 nmol of GA and 20 nmol of GB. This mixture was mixed vigorously and heated for 1 h at 75°C. A volume of 5 μl of deutero-trimethylsilylated GA and GB was added to derivatized fractions IIaE and IIb or to derivatized standards prior to GC–MS analysis. This mixture yielded final deutero-trimethylsilylated GA and GB concentrations of 3 pmol μl^{-1}. Quantitative analysis by GC–MS was done using the ratio of the peak area of known concentrations of derivatized GA and GB to that of deutero-derivatized GA and GB internal standards. These calibration curves were linear from 0 to 120 pmol μl^{-1} with correlation coefficients of ~0.99 for both GA and GB. They were used to assess the concentration of ginkgolides in fractions IIaE and IIb.

RESULTS AND DISCUSSION

GC–FID analysis

Derivatization reaction. Ginkgolides are non-volatile compounds and need to be derivatized to be made volatile and analysed by GC–FID. Derivatization using trimethylsilylating agent (BSA) was

chosen since a simple chemical reaction is involved. A typical procedure for derivatization with BSA recommends the use of 1200–2400 nmol of compound per 100 μl of BSA reagent [11]. In the present study, the quantity of BSA required to achieve complete trimethylsilylation of ginkgolides contained in purified biomass extracts needed to be determined. Since actual cultured biomass extracts were known to contain low quantities of ginkgolides (~ pmol g^{-1} dry weight) [9], this was done by adding different excess amounts of pure GA and GB (~7–60 nmol) to various purified fraction I mixtures not enriched with these compounds before purification. These mixtures were derivatized with a constant volume of BSA (100 μl) and analysed by GC–FID. The resulting GA and GB peak areas were divided by the amount of GA and GB added to the purified extracts. The resulting ratios were constant [125 mV s $nmol^{-1}$ for GA and 135 mV s $nmol^{-1}$ for GB, with a relative standard deviation (R.S.D.) of 10 mV s $nmol^{-1}$ calculated from four different assays], indicating that BSA was in excess and complete trimethylsilylation was achieved. Consequently, sample preparation required at most 100 μl of BSA per 60 nmol of ginkgolides in purified extracts.

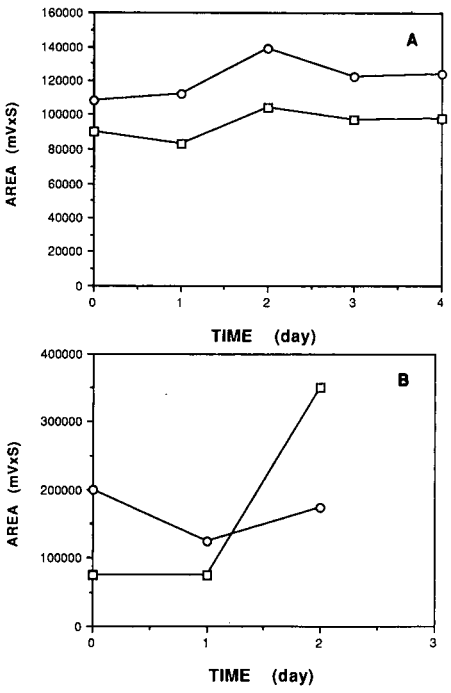

Fig. 2. Stability of trimethylsilylated derivatives (A) Pure ginkgolides. (B) Ginkgolides in enriched cell extracts. □ = GA; ○ = GB.

The chemical stability with time of trimethylsilylated GA and GB was evaluated. As shown in Fig. 2A, derivatized pure GA and GB were stable for at least four days. On the other hand, ginkgolides present in biomass extracts (fraction IIE) appeared to be degraded after one day, as indicated by significant differences in peak areas (Fig. 2B). This degradation may be attributed to hydrolysis since trimethylsilylated compounds are known to be moisture-sensitive [11] and/or appears to result in the formation other compound(s) interfering with ginkgolide detection. Consequently, purified biomass extracts needed to be analysed on the day of derivatization.

Purification procedure. Initially, the elution and recovery of pure ginkgolides from silica gel columns prepared as described above using a solvent system of 50:50 (v/v) cyclohexane–ethyl acetate, as suggested by Lobstein-Guth *et al.* [4], was evaluated. The rate of desorption of GA (~60 nmol) and GB (~60 nmol) was determined by collecting the effluent from the silica gel column in ~10-ml fractions which were analysed by GC–FID after derivatization. Recovery of GA was ~45%. However, GB, being more polar, was dispersed in many fractions, impairing its proper recovery. A more efficient scheme was devised using initially 60 ml of 50:50 (v/v) cyclohexane–ethyl acetate to separate hydrophobic products suspected to be present in actual extracts from ginkgolides. Thereafter, a 20:80 (v/v) cyclohexane–ethyl acetate solvent was used to elute GA and GB, which were recovered mainly between volumes of 65 and 120 ml with efficiencies of 90 ± 10% and 35 ± 10%, respectively (R.S.D. from three independent experiments). A more polar solvent (100% ethyl acetate) did not improve GB recovery.

Similarly, fraction IE purified on silica columns showed GA and GB to be eluted with 20:80 (v/v) cyclohexane–ethyl acetate at fractions between 70 and 130 ml. Fractions between 40 and 60 ml could not be analysed by GC–FID since a precipitate formed upon derivatization. Fig. 3, presenting the GC–FID chromatogram of derivatized fraction IIE, shows many organic compounds eluting together with GA and GB, rendering difficult their identification and quantification.

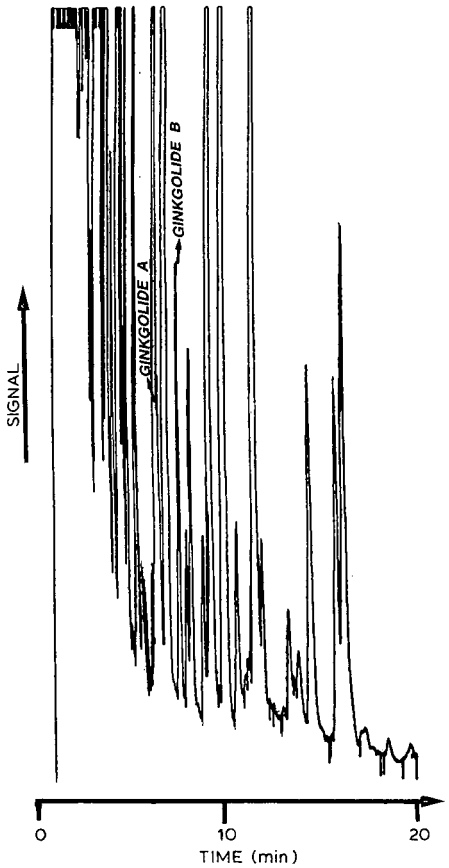

Fig. 3. GC–FID profile of trimethylsilylated ginkgolides in fraction IIE.

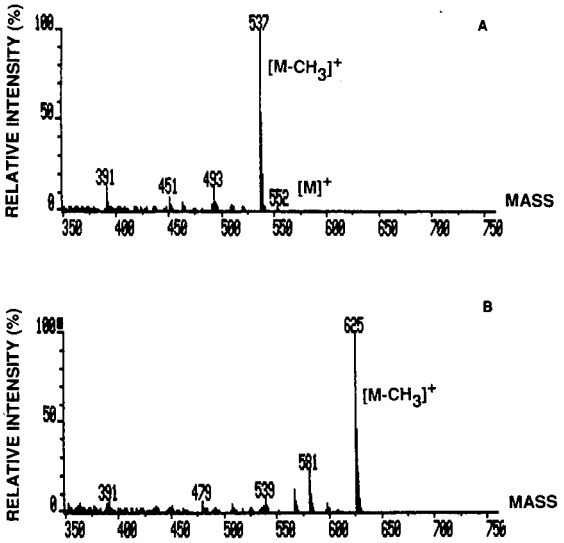

Fig. 4. Partial mass spectrum of trimethylsilylated ginkgolides measured at −70 eV EI. (A) GA. (B) GB.

The purification procedure converted resinous fraction I into a clear, injectable extract but was not sufficient to permit GC–FID analysis of GA and GB in the purified biomass extract. A more selective and sensitive detection technique, such as GC–MS, was preferred over further purification steps since cultured *G. biloba* cells were suspected to yield low concentrations of GA and GB.

GC–MS analysis

MS analysis of GA and GB. Derivatized GA and GB standards were analysed by GC–MS to evaluate their fragmentation pattern in the experimental conditions used. Fig. 4A presents the partial mass spectrum of trimethylsilylated GA, which displayed a weak molecular ion M^+ with *m/z* 552.221 in the 70-eV electron-impact (EI) spectrum. The major fragment with *m/z* 537.197 resulted from the loss of a methyl group. Trimethylsilylated GB displayed no molecular ion M^+ with *m/z* 640.256, as shown in Fig. 4B. The major fragment ion with *m/z* 625.232 resulted, as for derivatized GA, from the loss of a methyl group. The fragmentation patterns of trimethylsilylated GA and GB were very similar, consisting mainly of losses of 15, 59 and 101 a.m.u. from their respective molecular ion M^+. Deuterated trimethylsilylated GA and GB displayed weak molecular ions with *m/z* 570.334 and *m/z* 667.4245. Major ions resulting from the loss of a deuterated methyl group were observed at *m/z* 552.298 and *m/z* 649.383 for deuterated GA and GB, respectively.

The intense fragments resulting from the loss of methyl groups from the molecular ions were chosen for quantitative analysis in the SIM mode. Fig. 5A and B presents the mass chromatograms of non-deuterated and deuterated trimethylsilylated GA with retention times of 11.0 and 10.8 min, respectively. Mass chromatograms of non-deuterated and deuterated trimethylsilylated GB with retention times of 12.5 and 12.2 min, respectively, are shown in Fig. 5C and D.

The response factors [RF = (signal of the analyte × amount of the internal standard)/(signal of internal standard × amount of analyte)] were

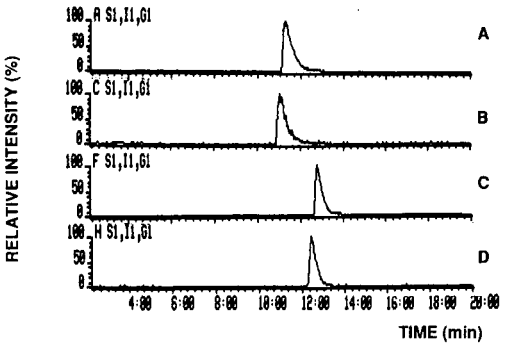

Fig. 5. Mass chromatograms of non-deuterated and deuterated trimethylsilylated ginkgolide standards. Each trace was normalized to the largest peak within the time window. (A) Trimethylsilylated GA: $[M-CH_3]^+$ at *m/z* 537.197. (B) Deutero-trimethylsilylated GA: $[M-C^2H_3]^+$ at *m/z* 552.221. (C) Trimethylsilylated GB: $[M-CH_3]^+$ at *m/z* 625.232. (D) Deutero-trimethylsilylated GB: $[M-C^2H_3]^+$ at *m/z* 649.383.

1.1 ± 0.1 and 1.0 ± 0.1 for GA and GB, respectively. These RF values near unity indicate that non-deuterated and deuterated trimethylsilylated ginkgolides behave similarly, satisfying an important criterion for selecting a good internal standard.

Analysis of cultured G. biloba cell extracts. Biomass extracts were purified and analysed by GC–MS. Fig. 6 presents typical mass chromatograms of a purified cell extract (fraction IIb) supplemented with internal standards. The retention times of fragment ions *m/z* 537.197 and *m/z* 552.221 were 10.7 and 10.6 min, respectively, which are similar to those of non- and deuterated derivatized GA standard. The retention times of ions *m/z* 625.232 and 649.383 were 12.0 and 11.7 min, respectively, in accordance with the retention times found for GB standards. Slight differences in retention times of GA and GB from standards and samples can be attributed to variations in the experimental conditions.

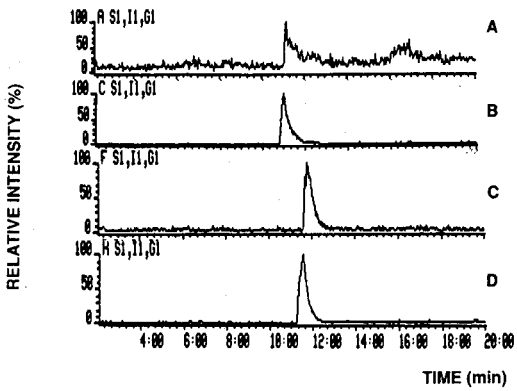

Fig. 6. Mass chromatograms of non-deuterated and deuterated trimethylsilylated ginkgolides in fraction IIb. Each trace was normalized to the largest peak within the time window. (A) Trimethylsilylated GA: $[M-CH_3]^+$ at *m/z* 537.197. (B) Deutero-trimethylsilylated GA: $[M-C^2H_3]^+$ at *m/z* 552.221. (C) Trimethylsilylated GB: $[M-CH_3]^+$ at *m/z* 625.232. (D) Deutero-trimethylsilylated GB: $[M-C^2H_3]^+$ at *m/z* 649.383.

The addition of deutero-trimethylsilylated ginkgolides to samples allowed normalization of the results of the GC–MS analysis and evaluation of GA and GB concentration in fraction IIb. As shown in Table I, GC coupled to electron-impact high-resolution MS allowed the quantitative determination of GA and GB in the range of 10^{-1} pmol μl^{-1} purified extracts. The addition of the internal standards prior to GC–MS prevented evaluation of the recovery efficiency of the whole procedure (purification and chromatographic separation). The use of a different internal standard before the purification of fraction I may have been a better method of evaluating the efficiency of recovery of the whole procedure. However, no chemical product that behaved to some extent like ginkgolides was found. The efficiency of the purification step was estimated by comparing results obtained from the analysis of enriched fraction II (fraction IIaE) and non-enriched fraction II (fraction IIb). As reported in Table I, recovery of GA and GB were 85 ± 10% and 30 ± 13%, respectively. These values are in the same range as those determined by GC–FID for pure GA and GB.

Ginkgolide yields of various *G. biloba* cell samples are presented in Table I. These figures were normalized by taking into account the recovery efficiency of the purification procedure. These low yields confirm the non-suitability of HPLC and TLC methods with refractive index or UV detection for the determination of ginkgolides produced by *G. biloba* cultured cells at this stage of development of this biological system. The procedures developed herein confirmed that GA and GB are produced by cell cultures, although in the pmol g^{-1} dry weight range presently. This method is used in our laboratory to screen different cell lines and culture con-

TABLE I

GC–MS ANALYSIS OF GA AND GB IN FOUR *G. BILOBA* CULTURED CELL SAMPLES

Sample No.	Concentration in prepurified extract (fraction IIb) (pmol μl^{-1})		Recovery from the extraction procedure [a] (%)		Concentration in cultured cells[b] (pmol g^{-1} dry weight)	
	GA	GB	GA	GB	GA	GB
1	0.6	0.2	97	32	6.4	5.8
2	2.9	0.5	81	22	56	35
3	2.7	0.9	75	23	56	52
4	0.4	0.7	85	40	5.3	17

[a] Recovery of GA and GB from the extraction procedure was evaluated using the enriched fraction (fraction IIa).

[b] Concentration in cells reported on a dry weight basis are normalized by taking into consideration the efficiency of the recovery of GA and GB from the extraction procedure.

ditions to optimize production of ginkgolides by *G. biloba* cell cultures.

ACKNOWLEDGEMENTS

The authors wish to thank Dr. Ian Reid for useful editorial comments. D. J. Carrier was the recipient of an F.C.A.R. scholarship.

REFERENCES

1 P. Braquet, *Drugs Future*, 12 (1987) 643.
2 E. Corey, M. Kang, M. Desai, A. Ghosh and I. Houpis, *J. Am. Chem. Soc.*, 110 (1988) 649.
3 K. Drieu, *Presse Med.*, 15 (1986) 1455.
4 A. Lobstein-Guth, F. Briancon-Scheid and R. Anton, *J. Chromatogr.*, 267 (1983) 431.
5 T. A. van Beek, H. A. Scheeren, T. Rantio, F. C. Griepink and W. C. Melger, *Planta Med.*, 56 (1990) 509.
6 S. G. Tallevi and W. G. W. Kurz, *J. Nat. Prod.*, 54 (1991) 624.
7 K. Nakanishi and K. Habaguchi, *J. Am. Chem. Soc.*, 93 (1971) 546.
8 K. Nakanishi, *Pure Appl. Chem.*, 8 (1967) 89.
9 D. J. Carrier, N. Chauret, P. Coulombe, M. Mancini, R. Neufeld, M. Weber and J. Archambault, *Plant Cell Rep.*, in press.
10 D. J. Carrier, G. Consentino, R. Neufeld, D. Rho, M. Weber and J. Archambault, *Plant Cell Rep.*, 8 (1990) 635.
11 *Pierce Handbook and General Catalog*, Rockford, Il, 1988, pp. 144–153.

Journal of Chromatography, 588 (1991) 289–294
Elsevier Science Publishers B.V., Amsterdam

CHROM. 23 606

Determination of the hold-up time and column outlet density for capillary supercritical fluid chromatography

R. L. Riester, C. Yan and D. E. Martire*

Department of Chemistry, Georgetown University, Washington, DC 20057 (USA)

(First received April 10th, 1991; revised manuscript received July 4th, 1991)

ABSTRACT

The column hold-up time (t_u) was determined for a capillary supercritical fluid chromatographic system over a range of temperatures and densities using methane as a marker and using homologous series extrapolations. At low temperatures, t_u was found to pass through a maximum with increasing density. To establish that this phenomenon is not due to a retention effect, t_u was also calculated from flow-rate measurements. The measured hold-up times and Darcy's law were used to calculate the outlet densities for different inlet pressures at two temperatures.

INTRODUCTION

The accurate determination of the column hold-up time, t_u, is a chronic problem for chromatographers, especially when mass spectrometric detection is not available or feasible. Theoretically, the hold-up time for an open-tubular column can be calculated if the pressure drop is known [1,2]. Perrut [2] has calculated hold-up times for packed columns with 5–40 bar pressure drops. However, the pressure drops in capillary supercritical fluid chromatography (SFC) are generally too small to be determined accurately. Hence, it is usually assumed that the pressure drop is negligible and the average density is closely approximated by the inlet density. Roth and Ansorgova [3] have calculated pressure profiles for capillary SFC and found them to be nearly linear. They have also demonstrated that secondary effects (thermal effects, turbulence effects, end effects and column coiling effects) can safely be neglected under capillary SFC conditions.

Here, we report the determination of t_u on a capillary SFC system with carbon dioxide as a mobile phase using four methods. In the first method, methane was assumed to be an "unretained" solute and was used as a t_u marker. Other compounds often used for this purpose (such as methylene chloride) were found to exhibit significant retention compared with methane, especially at low densities and temperatures. Methods 2 and 3 are based on the linearity of ln k' (capacity factor) with carbon number [4,5]. In method 2, retention times were measured for two different homologous series, alkanes and alkylbenzenes, and t_u was determined using the method of homologous series extrapolation described by Berendsen *et al.* [5]:

$$t_{R,n+1} = At_{R,n} - (A - 1)t_u \quad (1)$$

where $t_{R,n}$ is the retention time of the nth member of a homologous series and $t_{R,n+1}$ is the retention time for the next member of the series. A plot of $t_{R,n+1}$ *vs.* $t_{R,n}$ gives the slope A and the intercept $-(A - 1)t_u$. The hold-up time is determined from

$$t_u = \frac{\text{intercept}}{1 - \text{slope}} \quad (2)$$

In method 3, retention data for a homologous series of alkanes is fitted directly to the non-linear equation

$$t_R = t_u + t_u \exp a \exp bM \quad (3)$$

where M is the number of methylene groups and t_u, a

0021-9673/91/$03.50

and b are determined by fitting retention data for each density and temperature.

Using each of these methods, we found that t_u passes through a maximum with increasing density at low column temperatures. The maximum occurs near the critical density. This result was contrary to expectation, as t_u decreases with increasing pressure for both gas and liquid chromatography. In order to verify that the maximum was not an artifact caused by solute retention, in method 4, we used flow-rate measurements to determine t_u. The column-outlet volumetric flow-rate was measured and the mass flow-rate, $\dot{m}$, was determined from

$$\dot{m} = \rho_A F \tag{4}$$

where ρ_A is the density of the mobile phase in g/cm^3 under ambient conditions, as calculated from the extended BWR equation of state [6], and F is the measured volumetric flow-rate in cm^3/min. Then t_u is calculated from [1]

$$t_u = \frac{V_0 \rho_i}{\dot{m}} \tag{5}$$

where ρ_i is the column inlet density in g/cm^3 and V_0 is the column void volume in cm^3. With minimal error, the inlet density has been substituted for the spatial average density in eqn. 5 (see below).

In this study, we compared the column hold-up times obtained by the four methods outlined above and used the t_u values to calculate the column outlet density using equations derived from Darcy's law [1].

The derived expression for t_u is

$$t_u = \int_0^{t_u} dt = \frac{B}{(\upsilon_0 \rho_0)^2} \int_{\rho_0}^{\rho_i} D_t(\rho) d\rho \tag{6}$$

where υ is the velocity, ρ is the density and $D_t(\rho)$ is the temporal distribution function; the subscripts i and o refer to inlet and outlet conditions, respectively. For open-tubular columns, B is a constant which can be calculated:

$$B = \frac{\pi r^2}{8} \tag{7}$$

where r is the column radius. Making use of the equation

$$L = \int_0^L dx = \frac{B}{\upsilon_0 \rho_0} \int_{\rho_0}^{\rho_i} D_x(\rho) d\rho \tag{8}$$

where L is the column length and $D_x(\rho)$ is the spatial distribution function, $\upsilon_0 \rho_0$ can be eliminated from eqn. 6, resulting in

$$t_u = \frac{L}{B} \cdot \frac{\int_{\rho_0}^{\rho_i} D_t(\rho) d\rho}{\left[\int_{\rho_0}^{\rho_i} D_x(\rho) d\rho\right]^2} \tag{9}$$

The density distribution functions, $D_x(\rho)$ and $D_t(\rho)$, have been calculated for the given densities and temperatures in previous work [6]. An iterative procedure was used to solve this equation for the column outlet density. The outlet pressure corresponding to this density was then calculated using the extended BWR equation of state.

EXPERIMENTAL

The instrument used was a Model 501 capillary supercritical fluid chromatographic system with a flame ionization detector from Lee Scientific (Salt Lake City, UT, USA). The injection valve with a 200-nl sample loop was pneumatically operated. The sample was split on injection with a splitting ratio of *ca.* 20:1.

The capillary column was supplied by Lee Scientific. The stationary phase was SB-Octyl-50 with a film thickness of 0.25 μm. The column was 10 m × 50 μm I.D. A 30-cm frit restrictor was attached between the end of the column and the detector.

The mobile phase was supercritical-grade carbon dioxide obtained from Matheson Gas Products (Baltimore, MD, USA). Other gases (helium, used for valve actuation; nitrogen, used as a make-up gas; hydrogen and air, used for the flame ionization detector) were obtained from Roberts Oxygen (Rockville, MD, USA). Methane, used as the marker for the first t_u determination method, was obtained from natural gas piped into the laboratory. The alkanes and alkylbenzenes used for the homologous series studies were obtained from various standard sources. It was not deemed necessary to use highly purified solutes for these studies since trace impurities are resolved during the chromatographic process and easily identified.

The detector temperature was set at 325°C; the range and attenuation were adjusted for each set of conditions. The signal output was recorded on a Linear strip-chart recorder.

All experiments were performed under isothermal, isobaric (*i.e.*, non-programmed) conditions. Settings were selected to provide measurements at 10 K intervals from 320 to 380 K and 0.05 g/cm^3 density increments from 0.2 to 0.7 g/cm^3. Pressure settings were determined by calculating each pressure from the extended BWR equation of state for the selected temperature and density.

Replicate injections (usually three) were performed at each temperature and density setting. The system was allowed to equilibrate between each change of settings.

The low column flow-rates in capillary SFC are difficult to measure accurately. The solubility of carbon dioxide and its diffusion into the connective tubing make the determination of flow-rates with the usual soap-bubble flow meter semi-quantitative at best. A flow meter modified to minimize these problems was devised using a standard 50-ml buret with side-arm (Fig. 1). The glass side-arm is connected to the flame ionization detector directly to prevent diffusion of carbon dioxide through the connective tubing. The stopcock is closed after introduction of the bubble to prevent dissolution of the carbon dioxide in the soap solution and the flow meter is stoppered to minimize the effects of air currents and pressure fluctuations. Flow-rate measurements were made at 310, 320 and 360 K, with the detector flame extinguished. The reproducibility was significantly improved with the modified flow meter, but the relative uncertainty is still about 7%.

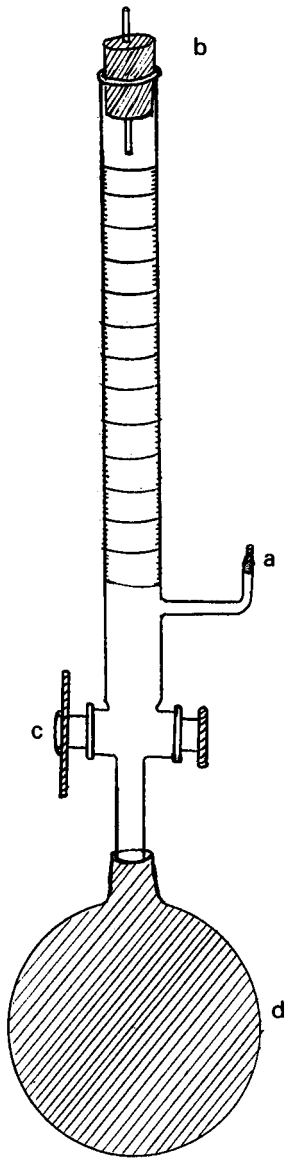

Fig. 1. Modified soap-bubble flow meter: (a) glass side-arm; (b) stopper with capillary; (c) stopcock; (d) rubber bulb containing soap solution.

RESULTS AND DISCUSSION

Selected results of the t_u determinations are given in Table I and Fig. 2. With a few exceptions, there is very good agreement among the values obtained using the first three methods. The t_u values obtained by fitting the alkane data and the alkylbenzene data by method 2 are also in good agreement. The hold-up times calculated using method 3 are in excellent agreement with those calculated using method 2. Method 2 has the advantage of being a linear fit but the disadvantage of requiring retention data for a series of sequential homologs. It also has the disadvantage of having errors in both "x" and "y", thus making the errors in t_u difficult to estimate. A non-linear fitting routine must be available in order to use method 3. We used SAS NLIN for this purpose. A series of homologs is necessary for this fit, but the series need not be sequential. Also, the

TABLE I

COLUMN HOLD-UP TIMES

Temperature (K)	ρ_i (g/cm^3)	Column hold-up time (min)				
		Method 1	Method 2		Method 3	Method 4
			a	b		
310	0.25	15.90	15.26			
	0.30	20.40	19.90			17.63
	0.35	24.90	24.80			
	0.40	26.00	25.95			20.68
	0.45	26.38	26.33			
	0.50	26.40	26.38			25.07
	0.55	26.39	26.30			
	0.60	25.40	25.70			27.11
	0.65	24.50	24.44	23.79	23.81	
	0.70	21.81	21.80	21.20	21.20	22.55
320	0.20	12.10	12.19			12.48
	0.25	12.60	12.62	12.42	12.43	
	0.30	13.50	13.47	13.20	13.16	13.51
	0.35	14.50	14.35	14.34	14.33	
	0.40	15.50	15.39	15.27	15.28	15.38
	0.45	16.21	16.17	16.00	16.01	
	0.50	16.55	16.36	16.37	16.35	15.76
	0.55	16.50	16.32	16.37	16.36	
	0.60	15.95	15.86	15.88	15.88	15.01
	0.65	14.80	14.66	14.77	14.76	
	0.70	12.95	12.79	12.87	12.91	12.94
360	0.20	7.72	7.79	7.40	7.42	8.06
	0.25	7.12	7.27	7.11	7.10	
	0.30	7.00	7.90	6.83	6.83	7.21
	0.35	6.80	6.78	6.73	6.75	
	0.40	6.63	6.58	6.58	6.64	6.29
	0.45	6.40	6.34	6.26	6.31	
	0.50	6.10	6.08	6.04	6.05	5.76
	0.55	5.71	5.68	5.62	5.66	
	0.60	5.22	5.20	4.93	5.15	4.84

errors are contained in "y" and errors in t_u are estimated by the program.

Using method 4, the calculated hold-up times are not in particularly good agreement with the results from the other methods. However, these measurements do follow the same trend and also exhibit a maximum in t_u near the critical density for low temperatures. The discrepancies are probably due to the reproducibility and accuracy of the flow-rate measurements. Mass flow-rates are plotted in Fig. 3. It can be seen that a small error in the flow-rate determination leads to a large error in t_u. Also, V_0 was assumed to be constant for this calculation, whereas it may change slightly with temperature and density of the mobile phase.

Eqn. 8 and the hold-up times determined by method 2 were used to calculate the column outlet densities. The extended BWR equation of state was then used to calculate the column outlet pressures with the assumption that the residence time of the mobile phase in the restrictor is negligible. The calculated outlet densities and pressures for 320 and 360 K are given in Table II.

The effect of the density drop on ln k' was

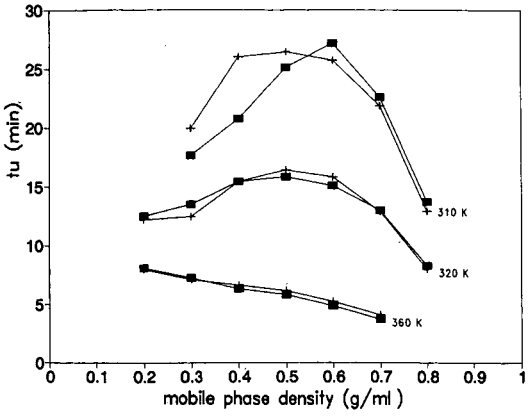

Fig. 2. Hold-up times *versus* mobile phase density at 310, 320 and 360 K. ■ = Method 1; + = method 4.

determined by comparing the ln k' values using the inlet density:

$$\ln k'(\rho_i) = \ln k'_0 + a\rho_i + b\rho_i^2 \quad (10)$$

and using the temporal average density:

$$\ln k'(<\rho>_t) = \ln k'_0 + a<\rho>_t + b<\rho^2>_t \quad (11)$$

where a and b are arbitrarily chosen constants. These results for $\ln k'_0 = 9.55$, $a = -29.38$, $b = 19.90$ are given in Table III. The pressure drops were found to be very small and the density drops insignificant. Therefore, the effect of using the inlet

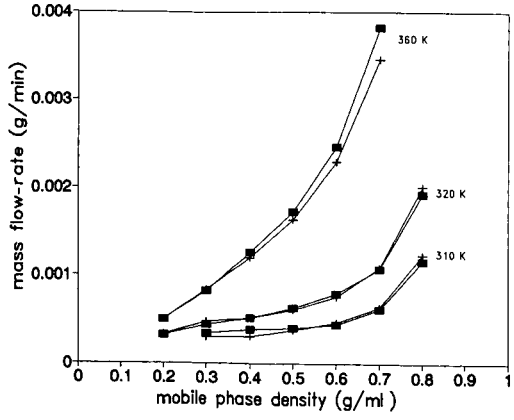

Fig. 3. Mass flow-rates *versus* mobile phase density at 310, 320 and 360 K. ■ = Method 1; + = method 4.

TABLE II

CALCULATED PRESSURE AND DENSITY DROPS

Temperature (K)	ρ_i (g/cm^3)	P_i (bar)	$\Delta\rho$ (g/cm^3)	ΔP (bar)
320	0.25	82.74	0.003	0.38
	0.30	88.65	0.004	0.38
	0.35	93.07	0.005	0.40
	0.40	96.70	0.006	0.42
	0.45	100.12	0.006	0.45
	0.50	103.78	0.006	0.48
	0.55	108.19	0.005	0.52
	0.60	114.25	0.004	0.58
	0.65	123.42	0.003	0.72
	0.70	138.00	0.003	0.94
360	0.20	97.32	0.002	0.54
	0.25	113.27	0.002	0.63
	0.30	127.45	0.003	0.71
	0.35	140.58	0.003	0.79
	0.40	155.39	0.004	0.89
	0.45	166.70	0.004	1.01
	0.50	181.40	0.004	1.14
	0.55	198.64	0.004	1.31
	0.60	220.01	0.003	1.59

TABLE III

CALCULATED CAPACITY FACTORS (k')

Temperature (K)	ρ_i (g/cm^3)	ln $k'(\rho_i)$	ln $k'(<\rho>_t)$
320	0.20	4.47	4.49
	0.25	3.45	3.48
	0.30	2.53	2.56
	0.35	1.71	1.75
	0.40	0.98	1.03
	0.45	0.36	0.40
	0.50	−0.16	−0.13
	0.55	−0.59	−0.57
	0.60	−0.91	−0.90
	0.65	−1.14	−1.13
	0.70	−1.26	−1.26
360	0.20	4.47	4.49
	0.25	3.45	3.47
	0.30	2.53	2.55
	0.35	1.71	1.73
	0.40	0.98	1.01
	0.45	0.36	0.38
	0.50	−0.16	−0.15
	0.55	−0.59	−0.57
	0.60	−0.91	−0.90

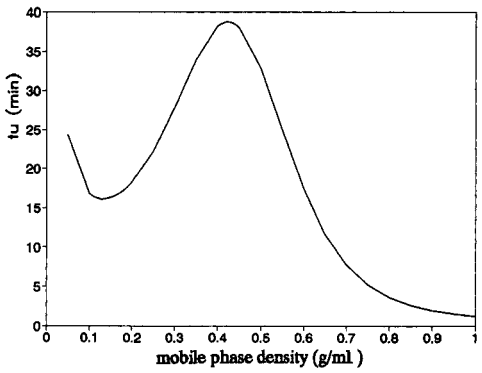

Fig. 4. Hold-up times calculated from eqn. 9 for 320 K, assuming $\rho_0 = 0.994\rho_i$.

density instead of the temporal (or spatial) average density is seen to be minimal.

In order to examine the behavior of t_u over a full range of densities, including those normally encountered in gas and liquid chromatography, a constant relative density drop was assumed ($\rho_0 = 0.994\rho_i$) and t_u was calculated at 320 K from eqn. 9 (see Fig. 4). This curve has the same general pattern in the vicinity of the critical density although the maximum is exaggerated. A minimum is also predicted at lower density. This behavior of t_u is peculiar to dense gases. As expected, the equation predicts a decrease in t_u with increasing pressure for both ideal gases and liquids.

CONCLUSIONS

Measurements of t_u as a function of inlet density for several temperatures indicate that, at low supercritical temperatures, the hold-up time increases with increasing density, reaches a maximum at or near the critical density, then decreases as the inlet density is further increased. At higher temperatures, t_u decreases with increasing density. This behavior, which is related to the dependence of the density distribution functions, $D_x(\rho)$ and $D_t(\rho)$, on the isothermal compressibility and viscosity of the mobile phase [1,6], can be predicted from eqn. 9, provided that both the inlet and outlet densities are known. Alternatively, it can be confirmed from eqn. 5, provided that sufficiently accurate mass flow-rates are available.

ACKNOWLEDGEMENT

This material is based on work supported by the National Science Foundation under Grant CHE-8902735.

REFERENCES

1 D. E. Martire, *J. Chromatogr.*, 461 (1989) 165.
2 M. Perrut, *J. Chromatogr.*, 396 (1987) 1.
3 M. Roth and A. Ansorgova, *J. Chromatogr.*, 465 (1989) 169.
4 D. E. Martire and R. E. Boehm, *J. Phys. Chem.*, 91 (1987) 2433.
5 G. E. Berendsen, P. J. Schoenmakers, L. de Galan, G. Vigh, Z. Varga-Puchony and J. Inczedy, *J. Liq. Chromatogr.*, 3 (1980) 1669.
6 D. E. Martire, R. L. Riester, T. J. Bruno, A. Hussam and D. P. Poe, *J. Chromatogr.*, 545 (1991) 135.

Journal of Chromatography, 588 (1991) 295–301
Elsevier Science Publishers B.V., Amsterdam

CHROM. 23 609

Use of hematoporphyrin as a fluorescent stain for detection of lipids in high-performance thin-layer chromatography

Joseph H. Aiken and Carmen W. Huie*

Department of Chemistry, State University of New York at Binghamton, Binghamton, NY 13902-6000 (USA)

(First received March 13th, 1991; revised manuscript received July 2nd, 1991)

ABSTRACT

The use of hematoporphyrin as a sensitive and selective fluorescent dye for the detection of various lipids after separation by high-performance thin-layer chromatography is reported. To maximize the fluorescence signal, one of the visible lines of an argon ion laser is used for fluorimetric excitation; to minimize background noise, a novel approach involving the rapid treatment of the chromatogram with a dilute solution of copper(II) nitrate for the efficient quenching of background fluorescence from hematoporphyrin adsorbed on the silica gel substrate is presented. Excellent limits of detection in the low nanogram range are obtained for the detection of cholesterol, cholesteryl esters, sphingomyelin, lecithin and triolein. Some preliminary investigations regarding visual detection limits, selectivity and photostability of hematoporphyrin are also reported.

INTRODUCTION

Thin-layer chromatography (TLC) is an important separation method for the qualitative and quantitative determination of lipids in various biological materials [1]. For the *in situ* visualization or quantification of lipids on thin-layer chromatograms, chromogenic reagents such as molybdophosphoric acid, bromothymol blue and copper(II) sulfate can be used for the production of colored compounds with lipids of interest [2]. The major disadvantage of these reagents is that an acid charring process is often necessary, which is time consuming and, more important, the charring process is difficult to control and could lead to destruction of the lipid samples. To increase the detection sensitivity and to simplify the sample treatment procedure, methods involving fluorogenic reagents can be used [3]. These include treating the chromatogram with fluorescent dyes such as 8-anilino-1-naphthalenesulfonate (ANS), 2′,7′-dichlorofluorescein and rhodamine B. Among these fluorescent dyes, only rhodamine has been shown to be a popular fluorogenic reagent owing to its high fluorescent quantum yield and photostability; however, destructive sample treatment procedures involving preliminary hydrogenation of samples are required before separation and detection can be performed [4]. Recently, a new fluorescent dye, nile red, has been introduced as a general-purpose reagent for the detection of lipids and other hydrophobic compounds after separation by TLC [5]. Among the major advantages of this reagent are that it is intensely fluorescent, the fluorescence is relatively photostable and fades slowly and the dye preferentially dissolves in hydrophobic compounds. A common disadvantage among almost all fluorescent dyes, including nile red, is that significant background fluorescence can be observed from dyes adsorbed directly on the stationary phase, resulting in a noisy background and a decrease in detectability and reproducibility. Quantification of lipids on thin-layer chromatograms using nile red staining requires the use of a dilute bleach solution for the

0021-9673/91/$03.50

reduction of background fluorescence. However, careful selection of the bleach concentration is necessary to prevent oxidation of lipids and/or dye dissolved in the lipid bands.

It has been known for a long time that protoporphyrin possesses affinity for certain lipids [6], and it has been used as a selective fluorogenic reagent for the detection of a number of lipids on paper chromatograms [7]. It has shown that the use of protoporphyrin as a fluorescent stain offers several advantages over rhodamine dyes for the visualization of lipids on paper chromatograms, the most significant of which is the enhancement in detectability due to the relatively high fluorescent quantum yield of protoporphyrin and the appearance of a very low background fluorescence. Further, it has been shown recently that hydrophobic porphyrins, including protoporphyrin and hematoporphyrin, bind strongly to serum lipoprotein and are responsible for the photosensitivity of patients suffering from porphyrias and the accumulation of hematoporphyrin derivatives in tumors accompanying the phototherapy of cancer [8].

The separation of different individual components of lipid subclasses usually involves the use of two-dimensional TLC techniques [9]. However, with the improvement in separation efficiency in high-performance (HP) TLC, the rapid separation of several lipid fractions with good resolution can be achieved in one-dimensional development [10]. Compared with conventional TLC plates, the decrease in particle size in HPTLC requires the application of smaller sample volumes, which places a greater demand on the detection system to achieve the best sensitivity possible. The ease with which the laser beam can be focused to a very small spot while maintaining sufficient power makes it an attractive light source for the fluorimetric excitation of sample spots on HPTLC plates. Excellent detectabilities have already been reported in the use of laser fluorimetric techniques for the determination of biologically important molecules such as aflatoxins after separation by TLC [11]. Further, other laser-based techniques such as photoacoustic spectroscopy, non-linear luminescence and photothermal deflection spectroscopy have also been successfully applied to improve analytical performances in TLC [12].

In this paper we report the use of hematoporphyrin as a sensitive and selective fluorescent dye for the detection of certain lipids separated on HPTLC plates. To reduce the background fluorescence, a novel approach involving the rapid and mild treatment of the chromatogram with a dilute copper(II) nitrate solution for the efficient quenching of hematoporphyrin molecules adsorbed on a silica gel substrate is presented. Using the 488-nm line of an argon ion laser for excitation, low nanogram amounts of cholesterol, cholesteryl esters, triolein, sphingomyelin and lecithin are detected fluorimetrically. Similar amounts of cholesterol and cholesteryl esters are also detected visually using a conventional ultraviolet (UV) light source for fluorimetric excitation.

EXPERIMENTAL

Chemicals

Hematoporphyrin and protoporphyrin were obtained from Fluka Biochemicals (Ronkonkoma, NY, USA). All the lipids (cholesterol, choslesteryl oleate, cholesteryl linoleate, cholesteryl linolenate, cholesteryl palmitate, sphingomyelin, lecithin, triolein and testosterone) were of research grade and purchased from Sigma (St. Louis, MO, USA). Chloroform, carbon tetrachloride and methanol were of HPLC grade and other organic solvents were of analytical-reagent grade; all were obtained from Fisher Scientific (Pittsburgh, PA, USA). Copper(II) nitrate, *n*-octanol, caproic acid and acetic acid were purchased from Eastman Kodak (Rochester, NY, USA).

Chromatography

Separations of various lipids were performed on 5-μm silica gel HPTLC plates equipped with a pre-adsorbent area (Whatman, Hillsboro, OR, USA). The plates had dimensions of 10 × 10 cm and a layer thickness of 200 μm. To minimize background fluorescence from impurities on the plates, the plates were first washed with methanol followed by an additional wash with the development solvents. A sample volume of 100 nl was spotted on the plates with a 0.5-μl syringe. Before development, the silica gel plates were activated at 100°C for 30 min. The plates were developed in a nano-developing chamber designed to accept 10 × 10 cm HPTLC plates (Anspec, Ann Arbor, MI, USA) and equipped with

a heavy glass lid to fit the chamber flanged top. The chamber was lined with four filter-papers and then filled with the appropriate solvent system to allow saturation of the chamber atmosphere for about 60 min before introduction of the spotted plate. The chromatographic solvent systems described recently which allow the rapid HPTLC separation of 21 different lipid components within 15 min [10] were adopted in our experiments for the separation of various lipids. For the separation of cholesteryl esters, solvent A (carbon tetrachloride) was used; sphingomyelin and lecithin were separated with solvent B, chloroform–methanol–methyl acetate–water (100:60:16:8, v/v), and cholesterol and triolein with solvent C, chloroform–ethylacetate (94:6, v/v).

Staining

A stock solution of 0.33 m*M* hematoporphyrin was prepared by first dissolving appropriate amounts of hematoporphyrin in a small amount of 2 *M* sodium hydroxide solution and then diluting to an appropriate volume with 0.01 *M* phosphate buffer (pH 7.4). A stock solution of 100 m*M* copper(II) nitrate was prepared in doubly distilled, deionized water (DDW). To stain lipids for either laser-based or visual detection, the plate was dipped for 10 s in a tank of 0.25 m*M* hematoporphyrin solution followed by rinsing with DDW. To reduce background fluorescence by chelation with copper (II) ions, the plate was dipped for another 10 s in a 10 m*M* solution of copper(II) nitrate. The plate was dried by heating at 100°C for about 5 min for the laser-based experiment; however, the plate was inspected wet for the visual experiment.

Detection

Fluorimetric detection of the hematoporphyrin-stained lipids was accomplished with the apparatus used in previous work [13]. Briefly, radiation from a Coherent Innova 90-4 argon ion laser was first passed through a 488-nm line filter before it was focused with a 90-mm focal length lens and directed at an angle of almost 45° relative to the plate surface. The excitation and emission wavelengths were found to be optimum at 488 and 630 nm, respectively. Typical output power of the laser was 80 mW. To obtain a chromatogram, the thin-layer plate was scanned in front of the focused laser beam at *ca.* 30 mm/min using a precision d.c. motor-driven translational stage (Newport Research, Fountain Valley, CA, USA). The fluorescence signal was collected normal to the plate with an *f*/1, 25-mm focal length lens. The signal was then focused by an 80-mm focal length lens onto the entrance slit of an *f*/4 monochromator (PTR Optics, Waltham, MA, USA). The monochromator was fitted with 600-μm slits and the band pass was *ca.* 3 nm. Further fluorescence isolation was provided by a Corion 10-nm band-pass filter centered at 620 nm. The signal was measured with an R928 photomultiplier tube (Hamamatsu, Bridgewater, NJ, USA) operated at 800 V. The photocurrents were fed to a picoammeter (Oriel, Stratford, CT, USA) and the output signal was filtered through a 1.0-s time constant before recording on a strip-chart recorder. To reveal lipids separated on HPTLC plates, the plates were excited with a UV hand lamp (UVP, San Gabriel, CA, USA) which was held *ca.* 5 cm from the surface of the plate. This lamp was operated at a wavelength of 366 nm ("long-wave" mode) and produced a typical peak 366-nm intensity of *ca.* 200 μW/cm^2 at a 15-cm distance. The visual detection limits were established by observing the pink fluorescence from the sample spots and recording the lowest lipid concentrations at which the fluorescence could no longer be seen in a dark room.

RESULTS AND DISCUSSION

In general, the fluorescence of porphyrins is most efficiently excited at the major absorption band at about 400 nm (the so-called "Soret" band) using a conventional light source; however, fluorimetric excitation using a laser light source at one of the minor absorption bands, which centers around 500 nm in the blue-green region of the visible spectrum and happens to fall conveniently within the most intense emission region of an argon ion laser, can be of great advantage for improved sensitivity and selectively as the high intensity of the laser will more than compensate for the sacrifice in the magnitude of the molar absorptivity and only a small number of organic molecules present in biological samples absorb efficiently in the visible region and yield appreciable fluorescence signals. These advantages have already been demonstrated in our earlier work on the determination of porphyrin profiles in human urine using HPTLC for separation and visible laser

fluorimetry for excitation and detection [13]. Another interesting spectroscopic property of porphyrins is that chelation of iron and other transition metal ions with porphyrins usually leads to severe quenching of the fluorescence [14]. For example, heme (iron protoporphyrin) has a fluorescence yield that is probably smaller than 10^{-10}. To the best of our knowledge, analytical exploitation of this particular property has not been reported.

In our experiments, a significant reduction in the background fluorescence on HPTLC plates is accomplished by the rapid chelation of Cu(II) ions with hematoporphyrin bound to the silica gel substrate. It should be noted that for most metal-free porphyrins, Cu(II) is the most rapidly incorporated ion in aqueous solution followed by Zn(II), Co(II), Fe(II) and Ni(II) [14]. Fig. 1a shows a chromatogram of 25 ng of cholesterol eluted on an HPTLC plate. Using hematoporphyrin as the fluorescent stain and the 488-nm line of an argon ion laser for fluorimetric excitation, it is clear that the intensity of the fluorescence signal from hematoporphyrin bound to the lipid band is higher than that of hematoporphyrin adsorbed directly on the stationary phase, partly owing to more efficient quenching of the stain by the silica gel. Fig. 1b shows the efects of treating the chromatogram as shown in Fig. 1a with a dilute solution of copper(II) nitrate. It is obvious that background fluctuations are significantly reduced owing to efficient chelation of Cu(II) ions and subsequent quenching of the hematoporphyrin molecules that are adsorbed on the silica gel. However, the intensity of the fluorescence signal arising from hematoporphyrin bound to the lipid also seems to decrease, but certainly to a much lesser extent. It should be noted that in order to record the chromatogram without changing the sensitivity on the recorder and the picoammeter, a suppression current provided by the internal circuitry of the picoammeter was used to attenuate the larger d.c. background obtained from plates that have not been treated with copper(II) nitrate solution. The results presented in Fig. 1a and b suggest that the rate of copper chelation with hematoporphyrin is sensitive to the microenvironment. When compared with the relatively polar silica gel substrate, the hydrophobic environment of the lipid band appears to provide a medium in which the rate of copper chelation with hematoporphyrin is slower, resulting in enhancement in signal-to-noise ratio (S/N). By comparing the average peak heights and peak-to-peak noise for five sets of chromatograms similar to that shown in Fig. 1a and b for the detection of cholesterol, an average improvement in S/N by a factor of *ca.* 5 can be estimated. This improvement factor remains relatively constant over a period of 30 min while keeping the chromatograms in a dark room. However, it is likely that the rate of copper chelation with hematoporphyrin dissolved in other lipids would be slightly different, resulting in varying degrees of S/N improvement.

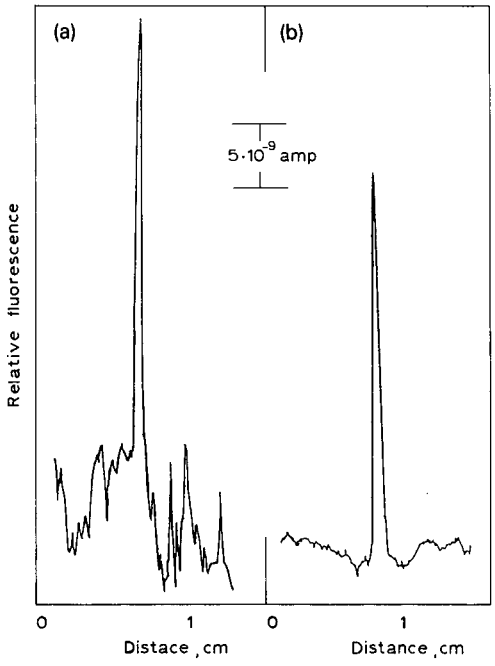

Fig. 1. HPTLC of 25 ng of cholesterol (a) without treatment and (b) with treatment in copper(II) nitrate solution. amp = Ampere.

The fluorescence of hematoporphyrin is pH and concentration dependent; the influence of these factors on the detection of lipids separated on HPTLC plates was investigated. Buffered hematoporphyrin solutions with pH in the range 2–11 were used for the study and the results indicated that the fluorescence of hematoporphyrin dissolved in lipid bands increased non-linearly with increasing pH and reached a plateau between pH 7 and 11. The concentrations of hematoporphyrin and copper(II) nitrate which gave the best S/N in our experiments

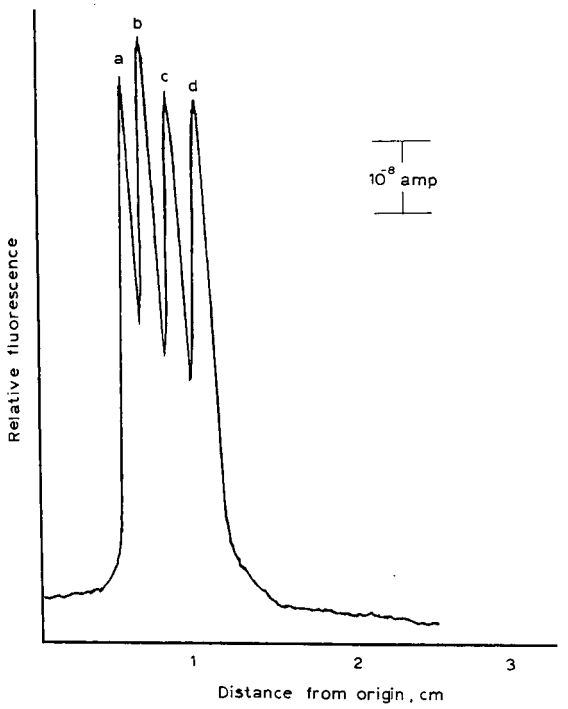

Fig. 2. HPTLC of 50 ng each of (a) cholesteryl palmitate, (b) cholesteryl oleate, (c) cholesteryl linoleate and (d) cholesteryl linolenate.

were found to be 0.25 and 10 m*M*, respectively. Also, a dipping time of 10 s appeared to offer the optimum S/N for the treatment of the plates with either hematoporphyrin or copper(II) nitrate solution.

Figs. 2, 3 and 4 show the HPTLC of cholesteryl esters, phospholipids and neutral lipids, respectively. The corresponding limits of detection (LOD) determined for each of these lipids are presented in Table I. These LOD values are about one to two orders of magnitude better than those reported for TLC [1,5,9] in the determination of lipids using densitometry or other fluorescence techniques. For example, using nile red as the fluorescent stain and a conventional UV light source for fluorimetric excitation, the minimum amount of cholesterol and sphingomyelin detectable is 100–200 ng; for cholesteryl oleate and trioleoylglycerol, the minimum amount detectable is about 50 ng [15]. The improvements in LOD in our method are made possible by the highly fluorescent nature of hematoporphyrin, the enhancement in fluorescence signal derived from the increase in photon flux using a laser source and the reduction in noise from effective quenching of background fluorescence through the rapid chelation of hematoporphyrin with copper(II) ion. It should be noted that hematoporphyrin is the least expensive metal-free porphyrin and contains a mixture of dicarboxylic acid porphyrins. We have compared the S/N for the detection of cholesterol separated on HPTLC plates using hematoporphyrin and protoporphyrin as the fluorescent stain and found that the detection limit obtained by hematoporphyrin staining is better by a factor of 2–3. Calibration graphs drawn for the various lipids exhibited linearity from the LOD up to the amount indicated in Table I, and the corresponding linear regression contents are also tabulated. At higher concentrations, non-linearity may arise from insufficient staining of the larger lipid mass, variation in quenching efficiency of the hematoporphyrin bound to the larger lipid bands and/or a mismatch between the dimension of the focused laser beam and the sample spot size and shape.

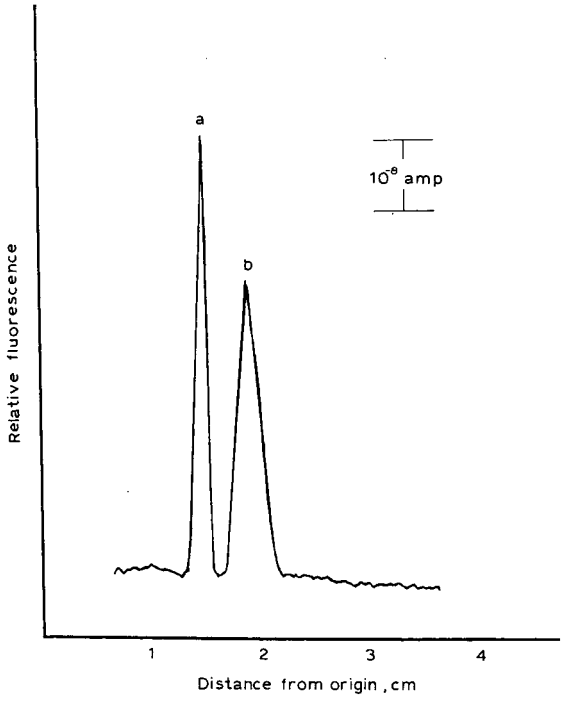

Fig. 3. HPTLC of 50 ng each of (a) sphingomyelin and (b) lecithin.

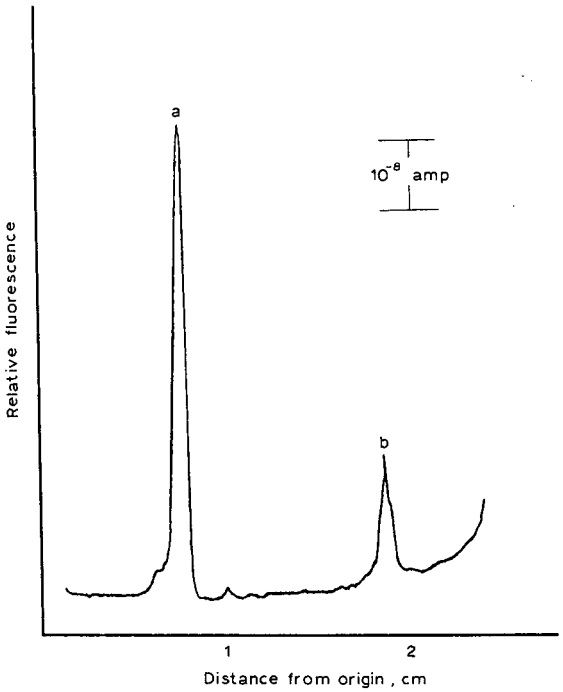

Fig. 4. HPTLC of 50 ng each of (a) cholesterol and (b) triolein.

A major limitation of most *in situ* TLC methods for the quantification of lipids is the varying effect of saturated *versus* unsaturated fatty acid moieties on the level of staining produced. Fig. 2 shows that the relative fluorescence intensity of cholesteryl esters with varying fatty acid composition is similar, suggesting that the influence of saturation of fatty acid moieties of lipids on the observed hematoporphyrin fluorescence is minimum. Fig. 2 also shows that there are some overlaps between the individual cholesteryl ester bands because the laser beam was focused to a diameter of *ca.* 2 mm on the plate surface to maximize the overlap between the laser spot and the various sample spots that are developed on the plate. To improve the resolution, sensitivity and linearity, two-dimensional scanning of the sample spots with a tightly focused laser beam can be performed either along a mutually perpendicular direction or in "meander-scanning" mode by interfacing the scanning table to a computer [16].

We have done some preliminary investigations on the photostability of hematoporphyrin as a fluorescent stain. Under the influence of ambient room light, the intensity of the fluorescence signal obtained from a chromatogram as shown in Fig. 1a remains relatively constant for at least 1 h. The intensity decrease by about *ca.* 5 and 10% in periods of 6 and 12 h, respectively. If the chromatogram is kept in the dark, the hematoporphyrin appears to be stable for at least 24 h. Under the influence of laser radiation (a laser power of 80 mW and laser spot diameter of *ca.* 2 mm), there is less than a 3% decrease in the peak height for the detection of 25 ng

TABLE I

DETECTION LIMITS AND LINEARITY AT GIVEN R_F VALUES

Lipid	R_F	Detection limit[a] (ng)	Linearity	
			Upper limit (ng)	Linear regression constant[b]
Cholesteryl palmitate	0.07	7.0	300	0.993
Cholesteryl oleate	0.09	3.3	300	0.993
Cholesteryl linoleate	0.12	7.7	300	0.993
Cholesteryl linolenate	0.14	5.2	300	0.993
Cholesterol	0.30	6.8	600	0.995
Sphingomyelin	0.45	6.8	300	1.000
Lecithin	0.53	10.4	300	1.000
Triolein	0.75	13.8	300	0.997

[a] Detection limits based on a signal-to-noise ratio of 3 according to peak heights.
[b] Linear regression constants determined from detection limits up to the amounts listed for the upper limits.

of cholesterol after five consecutive scans over the same spot while scanning the plate at *ca.* 30 mm/min.

Some preliminary studies have also been conducted in evaluating the visual LOD and the selectivity of hematoporphyrin for the detection of lipids. After dipping an HPTLC plate into a solution of hematoporphyrin for 10 s and subsequently observing the wet plate under UV radiation, cholesterol and cholestryl esters appears as brilliant pink spots on a background with similar color but dimmer intensity. A much better contrast was obtained after further treatment of the plate by dipping it in dilute copper(II)intrate solution for another 10 s, which gave a pink spot for the sample over a dark background. However, no significant improvements in our ability to detect visually the smallest concentrations of lipids was achieved, as hematoporphyrin bound to the lipids was also quenched but to a lesser extent. The visual LOD for cholesterol and cholesteryl esters using either procedure [with or without treatment with copper(II) nitrate] is *ca.* 10 ng, which is slightly better than those obtained by some of the more popular fluorogenic agents such as rhodamine B, ANS and dichlorofluorescein [3]. A number of substances have already been tested with protoporphyrin to determine its selectivity, and certain structural characteristics appear to be necessary for staining by protoporphyrin [7]. Most notably, a carboxyl group in aliphatic compounds of at least eight carbons is necessary. Among the polynuclear compounds, steroids without an isooctane side-chain are negative. In our experiments, testosterone, caproic acid and *n*-octanol were tested with hematoporphyrin to determine its selectivity. Negligible fluorescence signals were observed for these compounds spotted onto HPTLC plates. It appears that hematoporphyrin, having a similar structure to protoporphyrin, would have a similar selectivity to protoporphyrin for the detection of lipids. However, the structural requirements for staining with hematoporphyrin need further investigation.

It should be realized that the excellent LOD obtained for the detection of various lipids on HPTLC plates requires only 80 mW of continuous-wave radiation for fluorimetric excitation, which could be easily provided by a low-cost, air-cooled argon ion laser. Moreover, it is possible that small and inexpensive semiconductor lasers, which provide radiation in the yellow-red region of the visible spectrum, will be available in the near future [17]. Since hematoporphyrin possesses minor absorption bands in the blue-green and yellow-red regions, fluorimetric excitation of one of the minor absorption bands in the longer wavelength region may allow for the application of visible semiconductor laser fluorimetry for the detection of lipids. It should also be noted that the use of a laser is not a requirement, especially for hematoporphyrin-stained lipids separated on conventional TLC plates. As suggested by the excellent LOD obtained for the visual detection of cholesterol and cholesteryl esters, fluorimetric excitation with a conventional light source at the Soret band should provide LODs that are not significantly higher than those reported in Table I for the detection and quantification of certain lipids.

REFERENCES

1 C. F. Poole and S. Khatib, in E. Katz (Editor). *Quantitative Analysis Using Chromatographic Techniques*, Wiley, Chichester, 1987.
2 J. Sherma and S. Bennett, *J. Liq. Chromatogr.*, 6 (1983) 1193.
3 J. A. Vinson and J. E. Hooyman, *J. Chromatogr.*, 135 (1977) 226.
4 R. J. Nicolosi, S. C. Smith and R. F. Santerre, *J. Chromatogr.*, 60 (1971) 111.
5 S. D. Fowler, in J. C. Touchstone (Editor), *Planar Chromatography in the Life Sciences*, Wiley, New York, 1990.
6 T. Kosaki, T. Ikeda, Y. Kotani, S. Nakagawa and T. Saka, *Mie Med. J.*, 7 (1957) 305.
7 L. L. Sulya and R. R. Smith, *Biochem. Biophys. Res. Commun.*, 2 (1960) 59.
8 J. P. Reyftmann, P. Morliere, S. Goldstein, R. Santus, L. Dubertret and D. Lagrange, *Photochem. Photobiol.*, 40 (1984) 721.
9 W. W. Christie, *Lipid Analysis*, Pergamon Press, Oxford, 1982.
10 L. Kovacs, J. Pick and J. Pucsok, *J. Planar Chromatogr.*, 2 (1989) 389.
11 M. R. Berman and R. N. Zare, *Anal. Chem.*, 47 (1975) 1200.
12 M. K. L. Bicking, in J. C. Touchstone and J. Sherma (Editors), *Techniques and Applications of Thin Layer Chromatography*, Wiley, New York, 1985.
13 C. W. Huie and W. R. Williams, *Anal. Chem.*, 61 (1989) 2288.
14 J. E. Falk, *Porphyrins and Metalloporphyrins*, Elsevier, New York, 1964.
15 S. D. Bowler, W. J. Brown, J. Warfel and P. Greenspen, *J. Lipid Res.*, 28 (1987) 1225.
16 B. G. Belenkii, E. S. Gankina, T. B. Adamovich, A. Ph. Zobazov, S. V. Necheav and M. G. Solonenko, *J. Chromatogr.*, 365 (1986) 315.
17 T. Imasaka and N. Ishibashi, *Anal Chem.*, 62 (1990) 363A.

Journal of Chromatography, 588 (1991) 303–305
Elsevier Science Publishers B.V., Amsterdam

CHROMSYMP. 2375

Quantitative planar chromatography of phospholipids with different fatty acid compositions☆

G. Lendrath

Department of Pharmacognosy, Hamburg University, Bundesstrasse 43, W-2000 Hamburg 13 (Germany)

A. Bonekamp

Lucas Meyer GmbH & Co., Ausschläger Elbdeich 62, W-2000 Hamburg 26 (Germany)

Lj. Kraus*

Department of Pharmacognosy, Hamburg University, Bundesstrasse 43, W-2000 Hamburg 13 (Germany)

(First received September 24th, 1990; revised manuscript received June 25th, 1991)

ABSTRACT

A method was developed for the determination of phospholipids irrespective of their origin.

INTRODUCTION

Lecithin is a mixture of different phospholipids including phospatidylcholine (PC), phosphatidylethanolamine (PE), phosphatidylinositol (PI) and phosphatidic acid (PA), and it is used as an emulsifier in a wide variety of food, in pharmaceuticals and in technical applications. The origin, soybean, rapeseed, sunflower and egg yolk, influences the fatty acid composition. Phospholipids have different fatty acid compositions in lecithin. The determination of individual phospholipids is commonly based either on spectrophotometric determination of fatty acids (high-performance liquid chromatography with UV detection at 206 nm [1]) or on densitometric determination {thin-layer chromatographic (TLC) separation and detection with lipid-specific reagents [2–8]}.Therefore, is it necessary to use phospholipid standards separated from the same origin. We report here a TLC method for the determination of phospholipids independent of their origin.

EXPERIMENTAL AND RESULTS

Fatty acid composition of phospholipids

We separated individual phospholipid standards (PC, PE, PI, PA) from different sources (soybean, rapeseed, sunflower, egg yolk) by using various chromatographic procedures (Table I). Based on the known fatty acid composition of individual phospholipids, it is possible to calculate their average molecular weights (Table II).

Detection of phospholipids

For our purpose we used the group-specific Dittmer–Lester reagent, which reacts only with the

☆ Presented at the *18th International Symposium on Chromatography, Amsterdam, September 23–28, 1990*. The majority of the papers presented at this symposium have been published in *J. Chromatogr.*, Vols. 552 and 553 (1991).

0021-9673/91/$03.50

TABLE I

FATTY ACID COMPOSITIONS OF PHOSPHOLIPIDS

Phospholipid class	Source	Fatty acid					
		16:0	18:0	18:1	18:2	18:3	Others
PC	Soybean	14.5	4.2	8.9	59.6	6.3	4.5
	Rapeseed	9.6	1.2	44.5	28.5	4.1	8.6
	Sunflower	11.1	3.7	12.3	63.3	5.5	3.5
	Egg	26.9	9.4	24.3	24.2	2.1	12.0
PE	Soybean	19.1	3.0	7.7	58.9	6.4	3.1
	Rapeseed	9.5	0.7	45.1	37.8	4.4	2.2
	Sunflower	13.3	3.4	9.2	71.2	0.3	2.5
PI	Soybean	32.7	5.7	5.6	47.0	6.8	1.9
	Rapeseed	17.2	1.6	37.7	35.1	5.6	2.7
	Sunflower	32.6	4.7	6.9	47.2	5.1	2.9
PA	Soybean	20.4	3.6	10.8	55.9	5.7	3.1
	Rapeseed	9.0	0.9	48.3	35.5	4.1	1.5
	Sunflower	12.3	3.8	10.3	67.8	0.9	4.7

phosphorus that is common to all phospholipids [9]. In order to be able to use the reagent as dip-in reagent and thus to enhance the quantitative evaluation, we added ethanol. Impregnation of the silica gel layer with phosphoric acid enhanced the separation of phospholipids. It also improved the stability of the chromogenic response with the Dittmer–Lester reagent [4,10].

We detected the same relative peak areas at 720 nm for phosphatidylcholines from soybean, rapeseed, sunflower and egg lecithin. Similar quantitative results were obtained for PE, PI and PA (Table III).

Quantitative analysis of lecithin samples

For the quantitative analysis of different lecithin samples, Merck silica gel high-performance TLC plates (5 × 5 cm) were impregnated with phosphoric acid. For the separation a Desaga H-chamber was used [11]. Detection was effected with modified Dittmer–Lester reagent, with measurement at 720 nm. Calibration was carried out by using either standards (weight ranges) from the same origin as the sample or from the other origins. The results are given in Table IV.

TABLE II

AVERAGE MOLECULAR WEIGHTS OF PHOSPHOLIPIDS

Phospholipid class	Source			
	Soybean	Rapeseed	Sunflower	Egg
PC	770	768	778	771
PE	724	735	736	
PI	834	850	843	
PA	687	691	695	

TABLE III

RELATIVE PEAK AREAS OF PHOSPHOLIPIDS (n = 20)

Phospholipid class	Source			
	Soybean	Rapeseed	Sunflower	Egg
PC	100	101.4	98.1	99.6
PE	100	97.0	97.7	–
PI	100	96.0	95.4	–
PA	100	104.0	101.5	–

CONCLUSIONS

Phospholipids have different fatty acid compositions according to their origin. For densitometric determination phospholipids the Dittmer–Lester reagent was selected, which reacts with the phosphate group that is component of all phospholipids. The signal obtained by this method for each class of

TABLE IV

PHOSPHOLIPID DETERMINATION IN LECITHIN SAMPLES: COMPARISON BETWEEN STANDARDS OF DIFFERENT ORIGIN (%)

Lecithins	Sample	Standard[a]												
		Soybean				Rapeseed				Sunflower				Egg
		PC	PE	PI	PA	PC	PE	PI	PA	PC	PE	PI	PA	PC
Soybean	a	12.6	10.8	7.4	7.1	11.8	11.5	8.6	6.4	12.9	11.2	7.3	5.7	13.1
		12.3	9.9	7.0	6.5	12.0	11.6	9.1	6.3	13.3	10.6	7.8	6.2	13.2
	b	12.5	11.7	8.6	6.1	13.5	11.9	9.5	6.6	13.8	11.1	8.9	5.9	13.2
		12.9	12.1	7.8	6.0	12.9	11.5	9.0	6.6	13.6	11.9	8.1	6.3	13.6
Rapeseed	c	8.7	4.9	6.9	6.9	9.3	5.1	7.7	5.6	10.1	5.1	8.3	8.5	8.5
		8.8	4.5	7.0	6.5	9.4	5.3	7.6	5.3	9.9	5.3	8.5	8.6	8.5
	d	7.7	5.2	6.6	8.3	7.4	5.2	7.6	7.4	8.5	5.0	7.8	8.8	8.1
		8.1	5.3	6.8	8.5	7.5	5.2	7.9	7.8	8.3	4.7	7.2	8.5	8.1
Sunflower	e	2.8	1.4	2.4	3.7	2.7	1.2	2.6	3.9	3.3	1.3	2.6	3.8	3.2
		2.8	1.4	2.6	3.9	2.8	1.2	2.7	3.9	3.5	1.2	2.5	3.8	3.1
	f	5.4	2.9	3.9	5.5	5.1	2.5	4.2	4.9	5.1	2.7	4.5	4.9	5.1
		5.3	3.0	3.9	5.4	5.2	2.6	4.4	5.1	5.3	2.9	4.4	4.9	5.2
Egg	g	39.8	–	–	–	42.8	–	–	–	40.6	–	–	–	38.3
		40.2	–	–	–	42.0	–	–	–	38.4	–	–	–	39.2
	h	41.0	–	–	–	39.6	–	–	–	41.9	–	–	–	41.0
		41.0	–	–	–	40.7	–	–	–	42.5	–	–	–	40.3

[a] Standards are from the same origin as the sample or from the other origins.

phospholipids is independent of the origin of the lecithin and of the fatty acid composition, because the same phospholipid classes of different origin have similar molecular weights. By application of this method it is possible to determine individual phospholipids using standards not obtained from the same origin as the samples.

REFERENCES

1 A. Nasner, *Dissertation*, Hamburg University, Hamburg, 1983.
2 A. Nasner and Lj. Kraus, *Dtsch. Apoth.-Ztg.*, 122 (1982) 2407–2415.
3 G. Klatt, A. Nasner and Lj. Kraus, *Planta Med.*, 5 (1986) 415–416.
4 G. Lendrath, *Dissertation*, Hamburg University, Hamburg, 1989.
5 J. Sherma and S. Bennet, *J. Liq. Chromatogr.*, 6 (1983) 1193–1211.
6 M. Goppelt and K. Resch, *Anal. Biochm.*, 140 (1984) 152–156.
7 J. C. Touchstone, S. S. Levin, M. F. Dobbins and P. C. Beers, *J. Liq. Chromatogr.*, 6 (1983) 179–192.
8 E. Hedegaard and B. Jensen, *J. Chromatogr.*, 225 (1981) 450–454.
9 J. C. Dittmer and R. L. Lester, *J. Lipid Res.*, 5 (1964) 126–127.
10 G. Lendrath, A. Nasner and Lj. Kraus, *J. Chromatogr.*, 502 (1990) 385–392.
11 Lj. Kraus, *Kleines Praktikumsbuch der Dünnschichtchromatographie*, Desaga, Heidelberg, 3rd ed., 1990.

Journal of Chromatography, 588 (1991) 307–313
Elsevier Science Publishers B.V., Amsterdam

CHROM. 23 584

Application of the iodine–azide reagent for selective detection of thiophosphoryl compounds in thin-layer chromatography☆

Zbigniew H. Kudzin*

Institute of Chemistry, University of Łódź, Łódź, Narutowicza 68, Łódź 90-136 (Poland)

Andrzej Kotyński

Institute of Chemistry, Faculty of Pharmacy, Medical Academy of Łódź, Narutowicza 120A, Łódź 90-151 (Poland)

Piotr Kiełbasiński

Centre of Molecular and Macromolecular Studies, Polish Academy of Sciences, Department of Organic Sulphur Compounds, Sienkiewicza 112, Łódź 90-363 (Poland)

(First received September 10th, 1990; revised manuscript received April 24th, 1991)

ABSTRACT

The application of the iodine–azide-induced reaction for the detection of thiophosphoryl compounds in thin-layer chromatographic systems is described. The detection limits of the derivatives tested were found to be at the nanomole level and depend on the nature of the $P(S)_n$ function, particularly on the degree of polarity of the P–S bond and the number of sulphur atoms in the molecule. A comparison of the iodine–azide test reaction with other procedures used for thiophosphoryl compounds is presented. A procedure for the differentiation of thiophosphoryl compounds and sulphur compounds based on the combined molybdate procedure preceded by a preoxidation stage is demonstrated.

INTRODUCTION

Organophosphorus compounds, especially those containing P–S bonds, are of significant industrial interest [1,2]. Many of these compounds exhibit strong biological activity (*e.g.*, organophosphorus plant protection agents) and for this reason their occurrence is of significant environmental concern [3,4]. Analytical methods for thiophosphoryl compounds are numerous, most being based on chromatography-related techniques [4,5]. In this field, thin-layer chromatography (TLC) combined with chemoselective detection has been considered as the method of choice, especially for non-volatile and thermally unstable organophosphorus derivatives [4–7]. Thus, phosphorothioates and phosphorodithioates were detected by TLC using silver nitrate solution alone [8] or in conjunction with chelating indicators (*e.g.*, bromocresol green) [8–11] and using copper(II) chloride solution and potassium hexacyanoferrate(III) solution [12] as subsequent spray reagents. Also, potassium iodoplatinate [4], palladium(II) chloride [4,13,14] and palladium(II) complexes with fluorescent indicators [*e.g.*, palladium(II)–calcein] [15] have been widely used for the detection of thiophosphoryl insecticides. Phosphi-

☆ Presented at the *14th International Symposium on the Organic Chemistry of Sulfur, Łódź, Poland, September 2–7, 1990.*

0021-9673/91/$03.50

nothioate complexes with metals were localized on TLC plates by means of a dithizone reagent [16,17].

The detection of thiophosphoryl compounds has also been achieved using 2,6-dibromobenzoquinone-4-chlorimine (DCQ) [18,19], an ammoniacal solution of 4-methyl umbelliferone preceded by bromine vapour treatment [19], fluorescein [20], ammonium molybdate reagent [12,21,22] and by potassium iodate solution [23] as spray reagents.

These compounds are visible in the UV region (254 nm) using fluorescent chromatoplates [24]. Phosphorothioates can be also monitored in eluates by means of conductivity or spectrophotometric detectors [25]. Several reports have described the use of the TLC–enzyme inhibition (TLC–EI) technique for the detection of a variety of organophosphorus compounds, including the P–S type [4,26–28].

However, most of the procedures cited above seem to employ general rather than specific detection reagents for thiophosphoryl compounds [4–7,12,21,22]. Considering this, the application of the iodine–azide reaction, selectively induced by the presence of sulphur-containing compounds, offers the opportunity for the differentiation of thiophosphoryl compounds from other organophosphorus derivatives. This reaction:

$$2\,N_3^- + I_2 \xrightarrow[\text{inductor}]{\text{P–S}} 3\,N_2 + 2\,I^- \qquad (1)$$

originally carried out by Raschig [29], has been explored extensively for decades in analytical chemistry [30–36], but there are only two reports on the chromatographic detection of phosphorothiono ester-based pesticides [32,36]. Recently we described the induction activity of P–S-containing compounds in the iodine–azide-induced reaction (eqn. 1) and its analytical applications [37]. As a continuation of this research, we present here results on the TLC detection of thiophosphoryl compounds using the iodine–azide spray reagent.

EXPERIMENTAL

Materials

All organophosphorus compounds were prepared according to ref. 38 and were all of the same purity as reported previously. Other reagents were prepared from chemicals purchases from Aldrich (Milwaukee, WI, USA).

Solutions and reagents

The concentrations of the compounds chromatographed were *ca.* $5 \cdot 10^{-2}$–$1 \cdot 10^{-3}$ *M* in anhydrous dioxane [or in methanol (**5b**, **6b**) or benzene (**12**)].

A 1 *M* aqueous solution of sodium azide and a 1 *M* solution of iodine (in a 1 *M* aqueous solution of potassium iodide) were employed.

Dragendorff reagent (Bi) contained 0.11 g of bismuth(III) nitrate pentahydrate and 0.88 g of potassium iodide in 100 ml of 16% aqueous acetic acid. DDQ reagent was a 2% solution of 2,6-dibromo-*p*-benzoquinone-4-chlorimine in benzene. Fluorescein reagent (Flc) was a 0.25% solution of sodium fluorescein in dimethylformamide. Ninhydrin (Ninh) was a 0.1% solution of ninhydrin in ethanol. Copper(II) hexacyanoferrate(III) reagent (CFCN) was applied as a 2% aqueous solution of copper(II) chloride, followed by a 0.5% aqueous solution of potassium hexacyanoferrate(III). Palladium reagent (Pd) was a 0.5% solution of palladium(II) chloride in *ca.* 0.2 *M* hydrochloric acid. Silver reagent (Ag) was a 1% aqueous solution of silver nitrate. Iodate reagent (KIO_3) was applied as a mixture of a 5% aqueous solution of potassium iodate (25 ml) and a 1% aqueous starch solution (2 ml); the plates were pretreated with 20% hydrochloric acid.

Molybdate reagent (Mo) was prepared by dissolving 1 g of ammonium molybdate in 40 ml of water, followed by 3 ml of concentrated hydrochloric acid and 5 ml of 70% perchloric acid, and diluted while cooling with 100 ml of acetone. Tin(II) chloride reagent (Sn) was prepared by heating 1 g of tin(II) chloride dihydrate in 10 ml of concentrated hydrochloric acid until dissolved, followed by dilution with 40 ml of water and 50 ml of acetone. Perchloric acid was a 20% solution in ethanol, nitric acid (fuming) was a 90% solution, aqueous bromine solution was a saturated solution of bromine in water and hydrogen peroxide was a 10% aqueous solution.

Thin-layer chromatography

Precoated silica gel 60 F_{254} aluminium sheets (10 cm × 5 cm) with a 0.2 mm thick layer (Merck, Darmstadt, Germany) were used for all TLC experiments. The plates were spotted with an appropriate amount of compound (deposition area *ca.* 0.2 cm^2), developed for a distance of 8 cm with acetone, air

dried and sprayed with a freshly prepared 1:1 mixture of sodium azide and iodine solutions. Thiophosphoryl compounds appeared due to the catalytic effect of the P–S bond as white spots on a yellow background, and were stable for more than 20 min.

TABLE I

DETECTION LIMITS OF THIOPHOSPHORYL COMPOUNDS WITH UV DETECTION (254 nm) AND USING IODINE (VAPOUR) AND THE IODINE–AZIDE SPRAY REAGENT

No.	Compound[a,b]	I_2[c] (μg)	UV (μg)	I_2–N_3[d]		R_F
				μg	nmol	
1a	$(EtO)_2PSH$	1	–[e]	5	32	0.72
1b	(EtO)(MenO)PSH	1	–[e]	5	19	0.75
2	$(EtO)_2(EtS)P$	1	–[e]	10	160	0.52
3	$(EtS)_3P$	3	30	30	140	0.63
4	Ph_2PSH	1	2	10	46	0.69
5a	$(EtO)_2P(S)OH$	1	–[e]	2	12	0.07
5b	$(EtO)_2P(S)ONa$	1	–[e]	2	10	0.08
6a	$(EtO)_2P(S)SH$	1	50	0.5	2.6	0.36
6b	$(EtO)_2P(S)SNa$	1	50	0.2	2.4	0.51
7	$(EtO)_2P(S)SMe$	10	50	–[e]		0.49
8	$(EtO)_3PS$	10	10	–[e]		0.72
9	$(EtS)_3PS$	1	3	50	200	0.62
10	$[(EtO)_2P(S)S]_2$	1	1	0.1	0.3	0.73
11	$(EtO)_2P(S)OP(O)(OEt)_2$	0.3	–[e]	10	33	0.67
12	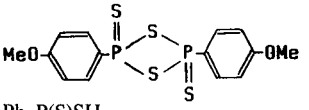	0.2	0.1	0.2	0.5	0.10; 0.50
13	$Ph_2P(S)SH$	0.2	1	0.1	0.4	0.74
14	$[Ph_2P(S)S]_2$	0.2	0.2	0.1	0.2	0.71
15	$Ph_2P(S)SMe$	1	1	10	38	0.70
16	*t*-Bu(Ph)P(S)OH	0.2	10	10[c]	47	0.22
17a	Me_3PS	0.3	–[e]	0.03	0.3	0.65
17b	Bu_3PS	0.3	–[e]	0.3	1.3	0.69
17c	Oct_3PS	0.3	–[e]	1	2.5	0.81
17d	Me_2PhPS	0.3	1	0.03	0.2	0.65
17e	$MePh_2PS$	0.3	1	0.3	1.3	0.65
17f	Ph_3PS	0.1	0.3	50[c]		0.69
18	$Ph_2(EtO)PS$	0.3	0.3	50[c]		0.71
19	$(Me_2N)_3PS$	1	1	10[c]	51	0.68
20b	$Ph(MeNH)_2PS$	0.3	0.3	0.5	2.5	0.68
20c	$Ph(PhNH)_2PS$	0.1	3.0	10	31	0.69
20d	$Ph(Me_2N)_2PS$	0.3	0.3	–[e]		0.70
21a	$Ph_2(NH_2)PS$	0.1	0.3	0.1	0.4	0.70
21b	$Ph_2(MeNH)PS$	0.3	0.3	0.5	2.2	0.69
21c	$Ph_2(PhNH)PS$			0.5	1.6	0.69
21d	$Ph_2(Me_2N)PS$	0.3	0.3	–[e]		0.70

[a] Bu = *n*-Butyl; *t*-Bu = *tert.*-butyl; Et = ethyl; Me = methyl; Men = menthyl; Oct = *n*-octyl; Ph = phenyl; Naphth = 2-naphthyl.
[b] Diethylphosphoric acid, diphenylphosphinic acid and triphenylphosphine oxide were undetectable using iodine–azide reagent.
[c] Brown spots.
[d] White spots.
[e] Undetectable at 50 μg per spot.

Detection of thiophosphoryl compounds by the preoxidation–molybdate procedure

The chromatographic plates were treated with the oxidation agent (described in Table II), allowed to react for 10 min, sprayed with perchloric acid and finally haeted in an oven to 180°C for 30 min. The plates were removed from the oven, cooled to room temperature, sprayed with the molybdate reagent and replaced in the oven for 5 min. After cooling, the plates were sprayed with tin(II) chloride solution. Phosphates and phosphonates (resulting from the corresponding P–S compounds) appeared as blue spots on a buff background (the background can be bleached by placing the plate in a tank containing an atmosphere of ammonia vapour).

RESULTS AND DISCUSSION

The results of the application of the iodine–azide reagent for the detection of various types of thio-

TABLE II

DETECTION OF SULPHUR COMPOUNDS AND THIOPHOSPHORYL COMPOUNDS BY MEANS OF THE IODINE–AZIDE, THE MOLYBDATE AND THE PREOXIDATION–MOLYBDATE PROCEDURES

− = Not detected; +− = spot is detectable; + = distinct detection; ++ = strong detection.

Compound[a]	Amount (μg per spot)	Detection procedure (reagent)				
		I_2–N_3	Mo[b]	(1) Br_2 (aq.), (2) Mo	(1) HNO_3, (2) Mo	(1) H_2O_2, (2) Mo
$HOCH_2CH_2SH$	1	+	+	−	−	−
	10	++	++	−	−	−
$HSC_6H_4CO_2H$-*m*	1	+	−	−	−	−
	10	++	++	+[c]	+−[c]	+−[c]
Naphth-SH	1	+	+	+[c]	+[c]	−
	10	++	++	+[c]	+[c]	+[c]
$S(CH_2CH_2OH)_2$	1	−	−			
	10	−	−			
PhSSPh	1	+	−	−	−	−
	10	+	−	+[c]	+[c]	+[c]
$PhNHC(=S)NH_2$	1	+	+	+[c]	+[c]	−
	10	++	++	+[c]	+[c]	+[c]
DMSO	1	−	−			
	10	−	−			
$(EtO)_2PSH$	1	−	+	−	−	−
	10	+	++	+[b]	+[b]	+[b]
$(EtO)_2P(S)ONa$	1	+−	+	+−[b]	+−[b]	+−[b]
	10	+	++	+[b]	+[b]	+[b]
$(EtO)_2P(S)SNa$	1	+	+	+[b]	+−[b]	+−[b]
	10	++	++	+[b]	+[b]	+[b]
$[(EtO)_2P(S)S]_2$	1	+	+	+[b]	+[b]	+[b]
	10	++	++	++[b]	++[b]	++[b]
t-Bu(Ph)P(S)OH	1	+	−	−	−	−
	10	+	+	+[b]	+[b]	+[b]
$PhP(S)(NHMe)_2$	1	+	−	−	−	−
	10	+	+	+[b]	+[b]	+[b]
$PhP(S)(NMe)_2$	1	−	−	−	−	−
	10	−	+	+[b]	+[b]	+[b]
$[Ph_2P(S)S]_2$	1	+	+	−	−	−
	10	++	+	+[b]	+[c]	+[c]

[a] Abbreviations as in Table I.
[b] Blue spots.
[c] Brown spots with or without molybdate spray.

phosphoryl compounds in comparison with their UV detection (254 nm) and using iodine are summarized in Table I.

It is evident that the detection limits of organophosphorus compounds, resulting from their own induction activity, are strongly dependent on their

TABLE III

COMPARISON OF REAGENTS FOR THE DETECTION OF THIOPHOSPHORYL COMPOUNDS BY TLC

− = Not detected; +− = spot is detectable; + = distinct detection; ++ = strong detection.

Compound	Amount (μg per spot)	Detection reagent								
		I_2–N_3[a]	Pd[c]	Ag[d]	CFCN[g]	Bi[h]	KIO_3[i]	DDQ[m]	Ninh[n]	Flc[q]
$(EtO)_2PSH$	3	+−	+	+	+−	−	−	+−[k]	−	−
	30	+	+	++	+	+	+[j]	+[k]	+[o]	+
Ph_2PSH	3	−	+	+	+	−	−	−	−	−
	30	+	+	+	+	+	+	+	+	+
$(EtO)_2(EtS)P$	3	−	+	+	−	−	−	−	−	−
	30	−	+	+	−	−	+	+[k]	−	−
$(EtS)_3P$	3	−	+	+	−	−	+	−	+[p]	−
	30	−	+	+	−	+	+	−	+[p]	+
$(EtO)_3PS$	3	−	+	+[f]	−	−	+[j]	−	−	−
	30	−	+	+[f]	−	−	+[j]	−	−	−
$(EtS)_3PS$	3	−	+	+	+	−	+	−	−	
	30	+[b]	++	+	+	+−	++	+−[l]	−	
$(EtO)_2P(S)SH$	3	+	+	−	+	−	−	+	+−[o]	
	30	+	+	+[f]	+	−	+[j]	+	+[o]	
$(EtO)_2P(S)SMe$	3	−	+	+−	−	−	−	−	−	−
	30	−	+	+	+	−	+[j]	−	−	−
$(EtO)_2P(S)OH$	3	+	+	−	−	−	−	−	+−[o]	−
	30	+	+	−	−	+	+[j]	+	+[o]	+
Ph_3PS	3	−	+	+[f]	−	+−	+	+[l]	−	−
	30	+[b]	+	+[f]	+[e]	+	++	+[l]	−	+−
Bu_3PS	3	+	+	+	+	+	+	+−	−	−
	30	+	++	+	++	+	+	+	−	+
$(Me_2N)_3PS$	3	−	+	−	+	+	+	+−	−	−
	30	+[b]	+	+[f]	+	++	+	+	−	+
$Ph_2P(S)SH$	3	+	+	+	−	+	+	+	−	−
	30	++	+	+	−	+	+	+	−	+
t-Bu(Ph)P(S)OH	3	−	+	+	−	+	−	−	−	−
	30	+	+	+	−	+	+	−	−	+

[a] White spots.
[b] Brown spots.
[c] Yellow-brown spots.
[d] Dark yellow-brown spots.
[e] After 0.5 h of exposure.
[f] After 1 h of exposure.
[g] Brown spots on grey-green background.
[h] Orange spots.
[i] Brown spots.
[j] Grey spots after saturation with ammonia vapour.
[k] Navy-blue spots after saturation with ammonia vapour.
[l] Lilac spots.
[m] Green spots.
[n] Spots appeared after preheating to *ca.* 80°C.
[o] Yellow spots.
[p] Pink spots.
[q] Lilac spots on yellow-green background.

structure and element contributions. Thus, organophosphorus compounds which do not contain a sulphur atom in the molecule exhibit no induction activity and are not detectable with the iodine–azide reagent (Table I). The activity of thiophosphoryl derivatives was found to be dependent on the nature of the $P(S)_n$ function. The results (Table I) reveal that the induction activity (resulting from this detection) of thiophosphoryl compounds is attributable more to the thiolate ($P-S^-$) function than to thiol ester (P–S–R) or thiono (P=S) functions. Thus, the lowest detection limits are exhibited by phosphorodithioates **6a** and **6b**, the disulphide **9** (0.3–5 nmol) and alkyl and aralkyl phosphines sulphides (**17a–e**) (0.2–2.5 nmol). Triphenylphosphine sulphide (**17f**) and diphenylethoxyphosphine sulphide (**18**) exhibit high detection limits (>100 nmol), presumably owing to the influence of their electronegative substituents on polarization of the P=S function. The detection of thioamides of organophosphorus acids was found to be dependent on the type of the amide moiety. Thus, primary (**21a**) and secondary thioamides (**20b**, **20c**, **21b**, **21c**) present show low to moderate detection limits (0.1–2.5 nmol) whereas tertiary thioamides (**20d** and **21d**) are inactive. Monothioacids **5a** and **16**, phosphorothioate **5b** and tetraethyl monothiopyrophosphate (**11**) exhibit moderate detection limits (10–30 nmol), whereas thiophosphate **8**, dithiophosphate **7** and perthiophosphate **9** exhibit very poor detection limits (>100 nmol). A similar trend is observed for thiophosphoryl derivatives of trivalent phosphorus. Thus, dialkyl thiophosphites **1a** and **1b** [$P(S)H \rightleftharpoons P-SH$] exhibit low detection limits (5 nmol) whereas triethyl thiophosphite (**2**) and triethyl trithiophosphites (**3**) exhibit high detection limits (>100 nmol). Hence the iodine–azide reagent allows the microdetection of aliphatic and mixed alkyl–aryl phosphine sulphides. The reagent also gives low detection limits of organophosphorus thioacids, their salts, partial esters and thioamides (primary and secondary) and disulphides, namely compounds with $P-S^-$ or P–S–S–P functions. The other compounds tested, bearing P=S or P–S–R functions, exhibit a poor to moderate detection limits and the application of the iodine–azide reagent requires their prior hydrolytic activation to the $P-S^-$ function. The reagent shows no activity towards phosphoric acid and its partial or full esters, alkanephosphonic acids, dialkylphosphinic acids and phosphine oxides.

It should be mentioned that the iodine–azide test reaction with thiophosphoryl derivatives is subject to interference from the presence of some sulphur compounds that do not contain phosphorus in the molecule. A similar interference problem also exists in the molybdate test, the most common test for phosphorus compounds [39,40]. Thus the application of the iodine–azide reagent or the molybdate reagent gives indiscriminately positive results for several thiophosphoryl and sulphur derivatives (Table II).

To overcome this lack of selectivity, we additionally developed a modified molybdate procedure based on the phosphoro–molybdate reaction but preceded by the oxidative elimination of potential sulphur reductants of molybdate (Table II). As a consequence, the combination of the iodine–azide test and the modified molybdate test permits the differentiation of thiophosphoryl and phosphoryl compounds and also phosphorus compounds from sulphur compounds.

The detection of various classes of thiophosphoryl compounds by means of the iodine–azide reagent and other representative spray reagents is presented in Table III.

ACKNOWLEDGEMENT

This project was partially supported by the Polish Academy of Science, grant CPBP 01.13.

REFERENCES

1 E. E. Reid, *Organic Chemistry of Bivalent Sulfur*, Vol. I, Chemical Rubber Publishing, New York, 1962.
2 K. A. Hassall, *The Chemistry of Pesticides*, Verlag Chemie, Weinheim, Deerfield Beach, Basle, 1982.
3 G. Zweig, *Analytical Methods for Pesticides, Plant Growth Regulators and Food Additives*, Vol. II, Academic Press, New York, 1964.
4 L. Fishbein, *Chromatography of Environmental Hazards*, Vol. III, Elsevier, Amsterdam, 1972.
5 F. Eisenberg (a), Y. Kiso, H. Kobayashi, Y. Kitaoka (b), N. Anaronson and Ch. Resnick (c), in M. Halmann (Editor), *Analytical Chemistry of Phosphorus Compounds*, Wiley-Interscience, New York, 1972, pp. 69–93 (a), pp. 93–151 (b) and pp. 793–831 (c).
6 K. G. Krebs, D. Heusser and H. Wimmer, in E. Stahl (Editor), *Thin-Layer Chromatography*, Springer, Berlin, Heidelberg, New York, 1969, p. 855.
7 H. Jork, W. Funk, W. Fischer and H. Wimmer, *Dünnschicht Chromatographie*, Band 1A, VCH, Weinheim, 1989, p. 342.

8 R. Klement and A. Wild, *Fresenius' Z. Anal. Chem.*, 195 (1963) 180.
9 M. E. Getz, *J. Assoc. Off. Agric. Chem.*, 45 (1962) 393.
10 M. F. Kovacs, Jr., *J. Assoc. Off. Anal. Chem.*, 47 (1964) 1097.
11 M. E. Getz and H. G. Wheeler, *J. Assoc. Off. Anal. Chem.*, 51 (1968) 1.
12 F. W. Plapp and J. E. Cassida, *Anal. Chem.*, 30 (1958) 1622.
13 R. Cox, *J. Chromatogr.*, 105 (1975) 57.
14 V. Trdlická and J. Mostecký, *J. Chromatogr.*, 130 (1977) 437.
15 T. F. Bildman, B. Nowlan and R. W. Frei, *Anal. Chim. Acta*, 60 (1972) 13.
16 R. A. C. Marschall, *J. Electroanal. Chem.*, 56 (1974) 313.
17 T. R. Timberbaev, V. V. Salov and O. H. Petrukhin, *Zh. Anal. Khim.*, 40 (1985) 61.
18 D. P. Braithwaite, *Nature (London)*, 200 (1963) 1011.
19 M. Ramasamy, *Analyst (London)*, 94 (1969) 1078.
20 R. T. Wang and S. S. Chou, *J. Chromatogr.*, 42 (1969) 416.
21 J. Asken, J. H. Ruzicka and B. B. Wheals, *Analyst (London)*, 94 (1969) 275.
22 A. Lamotte, A. Francina and J. C. Merlin, *J. Chromatogr.*, 44 (1969) 75.
23 V. B. Patil, S. V. Padalikar and G. B. Kawale, *Analyst (London)*, 112 (1987) 1765.
24 W. Steurbaut, W. Dejonckheere and R. H. Kips, *J. Chromatogr.*, 160 (1978) 37.
25 S. A. Bouyouces and D. R. Arkmentrout, *J. Chromatogr.*, 189 (1980) 61.
26 J. Schneider, *Nährung*, 30 (1986) 859.
27 M. A. Kusenko and M. V. Pismennaya, *Zh. Anal. Khim.*, 43 (1988) 354.
28 P. E. F. Zoun and T. S. Spierenburg, *J. Chromatogr.*, 462 (1989) 448.
29 F. Raschig, *Chem. Ztg.*, 32 (1908) 1203.
30 F. Feigl and E. Chargaff, *Fresenius' Z. Anal. Chem.*, 74 (1924) 376.
31 E. Chargaff, C. Levine and C. Green, *J. Biol. Chem.*, 175 (1948) 67.
32 R. Fischer and N. Otterbeck, *Sci. Pharm.*, 27 (1959) 1.
33 Z. Kurzawa, *Chem. Anal. (Warsaw)*, 5 (1960) 551.
34 B. Karska and L. Balcerkiewicz, *Chem. Anal. (Warsaw)*, 19 (1974) 421.
35 N. Kiba, T. Suto and M. Furusawa, *Talanta*, 28 (1981) 115 and 385.
36 T. Cserhati and F. Orsi, *Period. Polytech. (Budapest)*, 26 (1982) 111.
37 W. Ciesielski, W. Jędrzejewski, Z. H. Kudzin, P. Kiełbasiński and M. Mikołajczyk, *Analyst (London)*, 116 (1991) 85.
38 *Methoden der Organischen Chemie (Houben-Weyl)*, 4 Aufl., Vol. XIII, Georg Thieme, Stuttgart, 1963.
39 E. R. Cole and R. F. Bayfield, in A. Senning (Editor), *Sulphur in Organic and Inorganic Chemistry*, Vol. II, Marcel Dekker, New York, 1972, ch. 20.
40 F. Feigl and V. Anger, *Spot Tests in Inorganic Analysis*, Elsevier, Amsterdam, 1972; Russian edition, MIR, Moscow, 1976, Vol. 2, p. 178.

Journal of Chromatography, 588 (1991) 315–320
Elsevier Science Publishers B.V., Amsterdam

CHROM. 23 657

Optimization of resolution in capillary zone electrophoresis: combined effect of applied voltage and buffer concentration

Ibrahim Z. Atamna, Haleem J. Issaq, Gary M. Muschik and George M. Janini*

Program Resources, Inc./Dyncorp, NCI-Frederick Cancer Research and Development Center, P.O. Box B, Frederick, MD 21702-1201 (USA)

(First received April 4th, 1991; revised manuscript received June 11th, 1991)

ABSTRACT

Expressions are formulated for the prediction of solute migration time and resolution as a function applied voltage and buffer concentration in capillary zone electrophoresis. The resolution equation assumes that solute diffusion is the only operative zone-broadening mechanism. A resolution surface in applied voltage and buffer concentration space is presented featuring isochrones that are used to predict the behavior of resolution under constant analysis time. In the resolution–voltage planes the resolution increases continuously with increasing voltage. At the high-voltage border, the resolution decreases continuously with increasing concentration, however, at the low-voltage border the resolution passes through a shallow maximum as the buffer concentration is increased. At constant analysis time, resolution is optimized by simultaneously increasing the voltage and the buffer concentration. In comparison, this theoretical approach, which predicts resolution from solute migration times only, gives values that are consistently about 40–50% higher than experimentally determined resolution.

INTRODUCTION

Since its introduction in 1937 [1] electrophoresis has witnessed tremendous advances and a variety of methods and modes of operation were developed [2]. In particular, capillary zone electrophoresis (CZE) is now recognized as a highly efficient and sensitive microanalytical technique. It has rapidly developed since Jorgenson and Lukacs [3,4] realized the advantage of using small-diameter (< 100 μm) fused-silica columns. Although CZE is compared to liquid chromatography yet it has a completely different separation mechanism. Charged substances are resolved according to their differential migration in semiconducting buffers under the influence of an electric field gradient.

Resolution in CZE, as is the case in chromatography, is a function of three parameters: selectivity, column efficiency and migration time. Each of these parameters is influenced by many factors including applied voltage, buffer pH, type, concentration and ionic strength, modifiers, and inner capillary wall treatment. The pH is a dominant factor that could be manipulated to control resolution [5–7]. Surface modification of capillary walls by either masking or deactivating the surface silanol groups is another factor that greatly influences migration time and peak shape [8–11]. In previous studies from this laboratory we studied the role of applied voltage, buffer type and concentration in CZE [12–15]. The objective of this work is to investigate the effect of applied voltage and buffer concentration on resolution under ideal experimental conditions where the only operative solute zone-broadening mechanism is solute diffusion. An optimization procedure for the attainment of the best performance for a system by adjusting these two variables either independently or under isochronal (time normalization) conditions is presented. Isochronal methods have been developed and successfully used for the optimization of resolu-

tion in gas–liquid chromatography [16] and high-performance liquid chromatography [17,18]. This work represents an effort on our part to extend the utility of this procedure to CZE.

THEORETICAL

The resolution (R_s) of two close-lying zones in an electropherogram is given by [19]:

$$R_s = \frac{1}{4}(N)^{\frac{1}{2}}\frac{\Delta v}{\bar{v}} \tag{1}$$

where N is the number of theoretical plates and $\Delta v/\bar{v}$ is the relative migration velocity difference of the two zones. The migration time (t_m), which is directly measured from the electropherogram, is related to the migration velocity (v) by the following equation:

$$v = \frac{l}{t_m} \tag{2}$$

where l is the column length from injector to detector. The number of theoretical plates is given by [19]

$$N = \frac{L^2}{\sigma^2} \tag{3}$$

where L is the column length and σ^2 is the zone variance. If longitudinal diffusion is the only source of zone broadening, which seems to be the case under conditions where Joule's heating effects are minimized, then zone variance is given by the Einstein equation [19]:

$$\sigma^2 = 2Dt_m \tag{4}$$

where D is solute diffusion coefficient. Substituting eqn. 4 in eqn. 3 yields an expression for N in terms of experimental electrophoretic parameters and solute intrinsic diffusion.

$$N = \frac{L^2}{2Dt_m} \tag{5}$$

It is to be noted that L^2 should be substituted by $L \cdot l$ if the total column length and the injector-to-detector length are not identical. If the relation expressed in eqn. 5 as well as the fact that $\Delta v/\bar{v} \simeq \Delta t/t_2$ for two close-lying zones are taken into consideration then the resolution equation could be rewritten as:

$$R = \left(\frac{L^2}{32D}\right)^{\frac{1}{2}}\frac{1}{\sqrt{t_{m,2}}}\frac{\Delta t}{t_{m,2}} \tag{6}$$

where Δt is the migration time difference of the two zones and $t_{m,2}$ is the migration time of the slower-migrating solute. Note that this resolution equation neglects some experimental parameters which, if present, can adversely affect column performance such as sample injection artifacts, Joule's heating effects and possible solute adsorption onto the capillary wall.

In a previous communication from this laboratory [15] we have demonstrated that, under ideal electrophoretic conditions (*i.e.* the Joule's heat generated inside the column is efficiently dissipated), both the electrophoretic and electroosmotic mobilities are directly proportional to the applied voltage and inversely proportional to the square root of concentration. Accordingly the following relations are obeyed.

(i) At constant applied voltage (V)

$$t_m = a + b\sqrt{C} \tag{7}$$

where a and b are constants.

(ii) At constant buffer concentration (C)

$$\frac{l}{t_m V} = m + nV \tag{8}$$

where m and n are constants. The excellent linearity of the plots presented in Figs. 2–4 testify to the validity of these relationships.

In this work we attempt to formulate an expression for migration time as a function of applied voltage and buffer concentration, $t_m(C,V)$, as follows: a and b of eqn. 7 are each fitted to a second-degree polynomial in V:

$$a = a_0 + a_1V + a_2V^2 \tag{9a}$$

$$b = b_0 + b_1V + b_2V^2 \tag{9b}$$

Similarly m and n of eqn. 8 are fitted to a polynomial in C:

$$m = m_0 + m_1C + m_2C^2 \tag{10a}$$

$$n = n_0 + n_1C + n_2C^2 \tag{10b}$$

By substituting for a and b in eqn. 7 and for m and

n in eqn. 8 and solving for t_m the following expression is obtained:

$$t_m(C,V) = \left[\frac{a_0 + a_1V + a_2V^2 + b_0\sqrt{C} + b_1V\sqrt{C} + b_2V^2\sqrt{C}}{m_0V + m_1CV + m_2C^2V + n_0V^2 + n_1CV^2 + n_2C^2V^2}\right]^{\frac{1}{2}} \quad (11)$$

Finally, utilizing eqn. 11, the expression for resolution (eqn. 6) could be rewritten as:

$$R_s(C,V) = \left(\frac{L^2}{32D}\right)^{\frac{1}{2}} \frac{\Delta t_m(C,V)}{[t_{m,2}(C,V)]^{\frac{3}{2}}} \quad (12)$$

where $\Delta t_m(C,V) = t_{m,2}(C,V) - t_{m,1}(C,V)$.

EXPERIMENTAL

A Beckman CZE System 2000 (Model P/ACE) equipped with a UV detector, an automatic injector, a column cartridge (50 cm × 75 μm I.D., surrounded by coolant), an autosampler and a printer was used in this study. All experiments were carried out at 25°C and were run at least in triplicates to insure reproducibility. Injections were made using the pressure mode for 1 s each. The acetate buffer solutions were degassed and filtered through 0.2-μm Nylon 66 filters. All experiments were conducted at pH 5.0. Solute standards were prepared to be about 10 μg/ml and were monitored at 254 nm with the highest instrument sensitivity setting. Water was distilled and deionized. Dansyl leucine and dansyl methionine were purchased from Sigma (St. Louis, MO, USA), sodium acetate and acetic acid were purchased from Johson Matthey Alpha Products (Danvers, MA, USA) and mesityl oxide was obtained from Aldrich (Milwaukee, WI, USA). All solutes were dissolved in the eluent buffer.

The migration times for the solutes dansyl leucine and dansyl methionine and for the marker mesityl oxide were measured at four different applied voltages (10–25 kV) using water and five different buffer concentrations (10–50 mM).

RESULTS AND DISCUSSION

Table I lists the migration times for the probe solutes used in this study at different applied voltages in water and acetate buffers. Each data point is an average of at least three readings with a standard deviation of ±1%. Fig. 1 shows plots of the data collected at 20 kV according to eqn. 7. All plots were linear with correlation coefficients in excess of 0.995. It is important to note that if the data are plotted as t_m *vs.* C or t_m *vs.* log C the plots will be linear only if the data point for pure water is excluded. Even then the correlation coefficients are not as good as reported for Fig. 1. It is more important to note that these plots will not extrapolate to a single point at infinite buffer dilution as is the case in Fig. 1. The data for dansyl methionine were plotted according to eqn. 7 (Fig. 2) and eqn. 8 (Fig. 3). The values of a and b obtained from plots of t_m *vs.* $C^{1/2}$ at different voltages were fitted to a polynomial in V according

TABLE I

SOLUTE MIGRATION TIMES AT DIFFERENT APPLIED VOLTAGES IN WATER AND ACETATE BUFFERS

All measurements except pure water were conducted at pH = 5.0.

Applied voltage (kV)	Buffer concentration (mM)	Migration time[a] (min)		
		Mesityl oxide	Dansyl leucine	Dansyl methionine
10	0	3.21	3.21	3.21
15	0	1.99	1.99	1.99
20	0	1.49	1.49	1.49
25	0	1.28	1.28	1.28
10	10	6.52	9.75	9.90
15	10	4.20	6.22	6.32
20	10	3.21	4.27	4.34
25	10	2.55	3.36	3.42
10	20	8.54	11.89	12.08
15	20	5.43	7.46	7.58
20	20	3.88	5.29	5.36
25	20	3.01	4.09	4.15
10	30	9.65	13.99	14.29
15	30	6.02	8.77	8.95
20	30	4.08	5.89	6.01
25	30	3.17	4.51	4.60
10	40	10.71	15.83	16.19
15	40	6.69	9.77	9.98
20	40	4.67	6.74	6.86
25	40	3.45	4.93	5.01
10	50	11.47	17.36	17.80
15	50	7.05	10.53	10.76
20	50	4.92	7.26	7.41
25	50	3.60	5.24	5.34

[a] Migration times ± 1.0%.

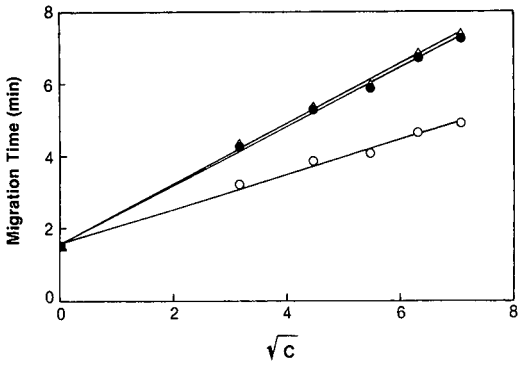

Fig. 1. Migration time as a function of the square root of buffer concentration. Buffer: acetate at pH 5.0; field strength: 400 V/cm; column: 50 cm × 75 μm I.D. fused silica; instrument: Beckman Model P/ACE System 2000. ○ = Mesityl oxide; ● = dansyl leucine; △ = dansyl methionine.

to eqns. 9a and 9b. Similarly the values of m and n obtained from plots of $1000/tV$ *vs.* V at different concentrations were fitted to a polynomial in C according to eqns. 10a and 10b. The coefficients thus obtained are reported in Table II. By substituting the values of the parameters for the appropriate solutes from Table II in eqns. 11 and 12 one could calculate the migration times and the resolution at any applied voltage and buffer concentration. In order to validate the fitting procedure described above the migration times for leucine and methionine were calculated according to eqn. 11. The results agreed with the experimental data reported in Table I to within ±2%.

It is important to emphasize that this treatment is based on the assumption that solute molecular diffusion is the only band-broadening mechanism in CZE. In practice many experimental parameters such as sample introduction [20], distortion of the flat flow profile by capillary walls [21], solute concentration, column length and diameter [5] and Joule's heating [22,23] can adversely affect column efficiency. Nevertheless, it is instructive to look at column efficiency and resolution based on this assumption since it is believed that all of these disruptive factors could be experimentally minimized or perhaps eliminated.

The resolution as a function of applied voltage and buffer concentration $R_s(C,V)$ is given by eqn. 12. Unlike chromatographic techniques where better resolution is achieved at the expense of longer analysis time, eqn. 12 suggests that resolution in CZE is not necessarily compromised if the analysis time is shortened. This appears to be in apparent contradiction with the Jorgenson and Lukacs [3] conclusion that resolution improves with increase in analysis time; however, it is to be noted that in their analysis they compared different columns with different electroosmotic properties while our analysis is based on using the same column and keeping all experimental parameters except applied voltage and buffer concentration constant.

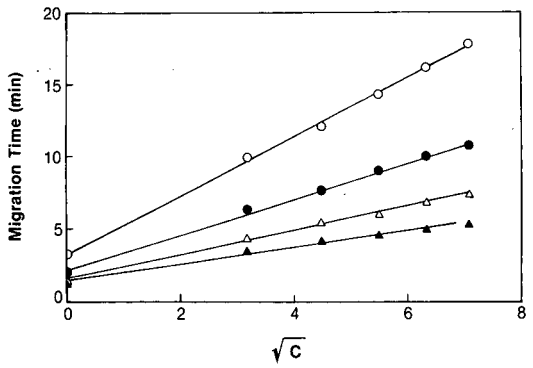

Fig. 2. Migration time for dansyl methionine *versus* square root of buffer concentration at different constant applied voltages. Experimental conditions as in Fig. 1. ○ = 10 kV; ● = 15 kV; △ = 20 kV; ▲ = 25 kV.

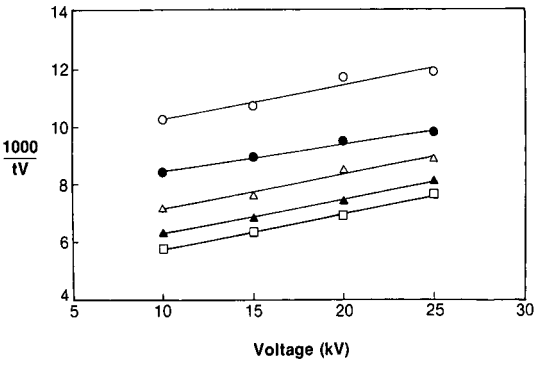

Fig. 3. Migration time for dansyl methionine as a function of applied voltage at different buffer concentrations. Experimental conditions as in Fig. 1. ○ = 10 mM; ● = 20 mM; △ = 30 mM; ▲ = 40 mM; □ = 50 mM.

TABLE II

VALUES OF THE COEFFICIENTS OF EQNS. 9 AND 10

Solute	a_0	a_1	a_2 ($\times 10^3$)	b_0	b_1	b_2 ($\times 10^3$)	m_0 ($\times 10^3$)	m_1 ($\times 10^3$)	m_2 ($\times 10^4$)	n_0 ($\times 10^4$)	n_1 ($\times 10^5$)	n_2 ($\times 10^5$)
Leucine	6.716	−0.456	9.680	4.246	−0.279	5.280	10.998	−0.217	0.017	0.744	0.156	−0.001
Methionine	6.662	−0.452	9.590	4.387	−0.289	5.480	10.917	−0.220	0.018	0.705	0.183	−0.001

The effect of applied voltage on resolution was investigated by several groups [5,6,24–27]. By all accounts experimentally determined resolution improves with increasing voltage, up to a certain point beyond which the voltage is so high as to contribute to zone broadening by Joule's heating effect. The effect of buffer concentration is not as dramatic as that of applied voltage [15,25,27]; however, it has been reported that resolution slightly increases with increasing buffer concentration [15,27].

In this work R_s values for dansyl methionine/dansyl alanine were calculated according to eqn. 12 given that the length of column used is 50 cm and assuming a value of $1 \cdot 10^{-5}$ cm^2 s^{-1} for the solute diffusion coefficient. The resolution was, then, plotted as a function of C and V resulting in the resolution surface shown in Fig. 4. Isochrons (*i.e.* lines of constant analysis time) were also calculated and plotted in Fig. 4 (dark lines). These lines are used

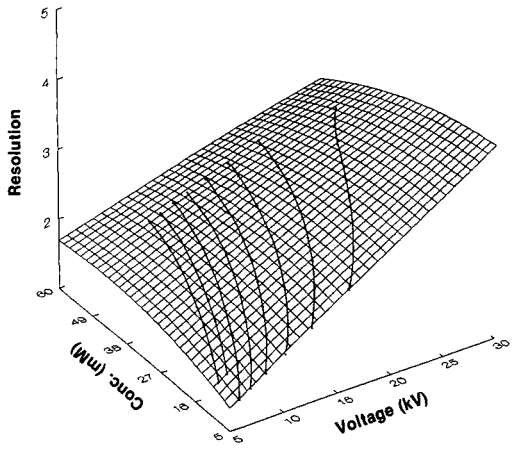

Fig. 4. Calculated resolution surface for dansyl methionine/dansyl leucine in applied voltage and buffer concentration space. The dark non-grid lines on the surface are isochrons, from 300 s (lower border) to 1000 s (higher border) in increments of 100 s.

for the prediction of the behavior of the resolution under constant analysis time. The R_s–V plane in this figure is featureless since R_s continuously increase with increase in V at all concentrations. With regards to buffer concentration effects the following observations are noted. At the high-voltage border, R_s decreases continuously with increasing concentration; however, at the low-voltage border R_s passes through a shallow maximum as the concentration is increased. For example, at 10 kV, R_s is maximum at $C = 35$ mM, while at 15 kV the maximum R_s value is at $C = 20$ mM. This behavior is mainly due to the fact that $\Delta T(C,V)$ is small at high voltages and only marginally increases with increasing concentration, while at low voltages ΔT is large and shows a relatively larger increase with increasing concentration. The isochronal lines show that at constant analysis time resolution is optimized by simultaneously increasing the voltage and the buffer concentration. A slight increase in voltage necessitates a large increase in buffer concentration in order to achieve higher resolution under isochronal conditions.

Finally, in order to compare this theoretical prediction of R_s with experimental determination we measured R_s from migration times and peak widths at half-height, and examined the trends in R_s as V and C are changed. It is observed that: (a) the experimental R_s values are consistently about 40–50% lower than the theoretical calculation, indicating that zone-broadening mechanisms other than solute diffusion are also operative in the experimental set-up used in this study; (b) R_s increases with increasing V in agreement with theory, however, R_s levels off at the high-voltage border; and (c) R_s increases with increasing buffer concentration in agreement with the theoretical prediction at the low-voltage border.

ACKNOWLEDGEMENTS

The help of W. Gregory Alvord with the statistical analysis is appreciated.

This project has been funded at least in part with Federal funds from the Department of Health and Human Services under Contract NO1-CO-74102. The content of this publication does not necessarily reflect the views or policies of the Department of Health and Human Services, nor does mention of trade names, commercial products or organizations imply endorsement by the U.S. Government.

REFERENCES

1 A. Tiselius, *Trans. Faraday. Soc.*, 33 (1937) 524.
2 D. Rickwood and B. D. Hames (Editors), *Gel Electrophoresis of Nucleic Acids: A Practical Approach*, IRL Press, Washington, DC, 1983.
3 J. W. Jorgenson and K. D. Lukacs, *Anal. Chem.*, 53 (1981) 1298.
4 J. W. Jorgenson and K. D. Lukacs, *J. Chromatogr.*, 218 (1981) 209.
5 K. D. Lukacs and J. W. Jorgenson, *J. High Resolut. Chromatogr. Chromatogr. Commun.*, 8 (1985) 407.
6 G. J. M. Bruin, J. P. Chang, R. H. Kuhlman, K. Zegers, J. C. Kraak and H. J. Poppe, *J. Chromatogr.*, 471 (1989) 429.
7 W. J. Lambert and D. L. Middleton, *Anal. Chem.*, 62 (1990) 1585.
8 S. Hjerten, *J. Chromatogr.*, 347 (1985) 191.
9 M. M. Bushey and J. W. Jorgenson, *J. Chromatogr.*, 480 (1989) 301.
10 R. M. McCormick, *Anal. Chem.*, 60 (1988) 2322.
11 J. K. Towns and F. E. Regnier, *J. Chromatogr.*, 516 (1999) 69.
12 H. J. Issaq, I. Z. Atamna, C. J. Metral and G. M. Muschik, *J. Liq. Chromatogr.*, 13 (1990) 1247.
13 I. Z. Atamna, C. J. Metral, G. M. Muschik and H. J. Issaq, *J. Liq. Chromatogr.*, 13 (1990) 2517.
14 I. Z. Atamna, C. J. Metral, G. M. Muschik and H. J. Issaq, *J. Liq. Chromatogr.*, 13 (1990) 3201.
15 H. J. Issaq, I. Z. Atamna, G. M. Muschik and G. M. Janini, *Chromatographia*, submitted for publication.
16 E. Grushka and G. Guiochon, *J. Chromatogr. Sci.*, 10 (1972) 649.
17 I. Atamna and E. Grushka, *J. Chromatogr.*, 355 (1986) 41.
18 E. Grushka and I. Atamna, *J. Chromatogr.*, 400 (1987) 5.
19 J. C. Giddings, *Sep. Sci.*, 4 (1969) 181.
20 E. Grushka and R. M. McCormick, *J. Chromatogr.*, 471 (1989) 421.
21 M. Martin and G. Guiochon, *Anal. Chem.*, 56 (1984) 614.
22 J. H. Knox and I. H. Grant, *Chromatographia*, 24 (1987) 135.
23 E. Grushka, R. M. McCormick and J. Kirkland, *Anal. Chem.*, 61 (1989) 241.
24 T. Tsuda, K. Nomura and G. Nakagawa, *J. Chromatogr.*, 264 (1983) 385.
25 K. D. Altria and C. F. Simpson, *Chromatographia*, 24 (1987) 527.
26 P. D. Grossman and D. S. Soane, *Anal. Chem.*, 62 (1990) 1593.
27 H. T. Rasmussen and H. M. McNair, *J. Chromatogr.*, 516 (1990) 223.

Journal of Chromatography, 588 (1991) 321–326
Elsevier Science Publishers B.V., Amsterdam

CHROM. 23 625

Quantitative aspects of indirect UV detection in capillary zone electrophoresis

M. W. F. Nielen

AKZO Research Laboratories Arnhem, Corporate Research, Analytical Chemistry Department, P.O. Box 9300, 6800 SB Arnhem (Netherlands)

(First received April 29th, 1991; revised manuscript received July 5th, 1991)

ABSTRACT

Quantitative aspects of indirect UV absorbance detection in capillary zone electrophoresis were studied using the separation of sodium alkylsulphate surfactants as a model system. Nearly uniform response factors, excellent reproducibility of electrophoretic mobilities and linearity of the detection signal can be obtained when veronal buffer is used as the UV-absorbing background electrolyte. The feasibility of the system for the analysis of commercial mixtures of primary sodium alkyl sulphates is demonstrated.

INTRODUCTION

Capillary zone electrophoresis (CZE) offers rapid and efficient separations of ionic and ionizable compounds [1]. One of the major weak points in CZE is the lack of a sensitive and universal detection system. Indirect detection modes [2] might be a relatively simple solution to the detection of both organic and inorganic compounds without a suitable chromophore.

Several indirect detection approaches have been described, including indirect UV absorbance [3–5], indirect fluorescence [6–8] and indirect amperometric [9] detection.

Despite the impressive detection limits obtained and the interesting applications shown, the applicability of indirect detection in CZE in quantitative analysis might be questioned. Foret *et al.* [4] discussed the selection of a suitable UV-absorbing background electrolyte and the relationship with electromigration dispersion. They concluded that the highest sensitivity is obtained for those analytes having an effective electrophoretic mobility close to the mobility of the absorbing background ion. However, for a given background ion, the useful dynamic range of this detection mode was reduced to approximately one order of magnitude for analytes with mobilities deviating from the mobility of the background ion.

A second drawback for quantitative analysis using the (universal) indirect detection mode follows from the Kohlrausch theory [10]. The change in concentration of the absorbing background ion, d[B], caused by an analyte concentration [A] can be calculated using the following equation:

$$d[B] = -\frac{\mu(B)\{\mu(A) + \mu(C)\}}{\mu(A)\{\mu(B) + \mu(C)\}} \cdot [A]$$

where the μ terms are the effective electrophoretic mobility of the analyte (A), the UV-absorbing background ion (B) and the counter ion (C). Consequently, one-to-one displacement will only occur for analytes having the same mobility as the background ion. Other analytes will have different response factors, which have to be calculated from accurately determined mobility data.

An additional disadvantage of indirect detection systems is their poor stability. Owing to the low concentrations of the background electrolyte usually applied, electroosmosis is very sensitive towards

0021-9673/91/$03.50

impurities, pH shifts, etc. Baseline problems and irreproducible mobilities might be observed [5].

In this work, we used indirect UV absorbance detection with veronal buffer as a background electrolyte. The CZE separation of aliphatic anionic surfactants was used as a model system, in order to study quantitative aspects such as the dependence of the response factor on the mobilities of the analytes, the reproducibility of the electrophoretic mobilities and the coefficient of electroosmotic flow, and the linear dynamic range. The feasibility of the analysis of commercial mixtures of primary sodium alkyl sulphates is demonstrated.

EXPERIMENTAL

Apparatus

An Applied Biosystems (San Jose, CA, USA) Model 270A capillary electrophoresis system [11] was used, equipped with a variable-wavelength UV absorbance detector, operated at 240 nm and a 0.2 s rise time. CZE was performed in a 70 cm × 50 μm I.D. fused-silica capillary (Applied Biosystems) at +25 kV (constant-voltage mode), thus yielding a current of 2–6 μA, depending on the buffer concentration used. The capillary was thermostated at 30.0°C. Samples were introduced into the capillary via a controlled vacuum system; the injection time was 0.5 s, which corresponds to a volume of *ca.* 1.5 nl.

The coefficient of electroosmotic flow was calculated using the migration time of the system peak. The effective electrophoretic mobilities and the plate numbers were calculated using the equations in ref. 12. Data were recorded using a Nelson Analytical Model 4400 integration system.

Chemicals

Ultrex-grade water was obtained from J. T. Baker (Deventer, Netherlands). Veronal (5,5-diethylbarbituric acid) buffer, Teepol HB7 and sodium octanesulphonate (further referred to as C_8) were obtained from Sigma (St. Louis, MO, USA). Sodium *n*-dodecyl sulphate (C_{12}), sodium decyl hydrogensulphate (C_{10}) and sodium nonyl hydrogensulphate (C_9) were obtained from Merck (Darmstadt, Germany). Technical-grade sodium chloroethylsulphonate (C_2) was obtained from laboratory stock.

Methods

The UV-absorbing veronal buffers were prepared in water, yielding either 6 or 12 m*M* solutions having a pH value of 8.6. Buffers were filtered through 0.45-μm Spartan 30/B membrane filters (Schleicher & Schüll, Dassel, Germany) prior to use. A stock solution of the C_2–C_{12} analytes, $2 \cdot 10^{-3}$ *M* each (except C_2, *ca.* $4 \cdot 10^{-3}$ *M*) was prepared in water. Sample solutions were prepared by dilution of the stock solution with the veronal buffer.

RESULTS AND DISCUSSION

Performance of the separation and detection limit

The performance of the CZE system using indirect UV absorbance detection is clearly shown in Fig. 1. All components of the test mixture (10^{-4} *M* of each C_8–C_{12} surfactant and *ca.* $2 \cdot 10^{-4}$ *M* of C_2) were baseline resolved, even those differing by only one CH_2 group. The efficiencies of the C_8–C_{12} peaks were 360 000–440 000 theoretical plates in the 12 m*M* and 350 000–390 000 in the 6 m*M* veronal system. The lower plate numbers in the latter situation and also the lower plate number for C_2 (*cf.*, Tables I and II) have to be attributed to electromigration dispersion caused by the less favourable analyte-to-buffer concentration ratio (60 *versus* 120).

The dynamic reserve, as determined for the 6 m*M* veronal system, was calculated to be 1100, yielding a theoretical detection limit of *ca.* $1 \cdot 10^{-5}$ *M* or

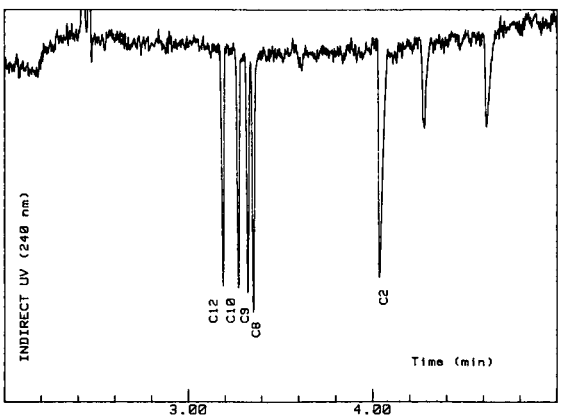

Fig. 1. CZE separation of a mixture of C_2–C_{12} alkyl sulphates using 12 m*M* veronal buffer at pH 8.6. For other conditions, see Experimental.

TABLE I

REPEATABILITY OF MOBILITIES AND DETECTION SIGNAL

Mean values of six analyses ± relative standard deviation (R.S.D.). μ(eo) = 0.849 · 10^{-3} cm^2 V^{-1} s^{-1} ± 0.14% R.S.D. Conditions: 12 m*M* veronal buffer (pH 8.6); other conditions as under Experimental.

Component	μ(ep) (10^{-3} cm^2 V^{-1} s^{-1})	Peak height (μV)	Area/time (μV)	Plate number
C_{12}	−0.2172 ± 0.15%	117 ± 2.2%	4.59 ± 3.0%	360 000
C_{10}	−0.2352 ± 0.15%	112 ± 2.9%	4.46 ± 3.1%	380 000
C_9	−0.2458 ± 0.15%	108 ± 4.8%	4.24 ± 4.4%	395 000
C_8	−0.2520 ± 0.15%	114 ± 4.4%	4.55 ± 3.9%	440 000
C_2	−0.3569 ± 0.14%	128 ± 2.6%	6.85 ± 4.3%	230 000

15 fmol (signal-to-noise ratio 2). The detection limits obtained experimentally [(1–2) · 10^{-5} *M*] were in good agreement with this value.

Repeatability of the mobilities and the detection

The repeatability of the system was evaluated for both 12 and 6 m*M* veronal buffers. The test mixture (10^{-4} *M* each, except C_2, *ca.* 2 · 10^{-4} *M*) was analysed six times and the coefficient of electroosmotic flow, μ(eo), the electrophoretic mobilities, μ(ep), the peak heights and the peak areas were determined.

Contrary to ref. 8, the peak areas were corrected for the different velocities of the zones in the detection window by dividing their values by the corresponding migration times [3]. The calculated mean values and standard deviations are presented in Table I (12 m*M* buffer) and Table II (6 m*M* buffer).

It can be concluded from Tables I and II that the mobilities are very constant. Obviously, a buffering UV-absorbing background ion is very beneficial, even at concentrations as low as 6 m*M*. Both peak heights and corrected peak areas can be used for precise quantification. The detector signal decreased by a factor of *ca.* 1.5 (instead of 2) on changing from 6 to 12 m*M* buffer. This discrepancy can be explained when the corresponding UV background levels are taken into account; 0.11 absorbance for 6 m*M* and 0.20 absorbance for 12 m*M* veronal at 240 nm. According to Foret *et al.* [4], it can be calculated that the linearity of Beer's law is limited in CZE to *ca.* 0.1 absorbance. From this point of view, a background electrolyte of 6 m*M* veronal will be the practical upper limit at 240 nm.

An impression of the reproducibility was obtained by the analysis of a freshly prepared C_9–C_{12} mixture using a 12 m*M* veronal CZE system, re-assembled 1 year later. The coefficient of electroosmotic flow, μ(eo), was 0.810 · 10^{-3} cm^2 V^{-1} s^{-1}, only 5% less than the value given in Table I. The electrophoretic mobilities of C_{12}, C_{10} and C_9 were calculated to be −0.221 · 10^{-3}, −0.239 · 10^{-3} and −0.250 · 10^{-3} cm^2 V^{-1} s^{-1}, respectively; only 2% less than

TABLE II

REPEATABILITY OF MOBILITIES AND DETECTION SIGNAL

Conditions: 6 m*M* veronal buffer (pH 8.6); other conditions and explanation as in Table I.

Component	μ(ep) (10^{-3} cm^2 V^{-1} s^{-1})	Peak height (μV)	Area/time (μV)	Plate number
C_{12}	−0.2203 ± 0.17%	150 ± 3.3%	6.20 ± 3.4%	365 000
C_{10}	−0.2382 ± 0.14%	151 ± 3.0%	6.01 ± 3.9%	350 000
C_9	−0.2488 ± 0.16%	145 ± 2.7%	5.73 ± 3.3%	395 000
C_8	−0.2550 ± 0.13%	159 ± 1.8%	6.07 ± 3.0%	370 000
C_2	−0.3678 ± 0.08%	151 ± 1.7%	9.10 ± 2.2%	175 000

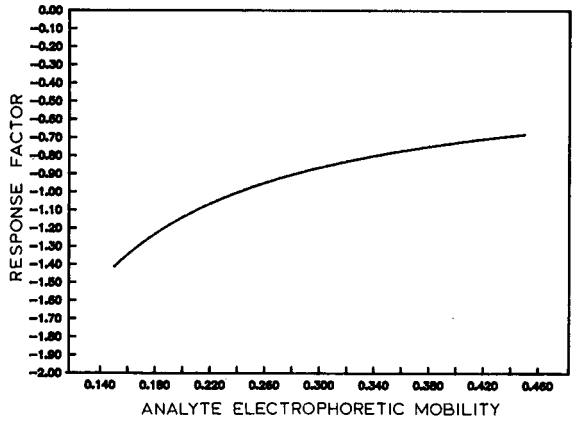

Fig. 2. Theoretical dependence of the response factor of an individual analyte on its electrophoretic mobility. The mobilities of the background ion and the counter ion are assumed to be $-0.241 \cdot 10^{-3}$ and $0.528 \cdot 10^{-3}$ cm^2 V^{-1} s^{-1}, respectively.

the values in Table I. The corresponding area/time data were found to be 5–10% less than the data presented in Table I.

Response factors

The effective electrophoretic mobility of veronal was determined using 12 m*M* borate buffer and found to be $-0.241 \cdot 10^{-3}$ cm^2 V^{-1} s^{-1}. The electrophoretic mobility of the counter ion, sodium, was taken from the literature ($0.528 \cdot 10^{-3}$). Assuming that these mobility data are applicable to the CZE veronal system, and using the equation presented in the Introduction, a theoretical curve showing the dependence of the individual response factor of an analyte on its corresponding electrophoretic mobility can be derived (Fig. 2).

From Fig. 2, it can be seen that this dependence is very moderate for analytes differing only slightly in mobility. The C_8–C_{12} surfactants would show a difference in response factor of less than 10%. Consequently, one can conclude that indirect UV detection of homologues, such as alkyl sulphates, might yield nearly uniform response factors, provided that the effective electrophoretic mobility of the veronal ion is carefully adjusted using the pH value.

The experimental data presented in Table I show a significantly higher peak height and area/time for C_{12} than for C_9 and C_2 (after correction for the two-fold higher concentration of C_2) and are in good agreement with the theoretical differences in the response factors, as shown by Fig. 2. The other data (except for C_8, which showed too high response factors throughout this study, possibly owing to a concentration error) show the same theoretical trend but more data will be required to support the significance of these differences statistically. The peak-height data for C_9, C_{10}, C_{12} and C_2 in Table II show significantly lower response factors than C_8. This discrepancy must be attributed to electromigration dispersion of the former components (the ratio of the concentrations of the background ion and the analytes is only 60 in Table II). Note that this discrepancy also implies that the electrophoretic mobility of C_8 must be very close to the effective electrophoretic mobility of veronal, *i.e.*, the mobility of veronal in the present CZE system will be *ca.* $-0.255 \cdot 10^{-3}$ instead of $-0.241 \cdot 10^{-3}$ cm^2 V^{-1} s^{-1} (which value had been determined in a borate CZE system; see above).

The area/time data in Table II show again for C_{12} a significantly higher response than for C_9 and C_2: C_{12} shows an 8% higher area/time than C_9 (8–9% predicted by Fig. 2); the area/time of C_2 is 79% relative to C_9 (80–81% is predicted by Fig. 2). As in Table I, the other data (except for C_8) showed the same theoretical trend, but the differences were statistically too small to be significant.

Linearity of the detector response

The linearity of the detection of the C_8–C_{12} surfactants was studied using a 6 m*M* veronal buffer and sample concentrations of 0, $2 \cdot 10^{-5}$, $6 \cdot 10^{-5}$, $2 \cdot 10^{-4}$, $6 \cdot 10^{-4}$ and $2 \cdot 10^{-3}$ *M*. Each analysis was carried out in duplicate.

The data for C_8, C_9 and C_{10} at $2 \cdot 10^{-3}$ *M* and for C_8 and C_9 at $2 \cdot 10^{-4}$ *M*, representing partially overlapping asymmetric peaks, could not be integrated reliably with our integration software and the corresponding area/time data were therefore rejected from the data sets.

Curve fitting of the mean peak heights yielded a second-order equation owing to eletromigration dispersion (overloading) at higher concentrations. Interestingly, curve fitting of the mean area/time data yielded straight lines, regression data for which are shown in Table III. The slopes for C_{12} and C_{10} are higher, which supports the theory about the response factors. However, correlations of the slopes

TABLE III

CURVE FITTING OF THE MEAN AREA/TIME DATA

Concentrations ranging from 0 up to $2 \cdot 10^{-3}$ *M*. For other conditions, see text.

Component	Slope	Intercept	Regression (r^2)
C_{12}	0.63	+0.53	1.000
C_{10}	0.64	−0.01	0.999
C_9	0.54	+0.15	1.000
C_8	0.57	+0.12	1.000

with the theoretical response factors are risky because of the curve fitting data, which are based on duplicate measurements only (contrary to the repeatability data above and the associated discussion about response factors), and the impact of the lower accuracy of the data points at concentrations near the detection limit on the regression analysis.

Application

As an application, we analysed a commercial sample of C_9–C_{13} primary sodium alkyl sulphates. The Teepol HB7 sample was diluted 5000-fold with veronal buffer and analysed using the 6 m*M* veronal system. The electropherogram thus obtained is shown in Fig. 3. The relative content of each surfactant in the sample was calculated using both peak-height and area/time data, and using both assumed uniform response factors and the real response factors, as calculated with the theoretical equation. The results are presented in Table IV. It can be concluded that the use of uniform response factors yields only small errors (less than 1% absolute). The area/time data will be less influenced by electromigration dispersion and are to be preferred.

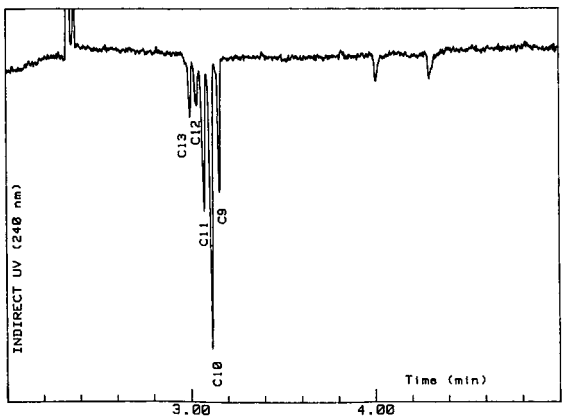

Fig. 3. CZE separation of primary sodium alkyl sulphates in Teepol using 6 m*M* veronal buffer at pH 8.6. For other conditions, see Experimental.

TABLE IV

RELATIVE COMPOSITION OF A COMMERCIAL SAMPLE

Conditions: 6 m*M* veronal CZE system; sample, Teepol HB7; calculation with either assumed uniform response factors or after correction for the theoretical factors.

Component	Relative content (%) based on			
	Peak height		Area/time	
	Uncorrected	Corrected	Uncorrected	Corrected
C_{13}	9.1	8.4	8.6	8.0
C_{12}	7.2	6.9	6.1	5.8
C_{11}	22.2	21.8	23.7	23.3
C_{10}	42.1	42.7	44.2	44.9
C_9	19.4	20.1	17.2	17.9

CONCLUSIONS

CZE with indirect UV absorbance detection can provide constant mobility data provided that a UV-absorbing ion is selected with buffering capability under the pH conditions used. Veronal buffer was found to fulfil this requirement. Quantitative analysis with nearly uniform response factors can be achieved for a series of homologues, *e.g.*, sodium alkyl sulphates, provided that the effective electrophoretic mobility of veronal is carefully adjusted. The linear dynamic range of indirect UV detection in CZE covers more than two orders of magnitude, as long as area/time data are considered. The veronal system can be successfully applied to the determination of the relative composition of technical mixtures of aliphatic anionic surfactants.

REFERENCES

1 J. Jorgenson and K. D. Lukacs, *Anal. Chem.*, 53 (1981) 1298.
2 E. S. Yeung and W. G. Kuhr, *Anal. Chem.*, 63 (1991) 275A.

3 S. Hjerten, K. Elenbring, F. Kilar, J.-L. Liao, A. J. C. Chen, C. J. Siebert and M. D. Zhu, *J. Chromatogr.*, 403 (1987) 47.
4 F. Foret, S. Fanali, L. Ossicini and P. Bocek, *J. Chromatogr.*, 470 (1989) 299.
5 G. J. Bruin, A. C. van Asten, J. C. Kraak and H. Poppe, presented at the *3rd International Symposium on High-Performance Capillary Electrophoresis, San Diego, CA, February 3–6, 1991*, poster PM57.
6 W. G. Kuhr and E. S. Yeung, *Anal. Chem.*, 60 (1988) 1832.
7 W. G. Kuhr and E. S. Yeung, *Anal. Chem.*, 60 (1988) 2642.
8 L. Gross and E. S. Yeung, *J. Chromatogr.*, 480 (1989) 169.
9 T. M. Olefirowicz and A. G. Ewing, *J. Chromatogr.*, 499 (1990) 713.
10 F. Kohlrausch, *Ann. Phys. (Leipzig)*, 62 (1987) 208.
11 S. E. Moring, J. C. Colburn, P. D. Grossman and H. H. Lauer, *LC · GC Int.*, 3 (1990) 46.
12 M. W. F. Nielen, *J. Chromatogr.*, 542 (1991) 173.

Journal of Chromatography, 588 (1991) 327–333
Elsevier Science Publishers B.V., Amsterdam

CHROM. 23 655

High-performance capillary zone electrophoresis of carbohydrates in the presence of alkaline earth metal ions

Susumu Honda*

Faculty of Pharmaceutical Sciences and Pharmaceutical Research and Technology Institute, Kinki University, 3-4-1 Kowakae, Higashi-osaka (Japan)

Keiko Yamamoto, Shigeo Suzuki, Minako Ueda and Kazuaki Kakehi

Faculty of Pharmaceutical Sciences, Kinki University, 3-4-1 Kowakae, Higashi-osaka (Japan)

(First received June 12th, 1991; revised manuscript received July 26th, 1991)

ABSTRACT

1-Phenyl-3-methyl-5-pyrazolone (PMP) derivatives of reducing carbohyrates were analyzed by capillary zone electrophoresis with on-tube ultraviolet detection, by using a capillary tube of fused silica and carriers containing alkaline earth metal salts. The direction (from cathode to anode) of electro-osmotic flow was the reverse of that observed for ordinary carriers not containing such metal salts, and the PMP derivatives of isomeric aldopentoses were completely separated from each other by the interaction with these metal ions. The order of mobility for the derivatives of aldopentose isomers was different from that observed in borate buffer, suggesting formation of different types of complexes. Examples of the application of this method to other monosaccharides and several oligosaccharides are also presented. It was demonstrated that this method allows quantification of reducing carbohydrates with high accuracy and high reproducibility.

INTRODUCTION

High-performance capillary electrophoresis (HPCE) is one of the epoch-making methodologies in separation science, and has been gaining in popularity for the analysis of biological substances. Application to carbohydrates, however, has the following two problems. First, carbohydrates lack functional groups which give signals in the detection system. Secondly, they have no electric charge, and hence cannot be separated by plain zone electrophoreis mode in the intact state. Micellar electrokinetic chromatography, another separation mode of HPCE, also does not allow separation of carbohydrates, since they are too hydrophilic to be solubilized in ionic surfactants as additives.

One of the solutions to the first problem is the introduction of chromophores or fluorophores by pre-column derivatization, such as condensation with 1-phenyl-3-methyl-5-pyrazolone [1], reductive pyridylamination [2] or reductive amination followed by coupling to 3-(4-carboxybenzoyl)-2-quinolinecarboxaldehyde [3].

The second problem was partly solved by *in situ* conversion to ionic derivatives such as borate complexes [4,5]. In this case carbohydrate derivatives introduced into a capillary tube filled with borate buffer were almost instantaneously converted to anionic borate complexes, which were separated by means of the differences in their electric charge and molecular size, as well as by the differences in the ease of complexation of the complexes formed. This principle of *in situ* conversion to ionic species permits analysis of neutral molecules by zone electrophoresis. In this paper we describe another attempt to analyze carbohydrates by utilizing interaction with metal ions.

0021-9673/91/$03.50

EXPERIMENTAL

Chemicals

1-Phenyl-3-methyl-5-pyrazolone (PMP) was purchased from Kishida (Osaka, Japan) and used without further purification. This reagent is also available from Aldrich (Milwaukee, WI, USA) under the name 3-methyl-1-phenyl-2-pyrazolin-5-one. Other reagents and carbohydrates samples were of the highest grade commercially available.

Pre-column derivatization of reducing carbohydrates with PMP

This was done according to our published procedure [1]. In short a 0.5 *M* methanolic solution (50 μl) of PMP and 0.3 *M* sodium hydroxide (50 μl) were added to a reducing carbohydrate (100 nmol) or a mixture of reducing carbohydrates (100 nmol each), and the mixture was maintained at 70°C for 30 min with occasional swirling. The reaction mixture was cooled to room temperature, 0.3 *M* hydrochloric acid (50 μl) was added for neutralization, and the whole was evaporated to dryness. The residue was dissolved in water (200 μl) and the solution was extracted with chloroform (200 μl). The aqueous layer was analyzed by HPCE.

Apparatus for HPCE

A laboratory-made apparatus was used, which was constructed from a high-voltage power supply from Yamabishi Electric (Tokyo, Japan), a Σ 873 UV spectrometer from Irika Instruments (Kyoto, Japan), initially designed for high-performance liquid chromatography but slightly modified for HPCE, and a Chromatopak RC-6A data processor from Shimadzu (Kyoto, Japan). The greater part of the UV beam of the spectrometer was cut off by setting a narrow slit (50 μm × 500 μm) in the center of the beam. A capillary tube of fused silica (50 μm I.D.) was obtained from Polymicro Technologies (Phoenix, AZ, USA). A small portion of the polyimide coating was removed by burning at 15 cm from one end of the tube, and the transparent portion was glued to the slit. Sample solutions were introduced into the tube by gravity flow by raising one end of the tube 10 cm higher than the level of the opposite electrode solution for 10 s. The PMP derivatives of reducing carbohydrates were monitored by measuring UV absorption at 245 nm.

RESULTS AND DISCUSSION

Reducing carbohydrates react with excess PMP to give bis-PMP derivatives, which strongly absorb UV light at 245 nm [1]. When they are introduced into the anodic end of a capillary tube of fused silica filled with 100 m*M* sodium acetate and a high voltage is applied, they migrate to the cathodic end by the combined effects of electrophoresis and electro-osmosis. Electro-osmotic flow drives them to the cathode at a uniform velocity regardless of carbohydrate species, because the inner wall of the capillary tube is negatively charged under these conditions. Electrophoresis pulls them back to the anode, because they are negatively charged, presumably as a result of dissociation of the enolic hydroxyl group (s). Under these conditions the PMP derivatives of isomeric aldopentoses have the same electric charge and molecular size. Therefore, they were held back at the same velocity without separation, as shown in Fig. 1.

The PMP derivatives of aldopentoses (pentose-PMPs) were migrated at the same velocity, giving a single peak at 9.3 min. The peak at 10.0 min is due to the remaining reagent which was not extracted with chloroform. An aqueous 100 m*M* solution of potassium acetate as well as a 100 m*M* solution of ammonium acetate, used as carrier, gave similar electropherograms.

The carrier was changed to an aqueous 20 m*M* solution of calcium acetate and the tube was allowed to stand for 2 h. Introduction of a mixture of PMP derivatives of some monosaccharides from the anodic end, followed by application of a high voltage, gave an electropherogram as shown in Fig. 2a, in which the PMP derivatives of these monosaccharides were well separated from each other.

The separation was presumably due to interaction, possibly complexation, of these derivatives with the calcium ion in the carrier. However, there was a tendency for migration time to become longer as time elapsed after changing carrier. The tube was rinsed with 20 m*M* calcium acetate for 0.3 h and allowed to stand for a further 6.7 h. Analysis of the same sample gave only the peak of mesityl oxide (an internal neutral marker) in 60 min (Fig. 2b). Repeated analysis after a further 0.3-h rinse and 4.7 h standing finally gave no peaks in 60 min (Fig. 2c). Nevertheless, introduction of this sample from the

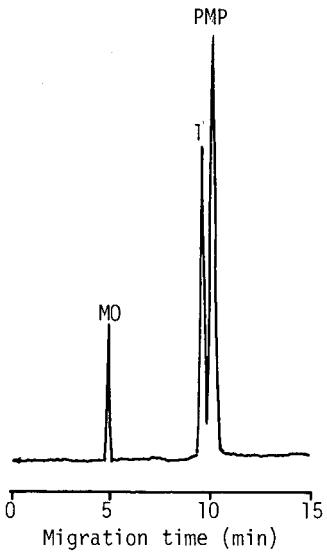

Fig. 1. Analysis of a mixture of pentose-PMPs in 100 m*M* sodium acetate. Capillary, fused silica (49 cm × 50 μm I.D.); applied voltage, 10 kV; detection, UV absorption at 245 nm. An aqueous solution was introduced from the anodic end of the tube. Peaks: MO = mesityl oxide (internal neutral marker); PMP = 1-phenyl-3-methyl-5-pyrazolone (reagent); 1 = pentose-PMPs ($1 \cdot 10^{-3}$ *M* each).

cathodic end gave rise to peaks of the monosaccharide derivatives in *ca.* 10 min, fairly well separated from each other (Fig. 2d). The remaining reagent and mesityl oxide gave peaks before and after, respectively, this group of peaks.

This series of experiments suggests that the velocity of electro-osmotic flow gradually reduced to zero, then the direction was reversed and the velocity continued to increase to a maximal value. Use of higher concentrations of calcium acetate facilitated such a change of electro-osmotic flow; continuous rinsing with 100 m*M* calcium acetate allowed rapid reversal of direction to give a steady-state flow in the opposite direction in only 2 h. Incidentally the original state was restored by continuous rinsing of the tube with the original carrier. The reversal of the direction of electro-osmotic flow is phenomenon similar to that observed when quaternary ammonium salts are added to carrier [6], and is considered to be the result of localization of the divalent metal ions on the surface of capillary inner wall by binding to the silanol group.

Fig. 3a shows complete separation of pentose-PMPs, achieved by introducing the sample solution from the cathodic end after equilibration of the inner wall of the tube with 100 m*M* calcium acetate. The reproducibility of migration time was high (*e.g.*

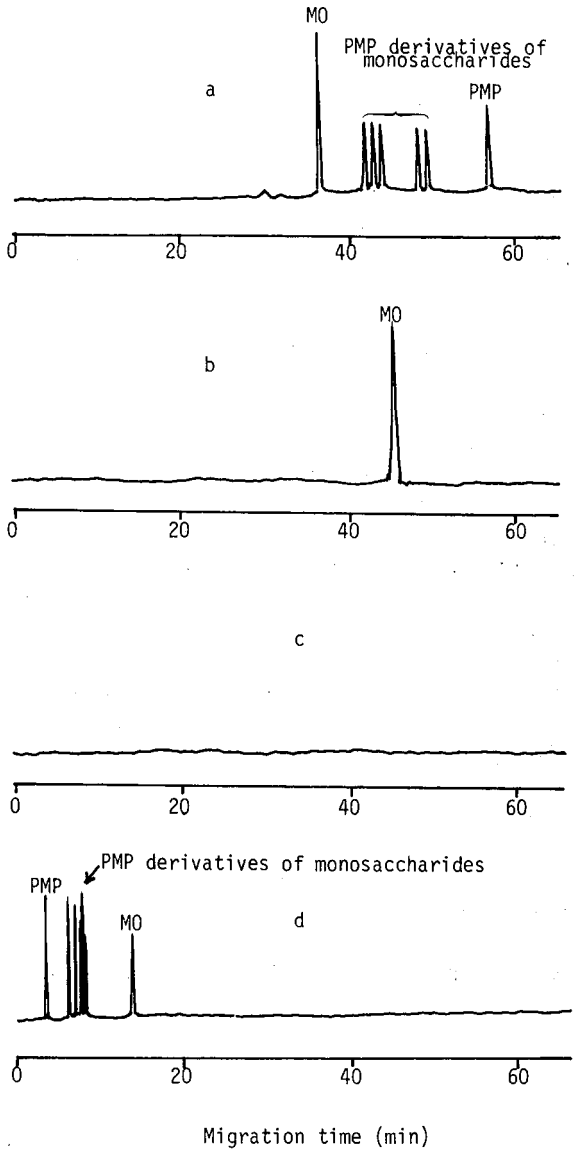

Fig. 2. Change in the electropherogram of the analysis of PMP derivatives of several monosaccharides with time after changing the carrier from 100 m*M* sodium acetate to 20 m*M* calcium acetate. (a) 2 h, (b) 7 h, (c) 12 h and (d) 13 h after the change of carrier. For details see the text. Sample, a mixture of PMP derivatives of arabinose, ribose, galactose, glucose and mannose ($1 \cdot 10^{-3}$ *M* each). An aqueous sample solution was introduced from the anodic (a–c) or cathodic (d) end of the tube. Other analytical conditions and abbreviations as in Fig. 1.

the relative standard deviation of the xylose-PMP peak was 1.5% for $n = 8$) under such equilibrated conditions.

The good separation of the peaks of pentose-PMPs is presumably because of complexation with the calcium ion. Since complexation naturally gives rise to positive charge around the calcium nucleus of the complexes, it causes a reduction in total negativity. As a result the migration velocities of the complexes (from cathode to anode) are lower than that of the reagent. The difference in the ease of complexation is at least a cause of difference in apparent electrophoretic mobility, which leads to separation of peaks.

The reversal of the direction of electro-osmotic flow and good separation of the peaks of pentose-PMPs were also observed with carriers containing other kinds of alkaline earth metal salts. Fig. 3b and c shows the electropherograms of pentose-PMPs in aqueous 100 m*M* solutions of barium acetate and strontium acetate. The barium salt-containing carrier gave sharper peaks and better separation of pentose-PMPs than the calcium salt-containing carrier. The strontium salt-containing carrier also gave good separation, but migration times were rather longer. A magnesium salt-containing carrier showed a tendency to tailing, and separation was rather worse, possibly because of weaker binding (Fig. 4).

The variation in the migration times of these metal salts is the result of variations in the velocities of electro-osmotic flow caused by the difference in the positivity of the capillary inner wall. The variation in peak resolution is mainly attributable to the ease of complexation based on the difference in electronegativity and valence angle among metal nuclei.

Table I lists the difference between apparent mobility of each pentose-PMP and that of PMP ($\Delta\mu_{ep}$), since it compares the effects of metal salts on sugar moieties.

The order of $\Delta\mu_{ep}$ values in divalent metal salt-containing carriers (ribose-PMP, lyxose-PMP, arabinose-PMP, xylose-PMP) is the same for all these metal salts, but is different from that in borate buffer (ref. 5, xylose-PMP, arabinose-PMP, ribose-PMP, lyxose-PMP). This discordance is obviously due to the difference in the mode of interaction. Since the present mode of separation is comparable to ligand exchange in liquid chromatography (*e.g* ref. 7), a mixture of pentose-PMPs was applied to a column of Shodex Sugar SP-0810, a sulfonated styrene–divinylbenzene copolymer, in the calcium form. However, elution with 100 m*M* calcium acetate gave no peaks because of strong retention on the column. Therefore, direct comparison of the present mode with ligand exchange was unsuccessful. Further discussion of this problem will be published elsewhere based on additional data.

The foregoing results indicate that aqueous solutions of the acetates of some divalent metals, especially barium, give excellent separation of pentose-PMPs. Therefore, other combinations of monosaccharides were analyzed as PMP derivatives in barium salt-containing carrier. Fig. 5 shows an example obtained for a mixture of five reducing monosaccharides (galactose, mannose, fucose, N-acetylgalactosamine and N-acetylglucosamine), ubiquitously found in animal glycoproteins.

Mannose gave a single peak with the shortest migration time (5.51 min), but the N-acetylgalactosamine–N-acetylglucosamine and gallactose–fucose couples were not separated from each other, giving

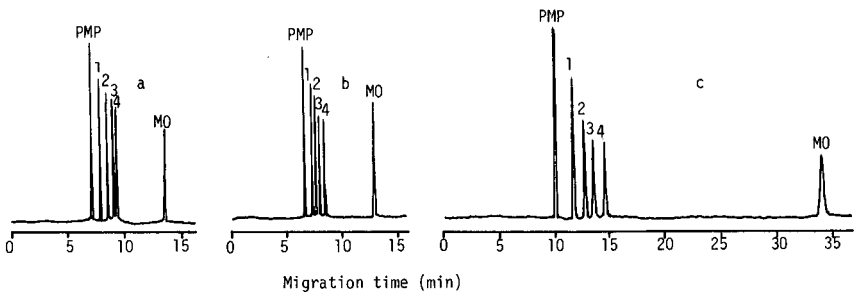

Fig. 3. Separation of pentose-PMPs in aqueous 100 m*M* solutions of calcium acetate (a), barium acetate (b) and strontium acetate (c). Capillary, fused silica (53 cm × 50 μm I.D.). An aqueous sample solution was introduced from the cathodic end of the tube. Other analytical conditions and abbreviations as in Fig. 1. Peaks: 1 = ribose-PMP; 2 = lyxose-PMP; 3 = arabinose-PMP; 4 = xylose-PMP.

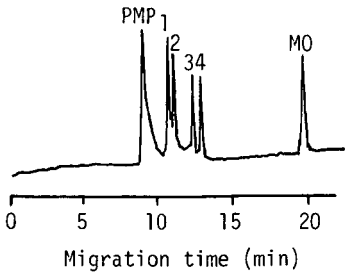

Fig. 4. Separation of pentose-PMPs in 100 m*M* magnesium acetate. Other analytical conditions, abbreviations and peak assignment as in Fig. 3.

superimposed peaks at 5.75 and 5.84 min, respectively.

Fig. 6 shows an electropherogram of partially hydrolyzed dextran containing isomaltooligosaccharides having various values of degree of polymerization (d.p.), analyzed under the same conditions as those used for the component monosaccharides of glycoproteins.

It is observed that these homologous series of oligosaccharides were separated from each other up to d.p. 9, but the separation was not so good as that in borate buffer (ref. 5, separable up to d.p. 13).

Fig. 7 shows an example of disaccharide analysis obtained under the same conditions. Maltose was separated from other disaccharides, but the cellobiose–melibiose and gentiobiose–lactose couples failed to be separated. Thus, the barium salt-containing carrier was unfavorable for differentiation of the 1,4-β-glucose–glucose and 1,6-β-galactose–glucose pair as well as the 1,6-β-glucose–glucose and 1,4-β-galactose–glucose pair.

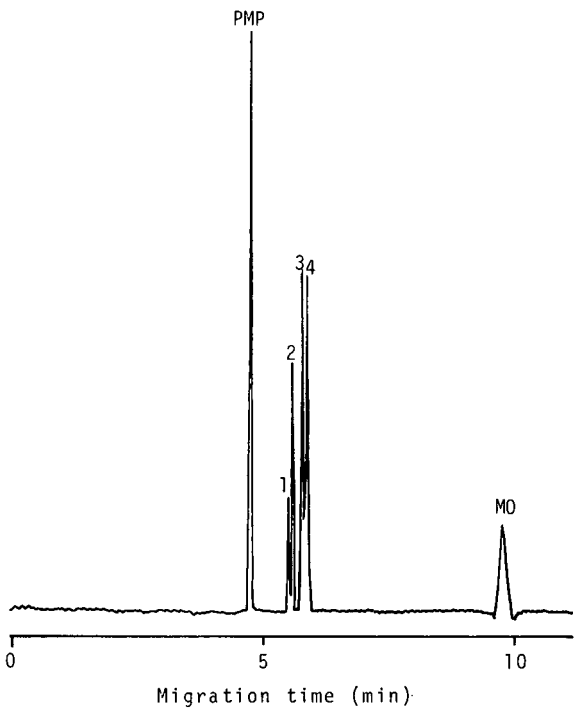

Fig. 5. Separation of the PMP derivatives of the component monosaccharides commonly found in glycoproteins. Capillary, fused silica (49 cm × 50 μm I.D.). Other analytical conditions as in Fig. 3d. Peaks: 1 = rhamnose (internal standard); 2 = mannose; 3 = N-acetylgalactosamine + N-acetylglucosamine; 4 = galactose + fucose.

Determination of reducing carbohydrates by this method was promising. In this case a reducing car-

TABLE I

μ_{ep} VALUES OF PENTOSE-PMPs

Ion in carrier[a]	$\Delta\mu_{ep}$[b] (× 10^{-2}, $cm^2\ min^{-1}\ V^{-1}$)			
	Ribose-PMP	Lyxose-PMP	Arabinose-PMP	Xylose-PMP
Ca^{2+}	3.0	4.9	6.2	6.7
Ba^{2+}	2.6	3.4	4.3	5.5
Sr^{2+}	3.3	4.8	5.5	6.9
Mg^{2+}	3.4	3.9	5.9	6.5
BO_2^-	2.9	3.5	2.2	1.7

[a] The concentration of ions were commonly 100 m*F*.

[b] $\Delta\mu_{ep}$ is the difference between the apparent mobility of pentose-PMP and that of PMP.

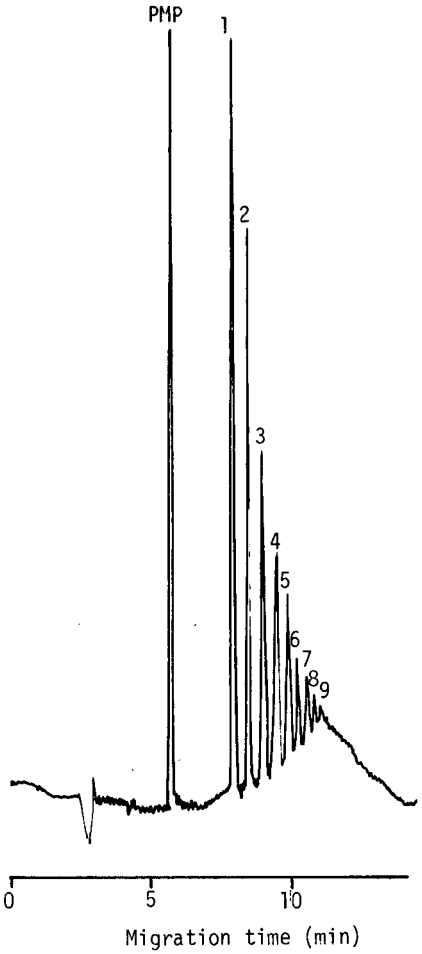

Fig. 6. Separation of the PMP derivatives of isomaltooligosaccharides. Analytical conditions and abbreviations as in Fig. 5. The peak numbers correspond d.p.s.

bohydrate or a mixture of reducing carbohydrates was derivatized with PMP in a similar manner as that described in the Experimental section, and derivatives were analyzed in divalent metal salt-containing carriers. Calibration curves showed excellent linearity over wide ranges of sample amount and they passed through the origin. For example, linearity was observed for galactose and glucose at least in the range 10–200 nmol (injected amount, 50–1000 fmol) under the conditions in Fig. 5. The respective coefficients of correlation were 0.997 and 0.999. The relative standard deviations (R.S.D., n = 8) of galactose and glucose at the 50-nmol level were 2.36 and 2.11%, respectively. The R.S.D. values of galactose and glucose, relative to rhamnose (internal standard) were much smaller: 0.69 and 0.85%, respectively. Based on these results, commercial samples of lactose and melibiose were hydrolyzed in 2 *M* trifluoroacetic acid at 100°C for 6 h under a nitrogen atmosphere, and the monosaccharides in the hydrolysates were determined. The galactose-to-glucose molar ratios obtained under the conditions in Fig. 5 were 1.05 and 1.08, respectively, both in fairly good agreement with the theoretical values. An example of the electropherograms is shown in Fig. 8.

The present method employing solutions of divalent metal salts as carrier offers a new mode of separation for carbohydrate derivatives, based on the interaction of solutes with the metal ions and the reversal effect of electro-osmotic flow. Some ex-

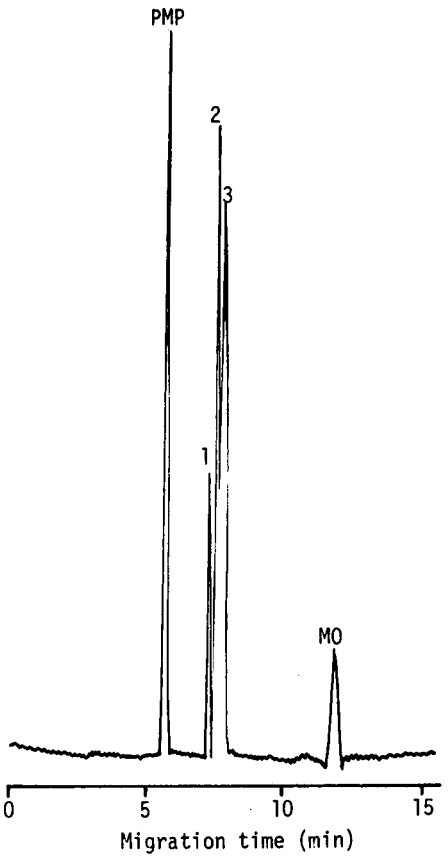

Fig. 7. Separation of the PMP derivatives of a few disaccharides. Analytical conditions and abbreviations as in Fig. 5. Peaks: 1 = maltose; 2 = cellobiose + melibiose; 3 = gentiobiose + lactose.

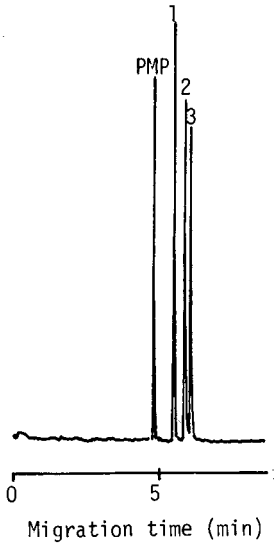

Fig. 8. Analysis of the component monosaccharides in melibiose. Capillary, fused silica (49 cm × 50 μm I.D.); carrier, 100 m*M* calcium acetate; applied voltage, 10 kV; detection, UV absorption at 245 nm.

amples presented above did not give complete separation of PMP derivatives of carbohydrates, but separation will be improved by changing the analytical conditions by using buffer solutions or additives.

REFERENCES

1 S. Honda, E. Akao, S. Suzuki, M. Okuda, K. Kakehi and J. Nakamura, *Anal. Biochem.*, 180 (1989) 351–357.
2 S. Hase, T. Ikenaka and Y. Matsushima, *Biochem. Biophys. Res. Commun.*, 85 (1978) 257–263.
3 M. Novotny, J.-P. Liu, O. Shirota and D. Wiesler, presented at *HPCE '91, San Diego, CA, February, 1991.*
4 S. Honda, S. Iwase, A. Makino and S. Fujiwara, *Anal. Biochem.*, 176 (1989) 72–77.
5 S. Honda, S. Suzuki, A. Nose, K. Yamamoto and K. Kakehi, *Carbohydr. Res.*, 215 (1991) 193–198.
6 T. Kaneta, S. Tanaka and H. Yoshida, *J. Chromatogr.*, 538 (1991) 385–391.
7 R. W. Goulding, *J. Chromatogr.*, 103 (1975) 119–139.

Journal of Chromatography, 588 (1991) 335–339
Elsevier Science Publishers B.V., Amsterdam

CHROM. 23 616

Determination of antihistamines in pharmaceuticals by capillary electrophoresis

C. P. Ong, C. L. Ng, H. K. Lee and S. F. Y. Li*

Department of Chemistry, National University of Singapore, Kent Ridge, Singapore 0511 (Singapore)

(First received April 18th, 1991; revised manuscript received July 4th, 1991)

ABSTRACT

Capillary electrophoresis with on-column UV detection at 214 nm was used to separate a group of nine antihistamines. All these compounds were satisfactorily separated within *ca.* 6 min using a mixed carrier system containing sodium dodecyl sulphate with β-cyclodextrin and tetrabutylammonium hydrogensulphate as modifiers. The application of the method to the determination of the amount of antihistamines present in commercial pharmaceutical samples was demonstrated. In addition, the migration behaviour of the antihistamines in the mixed carrier system was examined.

INTRODUCTION

Micellar electrokinetic chromatography (MEKC), since first initiated by Terabe *et al.* [1], has attracted much attention as an efficient separation technique in recent years [2–6]. This technique possesses both the advantages of capillary zone electrophoresis (CZE) in the separation of charged species and the selectivity required for the separation of neutral compounds [4–6]. This method is based on micellar solubilization and electrophoretic migration of the micelle. Solutes are separated by their differential distribution between the micelle and the surrounding aqueous phase and the differential migration of the two phases. To date MEKC has been successfully employed for the separation of environmental pollutants [7,8], biological compounds [3,5] and pharmaceutical products [9–13].

Most of these applications involve the use of a single surfactant, namely sodium dodecyl sulphate. To enhance further the selectivity of the system, the use of modifiers has been reported. Bushey and Jorgenson [14] found in their separation of dansylated methylamine and dansylated methyl-d_3-amine that the addition of methanol increases the elution range of the system. The introduction of cyclodextrin in the buffer system has been reported to provide additional selectivity for chiral separation via host–guest-type complexation [15].

In this work, the separation of nine antihistamines using MEKC with both β-cyclodextrin and tetrabutylammonium hydrogensulphate (TBA) as modifiers was examined. The method was applied to the determination of antihistamines in two commercial drug samples. In addition, the migration behaviour of the antihistamines in the mixed carrier system was investigated.

EXPERIMENTAL

Equipment

Capillary electrophoresis was performed using a P/ACE 2000 system (Beckman, Palo Alto, CA, USA). The system is equipped with a capillary cartridge containing a 47 cm × 50 μm I.D. (effective length 40 cm) capillary tubing (Polymicro Technologies, Phoenix, AZ, USA). The column temperature was maintained at 25°C throughout the investigation. On-column UV detection with the wavelength set at 214 nm was employed. Chromatographic data were collected and analysed using a Shimadzu (Kyoto, Japan) Chromatopac C-R6A data processor.

0021-9673/91/$03.50

Chemicals

All chemicals were of analytical-reagent grade or better. The buffer solution was prepared by dissolving sodium dihydrogenphosphate dihydrate and sodium tetraborate in water purified by a Millipore Milli-Q system. The electrophoretic media containing sodium dodecyl sulphate (SDS) and the modifiers were prepared as described previously [6]. SDS, β-cyclodextrin and TBA of the purest grade were purchased from Fluka (Buchs, Switzerland). The nine antihistamines used as test standards are listed in Table I. Standard solutions at a concentration of 500 ppm were prepared in high-performance liquid chromatographic-grade methanol (J. T. Baker, Phillipsburg, NJ, USA). All nine antihistamines were supplied by Sigma (St. Louis, MO, USA). Sample solutions were introduced using pressure injection with a pressure of 0.5 p.s.i. (3.5 kPa) and an injection time of 1 s. The amount injected is estimated to be 5.2 nl.

Sample preparation

The procedure for the determination of the active component in commercial antihistamine tablets is as follows. Each tablet was first ground and then extracted twice with a known amount of methanol in an ultrasonic bath kept at low temperature throughout the extraction. The extracted samples were then subjected to centrifugation followed by filtration through a 0.45-μm membrane before injection into the system for analysis.

RESULTS AND DISCUSSION

MEKC and CZE

Preliminary experiments carried out to separate the antihistamines using CZE and MEKC with SDS failed to provide satisfactory results. Because of the similar structural groups present in most of the antihistamines investigated, these methods did not provide adequate selectivity for satisfactory separation of this group of compounds. As a result, even for MEKC, only two broad distorted peaks were observed.

MEKC with β-cyclodextrin

The introduction of β-cyclodextrin to the micellar electrophoretic media resulted in a slight improvement in the overall resolution of the antihistamines. At the same time, it was found that the migration times decreased with increasing β-cyclodextrin concentration. This is consistent with the fact that the β-cyclodextrin molecules would compete with the micelles for the solutes. As the β-cyclodextrin moiety carries no charges, its mobility would not be influenced by electrophoretic attraction and hence its migration velocity would be exclusively governed by the bulk movement of the aqueous phase. Therefore species that were originally affected by the presence fo SDS either through Van der Waals solubilization or by electrostatic ion-pair formation with SDS would now be experiencing an additional partition mechanism via a host–guest type of interaction with the β-cyclodextrin moiety. This additional interaction present in the system would subsequently lead to an increase in selectivity and a considerable reduction in the migration times. However, in spite of the improvement in the resolution with the inclusion of β-cyclodextrin, the selectivity provided in this system was still insufficient to resolve all the peaks completely.

MEKC with tetrabutylammonium salts

Nishi *et al.* [17] in an investigation of some charged species observed an improvement in the resolution and the shape of the peaks using tetraalkylammonium salts in the MEKC mode. Unfortunately, our attempts to use this system again failed to achieve satisfactory results for the separation of the antihistamines, despite a marked improvement in the peak shape for most of the peaks. As all our attempts to separate this group of antihistamines with the known mixed carrier systems were not very successful, a new approach was subsequently adopted to overcome the problem of poor selectivity for this group of compounds.

MEKC with β-cyclodextrin and tetrabutylammonium salts

The new scheme involved the use of a mixed carrier system which includes SDS, β-cyclodextrin and TBA in the electrophoretic medium. With this new carrier system, enhanced selectivity was observed for the separation of the antihistamines. A typical electropherogram for the nine antihistamines is shown in Fig. 1. It can be seen that all peaks were satisfactorily separated within an extremely short analysis time of *ca.* 6 min, which is much shorter

than the time required for most of the systems used previously in this study. At the same time, the pair of enantiomers included in the mixture, (±)-chlorpheniramine (peak 10 in Fig. 1), were also satisfactorily separated using this mixed carrier system.

An unusual observation noted was that the methanol peak (*i.e.*, the insolubilized marker normally used in MEKC work) migrated out much later than some of the antihistamine peaks (peaks 1, 2 and 3). Under normal circumstances, in MEKC and other MEKC applications involving the use of modifiers such as cyclodextrin, the methanol peak would be the first solute to migrate out. In fact, the work carried out by Nishi *et al.* [17] employing tetraalkyammonium salts did not reveal the peculiar trend observed in this work. In order to explain this anomalous behaviour, the separation mechanism for this mixed carrier system needs to be considered.

It is known that the addition of the tetraalkylammonium salts (TAA) would increase the ionic strength of the electrophoretic media, which in turn would result in an increase in current, I (current due to transport of charge by the fluid). Consequently, an increase in the electric field strength (E) could be observed. As a result, the electroosmotic velocity, v_{eo}, of the system would also increase (v_{eo} is proportional to E). Therefore, this increase would contribute to the short analysis time observed in Fig. 1. At the same time, the cationic TAA would tend to combine with the anionic surfactant via ion pairing. As a result, the properties of the anionic surfactant would be considerably altered. The extent of surface binding of the TAA on the anionic site of the surfactant molecules would be largely governed by the size and nature of the alkyl chain. It has been reported that TAA salts with longer alkyl chains, such as the TBA salt used in this investigation, would tend to bind strongly to the negative sites of the micelle [17]. Subsequently, the negative charges present on the SDS micelle would be greatly reduced and therefore the modified SDS would now be experiencing a weaker electrophoretic pull towards the anode. As a result, the micellar velocity towards the cathode would be increased. This effect would also contribute to the increase in the bulk movement, thus increasing the current through the electrophoretic medium. Hence an overall decrease in the migration times of the solutes was observed.

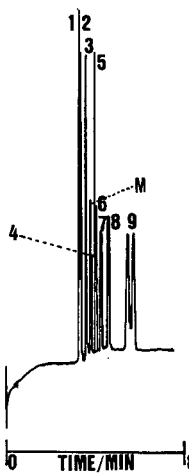

Fig. 1. Electropherogram of antihistamines. Electrophoretic solution, 10 mM SDS in 0.05 M borate–0.05 M phosphate buffer with 10 mM TBA and 10 mM β-cyclodextrin (pH 7.5); separation tube, 47 cm × 50 μm I.D. capillary tube kept at 25°C; voltage, 21.5 kV; detection wavelength, 214 nm. Peak numbers as in Table I; M = methanol.

A more important consequence of this modification is that ion-pair formation between the positively charged antihistamines and the SDS micelles would be inhibited. Therefore, the ion pairing of the positively charged antihistamines with the SDS molecules would be excluded. Further, these positively charged species would also experience electrophoretic repulsion from the anode. Hence they would migrate out much earlier than the remainder of the neutral species such as methanol. A point to note is that such an observation was not seen in the previous investigation involving the use of TAA [17]. The reason could be that in the previous study the ratio of TBA salt to the SDS concentration was much lower than that used in this work. As TBA salts are reported to bind strongly to SDS, it seems that it is only at higher concentrations of TBA salt that this anomalous behaviour can be observed.

In general, the results obtained showed that in spite of the slight modification, the mixed carrier system still possessed the characteristics of both CZE and MEKC. The separation of the charged species was found to be governed by the nature of the charges as in CZE separations, while the migration behaviour of the neutral species was found to be governed by the differential partition mechanism as in MEKC. This is evident from the results shown in Fig. 1. The earlier migrating species are the anti-

TABLE I

ANTIHISTAMINES INVESTIGATED, ABBREVIATIONS AND DETECTION LIMITS

No.	Compound	Abbreviation	Detection limit (pg)
1	Pheniramine	Phen	53.3
2	Doxylamine	Doxyl	55.9
3	Methapyrilene	Meth	57.2
4	Thonylamine	Thon	152.0
5	Triprolidine · HCl	Trip	76.1
6	Dimenhydrinate	Dimen	133.3
7	Cyclizine	Cycl	130.0
8	Promethazine	Prom	139.8
9	(±)-Chloropheniramine	Chlo	143.0

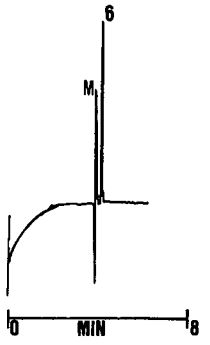

Fig. 2. Electropherogram of dimenhydrinate drug samples. Electrophoretic conditions as in Fig. 1. Peaks: M = methanol; 6 = Dimen.

Fig. 3. Electropherogram of promethazine drug samples. Electrophoretic conditions as in Fig. 1. Peaks: M = methanol; 8 = Prom.

histamines, which normally possess basic groups which favour protonation. The migration order of these positively charged species would, as in many CZE separations, be influenced by the extent of protonation (*i.e.* highly positively charged species would migrate out faster). On the other hand, the neutral antihistamines, the species migrating out later than methanol, would be separated by differential partition between the β-cyclodextrin and the modified SDS. This group of compounds usually consists of the species which contained substituent groups that inhibit protonation. For example, with chloropheniramine and promethazine, owing to the presence of electron-withdrawing groups in these compounds (*i.e.*, chloride and sulphur, respectively), protonation would be hindered. As a result, they were found to migrate slower than most of the other species. The additional partition mechanism would enhance the selectivity of the system. As in this instance the migration of the modified SDS would not be directly affected by the electrophoretic attraction of the high potential end, the overall migration times of the neutral species would be reduced. Even though negatively charged species were not investigated, it would be reasonable to expect that ion-pair formation between these species and the TBA salt would be likely to occur. As a result, faster analysis would also be expected.

Therefore, the major advantage of the use of such a mixed carrier system over other reported systems used in previous investigations is that the combined advantages of CZE and MEKC for the separation of charged and neutral species are present in this system. At the same time, by simply varying the TAA salt and SDS concentrations, in addition to the type of TAA salt used, the extent of modification of the SDS surface can be manipulated. As a result, higher selectivity could be readily achieved within a short analysis time.

TABLE II

AMOUNTS OF ANTIHISTAMINES FOUND IN PHARMACEUTICALS

Type of tablet	Amount indicated per tablet (mg)	Amount found ± S.D. (mg) (n = 5)		
		Tablet 1	Tablet 2	Tablet 3
Dimenhydrinate	50	45.00 ± 0.04	46.53 ± 0.03	46.01 ± 0.03
Promethazine	25	24.50 ± 0.03	25.03 ± 0.02	25.05 ± 0.01

Determination of antihistamines in pharmaceutical samples

The method developed was subsequently used for the determination of antihistamines present in drugs. Linear calibration graphs in the range 100–500 ppm were obtained. The correlation coefficients obtained were better than 0.99 for the nine antihistamines. The detection limits for these compounds are given in Table I. Typical electropherograms of the extracted samples are shown in Figs. 2 and 3 and the results of quantitation are given in Table II. The results obtained suggested that the proposed method can be a useful procedure for the routine determination of antihistamines in pharmaceuticals.

CONCLUSIONS

The usefulness of a mixed carrier system in capillary electrophoresis for the separation of antihistamines has been demonstrated. A major advantage of such a system is its high selectivity, which permits the separation of the antihistamines in a short analysis time with no significant losses in resolution. We believe that this is the first use of a mixed carrier system in capillary electrophoresis for the separation of antihistamines. From the promising results obtained, it can be expected that there will be great potential in the use of this type of technique for the separation of other pharmaceutical products and biological compounds.

ACKNOWLEDGEMENTS

The authors thank Beckman (Singapore) Pte. Ltd. for their generous loan of the P/ACE 2000 system.

REFERENCES

1 S. Terabe, K. Otsuka, K. Ichikawa, A. Tsuchiya and T. Ando, *Anal. Chem.*, 56 (1984) 111.
2 A. S. Cohen, S. Terabe, J. A. Smith and B. L. Karger, *Anal. Chem.*, 59 (1987) 1021.
3 D. E. Burton, M. J. Sepaniak and M. P. Maskarinee, *Chromatographia*, 21 (1986) 583.
4 S. Fujiwara and S. Honda, *Anal. Chem.*, 59 (1987) 2773.
5 K. Otsuka, S. Terabe and T. Ando, *J. Chromatogr.*, 332 (1985) 219.
6 K. Otsuka, S. Terabe and T. Ando, *J. Chromatogr.*, 348 (1985) 39.
7 C. P. Ong, C. L. Ng, N. C. Chong, H. K. Lee and S. F. Y. Li, *J. Chromatogr.*, 516 (1990) 263.
8 Y. F. Yik, C. L. Ng, C. P. Ong, S. B. Khoo, H. K. Lee and S. F. Y. Li, *Bull. Singapore Natl. Inst. Chem.*, 18 (1990) 91.
9 S. Fujiwara and S. Honda, *Anal. Chem.*, 59 (1987) 2773.
10 H. Nishi, N. Tsumagari, T. Nakimoto and S. Terabe, *J. Chromatogr.*, 477 (1989) 259.
11 K. D. Altria and C. F. Simpson, *J. Pharm. Biomed. Anal.*, 6 (1988) 801.
12 T. Nakagawa, Y. Oda, A. Shibukawa, H. Fukuda and H. Tanaka, *Chem. Pharm. Bull.*, 37 (1989) 707.
13 H. Nishi, T. Fukuyama, M. Matsuo and S. Terabe, *J. Chromatogr.*, 498 (1990) 313.
14 M. M. Bushey and J. W. Jorgenson, *J. Microcolumn Sep.*, 1 (1989) 125.
15 S. Fanali, *J. Chromatogr.*, 474 (1989) 441.
16 S. Terabe, K. Otsuka, K. Ichikawa and T. Ando, *J. Chromatogr.*, 264 (1983) 385.
17 H. Nishi, N. Tsumagari and S. Terabe, *Anal. Chem.*, 61 (1989) 2434.

Journal of Chromatography, 588 (1991) 340–343
Elsevier Science Publishers B.V., Amsterdam

CHROM. 23 715

Short Communication

Synthesis and characterization of stationary phases on the basis of silicas modified with epoxidized polybutadienes

IV☆. Chromatographic experiments on a new amino-functionalized stationary phase for high-performance liquid chromatography

U. Erler* and G. Heublein☆☆

Department of Chemistry, Friedrich-Schiller-University of Jena, Humboldt-Strasse 10, D-6900 Jena (Germany)

(First received July 12th, 1991; revised manuscript received August 29th, 1991)

ABSTRACT

Amino-functionalized stationary phases derived from polybutadiene epoxide-coated silica possess a good stability in aqueous buffer solutions at different pH. Pressure stability of the highly polymer-loaded support, separation of carbohydrates, purines and pyrimidines, and the influence of the pH of the eluent mixture on the retention behaviour of ionisable samples, such as substituted benzoic acids, are demonstrated.

INTRODUCTION

In our last paper [1] we described different ways of synthesizing amino-functionalized stationary phases within our concept of heterogeneous polymer-analogous reactions of epoxidized polybutadienes and silicas [2–4]. The aim of the present paper is to prove some characteristic properties of those amino-functionalized stationary phases under conditions of high-performance liquid chromatography.

EXPERIMENTAL

The following chromatographic equipment was used: an LC-6A pump, an SCL-6B system controller, an SPD-6AV UV spectrophotometric detector, an RID-6A differential refractometer and a C-R4A Chromatopac multifunctional data processor, all from Shimadzu. The chromatographic experiments were carried out at ambient temperature. The solvent acetonitrile was of UV grade. The test compounds were obtained from various chemical suppliers and were used as received.

Silica used was LiChrosorb Si 100 (Merck 9340, 7 μm, LC 100). The modification of the surface of LC 100 with epoxidized Polyöl 110 (Chemische Werke

☆ For Part III, see ref. 1.
☆☆ Author deceased.

0021-9673/91/$03.50

Hüls) was carried out according to an optimized variant for the synthesis of polymer-modified supports [4]. This procedure gave the following product: LC 100 P(EPO): 16.90% C, $O_{Spec.}$(BET) = 65 $m^2 g^{-1}$. The reaction of epoxide groups on the surface of the composite LC 100 P(EPO) with ethylene diamine was carried out at 80°C as described in ref. 1.

The resulting material was LC 100 P(NH): 19.54% C, 3.07% N, $O_{Spec.}$(BET) = 58 $m^2 g^{-1}$. LC 100 P(NH) was used to fill a 250 × 4 mm I.D. column using a high-pressure, balanced-density slurry-packing technique [5,6]. The column was rinsed with 200 ml of methanol after packing, followed by rinsing with the elution mixture until equilibration was attained. The ion-exchange capacities (IEC) of amino-functionalized stationary phases were determined by means of potentiometric titration in 1 *M* sodium chloride with 0.1 *M* hydrochloric acid after washing with acetic acid (10%), sodium hydrogencarbonate (10%), water, methanol and diethyl ether and drying at room temperature.

RESULTS AND DISCUSSION

One of the advantages of polymer-modified stationary phases in high-performance liquid chromatography (HPLC) is the combination of the properties of the organic polymer (high pH stability, functionality) with those of the inorganic support (porosity, pressure stability). However, highly polymer-loaded materials could show some disadvantages of polymer packing materials, such as swelling in certain organic solvents and poor pressure stability. In our first attempt we tested the pressure stability of LC 100 P(NH), measuring the dependence of the column pressure on the chosen flow-rate. We found a linear relationship between column pressure and flow-rate in the investigated range (0.1–3 ml/min, p = 0.2–26 MPa). On increasing the flow-rate several times, the measured pressures remained on the same straight line, demonstrating the pressure stability and incompressibility of the highly polymer-loaded and amino-functionalized support.

The separation, identification and quantitative determination of carbohydrates by liquid chromatography have received increasing attention in recent years. Verzele *et al.* [7] published a critical review of some liquid chromatographic (LC) systems for the separation of sugars. Other reviews were published by, for example, Heyrand and Rinando [8], Robards and Whitelaw [9], Hicks [10] and Hanai [11]. Silica gels, derivatized with aminopropyl- or aminoethylaminopropyl-trialkoxysilanes are the most widely used stationary phases for carbohydrate and sugar LC. These stationary phases separate mono-, di- and trisaccharides with eluent compositions such as acetonitrile–water in the ratio 80:20 or 75:25 [7]. We tried to separate some carbohydrates on our amino-functionalized stationary phase LC 100 P(NH) using acetonitrile–water in the ratio 75:25 as an eluent. Fig. 1 demonstrates the ability of the material to separate some mono- and disaccharides as well as other sugar derivatives. As expected, splitting of the peaks because of separation of the anomers was not a problem with the amino-functionalized stationary phase. The comparison of the k' values in Fig. 2 demonstrates the possibility of separating groups of compounds (mono- from disaccharides, desoxy sugars from monosaccharides, ketohexose fructose from aldohexoses, aldopentoses from aldohexoses) as well as compounds within groups (for example separation of individual mono- or disaccharides).

One of the drawbacks of aminopropyl-derivatized silica gel phases is the rather short life expectancy due to the self-hydrolysis of the basic material. Some reports on the hydrolytic stability of ami-

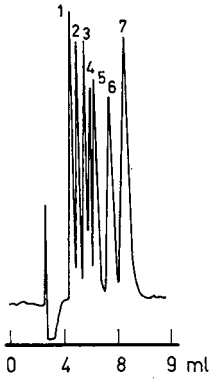

Fig. 1. Separation of rhamnose (1), arabinose (2), fructose (3), sorbitol (4), glucose (5), saccharose (6) and maltose (7). Column, LC 100 P(NH), 7 μm, 250 × 4 mm I.D.; eluent, acetonitrile–water (75:25); flow-rate, 1 ml/min; refractive index detector; 5-mg sample in 2 ml of eluent; dosier volume, 20 μl.

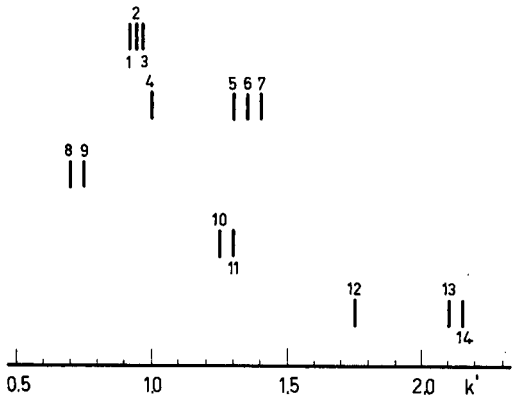

Fig. 2. Comparison of k' values of lyxose (1), xylose (2), arabinose (3), fructose (4), mannose (5), glucose (6), galactose (7), rhamnose (8), fucose (9), sorbitol (10), mannitol (11), saccharose (12), lactose (13) and maltose (14). Conditions as in Fig. 1.

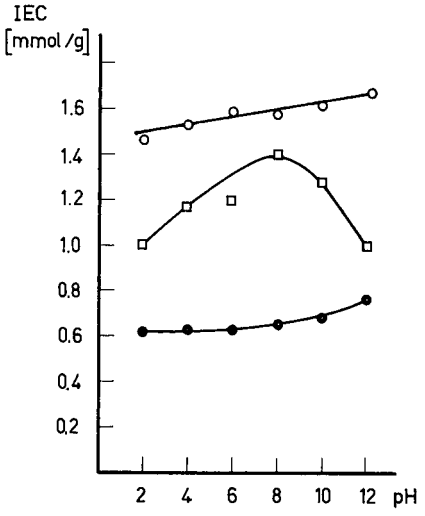

Fig. 3. Comparison of the stability of amino-functionalized stationary phases in aqueous buffer solutions at room temperature (10 days). □ = Kieselgel 60 (Merck, d = 0.04–0.063 mm), modified with aminoethylaminopropyl-triethoxysilane (Wacker, GF 94). Starting material: 7.1% C, 2.31% N, IEC = 1.65 mmol/g; after 10 days at pH 2: 4.5% C, 1.38% N; after 10 days at pH 12: 4.8% C, 1.35% N. ○ = Kieselgel 60, modified with epoxidized polybutadiene and functionalized with ethylene diamine [1]. Starting material: 18.21% C, 2.38% N, IEC = 1.68 mmol/g; after 10 days at pH 2: 16.10% C, 2.10% N; after 10 days at pH 12: 18.02% C, 2.35% N. ● = Kieselgel 60, modified with epoxidized polybutadiene and functionalized with ethylene diamine [1]. Starting material: 13.26% C, 1.05% N, IEC = 0.75 mmol/g; after 10 days at pH 2: 12.12% C, 0.88% N; after 10 days at pH 12: 13.10% C, 1.03% N.

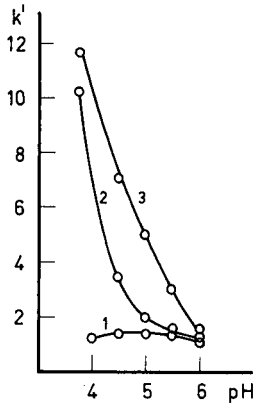

Fig. 4. Dependence of the retention behavior of phenol (1), 4-hydroxybenzoic acid (2) and 2,4-dihydroxybenzoic acid (3) on the pH of the eluent mixture. Column, LC 100 P(NH), 7 μm, 250 × 4 mm I.D.; eluent, phosphate buffer pH 4–6, (I = 0.1)–acetonitrile (80:20); flow-rate, 1 ml/min; UV detection at 280 nm.

no-functionalized stationary phases and reversed-phase materials are given in refs. 12 and 13. In contrast to aminosilane-modified silicas amino-functionalized stationary phase based on silicas modified with expoxidized polybutadienes possess good stability in aqueous buffer solutions at different pH values (Fig. 3).

As is well known, the pH of the buffer solution used as a mobile phase in ion-exchange chromatography influences the retention behavior of ionizable solutes. Fig. 4 demonstrates the increasing resolution of three ionizable samples with decreasing pH value of the mobile phase in the pH range 6–4. The order phenol, 4-hydroxybenzoic acid, 2,4-dihydroxybenzoic acid shows that the higher the possibility of ionization of the test solute, the more changes in the pH value of the eluent mixture influence the retention behavior. These results are in good agreement with those obtained by Heinemann *et al.* [14] on similar stationary phases.

Previously we demonstrated the possibility of separating some xanthine derivatives on columns filled with a new polyhydroxy-functionalized stationary phase derived from poly(butadiene)epoxide-modified silica [15]. We obtained a good separation of the test solutes caffeine, theophylline and 1,3-dimethyl-4-amino-5-formylaminouracil. Because of the strong tendency for xanthine or hypoxanthine to form hydrogen bonds, the system was not suitable for separating these samples in an ac-

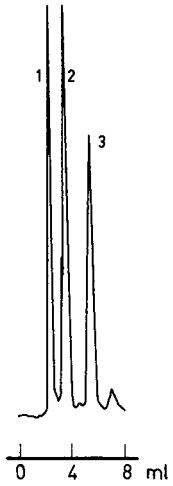

Fig. 5. Separation of caffeine (1), xanthine (2) and hypoxanthine (3). Column, LC 100 P(NH), 7 μm, 250 × 4 mm I.D.; eluent, phosphate buffer pH 5 (I = 0.1)–acetonitrile (80:20); flow-rate, 1 ml/min; UV detection at 280 nm.

ceptable time. As shown in Fig. 5, separation of caffeine, xanthine and hypoxanthine was achieved on LC 100 P(NH) at pH 5 with good efficiency. An important property of purines and pyrimidines is their ability to undergo tautomerization, affecting the chromatographic behavior of those compounds. In addition, the acid–base character of those molecules plays an important role in their chromatographic behavior.

ACKNOWLEDGEMENT

We greatly appreciate the support of Professor Dr. S. Reissmann (Friedrich-Schiller-University of Jena, Department of Biochemistry) for placing the chromatographic equipment at our disposal.

REFERENCES

1 U. Erler and G. Heublein, *Angew. Makromol. Chem.*, 182 (1990) 43.
2 G. Heublein, B. Heublein, P. Hortschansky, H. Meissner and H. Schütz, *J. Macromol. Sci.*, A25 (1988) 183.
3 G. Heublein, B. Heublein, P. Hortschansky, H. Schütz and H.-J. Flammersheim, *Makromol. Chem.*, 190 (1989) 9.
4 G. Heublein, U. Erler, A. Ulbricht and H. Winkelmann, *Angew. Makromol. Chem.*, 182 (1990) 29.
5 R. E. Majors, *Anal. Chem.*, 44 (1972) 1722.
6 J. J. Kirkland, *Chromatographia*, 8 (1975) 661.
7 M. Verzele, G. Simoens and F. Van Damme, *Chromatographia*, 23 (1987) 292.
8 A. Heyrand and M. Rinando, *J. Liq. Chromatogr.*, 4 (Suppl. 2) (1981) 175.
9 K. Robards and M. Whitelaw, *J. Chromatogr.*, 373 (1986) 81.
10 K. B. Hicks, *Adv. Carbohydrate Chem. Biochem.*, 46 (1987) 17.
11 T. Hanai, *Adv. Chromatogr.*, 25 (1986) 280.
12 D. M. Wonnacott and E. V. Patton, *J. Chromatogr.*, 389 (1987) 103.
13 J. L. Glajch, J. J. Kirkland and J. Köhler, *J. Chromatogr.*, 384 (1987) 81.
14 G. Heinemann, J. Köhler and G. Schomburg, *Chromatographia*, 23 (1987) 435.
15 U. Erler, S. Spange and G. Heublein, *Acta Polym.*, 42 (1991) 389.

Journal of Chromatography, 588 (1991) 344–347
Elsevier Science Publishers B.V., Amsterdam

CHROM. 23 765

Short Communication

Simultaneous determination of yohimbine hydrochloride, strychnine nitrate and methyltestosterone by ion-pair high-performance liquid chromatography

Ryoko Chiba* and Yoko Ishii

Department of Pharmaceutical Analytical Chemistry, Showa College of Pharmaceutical Sciences, 3-3165, Higashitamagawagakuen, Machida-shi, Tokyo 194 (Japan)

(First received April 2nd, 1991; revised manuscript received September 24th, 1991)

ABSTRACT

A reversed-phase ion-pair chromatographic method was developed for the simultaneous determination of yohimbine hydrochloride (YOH), strychnine nitrate (SN) and methyltestosterone (MT) in a pharmaceutical preparation (tablet). YOH, SN and MT were extracted and separated within 15 min on an octadecylsilano-silica gel column (15 cm × 4.6 mm I.D., 5 μm particle size). The mobile phase was a mixture of $5 \cdot 10^{-3}$ *M* sodium octanesulphonate solution (pH 5.5) and methanol (40:60, v/v). The ultraviolet absorption detector was set at 254 nm, and noscapine was used as an internal standard. The recoveries of YOH, SN and MT from a known sample were 101.9 and 101.8 and 99.4%, respectively. By this method, these components in commercial tablets could be simultaneously determined without any interference. The method is sufficiently sensitive, reproducible and accurate.

INTRODUCTION

Yohimbine hydrochloride (YOH) is an indole alkaloid isolated from the bark of *Corynante yohimbe*. Because it is a vasodilator, this alkaloid has been used alone or in combination with strychnine nitrate (SN) or methyltestosterone (MT) as an aphrodisiac. In recent years, analyses of samples containing YOH alone and in combination with either SN of MT have been carried out by high-performance liquid chromatography (HPLC) [1–6].

No report has dealt with the analysis of a mixture of YOH, SN and MT. In the present study, which attempted the simultaneous determination of YOH, SN and MT in a pharmaceutical tablet preparation, ion-pair HPLC with a column packed with octadecylsilane (ODS)-gel was used. A simple and reproducible procedure was established. This is described in the following section.

EXPERIMENTAL

Chemicals and reagents

YOH was the product of Tokyo-Kasei Kogyo (Tokyo, Japan). SN and noscapine were purchased from Sanko Seiyaku (Tokyo, Japan). MT was purchased from Wako Junyaku Kogyo (Osaka, Japan). YOH, SN, MT were used as standard substances. Noscapine was used as an internal standard for HPLC. The other chemical reagents and solvents were of analytical grade.

Conditions of chromatography

The HPLC system used consisted of 880 PU-In-

0021-9673/91/$03.50

telligent pumps, an 875 UV variable-wavelength detector, a 7125 Rheodyne injector, an RC 150 recorder, an 860-CO column oven and a column packed with Fine Pak SIL-C_{18}S (15 cm × 4.6 mm I.D., 5 μm particle size). All these parts were manufactured by Nippon Bunko Kogyo (Tokyo, Japan). The elution was carried out with an ultrasonicated mobile phase, a mixture of methanol and $5 \cdot 10^{-3}$ *M* sodium octanesulphonate solution (pH 5.5, 60:40, v/v), at a flow-rate 1.5 ml/mm and with a column temperature of 45°C. The eluate was monitored at 254 nm.

Preparation of standard solution

YOH, SN and MT were separately dissolved in the 60:40 (v/v) mixture of methanol and water, and standard solutions of 30, 200 and 600 μg/ml were prepared. Noscapine was dissolved in the same solvent as described above, and two internal standard solutions containing it at (1) 5000 μg/ml and (2) 100 μg/ml were prepared.

Preparation of sample solution

At least twenty tablets were weighed accurately and finely powdered. A portion of the powder, corresponding to about ten tablets, was weighed accurately, 40 ml of 10% sodium hydroxide solution were added, and the mixture was shaken for 10 min on a mixer. After centrifugation (3000 rpm, 10 min, 1500 *g*), the residue was collected and the supernatant liquid decanted [containing L-methionine (ME), thianine hydrochloride (VB_1), riboflavin (VB_2) and folic acid (FA)] as thoroughly as possible. Two aliquots of 20 ml of 10% sodium hydroxide solution were then added to the residue, and the mixture was shaken for 10 min on a mixer, centrifuged again, and the supernatant liquid decanted as thoroughly as possible. The residue was extracted with four 50-ml portions of chloroform. The chloroform extracts were combined, and the chloroform was evaporated on a water bath. A 10-ml volume of methanol was added just when the odour of chloroform was no longer apparent, and the solution was evaporated to dryness. An accurately measured aliquot of 25 ml of methanol–water mixture (60:40, v/v) was added to the residue, and this solution was filtered through a disposable filter unit and used to prepare sample solutions. The determination was performed using the same method (HPLC).

Quantitation

According to the formulation of pulspin tablet (Ishihara Pharmaceutical Industry, Chiba, Japan), the portions of YOH, SN, and MT corresponding to their weight in ten tablets were accurately weighed. These portions were combined in a mortar, thoroughly mixed until a uniform powder was obtained, and dissolved in the mixture of methanol and water (60:40, v/v). This solution was diluted with the mixture accurately to 25 ml, filtered through a disposable filter unit (0.45 μm, Chromatodisk 13A, for aqueous systems, Kurabo), and used to prepare sample solutions.

Sample solution A (for the determination of YOH and MT). A 5-ml portion of the sample solution and 2 ml of the internal standard solution 1 were accurately combined, and the mixture was diluted accurately to 20 ml with the mixture of methanol and water (60:40, v/v). A 5-μl portion of this solution was analysed for YOH and MT by HPLC.

Sample solution B (for the determination of SN). A 5-ml portion of the sample solution and 0.1 ml of the internal standard solution 2 were accurately combined, and the mixture was diluted accurately to 20 ml with the mixture of methanol and water (60:40, v/v). A 20-μl portion of this solution was analysed for SN by HPLC. Based on the peak-height ratio of the substance to be determined to the internal standard, the concentrations of YOH, SN and MT were calculated by a conventional procedure with the relevant calibration curves.

RESULTS AND DISCUSSION

Choice of system

An ODS-silica gel column was used for the ion-pair HPLC. Mobile phases varying in composition were examined in order to achieve the complete separation of YOH, SN and MT in a compound preparation. The best separation was obtained with the mixture of methanol and $5 \cdot 10^{-3}$ *M* sodium octanesulphonate solution (60:40, v/v). The effects of column temperature were studied at 40–50°C, the column temperature being maintained by means of a column oven. The best separation within a reasonable retention time (t_R) was obtained at 45°C.

Fig. 1 shows chromatograms obtained under the conditions as described above.

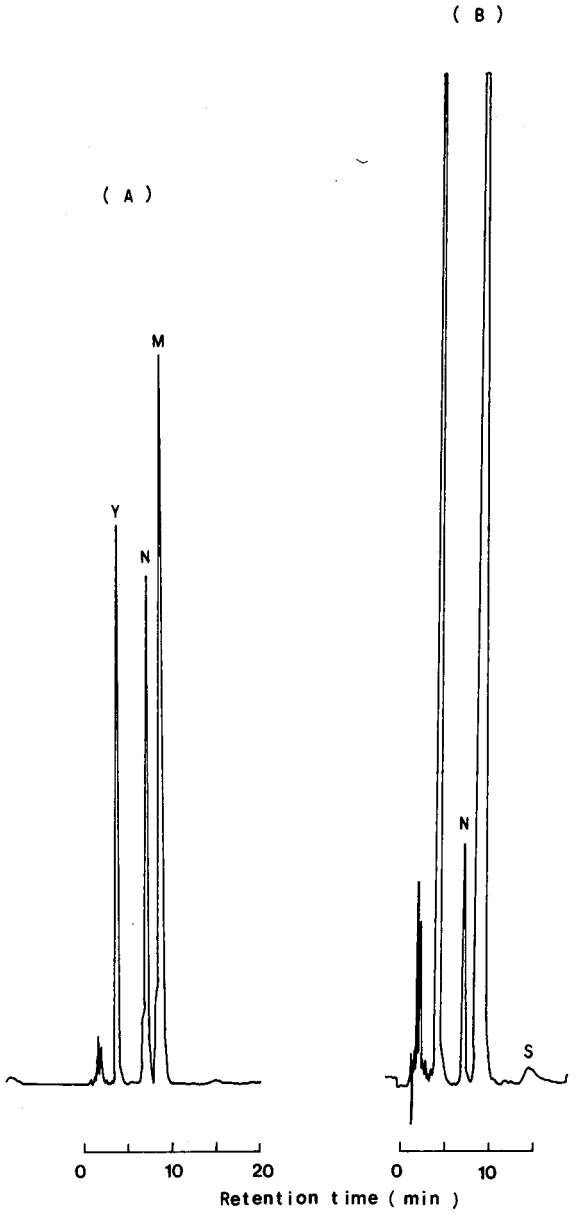

Fig. 1. Chromatograms of (A) yohimbine hydrochloride and methyltestosterone and (B) strychine nitrate in commercial tablets. Peaks: Y = yohimbine hydrochloride; N = noscapine; M = methyltestosterone; S = strychnine nitrate. Retention time: Y = 4 min; N = 7.3 min; M = 9.3 min; S = 15 min.

Calibration

Calibration curves were linear between 60 and 300 μg/ml for YOH ($y = 0.945x + 0.058$, $r = 0.999$), between 5 and 30 μg/ml for SN ($y = 12.408x - 0.034$, $r = 0.999$) and between 20 and 100 μg/ml for MT ($y = 3.608x - 0.009$, $r = 0.999$). Detection limits at a signal-to-noise ratio of 3 were 10 μg/ml for YOH, 1.5 μg/ml for SN and 2.86 μg/ml for MT.

TABLE I

RECOVERIES OF YOHIMBINE HYDROCHLORIDE, STRYCHNINE NITRATE AND METHYLTESTOSTERONE FROM A MIXTURE OF STANDARDS

Compound	Added (mg)	Recovery (%) ($n = 8$)	C.V. (%) ($n = 8$)
YOH	3.00	101.9	1.48
SN	0.30	101.8	1.06
MT	1.50	99.4	0.94

Recovery

Using the formulation of a commercially available compound preparation, a sample was prepared by combining known amounts of these three drugs and was analysed to assess their recovery. As shown in Table I, more than 99% of added YOH, SN and MT could be recovered. The coefficients of variation (C.V.) for the recovery tests were less than 1.5%.

Application

A chromatogram of commercial tablet extract is shown in Fig. 1A and B. The determination of YOH, SN and MT in commercial tablets is shown in Table II. Other ingredients, such as ME, VB_1, VB_2 and FA, did not interfere with the analysis.

TABLE II

DETERMINATION OF YOHIMBINE HYDROCHLORIDE, STRYCHNINE NITRATE AND METHYL TESTOSTERONE IN COMMERCIAL TABLETS

Tablets: according to the label, one tablet contains 3 mg of yohimbine hydrochloride, 1.5 mg of methyltestosterone, 0.3 mg of strychnine nitrate, 100 mg of L-methionine, 3 mg of thiamine hydrochloride, 3 mg of riboflavin and 0.1 mg of folic acid.

Compound	Label claim (mg per tablet)	Amount found (mean ± S.D., $n = 5$) (mg per tablet)
YOH	3.00	3.10 ± 0.17
SN	0.30	0.31 ± 0.02
MT	1.50	1.54 ± 0.08

In brief, the ion-pair HPLC method described is an excellent method which affords a simple simultaneous determination of YOH, SN and MT. The results were satisfactorily reproducible.

REFERENCES

1 O. Salama and F. Belal, *Analyst (London)*, 111 (1986) 581.
2 R. Chiba and Y. Ishii, *Bunseki Kagaku*, 35 (1986) 323.
3 A. Akbari, A. D. Jernigan, P. B. Bush and N. H. Booth, *J. Chromatogr.*, 361 (1986) 400.
4 J. A. Owen, S. L. Nakatsu, M. Condra, D. H. Surridge, J. Fenemore and A. Morales, *J. Chromatogr.*, 342 (1985) 333.
5 R. Chiba and Y. Ishii, *Yakugaku Zasshi*, 110 (1990) 289.
6 R. Chiba and Y. Ishii, *Bunseki Kagaku*, 39 (1990) 313.

Journal of Chromatography, 588 (1991) 348–351
Elsevier Science Publishers B.V., Amsterdam

CHROM. 23 772

Short Communication

High-performance liquid chromatographic analysis of diastereomers and enantiomers of pyrroloisoquinoline antidepressants

Rekha D. Shah and Cynthia A. Maryanoff*

The R. W. Johnson Pharmaceutical Research Institute, Chemical Development Department, Spring House, PA 19477 (USA)

(First received September 10th, 1991; revised manuscript received September 26th, 1991)

ABSTRACT

To determine the diastereomeric and enantiomeric purity of different sets of isomers of pyrroloisoquinoline compounds in a reaction mixture, two general direct high-performance liquid chromatographic (HPLC) methods were developed: a reversed-phase HPLC method for diastereomers and a normal-phase HPLC method for enantiomers. These methods allowed us to monitor the course of reactions; changes in reaction variables were made until optimized conditions were identified to provide enantiomerically pure products.

INTRODUCTION

Hexahydropyrrolo[2,1-a]isoquinoline compounds (**1**) were developed as potential antidepressant agents [1–5]. Biological activity in the series resides with the *trans*-[6a,10b] diastereomers [3]. In general, the active enantiomer has the *R* configuration at the 10b position [6,7]. Herein we present methods to determine diastereomeric and enantiomeric purity in the series.

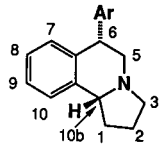

1

For this study, three sets of pyrroloisoquinoline compounds (**1A**,**1B** and **1C**) were prepared [7–9]. A reversed-phase high-performance liquid chromatography (HPLC) method, using a 25 cm × 4.6 mm Supelcosil-LC-18-DB (5 μm) column, was developed to determine the diastereomeric purity of each set. A normal-phase system, using a 25 cm × 4.6 mm Chiralcel OD (10 μm) column, was developed to determine the enantiomeric purity.

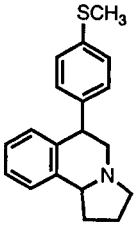

1A

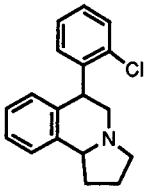

1B

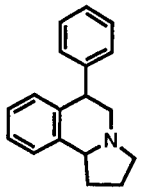

1C

These methods do not require derivatization of a compound before and/or after analysis. Both methods are linear in the tested concentration range

0021-9673/91/$03.50

(0.01–0.50 mg/ml for diastereomeric purity and 0.01–0.15 mg/ml for enantiomeric purity) with a correlation coefficient of 0.99. The lower detection limit of both methods is 0.006 mg.

EXPERIMENTAL

Materials

Pure standards of sets **1A** [McN-5652 (RWJ 35652) and McN-5655 (RWJ 35655)], sets **1B** [McN-4612 (RWJ 34612) and McN-4111 (RWJ 34111)], and sets **1C** [McN-5707 (RWJ 35707) and McN-5706 (RWJ 35706)] were prepared in our laboratory [7–9]. HPLC-grade acetonitrile, hexane, isopropanol and reagent-grade triethylamine were purchased from Fisher Scientific. Water was purified with a Millipore Milli-Q system.

Instrumentation

The chromatographic system consisted of a Waters (Milford, MA, USA) Model 600 pump, Model 490 variable-wavelength detector, U6K injector and Model 740 data system. The 25 cm × 4.6 mm Supelcosil-LC-18-DB (5 μm) column was purchased from Supelco (Bellefonte, PA, USA) and 25 cm × 4.6 mm Chiralcel OD (10 μm) column was purchased from J. T. Baker (Phillipsburg, NJ, USA).

Chromatographic conditions

The HPLC conditions are listed below.

(1) Diastereomeric purity method: mobile phase, 0.01 *M* triethylamine buffer (pH 6.2)–acetonitrile (25:75), flow-rate, 2.0 ml/min; injection volume, 10 μl; detection wavelength, 220 nm; detector sensitivity, 0.5 a.u.f.s.; column temperature, 35°C.

(2) Enantiomeric purity method: mobile phase, hexane–isopropanol–triethylamine (80:20:0.1); flow-rate, 1.0 ml/min; injection volume, 10 μl; detection wavelength, 220 nm; detector sensitivity, 0.5 a.u.f.s.; column temperature, ambient.

Calibration graphs

(1) Diastereomeric method: stock solutions of three sets of diastereomers, **1A**, **1B** and **1C** (as defined above), were prepared in acetonitrile at 2.0 mg/ml each. A series of dilutions were made to obtain the concentration range of 0.01–0.40 mg/ml. Four standards were analyzed and the calibration graphs of concentration *versus* area were plotted to check the linearity of the method. Using a least-squares analysis it was determined that the method is linear with a correlation coefficient of 0.99 in the tested concentration range. The calibration graphs were straight lines passing through the origin.

(2) Enantiomeric method: stock solution of racemic McN-5652 (RWJ 35652), McN-5707 (RWJ 35707) and McN-4612 (RWJ 34612) were prepared at 1.0 mg/ml concentration in hexane–isopropanol (80:20) solution. Four standards of each in the concentration range of 0.01–0.15 mg/ml were prepared by serial dilution and analyzed. The graph of concentration *versus* area was plotted to check the linearity of the method. Using a least-squares analysis it was determined that the method is linear with a correlation coefficient of 0.99 in the tested concentration range. The calibration graphs were straight lines which passed through the origin.

RESULTS AND DISCUSSION

Figs. 1–3 represent typical chromatograms of each set of diastereomers illustrating the separation achieved in the diastereomeric method. In each set of diastereomers, the *trans*-[6a,10b] diastereomer eluted as the second peak.

Figs. 4–6 represent typical chromatograms of McN-5652 (RWJ 35652), McN-5707 (RWJ 35707)

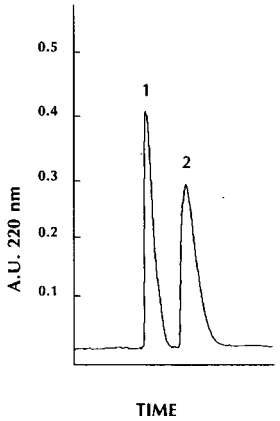

Fig. 1. Separation of McN-5652 (RWJ 35652) and McN-5655 (RWJ 35655) diastereomers. Chromatographic conditions: 25 cm × 4.6 mm I.D. Supelcosil-LC-18-DB (5 μm) column; 0.01 *M* triethylamine buffer (pH 6.2)–acetonitrile (25:75); flow-rate 2.0 ml/min; column temperature 35°C; detector wavelength 220 nm. Peaks: 1 = McN-5655 (retention time 3.25 min); 2 = McN-5652 (retention time 4.13 min).

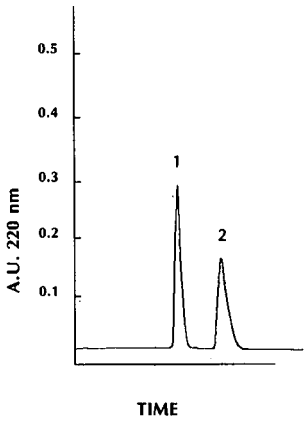

Fig. 2. Separation of McN-5707 (RWJ 35707) and McN-5706 (RWJ 35706) diastereomers. Chromatographic conditions as in Fig. 1. Peaks: 1 = McN-5706 (retention time 5.47 min); 2 = McN-5707 (retention time 7.46 min).

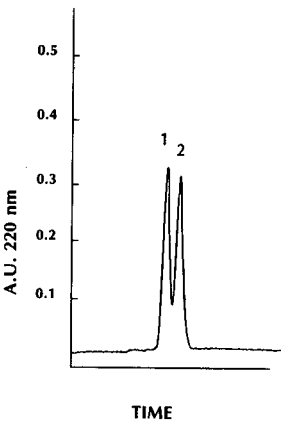

Fig. 4. Separation of McN-5652 (RWJ 35652) enantiomers. Chromatographic conditions: 25 cm × 4.6 mm I.D. Chiralcel OD (10 μm) column; hexane–isopropyl alcohol–triethylamine (80:20:1); flow-rate 1.0 ml/min; column temperature ambient; detector wavelength 220 nm. Peaks: 1 = 4.09 min; 2 = 4.40 min.

and McN-4612 (RWJ 34612) enantiomers demonstrating the separation achieved in the enantiomeric method. In each set of enantiomers the active enantiomer (*R*-configuration at the 10b position) eluted as the second peak.

Using calibration graphs of each with a linear regression equation we determined that both methods are linear throughout the concentration range studied with the correlation coefficient of 0.99.

These methods allowed us to monitor the course of reactions; changes in experimental conditions were made until optimized conditions were identified to provide enantiomerically pure products.

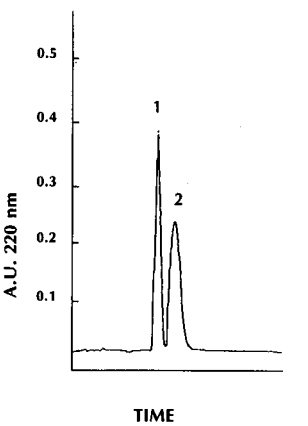

Fig. 3. Separation of McN-4612 (RWJ 34612) and McN-4111 (RWJ 34111) diastereomers. Chromatographic conditions as in Fig. 1. Peaks: 1 = McN-4111 (retention time 4.21 min); 2 = McN-4612 (retention time 5.34 min).

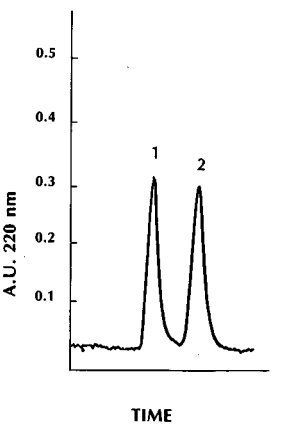

Fig. 5. Separation of McN-5707 (RWJ 35707) enantiomers. Chromatographic conditions as in Fig. 4. Peaks: 1 = 3.75 min; 2 = 4.37 min.

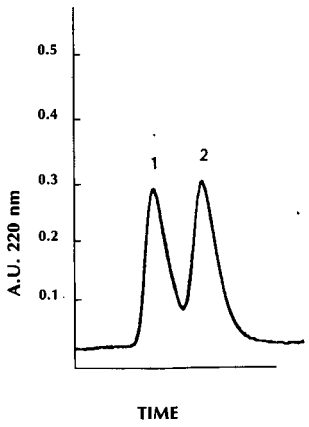

Fig. 6. Separation of McN-4612 (RWJ 34612) enantiomers. Chromatographic conditions as in Fig. 4. Peaks: 1 = 4.12 min; 2 = 4.47 min.

ACKNOWLEDGEMENTS

We thank B. E. Maryanoff, K. L. Sorgi and D. F. McComsey for supplying samples for analysis.

REFERENCES

1 B. E. Maryanoff, R. P. Shank and J. F. Gardocki, *Drugs Fut.*, 11 (1986) 18–20.
2 R. P. Shank, C. R. Schneider, W. B. Baldy, P. E. Setler, B. E. Maryanoff and D. F. McComsey, *Trans. Am. Soc. Neurochem.*, 16 (1985) 198.
3 R. P. Shank, J. L. Vaught, C. R. Schneider, J. R. Mathiasen, J. F. Gardocki, C. Cambarana, B. E. Maryanoff and D. F. McComsey, *Soc. Neurosci. Abs.*, 12 (1986) 1237.
4 R. P. Shank, J. L. Vaught, J. F. Gardocki, K. A. Pelley, B. E. Maryanoff and D. F. McComsey, *Int. J. Neurosci.*, 32 (1987) 537–538.
5 R. P. Shank, J. F. Gardocki, C. R. Schneider, J. L. Vaught, P. E. Setler, B. E. Maryanoff and D. F. McComsey, *J. Pharmacol. Exp. Ther.*, 242 (1987) 74–84.
6 B. E. Maryanoff, D. F. McComsey, M. J. Costanzo, P. E. Setler, J. G. Gardocki, R. P. Shank and C. R. Schneider, *J. Med. Chem.*, 27 (1984) 943–945.
7 K. L. Sorgi, C. A. Maryanoff, D. F. McComsey, D. W. Graden and B. E. Maryanoff, *J. Am. Chem. Soc.*, 112 (1990) 3567–3579.
8 B. E. Maryanoff and D. F. McComsey, *J. Heterocycl. Chem.*, 22 (1985) 911–914.
9 B. E. Maryanoff, D. F. McComsey, M. S. Mutter, K. L. Sorgi and C. A. Maryanoff, *Tetrahedron Lett.*, 29 (1988) 5073.
10 B. E. Maryanoff, D. F. McComsey, J. F. Gardocki, R. P. Shank, M. J. Costanzo, S. O. Nortey, C. R. Schneider and P. E. Setler, *J. Med. Chem.*, 30 (1987) 1433–1454.

Journal of Chromatography, 588 (1991) 352–355
Elsevier Science Publishers B.V., Amsterdam

CHROM. 23 692

Short Communication

Enantiomeric separation of racemic hydroperoxides and related alcohols

Annamarie Kunath*, Eugen Höft and Hans-Jürgen Hamann

Central Institute of Organic Chemistry, Rudower Chaussee 5, O-1199 Berlin (Germany)

Jürgen Wagner

Humboldt University, Institute of Bioorganic Chemistry, Hessische Strasse 1-2, O-1040 Berlin (Germany)

(First received July 12th, 1991; revised manuscript received August 15th, 1991)

ABSTRACT

Racemic hydroperoxides and alcohols were chromatographed on a chiral stationary phase consisting of cellulose tris(3,5-dimethylphenyl carbamate) coated on macroporous silica using hexane–2-propanol mobile phases. It was found that the retention (k') and the stereoselectivity (α) of secondary and tertiary chiral hydroperoxides and related alcohols are influenced by both the ambient temperature and water saturation of the mobile phase. The results indicate that water saturation of the mobile phase leads to decreased k' values and increased α. Increasing the temperature causes a clear decrease in k' but only a slightly decrease in α.

INTRODUCTION

Organic hydroperoxides are useful oxidants for many organic substrates. In some instances non-racemic hydroperoxides have been used for the asymmetric oxidation of sulphides, but up to now with low enantioselectivity. Such optically active hydroperoxides were obtained in solution by singlet oxygenation of thiazolidine derivatives [1], as stable substances by oxidation of 2,3-unsaturated glycosides [2] or by resolution of racemic hydroperoxides by means of liquid chromatography of diastereomeric derivatives [3]. The optical purity of the hydroperoxides obtained was proved by optical rotation data or by derivatization and high-performance liquid or capillary gas chromatography of the diastereomers [3].

A direct enantiomeric separation of chiral hydroperoxides has not been described so far, but chiral aromatic alcohols have been separated on cellulose tribenzoate and cinnamate chiral stationary phases (CSP) [4,5]. In this work, we used a CSP consisting of cellulose . tris(3,5-dimethylphenyl carbamate) coated on macroporous silica and hexane–2-propanol mobile phases. The method was found suitable for analysing enantiomers of hydroperoxides and related alcohols in the same solution.

EXPERIMENTAL

Reagents and chemicals

The racemic alcohol **1** (Fig. 1) was purchased from E. Merck (Darmstadt, Germany); **2** was obtained by reduction of 1,2,3,4-tetrahydro-1-naphthalenone with $LiAlH_4$ and **3** was purchased from Aldrich (Milwaukee, WI, USA). Compounds **4** and

0021-9673/91/$03.50

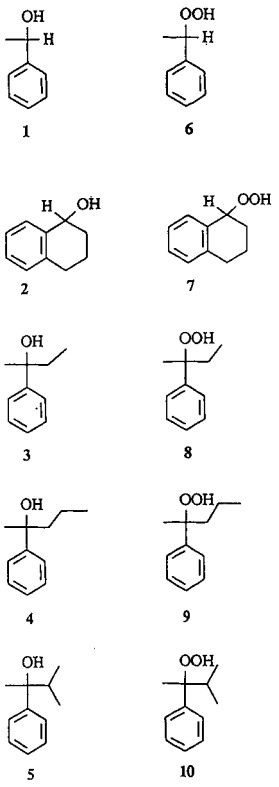

Fig. 1. Structures of racemic alcohols and hydroperoxides used.

5 were synthesized by reaction of the Grignard reagents of 1- and 2-propyl bromide, respectively, with acetophenone. The hydroperoxides **6** and **7** were obtained by autoxidation of the corresponding aralkanes [6,7]. Tertiary hydroperoxides **8–10** were prepared by the known reaction of the appropriate tertiary alcohols with hydrogen peroxide (44%) in the presence of a trace amount of sulphuric acid [8]. The purity of the hydroperoxides was determined by iodometric titration and found to be 70–95%.

The CSP cellulose tris(3,5-dimethylphenyl carbamate)-coated Nucleosil-4000-NH_2 (CDMPC) was prepared according to a procedure described by Okamoto *et al.* [9]. The column (250 × 4.6 mm I.D.) was packed by a slurry method at 300 kg/cm^2 with hexane as the eluent. The plate number [N for benzene; hexane–2-propanol (90:10), 0.5 ml/min] and the dead time (t_0 of 1,3,5-tri-*tert.*-butylbenzene as a non-retained compound [10]) of the column were estimated to be 3800 and 6.0 min, respectively.

The mobile phase was composed of UV-grade hexane (PCK, Schwedt, Germany) and analytical reagent grade 2-propanol (Riedel-de Haën, Seelze-Hannover, Germany).

Apparatus and chromatographic conditions

The high-performance liquid chromatographic equipment consisted of a Type 7095 injection valve (20-μl loop), a Type 364.00 pump, a Type 287.00 variable-wavelength spectrophotometer, a Model A1000 chiral detector (all from Knauer, Berlin, Germany) and a Model K201 recorder (Carl Zeiss, Jena, Germany).

The detection wavelength and the flow-rate were set at 254 nm and 1 ml/min, respectively. The column temperature was maintained either using a column oven (25 and 52°C) or by cooling the column in a Dewar container with ice–water (0°C). The solutes were dissolved in hexane–2-propanol (90:10) at a concentration of 0.1 and 1 mg/ml, respectively, when the UV and chiral detector were used in series.

RESULTS AND DISCUSSION

The chiral alcohols and hydroperoxides used as solutes are shown in Fig. 1. The chromatographic results obtained with dried and water-saturated mobile phase on the one hand and changing the column temperature on the other are given in Tables I and II, respectively. Fig. 2 shows the chromatogram

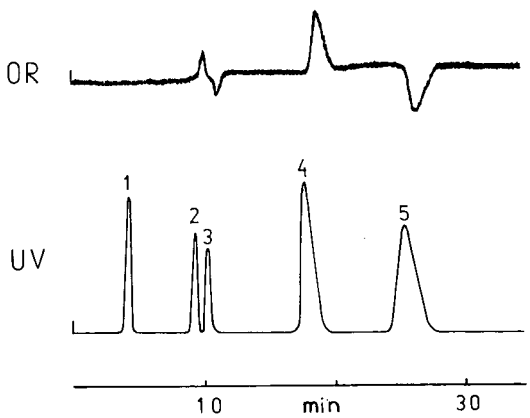

Fig. 2. Optical resolution of partly decomposed 1-methyl-1-phenylpropyl hydroperoxide (**8**). Eluent: water-saturated hexane–2-propanol (98:2, v/v). Top, optical rotation; bottom, UV detection. Peaks: (1) unknown; (2) (+)-enantiomer and (3) (−)-enantiomer of the related alcohol; (4) (+)-enantiomer and (5) (−)-enantiomer of the hydroperoxide.

TABLE I

EFFECT OF WATER SATURATION OF THE MOBILE PHASE ON THE RETENTION AND STEREOCHEMICAL RESOLUTION OF RACEMIC ALCOHOLS AND HYDROPEROXIDES (**1–10**)

Mobile phase: hexane–2-propanol (98:2, v/v). Column temperature: 25°C.

Compounds	Solute[a]	A[b]			B[b]			Enantiomeric elution order
		k'_1[c]	α	R_s	k'_1[c]	α	R_s	
Alcohols	**1**	4.34	1.28	2.69	3.78	1.44	3.34	+/−
	2	4.18	1.11	1.03	3.51	1.21	1.97	+/−
	3	2.09	1.00	0.00	1.88	1.24	1.83	+/−
	4	2.63	1.04	0.52	2.27	1.22	1.85	+/−
	5	1.91	1.21	1.94	1.50	1.34	2.71	+/−
Hydroperoxides	**6**	8.15	1.33	3.70	6.82	1.35	4.09	+/−
	7	10.76	1.17	1.86	8.65	1.20	2.24	+/−
	8	5.84	1.49	4.16	4.86	1.53	4.62	+/−
	9	7.06	1.49	4.42	5.49	1.56	4.95	+/−
	10	5.82	1.96	6.25	4.41	2.22	7.17	+/−

[a] See Fig. 1 for structures.
[b] A, mobile phase dried with molecular sieve; B, mobile phase water saturated.
[c] Capacity factor of the first-eluted enantiomer.

of the partly decomposed hydroperoxide **8**. In all instances the optical rotation of the first-eluting enantiomer of the alcohols and of the hydroperoxides was positive. Generally, a better optical resolution and longer retention times were obtained for appropriate hydroperoxides.

Effect of water on retention and stereoselectivity

As can be seen from Table I, the amount of water in the mobile phase influences the retention (k'), the

TABLE II

EFFECT OF COLUMN TEMPERATURE ON THE RETENTION AND STEREOCHEMICAL RESOLUTION OF RACEMIC ALCOHOLS AND HYDROPEROXIDES (**1–10**)

Mobile phase: hexane–2-propanol (98:2, v/v) dried with molecular sieve.

Solute[a]	52°C			25°C			0°C		
	k'_1[b]	α	R_s	k'_1[b]	α	R_s	k'_1[b]	α	R_s
1	3.69	1.22	2.24	4.34	1.28	2.69	4.90	1.38	2.81
3	3.54	1.11	1.37	4.18	1.11	1.03	4.59	1.12	0.94
3	1.95	1.00	0.00	2.09	1.00	0.00	2.82	1.08	0.69
4	ND[c]	ND	ND	2.63	1.04	0.52	3.13	1.13	1.15
5	1.58	1.11	1.02	1.91	1.21	1.94	2.78	1.00	0.00
6	6.70	1.28	3.14	8.15	1.33	3.70	10.34	1.41	3.94
7	9.11	1.12	1.64	10.76	1.17	1.86	12.74	1.20	1.68
8	4.69	1.42	3.89	5.84	1.49	4.16	7.77	1.60	4.95
9	ND	ND	ND	7.06	1.49	4.42	8.77	1.68	5.02
10	ND	ND	ND	5.82	1.96	6.25	7.59	3.01	7.97

[a] See Fig. 1 for structures.
[b] Capacity factor of the first-eluted enantiomer.
[c] ND: not determined.

separation factor (α) and the resolution (R_s) considerably. Generally, retention times decreased and α increased when water-saturated eluents were used. Without water **3** could not be separated and only a poor optical resolution of **4** could be achieved. Hydrogen bonding of the OH groups of alcohols and of hydroperoxides with the CSP is one factor affecting the separation of enantiomers. There are not only interactions possible with the cellulose carbamate but also those with the residual OH groups of the silica, which also contribute to retention too. If water interacts with silanol groups, the indifferent interaction of the solutes should become smaller and the retention time could decrease. The chiral interaction with the cellulose carbamate becomes predominant and α increases.

The most bulky alcohol **5**, was separated with a relatively high α at a relatively short retention time also without water. This can be caused on the one hand by a better steric fit in the chiral phase and on the other hand by the difficulty of reaching the OH groups of the silica.

We also performed a normal-phase separation (Si-60 column) of a mixture of 1-methyl-1-phenylpropanol (**3**) and the related hydroperoxide **8** in order to obtain more information about the influence of water or indifferent interactions with silanol groups, respectively. Using dried eluent [hexane–2-propanol (99.5:0.5)], the capacity factors of **8** and **3** were 3.31 and 4.02, respectively, whereas with water saturation the k' values were 4.54 and 4.10, respectively. Hence traces of water in the eluent in a normal-phase separation led to increasing retention times and a reversed elution order, *i.e.*, the retention mechanism changes. Moreover, in a normal-phase separation a much stronger effect of water addition on the hydroperoxide solute compared with the corresponding alcohol was found, the opposite of what happened with the chiral column. However, the effect of water on the retention and stereoselectivity seems to be caused by a more complex retention mechanism and further investigations are necessary.

Effect of temperature

As can be seen from Table II, there is also an influence of the ambient temperature on the retention (k'), separation factor (α) and stereochemical resolution (R_s) of solutes **1–10**. Increasing the temperature leads in all instance to decreased k' values, which means that the mobility of the solutes increases with increasing temperature and the interactions with the CSP decrease.

In most instances, except for **5**, α decreases slightly with increasing temperature. These findings correspond to a longer retention time at lower temperature, *i.e.*, a longer interaction with the CSP occurs. Most striking is the resolution behaviour of **5**. No separation at all occurs at 0°C, whereas for the corresponding hydroperoxide **10** the highest separation factor of all (α = 3.01) was obtained. No explanation can be given.

CONCLUSIONS

The CDMPC CSP is suitable for the separation of chiral hydroperoxides and alcohols. Water-saturated eluents effect increasing separation factors of the solutes investigated.

ACKNOWLEDGEMENT

The authors thank the Knauer KG for providing the chiral detector.

REFERENCES

1 T. Takata and W. Ando, *Bull. Chem. Soc. Jpn.*, 59 (1986) 1275.
2 M. Chmielewski, J. Jurczak and S. Maciejewski, *Carbohydr. Res.*, 165 (1987) 111.
3 P. Dussault and N. A. Porter, *J. Am. Chem. Soc.*, 110 (1988) 6276.
4 T. Shibata, I. Okamoto and K. Ishii, *J. Liq. Chromatogr.*, 9 (1986) 313.
5 J. W. Wainer, R. M. Stiffin and T. Shibata, *J. Chromatogr.*, 411 (1987) 139.
6 H. Hock and W. Susemiehl, *Chem. Ber.*, 66 (1933) 61.
7 H. Hock and S. Lang, *Chem. Ber.*, 75 (1942) 713; 76 (1943) 169.
8 E. Hägel, H. Kropf and S. Munke, in H. Kropf (Editor), *Methoden der organischen Chemie (Houben-Weyl)*, Georg Thieme, Stuttgart, 1988, Vol. E 13, p. 144.
9 Y. Okamoto, M. Kawashima and K. Hatada, *J. Chromatogr.*, 363 (1986) 173.
10 H. Koller, K.-H. Rimböck and A. Mannschreck, *J. Chromatogr.*, 282 (1983) 89.

Journal of Chromatography, 588 (1991) 356–360
Elsevier Science Publishers B.V., Amsterdam

CHROM. 23 709

Short Communication

High-performance liquid chromatography of heptaene polyenes: assay of heptaene produced by *Streptomyces griseoviridis*

Olavi Raatikainen*

Department of Pharmacology and Toxicology, University of Kuopio, P.O. Box 1627, SF-70211 Kuopio, and Department of Environmental Hygiene and Toxicology, National Public Health Institute, Kuopio (Finland)

(First received May 31st, 1991; revised manuscript received August 27th, 1991)

ABSTRACT

The antibiotic complex of a new heptaene polyene produced in *Streptomyces griseoviridis*, which is antagonistic to phytopathogenic fungi, was analysed by high-performance liquid chromatography (HPLC) and monitored with a diode-array detector. For reference six known heptaenes were also assayed. The individual components were separated on ODS Hypersil C_{18} using gradient or isocratic elution. Gradient elution was performed using 0.005 *M* EDTA buffer modified with methanol and acetonitrile. Isocratic separations were made with 0.05 *M* ammonium acetate modified with acetonitrile. Both elution systems separated the main components, but the gradient system eluted the long-retained components faster. The chromatogram of the heptaene isolated from *S. griseoviridis* was compared with those of aureofungin, candicidin, candimycin, hamycin and trichomycin. The heptaene synthesized by *S. griseoviridis* is a candicidin type, as indicated by HPLC.

INTRODUCTION

Polyenes are mixtures of compounds having a characteristic chromophore which contains 3–8 conjugated double bonds in the macrolide ring. The structures of various heptaenes possess seven conjugated double bonds and differ in the number of hydroxyl, keto and methyl groups attached to the ring. The absence or presence of an aromatic moiety indicates the aromatic nature of heptaenes, and typically they also contain an amino sugar moiety, mycosamine [1]. The aromatic character and sugar moiety can be evaluated by using modern chromatographic techniques [2]. Heptaenes and other polyenes are synthesized mainly in *Streptomyces* bacteria as multi-component complexes which can be separated by counter-current distribution or thin-layer or high-performance liquid chromatography (HPLC) [3,4].

Several column liquid chromatographic methods for qualitative and quantitative analyses of various polyene antibiotics have been published. Amphotericin B, a clinically used antifungal antibiotic against systemic fungal infections, has been determined quantitatively by an HPLC technique [5]. Other polyene antibiotics are generally analysed by HPLC [3,4].

In this paper I present an HPLC method suitable

* Present address: Department of Pharmaceutical Chemistry, University of Kuopio, P.O. Box 1627, SF-70211 Kuopio, Finland.

0021-9673/91/$03.50

for the assay of heptaene polyenes. The method was used for the assay of the heptaene complex formed in suppressive *Streptomyces griseoviridis* strains isolated from Finnish sphagnum peat [6]. One of these strains was introduced as a biological pesticide against fungal plant diseases [7], and an assay method is necessary for residue analysis.

EXPERIMENTAL

Polyenes

Seven heptaene polyenes were analyzed (Table I). The antibiotics were dissolved in dimethyl sulphoxide (DMSO) (Merck, Darmstadt, Germany) at a concentration of 1 mg/ml for HPLC analysis and were used within 1 day because of the instability of the DMSO solution of polyenes. The heptaene from *S. griseoviridis* (obtained from Dr. R. Tahvonen, Agricultural Research Centre, Jokioinen, Finland) was extracted from mycelium grown for 50 h (at 28°C) in a medium containing yeast extract, malt extract and glucose (1% each). This extract was used for HPLC analysis.

HPLC analysis

The HPLC equipment for gradient elution was a Hewlett-Packard (Waldbron, Germany) Model 1090 equipped with a diode-array detector and autosampler, integrator (HP 3392A) and computer (HP 85B) combined with a double disk drive (HP 9121). All the solvents used were of HPLC purity and water was purified with a Milli-Q system (Millipore, Molsheim, France).

All analyses were done by using columns (125 × 4.0 mm I.D.) filled with Shandon ODS Hypersil (5-μm particles) (Bischoff Chromatography, Leonberg, Germany) reversed-phase packing material.

Two solutions were used in the gradient separations: (A) 80% (v/v) 0.005 *M* ethylenediaminetetraacetic acid (EDTA) (pH 7.0) and 20% (v/v) acetonitrile–methanol (30:70) and (B) acetonitrile. The gradient (Fig. 1) was as follows:

$$0\ \text{min} \xrightarrow{20\%} 3 \xrightarrow{20\text{–}35\%} 3.1 \xrightarrow{35\text{–}40\%} 15 \xrightarrow{40\text{–}60\%} 20 \xrightarrow{60\text{–}60\%} 25 \xrightarrow{60\text{–}20\%} 25.1 \xrightarrow{20\text{–}20\%} 30\ \text{min}$$

where the percentages represent the amount or linear change in acetonitrile (B) in the mobile phase (1 ml/min) during the indicated periods.

Isocratic assays (Fig. 1) were performed with the HP 1090 system or using a system equipped with a Model T 414 LC pump (Kontron, Zürich, Switzerland), a Uvicon 735 LC detector (Kontron) at 380 nm, and an Enica 21 integrator (Delsi Instruments, Suresnes, France) using a normal injection system (Rheodyne). The mobile phase (1 ml/min) used in the isocratic elution was usually acetonitrile–0.05 *M* ammonium acetate, (pH 3.8) (40:60).

TABLE I

DESCRIPTION AND SOURCES OF THE ANALYSED HEPTAENE POLYENES[a]

Heptaene polyene	Sugar moiety	Aromatic moiety	Source[b]
Amphotericin B	Mycosamine	None	1
Aureofungin	Mycosamine	*p*-Aminoacetophenone N-Methyl-*p*-aminoacetophenone[c]	2
Candicidin	Mycosamine	*p*-Aminoacetophenone	1
Candimycin	Mycosamine	*p*-Aminoacetophenone N-Methyl-*p*-aminoacetophenone[c]	3
Hamycin	Mycosamine	*p*-Aminoacetophenone	2
Trichomycin	Mycosamine	*p*-Aminoacetophenone	4
Heptaene	Not assayed	Not assayed	5

[a] Data from ref. 1.

[b] 1 = Dumex (Copenhagen, Denmark); 2 = Hindustan Antibiotics (Pimpri, India); 3 = Takeda Chemical Industries (Osaka, Japan); 4 = Fujisawa Pharmaceutical (Osaka, Japan); 5 = this study.

[c] Data from ref. 2.

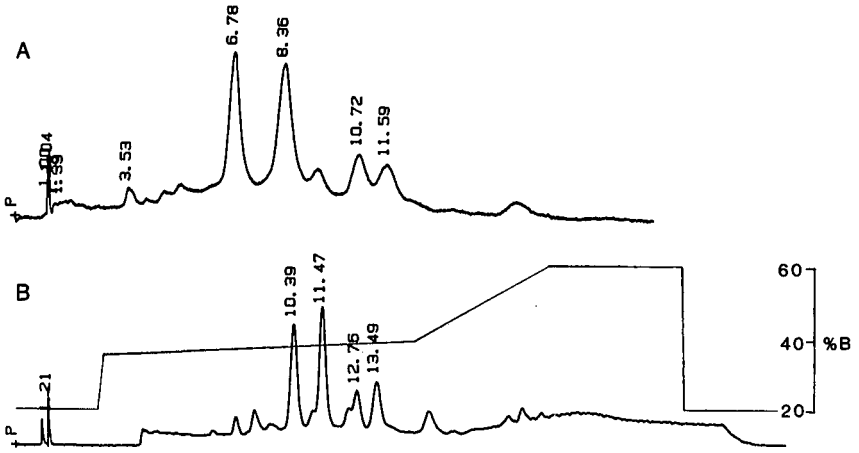

Fig. 1. HPLC separation of the individual components of candicidin complex (0.5 μg) with (A) isocratic or (B) gradient elution. The components were separated on ODS Hypersil C_{18}, monitored at 380 nm and eluted with the solvent compositions described in the text. Numbers at peaks indicate retention times in min.

RESULTS AND DISCUSSION

The chromatogram of a new heptaene isolated from *S. griseoviridis* was compared with those of the heptaene polyenes amphotericin B, aureofungin, candicidin, candimycin, hamycin and trichomycin. The chromatography of each (0.5 or 1.0 μg per injection) was performed using gradient or isocratic elution on 125 × 4 mm I.D. ODS Hypersil C_{18} columns and monitored at 380 nm (Fig. 1). The gradient system eluted all components in less than 30 min.

The heptaene produced by *S. griseoviridis* has one main component, but the pattern of the individual components is of the candicidin type. The relative intensities of the peaks differ from those of candicidin used as a reference standard (Fig. 2). This may be due to differences in the producer strains and in the composition of the culture media. The chromatogram shows also that there are many long-retained compounds dissimilar to candicidin. It is possible, however, that these long-retained components are produced by decomposition during

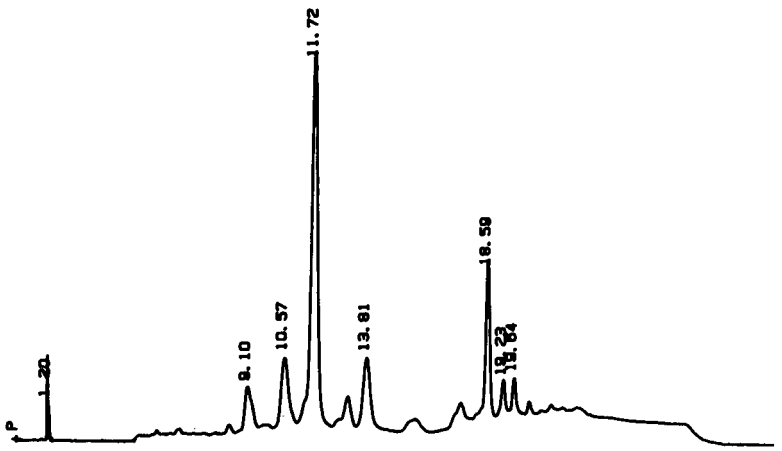

Fig. 2. HPLC of the heptaene polyene complex (1 μg) isolated from *S. griseoviridis*. Conditions as in Fig. 1B.

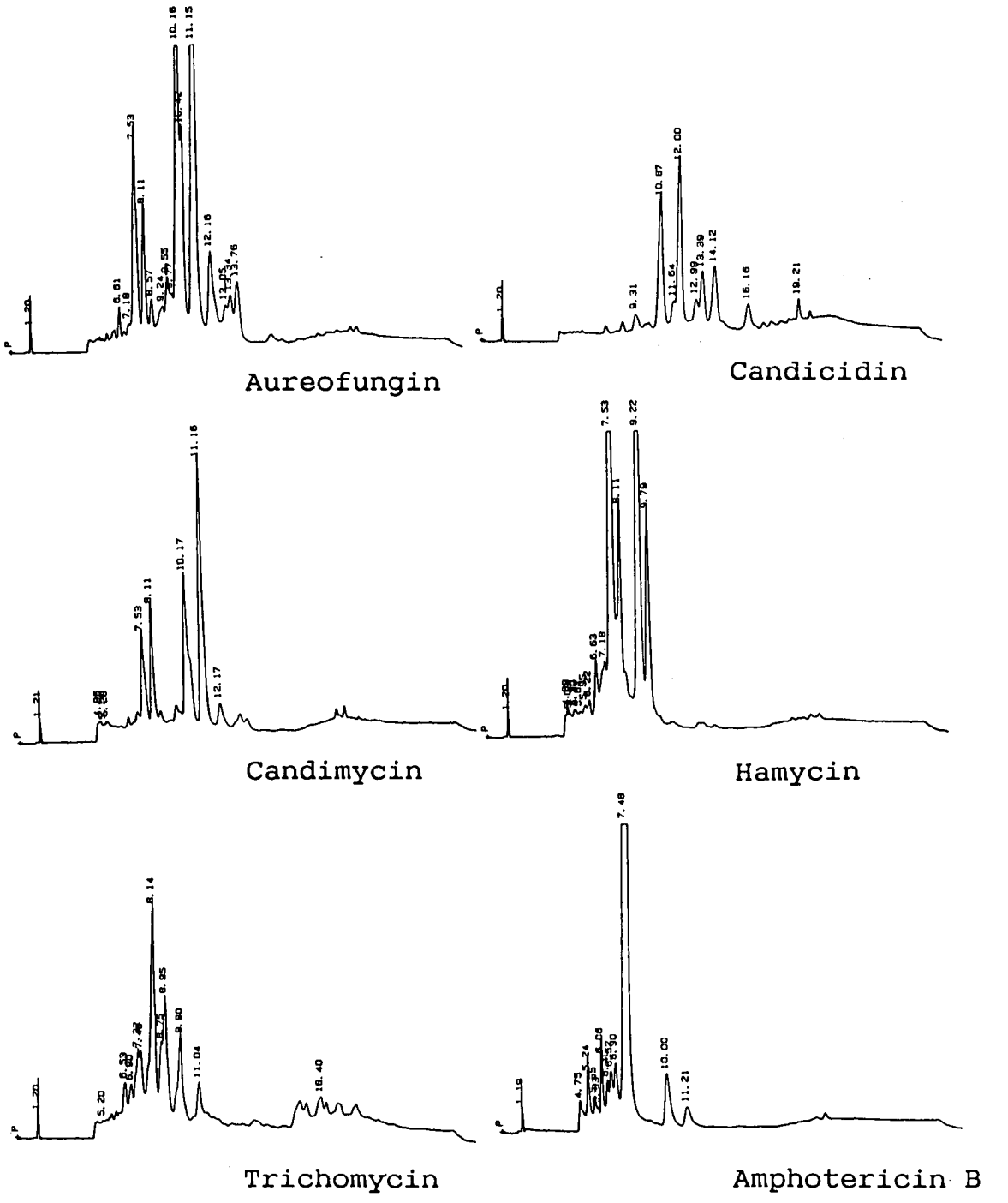

Fig. 3. HPLC of aureofungin, candicidin, candimycin, hamycin, trichomycin and amphotericin B (1.0 μg each). Conditions as in Fig. 1B.

the isolation of the polyene complex. By using the diode-array detector the heptaene character of these and the main peaks was also verified (data not shown).

Amphotericin B, a clinically used non-aromatic heptaene, consists of one major heptaene component and several other insignificant heptaene components (Fig. 3). Four aromatic heptaenes (hamycin, aureofungin, trichomycin, and candimycin) include 3–5 main components and all of them have many minor components (Fig. 3). The chromatograms of hamycin, aureofungin, trichomycin and candimycin were different from that of candicidin, but the HPLC data indicate that candimycin has the same individual components as aureofungin.

The further chemical characterization and biological effects of the heptaene produced by *S. griseoviridis* will be published separately.

ACKNOWLEDGEMENTS

I thank professor Dr. Jouko Tuomisto for obtaining the reference antibiotics. This work was financially supported by Kemira Research Centre (Espoo, Finland) and the Kemira Foundation (Helsinki, Finland). The skilful technical assistance of Mrs. A. Kinnunen is acknowledged.

REFERENCES

1 S. Ōmura and H. Tanaka, in S. Ōmura (Editor), *Macrolide Antibiotics, Chemistry, Biology, and Practice*, Academic Press, New York and London, 1984, p. 351.
2 O. Raatikainen, S. Auriola and J. Tuomisto, *J. Chromatogr.*, 585 (1991) 247.
3 A. H. Thomas, *Analyst (London)*, 101 (1976) 321.
4 A. Thomas and P. Newland, *J. Chromatogr.*, 354 (1986) 317.
5 J. W. Mayhew, C. Fiore, T. Murray and M. Barza, *J. Chromatogr.*, 274 (1983) 271.
6 R. Tahvonen, *J. Sci. Agric. Soc. Finl.*, 54 (1982) 345.
7 R. Tahvonen, *Bull. OEPP*, 18 (1988) 55.

Journal of Chromatography, 588 (1991) 361–364
Elsevier Science Publishers B.V., Amsterdam

CHROM. 23 756

Short Communication

Hydrogen bonding

XIX. The characterisation of two poly(methylphenylsiloxane)s

Michael H. Abraham*, Gary S. Whiting, Jenik Andonian-Haftvan and Jonathan W. Steed

Department of Chemistry, University College London, 20 Gordon Street, London WC1H 0AJ (UK)

Jay W. Grate

Chemistry Division, Naval Research Laboratory, Washington, DC 20375-5000 (USA)

(Received July 16th, 1991)

ABSTRACT

Two commercial samples of poly(methylphenylsiloxane) were characterised using our solvation equation,

$$\log L = c + rR_2 + s\pi_2^H + a\alpha_2^H + b\beta_2^H + l \log L^{16}$$

where L is the gas–liquid partition coefficient for a series of solutes on a given stationary phase, and the explanatory variables are R_2 an excess molar refraction, π_2^H the solute dipolarity/polarisability, α_2^H and β_2^H the solute hydrogen-bond acidity and basicity, and log L^{16} where L^{16} is the solute gas–liquid partition coefficient on hexadecane at 25°C. For both samples, a substantial b- constant was found, *viz.* 1.22 ± 0.07 and 0.49 ± 0.08 at 25°C, suggesting that they can act as hydrogen-bond acid (contrary to their chemical formulation). Examination of the bulk liquid stationary phases by IR showed the presence of OH groups and confirmed our analysis by the solvation equation. It is suggested that workers using the OV or SE series of siloxanes routinely check the bulk stationary phases by IR in order to assess the presence or absence of OH groups.

INTRODUCTION

Poly(methylsiloxanes) and poly(methylphenylsiloxanes), especially as the OV and SE series, are amongst the most common stationary gas–liquid chromatography phases, both as regards general analytical applications and more fundamental physico-chemical studies [1–5]. As part of our studies on solute–solvent interactions, we were interested in a liquid phase in which large dispersion interactions might be set up. Of the various poly(methylphenylsiloxanes), OV-25, which is a poly(diphenylphenylmethylsiloxane) with 75% phenyl substitution, seemed the most likely candidate for such a phase. Our method of characterising liquid phases, and of identifying solute–solvent interactions has been set out in detail before [6–8]. Retention data are obtained for a series of solutes on a given phase at a given

0021-9673/91/$03.50

temperature. These solute data, *SP*, can be specific retention volumes either at the column temperature, V_G, or corrected to 0°C, V_G^0, or they can be gas–liquid partition coefficients, *L*, or even relative retention times, *t*. Values of log *SP* for a series of solutes are then regressed against various solute parameters as explanatory variables through the multiple linear regression eqn. 1. These solute parameters are R_2 an excess solute molar volume [9], π_2^H our new solute dipolarity/polarisability parameter [7], α_2^H and β_2^H the solute hydrogen-bond acidity and basicity (more correctly these are effective or summation values, $\sum\alpha_2^H$ and $\sum\beta_2^H$ [7]), and log L^{16} where L^{16} is the solute gas–liquid partition coefficient on hexadecane at 25°C [10].

$$\log SP = c + rR_2 + s\pi_2^H + a\alpha_2^H + b\beta_2^H + l\log L^{16} \quad (1)$$

The constants in eqn. 1 are found by multiple linear regression analysis and serve to characterise the stationary phase as follows: *r* is the tendency of the phase to interact with solute π- and n-electron pairs, *s* is the phase dipolarity/polarisability, *a* is the phase hydrogen-bond basicity (because basic phases will interact with acidic solutes), *b* is the phase hydrogen-bond acidity, and *l* is an important constant that indicates how well the phase will separate homologues in any homologous series [6]. Each term in eqn. 1 thus corresponds to a specific solute–solvent interaction. We expected that OV-25 would give rise to rather large *r*- and *s*-constants due to the phenyl groups in the siloxane, to a small *a*-constant because OV-25 will be slightly basic, and to a zero *b* constant because the phase will not be a hydrogen-bond acid at all.

EXPERIMENTAL

Gas–liquid partition coefficients were obtained in the usual way [10] at 25°C; in the calculation of *L* values we took the density of the stationary phase as 1.15 g cm^3. Two samples were used. One from Petrach Chemicals we denote as SXPHA and one from Phase Separations we denote as SXPHB. In addition, we obtained relative retention times on an SXPHA column, modified by successive injections of trimethylchlorosilane: this column we denote as SXPHC. Stationary phases were coated onto Chromosorb GAW DMCS, 40–60 mesh, and column loadings were obtained by carefully weighing the stationary phase and the support into grease-free vessels prior to addition of acetone solvent, followed by careful evaporation. In addition, the dried coated support was extracted by acetone, and the residual support filtered off through a pre-weighed glass sinter. A blank experiment using an uncoated sample of inert support was run as a check. Column loadings by the original direct method were 9.99% on SXPHA and 9.93% on SXPHB. The extraction method gave loadings of 9.06% on SXPHA and 8.66% on SXPHB. Since the extractive method leads to the minimum loading, we have used the direct loadings in the calculation of *L* values. Use of the (lower) extraction method values would lead to log *L* values larger by 0.04 units on SXPHA and by 0.06 units on SXPHB. These would simply alter the *c* constant in the general eqn. 1 by the same amount. All results are collected in Table I.

Bulk samples of SXPHA and SXPHB were examined by *IR* as films between sodium chloride plates in the usual way.

$$\log L(\text{SXPHA}) = \underset{(0.06)}{-0.48} + \underset{(0.06)}{0.22R_2} + \underset{(0.07)}{0.95\pi_2^H} + \underset{(0.09)}{0.70\alpha_2^H} + \underset{(0.07)}{1.22\beta_2^H} + \underset{(0.014)}{0.815\log L^{16}} \quad (2)$$

$$n = 78 \quad R = 0.9928 \quad \text{S.D.} = 0.12$$

$$\log L(\text{SXPHB}) = \underset{(0.08)}{-0.79} + \underset{(0.08)}{0.24R_2} + \underset{(0.08)}{1.23\pi_2^H} + \underset{(0.09)}{0.63\alpha_2^H} + \underset{(0.08)}{0.49\beta_2^H} + \underset{(0.020)}{0.866\log L^{16}} \quad (3)$$

$$n = 42 \quad R = 0.9932 \quad \text{S.D.} = 0.10$$

$$\log t(\text{SXPHC}) = \underset{(0.10)}{-2.96} + \underset{(0.10)}{0.21R_2} + \underset{(0.09)}{1.03\pi_2^H} + \underset{(0.11)}{0.61\alpha_2^H} + \underset{(0.10)}{0.79\beta_2^H} + \underset{(0.030)}{0.800\log L^{16}} \quad (4)$$

$$n = 24 \quad R = 0.9923 \quad \text{S.D.} = 0.09$$

TABLE I

VALUES OF LOG L OR LOG t ON POLY(METHYLPHENYLSILOXANE) COLUMNS AT 25°C

Compound	Log L (SXPHA)	Log L (SXPHB)	Log t (SXPHC)	Compound	Log L (SXPHA)	Log L (SXPHB)	Log t (SXPHC)
Pentane			−1.13	Butyl propanoate	3.84	3.53	
Hexane	1.52	1.38	−0.86	Methyl trimethyl-acetate	2.69		
Heptane	2.02	1.92	−0.48	Acetonitrile		2.16	
Octane	2.51	2.37	0.00	Triethylamine	3.49		
Nonane	2.93	2.90		Nitromethane	2.55	2.40	−0.10
Decane	3.39	3.37	0.86	Nitroethane	2.90	2.78	0.30
Undecane	3.81			Methanol	1.82	1.42	−0.90
Dodecane	4.05			Ethanol	2.15		−0.59
Tetradecane	4.98			Propan-1-ol	2.58	2.03	−0.18
Cyclohexane	1.86			Propan-2-ol	2.24		
Dichloromethane	1.98	1.93		Butan-1-ol	3.01	2.53	0.28
Trichloromethane	2.32	2.24		2-Methylpropan-1-ol	2.67	2.31	−0.05
Tetrachloromethane	2.30	2.19		Butan-2-ol	2.67		
1,1-Dichloroethane	2.09			2-Methylpropan-2-ol	2.12	1.64	−0.54
1,2-Dichloroethane	2.60			Pentan-1-ol	3.43	2.98	
1,1,2,2-Tetrachloro-ethane	3.87			Hexan-1-ol	3.86	3.45	
1-Chlorobutane	2.31	2.21		Heptan-1-ol	4.28	3.87	
1-Chloropentane	2.78	2.66		Octan-1-ol	4.64		
1,5-Dichloropentane	4.33			Trifluoroethanol	1.60	1.34	−1.02
Trichloroethene	2.56			Hexafluoropropan-2-ol	1.53	1.36	−0.86
Tetrachloroethene	3.06			Benzene	2.51	2.45	0.00
Dibromomethane	2.91			Toluene	3.00	2.92	0.40
1-Bromobutane	2.75	2.67		Ethylbenzene	3.39		
1-Bromooctane	4.34			o-Xylene	3.52	3.46	
Diethyl ether	1.97	1.43	−0.83	Propylbenzene	3.71		
Di-n-butyl ether	3.36	3.12	0.75	Butylbenzene	4.13	4.11	
1,4-Dioxane		2.85	0.66	1,2,3,4-Tetramethyl-benzene	4.63		
Propanone	2.29	1.82	−0.39	Phenylethyne	3.58		
Butanone	2.69	2.28		Chlorobenzene	3.37		
Pentan-2-one	3.01	2.67		1,2-Dichlorobenzene	4.19		
Pentan-3-one	3.03			1,4-Dichlorobenzene	4.16		
Heptan-2-one	3.89	3.57		2-Chlorotoluene	3.81	3.77	
Octan-2-one	4.26	3.99		Bromobenzene	3.76	3.78	1.27
Nonan-2-one	4.67			Methylphenyl ether	3.87		
Cyclohexanone	4.21			Acetophenone	4.90		
Methyl formate	1.60			Methylbenzyl ketone	5.19		
Ethyl formate		1.82	−0.56	Methyl benzoate	4.86		
Propyl formate	2.50			Aniline	4.51		
Butyl formate	2.95	2.71		N,N-Dimethylaniline	4.67		
Methyl acetate	2.27			Pyrrole	3.30		
Pentyl acetate	3.64						
Ethyl propanoate	3.05	2.69	0.38				

RESULTS AND DISCUSSION

For the first commercial sample, denoted as SXPHA, we have log L values for 78 solutes at 25°C. We chose 25°C as the standard temperature so that in future we can compare results with those for numerous liquid phases that we are at present investigating. The various solute parameters were taken from our previous compilation [7]. Although we expected the b constant in eqn. 1 to be zero, we first regressed the log L values against all five solute parameters as a matter of course. We were thus very surprised to obtain eqn. 2. Here, the standard deviations of the constants are in parentheses, n is

the number of solutes, R is the overall correlation coefficient and $S.D.$ is the overall standard deviation in log L[16].

It seems clear that the b constant, 1.22 $\pm$ 0.07, is highly significant and therefore that SXPHA is quite acidic. This is not at all consistent with the chemical formulation of SXPHA as a copolymer of (45–55%) methylphenyl- and (45–55%) diphenyl-siloxane that is trimethylsiloxy terminated, and so we repeated measurements on a commercial sample of OV-25 intended for use as a GLC stationary phase; we denote this as SXPHB. The corresponding regression equation for 42 log L values is given as eqn. 3.

Although the b constant in eqn. 3 is much smaller than that in eqn. 2, it is still not zero. Hence either our methodology has produced spurious results or, indeed, our two samples contain hydrogen-bond acidic sites capable of interacting with solute hydrogen-bond bases (and these acidic sites could be part of the actual bulk liquid phase, or they could be sites on the solid support used to pack the columns). We resolved this problem by simply running the IR spectra of the original bulk liquid phases. Fig. 1 shows the spectra obtained between 1600 and 4000 cm^{-1}. Both phases show absorption at round 3500 cm^{-1}, the characteristic OH stretch wavenumber. Absorption is much stronger with sample SXPHA than with SXPHB. This result indicates that both bulk samples contain OH groups, and hence will act as hydrogen-bond acids. The regression equations, above, are hence not artifacts of our methodology but do serve as characteristic equations of the liquid phases. We checked our IR result by treating a packed column of SXPHA with trimethylchlorosilane in order to remove OH. Values of relative retention times, as log t, were regressed as usual to obtain eqn. 4.

This treatment indeed reduces the b constant from 1.22 in eqn. 2 to 0.79 in eqn. 4, as would be expected if the SXPHA column did contain OH groups. We therefore conclude that both our samples, SXPHA and SXPHB, contain OH groups and that our methodology has correctly shown this via the b-constant in eqns. 2–4. As far as our original aim is concerned, the r-constant in eqn. 3 is not particularly large, but the s-constant, 1.23 $\pm$ 0.08, must reflect the rather large dipolar/polarisability effect of the aromatic rings and the OH groups. More important, we feel, is our finding that samples of OV-25 may contain previously unsuspected OH groups, that measurably influence sorption at 25°C, and we suggest that workers who use the OV or SE series of siloxanes, examine the bulk liquid phases by IR in order to define better the chemical nature of the stationary phases they are using.

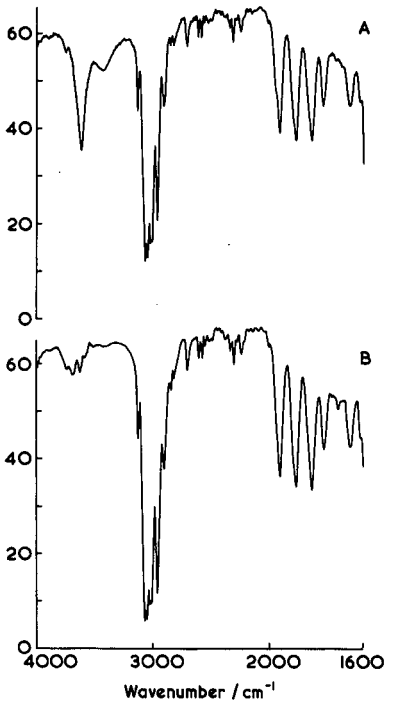

Fig. 1. The IR spectrum of the two samples of (A) SXPHA and (B) SXPHB.

ACKNOWLEDGEMENT

We thank the US Navy for support under contract N60921-87-D-A315.

REFERENCES

1 J. F. Parcher, J. R. Hansbrough and A. M. Koury, *J. Chromatogr. Sci.*, 16 (1978) 183.
2 C.-F. Chien, M. M. Kopečni and R. J. Laub, *J. High Resolut. Chromatogr. Chromatogr. Commun.*, 4 (1981) 539.
3 C.-F. Chien, D. L. Furio, M. M. Kopečni and R. J. Laub, *J. High Resolut. Chromatogr. Chromatogr. Commun.*, 6 (1983) 577, 669.
4 C.-F. Chien, M. M. Kopečni and R. J. Laub, *J. Chromatogr. Sci.*, 22 (1984) 1.
5 R. J. Laub, *J. High Resolut. Chromatogr. Chromatogr. Commun.*, 10 (1987) 565.
6 M. H. Abraham, G. S. Whiting, R. M. Doherty and W. J. Shuely, *J. Chromatogr.*, 518 (1990) 329.
7 M. H. Abraham, G. S. Whiting, R. M. Doherty and W. J. Shuely, *J. Chromatogr.*, 587 (1991) 213.
8 M. H. Abraham, G. S. Whiting, R. M. Doherty and W. J. Shuely, *J. Chromatogr.*, 587 (1991) 229.
9 M. H. Abraham, G. S. Whiting, R. M. Doherty and W. J. Shuely, *J. Chem. Soc., Perkin Trans. 2*, (1990) 1451.
10 M. H. Abraham, P. L. Grellier and R. A. McGill, *J. Chem. Soc., Perkin Trans. 2*, (1987) 797.

Journal of Chromatography, 588 (1991) 365–366
Elsevier Science Publishers B.V., Amsterdam

CHROM. 23 741

Book Review

Handbook of thin-layer chromatography, edited by J. Sherma and B. Fried, Marcel Dekker, New York, 1991, VIII + 1047 pp., price US$ 165, ISBN 0-8247-8335-2.

In the *Chromatographic Science Series*, edited by Jack Cazes, several monographs devoted to the techniques and applications of thin-layer chromatography (TLC) have been published. Less than 1 year after publishing the book by Grinberg in this series, there now appears another monograph (so far the largest), entitled *Handbook of Thin-Layer Chromatography*. The editors of this monograph, J. Sherma and B. Fried, decided to follow the now classical handbook on TLC by Egon Stahl, the last English edition of which appeared in 1969. Sherma and Fried's book covers mainly the last 20 years. On 1047 pages, 44 authors (31 from Europe, where TLC accommodated itself most, 8 from the USA, 4 from India and 1 from Canada) present the theory and general practice of TLC (13 chapters, 350 pages) followed by applications (18 chapters, 670 pages). The book also contains a glossary, selective directory of manufacturers and suppliers of instruments and products for TLC (68 from the USA, 16 from Europe and 1 from Canada) and finally a Subject Index. The bibliography of the individual chapters contains altogether over 2700 references, predominantly from the period 1975–88.

There is no doubt that this is the most voluminous monograph in the area of TLC since Kirchner's book published in 1978. Although Sherma and Fried are experienced Editors of recognized journals and monographs, unfortunately it must be concluded that in this case their intentions have not been fully materialized. Their aim was, as stated in the Preface, to have a book of uniform style, but this is reflected only in the formal categorization of the subjects in individual chapters, with endless repetition of subjects such as layer preparation and sorbents. Considerable attention was paid to the tables which, however, some authors took from the literature without appropriate judgement (the longest chapter on inorganic TLC has 78 pages, of which there are 67 pages of tables, 6 pages of references and only 5 pages of text). Generalization of results and recommendations of the most advantageous procedures are mostly missing. In addition, the sizes of individual chapters in both the general and application parts are considerably unbalanced and the size of a chapter does not always correspond to its importance. If we take the bibliographic reviews in the *Journal of Chromatography* (which are not quoted in this monograph at all) as a certain criterion of how TLC has spread for a particular group of compounds, then within the last 5 years most attention has been paid to the TLC of drugs, lipids and steroids. In this monograph, however, these categories of compounds are paid much less attention than, *e.g.*, polymers or inorganic compounds (lipids, 32 pages; inorganic ions, 78 pages). Also, as far as the bibliographic data are concerned, there is a lack of balance (46 quotations on drugs compared with 224 quotations on phenols, aromatic acids and indoles). In the selection of chapters I really missed the coverage of alkaloids (some of them are included under toxins) and amines (*e.g.*, polyamines and catecholamines).

As in most multi-author books, here also there are chapters which are very good and others which do not reach the expected quality. In the general part, the authors of some chapters have used the allotted space mainly for commercial purposes. Others have tried hard to avoid this, as in the chapter on sorbents, although here a table comparing different commercial products and their properties would have been welcomed by potential readers. In the application part the chapter on pharmaceuticals and drugs is one of the weakest, although this is the most important area of applications of chromatography. Not only is this chapter far too short, but

out of the 36 pages half are devoted to a table presenting the structures of 153 drugs taken from the Merck Index. This table lacks any data about chromatographic behaviour and, what is more, the majority of these compounds are not mentioned in this chapter at all! It is surprising that experienced Editors could have accepted such a chapter for inclusion.

In books of this type, a glossary is generally useful; however, here the authors underestimate the reader. How can one otherwise explain entries such as homologue, isomer, nanogram, conjugate, metabolite and a number of others? On the other hand, some chromatographically important terms are missing and some definitions are not correct. The Subject Index is another weakness: it is compiled very superficially mainly from the subchapter headings. The reader has no chance of finding here either the basic entries relating to the theory and techniques of TLC, or entries about individual categories of compounds and individual chemical entities. With a book of this size and intention, where moreover the contents of all the subchapters are lacking, this is a considerable drawback. Typographically the book is well presented apart from two points: the subdivision is confusing, where instead of a decimal categorization of subchapters, here Roman numbering, then capitals, Arabic numbering and again Arabic numbering is used (*e.g.*, Chapter III–C–1–1), and the size of figures does not correspond to the amount of information contained in them (compare, *e.g.*, the chromatograms on pages 125 and 573).

It is pity that this large and in many respects timely monograph which was surely to be sought particularly by the younger and starting professionals in the TLC field is likely not to satisfy their expectations.

Prague (Czechoslovakia) Karel Macek

Journal of Chromatography, 588 (1991) 367–368
Elsevier Science Publishers B.V., Amsterdam

CHROM. 23 768

Book Review

Luminescence techniques in chemical and biochemical analysis (*Practical Spectroscopy Series*, Vol. 12), edited by W. R. G. Bayens, D. De Keukeleire and K. Korkides, Marcel Dekker, New York, 1991, XV + 654 pp., price US$ 150.00 (USA and Canada), US$ 180.00 (rest of world), ISBN 0-8247-8369-7.

In liquid chromatography (LC), without any doubt fluorescence is the best known mode of molecular luminescence spectrometry, frequently applied for detection purposes. For natively fluorescent analytes high sensitivities are attained; further, for real sample analyses the inherent selectivity of fluorescence detection is appropriate: various potentially interfering compounds do not emit any fluorescence and, additionally, two wavelength settings are available, *i.e.*, the emission and the excitation wavelengths. For non-fluorescent analytes, chemical derivatization can be involved.

The book reviewed here illustrates that luminescence techniques have far more potential than the conventional fluorescence method described above. In fact, only a few out of the nineteen chapters are more or less related to luminescence detection in LC. Del Castillo, Alverez-Builla and Lerner present an extensive overview on fluorogenic reagents and fluorescent probes, not only considering chemical modifications of non-fluorescent analytes, but also physico-chemical modifications. The latter are directed to the improvement of quantum yields of already fluorescent molecules, for instance by changing the molecular environment. Applications in high-performance LC, thin-layer chromatography and fluoroimmunoassays and studies of proteins and other macromolecules and biological membranes are treated. A fairly complete, clearly written overview of the developments in laser-based detection in LC, covering the literature up to 1988, is presented by Van den Beld and Lingeman. They do not confine themselves to fluorescence detection as other laser techniques are also discussed. There is a chapter on sample clean-up for LC directed to bioactive substances and drugs in biological materials written by Takahagi and Imai, a useful paper but a little outside the scope of the book. Finally, there is a compact but nevertheless complete chapter by Nieman on chemiluminescence (CL) in flow-injection analysis and LC.

Including Nieman's paper, five chapters are devoted to CL. Jansen *et al.* consider CL immunoassays in veterinary and food analysis, where the applications are primarily directed to the analysis of anabolic agents. In another chapter, written by Zomer *et al.*, the attention is focused on acridinium ester-labelled compounds for CL immunoassays and detailed experimental information is provided. Kricka, Stott and Thorpe survey the developments and applications of a new type of chemiluminescence assay, enhanced CL of the luminol–hydrogen peroxide system, for horseradish peroxidase. An interesting paper is devoted to the CL of 1,2-dioxetanes, with emphasis on chemical behaviour, *i.e.*, synthesis, decomposition and mechanisms, written by the physical-organic chemists Hummelen, Wijnberg, *et al.* Of course, the state of the art concerning fluoroimmunoassays is also discussed in the book, in a contribution by Schulman, Hochhaus and Karnes.

Apart from the chapter on laser-based detection in LC, the techniques mentioned above do not require specialized, highly sophisticated instrumentation. This is completely different for the other subjects to be discussed, chapters written by specialists and devoted to relatively novel and not readily conceivable luminescence techniques. Three chapters are focused on time-resolved measurements in fluorescence spectroscopy. In contrast to phosphorescence and lanthanide luminescence, where the luminescence decays slowly, in fluorescence the lifetimes can be as short as 1 ns so that complicated instrumentation is required, almost exclusively used by

experts in the field. Two approaches are discussed, *i.e.*, measurements in the time domain (pulse fluorimetry) and in the frequency domain. The former, described by Boens, is usually denoted the single-photon timing technique. Repetitive excitation of the sample is performed, for instance, by a mode-locked tunable dye laser with a high pulse repetition rate and pulses of picosecond duration; the time delay between the start of the excitation pulse and the moment the photon is emitted from the sample is measured. Currently, decay times as short as a few picoseconds can be determined and the dynamic range of the technique is phenomenal. In the frequency-domain approach, the light source is modulated sinusoidally at a given frequency and both the phase delay and the relative modulation of the fluorescence with respect to the exciting light are determined. Two chapters are devoted to frequency-domain fluorimetry: Gratton *et al.* focus their attention on the technique as such, while Lakowicz *et al.* provide some applications.

The polarization of luminescence radiation also provides interesting analytical potential. One chapter (written by Brittain) is concerned exclusively with circularly polarized luminescence of chiral lanthanide complexes in solution, an important aid in characterizing lanthanide coordination chemistry. Furthermore, fluorescence detection can be utilized to measure circular dichroism (CD) in biochemical analysis, as outlined by Thomas, Patonay and Warner. Thus, chiral fluorophores are detected very sensitively. Especially the combination of CD absorption measurements and fluorescence-detected CD is interesting.

Leiner, Hubmann and Wolfbeis discuss the potential of total luminescence spectrometry with emphasis on biochemical analysis. Whereas in conventional luminescence spectrometry usually spectra of complex mixtures cannot be resolved satisfactorily, a multiparametric presentation of luminescence is frequently very helpful: mostly the fluorescence intensity as a function of excitation and emission wavelengths is presented as an excitation–emission matrix (EEM). The availability of multi-channel detectors has greatly reduced the recording time of EEMs.

Even more detailed spectral information can be obtained by utilizing fluorescence line narrowing, a cryogenic, laser-based fluorescence technique, revealing extremely narrow-line spectra. Cooper, Jankowiak and Small discuss the potential of this technique in studying the adducts between metabolites of benzo[*a*]pyrene and DNA. The same type of interaction is the subject of the chapter written by Geacintov and Kim, but these authors confine themselves to fluorescence quenching and optical detection of magnetic resonance (ODMR), a rather specialized phosphorescence technique.

To summarize, this book provides a wealth of information on the achievements and potential of a wide variety of luminescence techniques. As such, it should be available in any large library. Its main shortcoming is that the chapters are completely independent. In order to understand the specialized subjects, the reader will probably need to consult the basic literature fairly frequently.

Amsterdam (Netherlands) Cees Gooijer

Author Index

PUBLICATION SCHEDULE FOR 1992

Journal of Chromatography and *Journal of Chromatography, Biomedical Applications*

MONTH	O 1991	N 1991	D 1991	J	
Journal of Chromatography	585/1	585/2 586/1 586/2 587/1	587/2 588/1+2	589/1+2 590/1 590/2	The publication schedule for further issues will be published later
Cumulative Indexes, Vols. 551–600					
Bibliography Section					
Biomedical Applications				573/1 573/2	

INFORMATION FOR AUTHORS

(Detailed *Instructions to Authors* were published in Vol. 558, pp. 469–472. A free reprint can be obtained by application to the publisher, Elsevier Science Publishers B.V., P.O. Box 330, 1000 AH Amsterdam, The Netherlands.)

Types of Contributions. The following types of papers are published in the *Journal of Chromatography* and the section on *Biomedical Applications:* Regular research papers (Full-length papers), Review articles and Short Communications. Short Communications are usually descriptions of short investigations, or they can report minor technical improvements of previously published procedures; they reflect the same quality of research as Full-length papers, but should preferably not exceed five printed pages. For Review articles, see inside front cover under Submission of Papers.

Submission. Every paper must be accompanied by a letter from the senior author, stating that he/she is submitting the paper for publication in the *Journal of Chromatography*.

Manuscripts. Manuscripts should be typed in double spacing on consecutively numbered pages of uniform size. The manuscript should be preceded by a sheet of manuscript paper carrying the title of the paper and the name and full postal address of the person to whom the proofs are to be sent. As a rule, papers should be divided into sections, headed by a caption (*e.g.*, Abstract, Introduction, Experimental, Results, Discussion, etc.). All illustrations, photographs, tables, etc., should be on separate sheets.

Introduction. Every paper must have a concise introduction mentioning what has been done before on the topic described, and stating clearly what is new in the paper now submitted.

Abstract. All articles should have an abstract of 50–100 words which clearly and briefly indicates what is new, different and significant.

Illustrations. The figures should be submitted in a form suitable for reproduction, drawn in Indian ink on drawing or tracing paper. Each illustration should have a legend, all the *legends* being typed (with double spacing) together on a *separate sheet*. If structures are given in the text, the original drawings should be supplied. Coloured illustrations are reproduced at the author's expense, the cost being determined by the number of pages and by the number of colours needed. The written permission of the author and publisher must be obtained for the use of any figure already published. Its source must be indicated in the legend.

References. References should be numbered in the order in which they are cited in the text, and listed in numerical sequence on a separate sheet at the end of the article. Please check a recent issue for the layout of the reference list. Abbreviations for the titles of journals should follow the system used by *Chemical Abstracts*. Articles not yet published should be given as "in press" (journal should be specified), "submitted for publication" (journal should be specified), "in preparation" or "personal communication".

Dispatch. Before sending the manuscript to the Editor please check that the envelope contains four copies of the paper complete with references, legends and figures. One of the sets of figures must be the originals suitable for direct reproduction. Please also ensure that permission to publish has been obtained from your institute.

Proofs. One set of proofs will be sent to the author to be carefully checked for printer's errors. Corrections must be restricted to instances in which the proof is at variance with the manuscript. "Extra corrections" will be inserted at the author's expense.

Reprints. Fifty reprints of Full-length papers and Short Communications will be supplied free of charge. Additional reprints can be ordered by the authors. An order form containing price quotations will be sent to the authors together with the proofs of their article.

Physical Sciences Data Volume 43

Vapor-Liquid Equilibrium Data - Salt Effect

by **S. Ohe**, Department of Engineering, Science University of Tokyo, Japan

Vapor-liquid equilibrium (VLE) data of solutions are necessary for the design of distillation and absorption processes. VLE exhibits various characteristics depending on the type of solution. In the case of nonideal solutions, an azeotropic mixture is formed which cannot be separated by ordinary distillation. The mixture must be separated by adding a third component, called an entrainer, which has the capability of breaking the azeotropic point. In most cases, a volatile component is employed as an entrainer for an azeotropic mixture. However, salt is also effective in breaking the point; this is called the salt effect on VLE. Much has been observed on salt effect, however very few commercial distillation plants use this method. This book aims to cover all reported data found in journals on salt effect on VLE.

Prediction methods for VLE at low and high pressures for systems composed of volatile substances are used routinely, However, no method to predict the salt effect on VLE is in use, because salts show entirely different behavior from volatile substances. A method to predict salt effect based on preferential solvation was reported by the author in 1976. 30 systems were examined and the formation of preferential solvates between the salt and one of the volatile components was shown. Continuing the work, the formation of preferential solvates for almost all salt effect data has been examined. As a result of this work, it has been found that preferential solvates are formed without exception.

In this volume, the preferential solvation numbers determined by least squares method are shown by processing the data of salt effect on VLE.

Contents:

1991 xxxii + 360 pages
Price: US $ 218.00 / Dfl. 425.00
ISBN 0-444-98687-1

Co-edition with and distributed in Japan by Kodansha Scientific Ltd.

Elsevier Science Publishers

P.O. Box 211, 1000 AE Amsterdam, The Netherlands
P.O. Box 882, Madison Square Station, New York, NY 10159, USA